frontiers | Research Topics

Recent advancements in musculoskeletal regenerative medicine

Edited by
Elizabeth Vinod, Csaba Matta and
Boopalan Ramasamy

Published in
Frontiers in Cell and Developmental Biology
Frontiers in Bioengineering and Biotechnology

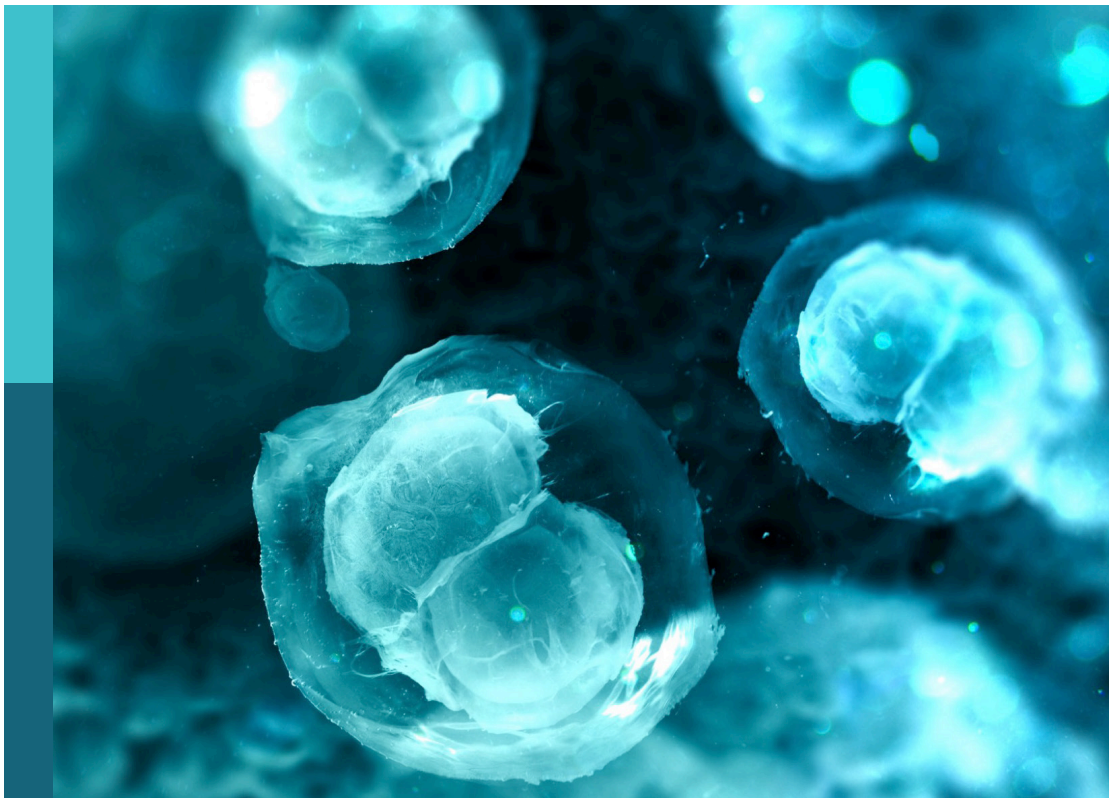

FRONTIERS EBOOK COPYRIGHT STATEMENT

The copyright in the text of individual articles in this ebook is the property of their respective authors or their respective institutions or funders. The copyright in graphics and images within each article may be subject to copyright of other parties. In both cases this is subject to a license granted to Frontiers.

The compilation of articles constituting this ebook is the property of Frontiers.

Each article within this ebook, and the ebook itself, are published under the most recent version of the Creative Commons CC-BY licence. The version current at the date of publication of this ebook is CC-BY 4.0. If the CC-BY licence is updated, the licence granted by Frontiers is automatically updated to the new version.

When exercising any right under the CC-BY licence, Frontiers must be attributed as the original publisher of the article or ebook, as applicable.

Authors have the responsibility of ensuring that any graphics or other materials which are the property of others may be included in the CC-BY licence, but this should be checked before relying on the CC-BY licence to reproduce those materials. Any copyright notices relating to those materials must be complied with.

Copyright and source acknowledgement notices may not be removed and must be displayed in any copy, derivative work or partial copy which includes the elements in question.

All copyright, and all rights therein, are protected by national and international copyright laws. The above represents a summary only. For further information please read Frontiers' Conditions for Website Use and Copyright Statement, and the applicable CC-BY licence.

ISSN 1664-8714
ISBN 978-2-8325-6941-2
DOI 10.3389/978-2-8325-6941-2

Generative AI statement
Any alternative text (Alt text) provided alongside figures in the articles in this ebook has been generated by Frontiers with the support of artificial intelligence and reasonable efforts have been made to ensure accuracy, including review by the authors wherever possible. If you identify any issues, please contact us.

About Frontiers

Frontiers is more than just an open access publisher of scholarly articles: it is a pioneering approach to the world of academia, radically improving the way scholarly research is managed. The grand vision of Frontiers is a world where all people have an equal opportunity to seek, share and generate knowledge. Frontiers provides immediate and permanent online open access to all its publications, but this alone is not enough to realize our grand goals.

Frontiers journal series

The Frontiers journal series is a multi-tier and interdisciplinary set of open-access, online journals, promising a paradigm shift from the current review, selection and dissemination processes in academic publishing. All Frontiers journals are driven by researchers for researchers; therefore, they constitute a service to the scholarly community. At the same time, the *Frontiers journal series* operates on a revolutionary invention, the tiered publishing system, initially addressing specific communities of scholars, and gradually climbing up to broader public understanding, thus serving the interests of the lay society, too.

Dedication to quality

Each Frontiers article is a landmark of the highest quality, thanks to genuinely collaborative interactions between authors and review editors, who include some of the world's best academicians. Research must be certified by peers before entering a stream of knowledge that may eventually reach the public - and shape society; therefore, Frontiers only applies the most rigorous and unbiased reviews. Frontiers revolutionizes research publishing by freely delivering the most outstanding research, evaluated with no bias from both the academic and social point of view. By applying the most advanced information technologies, Frontiers is catapulting scholarly publishing into a new generation.

What are Frontiers Research Topics?

Frontiers Research Topics are very popular trademarks of the *Frontiers journals series*: they are collections of at least ten articles, all centered on a particular subject. With their unique mix of varied contributions from Original Research to Review Articles, Frontiers Research Topics unify the most influential researchers, the latest key findings and historical advances in a hot research area.

Find out more on how to host your own Frontiers Research Topic or contribute to one as an author by contacting the Frontiers editorial office: frontiersin.org/about/contact

Recent advancements in musculoskeletal regenerative medicine

Topic editors
Elizabeth Vinod — Christian Medical College and Hospital, India
Csaba Matta — University of Debrecen, Hungary
Boopalan Ramasamy — Royal Adelaide Hospital, Australia

Citation
Vinod, E., Matta, C., Ramasamy, B., eds. (2025). *Recent advancements in musculoskeletal regenerative medicine*. Lausanne: Frontiers Media SA.
doi: 10.3389/978-2-8325-6941-2

Table of contents

frontiers | Frontiers in Cell and Developmental Biology

TYPE Editorial
PUBLISHED 22 September 2025
DOI 10.3389/fcell.2025.1688419

Check for updates

OPEN ACCESS

EDITED AND REVIEWED BY
Michael De Lisio,
University of Ottawa, Canada

*CORRESPONDENCE
Elizabeth Vinod,
elsyclarence@cmcvellore.ac.in

‡These authors have contributed equally to this work

RECEIVED 19 August 2025
ACCEPTED 29 August 2025
PUBLISHED 22 September 2025

CITATION
Matta C, Ramasamy B and Vinod E (2025) Editorial: Recent advancements in musculoskeletal regenerative medicine. *Front. Cell Dev. Biol.* 13:1688419. doi: 10.3389/fcell.2025.1688419

COPYRIGHT
© 2025 Matta, Ramasamy and Vinod. This is an open-access article distributed under the terms of the Creative Commons Attribution License (CC BY). The use, distribution or reproduction in other forums is permitted, provided the original author(s) and the copyright owner(s) are credited and that the original publication in this journal is cited, in accordance with accepted academic practice. No use, distribution or reproduction is permitted which does not comply with these terms.

Editorial: Recent advancements in musculoskeletal regenerative medicine

Csaba Matta [1‡], Boopalan Ramasamy [2‡] and Elizabeth Vinod [3,4*]

[1]Department of Anatomy, Histology and Embryology, Faculty of Medicine, University of Debrecen, Debrecen, Hungary, [2]Department of Orthopaedics, Royal Adelaide Hospital and Adelaide University, Adelaide, SA, Australia, [3]Department of Physiology, Christian Medical College, Vellore, India, [4]Centre for Stem Cell Research, (A unit of BRIC-InStem, Bengaluru), Christian Medical College, Vellore, India

KEYWORDS

musculoskeletal regenerative medicine, mesenchymal stem cells, cartilage and bone repair, single-cell transcriptomics, smart biomaterials and hydrogels, exosome-mediated signaling, inflammation and immunomodulation, translational orthobiologics

Editorial on the Research Topic
Recent advancements in musculoskeletal regenerative medicine

Introduction

Musculoskeletal regenerative medicine continues to evolve rapidly, offering renewed hope for patients with cartilage, bone, and joint disorders that currently lack durable treatments. This Research Topic features ten original contributions that collectively illustrate how the field is moving beyond traditional repair paradigms, integrating cellular engineering, smart biomaterials, immunomodulatory strategies, exosome signaling, and system-level insights. In this editorial, we contextualize these contributions, highlight their translational and clinical implications, and outline priorities for the future in musculoskeletal regeneration.

Highlights from the Research Topic

Kim et al. harnessed engineered MSCs expressing a doxycycline-inducible IL-1β "sticky-trap," a membrane-bound decoy receptor. The construct enables localized binding of IL-1β without systemic release, retaining it at joint surfaces. This innovative design allowed local, matrix-retained cytokine modulation while sparing systemic physiology. Intra-articular injection in a murine destabilization of the medial meniscus (DMM) model reduced cartilage degeneration, synovitis, and MMP-13 expression, while preserving type II collagen, illustrating the feasibility of durable, site-specific control of chronic inflammation, a major unmet need in osteoarthritis (OA).

Peng et al. created a single-cell RNA sequencing atlas of cystic lesions in steroid-induced osteonecrosis of the femoral head and identified eight chondrocyte subsets, including homeostatic, fibrocartilaginous, inflammatory, and hypertrophic. A reparative hypertrophic

population expressing *CLIC3* showed osteogenic potential transitioning toward bone. Histology confirmed a cartilage-to-bone interface within lesions, outlining a reparative trajectory involving chondrocyte hypertrophy preceding bone formation. This atlas is a blueprint of *in situ* repair processes in necrotic bone and identifies targetable cell populations for future therapy. This approach highlights how mapping cell states at disease interfaces can unveil targets for regeneration without the need for fully exogenous interventions.

Chen et al. explored the dual role of graphene oxide (GO) in skeletal muscle regeneration and its downstream effects on osteoblasts, showing that larger GO particles (>500 nm) enhanced myoblast proliferation and differentiation via PI3K–Akt signaling and NFATc1 upregulation. Also, exosomes from GO-treated myoblasts also stimulate osteoblastogenesis by upregulating osteogenic genes in MC3T3-E1 cells, suggesting muscle–bone crosstalk. GO acts both as a scaffold that supports myogenic maturation and a modulator of paracrine signaling, with potential to coordinate musculoskeletal repair. By positioning muscle regeneration within the broader musculoskeletal unit, this work underscores the systemic perspective required for tissue repair, where local interventions may have cascading effects across connected tissues.

Firoozi et al. compared meniscus-derived matrix scaffolds from healthy versus OA donors. While both supported fibro-chondrocyte viability and matrix deposition, only healthy donor scaffolds improved integration strength. Subtle biochemical or structural alterations in OA tissue may impair repair outcomes, even when decellularization is adequate. This work highlights the significance of donor tissue quality as an often-overlooked determinant of scaffold success, emphasizing the need for standardized screening or synthetic alternatives.

Ilyas Khan and Anderson-Watters demonstrated the ability of BMP9 in promoting cartilage maturation in immature cartilage explants. BMP9 improved collagen alignment, zonal organization, and proteoglycan content, resembling postnatal cartilage. These changes were accompanied by increased stiffness and matrix remodeling features often lacking in engineered constructs. The study supports BMP9 as a tool to accelerate functional maturation of engineered cartilage and addresses a critical translational gap between engineered and native tissues in load-bearing applications where constructs must not only survive implantation but also withstand mechanical load over time.

Santiago et al. conducted a systematic review and meta-analysis comparing platelet-rich plasma (PRP) versus PRP combined with hyaluronic acid (HA) for hip OA. While both treatments improved pain and function in the short term, PRP alone was more effective in pain relief. Since HA addition did not enhance outcomes and was occasionally linked to discomfort, the results question the additive value of HA and the need for protocol harmonization and evidence-based refinement of orthobiologic interventions before broad clinical uptake.

Desando et al. highlight the translational potential of mechanically isolated stromal vascular fraction (mctSVF) in OA. In a preclinical rabbit model, mctSVF promoted osteochondral repair, mitigated synovial inflammation, and preserved meniscal integrity, matching outcomes seen with expanded adipose stromal cells. By retaining native microarchitecture, mctSVF offers a minimally manipulated, clinically relevant approach to cartilage protection and joint regeneration.

Ivanovska et al. reveal that MSCs adapt dynamically to the OA joint environment. In a murine model, intra-articularly delivered MSCs persisted as a subset capable of modulating macrophage-driven inflammation and supporting cartilage repair. Transcriptomic analysis highlighted disease-stage -dependent activation and identified BRINP3 as a potential regulator of MSC function. These findings emphasize the context-specific plasticity of MSCs, offering insight into tailored cell-based interventions for OA.

Ossanna et al. demonstrate that mechanically isolated stromal vascular fraction (HT-SVF) combined with low -molecular-weight hyaluronic acid (ACP) markedly enhances bone regeneration in a murine calvarial defect model. Compared with enzymatically processed SVF, HT-SVF + ACP improved bone matrix maturity, reduced fibrosis, and accelerated healing. These results underscore the translational potential of mechanically processed SVF as a cost-effective, cell-based regenerative strategy for bone and tissue repair.

Finally, Velot et al. provided a perspective acknowledging the contributions of women in stem cell–based OA therapies and underscoring ongoing disparities in recognition and leadership roles. This piece calls for systemic solutions and reminds us that advancing regenerative medicine is not just a technical endeavor, but also a sociocultural one tied to equity and inclusive leadership.

Conclusion

Collectively, these contributions demonstrate how musculoskeletal regenerative medicine is shifting toward precision interventions featuring targeted modulation of inflammation, the development of smarter scaffolds and biomaterials, and system-level insights for the interconnected biology of musculoskeletal tissues. The collection emphasizes not only structural regeneration but also functional recovery and long-term integration, which are fundamental for successful clinical outcomes. Through cytokine-neutralizing cell therapies, engineered biomaterials, and exosome-mediated communication, these methods bring truly personalized and biologically informed treatments within reach.

Looking ahead, further progress will depend on robust models, standardized assessments, and a clear focus on both personalization and equity, ensuring the benefits of regenerative science extend widely. We thank all contributors for advancing the science and setting a foundation for the next-generation of clinically robust, translationally relevant, and socially conscious regenerative strategies.

Author contributions

CM: Writing – original draft, Writing – review and editing. BR: Writing – original draft, Writing – review and editing. EV: Writing – original draft, Writing – review and editing.

Funding

The author(s) declare that no financial support was received for the research and/or publication of this article.

Conflict of interest

The authors declare that the research was conducted in the absence of any commercial or financial relationships that could be construed as a potential conflict of interest.

Generative AI statement

The author(s) declare that no Generative AI was used in the creation of this manuscript.

Any alternative text (alt text) provided alongside figures in this article has been generated by Frontiers with the support of artificial intelligence and reasonable efforts have been made to ensure accuracy, including review by the authors wherever possible. If you identify any issues, please contact us.

Publisher's note

All claims expressed in this article are solely those of the authors and do not necessarily represent those of their affiliated organizations, or those of the publisher, the editors and the reviewers. Any product that may be evaluated in this article, or claim that may be made by its manufacturer, is not guaranteed or endorsed by the publisher.

frontiers | Frontiers in Cell and Developmental Biology

TYPE Review
PUBLISHED 19 December 2023
DOI 10.3389/fcell.2023.1209047

Check for updates

OPEN ACCESS

EDITED BY
Giovanna Orsini,
Marche Polytechnic University, Italy

REVIEWED BY
Matilde Cescon,
University of Padua, Italy

*CORRESPONDENCE
Émilie Velot,
emilie.velot@univ-lorraine.fr
Magali Cucchiarini,
mmcucchiarini@hotmail.com

RECEIVED 20 April 2023
ACCEPTED 18 September 2023
PUBLISHED 19 December 2023

CITATION
Velot É, Balmayor ER, Bertoni L, Chubinskaya S, Cicuttini F, de Girolamo L, Demoor M, Grigolo B, Jones E, Kon E, Lisignoli G, Murphy M, Noël D, Vinatier C, van Osch GJVM and Cucchiarini M (2023), Women's contribution to stem cell research for osteoarthritis: an opinion paper.
Front. Cell Dev. Biol. 11:1209047.
doi: 10.3389/fcell.2023.1209047

COPYRIGHT
© 2023 Velot, Balmayor, Bertoni, Chubinskaya, Cicuttini, de Girolamo, Demoor, Grigolo, Jones, Kon, Lisignoli, Murphy, Noël, Vinatier, van Osch and Cucchiarini. This is an open-access article distributed under the terms of the Creative Commons Attribution License (CC BY). The use, distribution or reproduction in other forums is permitted, provided the original author(s) and the copyright owner(s) are credited and that the original publication in this journal is cited, in accordance with accepted academic practice. No use, distribution or reproduction is permitted which does not comply with these terms.

Women's contribution to stem cell research for osteoarthritis: an opinion paper

Émilie Velot[1]*, Elizabeth R. Balmayor[2,3], Lélia Bertoni[4], Susan Chubinskaya[5], Flavia Cicuttini[6], Laura de Girolamo[7], Magali Demoor[8], Brunella Grigolo[9], Elena Jones[10], Elizaveta Kon[11,12], Gina Lisignoli[13], Mary Murphy[14], Danièle Noël[15], Claire Vinatier[16], Gerjo J. V. M. van Osch[17] and Magali Cucchiarini[18]*

[1]Laboratory of Molecular Engineering and Articular Physiopathology (IMoPA), French National Centre for Scientific Research, University of Lorraine, Nancy, France, [2]Experimental Orthopaedics and Trauma Surgery, Department of Orthopaedic, Trauma, and Reconstructive Surgery, RWTH Aachen University Hospital, Aachen, Germany, [3]Rehabilitation Medicine Research Center, Mayo Clinic, Rochester, MN, United States, [4]CIRALE, USC 957, BPLC, École Nationale Vétérinaire d'Alfort, Maisons-Alfort, France, [5]Rush University Medical Center, Chicago, IL, United States, [6]Musculoskeletal Unit, Monash University and Rheumatology, Alfred Hospital, Melbourne, VIC, Australia, [7]IRCCS Ospedale Galeazzi - Sant'Ambrogio, Orthopaedic Biotechnology Laboratory, Milan, Italy, [8]Normandie University, UNICAEN, BIOTARGEN, Caen, France, [9]IRCCS Istituto Ortopedico Rizzoli, Laboratorio RAMSES, Bologna, Italy, [10]Leeds Institute of Rheumatic and Musculoskeletal Medicine, Leeds, United Kingdom, [11]IRCCS Humanitas Research Hospital, Milan, Italy, [12]Department ofBiomedical Sciences, Humanitas University, Milan, Italy, [13]IRCCS Istituto Ortopedico Rizzoli, Laboratorio di Immunoreumatologia e Rigenerazione Tissutale, Bologna, Italy, [14]Regenerative Medicine Institute (REMEDI), School of Medicine, University of Galway, Galway, Ireland, [15]IRMB, University of Montpellier, Inserm, CHU Montpellier, Montpellier, France, [16]Nantes Université, Oniris, INSERM, Regenerative Medicine and Skeleton, Nantes, France, [17]Department of Orthopaedics and Sports Medicine and Department of Otorhinolaryngology, Department of Biomechanical Engineering, University Medical Center Rotterdam, Faculty of Mechanical, Maritime and Materials Engineering, Delft University of Technology, Delft, Netherlands, [18]Center of Experimental Orthopedics, Saarland University and Saarland University Medical Center, Homburg/Saar, Germany

KEYWORDS

osteoarthritis, regenerative medicine, orthobiologics, stem cells, extracellular vesicles, gene therapy, RNA therapeutics

1 Introduction

The overall burden associated with musculoskeletal (MSK) conditions surpasses that of tobacco-related health effects, cancer, and diabetes (Barbour et al., 2017; United States Bone and Joint Initiative, 2020). Osteoarthritis (OA) is the most common degenerative joint disorder and a major worldwide challenge for health systems. OA is the leading cause of chronic disability among older adults (Anderson et al., 2011; Oo et al., 2021). It is a heterogenous condition with the pathogenesis differing across different joints. For example, obesity and meta-inflammatory processes have a significant role in knee OA while the shape of the joint and determinants of this are important in hip OA. Targeting the underlying pathological processes will be important in order to develop effective therapies. Post-traumatic OA (PTOA) develops after joint injury and is responsible for 12% of the cases of OA in the US. According to the US Bone and Joint Initiative (https://www.usbji.org), 62% of individuals with OA are women, being more prone to peripheral OA (hand, foot, knee) and experiencing more severe pain and disabling than men (Hawker, 2019; Leifer et al., 2022; Peshkova et al., 2022). Available pharmacological treatments only provide symptomatic pain relief and fail to arrest the progressive degeneration of cartilage associated with PTOA or idiopathic OA (Anderson et al., 2011; de Girolamo et al., 2016; de Girola et al., 2019). Surgical

procedures that promote cartilage repair are expensive, require long rehabilitation, and might expose patients to the risk of complications. Thus, there is an imperative need to develop prophylactic novel biologic means that either prevent or treat early onset of the disease (Vincent, 2019; Vincent, 2020; Vincent et al., 2022).

The current management of OA is gradual and depends on the symptomatic evolution of the disease. Initially, a non-pharmacological approach can be proposed, mainly based on weight loss and the introduction of an adapted physical activity, accompanied by a general awareness of the patient to a healthy lifestyle (Skou and Roos, 2019). If insufficient symptom improvement is achieved with non-pharmacological approaches, pharmacological treatments using non-steroidal anti-inflammatory drugs (NSAIDs) are proposed to reduce pain and inflammation (Bannuru et al., 2019). Although their long-term efficacy and safety are still controversial, intra-articular injections of corticosteroids or hyaluronic acid, or a combination of both, are also being performed to improve the symptoms in patients who did not respond to conventional routes of analgesic administration (Fusco et al., 2021; Peck et al., 2021). Moreover, with the advent of orthobiologics, new potential therapeutic approaches are being exploited to preserve and, potentially restore, the articular surface (Kon et al., 2020; Kon and Di Matteo, 2021; Anzillotti et al., 2022). The group of S. Chubinskaya* has extensively studied the mechanisms of PTOA and the role of orthobiologics in cartilage repair and regeneration and successfully contributed to the clinical approval of the Agili-C implant (Anderson et al., 2011; de Girola et al., 2019). However, no drug can restore joint integrity or even stop the mechanisms leading to the development of OA and partial or total joint replacement by a prosthesis is considered for end-stage OA. Currently, 2,127 clinical trials related to OA (https://clinicaltrials.gov, accessed on 15 April 2023 under "OA+ drugs + interventional + female") are underway to identify disease-modifying OA drugs (DMOADs) (Dietz et al., 2021; Kennedy et al., 2022). Of those expected to have clinical value, sprifermin and lorecivivint (SM04690) recently entered phase II clinical trials. Still, despite encouraging preliminary results in preclinical models (Deshmukh et al., 2018; Deshmukh et al., 2019), these clinical trials showed mitigated results on the global population studied, with encouraging results obtained in one subtype of patients (Yazici et al., 2020; Li et al., 2021).

Women have had a significant role in the translation of stem cell studies to clinical trials including for OA. This required the development of measurement tools to assess progression of structural disease in OA. That cartilage loss can be detected in a valid and reproducible way over 2 years was first shown using magnetic resonance imaging (MRI) by Wluka *et al.* (Wluka et al., 2004). This method was shown to detect the clinically important outcomes of pain (Wluka et al., 2004) and knee replacement (Cicuttini et al., 2004), meaning that it was now possible to use this method for proof of concept trials in OA. This has led to the testing of stem cells in those at high risk of OA, such as knee PTOA, with favorable results (Wang et al., 2017). The trials in this area have been summarized in a number of systematic reviews (Gong et al., 2021). These have tended to find consistent evidence for a beneficial effect of intra-articular injections of stem cells on articular cartilage and subchondral bone, irrespective of the source or contents of the stem cells. However, among the trials there remains significant heterogeneity in the source and composition of the injected cells, small to modest sample sizes, and the potential for publication bias. The use of stem cells remains an exciting area of endeavor (Fortier, 2005), including for OA where there is a lack of effective therapies. However, more work is needed before such therapies can be recommended in the management of the pathology.

In parallel with ongoing human studies, stem cells have been employed in veterinary medicine (Fortier and Travis, 2011; Ferris et al., 2014; Colbath et al., 2020) and the European Drugs Regulations Agency already authorized the use of two products based on stem cells (Arti-Cell Forte® and HorStem®) to treat mild to moderate signs of OA associated with lameness in horses, following various safety and efficacy studies of intra-articular injections (Bertoni et al., 2019; Broeckx et al., 2019; Be et al., 2021). As for humans, MSK injuries are the most prevalent and debilitating condition responsible for pain (in the form of lameness) and loss of performance associated with highly negative economic impact on the equine industry (IVIS, 2010). A wider range of therapies are used in equine practice compared with human practice to reduce the clinical signs and progression of OA (Velloso Alvarez et al., 2020), although there is still no curative treatment. In a "One Health, One Medicine" concept (Kahn, 2017), preclinical studies in horses led to applications in humans and *vice versa*, as recently illustrated by the marketing of the intra-articular polyacrylamide hydrogel (Arthrosamid®) or of autologous conditioned serum (ACS) (Camargo Garbin and Morris, 2021). Large animals including livestock, dogs or horses have similar biomechanical constraints to humans, leading to the development of MSK diseases in a similar pathogenesis (Yazici et al., 2020). Therefore, they are considered suitable target species and translational models for researching new therapeutic approaches, while small animal models are typically employed for investigating pathophysiological processes (McCoy, 2015; Manivong et al., 2023). Horses in particular demonstrated many similarities to human joints regarding articular cartilage thickness, cellular structure, biochemical composition, and mechanical properties. It is however interesting to note that in major international equestrian competitions and races, all genders compete in the same category and females achieve great victories (Hanousek et al., 2018).

This opinion paper focuses on the manipulation of mesenchymal progenitor cells as a promising therapeutic source of cells to treat MSK disorders with a focus on OA. This initiative was established by women researchers, with the purpose of highlighting some of the critical women's contributions in the field of MSK tissue regeneration (including those of the current authors) as examples (Figure 1) with particular attention drawn in the text on outstanding women and on women (*) involved in the current opinion paper, and was performed under the umbrella of the International Cartilage Regeneration and Joint Preservation Society (ICRS; https://cartilage.org).

2 Cell-based therapies

2.1 Embryology and joint development, progenitor cells in the joint

The limb forms during embryogenesis as a limb bud, from the condensation of mesenchymal progenitor cells that

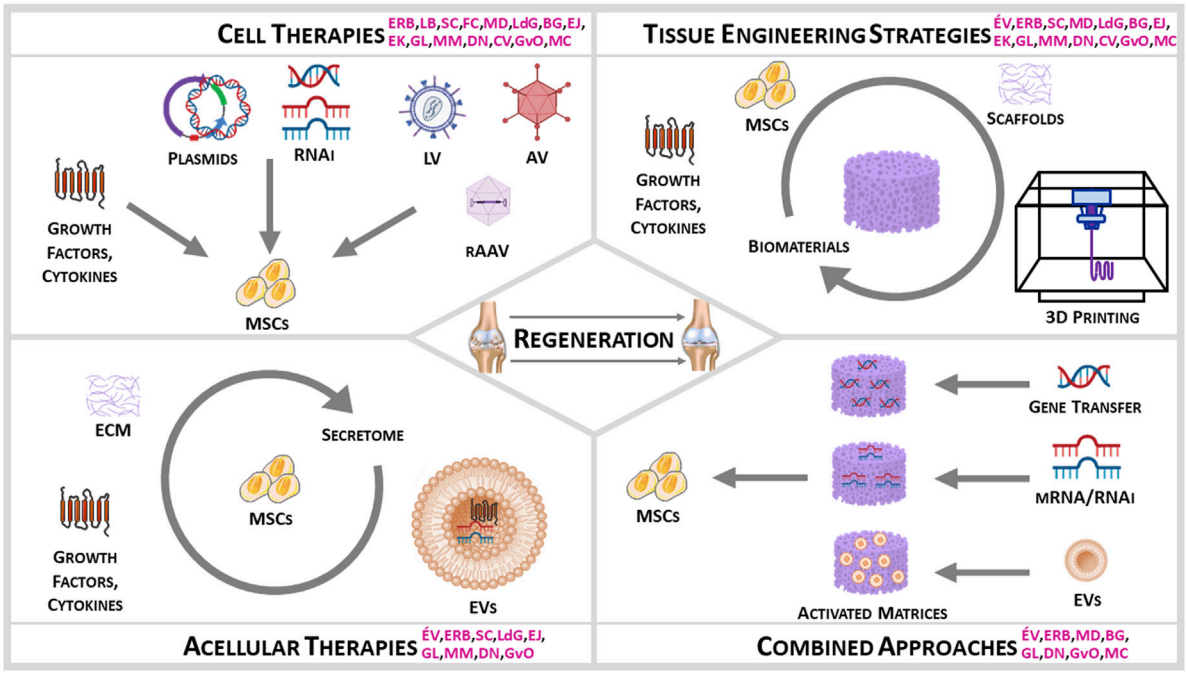

FIGURE 1
Women Input on Stem Cells for MSK Regeneration (initials in pink indicate the research contributions of the current authors).

chondrogenically differentiate into and form a cartilage anlage. This cartilage anlage will undergo endochondral ossification to form long bones, except at specific sites where an interzone is formed to give rise to the joint structures (Decker et al., 2014). The initial interzone consisting of growth and differentiation factor (*Gdf*)*5*$^{+}$ cells generated from descendants of chondrocytes which after cavitation will form the articular cartilage and intra-articular ligaments. Flanking cells recruited into the interzone from surrounding tissues also express *Gdf5* and will largely form the synovial lining and joint capsule. In adult mouse synovium, cells that originate from *Gdf5*-expressing joint interzone cells appear largely negative for the skeletal stem cell markers *Nestin*, Leptin receptor, and Gremlin1 (Roelofs et al., 2017), confirming a separate origin of these progenitor cells in synovium and skeletal progenitor cells. With different approaches, Decker *et al.* and Roelofs *et al.* demonstrated that upon osteochondral injury in adult mice, progenitor cells in the synovium proliferate and are recruited to the defect to contribute to tissue repair and articular chondrocytes have minimal contribution to tissue repair (Decker et al., 2017; Roelofs et al., 2017).

2.2 Joint MSC sources

Although initially referred to as stem cells, the definition of MSCs has been under discussion over the last decades (Viswanathan et al., 2019). The term "MSCs" is interchangeably used for Mesenchymal Stem Cells, Mesenchymal Stromal Cells, Medicinal Signaling Cells, or Multipotent Stromal Cells, and for the most part in connection to a potential clinical use. In this review, we use the term "MSCs" as such and the exact meaning refers to the context of their potential clinical use: either to generate tissue or to modulate tissue repair (Viswanathan et al., 2019). Distinct progenitor cells are present in the different joint tissues but it became clear that also within one tissue, different populations of progenitor cells exist. Generally, one can discriminate perivascular progenitor cell populations and populations located in the stroma or the lining. In the human synovium, the group of G. J. V. M. van Osch* (Sivasubramaniyan et al., 2019) described progenitor cells that are CD45^{-}CD31^{-}CD73^{+} and discriminated a CD90^{-} population in the intimal, synovial lining layer and a CD90^{+} population in the subintimal, perivascular area with distinct chondrogenic capacities. Similarly, synovial-derived MSCs have been reported in animal species by this group* (Teunissen et al., 2022). Moreover, as reported by this group in collaboration with the groups of E. Jones* (Sivasubramaniyan et al., 2018), in the human bone marrow, two different populations of CD45^{-}CD271^{+} mesenchymal progenitor cells were found: a perivascular CD56^{-} population with poor chondrogenic capacity and a CD56^{+} bone lining population with good chondrogenic capacity. In bone marrow aspirations, the less chondrogenic perivascular population is more abundant than the bone lining population. A higher abundance of the more chondrogenic bone lining populations was found when the bone marrow was collected after rasping the marrow canal before implanting a prosthesis (Sivasubramaniyan et al., 2018). Bone marrow-derived (BM) MSCs have also been isolated from animals (Fortier et al., 1998; Kisiday et al., 2020). Thus, the location and way of collecting MSCs is an important determinant for their capacity to generate tissues.

Subcutaneous adipose tissue has gained popularity as a source of MSCs more recently compared with bone marrow. Nevertheless, many research efforts have addressed it as an optimal tissue source for a variety of clinical applications, as well as for an impressive number of basic studies to clarify MSC properties. Adipose tissue is indisputably a convenient tissue to harvest, with potentially no limit in terms of quantity and it contains a higher number of MSCs (adipose-derived stem cells, i.e., ASCs) with a similar immunophenotype to BM MSCs, bar the higher expression of CD34 seen in freshly isolated ASCs as shown by the groups of F. J. van Milligen and of D. Noël* (Varma et al., 2007; Maumus et al., 2013). Also, adipose tissue-derived MSCs have been reported by the group of H. Roelofs (Melie et al., 2013) to possess a higher immunomodulatory capacity than their bone marrow counterparts, making ASCs a more appealing cell type compared with BM MSCs in some clinical applications. ASCs are associated with the so-called stromal vascular fraction (SVF), a heterogeneous collection of cells composed of pre-adipocytes, endothelial precursor cells, T regulatory cells, macrophages, smooth muscle cells, and MSCs/pericytes indeed. Nevertheless, the SVF is a versatile cellular system and the degree of heterogeneity depends on a variety of factors, such as the adipose tissue harvest site, the digestion protocol, and the patient's own pathological status. For this reason, there is no consensus on the exact definition and proportion of these cell types within the SVF. Also, culturing SVF cells for even one passage can profoundly alter their cellular composition as reported by Nunes *et al.* (Nunes et al., 2013) and observed by the group of D. Noël* (Domergue et al., 2016). From a therapeutic perspective, beyond exploiting the adipose tissue for the isolation and *in vitro* expansion of ASCs, the relatively higher abundance of MSCs within the adipose tissue has driven the development of several medical devices to isolate the SVF intra-operatively without the need for further cell expansion. These devices can either provide mechanical digestion of the adipose tissue resulting in a mechanical-SVF as reported by the group of Y. Kul (Tiryaki et al., 2022) and observed by the group of D. Noël* (Bony et al., 2016) or resize the adipose tissue into microfragments while removing oil and blood contaminants and resulting into microfragmented adipose tissue as shown by the group of L. de Girolamo* (Ulivi et al., 2022). Notably, in addition to the subcutaneous adipose tissue, other adipose sites have been investigated as MSC sources. In particular, in the MSK field ASCs isolated from the infrapatellar fat pad (or Hoffa's body) have been demonstrated to possess a differentiation ability equal or even superior to subcutaneous ASCs (Lopa et al., 2014; Sun et al., 2018).

MSCs have additionally been found in healthy and OA synovial fluid (SF) by the group of E. Jones* (Jones et al., 2004; Jones et al., 2008) and in patients with chondral defects by G. J. V. M. van Osch* and K. Wright (Garcia et al., 2020). Compared with BM MSCs, SF MSCs are highly proliferative and consistently chondrogenic (Jones et al., 2008). In OA human knees, as shown in the work of the group of E. Jones* (Ilas et al., 2019; Sanjurjo-Rodriguez et al., 2019), subchondral BM MSCs are driven towards osteogenesis in order to rapidly compensate for load distribution alterations following the loss of cartilage. In contrast, they showed that SF MSCs from the same knees express higher levels of cartilage formation and turnover genes, and lower levels of ossification molecules (Sanjurjo-Rodriguez et al., 2020). Furthermore, SF MSCs display a pro-chondrogenic and immunomodulatory response following a joint-sparing, knee joint distraction procedure (Sanjurjo-Rodriguez et al., 2020). Owing to their apparent ability to respond to biomechanical cues, both types of joint-resident MSCs can be manipulated towards cartilage regeneration using mechanically-competent scaffolds and smart biomaterials.

MSCs have also been isolated from the articular cartilage by the group of L. A. Vonk (Rikkers et al., 2021; Rikkers et al., 2022) and peripheral blood (PB-MSCs), both showing a certain ability for osteochondrogenic differentiation (Mödder and Khosla, 2008; Beane and Darling, 2012; Martinello et al., 2013; Orth et al., 2014; Frisch et al., 2015a; Rikkers et al., 2021; Rikkers et al., 2022). Other sources of MSCs include perinatal MSCs from the umbilical cord blood or connective tissue or from the amniotic fluid and membrane (El Omar et al., 2014; Gómez-Leduc et al., 2016; Borghesi et al., 2019; Lepage et al., 2019; Hyland et al., 2020; Perry et al., 2021) as well as embryonic stem cells (ESCs) (Hwang et al., 2008), all with chondrogenic abilities and showing a higher potential for self-renewal and lower immunogenic and tumorigenic activities relative to adult MSCs. Of further note, as shown by the groups of É. Velot*, of J. Elisseeff, and of S. J. Kimber and by Lepage *et al.* and Borghesi *et al.* (Hwang et al., 2006; Oldershaw et al., 2010; El Omar et al., 2014; Dostert et al., 2017; Borghesi et al., 2019; Lepage et al., 2019; Mesure et al., 2019; Velot et al., 2021), MSCs from birth tissues have a better accessibility and can be non-invasively isolated in large amounts relative to adult MSCs while showing fewer ethical issues compared with ESCs.

The number of MSCs that can be obtained from a donor is limited. ESCs and induced pluripotent stem cells (iPSCs) represent a potentially unlimited source of chondrocytes. Protocols from ESCs have been adapted for iPSCs with slight variations. These stem cells can be used to specifically generate hypertrophic or non-hypertrophic chondrocytes as shown in particular by the groups of S. J. Kimber, of R. A. Kandel, of S. Diederichs, and of W. Richter (Oldershaw et al., 2010; Craft et al., 2013; Cheng et al., 2014; Diederichs and Tuan, 2014; Diederichs et al., 2019a). Non-hypertrophic chondrocytes generated from human ESCs have been reported to promote the repair of focal cartilage defects in rats (Cheng et al., 2014). Hypertrophic chondrocytes are generally generated from iPSCs by first differentiating them into iPSC-derived MSC-like progenitor cells (iMPCs). iMPCs generated from human BM MSCs were comparable to the parental MSCs, although iMPCs appear less responsive to traditional MSC differentiation protocols (Diederichs and Tuan, 2014). The considerable heterogeneity in chondrogenesis found using iMPCs has been associated with variable SRY-related high-mobility-group-box gene 9 (SOX9) protein expression, with low SOX9 levels correlating to high levels of the SOX9-antagonizing hsa-miR-145 (Diederichs et al., 2016). Still, the clinical use of iPSCs remains controversial since these cells are potentially tumorigenic and immunogenic, with an instability of their genome (Hackett and Fortier, 2011; Guzzo et al., 2013; Schnabel et al., 2014; Vonk et al., 2015; Driessen et al., 2017; Xu et al., 2019; Velot et al., 2021). However, the secretome of iPSC-derived MSCs (iMSCs) primed with tumor necrosis alpha (TNF-α) and interferon gamma (IFN-γ) has a high resemblance to BM MSCs, with iMSC-derived extracellular vesicles (EVs) showing similar *in vitro* immunomodulation (Ramos et al., 2022).

2.3 MSCs *versus* tissue-specific cells for joint regeneration

Murphy* *et al.* were the first to intra-articularly inject BM MSCs and study their potential for the treatment of OA using a caprine model (Murphy et al., 2003). Many studies in animals and in human patients followed. Since cell tracking studies showed only limited cartilage formation by these cells (Murphy et al., 2003; Hamilton et al., 2019; Markides et al., 2019; Perry et al., 2021), the mechanism of action was hypothesized to be related to factors secreted by the MSCs (Hamilton et al., 2019; Markides et al., 2019; Perry et al., 2021). Given their established immunomodulatory and trophic properties, MSCs isolated from different sources have been proposed as a viable therapeutic option to treat cartilage damage and early OA (Lopa et al., 2019). The group of D. Noël* noted the therapeutic efficiency of human and equine ASCs in the inflammatory model of collagenase-induced OA (Ter Huurne et al., 2012; Maumus et al., 2016). Intra-articular injection of immune-selected allogeneic human mesenchymal precursor cells were reported by the group of F. Cicuttini* to improve symptoms and structure in PTOA, suggesting that they modulate some of the pathological processes responsible for the onset and progression of this phenotype (Wang et al., 2017). These cells help to establish a "regenerative microenvironment" through the paracrine secretion of bioactive molecules and promote tissue-specific progenitor proliferation while inhibiting cell apoptosis and tissue fibrosis as reported by the group of L. de Girolamo* (Colombini et al., 2019). Among the molecules that play a role in the chondroprotective effect of MSCs in OA, Fra-1, THBS1 and TGFβi have been noted by the group of D. Noël* (Schwabe et al., 2016; Maumus et al., 2017; Ruiz et al., 2020). Alternatively to MSCs, tissue-specific cells have been also proposed as a valuable regenerative alternative for decades. Autologous Chondrocyte Implantation or Transplantation (ACI/ACT) was first developed in the 90s and since then has been used to treat thousands of patients with satisfactory results compared with other available techniques (Kon et al., 2013). Over time, a number of implementations of the original techniques have been developed, including the association of suitable biomaterials acting as scaffolds for cell growth and colonization (MACI, matrix-assisted autologous chondrocyte implantation) as shown by the large case series published by the group of E. Kon* (Kon et al., 2012). Nevertheless, while ACI/MACI resulted in the successful treatment of focal isolated chondral injuries, the clinical outcomes in patients with diffuse chondral damages are still under debate (Colombini et al., 2022a). One of the possibilities to make these techniques more effective in patients with diffuse cartilage defects (i.e., early OA patients) is to focus on chondroprogenitors. Chondroprogenitors are represented within cartilage as cells with migratory, clonogenic ability, and differentiation potential, found both in healthy and damaged cartilage as reported by Vinod *et al.* (Vinod et al., 2023). In addition to their direct stimulation within the cartilage, cartilage progenitors, likewise MSCs, could indeed be exploited to improve the existing cell-based therapies for the treatment of cartilage defects. In this regard, the possibility to enrich the amount of cartilage progenitors throughout *in vitro* expansion of the whole cartilage cell population seems a valuable option to improve the current results in early OA patients. It was observed that, with increasing passages in culture, cartilage cell populations are characterized by a progressive enhancement of clonogenic ability and sustained expression of stemness markers. Moreover, these expanded cells revealed a noteworthy chondrogenic potential, an enhanced secretory response to inflammation compared with MSCs, and strong immunomodulatory functions after inflammatory priming as seen by De Luca *et al.* (De Luca et al., 2019). Although data derived from animal models also show that chondroprogenitors have the ability to attenuate OA, repair, chondral defects, and form stable cartilage, displaying better outcomes than BM MSCs, these preclinical data would require further studies to optimize their use before clinical translation (Vinod et al., 2023).

Another possibility would be to combine the favorable properties of chondrocytes and MSC into a combined treatment. Apart from anti-inflammatory or anti-catabolic effects, the secretome of MSCs can also have trophic effects and in co-culture with chondrocytes, both adipose tissue-derived and BM MSCs demonstrated to enhance cartilage generation by the chondrocytes as reported by the group of G. J. V. M. van Osch* (Pleumeekers et al., 2018). This property of MSCs might explain the potential of a proposed one-stage cell therapy for cartilage defects where 75% of the chondrocytes can be replaced by MSCs (US20140329316A1, US20100144036A1), although the initial claim referring to an effect of the chondrocytes on the differentiation of the MSCs cannot be fully excluded.

2.4 Differentiation and culture conditions for appropriate MSK differentiation of MSCs, priming, immunomodulation

MSCs can be differentiated into cartilage-like cells *in vitro*. A large body of research from the groups of W. Richter and of G. J. V. M. van Osch* have investigated the stability of the cartilage formed by these cells and ways to improve this. They demonstrated that chondrogenically differentiated MSCs, though, were shown to be prone to endochondral ossification when implanted *in vivo* (Pelttari et al., 2006; Farrell et al., 2009). This finding redirected the bone tissue engineering field since more bone could be generated by pre-differentiating MSCs chondrogenically than the original attempts of pre-differentiating them towards the osteogenic lineage. Whereas research mostly focused on stimulating the chondrogenic capacity of these cells, such as, for example, by addition of parathyroid hormone-related protein (PTHrP) (Fischer et al., 2014; Fischer et al., 2016), TGFβi, NMB, or miR-29a as noted by the group of D. Noël* (Ruiz et al., 2020; Maumus et al., 2021; Guérit et al., 2014), inhibition of the anti-chondrogenic regulators became an emerging area (Lolli et al., 2019a). Inhibition of SMAD1/5/9 (Helli et al., 2011), WNT (Narcisi et al., 2015; Diederichs et al., 2019b), or anti-chondrogenic miRNAs, such as, for example, miRNA221 (Lolli et al., 2016) and miR-574–3p as observed by the group of D. Noël* (Guérit et al., 2013), has shown promise to inhibit hypertrophic differentiation. In addition to modulating chondrogenesis during the differentiation phase, modulation of the MSC expansion medium, for example, by the addition of WNT (Narcisi et al., 2015) or of TNF-α (Voskamp et al., 2020) resulted in improvement of chondrogenic capacity. The fact that

these factors have demonstrated anti-chondrogenic properties during the differentiation phase demonstrates the complexity and importance of paying to the different stages of cell differentiation.

The immunomodulatory capacity of MSCs and ASCs can be influenced by disease status of the joint as noted by the groups of G. J. V. M. van Osch* and of G. Lisignoli* (Leijs et al., 2012; Manferdini et al., 2020). The immunomodulatory ability of ASCs was not affected by hypoxia as reported by the group of G. J. V. M. van Osch* (Roemeling-van Rhijn et al., 2013), whereas it was positively affected by an inflammatory stimulus such as interleukin 1 beta (IL-1β) as observed by the groups of L. de Girolamo* and of D. Noël* (Colombini et al., 2022b; Maumus et al., 2016). Similarly, the protein cargo of umbilical cord EVs was affected by their pro-inflammatory priming, but not in hypoxic conditions (Hyland et al., 2020).

2.5 Gene therapy

Stem cells are amenable to genetic modification to enhance their reparative potential in a variety of MSK disorders. Gene therapy is the transfer of candidate nucleic acid sequences as direct molecules or using a gene vector derived from nonviral material (most commonly a plasmid) or from viral material (adenoviral [AV], herpes simplex viral, retro-/lentiviral [LV], or recombinant adeno-associated viral [rAAV] vectors) to prolong the therapeutic effects of a gene product compared with recombinant agents with short pharmacological half-lives (Jorgensen et al., 2001; Noël et al., 2002; Jorgensen et al., 2003; Djouad et al., 2009; van Osch et al., 2009; Vinatier et al., 2009; Coleman et al., 2010; Ansboro et al., 2012; Cucchiarini et al., 2012; Demoor et al., 2014; Frisch et al., 2015a; Docheva et al., 2015; Balmayor, 2015; Cucchiarini, 2016; Fris et al., 2016; Jones et al., 2016; Rey-Rico and Cucchiarini, 2017; Poh et al., 2018; Mesure et al., 2019; Roseti et al., 2019; De la Vega et al., 2021; Amini et al., 2022). Gene therapy is performed *via* classical gene transfer or using genome editing methodologies such as use of the clustered regularly interspaced short palindromic repeats (CRIPSR)-associated 9 (CRISPR/Cas9) system (Tanikella et al., 2020). The contribution of women researchers in the field of gene therapy to target stem cells is broadly illustrated by reports showing the improved commitment of stem cell to MSK profiles using various classes of gene transfer vectors. Nonviral vectors carrying the SOX9 transcription factor were reported by the group of A. Rey-Rico to activate MSC chondrogenesis (Carball et al., 2022) (or the vascular endothelial growth factor - VEGF - to tackle MSC osteogenesis and bone healing as noted by the group of W. Richter (Geiger et al., 2007)). Adenoviral vectors carrying IL-10 were successfully used by the group of M. Murphy* to prevent OA (Farrell et al., 2016) (or bone morphogenetic proteins - BMP-2, BMP-6 - to modulate MSC osteogenesis and bone healing as reported by the group of A. L. Bertone (Zachos et al., 2006; Zachos et al., 2007; Murray et al., 2010; Ishihara et al., 2015)). rAAV vectors were manipulated by the groups of C. R. Chu, of L. R. Goodrich, and of M. Cucchiarini* to deliver the basic fibroblast growth factor (FGF-2) (Cucchiarini et al., 2005; Cucchiarini et al., 2011), transforming growth factor beta (TGF-β) (Pagnotto et al., 2007; Lee et al., 2011; Frisch et al., 2014a; Frisch et al., 2016; Frisch et al., 2017a; Cucchiarini et al., 2018), insulin-like growth factor I (IGF-I) alone (Frisch et al., 2014b; Cucchiarini and Madry, 2014; Frisch et al., 2015b; Frisch et al., 2017b) or with TGF-β (Morscheid et al., 2019a; Morscheid et al., 2019b), BMP-3 (Venkatesan et al., 2022), SOX9 (Cucchiarini et al., 2013), and chondromodulin (Klinger et al., 2011) to stimulate MSC chondrogenesis and cartilage repair (or BMP-2 for MSC osteogenesis (Ball et al., 2019)). Gene silencing in MSCs based on gene knockdown strategies using RNA interference (RNAi) technology is also a potent approach to modulate the reparative potential of these cells for MSK regeneration (Lolli et al., 2017; Demoor et al., 2014). For instance, silencing the antichondrogenic regulator microRNA 221 (miR-221) *via* specific antagomiR-221 or antimiR-221 oligonucleotides is capable of enhancing chondrogenesis and cartilage repair as seen in work from the group of G. J. V. M. van Osch* (Lolli et al., 2016; Lolli et al., 2019b).

2.6 Gene therapy modifications

Adenoviral- and rAAV-based vectors, while considered the most promising systems for OA, still have two main limitations: potential anti-viral host immune responses and the levels of efficiency and specificity of transgene expression in joint tissues. Targeting the joint cells of interest is still arduous even using intra-articular injections. Indeed, chondrocytes embedded in a dense extracellular matrix (ECM) are less accessible than synovial, ligament, or fat pad cells. In addition, disturbances in intracellular trafficking may decrease the efficiency of viral vector transduction. To address these issues, optimization of the carrier nucleic acid sequence and a modification of viral vectors have been considered with increasing interest. The capsids of adenoviral and rAAV vectors promote tropism but can also be recognized by neutralizing antibodies present in the circulation and synovial fluid as evidenced by the group of N. Bessis (Cottard et al., 2004) due to a pre-existing immunity, overall reducing the transduction efficiency. Yet, capsids may be engineered to escape such neutralization, and in this context, several improved hybrid AAV serotypes have emerged. Among them, the rAAV 2.5, a chimera of AAV1 and AAV2, evaluated in preclinical models of equine OA by Watson-Levings *et al.* (Watson Levings et al., 2018a) is currently being used in a clinical trial for OA (NCT05454566) and rAAV-DJ, which has been successfully used in a preclinical rat model of OA by Martinez-Redondo *et al.* (Martinez-Redondo et al., 2020). Also of interest in OA, Eichhoff *et al.* (Eichhoff et al., 2019) designed an rAAV preferentially targeting cells expressing the purinergic receptor ($P2X_7R$) overexpressed in OA chondrocytes. Chemical modification allowing a large panel of chemical compounds or peptides to be coupled may also improve capsids to limit off-target effects, overcome undesirable properties, and permit viral escape from neutralizing antibodies. For instance, the chondrocyte-affinity peptide (CAP) has been used by the group of P. Pothacharoen (Chongchai et al., 2023) to enhance rAAV targeting of chondrocytes. Finally, self-complementary AAV (scAAV) composed of a double-stranded DNA genome have been successfully used by Watson-Levings *et al.* (Watson Levings et al., 2018a; Watson Levings et al., 2018b) to target chondrocytes, bypassing their step-limiting, low rates of cell replication/proliferation.

2.7 Transcript therapy

Despite the clear advantages of gene therapy, safety concerns related to viral vectors and affordability issues have restricted their

clinical use as noted by the group of E. R. Balmayor* among others (Evans, 2019; De la Vega et al., 2021) In fact, affordability remains a pressuring issue, with gene therapy products tagged at $2 million a dose (Dyer, 2020) related to the manufacturing process under Good Manufacturing Practice (GMP). In addition, achieving efficient gene transfer and appropriate levels of transgene expression proved to be cumbersome for some applications as described by the group of E. R. Balmayor* (De la Vega et al., 2021), motivating researchers to explore alternatives to traditional MSK gene therapy. Applied to tissue regeneration, gene therapies commonly deliver protein-coding DNA. However, messenger RNA (mRNA), offers a more efficient way to achieve protein translation while accommodating numerous advantages as explained by Balmayor* *et al.* (Balmayor, 2022). Like traditional gene therapy, mRNA transcript therapy offers control over the production of therapeutic proteins. In addition, since mRNA function is conducted in the cell cytoplasm, it results in an immediate initiation of translation. Unlike viral gene therapy, mRNA transcript therapy is safe as it does not carry the risk of insertional mutagenesis and oncogenesis. Also, mRNA's transient nature is valuable in many regenerative medicine applications when long-term effects are not necessary as stated by others and by Balmayor* *et al.* (Sahin et al., 2014; Balmayor and Evans, 2019). mRNA is produced by *in vitro* transcription (IVT), a relatively simple, single-reaction procedure easily controllable and scalable and identical for all mRNAs, regardless of the sequence. Importantly, no cell or bacterial culture is required, reducing the risk of contamination. IVT allows the introduction of numerous chemical modifications and the use of modified nucleosides to produce defined mRNAs with reduced immunogenicity and low stability, with costs described as up to 10-fold lower that their protein therapeutic counterparts as demonstrated by K. Karikó among others (Karikó et al., 2005; Weissman, 2015). The recent use of mRNA in COVID-19 vaccines receiving approval in various countries demonstrates that this technology can be safe and efficient. Regarding MSK regeneration, local mRNA delivery has been investigated mostly for bone by the group of E. R. Balmayor* and by Badieyan *et al.* and Khorsand *et al.* (Elangovan et al., 2015; Badieyan et al., 2016; Balmayor et al., 2016; Balmayor et al., 2017; Khorsand et al., 2017; Zhang et al., 2019; Fayed et al., 2021; Geng et al., 2021; De La Vega et al., 2022; European Scoiety of Gene and Cell Therapy, 2022), with a strong focus on effective BMP-2 mRNAs but also with an emerging interest for BMP-9 (Khorsand et al., 2017), BMP-7 (European Scoiety of Gene and Cell Therapy, 2022), and VEGF mRNAs by Geng *et al.* (Geng et al., 2021). In one of the most translatable studies performed to date, a BMP-2 mRNA administered to rat femoral critical-size defects *via* a collagen carrier was reported by the group of E. R. Balmayor* (De La Vega et al., 2022) to remain local in a safe manner and to efficiently induce bone healing in a dose-dependent manner. For cartilage repair, mRNAs coding for the runt-related transcription factor 1 (Runx1) (Aini et al., 2016), Link N by the group of M. Avci-Adali (Tendulkar et al., 2019), and IGF-I (Wu et al., 2022) have been investigated as OA treatments. Direct injections of Runx1 mRNA in mouse OA knee joints significantly suppressed OA progression (Aini et al., 2016) while injection of stem cells transfected with an IGF-I mRNA in mouse knee joints safely enhanced cell survival and engraftment in the cartilage tissue (Wu et al., 2022). Overall, all these findings support the safety and efficacy of this emerging technology for MSK regeneration.

3 Tissue engineering strategies

3.1 Tissue engineering

New tissue engineering therapeutic strategies mainly based on the use of biomaterials combined with stem cells showed good potential both in preclinical and clinical studies as reported by the groups of G. Lisignoli*, of D. Noel* and of L. R. Goodrich and by Nooeaid *et al.*, Moradi *et al.*, Taraballi *et al.*, Armiento *et al.*, and Kwon *et al.* (Nooeaid et al., 2012; Moradi et al., 2017; Taraballi et al., 2017; Yang et al., 2017; Armiento et al., 2018; Kwon et al., 2019; Pascual-Garrido et al., 2019; Trucco et al., 2021, Valot et al., 2021; Manferdini et al., 2022). Regenerative scaffold-based methods are emerging as possible therapeutic alternatives for the treatment of various types of cartilage lesions as noted by the group of E. Kon* (Kon et al., 2015). In order to support the proliferation of live cells, a scaffold is a temporary three-dimensional (3D) framework made of biodegradable polymers that may replicate the highly structured functional architecture of the articular cartilage. Chondrogenic differentiation of MSCs can be achieved on different types of scaffolds provided that a growth factor can be released to induce the process as observed by the group of D. Noël* (Morille et al., 2013; Morille et al., 2016; Mathieu et al., 2014). Different types of chondral and osteochondral scaffolds have been used in the past, but the most promising results have being obtained with biodegradable scaffolds as observed by the group of E. Kon* (Kon et al., 2014; Kon et al., 2018; Kon et al., 2021; Altschuler et al., 2023). The use of scaffolds is often integrated with cells seeded on the scaffold itself. The group of E. Kon* (Kon et al., 2008; Kon et al., 2012) was the first to use articular chondrocytes in association with biomaterials for cartilage regeneration in clinical practice with discrete success in treating focal defects. Although some products containing chondrocytes and biomaterials are still on the market, the necessity of addressing different tissues and the need of modulating the joint environment pushed towards the use of stem cells instead of chondrocytes.

Both natural and synthetic biomaterials have been used to regenerate different joint tissues (cartilage, bone, meniscus) and cells have been mainly seeded or encapsulated into these structures for instance by Sanchez-Tellez *et al.*, Yang *et al.*, and Critchley *et al.* (Sánchez-Téllez et al., 2017; Li et al., 2019; Yang et al., 2019; Critchley et al., 2020; Rahman et al., 2022). However, the main limitation of this approach is the retention of stem cells in the target joint tissue that may be influenced by the presence of synovial fluid, inflammation, load, and joint movement as noted by the groups of E. Kon* and of G. J. V. M. van Osch* and by Bakhshandeh *et al.* (Fahy et al., 2014; Perdisa et al., 2014; Bakhshandeh et al., 2017; Dong et al., 2017). To overcome this issue, it is necessary to design advanced biomaterials capable of retaining cells *in situ*, with immunomodulating properties while at the same time, retaining the capacity to stably adhere to damaged joint tissues and boost their regeneration. Biomaterial stiffness and viscoelasticity, as other critical parameters, are selected depending on the anatomical characteristics of the regenerated joint tissues as reported for instance by Sarem *et al.* (Sarem et al., 2018; Zhang et al., 2020;

Huang et al., 2023). All biomaterial parameters directly control and influence the characteristics of the cells by acting through specific receptors directing their migration, proliferation, matrix synthesis, and differentiation as observed by the group of G. Lisignoli* and by Yang *et al.*, Sarem *et al.*, and Hafezi *et al.* (Sarem et al., 2018; Yang et al., 2019; Hafezi et al., 2021; Sartore et al., 2021). These strategies contribute to joint tissue regeneration by showing effects on different physiological processes including inflammation, metabolic processes, aging, apoptosis, and autophagy as shown by the groups of E. R. Balmayor* and of G. Lisignoli* and by Koh *et al.* (Amann et al., 2017; Chen et al., 2020; Koh et al., 2020; Gabusi et al., 2022).

Stem cells have also been reported to secrete an ECM that may be valuable for MSK regeneration. For instance, MSCs from the connective tissue of the umbilical cord (Wharton's jelly) produce ECM components similar to those of articular cartilage as reported by Russo *et al.* (Russo et al., 2022) and participate in MSC chondrogenic differentiation, offering a potential scaffold that may be used as an alternative to improve cartilage regeneration as noted by Ramzan *et al.* (Ramzan et al., 2022).

3.2 Bioprinting, sustainable automated manufacturing for therapeutic cells

Emerging technologies like additive manufacturing (three-dimensional [3D] printing) will lead future directions for tissue engineering therapeutic strategies. 3D printing replicates the damaged tissue shape starting from the patient medical image. It consists of the fabrication of living tissue/organ-like structures throughout the bottom-up deposition of either cell-laden droplets or cells embedded in a hydrogel, in both cases termed as "bioink" as described for instance by Abdollahiyan *et al.* (Abdollahiyan et al., 2020). Such a technology makes is possible to overcome issues associated with more conventional methods like static (manual) seeding onto scaffolds or dynamic seeding using bioreactors as shown by the group of B. Grigolo* (Roseti et al., 2018). In these cases, problems are due to cell accumulation at the surface of scaffold and to the low density in the inner part where cells tend to die because of the scarcity of nutrients. This may lead to inaccurate experimental results and consequent speculation. Differently, 3D bioprinting offers the advantage of fine control of cell spatial distribution in terms of homogeneity. When scaffolds were cultured with chondrogenic or osteogenic medium, cartilage and bone tissues were produced, respectively, as determined by specific gene and protein expression (Gao et al., 2015). Further benefits of 3D bioprinting techniques include reduced production times, an increased versatility, and the possibility to work at room temperature and "solvent-free" conditions, taking advantage of the features of water-based gels such as bioinks as reviewed by the groups of B. Grigolo* and of D. Noël* (Roseti et al., 2017; Montheil et al., 2022). 3D bioprinting also enables the fabrication of custom-made products based on patient's medical images. Such options improve the match between implant and defect size, thus shortening the time required for surgery and for patient recovery, and positively affecting the success of treatment.

Development and use of bio-inspired, fabricated bio-printed constructs will require validated and relevant cell sources and/or use of appropriate factors to attract endogenous stem cells to the constructs. The cost of producing GMP-grade MSCs, or even iMSCs, using manual processes is such that translation to patient use at scale to enable widespread use is prohibitive and a critical impediment in the field as noted by the group of M. Murphy* (Ochs et al., 2022). The automation of production of advanced therapy medicinal products (ATMPs), state-of-the-art medicines for human use based on genes, tissues or cell-derived EVs can address this hurdle to clinical translation as reported by the group of M. Murphy* (Ochs et al., 2022).

3.3 From biologic substitutes to organoids, 3D models, and organ-on-a-chip

In accordance with the 3Rs concept (replacement, reduction, refinement) and with the strategic directions of the European Medicines Agency (EMA) (announcement of 29 September 2021) to promote alternative approaches to animal models, the development and use of effective alternative *in vitro* methods before formal animal testing are now mandatory. Advanced techniques such as biomanufacturing (3D bioprinting and bioassembly) and organotypic models (organoids, organ-on-a-chip) are gaining interest due to their ability to mimic OA conditions. Although 2D and 3D cellular cultures have limitations, they are still useful in answering fundamental questions in a molecular, cellular, and tissue continuum and provide a cost-effective platform for rapid, high-throughput screening of new drugs, delivery systems, or biolubricants. This provides an efficient standardized functional qualification without the use of experimental animals for more ethical research (Manivong et al., 2023). Tissue engineering studies conducted since the emergence of ACT in 1994 by Brittberg (Brittberg et al., 1994) led to the development of suitable biological substitutes and refinement of organotypic models by the group of M. Demoor* (Demoor et al., 2014). These mini-tissues/organoids have been incorporated in some translational research studies by the same group* (Desancé et al., 2018; Cullier et al., 2022) to develop cell-based and cell-free orthobiological therapeutic approaches. Therefore, some *in vitro* studies have been transposed from humans (Legendre et al., 2013; Gómez-Leduc et al., 2016; Gómez-Leduc et al., 2017; Legendre et al., 2017) to horses (Desancé et al., 2018) again by this group* to demonstrate the therapeutic potential of chondrocytes and stem cells for cartilage engineering in both species and to have the possibility to carry out preparatory work in horses before transposing it to humans.

4 Acellular therapies

4.1 Secretome

MSC capacity to induce tissue regeneration is due to its secretome that comprises all cell secretions (growth factors, cytokines, EVs, etc.). Among regenerative medicine strategies, acellular or cell-free therapies requires the delivery of exogenous active molecules, such as synthetic molecules or MSC secretome, as therapeutic agents into the joint as reported by Velot* *et al.* (Dostert et al., 2017; Velot et al., 2021).

Indeed, the secretome of BM MSCs that were primed with inflammatory factors were shown to inhibit inflammatory processes in human OA synovial explants *in vitro* as observed by the group of G. J. V. M. van Osch* (van Buul et al., 2012). The activity of the secretome of MSCs is not specific for BM MSCs (Manferdini et al., 2020). The groups of G. Lisignoli* and of D. Noël* showed that adipose tissue-derived MSCs (ASCs) have similar effects *in vitro,* and their anti-inflammatory and anti-catabolic effects were indicated to be dependent on the inflammatory status of the chondrocytes or synoviocytes (Maumus et al., 2016). The secretome of human BM MSCs reduced pain and joint degeneration in a mouse model of OA (Khatab et al., 2018).

Most animal studies aimed at improving acellular MSC-based therapies, especially in horses, are still predominantly conducted *in vitro* as reported by Jammes *et al.* (Jammes et al., 2023). The same author participated in a study (Contentin et al., 2022) that specifically highlighted the pro-anabolic potential of equine MSC-conditioned media containing exosomes on a cartilage organoid model *in vitro*. Kearney *et al.* (Kearney et al., 2022) performed a recent study in acute inflammatory arthritis by injection of lipopolysaccharide (LPS) in horses, showing no difference between the injection of allogenic BM MSCs and of their secretome. Additionally, proofs of concept for the manufacturing of clinical-grade equine and canine freeze-dried secretome which present many advantages in terms of practical use (stability, easy to store and use) have been published by Mocchi *et al.* (Mocchi et al., 2021a; Mocchi et al., 2021b). These authors showed in a canine study that an intra-articular injection of secretome in five dogs with OA was safe, without significant adverse effects. These preliminary data suggest that clinical trials may be established to evaluate the potential of these therapies in the treatment of spontaneous OA in animals.

4.2 Extracellular vesicles

Research is also well underway in animals to characterize the MSC secretome in order to identify the most promising factors for treating OA and to explore the EVs as potential biomarkers for monitoring its progression (Anderson et al., 2022). In particular, techniques for isolating and characterizing EVs have been described for several types of MSCs and work on chondrocytes indicated that MSC-EVs reduce gene expression of inflammatory markers (Hotham et al., 2021; Arévalo-Turrubiarte et al., 2022).

MSCs produce large and small size EV subtypes that exert similar protective effects on chondrocytes and anti-inflammatory effects on macrophages *in vitro* as reported by Vonk *et al.* and *in vivo* in the collagenase-induced OA model of the group of D. Noël* (Cosenza et al., 2017; Vonk et al., 2018). However, small size EVs were more potent to suppress the clinical signs of inflammatory arthritis in the collagen-induced model of the group of D. Noël* (Cosenza et al., 2018). This observation was attributed to the induction of a regulatory response by small size EVs as shown by the upregulation of $CD19^{+}IL10^{+}$ Breg-like cells and the decrease in plasmablast cells in the lymph nodes of mice. Down-regulating the TGF-β-induced gene product-h3 (TGFBI/BIGH3) in MSCs partly inhibited their anabolic effects on chondrocytes and did not protect mice from developing OA. Although not demonstrated to be directly related, the detection of TGFBI/BIGH3 in the cargo of both small and large size EVs might explain the protective role of EVs in OA as seen by the group of D. Noël* (Ruiz et al., 2020). Priming MSCs was shown to modify their proteome and secretome as well as their content in miRNAs, thereby modulating their functional properties, in particular their immunoregulatory function as described by the group of D. Noël* (Pers et al., 2021). Parental cell priming also impacts the cargo of EVs and inflammatory priming was reported to modulate cytokine and miRNA levels in EVs and enhance their anti-inflammatory potency (Ragni et al., 2020). Another strategy is based on genetic engineering of MSCs to overexpress the hypoxia-inducible factor 1 alpha (HIF-1α) and telomerase to generate large-scale production of reproducible batches of MSC-derived EVs with higher immunosuppressive activity (Gómez-Ferrer et al., 2021). In addition, overexpression of several miRNAs in MSCs or in synovial fibroblasts, as shown with miR-126–3p, may suppress apoptosis and inflammation in chondrocytes and prevent cartilage degradation in a OA model (Zhou et al., 2021).

Indeed, miRNAs were shown to be a crucial player for MSC-EVs function. This paradigm has been confirmed for EVs released by MSCs obtained from several sources such as adipose tissue, bone marrow, and amniotic membrane as studied by the group of L. de Girolamo* (Ragni et al., 2020; Ragni et al., 2021a; Ragni et al., 2022a). With respect to EV-miRNA activity for orthopedic conditions, a complex scenario has emerged with respect to how they can function/contribute to MSC therapeutic potential. MSC-EVs are enriched in miRNAs, predicted to suppress the activation of immune cells and the production of OA-related inflammatory mediators, as well as to promote cartilage protection by acting on both chondrocyte homeostasis and extracellular matrix-degrading enzymes. Most importantly, pre-activation of MSCs with pro-inflammatory mediators allows for the release of EVs with increased amounts of protective miRNAs, as clearly shown for adipose MSCs (Ragni et al., 2020). These results were confirmed by the group of L. de Girolamo* (Ragni et al., 2021b; Ragni et al., 2022b) for EVs released from MSCs in the presence of synovial fluid from OA patients that is rich in pro-inflammatory molecules. Consistently, when envisioned as a cell-free therapy, MSC-EVs protected mice from developing OA, suggesting that these nanoparticles can reproduce the main therapeutic effects of secreting cells by reducing OA symptoms (Cosenza et al., 2017). Notably, inhibition of inflammation (Cosenza et al., 2018) and reduction of cartilage degradation (Cosenza et al., 2017) *in vivo* confirmed *in silico* molecular data on EV-miRNAs fingerprints, leading to the potential for new strategies using single miRNA modulation (Xi et al., 2021) as a means to improve therapeutic potential for both MSK disorders and other diseases where cutting-edge treatments are actively needed.

Native EVs or EVs from primed cells do not necessarily contain appropriate mediators to improve OA. The use of synthetic vesicles such as liposomes may be a means to encapsulate and deliver exogenous active molecules of interest to joint tissues via intra-articular injection. This drug delivery system may counteract the degradation of selected mediators and allow for their sustained release in the joint (Velot et al., 2022). However, liposomes can be silenced by immune cell phagocytosis. As the composition of EV membrane prevents phagocytosis, new delivery systems to carry selected active molecules may be developed by merging MSC-

derived EVs and liposomes to engineer a hybrid vesicle designed for joint healing as reported by Velot* *et al.* and by others (Velot et al., 2021; Elkhoury et al., 2022).

5 Combined approaches

5.1 Gene-activated matrices

MSK gene therapy has been further expanded by combining gene transfer technologies with tissue engineering to generate gene-activated matrices (GAMs), a powerful tool also referred to as biomaterial-guided gene therapy, improving the spatiotemporal, controlled delivery of therapeutic genes to their targets (Borghesi et al., 2019; Perry et al., 2021; Hyland et al., 2020; Hwang et al., 2008; Karikó et al., 2005; Weissman, 2015; Elangovan et al., 2015; Balmayor et al., 2016; Badieyan et al., 2016; Balmayor et al., 2017; Khorsand et al., 2017; Zhang et al., 2019; Geng et al., 2021; Fayed et al., 2021; De La Vega et al., 2022; European Scoiety of Gene and Cell Therapy, 2022; Aini et al., 2016; Tendulkar et al., 2019; Liu et al., 2022; Madry et al., 2020a; Venkatesan et al., 2019; Cucchiarini and Madry, 2019; Atasoy-Zeybek and Kose, 2018; Shapiro et al., 2018; Venkatesan et al., 2018; Rey-Rico et al., 2017a; D'Mello et al., 2017; Rey-Rico et al., 2016; Raisin et al., 2016; Cucchiarini et al., 2016; Raftery et al., 2016; Rey-Rico and Cucchiarini, 2016). Different systems (micelles, hydrogels, solid scaffolds) have been used to generate GAMs capable of delivering a variety of gene transfer vectors. Nonviral vectors were incorporated in GAMs by the groups of A. L. Bertone, of W. Richter, and of M. Murphy* and also by Curtin *et al.*, Raftery *et al.*, and Tierney *et al.* to carry PTH(1–34) (collagen) (Backstrom et al., 2004), VEGF (collagen) (Geiger et al., 2005), BMP-2 (collagen, nano-hydroxyapatite - nHA, alginate, chondroitin sulfate) (Curtin et al., 2012; Loozen et al., 2013; Nedorubova et al., 2022; Husteden et al., 2023), BMP-2/VEGF (collagen, nHA, chitosan) (Curtin et al., 2015; Raftery et al., 2017; Raftery et al., 2019; Walsh et al., 2021), BMP-2/BMP-7 (collagen, nHA, chitosan) (Raftery et al., 2018), SOX9 (collagen, alginate) (Ledo et al., 2020), ephrinB2 (collagen, nHA) (Tierney et al., 2013), and the stromal-derived factor 1 alpha (SDF-1α) (collagen, nHA) (Power et al., 2022) to stimulate MSC chondro-/osteogenesis and bone healing. GAMs formulating rAAV vectors carrying TGF-β (pluronics, carbon dots - CDs, poly (ε-caprolactone) - PCL) (Rey-Rico et al., 2017b; Meng et al., 2020; Venkatesan et al., 2021), IGF-I (alginate) (Maihöfer et al., 2021), and SOX9 (pluronics, PCL, CDs) (Rey-Rico et al., 2018; Madry et al., 2020b; Urich et al., 2020; Venkatesan et al., 2020) were also used by the group of M. Cucchiarini* to stimulate MSC chondrogenesis, cartilage repair, and prevent OA. Interestingly, GAM have been also tested by the groups of E. R. Balmayor*, of M. Murphy*, and of D. Noël* to deliver RNAs, like for instance an mRNA for BMP-2 (micro-macro biphasic calcium phosphate - MBCP - granules, fibrin gel, collagen sponge, titanium implants) (Tierney et al., 2013; Morille et al., 2016; Balmayor et al., 2017; Zhang et al., 2019; Fayed et al., 2021; De La Vega et al., 2022) to stimulate MSC osteogenesis and bone healing or siRNAs against Runx2 (pluronics, collagen) (Raisin et al., 2017; Salvador et al., 2022) to reduce MSC osteogenesis.

5.2 EVs and biomaterials

The use of MSC-derived EVs in combination with biomaterials represent a future MSK tissue engineering strategy to influence and facilitate local therapeutic release of EVs by means of their design and chemical characteristics (Yan et al., 2020; Casanova et al., 2021; Zhang et al., 2021). Nanofibrous substrates designed to immobilize EVs induce the chondrogenic differentiation of BM MSCs as seen by Casanova *et al.* (Casanova et al., 2021). Hydrogels containing MSC-derived EVs have the ability to integrate cartilage ECM and to promote MSC recruitment, resulting in cartilage defect repair (Liu et al., 2017; Zhang et al., 2021). The association of scaffolds with EVs and MSCs is also an alternative to improve cartilage regeneration as reported by Heirani-Tabasi *et al.* and by others (Heirani-Tabasi et al., 2021; Cho et al., 2023).

6 Discussion

The last 30 years of research in cartilage regeneration and its biology have been marked by numerous and essential steps forward in the technologies available to study and apply research aimed at joint regeneration. The fact that women have been a vital part of this effort, especially *via* work performed in interdisciplinary teams, is to be noted, as evidenced by the large (although non-exhaustive) body of literature cited here. It is critical for us to be at the forefront of research in a field of particular interest to us as doctors, researchers, and women (Alliston et al., 2020), but also as potential patients. If medicine has taught us anything, one must not only view one component of what we are trying to treat, but related components and how they all interact.

In the future, patients will benefit from a continuously maturing collaborative approach, combining the best biological research with robotics for biomaterial and scaffold development and printing. For example, 3D printing has already shown its relevance in creating patient-specific scaffolds based on defect evaluation *via* radiological evaluation, allowing for near-perfect replication and correction. Automated production systems for cells and cell-derived products synergize to provide relevant cells for these scaffolds in a cost effective manner. This personalized approach allows for a more precise correction and treatment, and better outcomes. Additionally, with potential for the continuous growth of the industry due to the increased incidence of OA in the general population, therapy production will be further facilitated and standardized; therefore, more patients will be able to benefit from a better access to improved technologies to treat OA.

We have also seen that OA and MSK research has diverged to genetic engineering, secretomes, and viral vectors. These approaches based on basic biological principles common to cells show promise, notably when combined with the application of stem cells. *In vitro* studies on MSC secretomes and EVs by the groups of G. Lisignoli*, of D. Noël*, and of G. J. V. M. van Osch* (van Buul et al., 2012; Manferdini et al., 2020; Ruiz et al., 2020) show promise in terms of anti-inflammatory properties and anti-catabolic effects dependent on the inflammatory status of chondrocytes and synoviocytes. These approaches allow for a more direct cellular-based approach to managing the degeneration leading to OA and the potential for slowing down the catabolic mechanisms leading to its advancement.

The future of MSK regeneration is based on a patient-centered approach. OA is a multimodal disease, with multiple factors leading

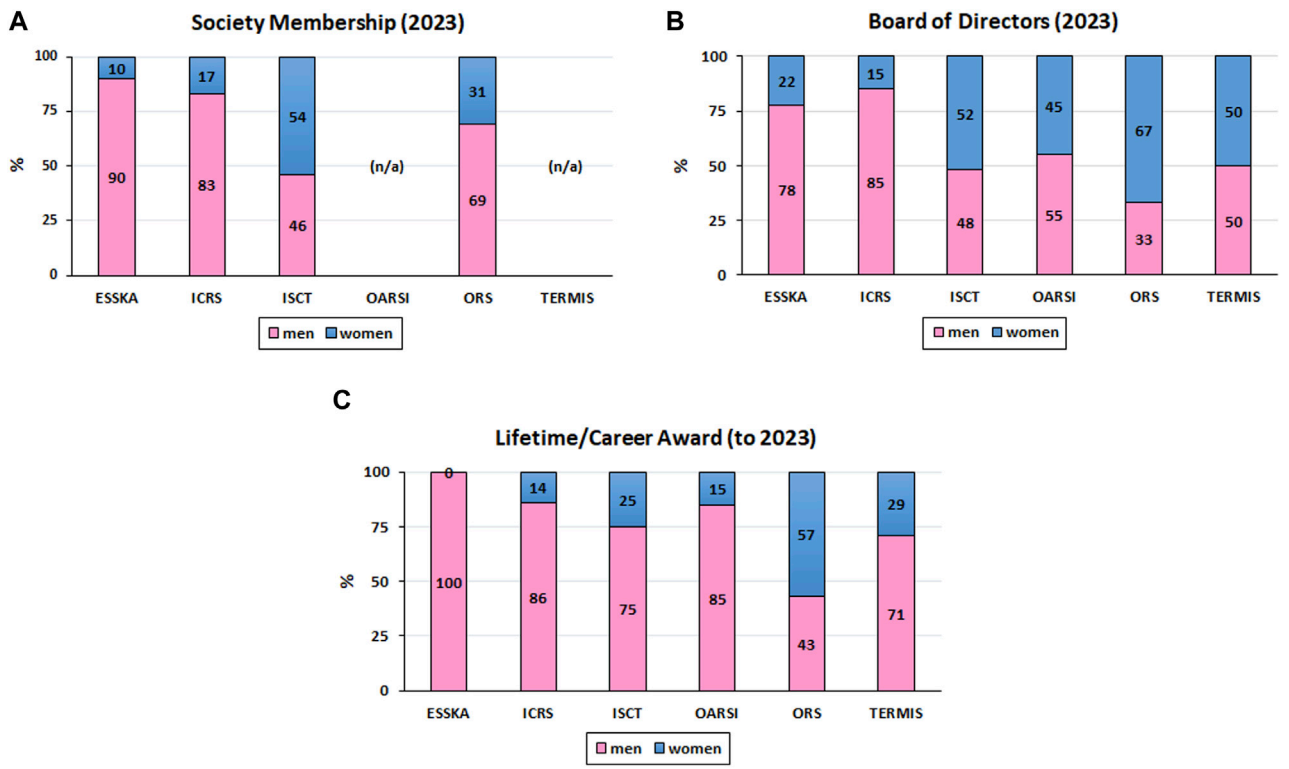

FIGURE 2
Representation of Women in MSK Societies. **(A)**: Society Membership; **(B)** Board of Directors; **(C)** Recipients of Lifetime/Career Awards; n/a: not available).

to its development and progression that can be targeted to delay or even prevent its progression. The ideal scenario for future patients is a multimodal approach from personalized lifestyle modifications informed by polygenic risk scores that characterize an individual genetic risk profile as reported by the group of F. Cicuttini* (Lacaze et al., 2022) to the study of the degenerative and inflammatory state of the joint down to a cellular level to counteract destructive processes and even stimulate regeneration. Combining these different levels of therapeutic impact, one could potentially modulate the disease progression by targeting therapies to different patient phenotype in OA. There remain some challenges regarding how to make such an approach applicable, but once a multimodal method can be applied, the results may be revolutionary by targeting therapies to those most likely to benefit.

Research in the MSK field has seen many breakthroughs in the last decades, with women being at the forefront of several, especially in the field of biology. Yet, a significant disparity remains due to the generally imbalanced ratio of women to men in the field as can be noted on the representation of women in the membership (Figure 2A), in the Board of Directors (Figure 2B), and as recipients of Lifetime/Career Awards (Figure 2C) of various MSK and cell therapy/tissue regeneration societies (data generously provided by the European Society for Sports Traumatology, Knee Surgery and Arthroscopy - ESSKA - https://www.esska.org, the ICRS with a woman current President - EK*, the International Society for Cell and Gene Therapy - ISCT - https://www.isctglobal.org/home, the Osteoarthritis Research Society International - OARSI - https://www.oarsi.org, the Orthopaedic Research Society - ORS - https://www.ors.org with a woman as Past President and a woman as Incoming President, and the Tissue Engineering and Regenerative Medicine International Society - TERMIS - https://www.termis.org with a woman as Incoming President). In particular, the societies associated to clinical orthopedics (i.e., ESSKA and ICRS) are still male-dominated. Since a majority of the 2023 Board of Directors of the societies presented here are well balanced, we can speculate that this token of involvement and recognition of women in the field will translate in a better gender balance of Lifetime/Career awards in the future. The current under-representation of women in MSK research, in particular when it involves orthopedics, has a number of reasons. These include the lack of female role models and mentors in the academic world and in industry is one aspect that makes it more challenging for women to see themselves pursuing careers in MSK research. Moreover, gender prejudice and discrimination might make it more difficult for women to excel in both academia and industry, particularly in male-dominated specialties such as orthopedic surgery.

Orthopedics remains the least diversified medical specialty, with the highest prevalence of men. In fact, only 7.4% and 7% of orthopedic surgeons in the United States and UK, respectively, are female (Ahmed and Hamilton, 2021; Peterman et al., 2022). This disparity also applies in academic and research fields, with only 20% of women assistant professors, 15% of women associate professors, and 9% of women full professors in orthopedics for instance (Gerull et al., 2020), although their impact should not be overlooked. Women are also under-represented in the biomedical engineering field (Barabino et al., 2020) which is key for MSK research and translation. It is therefore crucial to

take action to address these underlying problems. This can include campaigns to eliminate gender bias and discrimination as well as initiatives to raise the profile of female researchers and clinicians in academics and associated industries, such as the "Women in ESSKA" initiative that (*sic*) "wants to promote ESSKA's educational and research activities among female orthopedic surgeons during and after their specialization" (https://www.esska.org/page/WomeninESSKA) or the "ORS Women's Leadership Forum" that (*sic*) "will mentor, foster, encourage and inspire women at the start and throughout their careers in orthopedic research, and will assist women in obtaining leadership roles in orthopedic-related organizations" (https://www.ors.org/womens-leadership-forum).

Hope now lies in the upcoming generation of doctors and researchers, with medical and scientific Universities today having a higher prevalence of female students than males (Barabino et al., 2020; Ahmed and Hamilton, 2021). Moreover, gender should no longer be considered as binary. Hopefully, these developments will have a "butterfly" effect to increase diversity and to continue to open doors for women and minorities in the field of MSK research, including stem cell research. These new and upcoming colleagues also have the advantage of having grown up in parallel to all the new technologies of today. They have a different approach and mindset to search for opportunities, bringing a breath of fresh air and innovation to biomedical research in general. Although these newcomers may have suffered from a lack of mentorship and role models, we hope that this paper will have highlighted women who can illustrate the part and that it will inspire them to become the leaders of tomorrow in this disciplinary field (Barabino et al., 2020).

Author contributions

All authors participated in writing the Introduction and Discussion sections and in preparing and editing Figure 1 and Figure 2. ÉV wrote "EV and biomaterials" and parts of "Joint MSC sources", of "Tissue engineering", of "Secretome", and of "Extracellular vesicles"; EB wrote "Transcript therapy"; LB wrote parts of "Secretome"; SC wrote parts of the "Introduction"; FC wrote parts of the "Introduction"; LdG wrote parts of "Joint MSC sources", of "MSCs *versus* tissue-specific cells for joint regeneration", of "Differentiation and culture conditions for appropriate MSK differentiation of MSCs, priming, immunomodulation", and of "Extracellular vesicles"; MD wrote "From biologic substitutes to organoids, 3D models, and organ-on-a-chip" and parts of "Secretome"; BG wrote parts of "Bioprinting, sustainable automated manufacturing for therapeutic cells"; EJ wrote parts of "Joint MSC sources", of "Differentiation and culture conditions for appropriate MSK differentiation of MSCs, priming, immunomodulation", and of "Secretome"; EK wrote parts of "Tissue engineering"; GL wrote parts of "Tissue engineering"; MM wrote parts of "Joint MSC sources" and of "Bioprinting, sustainable automated manufacturing for therapeutic cells"; EJ wrote parts of "Joint MSC sources"; DN wrote parts of "MSCs *versus* tissue-specific cells for joint regeneration", "Joint MSC sources", "Differentiation and culture conditions for appropriate MSK differentiation of MSCs, priming, immunomodulation", "Tissue engineering", "Bioprinting, sustainable automated manufacturing for therapeutic cells" and "Extracellular vesicles"; CV wrote "Gene therapy modifications"; GJVMvO wrote "Embryology and joint development, progenitor cells in the joint" and parts of "Joint MSC sources", of "MSCs *versus* tissue-specific cells for joint regeneration", of "Differentiation and culture conditions for appropriate MSK differentiation of MSCs, priming, immunomodulation", of "Secretome", and of "Extracellular vesicles"; MC wrote "Gene therapy", "Gene-activated matrices", and parts of "Joint MSC sources" and edited all the sections and the complete manuscript. All authors contributed to the article and approved the submitted version.

Funding

This work was supported by the NIH (grant number R01AR074395, NIAMS) and the European Union's Horizon 2020 research and innovation program (grant "cmRNAbone", agreement number 874790) (EB), the NHMRC Investigator Grant (APP1194829) (FC), the European Union-funded project "OA-ACTIVE" within the framework of the Operational Program ERDF (European Regional Development Funds)/ESF 2014–2020, also supported by ERDF grants "EQUISTEM" 917CB210), by Fonds Eperon ("EQUISTEM" N80-2014) (MD, LB), the GIS CENTAURE-equine research, the ERDF and Regional Council of Normandy (France) grant in the CPER Centaure program (N°917CB213, 917CB224), the French National Research Agency (ANR/EuroNanoMedIII, ANR-20-ANM3-0006-02) (MD), the Italian Ministry of Health "Ricerca Corrente" (BG), the Centre of Excellence in Medical Engineering funded by the Wellcome Trust and EPSRC (WELMEC; grant number WT 088908/Z/09/Z) and the Foundation for Research in Rheumatology (FOREUM, grant number 104929) (EJ), the Italian Ministry of Health (BANDO RICERCA FINALIZZATA 2019 esercizio finanziario anni 2018–2019, "PATTERN" grant CO-2019–12370720) (EK), the Italian Ministry of Health "Ricerca Corrente" (GL), the European Union's Horizon 2020 research and innovation programmes (grant numbers 874671 and 667932), the Higher Education Authority Ireland (EpiHyper), the INTERREG Ireland Wales Programme (80885), the Science Foundation Ireland (2021/01/29FIDEC), and the European Union's Horizon 2020 research and innovation programme (grant agreements "AutoCRAT" 874671 and "AutoSTEM" 667932) (MM), the French National Research Agency (ANR) ("ECELLFRANCE " grant PIA/ANR-11-INSB-005) (DN), the French National Research Agency (ANR) through the ANR JCJC "KLOTHOA" (ANR-18-CE14-0024-01), the region Pays de la Loire ("RFI Bioregate", "GenOA"), the Arthritis Foundation, and the Société Française de Rhumatologie (CV), and the World Arthrosis Foundation (MC).

Conflict of interest

The authors declare that the research was conducted in the absence of any commercial or financial relationships that could be construed as a potential conflict of interest.

Publisher's note

All claims expressed in this article are solely those of the authors and do not necessarily represent those of their affiliated organizations, or those of the publisher, the editors and the reviewers. Any product that may be evaluated in this article, or claim that may be made by its manufacturer, is not guaranteed or endorsed by the publisher.

References

Abdollahiyan, P., Oroojalian, F., Mokhtarzadeh, A., and de la Guardia, M. (2020). Hydrogel-based 3D bioprinting for bone and cartilage tissue engineering. *Biotechnol. J.* 15, e2000095. doi:10.1002/biot.202000095

Ahmed, M., and Hamilton, L. C. (2021). Current challenges for women in orthopaedics. *Bone Jt. Open* 2, 893–899. doi:10.1302/2633-1462.210.BJO-2021-0089.R1

Aini, H., Itaka, K., Fujisawa, A., Uchida, H., Uchida, S., Fukushima, S., et al. (2016). Messenger RNA delivery of a cartilage-anabolic transcription factor as a disease-modifying strategy for osteoarthritis treatment. *Sci. Rep.* 6, 18743. doi:10.1038/srep18743

Alliston, T., Foucher, K. C., Frederick, B., Hernandez, C. J., Iatridis, J. C., Kozloff, K. M., et al. (2020). The importance of diversity, equity, and inclusion in orthopedic research. *J. Orthop. Res.* 38, 1661–1665. doi:10.1002/jor.24685

Altschuler, N., Zaslav, K. R., Di Matteo, B., Sherman, S. L., Gomoll, A. H., Hacker, S. A., et al. (2023). Aragonite-based scaffold versus microfracture and debridement for the treatment of knee chondral and osteochondral lesions: results of a multicenter randomized controlled trial. *Am. J. Sports Med.* 51, 957–967. doi:10.1177/03635465231151252

Amann, E., Wolff, P., Breel, E., van Griensven, M., and Balmayor, E. R. (2017). Hyaluronic acid facilitates chondrogenesis and matrix deposition of human adipose derived mesenchymal stem cells and human chondrocytes Co-cultures. *Acta Biomater.* 52, 130–144. doi:10.1016/j.actbio.2017.01.064

Amini, M., Venkatesan, J. K., Liu, W., Leroux, A., Nguyen, T. N., Madry, H., et al. (2022). Advanced gene therapy strategies for the repair of ACL injuries. *Int. J. Mol. Sci.* 23, 14467. doi:10.3390/ijms232214467

Anderson, D. D., Chubinskaya, S., Guilak, F., Martin, J. A., Oegema, T. R., Olson, S. A., et al. (2011). Post-traumatic osteoarthritis: improved understanding and opportunities for early intervention. *J. Orthop. Res.* 29, 802–809. doi:10.1002/jor.21359

Anderson, J. R., Jacobsen, S., Walters, M., Bundgaard, L., Diendorfer, A., Hackl, M., et al. (2022). Small non-coding RNA landscape of extracellular vesicles from a post-traumatic model of equine osteoarthritis. *Front. Vet. Sci.* 9, 901269. doi:10.3389/fvets.2022.901269

Ansboro, S., Greiser, U., Barry, F., and Murphy, M. (2012). Strategies for improved targeting of therapeutic cells: implications for tissue repair. *Eur. Cell Mater* 23, 310–318. doi:10.22203/ecm.v023a24

Anzillotti, G., Conte, P., Di Matteo, B., Bertolino, E. M., Marcacci, M., and Kon, E. (2022). Injection of biologic agents for treating severe knee osteoarthritis: is there a chance for a good outcome? a systematic review of clinical evidence. *Eur. Rev. Med. Pharmacol. Sci.* 26, 5447–5459. doi:10.26355/eurrev_202208_29413

Arévalo-Turrubiarte, M., Baratta, M., Ponti, G., Chiaradia, E., and Martignani, E. (2022). Extracellular vesicles from equine mesenchymal stem cells decrease inflammation markers in chondrocytes *in vitro*. *Equine Vet. J.* 54, 1133–1143. doi:10.1111/evj.13537

Armiento, A. R., Stoddart, M. J., Alini, M., and Eglin, D. (2018). Biomaterials for articular cartilage tissue engineering: learning from biology. *Acta Biomater.* 65, 1–20. doi:10.1016/j.actbio.2017.11.021

Atasoy-Zeybek, A., and Kose, G. T. (2018). Gene therapy strategies in bone tissue engineering and current clinical applications. *Adv. Exp. Med. Biol.* 1119, 85–101. doi:10.1007/5584_2018_253

Backstrom, K. C., Bertone, A. L., Wisner, E. R., and Weisbrode, S. E. (2004). Response of induced bone defects in horses to collagen matrix containing the human parathyroid hormone gene. *Am. J. Vet. Res.* 65, 1223–1232. doi:10.2460/ajvr.2004.65.1223

Badieyan, Z. S., Berezhanskyy, T., Utzinger, M., Aneja, M. K., Emrich, D., Erben, R., et al. (2016). Transcript-activated collagen matrix as sustained MRNA delivery system for bone regeneration. *J. Control Release* 239, 137–148. doi:10.1016/j.jconrel.2016.08.037

Bakhshandeh, B., Zarrintaj, P., Oftadeh, M. O., Keramati, F., Fouladiha, H., Sohrabi-Jahromi, S., et al. (2017). Tissue engineering; strategies, tissues, and biomaterials. *Biotechnol. Genet. Eng. Rev.* 33, 144–172. doi:10.1080/02648725.2018.1430464

Ball, A. N., Phillips, J. N., McIlwraith, C. W., Kawcak, C. E., Samulski, R. J., and Goodrich, L. R. (2019). Genetic modification of ScAAV-equine-BMP-2 transduced bone-marrow-derived mesenchymal stem cells before and after cryopreservation: an "off-the-shelf" option for fracture repair. *J. Orthop. Res.* 37, 1310–1317. doi:10.1002/jor.24209

Balmayor, E. R., and Evans, C. H. (2019). RNA therapeutics for tissue engineering. *Tissue Eng. Part A* 25, 9–11. doi:10.1089/ten.tea.2018.0315

Balmayor, E. R., Geiger, J. P., Aneja, M. K., Berezhanskyy, T., Utzinger, M., Mykhaylyk, O., et al. (2016). Chemically modified RNA induces osteogenesis of stem cells and human tissue explants as well as accelerates bone healing in rats. *Biomaterials* 87, 131–146. doi:10.1016/j.biomaterials.2016.02.018

Balmayor, E. R., Geiger, J. P., Koch, C., Aneja, M. K., van Griensven, M., Rudolph, C., et al. (2017). Modified MRNA for BMP-2 in combination with biomaterials serves as a transcript-activated matrix for effectively inducing osteogenic pathways in stem cells. *Stem Cells Dev.* 26, 25–34. doi:10.1089/scd.2016.0171

Balmayor, E. R. (2022). Synthetic MRNA - emerging new class of drug for tissue regeneration. *Curr. Opin. Biotechnol.* 74, 8–14. doi:10.1016/j.copbio.2021.10.015

Balmayor, E. R. (2015). Targeted delivery as key for the success of small osteoinductive molecules. *Adv. Drug Deliv. Rev.* 94, 13–27. doi:10.1016/j.addr.2015.04.022

Bannuru, R. R., Osani, M. C., Vaysbrot, E. E., Arden, N. K., Bennell, K., Bierma-Zeinstra, S. M. A., et al. (2019). OARSI guidelines for the non-surgical management of knee, hip, and polyarticular osteoarthritis. *Osteoarthr. Cartil.* 27, 1578–1589. doi:10.1016/j.joca.2019.06.011

Barabino, G., Frize, M., Ibrahim, F., Kaldoudi, E., Lhotska, L., Marcu, L., et al. (2020). Solutions to gender balance in STEM fields through support, training, education and mentoring: report of the international women in medical physics and biomedical engineering task group. *Sci. Eng. Ethics* 26, 275–292. doi:10.1007/s11948-019-00097-0

Barbour, K. E., Helmick, C. G., Boring, M., and Brady, T. J. (2017). Vital signs: prevalence of doctor-diagnosed arthritis and arthritis-attributable activity limitation - united states, 2013-2015. *MMWR Morb. Mortal. Wkly. Rep.* 66, 246–253. doi:10.15585/mmwr.mm6609e1

Bertoni, L., Jacquet-Guibon, S., Branly, T., Desancé, M., Legendre, F., Melin, M., et al. (2021). Evaluation of allogeneic bone-marrow-derived and umbilical cord blood-derived mesenchymal stem cells to prevent the development of osteoarthritis in an equine model. *Int. J. Mol. Sci.* 22, 2499. doi:10.3390/ijms22052499

Beane, O. S., and Darling, E. M. (2012). Isolation, characterization, and differentiation of stem cells for cartilage regeneration. *Ann. Biomed. Eng.* 40, 2079–2097. doi:10.1007/s10439-012-0639-8

Bertoni, L., Branly, T., Jacquet, S., Desancé, M., Desquilbet, L., Rivory, P., et al. (2019). Intra-articular injection of 2 different dosages of autologous and allogeneic bone marrow- and umbilical cord-derived mesenchymal stem cells triggers a variable inflammatory response of the fetlock joint on 12 sound experimental horses. *Stem Cells Int.* 2019, 9431894–9431917. doi:10.1155/2019/9431894

Borghesi, J., Ferreira Lima, M., Mario, L. C., de Almeida da Anunciação, A. R., Silveira Rabelo, A. C., Giancoli Kato Cano da Silva, M., et al. (2019). Canine amniotic membrane mesenchymal stromal/stem cells: isolation, characterization and differentiation. *Tissue Cell* 58, 99–106. doi:10.1016/j.tice.2019.04.007

Bony, C., Cren, M., Domergue, S., Toupet, K., Jorgensen, C., and Noël, D. (2016). Adipose mesenchymal stem cells isolated after manual or water-jet-assisted liposuction display similar properties. *Front. Immunol.* 6, 655. doi:10.3389/fimmu.2015.00655

Brittberg, M., Lindahl, A., Nilsson, A., Ohlsson, C., Isaksson, O., and Peterson, L. (1994). Treatment of deep cartilage defects in the knee with autologous chondrocyte transplantation. *N. Engl. J. Med.* 331, 889–895. doi:10.1056/NEJM199410063311401

Broeckx, S. Y., Seys, B., Suls, M., Vandenberghe, A., Mariën, T., Adriaensen, E., et al. (2019). Equine allogeneic chondrogenic induced mesenchymal stem cells are an effective treatment for degenerative joint disease in horses. *Stem Cells Dev.* 28, 410–422. doi:10.1089/scd.2018.0061

Camargo Garbin, L., and Morris, M. J. (2021). A comparative review of autologous conditioned serum and autologous protein solution for treatment of osteoarthritis in horses. *Front. Vet. Sci.* 8, 602978. doi:10.3389/fvets.2021.602978

Carballo-Pedrares, N., Sanjurjo-Rodriguez, C., Señarís, J., Díaz-Prado, S., and Rey-Rico, A. (2022). Chondrogenic differentiation of human mesenchymal stem cells via SOX9 delivery in cationic niosomes. *Pharmaceutics* 14, 2327. doi:10.3390/pharmaceutics14112327

Casanova, M. R., Osório, H., Reis, R. L., Martins, A., and Neves, N. M. (2021). Chondrogenic differentiation induced by extracellular vesicles bound to a nanofibrous substrate. *NPJ Regen. Med.* 6, 79. doi:10.1038/s41536-021-00190-8

Chen, M., Hu, Y., Hou, Y., Li, M., Chen, M., Tan, L., et al. (2020). Osteogenesis regulation of mesenchymal stem cells via autophagy induced by silica-titanium composite surfaces with different mechanical moduli. *J. Mater Chem. B* 8, 9314–9324. doi:10.1039/d0tb01412e

Cheng, A., Kapacee, Z., Peng, J., Lu, S., Lucas, R. J., Hardingham, T. E., et al. (2014). Cartilage repair using human embryonic stem cell-derived chondroprogenitors. *Stem Cells Transl. Med.* 3, 1287–1294. doi:10.5966/sctm.2014-0101

Cho, W. J., Ahn, J., Lee, M., Choi, H., Park, S., Cha, K.-Y., et al. (2023). Combinatorial effect of mesenchymal stem cells and extracellular vesicles in a hydrogel on cartilage regeneration. *Tissue Eng. Regen. Med.* 20, 143–154. doi:10.1007/s13770-022-00509-6

Chongchai, A., Waramit, S., Wongwichai, T., Kampangtip, J., Phitak, T., Kongtawelert, P., et al. (2023). Targeting human osteoarthritic chondrocytes with ligand directed bacteriophage-based particles. *Viruses* 221 (13), 2343. doi:10.3390/v13122343

Cicuttini, F. M., Jones, G., Forbes, A., and Wluka, A. E. (2004). Rate of cartilage loss at two years predicts subsequent total knee arthroplasty: A prospective study. *Ann. Rheum. Dis.* 63, 1124–1127. doi:10.1136/ard.2004.021253

Colbath, A. C., Dow, S. W., McIlwraith, C. W., and Goodrich, L. R. (2020). Mesenchymal stem cells for treatment of musculoskeletal disease in horses: relative merits of allogeneic versus autologous stem cells. *Equine Vet. J.* 52, 654–663. doi:10.1111/evj.13233

Coleman, C. M., Curtin, C., Barry, F. P., O'Flatharta, C., and Murphy, J. M. (2010). Mesenchymal stem cells and osteoarthritis: remedy or accomplice? *Hum. Gene Ther.* 21, 1239–1250. doi:10.1089/hum.2010.138

Colombini, A., Libonati, F., Cangelosi, D., Lopa, S., De Luca, P., Coviello, D. A., et al. (2022b). Inflammatory priming with IL-1β promotes the immunomodulatory behavior of adipose derived stem cells. *Front. Bioeng. Biotechnol.* 10, 1000879. doi:10.3389/fbioe.2022.1000879

Colombini, A., Libonati, F., Lopa, S., Peretti, G. M., Moretti, M., and de Girolamo, L. (2022a). Autologous chondrocyte implantation provides good long-term clinical results in the treatment of knee osteoarthritis: A systematic review. *Knee Surg. Sports Traumatol. Arthrosc.* 31, 2338–2348. doi:10.1007/s00167-022-07030-2

Colombini, A., Perucca Orfei, C., Kouroupis, D., Ragni, E., De Luca, P., ViganÒ, M., et al. (2019). Mesenchymal stem cells in the treatment of articular cartilage degeneration: new biological insights for an old-timer cell. *Cytotherapy* 21, 1179–1197. doi:10.1016/j.jcyt.2019.10.004

Contentin, R., Jammes, M., Bourdon, B., Cassé, F., Bianchi, A., Audigié, F., et al. (2022). Bone marrow MSC secretome increases equine articular chondrocyte collagen accumulation and their migratory capacities. *IJMS* 23, 5795. doi:10.3390/ijms23105795

Cosenza, S., Ruiz, M., Toupet, K., Jorgensen, C., and Noël, D. (2017). Mesenchymal stem cells derived exosomes and microparticles protect cartilage and bone from degradation in osteoarthritis. *Sci. Rep.* 7, 16214. doi:10.1038/s41598-017-15376-8

Cosenza, S., Toupet, K., Maumus, M., Luz-Crawford, P., Blanc-Brude, O., Jorgensen, C., et al. (2018). Mesenchymal stem cells-derived exosomes are more immunosuppressive than microparticles in inflammatory arthritis. *Theranostics* 8, 1399–1410. doi:10.7150/thno.21072

Cottard, V., Valvason, C., Falgarone, G., Lutomski, D., Boissier, M.-C., and Bessis, N. (2004). Immune response against gene therapy vectors: influence of synovial fluid on adeno-associated virus mediated gene transfer to chondrocytes. *J. Clin. Immunol.* 24, 162–169. doi:10.1023/B:JOCI.0000019781.64421.5c

Craft, A. M., Ahmed, N., Rockel, J. S., Baht, G. S., Alman, B. A., Kandel, R. A., et al. (2013). Specification of chondrocytes and cartilage tissues from embryonic stem cells. *Development* 140, 2597–2610. doi:10.1242/dev.087890

Critchley, S., Sheehy, E. J., Cunniffe, G., Diaz-Payno, P., Carroll, S. F., Jeon, O., et al. (2020). 3D printing of fibre-reinforced cartilaginous templates for the regeneration of osteochondral defects. *Acta Biomater.* 113, 130–143. doi:10.1016/j.actbio.2020.05.040

Cucchiarini, M., Asen, A.-K., Goebel, L., Venkatesan, J. K., Schmitt, G., Zurakowski, D., et al. (2018). Effects of TGF-β overexpression via RAAV gene transfer on the early repair processes in an osteochondral defect model in minipigs. *Am. J. Sports Med.* 46, 1987–1996. doi:10.1177/0363546518773709

Cucchiarini, M., Ekici, M., Schetting, S., Kohn, D., and Madry, H. (2011). Metabolic activities and chondrogenic differentiation of human mesenchymal stem cells following recombinant adeno-associated virus-mediated gene transfer and overexpression of fibroblast growth factor 2. *Tissue Eng. Part A* 17, 1921–1933. doi:10.1089/ten.TEA.2011.0018

Cucchiarini, M. (2016). Human gene therapy: novel approaches to improve the current gene delivery systems. *Discov. Med.* 21, 495–506.

Cucchiarini, M., and Madry, H. (2019). Biomaterial-guided delivery of gene vectors for targeted articular cartilage repair. *Nat. Rev. Rheumatol.* 15, 18–29. doi:10.1038/s41584-018-0125-2

Cucchiarini, M., Madry, H., Ma, C., Thurn, T., Zurakowski, D., Menger, M. D., et al. (2005). Improved tissue repair in articular cartilage defects *in vivo* by RAAV-mediated overexpression of human fibroblast growth factor 2. *Mol. Ther.* 12, 229–238. doi:10.1016/j.ymthe.2005.03.012

Cucchiarini, M., and Madry, H. (2014). Overexpression of human IGF-I via direct RAAV-mediated gene transfer improves the early repair of articular cartilage defects *in vivo*. *Gene Ther.* 21, 811–819. doi:10.1038/gt.2014.58

Cucchiarini, M., McNulty, A. L., Mauck, R. L., Setton, L. A., Guilak, F., and Madry, H. (2016). Advances in combining gene therapy with cell and tissue engineering-based approaches to enhance healing of the meniscus. *Osteoarthr. Cartil.* 24, 1330–1339. doi:10.1016/j.joca.2016.03.018

Cucchiarini, M., Orth, P., and Madry, H. (2013). Direct RAAV SOX9 administration for durable articular cartilage repair with delayed terminal differentiation and hypertrophy *in vivo*. *J. Mol. Med. Berl.* 91, 625–636. doi:10.1007/s00109-012-0978-9

Cucchiarini, M., Venkatesan, J. K., Ekici, M., Schmitt, G., and Madry, H. (2012). Human mesenchymal stem cells overexpressing therapeutic genes: from basic science to clinical applications for articular cartilage repair. *Biomed. Mater Eng.* 22, 197–208. doi:10.3233/BME-2012-0709

Cullier, A., Cassé, F., Manivong, S., Contentin, R., Legendre, F., Garcia Ac, A., et al. (2022). Functionalized nanogels with endothelin-1 and bradykinin receptor antagonist peptides decrease inflammatory and cartilage degradation markers of osteoarthritis in a horse organoid model of cartilage. *Int. J. Mol. Sci.* 23, 8949. doi:10.3390/ijms23168949

Curtin, C. M., Cunniffe, G. M., Lyons, F. G., Bessho, K., Dickson, G. R., Duffy, G. P., et al. (2012). Innovative collagen nano-hydroxyapatite scaffolds offer a highly efficient non-viral gene delivery platform for stem cell-mediated bone formation. *Adv. Mater* 24, 749–754. doi:10.1002/adma.201103828

Curtin, C. M., Tierney, E. G., McSorley, K., Cryan, S.-A., Duffy, G. P., and O'Brien, F. J. (2015). Combinatorial gene therapy accelerates bone regeneration: non-viral dual delivery of vegf and bmp2 in a collagen-nanohydroxyapatite scaffold. *Adv. Healthc. Mater* 4, 223–227. doi:10.1002/adhm.201400397

de Girolamo, L., Ragni, E., Cucchiarini, M., van Bergen, C. J. A., Hunziker, E. B., and Chubinskaya, S. (2019). Cells, soluble factors and matrix harmonically play the concert of allograft integration. *Knee Surg. Sports Traumatol. Arthrosc.* 27, 1717–1725. doi:10.1007/s00167-018-5182-1

de Girolamo, L., Kon, E., Filardo, G., Marmotti, A. G., Soler, F., Peretti, G. M., et al. (2016). Regenerative approaches for the treatment of early OA. *Knee Surg. Sports Traumatol. Arthrosc.* 24, 1826–1835. doi:10.1007/s00167-016-4125-y

De la Vega, R. E., Atasoy-Zeybek, A., Panos, J. A., Van Griensven, M., Evans, C. H., and Balmayor, E. R. (2021). Gene therapy for bone healing: lessons learned and new approaches. *Transl. Res.* 236, 1–16. doi:10.1016/j.trsl.2021.04.009

De La Vega, R. E., van Griensven, M., Zhang, W., Coenen, M. J., Nagelli, C. V., Panos, J. A., et al. (2022). Efficient healing of large osseous segmental defects using optimized chemically modified messenger RNA encoding BMP-2. *Sci. Adv.* 8, eabl6242. doi:10.1126/sciadv.abl6242

De Luca, P., Kouroupis, D., Viganò, M., Perucca-Orfei, C., Kaplan, L., Zagra, L., et al. (2019). Human diseased articular cartilage contains a mesenchymal stem cell-like population of chondroprogenitors with strong immunomodulatory responses. *J. Clin. Med.* 8, 423. doi:10.3390/jcm8040423

Decker, R. S., Koyama, E., and Pacifici, M. (2014). Genesis and morphogenesis of limb synovial joints and articular cartilage. *Matrix Biol.* 39, 5–10. doi:10.1016/j.matbio.2014.08.006

Decker, R. S., Um, H.-B., Dyment, N. A., Cottingham, N., Usami, Y., Enomoto-Iwamoto, M., et al. (2017). Cell origin, volume and arrangement are drivers of articular cartilage formation, morphogenesis and response to injury in mouse limbs. *Dev. Biol.* 426, 56–68. doi:10.1016/j.ydbio.2017.04.006

Demoor, M., Ollitrault, D., Gomez-Leduc, T., Bouyoucef, M., Hervieu, M., Fabre, H., et al. (2014). Cartilage tissue engineering: molecular control of chondrocyte differentiation for proper cartilage matrix reconstruction. *Biochim. Biophys. Acta* 1840, 2414–2440. doi:10.1016/j.bbagen.2014.02.030

Desancé, M., Contentin, R., Bertoni, L., Gomez-Leduc, T., Branly, T., Jacquet, S., et al. (2018). Chondrogenic differentiation of defined equine mesenchymal stem cells derived from umbilical cord blood for use in cartilage repair therapy. *Int. J. Mol. Sci.* 19, 537. doi:10.3390/ijms19020537

Deshmukh, V., Hu, H., Barroga, C., Bossard, C., Kc, S., Dellamary, L., et al. (2018). A small-molecule inhibitor of the wnt pathway (SM04690) as a potential disease modifying agent for the treatment of osteoarthritis of the knee. *Osteoarthr. Cartil.* 26, 18–27. doi:10.1016/j.joca.2017.08.015

Deshmukh, V., O'Green, A. L., Bossard, C., Seo, T., Lamangan, L., Ibanez, M., et al. (2019). Modulation of the wnt pathway through inhibition of CLK2 and DYRK1A by lorecivivint as a novel, potentially disease-modifying approach for knee osteoarthritis treatment. *Osteoarthr. Cartil.* 27, 1347–1360. doi:10.1016/j.joca.2019.05.006

Diederichs, S., Gabler, J., Autenrieth, J., Kynast, K. L., Merle, C., Walles, H., et al. (2016). Differential regulation of SOX9 protein during chondrogenesis of induced pluripotent stem cells versus mesenchymal stromal cells: a shortcoming for cartilage formation. *Stem Cells Dev.* 25, 598–609. doi:10.1089/scd.2015.0312

Diederichs, S., Klampfleuthner, F. A. M., Moradi, B., and Richter, W. (2019a). Chondral differentiation of induced pluripotent stem cells without progression into the endochondral pathway. *Front. Cell Dev. Biol.* 7, 270. doi:10.3389/fcell.2019.00270

Diederichs, S., Tonnier, V., März, M., Dreher, S. I., Geisbüsch, A., and Richter, W. (2019b). Regulation of WNT5A and WNT11 during MSC *in vitro* chondrogenesis: WNT inhibition lowers BMP and hedgehog activity, and reduces hypertrophy. *Cell Mol. Life Sci.* 76, 3875–3889. doi:10.1007/s00018-019-03099-0

Diederichs, S., and Tuan, R. S. (2014). Functional comparison of human-induced pluripotent stem cell-derived mesenchymal cells and bone marrow-derived mesenchymal stromal cells from the same donor. *Stem Cells Dev.* 23, 1594–1610. doi:10.1089/scd.2013.0477

Dietz, B. W., Nakamura, M. C., Bell, M. T., and Lane, N. E. (2021). Targeting nerve growth factor for pain management in osteoarthritis-clinical efficacy and safety. *Rheum. Dis. Clin. North Am.* 47, 181–195. doi:10.1016/j.rdc.2020.12.003

Djouad, F., Bouffi, C., Ghannam, S., Noël, D., and Jorgensen, C. (2009). Mesenchymal stem cells: innovative therapeutic tools for rheumatic diseases. *Nat. Rev. Rheumatol.* 5, 392–399. doi:10.1038/nrrheum.2009.104

D'Mello, S., Atluri, K., Geary, S. M., Hong, L., Elangovan, S., and Salem, A. K. (2017). Bone regeneration using gene-activated matrices. *AAPS J.* 19, 43–53. doi:10.1208/s12248-016-9982-2

Docheva, D., Müller, S. A., Majewski, M., and Evans, C. H. (2015). Biologics for tendon repair. *Adv. Drug Deliv. Rev.* 84, 222–239. doi:10.1016/j.addr.2014.11.015

Domergue, S., Bony, C., Maumus, M., Toupet, K., Frouin, E., Rigau, V., et al. (2016). Comparison between stromal vascular fraction and adipose mesenchymal stem cells in remodeling hypertrophic scars. *PLoS ONE* 11, e0156161. doi:10.1371/journal.pone.0156161

Dong, L., Wang, S.-J., Zhao, X.-R., Zhu, Y.-F., and Yu, J.-K. (2017). 3D- printed poly(ε-caprolactone) scaffold integrated with cell-laden chitosan hydrogels for bone tissue engineering. *Sci. Rep.* 7, 13412. doi:10.1038/s41598-017-13838-7

Dostert, G., Mesure, B., Menu, P., and Velot, É. (2017). How do mesenchymal stem cells influence or are influenced by microenvironment through extracellular vesicles communication? *Front. Cell Dev. Biol.* 5, 6. doi:10.3389/fcell.2017.00006

Driessen, B. J. H., Logie, C., and Vonk, L. A. (2017). Cellular reprogramming for clinical cartilage repair. *Cell Biol. Toxicol.* 33, 329–349. doi:10.1007/s10565-017-9382-0

Dyer, O. (2020). Health ministers condemn novartis lottery for zolgensma, the world's most expensive drug. *BMJ* 368, m580. doi:10.1136/bmj.m580

Eichhoff, A. M., Börner, K., Albrecht, B., Schäfer, W., Baum, N., Haag, F., et al. (2019). Nanobody-enhanced targeting of AAV gene therapy vectors. *Mol. Ther. Methods Clin. Dev.* 15, 211–220. doi:10.1016/j.omtm.2019.09.003

El Omar, R., Beroud, J., Stoltz, J.-F., Menu, P., Velot, E., and Decot, V. (2014). Umbilical cord mesenchymal stem cells: the new gold standard for mesenchymal stem cell-based therapies? *Tissue Eng. Part B Rev.* 20, 523–544. doi:10.1089/ten.TEB.2013.0664

Elangovan, S., Khorsand, B., Do, A.-V., Hong, L., Dewerth, A., Kormann, M., et al. (2015). Chemically modified RNA activated matrices enhance bone regeneration. *J. Control Release* 218, 22–28. doi:10.1016/j.jconrel.2015.09.050

Elkhoury, K., Chen, M., Koçak, P., Enciso-Martínez, E., Bassous, N. J., Lee, M. C., et al. (2022). Hybrid extracellular vesicles-liposome incorporated advanced bioink to deliver MicroRNA. *Biofabrication* 14, 045008. doi:10.1088/1758-5090/ac8621

European Scoiety of Gene and Cell Therapy, Human gene therapy, Proceedings of the ESGCT 29th annual congress in collaboration with BSGCT edinburgh, UK October, 2022, doi:10.1089/hum.2022.29225.abstracts

Evans, C. H. (2019). The vicissitudes of gene therapy. *Bone Jt. Res.* 8, 469–471. doi:10.1302/2046-3758.810.BJR-2019-0265

Fahy, N., de Vries-van Melle, M. L., Lehmann, J., Wei, W., Grotenhuis, N., Farrell, E., et al. (2014). Human osteoarthritic synovium impacts chondrogenic differentiation of mesenchymal stem cells via macrophage polarisation state. *Osteoarthr. Cartil.* 22, 1167–1175. doi:10.1016/j.joca.2014.05.021

Farrell, E., Fahy, N., Ryan, A. E., Flatharta, C. O., O'Flynn, L., Ritter, T., et al. (2016). VIL-10-Overexpressing human MSCs modulate naïve and activated T lymphocytes following induction of collagenase-induced osteoarthritis. *Stem Cell Res. Ther.* 7, 74. doi:10.1186/s13287-016-0331-2

Farrell, E., van der Jagt, O. P., Koevoet, W., Kops, N., van Manen, C. J., Hellingman, C. A., et al. (2009). Chondrogenic priming of human bone marrow stromal cells: A better route to bone repair? *Tissue Eng. Part C Methods* 15, 285–295. doi:10.1089/ten.tec.2008.0297

Fayed, O., van Griensven, M., Tahmasebi Birgani, Z., Plank, C., and Balmayor, E. R. (2021). Transcript-activated coatings on titanium mediate cellular osteogenesis for enhanced osteointegration. *Mol. Pharm.* 18, 1121–1137. doi:10.1021/acs.molpharmaceut.0c01042

Ferris, D. J., Frisbie, D. D., Kisiday, J. D., McIlwraith, C. W., Hague, B. A., Major, M. D., et al. (2014). Clinical outcome after intra-articular administration of bone marrow derived mesenchymal stem cells in 33 horses with stifle injury. *Vet. Surg.* 43, 255–265. doi:10.1111/j.1532-950X.2014.12100.x

Fischer, J., Aulmann, A., Dexheimer, V., Grossner, T., and Richter, W. (2014). Intermittent PTHrP(1-34) exposure augments chondrogenesis and reduces hypertrophy of mesenchymal stromal cells. *Stem Cells Dev.* 23, 2513–2523. doi:10.1089/scd.2014.0101

Fischer, J., Ortel, M., Hagmann, S., Hoeflich, A., and Richter, W. (2016). Role of PTHrP(1-34) pulse frequency versus pulse duration to enhance mesenchymal stromal cell chondrogenesis. *J. Cell Physiol.* 231, 2673–2681. doi:10.1002/jcp.25369

Fortier, L. A., Nixon, A. J., Williams, J., and Cable, C. S. (1998). Isolation and chondrocytic differentiation of equine bone marrow-derived mesenchymal stem cells. *Am. J. Vet. Res.* 59, 1182–1187.

Fortier, L. A. (2005). Stem cells: classifications, controversies, and clinical applications. *Vet. Surg.* 34, 415–423. doi:10.1111/j.1532-950X.2005.00063.x

Fortier, L. A., and Travis, A. J. (2011). Stem cells in veterinary medicine. *Stem Cell Res. Ther.* 2, 9. doi:10.1186/scrt50

Frisch, J., and Cucchiarini, M. (2016). Gene- and stem cell-based approaches to regulate hypertrophic differentiation in articular cartilage disorders. *Stem Cells Dev.* 25, 1495–1512. doi:10.1089/scd.2016.0106

Frisch, J., Orth, P., Venkatesan, J. K., Rey-Rico, A., Schmitt, G., Kohn, D., et al. (2017a). Genetic modification of human peripheral blood aspirates using recombinant adeno-associated viral vectors for articular cartilage repair with a focus on chondrogenic transforming growth factor-β gene delivery. *Stem Cells Transl. Med.* 6, 249–260. doi:10.5966/sctm.2016-0149

Frisch, J., Orth, P., Rey-Rico, A., Venkatesan, J. K., Schmitt, G., Madry, H., et al. (2017b). Peripheral blood aspirates overexpressing IGF-I via RAAV gene transfer undergo enhanced chondrogenic differentiation processes. *J. Cell Mol. Med.* 21, 2748–2758. doi:10.1111/jcmm.13190

Frisch, J., Rey-Rico, A., Venkatesan, J. K., Schmitt, G., Madry, H., and Cucchiarini, M. (2015b). Chondrogenic differentiation processes in human bone marrow aspirates upon RAAV-mediated gene transfer and overexpression of the insulin-like growth factor I. *Tissue Eng. Part A* 21, 2460–2471. doi:10.1089/ten.TEA.2014.0679

Frisch, J., Rey-Rico, A., Venkatesan, J. K., Schmitt, G., Madry, H., and Cucchiarini, M. (2016). TGF-B gene transfer and overexpression via RAAV vectors stimulates chondrogenic events in human bone marrow aspirates. *J. Cell Mol. Med.* 20, 430–440. doi:10.1111/jcmm.12774

Frisch, J., Venkatesan, J. K., Rey-Rico, A., Madry, H., and Cucchiarini, M. (2015a). Current progress in stem cell-based gene therapy for articular cartilage repair. *Curr. Stem Cell Res. Ther.* 10, 121–131. doi:10.2174/1574888x09666140922112326

Frisch, J., Venkatesan, J. K., Rey-Rico, A., Schmitt, G., Madry, H., and Cucchiarini, M. (2014a). Determination of the chondrogenic differentiation processes in human bone marrow-derived mesenchymal stem cells genetically modified to overexpress transforming growth factor-β via recombinant adeno-associated viral vectors. *Hum. Gene Ther.* 25, 1050–1060. doi:10.1089/hum.2014.091

Frisch, J., Venkatesan, J. K., Rey-Rico, A., Schmitt, G., Madry, H., and Cucchiarini, M. (2014b). Influence of insulin-like growth factor I overexpression via recombinant adeno-associated vector gene transfer upon the biological activities and differentiation potential of human bone marrow-derived mesenchymal stem cells. *Stem Cell Res. Ther.* 5, 103. doi:10.1186/scrt491

Fusco, G., Gambaro, F. M., Di Matteo, B., and Kon, E. (2021). Injections in the osteoarthritic knee: A review of current treatment options. *EFORT Open Rev.* 6, 501–509. doi:10.1302/2058-5241.6.210026

Gabusi, E., Lenzi, E., Manferdini, C., Dolzani, P., Columbaro, M., Saleh, Y., et al. (2022). Autophagy is a crucial path in chondrogenesis of adipose-derived mesenchymal stromal cells laden in hydrogel. *Gels* 8, 766. doi:10.3390/gels8120766

Gao, G., Schilling, A. F., Hubbell, K., Yonezawa, T., Truong, D., Hong, Y., et al. (2015). Improved properties of bone and cartilage tissue from 3D inkjet-bioprinted human mesenchymal stem cells by simultaneous deposition and photocrosslinking in PEG-GelMA. *Biotechnol. Lett.* 37, 2349–2355. doi:10.1007/s10529-015-1921-2

Garcia, J., Hulme, C., Mennan, C., Roberts, S., Bastiaansen-Jenniskens, Y. M., van Osch, G. J. V. M., et al. (2020). The synovial fluid from patients with focal cartilage defects contains mesenchymal stem/stromal cells and macrophages with pro- and anti-inflammatory phenotypes. *Osteoarthr. Cartil. Open* 2, 100039. doi:10.1016/j.ocarto.2020.100039

Geiger, F., Bertram, H., Berger, I., Lorenz, H., Wall, O., Eckhardt, C., et al. (2005). Vascular endothelial growth factor gene-activated matrix (VEGF165-GAM) enhances osteogenesis and angiogenesis in large segmental bone defects. *J. Bone Min. Res.* 20, 2028–2035. doi:10.1359/JBMR.050701

Geiger, F., Lorenz, H., Xu, W., Szalay, K., Kasten, P., Claes, L., et al. (2007). VEGF producing bone marrow stromal cells (BMSC) enhance vascularization and resorption of a natural coral bone substitute. *Bone* 41, 516–522. doi:10.1016/j.bone.2007.06.018

Geng, Y., Duan, H., Xu, L., Witman, N., Yan, B., Yu, Z., et al. (2021). BMP-2 and VEGF-A ModRNAs in collagen scaffold synergistically drive bone repair through osteogenic and angiogenic pathways. *Commun. Biol.* 4, 82. doi:10.1038/s42003-020-01606-9

Gerull, K. M., Kim, D. J., Cogsil, T., Rhea, L., and Cipriano, C. (2020). Are women proportionately represented as speakers at orthopaedic surgery annual meetings? A cross-sectional analysis. *Clin. Orthop. Relat. Res.* 478, 2729–2740. doi:10.1097/CORR.0000000000001359

Gómez-Ferrer, M., Villanueva-Badenas, E., Sánchez-Sánchez, R., Sánchez-López, C. M., Baquero, M. C., Sepúlveda, P., et al. (2021). HIF-1α and pro-inflammatory signaling improves the immunomodulatory activity of MSC-derived extracellular vesicles. *Int. J. Mol. Sci.* 22, 3416. doi:10.3390/ijms22073416

Gómez-Leduc, T., Desancé, M., Hervieu, M., Legendre, F., Ollitrault, D., de Vienne, C., et al. (2017). Hypoxia is a critical parameter for chondrogenic differentiation of human umbilical cord blood mesenchymal stem cells in type I/III collagen sponges. *IJMS* 18, 1933. doi:10.3390/ijms18091933

Gómez-Leduc, T., Hervieu, M., Legendre, F., Bouyoucef, M., Gruchy, N., Poulain, L., et al. (2016). Chondrogenic commitment of human umbilical cord blood-derived mesenchymal stem cells in collagen matrices for cartilage engineering. *Sci. Rep.* 6, 32786. doi:10.1038/srep32786

Gong, J., Fairley, J., Cicuttini, F. M., Hussain, S. M., Vashishtha, R., Chou, L., et al. (2021). Effect of stem cell injections on osteoarthritis-related structural outcomes: A systematic review. *J. Rheumatol.* 48, 585–597. doi:10.3899/jrheum.200021

Guzzo, R. M., Gibson, J., Xu, R.-H., Lee, F. Y., and Drissi, H. (2013). Efficient differentiation of human IPSC-derived mesenchymal stem cells to chondroprogenitor cells. *J. Cell Biochem.* 114, 480–490. doi:10.1002/jcb.24388

Guérit, D., Brondello, J.-M., Chuchana, P., Philipot, D., Toupet, K., Bony, C., et al. (2014). FOXO3A regulation by miRNA-29a controls chondrogenic differentiation of mesenchymal stem cells and cartilage formation. *Stem Cells Dev.* 23, 1195–1205. doi:10.1089/scd.2013.0463

Guérit, D., Philipot, D., Chuchana, P., Toupet, K., Brondello, J.-M., Mathieu, M., et al. (2013). Sox9-Regulated miRNA-574-3p inhibits chondrogenic differentiation of mesenchymal stem cells. *PLoS ONE* 8, e62582. doi:10.1371/journal.pone.0062582

Hackett, C. H., and Fortier, L. A. (2011). Embryonic stem cells and IPS cells: sources and characteristics. *Vet. Clin. North Am. Equine Pract.* 27, 233–242. doi:10.1016/j.cveq.2011.04.003

Hafezi, M., Nouri Khorasani, S., Zare, M., Esmaeely Neisiany, R., and Davoodi, P. (2021). Advanced hydrogels for cartilage tissue engineering: recent progress and future directions. *Polym. (Basel)* 13, 4199. doi:10.3390/polym13234199

Hamilton, A. M., Cheung, W.-Y., Gómez-Aristizábal, A., Sharma, A., Nakamura, S., Chaboureau, A., et al. (2019). Iron nanoparticle-labeled murine mesenchymal stromal cells in an osteoarthritic model persists and suggests anti-inflammatory mechanism of action. *PLoS One* 14, e0214107. doi:10.1371/journal.pone.0214107

Hanousek, K., Salavati, M., and Fouladi-Nashta, A. (2018). Effect of horse sex status on British eventing competition performance: an observational study between 1998 and 2016. *Vet. Rec.* 182, 666. doi:10.1136/vr.104719

Hawker, G. A. (2019). Osteoarthritis is a serious disease. *Clin. Exp. Rheumatol.* 37, 3–6.

Heirani-Tabasi, A., Hosseinzadeh, S., Rabbani, S., Ahmadi Tafti, S. H., Jamshidi, K., Soufizomorrod, M., et al. (2021). Cartilage tissue engineering by Co-transplantation of chondrocyte extracellular vesicles and mesenchymal stem cells, entrapped in chitosan-hyaluronic acid hydrogel. *Biomed. Mater* 16, 055003. doi:10.1088/1748-605X/ac0cbf

Hellingman, C. A., Davidson, E. N. B., Koevoet, W., Vitters, E. L., van den Berg, W. B., van Osch, G. J. V. M., et al. (2011). Smad signaling determines chondrogenic differentiation of bone-marrow-derived mesenchymal stem cells: inhibition of smad1/5/8p prevents terminal differentiation and calcification. *Tissue Eng. Part A* 17, 1157–1167. doi:10.1089/ten.TEA.2010.0043

Hotham, W. E., Thompson, C., Szu-Ting, L., and Henson, F. M. D. (2021). The anti-inflammatory effects of equine bone marrow stem cell-derived extracellular vesicles on autologous chondrocytes. *Vet. Rec. Open* 8, e22. doi:10.1002/vro2.22

Huang, D., Li, Y., Ma, Z., Lin, H., Zhu, X., Xiao, Y., et al. (2023). Collagen hydrogel viscoelasticity regulates MSC chondrogenesis in a ROCK-dependent manner. *Sci. Adv.* 9, eade9497. doi:10.1126/sciadv.ade9497

Husteden, C., Brito Barrera, Y. A., Tegtmeyer, S., Borges, J., Giselbrecht, J., Menzel, M., et al. (2023). Lipoplex-functionalized thin-film surface coating based on extracellular matrix components as local gene delivery system to control osteogenic stem cell differentiation. *Adv. Healthc. Mater* 12, e2201978. doi:10.1002/adhm.202201978

Hwang, N. S., Varghese, S., Lee, H. J., Zhang, Z., Ye, Z., Bae, J., et al. (2008). *In vivo* commitment and functional tissue regeneration using human embryonic stem cell-derived mesenchymal cells. *Proc. Natl. Acad. Sci. U. S. A.* 105, 20641–20646. doi:10.1073/pnas.0809680106

Hwang, N. S., Varghese, S., Zhang, Z., and Elisseeff, J. (2006). Chondrogenic differentiation of human embryonic stem cell-derived cells in arginine-glycine-aspartate-modified hydrogels. *Tissue Eng.* 12, 2695–2706. doi:10.1089/ten.2006.12.2695

Hyland, M., Mennan, C., Wilson, E., Clayton, A., and Kehoe, O. (2020). Pro-inflammatory priming of umbilical cord mesenchymal stromal cells alters the protein cargo of their extracellular vesicles. *Cells* 9, 726. doi:10.3390/cells9030726

Ilas, D. C., Churchman, S. M., Baboolal, T., Giannoudis, P. V., Aderinto, J., McGonagle, D., et al. (2019). The simultaneous analysis of mesenchymal stem cells and early osteocytes accumulation in osteoarthritic femoral head sclerotic bone. *Rheumatol. Oxf.* 58, 1777–1783. doi:10.1093/rheumatology/kez130

Ishihara, A., Weisbrode, S. E., and Bertone, A. L. (2015). Autologous implantation of BMP2-expressing dermal fibroblasts to improve bone mineral density and architecture in rabbit long bones. *J. Orthop. Res.* 33, 1455–1465. doi:10.1002/jor.22791

Ivis, (2010). AAEP annual convention - baltimore. Available online: https://www.ivis.org/library/aaep/aaep-annual-convention-baltimore-2010 (accessed on March 6, 2023).

Jammes, M., Contentin, R., Cassé, F., and Galéra, P. (2023). Equine osteoarthritis: strategies to enhance mesenchymal stromal cell-based acellular therapies. *Front. Vet. Sci.* 10, 1115774. doi:10.3389/fvets.2023.1115774

Jones, E. A., Crawford, A., English, A., Henshaw, K., Mundy, J., Corscadden, D., et al. (2008). Synovial fluid mesenchymal stem cells in health and early osteoarthritis: detection and functional evaluation at the single-cell level. *Arthritis Rheum.* 58, 1731–1740. doi:10.1002/art.23485

Jones, E. A., English, A., Henshaw, K., Kinsey, S. E., Markham, A. F., Emery, P., et al. (2004). Enumeration and phenotypic characterization of synovial fluid multipotential mesenchymal progenitor cells in inflammatory and degenerative arthritis. *Arthritis Rheum.* 50, 817–827. doi:10.1002/art.20203

Jones, E. A., Giannoudis, P. V., and Kouroupis, D. (2016). Bone repair with skeletal stem cells: rationale, progress to date and clinical application. *Ther. Adv. Musculoskelet. Dis.* 8, 57–71. doi:10.1177/1759720X16642372

Jorgensen, C., Djouad, F., Apparailly, F., and Noël, D. (2003). Engineering mesenchymal stem cells for immunotherapy. *Gene Ther.* 10, 928–931. doi:10.1038/sj.gt.3302019

Jorgensen, C., Noel, D., Apparailly, F., and Sany, J. (2001). Stem cells for repair of cartilage and bone: the next challenge in osteoarthritis and rheumatoid arthritis. *Ann. Rheum. Dis.* 60, 305–309. doi:10.1136/ard.60.4.305

Kahn, L. H. (2017). Perspective: the one-health way. *Nature* 543, S47. doi:10.1038/543S47a

Karikó, K., Buckstein, M., Ni, H., and Weissman, D. (2005). Suppression of RNA recognition by toll-like receptors: the impact of nucleoside modification and the evolutionary origin of RNA. *Immunity* 23, 165–175. doi:10.1016/j.immuni.2005.06.008

Kearney, C. M., Khatab, S., van Buul, G. M., Plomp, S. G. M., Korthagen, N. M., Labberté, M. C., et al. (2022). Treatment effects of intra-articular allogenic mesenchymal stem cell secretome in an equine model of joint inflammation. *Front. Vet. Sci.* 9, 907616. doi:10.3389/fvets.2022.907616

Kennedy, S., Tambiah, J. R. S., and Lane, N. E. (2022). Osteoarthritis today: lost in translation? *Best. Pract. Res. Clin. Rheumatol.* 2023, 101810. doi:10.1016/j.berh.2022.101810

Khatab, S., van Osch, G. J., Kops, N., Bastiaansen-Jenniskens, Y. M., Bos, P. K., Verhaar, J. A., et al. (2018). Mesenchymal stem cell secretome reduces pain and prevents cartilage damage in a murine osteoarthritis model. *Eur. Cell Mater* 36, 218–230. doi:10.22203/eCM.v036a16

Khorsand, B., Elangovan, S., Hong, L., Dewerth, A., Kormann, M. S. D., and Salem, A. K. (2017). A comparative study of the bone regenerative effect of chemically modified RNA encoding BMP-2 or BMP-9. *AAPS J.* 19, 438–446. doi:10.1208/s12248-016-0034-8

Kisiday, J. D., Liebig, B. E., and Goodrich, L. R. (2020). Adult ovine chondrocytes in expansion culture adopt progenitor cell properties that are favorable for cartilage tissue engineering. *J. Orthop. Res.* 38, 1996–2005. doi:10.1002/jor.24671

Klinger, P., Surmann-Schmitt, C., Brem, M., Swoboda, B., Distler, J. H., Carl, H.-D., et al. (2011). Chondromodulin 1 stabilizes the chondrocyte phenotype and inhibits endochondral ossification of porcine cartilage repair tissue. *Arthritis Rheum.* 63, 2721–2731. doi:10.1002/art.30335

Koh, R. H., Jin, Y., Kim, J., and Hwang, N. S. (2020). Inflammation-modulating hydrogels for osteoarthritis cartilage tissue engineering. *Cells* 9, 419. doi:10.3390/cells9020419

Kon, E., Delcogliano, M., Filardo, G., Montaperto, C., and Marcacci, M. (2008). Second generation issues in cartilage repair. *Sports Med. Arthrosc. Rev.* 16, 221–229. doi:10.1097/JSA.0b013e31818cdbc5

Kon, E., Di Matteo, B., Delgado, D., Cole, B. J., Dorotei, A., Dragoo, J. L., et al. (2020). Platelet-rich plasma for the treatment of knee osteoarthritis: an expert opinion and proposal for a novel classification and coding system. *Expert Opin. Biol. Ther.* 20, 1447–1460. doi:10.1080/14712598.2020.1798925

Kon, E., and Di Matteo, B. (2021). Editorial commentary: minimally invasive strategies for osteoarthritis: from platelets to mesenchymal stem cells. *Arthroscopy* 37, 2258–2261. doi:10.1016/j.arthro.2021.04.010

Kon, E., Di Matteo, B., Verdonk, P., Drobnic, M., Dulic, O., Gavrilovic, G., et al. (2021). Aragonite-based scaffold for the treatment of joint surface lesions in mild to moderate osteoarthritic knees: results of a 2-year multicenter prospective study. *Am. J. Sports Med.* 49, 588–598. doi:10.1177/0363546520981750

Kon, E., Filardo, G., Brittberg, M., Busacca, M., Condello, V., Engebretsen, L., et al. (2018). A multilayer biomaterial for osteochondral regeneration shows superiority vs microfractures for the treatment of osteochondral lesions in a multicentre randomized trial at 2 years. *Knee Surg. Sports Traumatol. Arthrosc.* 26, 2704–2715. doi:10.1007/s00167-017-4707-3

Kon, E., Filardo, G., Di Martino, A., Busacca, M., Moio, A., Perdisa, F., et al. (2014). Clinical results and MRI evolution of a nano-composite multilayered biomaterial for osteochondral regeneration at 5 years. *Am. J. Sports Med.* 42, 158–165. doi:10.1177/0363546513505434

Kon, E., Filardo, G., Di Martino, A., and Marcacci, M. (2012). ACI and MACI. *J. Knee Surg.* 25, 17–22. doi:10.1055/s-0031-1299651

Kon, E., Filardo, G., Di Matteo, B., Perdisa, F., and Marcacci, M. (2013). Matrix assisted autologous chondrocyte transplantation for cartilage treatment: A systematic review. *Bone Jt. Res.* 2, 18–25. doi:10.1302/2046-3758.22.2000092

Kon, E., Roffi, A., Filardo, G., Tesei, G., and Marcacci, M. (2015). Scaffold-based cartilage treatments: with or without cells? a systematic review of preclinical and clinical evidence. *Arthroscopy* 31, 767–775. doi:10.1016/j.arthro.2014.11.017

Kwon, H., Brown, W. E., Lee, C. A., Wang, D., Paschos, N., Hu, J. C., et al. (2019). Surgical and tissue engineering strategies for articular cartilage and meniscus repair. *Nat. Rev. Rheumatol.* 15, 550–570. doi:10.1038/s41584-019-0255-1

Lacaze, P., Wang, Y., Polekhina, G., Bakshi, A., Riaz, M., Owen, A., et al. (2022). Genomic risk score for advanced osteoarthritis in older adults. *Arthritis Rheumatol.* 74, 1480–1487. doi:10.1002/art.42156

Ledo, A. M., Vining, K. H., Alonso, M. J., Garcia-Fuentes, M., and Mooney, D. J. (2020). Extracellular matrix mechanics regulate transfection and SOX9-directed differentiation of mesenchymal stem cells. *Acta Biomater.* 110, 153–163. doi:10.1016/j.actbio.2020.04.027

Lee, H. H., Haleem, A. M., Yao, V., Li, J., Xiao, X., and Chu, C. R. (2011). Release of bioactive adeno-associated virus from fibrin scaffolds: effects of fibrin glue concentrations. *Tissue Eng. Part A* 17, 1969–1978. doi:10.1089/ten.TEA.2010.0586

Legendre, F., Ollitrault, D., Gomez-Leduc, T., Bouyoucef, M., Hervieu, M., Gruchy, N., et al. (2017). Enhanced chondrogenesis of bone marrow-derived stem cells by using a combinatory cell therapy strategy with BMP-2/TGF-B1, hypoxia, and COL1A1/HtrA1 SiRNAs. *Sci. Rep.* 7, 3406. doi:10.1038/s41598-017-03579-y

Legendre, F., Ollitrault, D., Hervieu, M., Baugé, C., Maneix, L., Goux, D., et al. (2013). Enhanced hyaline cartilage matrix synthesis in collagen sponge scaffolds by using SiRNA to stabilize chondrocytes phenotype cultured with bone morphogenetic protein-2 under hypoxia. *Tissue Eng. Part C Methods* 19, 550–567. doi:10.1089/ten.TEC.2012.0508

Leifer, V. P., Katz, J. N., and Losina, E. (2022). The burden of OA-health services and economics. *Osteoarthr. Cartil.* 30, 10–16. doi:10.1016/j.joca.2021.05.007

Leijs, M. J. C., van Buul, G. M., Lubberts, E., Bos, P. K., Verhaar, J. A. N., Hoogduijn, M. J., et al. (2012). Effect of arthritic synovial fluids on the expression of immunomodulatory factors by mesenchymal stem cells: an explorative *in vitro* study. *Front. Immunol.* 3, 231. doi:10.3389/fimmu.2012.00231

Lepage, S. I. M., Lee, O. J., and Koch, T. G. (2019). Equine cord blood mesenchymal stromal cells have greater differentiation and similar immunosuppressive potential to cord tissue mesenchymal stromal cells. *Stem Cells Dev.* 28, 227–237. doi:10.1089/scd.2018.0135

Li, J., Wang, X., Ruan, G., Zhu, Z., and Ding, C. (2021). Sprifermin: A recombinant human fibroblast growth factor 18 for the treatment of knee osteoarthritis. *Expert Opin. Investig. Drugs* 30, 923–930. doi:10.1080/13543784.2021.1972970

Li, L., Yu, F., Zheng, L., Wang, R., Yan, W., Wang, Z., et al. (2019). Natural hydrogels for cartilage regeneration: modification, preparation and application. *J. Orthop. Transl.* 17, 26–41. doi:10.1016/j.jot.2018.09.003

Liu, W., Madry, H., and Cucchiarini, M. (2022). Application of alginate hydrogels for next-generation articular cartilage regeneration. *Int. J. Mol. Sci.* 23, 1147. doi:10.3390/ijms23031147

Liu, X., Yang, Y., Li, Y., Niu, X., Zhao, B., Wang, Y., et al. (2017). Integration of stem cell-derived exosomes with *in situ* hydrogel glue as a promising tissue patch for articular cartilage regeneration. *Nanoscale* 9, 4430–4438. doi:10.1039/c7nr00352h

Lolli, A., Colella, F., De Bari, C., and van Osch, G. J. V. M. (2019a). Targeting anti-chondrogenic factors for the stimulation of chondrogenesis: A new paradigm in cartilage repair. *J. Orthop. Res.* 37, 12–22. doi:10.1002/jor.24136

Lolli, A., Narcisi, R., Lambertini, E., Penolazzi, L., Angelozzi, M., Kops, N., et al. (2016). Silencing of antichondrogenic MicroRNA-221 in human mesenchymal stem cells promotes cartilage repair *in vivo*. *Stem Cells* 34, 1801–1811. doi:10.1002/stem.2350

Lolli, A., Penolazzi, L., Narcisi, R., van Osch, G. J. V. M., and Piva, R. (2017). Emerging potential of gene silencing approaches targeting anti-chondrogenic factors for cell-based cartilage repair. *Cell Mol. Life Sci.* 74, 3451–3465. doi:10.1007/s00018-017-2531-z

Lolli, A., Sivasubramaniyan, K., Vainieri, M. L., Oieni, J., Kops, N., Yayon, A., et al. (2019b). Hydrogel-based delivery of AntimiR-221 enhances cartilage regeneration by endogenous cells. *J. Control Release* 309, 220–230. doi:10.1016/j.jconrel.2019.07.040

Loozen, L. D., Wegman, F., Öner, F. C., Dhert, W. J. A., and Alblas, J. (2013). Porous bioprinted constructs in BMP-2 non-viral gene therapy for bone tissue engineering. *J. Mater Chem. B* 1, 6619–6626. doi:10.1039/c3tb21093f

Lopa, S., Colombini, A., Moretti, M., and de Girolamo, L. (2019). Injective mesenchymal stem cell-based treatments for knee osteoarthritis: from mechanisms of action to current clinical evidences. *Knee Surg. Sports Traumatol. Arthrosc.* 27, 2003–2020. doi:10.1007/s00167-018-5118-9

Lopa, S., Colombini, A., Stanco, D., de Girolamo, L., Sansone, V., and Moretti, M. (2014). Donor-matched mesenchymal stem cells from knee infrapatellar and subcutaneous adipose tissue of osteoarthritic donors display differential chondrogenic and osteogenic commitment. *Eur. Cell Mater* 27, 298–311. doi:10.22203/ecm.v027a21

Madry, H., Gao, L., Rey-Rico, A., Venkatesan, J. K., Müller-Brandt, K., Cai, X., et al. (2020b). Thermosensitive hydrogel based on PEO-PPO-PEO poloxamers for a controlled *in situ* release of recombinant adeno-associated viral vectors for effective gene therapy of cartilage defects. *Adv. Mater* 32, e1906508. doi:10.1002/adma.201906508

Madry, H., Venkatesan, J. K., Carballo-Pedrares, N., Rey-Rico, A., and Cucchiarini, M. (2020a). Scaffold-Mediated gene delivery for osteochondral repair. *Pharmaceutics* 12, 930. doi:10.3390/pharmaceutics12100930

Maihöfer, J., Madry, H., Rey-Rico, A., Venkatesan, J. K., Goebel, L., Schmitt, G., et al. (2021). Hydrogel-guided, RAAV-mediated IGF-I overexpression enables long-term cartilage repair and protection against perifocal osteoarthritis in a large-animal full-thickness chondral defect model at one year *in vivo*. *Adv. Mater* 33, e2008451. doi:10.1002/adma.202008451

Manferdini, C., Gabusi, E., Saleh, Y., Lenzi, E., D'Atri, G., Ricotti, L., et al. (2022). Mesenchymal stromal cells laden in hydrogels for osteoarthritis cartilage regeneration: A systematic review from *in vitro* studies to clinical applications. *Cells* 11, 3969. doi:10.3390/cells11243969

Manferdini, C., Paolella, F., Gabusi, E., Cattini, L., Rojewski, M., Schrezenmeier, H., et al. (2020). Osteoarthritic milieu affects adipose-derived mesenchymal stromal cells. *J. Orthop. Res.* 38, 336–347. doi:10.1002/jor.24446

Manivong, S., Cullier, A., Audigié, F., Banquy, X., Moldovan, F., Demoor, M., et al. (2023). New trends for osteoarthritis: biomaterials, models and modeling. *Drug Discov. Today* 28, 103488. doi:10.1016/j.drudis.2023.103488

Markides, H., Newell, K. J., Rudorf, H., Ferreras, L. B., Dixon, J. E., Morris, R. H., et al. (2019). *Ex vivo* MRI cell tracking of autologous mesenchymal stromal cells in an ovine osteochondral defect model. *Stem Cell Res. Ther.* 10, 25. doi:10.1186/s13287-018-1123-7

Martinello, T., Bronzini, I., Perazzi, A., Testoni, S., De Benedictis, G. M., Negro, A., et al. (2013). Effects of *in vivo* applications of peripheral blood-derived mesenchymal stromal cells (PB-MSCs) and platlet-rich plasma (PRP) on experimentally injured deep digital flexor tendons of sheep. *J. Orthop. Res.* 31, 306–314. doi:10.1002/jor.22205

Martinez-Redondo, P., Guillen-Guillen, I., Davidsohn, N., Wang, C., Prieto, J., Kurita, M., et al. (2020). αKLOTHO and sTGFβR2 treatment counteract the osteoarthritic phenotype developed in a rat model. *Protein Cell* 11, 219–226. doi:10.1007/s13238-019-00685-7

Mathieu, M., Vigier, S., Labour, M.-N., Jorgensen, C., Belamie, E., et al. (2014). Induction of mesenchymal stem cell differentiation and cartilage formation by cross-linker-free collagen microspheres. *eCM* 28, 82–97. doi:10.22203/eCM.v028a07

Maumus, M., Fonteneau, G., Ruiz, M., Assou, S., Boukhaddaoui, H., Pastoureau, P., et al. (2021). Neuromedin B promotes chondrocyte differentiation of mesenchymal stromal cells via calcineurin and calcium signaling. *Cell Biosci.* 11, 183. doi:10.1186/s13578-021-00695-1

Maumus, M., Manferdini, C., Toupet, K., Chuchana, P., Casteilla, L., Gachet, M., et al. (2017). Thrombospondin-1 partly mediates the cartilage protective effect of adipose-derived mesenchymal stem cells in osteoarthritis. *Front. Immunol.* 8, 1638. doi:10.3389/fimmu.2017.01638

Maumus, M., Manferdini, C., Toupet, K., Peyrafitte, J.-A., Ferreira, R., Facchini, A., et al. (2013). Adipose mesenchymal stem cells protect chondrocytes from degeneration associated with osteoarthritis. *Stem Cell Res.* 11, 834–844. doi:10.1016/j.scr.2013.05.008

Maumus, M., Roussignol, G., Toupet, K., Penarier, G., Bentz, I., Teixeira, S., et al. (2016). Utility of a mouse model of osteoarthritis to demonstrate cartilage protection by ifnγ-primed equine mesenchymal stem cells. *Front. Immunol.* 7, 392. doi:10.3389/fimmu.2016.00392

McCoy, A. M. (2015). Animal models of osteoarthritis: comparisons and key considerations. *Vet. Pathol.* 52, 803–818. doi:10.1177/0300985815588611

Melief, S. M., Zwaginga, J. J., Fibbe, W. E., and Roelofs, H. (2013). Adipose tissue-derived multipotent stromal cells have a higher immunomodulatory capacity than their bone marrow-derived counterparts. *Stem Cells Transl. Med.* 2, 455–463. doi:10.5966/sctm.2012-0184

Meng, W., Rey-Rico, A., Claudel, M., Schmitt, G., Speicher-Mentges, S., Pons, F., et al. (2020). RAAV-mediated overexpression of SOX9 and TGF-β via carbon dot-guided vector delivery enhances the biological activities in human bone marrow-derived mesenchymal stromal cells. *Nanomater. (Basel)* 10, 855. doi:10.3390/nano10050855

Mesure, B., Menu, P., Venkatesan, J. K., Cucchiarini, M., and Velot, É. (2019). Biomaterials and gene therapy: A smart combination for MSC musculoskeletal engineering. *Curr. stem cell Res. Ther.* 14, 337–343. doi:10.2174/1574888X14666181205121658

Mocchi, M., Bari, E., Dotti, S., Villa, R., Berni, P., Conti, V., et al. (2021b). Canine mesenchymal cell lyosecretome production and safety evaluation after allogenic intraarticular injection in osteoarthritic dogs. *Anim. (Basel)* 11, 3271. doi:10.3390/ani11113271

Mocchi, M., Grolli, S., Dotti, S., Di Silvestre, D., Villa, R., Berni, P., et al. (2021a). Equine mesenchymal stem/stromal cells freeze-dried secretome (lyosecretome) for the treatment of musculoskeletal diseases: production process validation and batch release test for clinical use. *Pharm. (Basel)* 14, 553. doi:10.3390/ph14060553

Mödder, U. I., and Khosla, S. (2008). Skeletal stem/osteoprogenitor cells: current concepts, alternate hypotheses, and relationship to the bone remodeling compartment. *J. Cell Biochem.* 103, 393–400. doi:10.1002/jcb.21423

Montheil, T., Simon, M., Noël, D., Mehdi, A., Subra, G., and Echalier, C. (2022). Silylated biomolecules: versatile components for bioinks. *Front. Bioeng. Biotechnol.* 10, 888437. doi:10.3389/fbioe.2022.888437

Moradi, L., Vasei, M., Dehghan, M. M., Majidi, M., Farzad Mohajeri, S., and Bonakdar, S. (2017). Regeneration of meniscus tissue using adipose mesenchymal stem cells-chondrocytes Co-culture on a hybrid scaffold: *in vivo* study. *Biomaterials* 126, 18–30. doi:10.1016/j.biomaterials.2017.02.022

Morille, M., Toupet, K., Montero-Menei, C. N., Jorgensen, C., and Noël, D. (2016). PLGA-based microcarriers induce mesenchymal stem cell chondrogenesis and

stimulate cartilage repair in osteoarthritis. *Biomaterials* 88, 60–69. doi:10.1016/j.biomaterials.2016.02.022

Morille, M., Van-Thanh, T., Garric, X., Cayon, J., Coudane, J., Noël, D., et al. (2013). New PLGA–P188–PLGA matrix enhances TGF-β3 release from pharmacologically active microcarriers and promotes chondrogenesis of mesenchymal stem cells. *J. Control. Release* 170, 99–110. doi:10.1016/j.jconrel.2013.04.017

Morscheid, S., Rey-Rico, A., Schmitt, G., Madry, H., Cucchiarini, M., and Venkatesan, J. K. (2019a). Therapeutic effects of RAAV-mediated concomittant gene transfer and overexpression of TGF-β and IGF-I on the chondrogenesis of human bone-marrow-derived mesenchymal stem cells. *Int. J. Mol. Sci.* 20, 2591. doi:10.3390/ijms20102591

Morscheid, S., Venkatesan, J. K., Rey-Rico, A., Schmitt, G., and Cucchiarini, M. (2019b). Remodeling of human osteochondral defects via RAAV-mediated Co-overexpression of TGF-β and IGF-I from implanted human bone marrow-derived mesenchymal stromal cells. *J. Clin. Med.* 8, 1326. doi:10.3390/jcm8091326

Murphy, J. M., Fink, D. J., Hunziker, E. B., and Barry, F. P. (2003). Stem cell therapy in a caprine model of osteoarthritis. *Arthritis Rheum.* 48, 3464–3474. doi:10.1002/art.11365

Murray, S. J., Santangelo, K. S., and Bertone, A. L. (2010). Evaluation of early cellular influences of bone morphogenetic proteins 12 and 2 on equine superficial digital flexor tenocytes and bone marrow-derived mesenchymal stem cells *in vitro*. *Am. J. Vet. Res.* 71, 103–114. doi:10.2460/ajvr.71.1.103

Narcisi, R., Cleary, M. A., Brama, P. A. J., Hoogduijn, M. J., Tüysüz, N., ten Berge, D., et al. (2015). Long-term expansion, enhanced chondrogenic potential, and suppression of endochondral ossification of adult human MSCs via WNT signaling modulation. *Stem Cell Rep.* 4, 459–472. doi:10.1016/j.stemcr.2015.01.017

Nedorubova, I. A., Bukharova, T. B., Mokrousova, V. O., Khvorostina, M. A., Vasilyev, A. V., Nedorubov, A. A., et al. (2022). Comparative efficiency of gene-activated matrices based on chitosan hydrogel and PRP impregnated with BMP2 polyplexes for bone regeneration. *Int. J. Mol. Sci.* 23, 14720. doi:10.3390/ijms232314720

Noël, D., Djouad, F., and Jorgensen, C. (2002). Regenerative medicine through mesenchymal stem cells for bone and cartilage repair. *Curr. Opin. Investig. Drugs* 3, 1000–1004.

Nooeaid, P., Salih, V., Beier, J. P., and Boccaccini, A. R. (2012). Osteochondral tissue engineering: scaffolds, stem cells and applications. *J. Cell Mol. Med.* 16, 2247–2270. doi:10.1111/j.1582-4934.2012.01571.x

Nunes, S. S., Maijub, J. G., Krishnan, L., Ramakrishnan, V. M., Clayton, L. R., Williams, S. K., et al. (2013). Generation of a functional liver tissue mimic using adipose stromal vascular fraction cell-derived vasculatures. *Sci. Rep.* 3, 2141. doi:10.1038/srep02141

Ochs, J., Hanga, M. P., Shaw, G., Duffy, N., Kulik, M., Tissin, N., et al. (2022). Needle to needle ROBOT-ASSISTED manufacture of cell therapy products. *Bioeng. Transl Med* 7, e10387. doi:10.1002/btm2.10387

Oldershaw, R. A., Baxter, M. A., Lowe, E. T., Bates, N., Grady, L. M., Soncin, F., et al. (2010). Directed differentiation of human embryonic stem cells toward chondrocytes. *Nat. Biotechnol.* 28, 1187–1194. doi:10.1038/nbt.1683

Oo, W. M., Little, C., Duong, V., and Hunter, D. J. (2021). The development of disease-modifying therapies for osteoarthritis (DMOADs): the evidence to date. *Drug Des. Devel Ther.* 15, 2921–2945. doi:10.2147/DDDT.S295224

Orth, P., Rey-Rico, A., Venkatesan, J. K., Madry, H., and Cucchiarini, M. (2014). Current perspectives in stem cell research for knee cartilage repair. *Stem Cells Cloning* 7, 1–17. doi:10.2147/SCCAA.S42880

Pagnotto, M. R., Wang, Z., Karpie, J. C., Ferretti, M., Xiao, X., and Chu, C. R. (2007). Adeno-associated viral gene transfer of transforming growth factor-beta1 to human mesenchymal stem cells improves cartilage repair. *Gene Ther.* 14, 804–813. doi:10.1038/sj.gt.3302938

Pascual-Garrido, C., Aisenbrey, E. A., Rodriguez-Fontan, F., Payne, K. A., Bryant, S. J., and Goodrich, L. R. (2019). Photopolymerizable injectable cartilage mimetic hydrogel for the treatment of focal chondral lesions: A proof of concept study in a rabbit animal model. *Am. J. Sports Med.* 47, 212–221. doi:10.1177/0363546518808012

Peck, J., Slovek, A., Miro, P., Vij, N., Traube, B., Lee, C., et al. (2021). A comprehensive review of viscosupplementation in osteoarthritis of the knee. *Orthop. Rev. (Pavia)* 13, 25549. doi:10.52965/001c.25549

Pelttari, K., Winter, A., Steck, E., Goetzke, K., Hennig, T., Ochs, B. G., et al. (2006). Premature induction of hypertrophy during *in vitro* chondrogenesis of human mesenchymal stem cells correlates with calcification and vascular invasion after ectopic transplantation in SCID mice. *Arthritis Rheum.* 54, 3254–3266. doi:10.1002/art.22136

Perdisa, F., Filardo, G., Di Matteo, B., Marcacci, M., and Kon, E. (2014). Platelet rich plasma: A valid augmentation for cartilage scaffolds? A systematic review. *Histol. Histopathol.* 29, 805–814. doi:10.14670/HH-29.805

Perry, J., Roelofs, A. J., Mennan, C., McCarthy, H. S., Richmond, A., Clark, S. M., et al. (2021). Human mesenchymal stromal cells enhance cartilage healing in a murine joint surface injury model. *Cells* 10, 1999. doi:10.3390/cells10081999

Pers, Y.-M., Bony, C., Duroux-Richard, I., Bernard, L., Maumus, M., Assou, S., et al. (2021). MiR-155 contributes to the immunoregulatory function of human mesenchymal stem cells. *Front. Immunol.* 12, 624024. doi:10.3389/fimmu.2021.624024

Peshkova, M., Lychagin, A., Lipina, M., Di Matteo, B., Anzillotti, G., Ronzoni, F., et al. (2022). Gender-related aspects in osteoarthritis development and progression: A review. *IJMS* 23, 2767. doi:10.3390/ijms23052767

Peterman, N. J., Macinnis, B., Stauffer, K., Mann, R., Yeo, E. G., and Carpenter, K. (2022). Gender representation in orthopaedic surgery: A geospatial analysis from 2015 to 2022. *Cureus* 14, e27305. doi:10.7759/cureus.27305

Pleumeekers, M. M., Nimeskern, L., Koevoet, J. L. M., Karperien, M., Stok, K. S., and van Osch, G. J. V. M. (2018). Trophic effects of adipose-tissue-derived and bone-marrow-derived mesenchymal stem cells enhance cartilage generation by chondrocytes in Co-culture. *PLoS One* 13, e0190744. doi:10.1371/journal.pone.0190744

Poh, P. S. P., Seeliger, C., Unger, M., Falldorf, K., Balmayor, E. R., and van Griensven, M. (2018). Osteogenic effect and cell signaling activation of extremely low-frequency pulsed electromagnetic fields in adipose-derived mesenchymal stromal cells. *Stem Cells Int.* 2018, 5402853–5402911. doi:10.1155/2018/5402853

Power, R. N., Cavanagh, B. L., Dixon, J. E., Curtin, C. M., and O'Brien, F. J. (2022). Development of a gene-activated scaffold incorporating multifunctional cell-penetrating peptides for PSDF-1α delivery for enhanced angiogenesis in tissue engineering applications. *Int. J. Mol. Sci.* 23, 1460. doi:10.3390/ijms23031460

Raftery, R. M., Mencía Castaño, I., Chen, G., Cavanagh, B., Quinn, B., Curtin, C. M., et al. (2017). Translating the role of osteogenic-angiogenic coupling in bone formation: highly efficient chitosan-pdna activated scaffolds can accelerate bone regeneration in critical-sized bone defects. *Biomaterials* 149, 116–127. doi:10.1016/j.biomaterials.2017.09.036

Raftery, R. M., Mencía-Castaño, I., Sperger, S., Chen, G., Cavanagh, B., Feichtinger, G. A., et al. (2018). Delivery of the improved BMP-2-advanced plasmid DNA within a gene-activated scaffold accelerates mesenchymal stem cell osteogenesis and critical size defect repair. *J. Control Release* 283, 20–31. doi:10.1016/j.jconrel.2018.05.022

Raftery, R. M., Walsh, D. P., Blokpoel Ferreras, L., Mencía Castaño, I., Chen, G., LeMoine, M., et al. (2019). Highly versatile cell-penetrating peptide loaded scaffold for efficient and localised gene delivery to multiple cell types: from development to application in tissue engineering. *Biomaterials* 216, 119277. doi:10.1016/j.biomaterials.2019.119277

Raftery, R. M., Walsh, D. P., Castaño, I. M., Heise, A., Duffy, G. P., Cryan, S.-A., et al. (2016). Delivering nucleic-acid based nanomedicines on biomaterial scaffolds for orthopedic tissue repair: challenges, progress and future perspectives. *Adv. Mater* 28, 5447–5469. doi:10.1002/adma.201505088

Ragni, E., Colombini, A., Viganò, M., Libonati, F., Perucca Orfei, C., Zagra, L., et al. (2021b). Cartilage protective and immunomodulatory features of osteoarthritis synovial fluid-treated adipose-derived mesenchymal stem cells secreted factors and extracellular vesicles-embedded MiRNAs. *Cells* 10, 1072. doi:10.3390/cells10051072

Ragni, E., Papait, A., Perucca Orfei, C., Silini, A. R., Colombini, A., Viganò, M., et al. (2021a). Amniotic membrane-mesenchymal stromal cells secreted factors and extracellular vesicle-MiRNAs: anti-inflammatory and regenerative features for musculoskeletal tissues. *Stem Cells Transl. Med.* 10, 1044–1062. doi:10.1002/sctm.20-0390

Ragni, E., Perucca Orfei, C., and de Girolamo, L. (2022a). Secreted factors and extracellular vesicles account for the immunomodulatory and tissue regenerative properties of bone-marrow-derived mesenchymal stromal cells for osteoarthritis. *Cells* 11, 3501. doi:10.3390/cells11213501

Ragni, E., Perucca Orfei, C., De Luca, P., Mondadori, C., Viganò, M., Colombini, A., et al. (2020). Inflammatory priming enhances mesenchymal stromal cell secretome potential as a clinical product for regenerative medicine approaches through secreted factors and EV-MiRNAs: the example of joint disease. *Stem Cell Res. Ther.* 11, 165. doi:10.1186/s13287-020-01677-9

Ragni, E., Perucca Orfei, C., Valli, F., Zagra, L., and de Girolamo, L. (2022b). Molecular characterization of secreted factors and extracellular vesicles-embedded MiRNAs from bone marrow-derived mesenchymal stromal cells in presence of synovial fluid from osteoarthritis patients. *Biol. (Basel)* 11, 1632. doi:10.3390/biology11111632

Rahman, G., Frazier, T. P., Gimble, J. M., and Mohiuddin, O. A. (2022). The emerging use of ASC/scaffold composites for the regeneration of osteochondral defects. *Front. Bioeng. Biotechnol.* 10, 893992. doi:10.3389/fbioe.2022.893992

Raisin, S., Belamie, E., and Morille, M. (2016). Non-viral gene activated matrices for mesenchymal stem cells based tissue engineering of bone and cartilage. *Biomaterials* 104, 223–237. doi:10.1016/j.biomaterials.2016.07.017

Raisin, S., Morille, M., Bony, C., Noël, D., Devoisselle, J.-M., and Belamie, E. (2017). Tripartite polyionic complex (PIC) micelles as non-viral vectors for mesenchymal stem cell SiRNA transfection. *Biomater. Sci.* 5, 1910–1921. doi:10.1039/c7bm00384f

Ramos, Y. F. M., Tertel, T., Shaw, G., Staubach, S., de Almeida, R. C., Suchiman, E., et al. (2022). Characterizing the secretome of licensed HiPSC-derived MSCs. *Stem Cell Res. Ther.* 13, 434. doi:10.1186/s13287-022-03117-2

Ramzan, F., Ekram, S., Frazier, T., Salim, A., Mohiuddin, O. A., and Khan, I. (2022). Decellularized human umbilical tissue-derived hydrogels promote proliferation and

chondrogenic differentiation of mesenchymal stem cells. *Bioeng. (Basel)* 9, 239. doi:10.3390/bioengineering9060239

Rey-Rico, A., and Cucchiarini, M. (2016). Controlled release strategies for RAAV-mediated gene delivery. *Acta Biomater.* 29, 1–10. doi:10.1016/j.actbio.2015.10.015

Rey-Rico, A., Cucchiarini, M., and Madry, H. (2017a). Hydrogels for precision meniscus tissue engineering: A comprehensive review. *Connect. Tissue Res.* 58, 317–328. doi:10.1080/03008207.2016.1276576

Rey-Rico, A., and Cucchiarini, M. (2017). Smart and controllable RAAV gene delivery carriers in progenitor cells for human musculoskeletal regenerative medicine with a focus on the articular cartilage. *Curr. Gene Ther.* 17, 127–138. doi:10.2174/1566523217666170510162459

Rey-Rico, A., Madry, H., and Cucchiarini, M. (2016). Hydrogel-based controlled delivery systems for articular cartilage repair. *Biomed. Res. Int.* 2016, 1215263. doi:10.1155/2016/1215263

Rey-Rico, A., Venkatesan, J. K., Schmitt, G., Concheiro, A., Madry, H., Alvarez-Lorenzo, C., et al. (2017b). RAAV-mediated overexpression of TGF-β via vector delivery in polymeric micelles stimulates the biological and reparative activities of human articular chondrocytes *in vitro* and in a human osteochondral defect model. *Int. J. Nanomedicine* 12, 6985–6996. doi:10.2147/IJN.S144579

Rey-Rico, A., Venkatesan, J. K., Schmitt, G., Speicher-Mentges, S., Madry, H., and Cucchiarini, M. (2018). Effective remodelling of human osteoarthritic cartilage by Sox9 gene transfer and overexpression upon delivery of RAAV vectors in polymeric micelles. *Mol. Pharm.* 15, 2816–2826. doi:10.1021/acs.molpharmaceut.8b00331

Rikkers, M., Korpershoek, J. V., Levato, R., Malda, J., and Vonk, L. A. (2021). Progenitor cells in healthy and osteoarthritic human cartilage have extensive culture expansion capacity while retaining chondrogenic properties. *Cartilage* 13, 129S–142S. doi:10.1177/19476035211059600

Rikkers, M., Korpershoek, J. V., Levato, R., Malda, J., and Vonk, L. A. (2022). The clinical potential of articular cartilage-derived progenitor cells: A systematic review. *NPJ Regen. Med.* 7, 2. doi:10.1038/s41536-021-00203-6

Roelofs, A. J., Zupan, J., Riemen, A. H. K., Kania, K., Ansboro, S., White, N., et al. (2017). Joint morphogenetic cells in the adult mammalian synovium. *Nat. Commun.* 8, 15040. doi:10.1038/ncomms15040

Roemeling-van Rhijn, M., Mensah, F. K. F., Korevaar, S. S., Leijs, M. J., van Osch, G. J. V. M., Ijzermans, J. N. M., et al. (2013). Effects of hypoxia on the immunomodulatory properties of adipose tissue-derived mesenchymal stem cells. *Front. Immunol.* 4, 203. doi:10.3389/fimmu.2013.00203

Roseti, L., Cavallo, C., Desando, G., Parisi, V., Petretta, M., Bartolotti, I., et al. (2018). Three-dimensional bioprinting of cartilage by the use of stem cells: A strategy to improve regeneration. *Mater. (Basel)* 11, 1749. doi:10.3390/ma11091749

Roseti, L., Desando, G., Cavallo, C., Petretta, M., and Grigolo, B. (2019). Articular cartilage regeneration in osteoarthritis. *Cells* 8, 1305. doi:10.3390/cells8111305

Roseti, L., Parisi, V., Petretta, M., Cavallo, C., Desando, G., Bartolotti, I., et al. (2017). Scaffolds for bone tissue engineering: state of the art and new perspectives. *Mater Sci. Eng. C Mater Biol. Appl.* 78, 1246–1262. doi:10.1016/j.msec.2017.05.017

Ruiz, M., Toupet, K., Maumus, M., Rozier, P., Jorgensen, C., and Noël, D. (2020). TGFBI secreted by mesenchymal stromal cells ameliorates osteoarthritis and is detected in extracellular vesicles. *Biomaterials* 226, 119544. doi:10.1016/j.biomaterials.2019.119544

Russo, E., Caprnda, M., Kruzliak, P., Conaldi, P. G., Borlongan, C. V., and La Rocca, G. (2022). Umbilical cord mesenchymal stromal cells for cartilage regeneration applications. *Stem Cells Int.* 2022, 2454168. doi:10.1155/2022/2454168

Sahin, U., Karikó, K., and Türeci, Ö. (2014). MRNA-based therapeutics--developing a new class of drugs. *Nat. Rev. Drug Discov.* 13, 759–780. doi:10.1038/nrd4278

Salvador, J., Berthelot, J., Bony, C., Robin, B., Him, J. L. K., Noël, D., et al. (2022). Size-tunable lipid vectors for controlled local delivery of SiRNA from gene activated matrix. *Acta Biomater.* 153, 97–107. doi:10.1016/j.actbio.2022.09.016

Sánchez-Téllez, D. A., Téllez-Jurado, L., and Rodríguez-Lorenzo, L. M. (2017). Hydrogels for cartilage regeneration, from polysaccharides to hybrids. *Polym. (Basel)* 9, 671. doi:10.3390/polym9120671

Sanjurjo-Rodriguez, C., Altaie, A., Mastbergen, S., Baboolal, T., Welting, T., Lafeber, F., et al. (2020). Gene expression signatures of synovial fluid multipotent stromal cells in advanced knee osteoarthritis and following knee joint distraction. *Front. Bioeng. Biotechnol.* 8, 579751. doi:10.3389/fbioe.2020.579751

Sanjurjo-Rodriguez, C., Baboolal, T. G., Burska, A. N., Ponchel, F., El-Jawhari, J. J., Pandit, H., et al. (2019). Gene expression and functional comparison between multipotential stromal cells from lateral and medial condyles of knee osteoarthritis patients. *Sci. Rep.* 9, 9321. doi:10.1038/s41598-019-45820-w

Sarem, M., Arya, N., Heizmann, M., Neffe, A. T., Barbero, A., Gebauer, T. P., et al. (2018). Interplay between stiffness and degradation of architectured gelatin hydrogels leads to differential modulation of chondrogenesis *in vitro* and *in vivo*. *Acta Biomater.* 69, 83–94. doi:10.1016/j.actbio.2018.01.025

Sartore, L., Manferdini, C., Saleh, Y., Dey, K., Gabusi, E., Ramorino, G., et al. (2021). Polysaccharides on gelatin-based hydrogels differently affect chondrogenic differentiation of human mesenchymal stromal cells. *Mater Sci. Eng. C Mater Biol. Appl.* 126, 112175. doi:10.1016/j.msec.2021.112175

Schnabel, L. V., Abratte, C. M., Schimenti, J. C., Felippe, M. J. B., Cassano, J. M., Southard, T. L., et al. (2014). Induced pluripotent stem cells have similar immunogenic and more potent immunomodulatory properties compared with bone marrow-derived stromal cells *in vitro*. *Regen. Med.* 9, 621–635. doi:10.2217/rme.14.29

Schwabe, K., Garcia, M., Ubieta, K., Hannemann, N., Herbort, B., Luther, J., et al. (2016). Inhibition of osteoarthritis by adipose-derived stromal cells overexpressing fra-1 in mice. *Arthritis & Rheumatology* 68, 138–151. doi:10.1002/art.39425

Shapiro, G., Lieber, R., Gazit, D., and Pelled, G. (2018). Recent advances and future of gene therapy for bone regeneration. *Curr. Osteoporos. Rep.* 16, 504–511. doi:10.1007/s11914-018-0459-3

Sivasubramaniyan, K., Ilas, D. C., Harichandan, A., Bos, P. K., Santos, D. L., de Zwart, P., et al. (2018). Bone marrow-harvesting technique influences functional heterogeneity of mesenchymal stem/stromal cells and cartilage regeneration. *Am. J. Sports Med.* 46, 3521–3531. doi:10.1177/0363546518804807

Sivasubramaniyan, K., Koevoet, W. J. L. M., Hakimiyan, A. A., Sande, M., Farrell, E., Hoogduijn, M. J., et al. (2019). Cell-surface markers identify tissue resident multipotential stem/stromal cell subsets in synovial intimal and sub-intimal compartments with distinct chondrogenic properties. *Osteoarthr. Cartil.* 27, 1831–1840. doi:10.1016/j.joca.2019.08.006

Skou, S. T., and Roos, E. M. (2019). Physical therapy for patients with knee and hip osteoarthritis: supervised, active treatment is current best practice. *Clin. Exp. Rheumatol.* 37, 112–117.

Sun, Y., Chen, S., and Pei, M. (2018). Comparative advantages of infrapatellar fat pad: an emerging stem cell source for regenerative medicine. *Rheumatol. Oxf.* 57, 2072–2086. doi:10.1093/rheumatology/kex487

Tanikella, A. S., Hardy, M. J., Frahs, S. M., Cormier, A. G., Gibbons, K. D., Fitzpatrick, C. K., et al. (2020). Emerging gene-editing modalities for osteoarthritis. *Int. J. Mol. Sci.* 21, 6046. doi:10.3390/ijms21176046

Taraballi, F., Bauza, G., McCulloch, P., Harris, J., and Tasciotti, E. (2017). Concise review: biomimetic functionalization of biomaterials to stimulate the endogenous healing process of cartilage and bone tissue. *Stem Cells Transl. Med.* 6, 2186–2196. doi:10.1002/sctm.17-0181

Ter Huurne, M., Schelbergen, R., Blattes, R., Blom, A., De Munter, W., Grevers, L. C., et al. (2012). Antiinflammatory and chondroprotective effects of intraarticular injection of adipose-derived stem cells in experimental osteoarthritis. *Arthritis & Rheumatism* 64, 3604–3613. doi:10.1002/art.34626

Tendulkar, G., Ehnert, S., Sreekumar, V., Chen, T., Kaps, H.-P., Golombek, S., et al. (2019). Exogenous delivery of Link N MRNA into chondrocytes and MSCs-the potential role in increasing anabolic response. *Int. J. Mol. Sci.* 20, 1716. doi:10.3390/ijms20071716

Teunissen, M., Ahrens, N. S., Snel, L., Narcisi, R., Kamali, S. A., van Osch, G. J. V. M., et al. (2022). Synovial membrane-derived mesenchymal progenitor cells from osteoarthritic joints in dogs possess lower chondrogenic-and higher osteogenic capacity compared to normal joints. *Stem Cell Res. Ther.* 13, 457. doi:10.1186/s13287-022-03144-z

Tierney, E. G., McSorley, K., Hastings, C. L., Cryan, S.-A., O'Brien, T., Murphy, M. J., et al. (2013). High levels of EphrinB2 over-expression increases the osteogenic differentiation of human mesenchymal stem cells and promotes enhanced cell mediated mineralisation in a polyethyleneimine-EphrinB2 gene-activated matrix. *J. Control Release* 165, 173–182. doi:10.1016/j.jconrel.2012.11.013

Tiryaki, T., Cohen, S. R., Canikyan Turkay, S., Kocak, P., Sterodimas, A., Schlaudraff, K.-U., et al. (2022). Hybrid stromal vascular fraction (Hybrid-SVF): A new paradigm in mechanical regenerative cell processing. *Plast. Reconstr. Surg. Glob. Open* 10, e4702. doi:10.1097/GOX.0000000000004702

Trucco, D., Sharma, A., Manferdini, C., Gabusi, E., Petretta, M., Desando, G., et al. (2021). Modeling and fabrication of silk fibroin–gelatin-based constructs using extrusion-based three-dimensional bioprinting. *ACS Biomater. Sci. Eng.* 7, 3306–3320. doi:10.1021/acsbiomaterials.1c00410

Ulivi, M., Meroni, V., Viganò, M., Colombini, A., Lombardo, M. D. M., Rossi, N., et al. (2022). Micro-fragmented adipose tissue (MFAT) associated with arthroscopic debridement provides functional improvement in knee osteoarthritis: A randomized controlled trial. *Knee Surg. Sports Traumatol. Arthrosc.* 31, 3079–3090. doi:10.1007/s00167-022-07101-4

United States Bone and Joint Initiative, (2020). The burden of musculoskeletal diseases in the United States (BMUS). Available online: https://www.boneandjointburden.org (accessed on March 6, 2023).

Urich, J., Cucchiarini, M., and Rey-Rico, A. (2020). Therapeutic delivery of RAAV Sox9 via polymeric micelles counteracts the effects of osteoarthritis-associated inflammatory cytokines in human articular chondrocytes. *Nanomater. (Basel)* 10, 1238. doi:10.3390/nano10061238

van Buul, G. M., Villafuertes, E., Bos, P. K., Waarsing, J. H., Kops, N., Narcisi, R., et al. (2012). Mesenchymal stem cells secrete factors that inhibit inflammatory processes in short-term osteoarthritic synovium and cartilage explant culture. *Osteoarthr. Cartil.* 20, 1186–1196. doi:10.1016/j.joca.2012.06.003

van Osch, G. J. V. M., Brittberg, M., Dennis, J. E., Bastiaansen-Jenniskens, Y. M., Erben, R. G., Konttinen, Y. T., et al. (2009). Cartilage repair: past and future--lessons for regenerative medicine. *J. Cell Mol. Med.* 13, 792–810. doi:10.1111/j.1582-4934.2009.00789.x

Valot, L., Maumus, M., Brunel, L., Martinez, J., Amblard, M., Noël, D., et al. (2021). A collagen-mimetic organic-inorganic hydrogel for cartilage engineering. *Gels* 7, 73. doi:10.3390/gels7020073

Varma, M. J. O., Breuls, R. G. M., Schouten, T. E., Jurgens, W. J. F. M., Bontkes, H. J., Schuurhuis, G. J., et al. (2007). Phenotypical and functional characterization of freshly isolated adipose tissue-derived stem cells. *Stem Cells Dev.* 16, 91–104. doi:10.1089/scd.2006.0026

Velloso Alvarez, A., Boone, L. H., Braim, A. P., Taintor, J. S., Caldwell, F., Wright, J. C., et al. (2020). A survey of clinical usage of non-steroidal intra-articular therapeutics by equine practitioners. *Front. Vet. Sci.* 7, 579967. doi:10.3389/fvets.2020.579967

Velot, É., Elkhoury, K., Kahn, C., Kempf, H., Linder, M., Arab-Tehrany, E., et al. (2022). Efficient TGF-B1 delivery to articular chondrocytes *in vitro* using agro-based liposomes. *IJMS* 23, 2864. doi:10.3390/ijms23052864

Velot, É., Madry, H., Venkatesan, J. K., Bianchi, A., and Cucchiarini, M. (2021). Is extracellular vesicle-based therapy the next answer for cartilage regeneration? *Front. Bioeng. Biotechnol.* 9, 645039. doi:10.3389/fbioe.2021.645039

Venkatesan, J. K., Cai, X., Meng, W., Rey-Rico, A., Schmitt, G., Speicher-Mentges, S., et al. (2021). PNaSS-grafted PCL film-guided RAAV TGF-β gene therapy activates the chondrogenic activities in human bone marrow aspirates. *Hum. Gene Ther.* 32, 895–906. doi:10.1089/hum.2020.329

Venkatesan, J. K., Falentin-Daudré, C., Leroux, A., Migonney, V., and Cucchiarini, M. (2018). Controlled release of gene therapy constructs from solid scaffolds for therapeutic applications in orthopedics. *Discov. Med.* 25, 195–203.

Venkatesan, J. K., Meng, W., Rey-Rico, A., Schmitt, G., Speicher-Mentges, S., Falentin-Daudré, C., et al. (2020). Enhanced chondrogenic differentiation activities in human bone marrow aspirates via Sox9 overexpression mediated by PNaSS-grafted PCL film-guided RAAV gene transfer. *Pharmaceutics* 12, 280. doi:10.3390/pharmaceutics12030280

Venkatesan, J. K., Rey-Rico, A., and Cucchiarini, M. (2019). Current trends in viral gene therapy for human orthopaedic regenerative medicine. *Tissue Eng. Regen. Med.* 16, 345–355. doi:10.1007/s13770-019-00179-x

Venkatesan, J. K., Schmitt, G., Speicher-Mentges, S., Orth, P., Madry, H., and Cucchiarini, M. (2022). Effects of recombinant adeno-associated virus-mediated overexpression of bone morphogenetic *protein 3 on the chondrogenic fate of human bone marrow-derived mesenchymal stromal cells. *Hum. Gene Ther.* 33, 950–958. doi:10.1089/hum.2022.004

Vinatier, C., Bouffi, C., Merceron, C., Gordeladze, J., Brondello, J.-M., Jorgensen, C., et al. (2009). Cartilage tissue engineering: towards a biomaterial-assisted mesenchymal stem cell therapy. *Curr. Stem Cell Res. Ther.* 4, 318–329. doi:10.2174/157488809789649205

Vincent, T. L., Alliston, T., Kapoor, M., Loeser, R. F., Troeberg, L., and Little, C. B. (2022). Osteoarthritis pathophysiology: therapeutic target discovery may require a multifaceted approach. *Clin. Geriatr. Med.* 38, 193–219. doi:10.1016/j.cger.2021.11.015

Vincent, T. L. (2019). Mechanoflammation in osteoarthritis pathogenesis. *Semin. Arthritis Rheum.* 49, S36–S38. doi:10.1016/j.semarthrit.2019.09.018

Vincent, T. L. (2020). Of mice and men: converging on a common molecular understanding of osteoarthritis. *Lancet Rheumatol.* 2, e633–e645. doi:10.1016/S2665-9913(20)30279-4

Vinod, E., Padmaja, K., Ramasamy, B., and Sathishkumar, S. (2023). Systematic review of articular cartilage derived chondroprogenitors for cartilage repair in animal models. *J. Orthop.* 35, 43–53. doi:10.1016/j.jor.2022.10.012

Viswanathan, S., Shi, Y., Galipeau, J., Krampera, M., Leblanc, K., Martin, I., et al. (2019). Mesenchymal stem versus stromal cells: international society for cell and gene therapy (isct®) mesenchymal stromal cell committee position statement on nomenclature. *Cytotherapy* 21, 1019–1024. doi:10.1016/j.jcyt.2019.08.002

Vonk, L. A., de Windt, T. S., Slaper-Cortenbach, I. C. M., and Saris, D. B. F. (2015). Autologous, allogeneic, induced pluripotent stem cell or a combination stem cell therapy? Where are we headed in cartilage repair and why: A concise review. *Stem Cell Res. Ther.* 6, 94. doi:10.1186/s13287-015-0086-1

Vonk, L. A., van Dooremalen, S. F. J., Liv, N., Klumperman, J., Coffer, P. J., Saris, D. B. F., et al. (2018). Mesenchymal stromal/stem cell-derived extracellular vesicles promote human cartilage regeneration *in vitro*. *Theranostics* 8, 906–920. doi:10.7150/thno.20746

Voskamp, C., Koevoet, W. J. L. M., Somoza, R. A., Caplan, A. I., Lefebvre, V., van Osch, G. J. V. M., et al. (2020). Enhanced chondrogenic capacity of mesenchymal stem cells after TNFα pre-treatment. *Front. Bioeng. Biotechnol.* 8, 658. doi:10.3389/fbioe.2020.00658

Walsh, D. P., Raftery, R. M., Murphy, R., Chen, G., Heise, A., O'Brien, F. J., et al. (2021). Gene activated scaffolds incorporating star-shaped polypeptide-PDNA nanomedicines accelerate bone tissue regeneration *in vivo*. *Biomater. Sci.* 9, 4984–4999. doi:10.1039/d1bm00094b

Wang, Y., Shimmin, A., Ghosh, P., Marks, P., Linklater, J., Connell, D., et al. (2017). Safety, tolerability, clinical, and joint structural outcomes of a single intra-articular injection of allogeneic mesenchymal precursor cells in patients following anterior cruciate ligament reconstruction: A controlled double-blind randomised trial. *Arthritis Res. Ther.* 19, 180. doi:10.1186/s13075-017-1391-0

Watson Levings, R. S., Broome, T. A., Smith, A. D., Rice, B. L., Gibbs, E. P., Myara, D. A., et al. (2018b). Gene therapy for osteoarthritis: pharmacokinetics of intra-articular self-complementary adeno-associated virus interleukin-1 receptor antagonist delivery in an equine model. *Hum. Gene Ther. Clin. Dev.* 29, 90–100. doi:10.1089/humc.2017.142

Watson Levings, R. S., Smith, A. D., Broome, T. A., Rice, B. L., Gibbs, E. P., Myara, D. A., et al. (2018a). Self-complementary adeno-associated virus-mediated interleukin-1 receptor antagonist gene delivery for the treatment of osteoarthritis: test of efficacy in an equine model. *Hum. Gene Ther. Clin. Dev.* 29, 101–112. doi:10.1089/humc.2017.143

Weissman, D. (2015). MRNA transcript therapy. *Expert Rev. Vaccines* 14, 265–281. doi:10.1586/14760584.2015.973859

Wluka, A. E., Wolfe, R., Stuckey, S., and Cicuttini, F. M. (2004). How does tibial cartilage volume relate to symptoms in subjects with knee osteoarthritis? *Ann. Rheum. Dis.* 63, 264–268. doi:10.1136/ard/2003.007666

Wu, H., Peng, Z., Xu, Y., Sheng, Z., Liu, Y., Liao, Y., et al. (2022). Engineered adipose-derived stem cells with IGF-1-modified MRNA ameliorates osteoarthritis development. *Stem Cell Res. Ther.* 13, 19. doi:10.1186/s13287-021-02695-x

Xi, X.-M., Xia, S.-J., and Lu, R. (2021). Drug loading techniques for exosome-based drug delivery systems. *Pharmazie* 76, 61–67. doi:10.1691/ph.2021.0128

Xu, M., Shaw, G., Murphy, M., and Barry, F. (2019). Induced pluripotent stem cell-derived mesenchymal stromal cells are functionally and genetically different from bone marrow-derived mesenchymal stromal cells. *Stem Cells* 37, 754–765. doi:10.1002/stem.2993

Yan, H.-C., Yu, T.-T., Li, J., Qiao, Y.-Q., Wang, L.-C., Zhang, T., et al. (2020). The delivery of extracellular vesicles loaded in biomaterial scaffolds for bone regeneration. *Front. Bioeng. Biotechnol.* 8, 1015. doi:10.3389/fbioe.2020.01015

Yang, J., Li, Y., Liu, Y., Li, D., Zhang, L., Wang, Q., et al. (2019). Influence of hydrogel network microstructures on mesenchymal stem cell chondrogenesis *in vitro* and *in vivo*. *Acta Biomater.* 91, 159–172. doi:10.1016/j.actbio.2019.04.054

Yang, J., Zhang, Y. S., Yue, K., and Khademhosseini, A. (2017). Cell-laden hydrogels for osteochondral and cartilage tissue engineering. *Acta Biomater.* 57, 1–25. doi:10.1016/j.actbio.2017.01.036

Yazici, Y., McAlindon, T. E., Gibofsky, A., Lane, N. E., Clauw, D., Jones, M., et al. (2020). Lorecivivint, a novel intraarticular CDC-like kinase 2 and dual-specificity tyrosine phosphorylation-regulated kinase 1A inhibitor and wnt pathway modulator for the treatment of knee osteoarthritis: A phase II randomized trial. *Arthritis Rheumatol.* 72, 1694–1706. doi:10.1002/art.41315

Zachos, T. A., Shields, K. M., and Bertone, A. L. (2006). Gene-Mediated osteogenic differentiation of stem cells by bone morphogenetic proteins-2 or -6. *J. Orthop. Res.* 24, 1279–1291. doi:10.1002/jor.20068

Zachos, T., Diggs, A., Weisbrode, S., Bartlett, J., and Bertone, A. (2007). Mesenchymal stem cell-mediated gene delivery of bone morphogenetic protein-2 in an articular fracture model. *Mol. Ther.* 15, 1543–1550. doi:10.1038/sj.mt.6300192

Zhang, F.-X., Liu, P., Ding, W., Meng, Q.-B., Su, D.-H., Zhang, Q.-C., et al. (2021). Injectable mussel-inspired highly adhesive hydrogel with exosomes for endogenous cell recruitment and cartilage defect regeneration. *Biomaterials* 278, 121169. doi:10.1016/j.biomaterials.2021.121169

Zhang, J., Wehrle, E., Adamek, P., Paul, G. R., Qin, X.-H., Rubert, M., et al. (2020). Optimization of mechanical stiffness and cell density of 3D bioprinted cell-laden scaffolds improves extracellular matrix mineralization and cellular organization for bone tissue engineering. *Acta Biomater.* 114, 307–322. doi:10.1016/j.actbio.2020.07.016

Zhang, W., De La Vega, R. E., Coenen, M. J., Müller, S. A., Peniche Silva, C. J., Aneja, M. K., et al. (2019). An improved, chemically modified RNA encoding BMP-2 enhances osteogenesis *in vitro* and *in vivo*. *Tissue Eng. Part A* 25, 131–144. doi:10.1089/ten.TEA.2018.0112

Zhou, Y., Ming, J., Li, Y., Li, B., Deng, M., Ma, Y., et al. (2021). Exosomes derived from MiR-126-3p-overexpressing synovial fibroblasts suppress chondrocyte inflammation and cartilage degradation in a rat model of osteoarthritis. *Cell Death Discov.* 7, 37. doi:10.1038/s41420-021-00418-y

frontiers | Frontiers in Bioengineering and Biotechnology

TYPE Original Research
PUBLISHED 29 October 2024
DOI 10.3389/fbioe.2024.1495015

Check for updates

OPEN ACCESS

EDITED BY
Elizabeth Vinod,
Christian Medical College and Hospital, India

REVIEWED BY
Sumit Murab,
Indian Institute of Technology Mandi, India
Weibin Du,
Zhejiang Chinese Medical University, China

*CORRESPONDENCE
Amy L. McNulty,
alr@duke.edu

RECEIVED 11 September 2024
ACCEPTED 17 October 2024
PUBLISHED 29 October 2024

CITATION
Firoozi S, Ley JC, Chasse DAD, Attarian DE, Wellman SS, Amendola A and McNulty AL (2024) Healthy but not osteoarthritic human meniscus-derived matrix scaffolds promote meniscus repair.
Front. Bioeng. Biotechnol. 12:1495015.
doi: 10.3389/fbioe.2024.1495015

COPYRIGHT
© 2024 Firoozi, Ley, Chasse, Attarian, Wellman, Amendola and McNulty. This is an open-access article distributed under the terms of the Creative Commons Attribution License (CC BY). The use, distribution or reproduction in other forums is permitted, provided the original author(s) and the copyright owner(s) are credited and that the original publication in this journal is cited, in accordance with accepted academic practice. No use, distribution or reproduction is permitted which does not comply with these terms.

Healthy but not osteoarthritic human meniscus-derived matrix scaffolds promote meniscus repair

Saman Firoozi[1], Jon C. Ley[1], Dawn A. D. Chasse[1], David E. Attarian[1], Samuel S. Wellman[1], Annunziato Amendola[1] and Amy L. McNulty[1,2,3]*

[1]Department of Orthopaedic Surgery, Duke University School of Medicine, Durham, NC, United States, [2]Department of Pathology, Duke University School of Medicine, Durham, NC, United States, [3]Department of Biomedical Engineering, Duke University, Durham, NC, United States

Meniscus tissue is commonly injured due to sports-related injuries and age-related degeneration and approximately 50% of individuals with a meniscus tear will develop post-traumatic osteoarthritis (PTOA). Given that the meniscus has limited healing potential, new therapeutic strategies are required to enhance meniscus repair. Porcine meniscus-derived matrix (MDM) scaffolds improve meniscus integrative repair, but sources of human meniscus tissue have not been investigated. Therefore, the objectives of this study were to generate healthy and osteoarthritic (OA) MDM scaffolds and to compare meniscus cellular responses and integrative repair. Meniscus cells showed high viability on both healthy and OA scaffolds. While DNA content was higher in cell-seeded OA scaffolds than cell-seeded healthy scaffolds, CCK-8, and both sGAG and collagen content were similar between scaffold types. After 28 days in an *ex vivo* meniscus defect model, healthy and OA scaffolds had similar DNA, sGAG, and collagen content. However, the shear strength of repair was reduced in defects containing OA scaffolds compared to healthy scaffolds. In conclusion, healthy human allograft tissue is a useful source for generating MDM scaffolds that can support cellular growth, ECM production, and *ex vivo* integrative repair of the meniscus, highlighting the potential suitability for tissue engineering approaches to improve meniscus repair.

KEYWORDS

tissue engineering, proteoglycans, osteoarthritis, allograft, meniscus, age, collagen, meniscus repair

1 Introduction

Menisci are fibrocartilaginous tissues located between the femoral condyles and tibial plateau in the knee. The menisci transfer and distribute load across the articular cartilage, provide joint stability, and afford a low friction surface for joint articulation (Fox et al., 2012; Ahmed et al., 1983; Markolf et al., 1981; Wojtys and Chan, 2005; Carter et al., 2015). Proper meniscus function is necessary for maintaining performance and health of the knee joint (Ahmed et al., 1983; Markolf et al., 1981; Wojtys and Chan, 2005; Carter et al., 2015). Due to joint loading during activities of daily living and sports, the menisci must resist high forces in tension and compression and thus are highly susceptible to injury (Vignes et al., 2022).

The yearly incidence of meniscus injury is 66 tears per 100,000 people (Bansal et al., 2021). These tears can be primarily traumatic or degenerative due to sports-related injuries or age-related joint degeneration respectively (Terzidis et al., 2006; Englund et al., 2009). There is pain and disability associated with the meniscus injury but also nearly 50% of individuals with a meniscus tear develop post-traumatic osteoarthritis (PTOA) within 20 years of the injury (Blake and Johnson, 2018; Scotti et al., 2013; Lohmander et al., 2007; Badlani et al., 2013). Therefore, current orthopaedic treatments seek to restore meniscus structure and function through different approaches including meniscus repair, allograft transplantation, and biological augmentation strategies (Lin et al., 2017; Guo et al., 2015; Chevrier et al., 2018; Wang et al., 2024; Luvsannyam et al., 2022). Despite promising short-term results, these treatments fail to restore function of the injured meniscus tissue and are not able to prevent PTOA development (Scotti et al., 2013; Wang et al., 2024). Given that the meniscus has a limited healing potential due to its dense extracellular matrix (ECM) and minimal vascularity (Xia et al., 2021), new therapeutic strategies are required to enhance meniscus repair.

Meniscus tissue engineering is a promising approach to replace lost and/or damaged meniscus tissue. Various types of biomaterials, including natural and synthetic polymers, hydrogels, and tissue-derived materials, have been used to generate tissue-engineered scaffolds for meniscus regeneration (Makris et al., 2011; Li et al., 2021b; Ionescu and Mauck, 2013; Chen et al., 2019; Guo et al., 2021; Gao et al., 2017; Komatsu et al., 2024; An et al., 2021). Decellularized ECM is a promising choice because it contains the native components of the ECM, natural growth factors found in the matrix, and provides tissue specific epitopes to regulate cellular behavior and function (Hussey et al., 2018; Pati et al., 2014). To date, numerous forms of meniscus-derived matrix (MDM) scaffolds have been investigated including whole lyophilized tissue grafts (Gelse et al., 2017; Shimomura et al., 2017; Jiang et al., 2018), pulverized tissue reconstituted as porous or hydrogel scaffolds (Wu et al., 2015; Yuan et al., 2017; Ruprecht et al., 2019; Lyons et al., 2019; Xia et al., 2021; Salinas-Fernandez et al., 2024), 3D printed scaffolds composed of ECM-based bioinks (Pati et al., 2014; Ahn et al., 2017; Yang et al., 2017; Grogan et al., 2013; Bakarich et al., 2014; Lian et al., 2024; Wang et al., 2023), electrospun scaffolds (Baek et al., 2016; Venugopal et al., 2018; Mandal et al., 2011a; Li et al., 2021a), or a combination of these strategies (Baek et al., 2015; Yu et al., 2019). In our prior work, we showed that pulverized and reconstituted porcine MDM scaffolds can promote migration of endogenous meniscus cells and can improve the integrative repair of a porcine *ex vivo* meniscus defect (Ruprecht et al., 2019). For clinical applications, MDM can be isolated from allogeneic or xenogeneic meniscus tissues. However, there are concerns regarding the immunogenicity of xenogenic scaffolds for use in humans (Stone et al., 2017; Chen et al., 2024). Alternatively, there is limited availability of healthy human meniscus tissue. Prior work has shown that discarded human kidneys procured for transplantation were successfully used to generate ECM scaffolds for renal tissue engineering applications (Orlando et al., 2013). According to the 2024 report of the American College of Rheumatology, there are approximately 790,000 total knee joint replacement surgeries performed annually in the US (Ray, 2024), so there is a large abundance of human osteoarthritic (OA) menisci available as waste following surgery (Kremers et al., 2015). These tissues could be an abundant and useful source for human MDM scaffold fabrication.

Therefore, the objectives of this study were to generate healthy and OA MDM scaffolds and to compare *in vitro* meniscus cellular responses and meniscus integrative repair capacity of the scaffolds using an *ex vivo* human meniscus defect model. A new combination of physical and chemical methods was employed to fabricate decellularized healthy and OA scaffolds. Then, the response of human meniscus cells to healthy and OA scaffolds was evaluated using *in vitro* assays. Using a cell-free approach, healthy and OA scaffolds were implanted in an *ex vivo* human meniscus defect model to compare cellular migration of native cells, tissue formation, and integrative repair capacity of the healthy *versus* OA scaffolds.

2 Materials and methods

2.1 Human and OA meniscus samples

Deidentified OA human medial and lateral menisci (N = 31, 22F/9M) with a mean age of 65 ± 8.2 years old were obtained from subjects undergoing total knee replacement at Duke Hospital (IRB Pro00079807). Healthy human medial menisci (N = 10, 5F/5M) from donors with an average age of 25 ± 6 years old were generously donated by JRF Ortho. Photographs were taken of all menisci prior to storage at −80°C.

2.2 Gross grading

Gross grading (n = 5 healthy, n = 10 OA) was performed independently by four blinded graders from photographs and the results were averaged. The scoring criteria was previously published by Pauli et al. (2011). Briefly, each meniscus was divided into 3 zones and each zone was given a score between 1 and 4. The total for each zone was then summed, yielding a total of 3 for a normal intact meniscus and a maximum score of 12 for a meniscus with full/complete substance tears, loss of tissue, and/or tissue maceration in all zones.

2.3 Histological analyses

Healthy and OA menisci (n = 3/group) were sliced radially for cross-sectional analysis in the central portion of the menisci. These tissues and day 28 meniscus defect model explants (see Meniscus explant harvest and *ex vivo* meniscus defect below, n = 3/group) were fixed in formalin overnight at 4°C, dehydrated, and paraffin embedded. Then samples were cut into 8 μm sections and stained with Harris' hematoxylin (Electron Microscopy Sciences, #26754-01, United States), 0.02% aqueous fast green (Electron Microscopy Sciences, #15500, United States), and 0.1% Safranin-O (Sigma-Aldrich, #HT904-8FOZ) (Ruprecht et al., 2019).

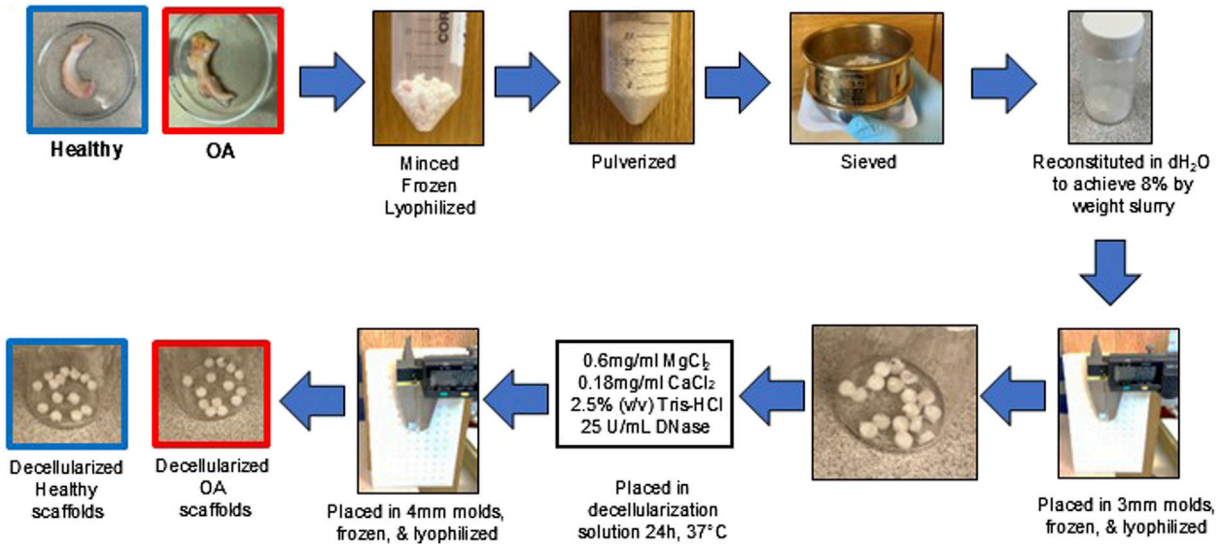

FIGURE 1
Fabrication procedure of healthy and OA MDM scaffolds.

2.4 MDM scaffold fabrication and decellularization

The healthy and OA menisci were thawed, minced into ≤5 mm pieces, frozen overnight at −80°C, and then lyophilized (FreeZone 2.5 L, Labconco, Kansas City, MO) for 24 h (Figure 1). The lyophilized meniscus pieces were pulverized (5 min pre-cool, 5 cycles of 1 min at 5 Hz and 2 min cool) in a 6770 freezer mill (SPEX SamplePrep, Metuchen, NJ) (Ruprecht et al., 2019). The healthy and OA meniscus powders were sieved at 500 μm and pooled into two separate superlots. Healthy and OA powders were rehydrated to 8% weight fraction by mixing 0.8 g MDM powder with distilled water to achieve 10 g total mass. After resuspension, the healthy and OA slurry was homogenized (VWR® 200 Homogenizer) at 30,000 rpm for 2 cycles of 2 min run then 2 min cool on ice (Rowland et al., 2016; Ruprecht et al., 2019; Lyons et al., 2019). Healthy and OA homogenized slurries were pipetted into delrin molds (1.9 mm deep × 3 mm diameter). Molds were then frozen at −80°C overnight and lyophilized for 24 h. Next, fabricated healthy and OA scaffolds were removed from the mold and incubated in decellularization solution composed of 0.6 mg/mL $MgCl_2$ (Sigma-Aldrich, M8266), 0.18 mg/mL $CaCl_2$ (Sigma-Aldrich, C3889), 2.5% (v/v) Tris-HCl (Sigma-Aldrich, T9285), and 25 U/mL DNase (Sigma-Aldrich, D5319) at 37°C for 24 h (Rowland et al., 2016). Scaffolds were gently placed into 4 mm diameter delrin molds using tweezers, frozen at −80°C overnight, lyophilized for 24 h, and kept in sterile containers. Both non-decellularized and decellularized scaffolds were washed 5 times with PBS prior to biochemical assessments and *in vitro* and *ex vivo* experiments.

2.5 Biochemical assays

In order to determine biochemical content of scaffolds before and after decellularization (n = 3–4/group), throughout *in vitro* culture (n = 3/group/timepoint), and following *ex vivo* culture (n = 18/group), meniscus inner cores and scaffolds were digested in 500 μL of papain (125 μg/mL papain (Sigma-Aldrich, P4762), 100 mM phosphate buffer (Sigma-Aldrich, S9638), 10 mM cysteine (Sigma-Aldrich, C1276), and 10 mM EDTA, pH 6.3 (Sigma-Aldrich, E7989) at 65°C overnight (Rowland et al., 2013; Collins et al., 2019; Hatcher et al., 2017). DNA content was measured by following the manufacturer's instructions for the picogreen assay (Invitrogen, P7589) (Lyons et al., 2019; Ruprecht et al., 2019). The sGAG content was determined by the dimethylmethylene blue assay (Farndale et al., 1986), using a bovine chondroitin sulfate standard (Sigma-Aldrich, C6737). Collagen content was measured by the hydroxyproline assay (Reddy and Enwemeka, 1996; Collins et al., 2019; Hatcher et al., 2017; Lyons et al., 2019; Ruprecht et al., 2019).

2.6 Human meniscus cell isolation and scaffold cell seeding

Human meniscal cells were isolated from joint replacement waste meniscus tissue (N = 3, 2F/1M, 54 ± 22.5 years old). Immediately after surgical removal, menisci were placed in sealed containers with sterile saline. The whole meniscus was minced into ~2 mm × 2 mm pieces and washed in Dulbecco's modified eagle medium-high glucose (DMEM-HG, Gibco) containing 10% antibiotic–antimycotic (penicillin–streptomycin–fungizone (PSF), Gibco). Meniscus pieces were then enzymatically digested (Riera et al., 2011; McNulty et al., 2013) with 0.5% pronase (Calbiochem, San Diego, CA, United States) for 1 h followed by overnight digestion with 0.2% collagenase type I (Worthington, Lakewood, NJ, United States) in DMEM-HG containing 10% PSF and 10% fetal bovine serum (FBS; Corning, Corning, NY, United States) at 37°C (Andress et al., 2021; Andress et al., 2022). Isolated cells were then filtered through a 70 μm cell strainer (Corning). Isolated meniscus

cells from three different patients were pooled together and expanded in meniscus growth medium consisting of DMEM-HG supplemented with 10% FBS, 1% PSF, 1% 4-(2-hydroxyethyl)-1-piperazine ethanesulfonic acid buffer (HEPES, Invitrogen, Carlsbad, CA, United States), 1% non-essential amino acids (Invitrogen), and 100 μg/mL ascorbic acid 2-phosphate (Sigma–Aldrich) at 37°C, 5% CO_2. Passage 1 meniscus cells were trypsinized, counted, and resuspended in meniscus growth medium at a density of 7.8×10^6 cells/mL (Lyons et al., 2019). Healthy and OA scaffolds were placed in ultra-low attachment 24 well plates (Corning). Then 8 μL of cell suspension was pipetted on the top of each scaffold. Scaffolds were placed into a vacuum chamber for 45 s to improve cell infiltration (Solchaga et al., 2006). Scaffolds were flipped and 8 μL of cells were pipetted onto the other side of the scaffolds and vacuum infiltration was repeated (Lyons et al., 2019). Then 1 mL of meniscus growth medium was added to each well and scaffolds were incubated at 37°C and 5% CO_2 for up to 14 days. Growth media was changed every 2–3 days.

2.7 Evaluation of meniscus cellular responses on scaffolds

2.7.1 Actin immunostaining

At 1, 3, 6, and 24 h after cell seeding, scaffolds were fixed in 4% paraformaldehyde (PFA, Electron Microscopy Sciences, 15,710) for 20 min to evaluate cellular attachment (n = 3/group/timepoint) as described previously (Xia et al., 2021). Scaffolds were subjected to antigen retrieval using the Universal antigen retrieval reagent (Abcam, ab208572) for 20 min. Next, samples were permeabilized with 0.5% Triton X-100 (Sigma-Aldrich) at RT for 30 min, blocked in 3% bovine serum albumin (Sigma-Aldrich, A9418) for 1 h at 37°C, and incubated overnight with 1 μg/mL recombinant anti-actin antibody (Abcam, ab213251) at 4°C. Then 1 μg/mL goat anti-human IgG-488 (Abcam, ab69907) was applied at 37°C for 1 h. Scaffolds were counterstained with DAPI (Invitrogen) and imaged using a fluorescent microscope (Olympus, IX83).

2.7.2 Live/dead staining

On days 3 and 7, healthy and OA cell-seeded scaffolds were stained with the Live/Dead Assay kit (Invitrogen, L34973) to assess cell viability (n = 3/group/timepoint) (Van Der Straeten et al., 2016; Wilusz et al., 2008). Scaffolds were incubated with 2 mM calcein AM and 4 mM ethidium homodimer-1 for 30 min and then washed in PBS. Images were acquired using a fluorescent microscope (Olympus, IX83). Images were deconvoluted and live and dead cells were counted using cellSens Dimension version 1.18 software (Olympus, Center Valley, PA). Percent cell viability was calculated as follows: % Cell viability = (live cells/total cells) × 100.

2.7.3 Edu staining

On days 3 and 13, fresh culture media was added containing 10 μM 5-ethylnyl-2′-deoxyuridine (EdU from the Click-iT™ EdU Alexa Fluor® 488 Imaging Kit; Invitrogen C10337). After 24 h, on days 4 and 14, EdU staining was performed to detect proliferative cells on cell-seeded scaffolds, according to the manufacturer's protocol (n = 3–4/group/timepoint). Samples were imaged using a fluorescent microscope (Olympus, IX83). Images were deconvoluted and the number of EdU-positive and total cells were counted using the cellSens Dimension version 1.18 software. The percent proliferative cells were calculated as follows: % Proliferative cells = (Edu^+ cells/total cells) × 100.

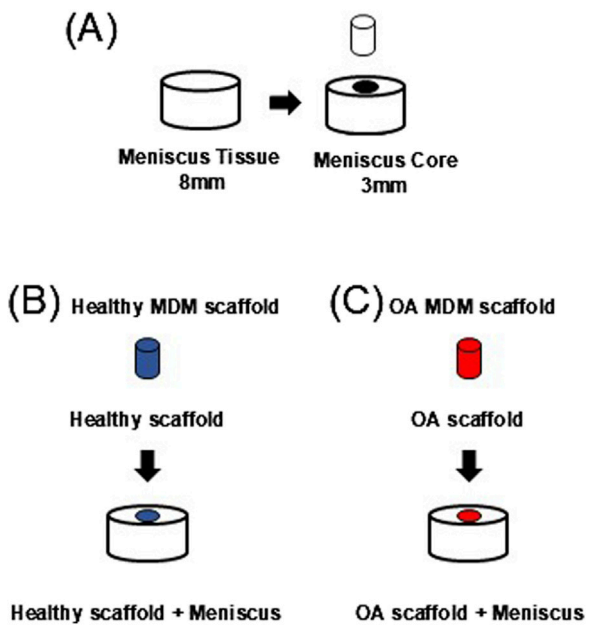

FIGURE 2
(A) Schematic of meniscal defect model. Implantation of **(B)** healthy and **(C)** OA scaffolds.

2.7.4 Biochemical assessment of cell viability

On days 1, 4, 7, and 14, cell counting kit-8 (CCK-8 kit, APExBIO, K1018) was used to evaluate cell viability within the healthy and OA scaffolds (n = 3/group/timepoint). Growth media containing CCK-8 solution at a final concentration of 10% was added to each cell-seeded scaffold (Chen et al., 2019). After 3 h at 37°C, the media was removed and read at 450 nm on a microplate reader (TECAN, Austria).

2.8 Meniscus explant harvest and *ex vivo* meniscus defect model

Waste human menisci (N = 11, 9F/2M, 69 ± 7.82 years old) from joint replacement surgeries were used to harvest meniscus defect model explants. For each subject, the grossly healthier meniscus (Pauli et al., 2011) was used. Tissue explants were harvested using 8 mm diameter biopsy punches and cut to 2 mm thick explants (Figure 2A). Then a 3 mm diameter core was removed from each explant to create a full-thickness defect (Hennerbichler et al., 2007a; McNulty et al., 2010; McNulty and Guilak, 2008; McNulty et al., 2007; McNulty et al., 2009; Ruprecht et al., 2019; Lyons et al., 2019). The defect was filled with either a healthy (Figure 2B, Healthy scaffold + Meniscus) or OA scaffold (Figure 2C, OA scaffold + Meniscus). All samples were cultured in meniscus growth media and incubated at 37°C and 5% CO_2 for up to 28 days. Growth media was changed every 2–3 days.

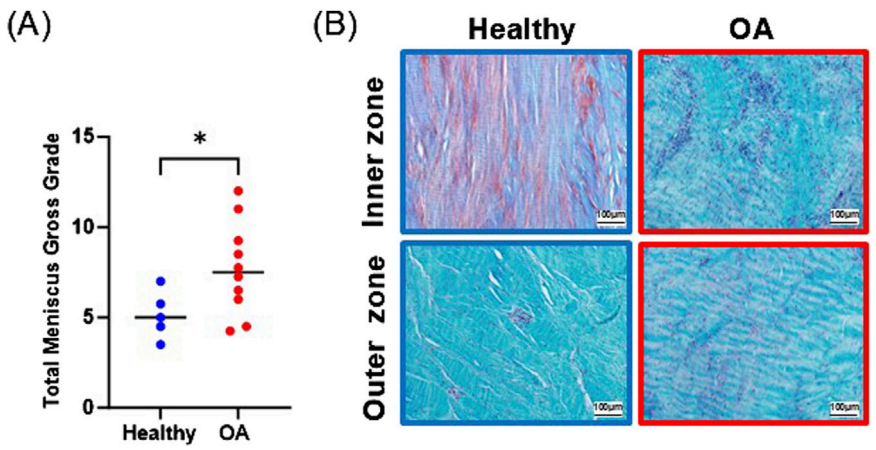

FIGURE 3
(A) Gross grading scores. The mean is indicated by a line for each group. *$p < 0.05$. **(B)** Safranin O and fast green staining of representative healthy and OA meniscus tissue.

2.9 Evaluation of meniscus defect model explants

2.9.1 Fluorescent imaging of meniscus defect model explants

Meniscal defect model explants were harvested at days 7, 14, 21, and 28 (n = 3/group/timepoint) to visualize migration of cells from the outer meniscus tissue to the inner core by staining of live cells using calcein AM (Invitrogen, L3224) and matrix with Alexa fluor 633 NHS ester (Invitrogen, A20005) (Lyons et al., 2019; Ruprecht et al., 2019). A fluorescent microscope (IX83, Olympus) was used to visualize the cells and matrix.

2.9.2 Shear strength of repair

After 28 days of culture, meniscus defect model explants were subjected to a push-out test to measure shear strength of repair (n = 12/group) (Hennerbichler et al., 2007a; McNulty et al., 2010; Ruprecht et al., 2019; Lyons et al., 2019; McNulty et al., 2007). Explants were loaded into a dish containing a central 4 mm hole and placed in the test frame (ElectroForce 3220 Series III, MN, United States). A 2 mm piston connected to a 225N load cell (Honeywell, Morris Plains, NJ) and centered directly above the inner core was used to push-out the inner core. A 0.5 g tare load was held for 10 s, and then the piston was displaced at a rate of 0.083 mm/sec to 5 mm. Images of each explant were collected and imported into ImageJ (NIH, United States) to measure sample height. Shear strength of repair was calculated as the peak force divided by the area of the repair interface. The displaced inner core scaffolds were papain digested for biochemical analyses (see Biochemical assays above).

2.10 Statistical analyses

Statistical analyses were performed using GraphPad Prism 10. All data was tested for normality. For gross grading and the *ex vivo* biochemical data, unpaired t-tests were performed. For decellularization DNA content and *in vitro* biochemical outcomes, two-way ANOVAs followed Tukey's *post hoc* testing were performed. For decellularization matrix content, cell viability, and proliferation, two-way ANOVAs with Sidak's multiple comparison testing was used. The data for the shear strength of repair was not normally distributed so Mann-Whitney U testing was performed. For all experiments $p < 0.05$ was considered statistically significant.

3 Results

3.1 Assessment of meniscus tissue

Gross grading revealed that OA meniscus tissue had significantly higher scores than healthy meniscus tissue, indicative of degradative changes in the OA tissues (Figure 3A, $p < 0.05$). Histological staining of the healthy meniscus tissue showed sparce cells distributed throughout the tissue and there was strong proteoglycan staining in the inner zone (Figure 3B). On the other hand, in OA meniscus tissue, there was hypercellularity and diminished proteoglycan staining.

3.2 Evaluation of decellularization of scaffolds

DNA content of the OA scaffolds was significantly higher than healthy scaffolds before decellularization (Figure 4A, $p < 0.0001$), indicating that the OA menisci contained more cells. Decellularization significantly decreased DNA content of both healthy and OA scaffolds ($p < 0.0001$). After decellularization, there were no detectable differences in the DNA content between the healthy and OA scaffolds. sGAG was not detectably different between scaffold types but was slightly reduced due to decellularization (Figure 4B, $p < 0.05$). On the other hand, collagen content was retained in both the healthy and OA scaffolds after decellularization and there were no detectable differences between the scaffold types (Figure 4C).

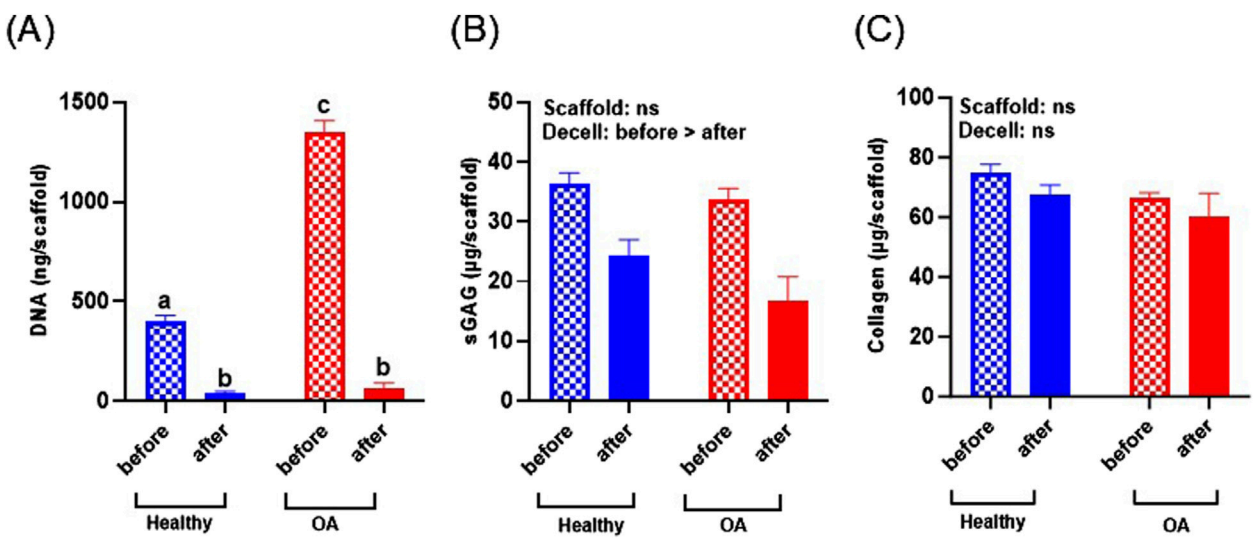

FIGURE 4
(A) DNA, **(B)** sGAG, and **(C)** collagen content of healthy and OA scaffolds before and after decellularization (Decell). Data are expressed as the mean +SEM for all groups. All groups not sharing the same letter have *p*-values <0.0001.

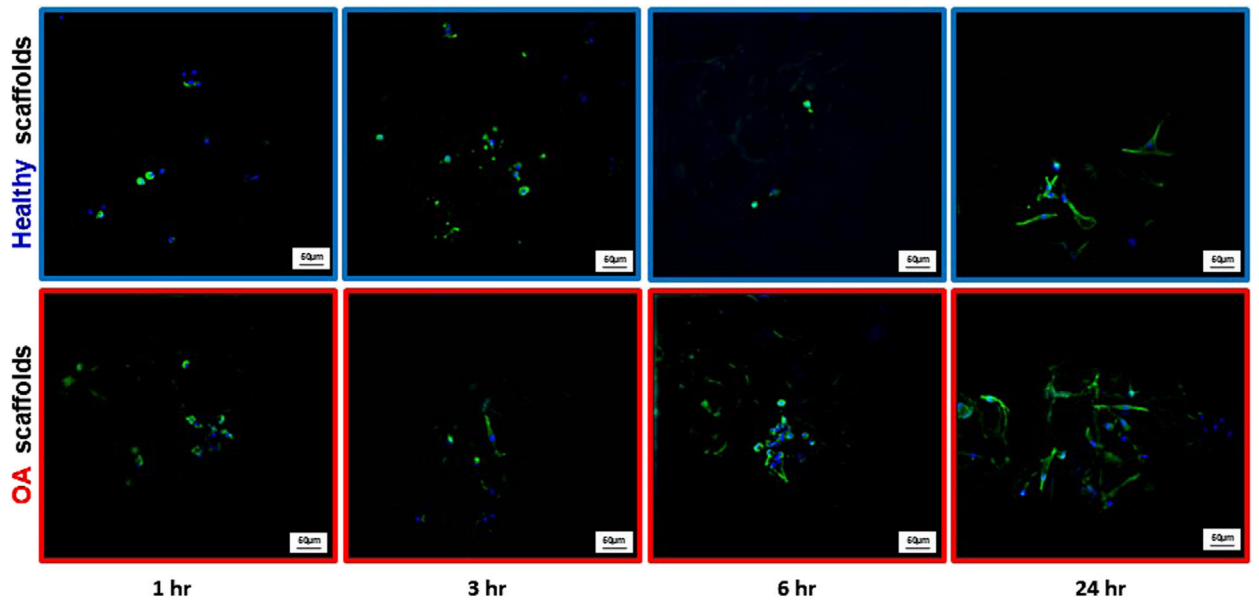

FIGURE 5
Representative images of actin (green) and DAPI (blue) staining of human meniscal cells seeded onto healthy and OA scaffolds.

3.3 Meniscus cellular responses on scaffolds

Actin immunostaining revealed the initial spherical shape of the human meniscus cells on both scaffold types at 1 and 3 h after seeding (Figure 5). For healthy scaffolds, the cells remained rounded at 6 h, while on the OA scaffolds the cells began to elongate. By 24 h, the cells appeared fibroblastic with cellular processes on both the healthy and OA scaffolds. Meniscus cells showed approximately 90% viability within both the healthy and OA scaffolds on both days 3 and 7 with no detectable differences between the scaffolds (Figures 6A,B). In both healthy and OA scaffolds, meniscus cells were more proliferative at day 4 than day 14 (Figures 7A,B, $p < 0.05$). There were no detectable differences in cellular proliferation between scaffold types.

3.4 Biochemical changes in meniscus cell seeded scaffolds

The DNA content of meniscus cell-seeded healthy and OA scaffolds was significantly increased over 14 days (Figure 8A, $p <$

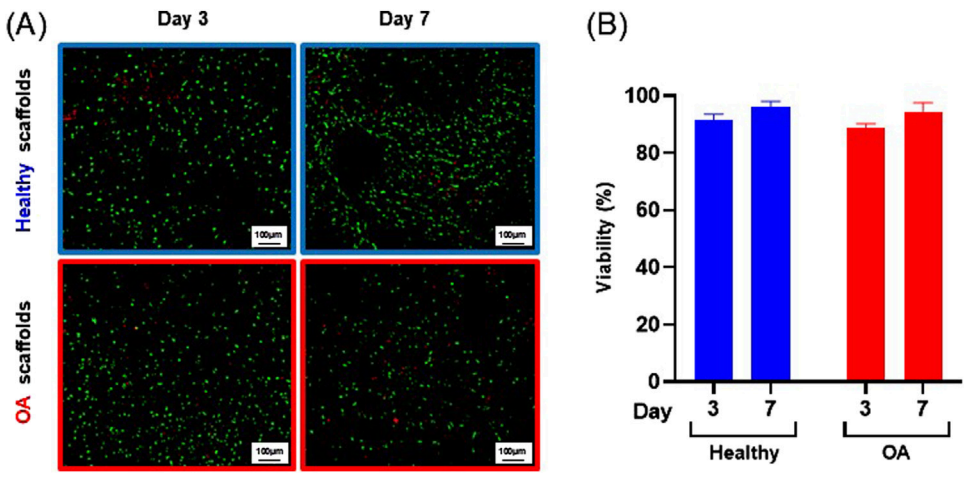

FIGURE 6
(A) Representative images of live (green) and dead (red) human meniscal cells seeded onto healthy and OA scaffolds. **(B)** Percent viability of cells on healthy and OA scaffolds. Data are expressed as the mean +SEM for all groups.

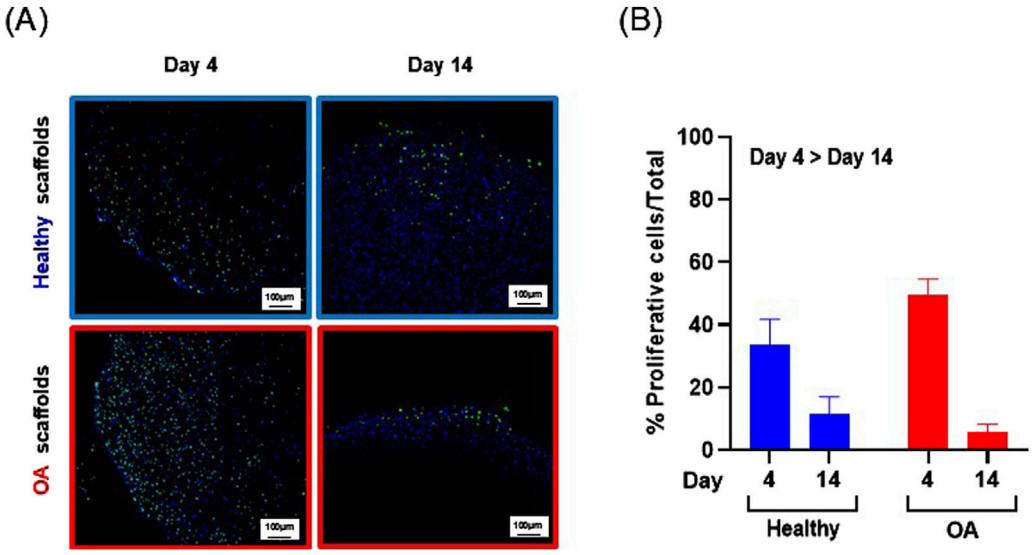

FIGURE 7
(A) Representative images of Edu+ (green) cells and total (blue) human meniscus cells seeded on healthy and OA scaffolds. **(B)** Percent proliferative cells per total cells on healthy and OA scaffolds. Data is expressed as the mean +SEM for all groups.

0.0001). Overall meniscus cell-seeded OA scaffolds contained higher DNA content than healthy scaffolds ($p < 0.05$). Generally, CCK-8 measurements, indicative of viable cell number, significantly increased over the 14 days of culture for both scaffolds (Figure 8B, $p < 0.0001$). However, there were no detectable differences in CCK-8 between OA and healthy scaffolds. sGAG content trended towards an increase from days 7–14 for both meniscus cell-seeded scaffold types (Figure 8C). There were no detectable differences in collagen content between scaffold types or over time in meniscus cell-seeded scaffolds (Figure 8D).

3.5 Meniscus cellular responses in the *ex vivo* defect model

Fluorescent imaging on day 7 demonstrated that cells were located throughout the meniscus tissue outer ring but not in the healthy and OA scaffold inner cores (Figure 9). On day 14, while no cells were detectable in the healthy scaffolds, there were meniscus cells that had migrated from the outer ring into the edge of the implanted OA scaffold. On day 21 few cells had migrated into the healthy scaffolds but there were abundant meniscal cells distributed throughout the OA scaffolds. By day 28, both scaffold groups

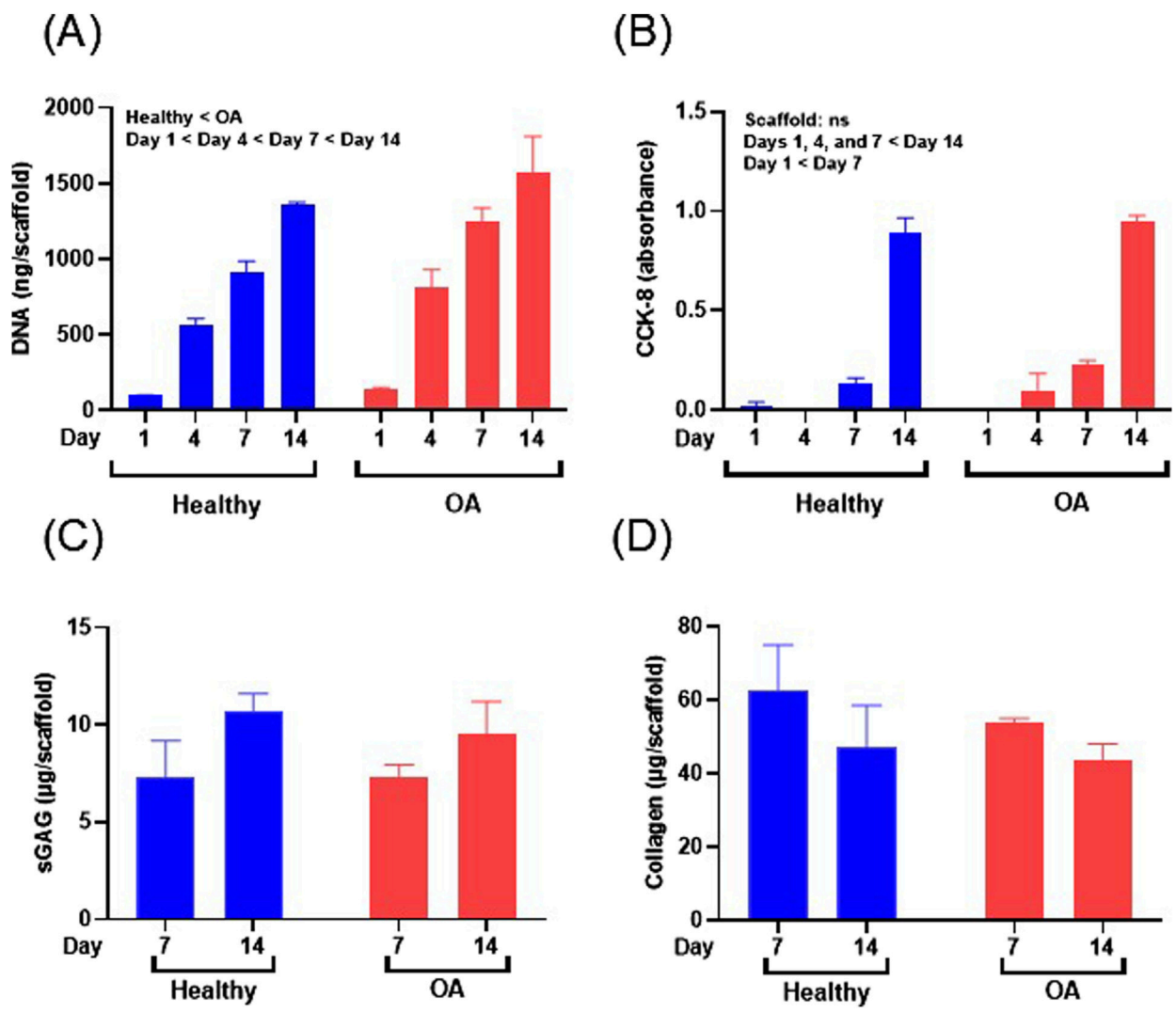

FIGURE 8
(A) DNA content, **(B)** CCK-8, **(C)** sGAG, and **(D)** collagen content of human meniscus cell-seeded healthy and OA scaffolds. Data are expressed as the mean +SEM for all groups.

showed cellular infiltration throughout the core and at the interface between the outer ring and inner core. However, there was greater visible cellular bridging between the inner core scaffolds and the outer ring meniscus tissue in the Healthy + Meniscus samples than the OA + Meniscus samples.

3.6 Biochemical and shear strength evaluation in the *ex vivo* defect model

After 28 days of culture in the *ex vivo* repair model, there were no detectable differences between the DNA (Figure 10A), sGAG (Figure 10B), or collagen (Figure 10C) content between the healthy and OA scaffolds. However, the shear strength of repair was significantly lower in the defects filled with OA scaffolds compared to defects filled with healthy scaffolds (Figure 10D, $p < 0.005$).

3.7 Histological analysis of the *ex vivo* defect model

Histological analysis revealed that both the healthy and OA scaffolds integrated with the surrounding meniscus tissue (Figure 10E). While proteoglycan staining was detectable in the surrounding meniscus tissue, the healthy and OA scaffolds predominately stained for collagen. Both scaffold types were porous; however, there was more collagenous matrix present in the healthy scaffolds compared to the OA scaffolds.

4 Discussion

To our knowledge, this is the first study to compare the biocompatibility and functionality of healthy and OA MDM scaffolds that have potential for clinical practice as a cell-free

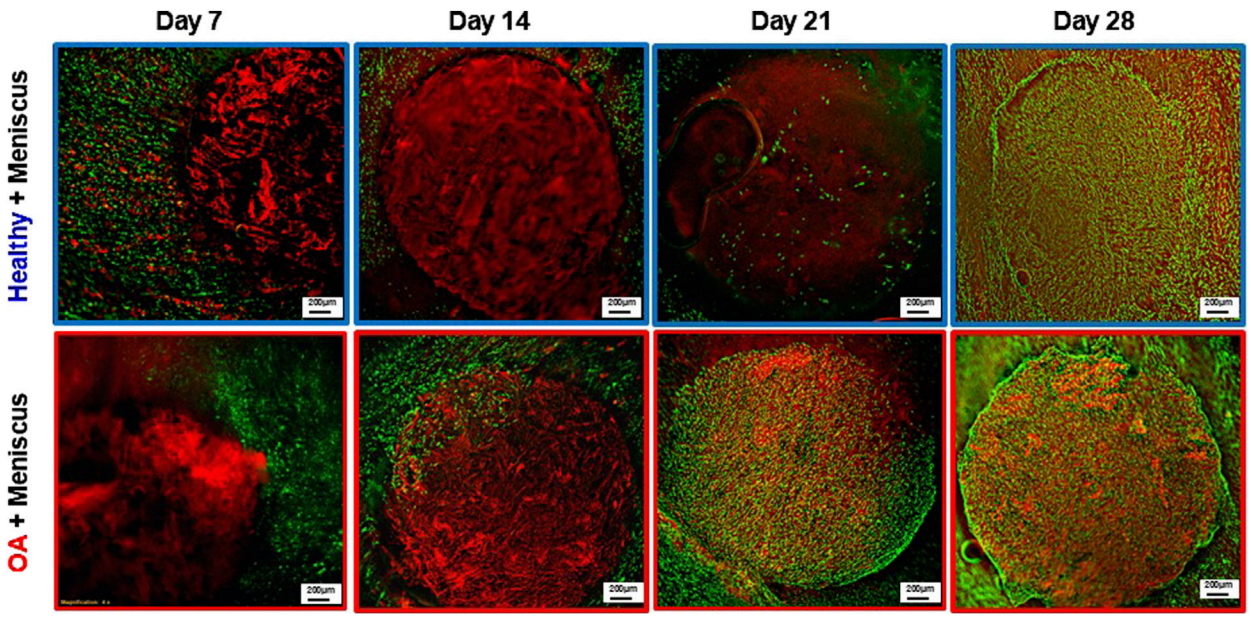

FIGURE 9
Representative fluorescent images of the Healthy scaffold + Meniscus and OA scaffold + Meniscus in the *ex vivo* defect model. Live cells (green) and matrix (red) are stained.

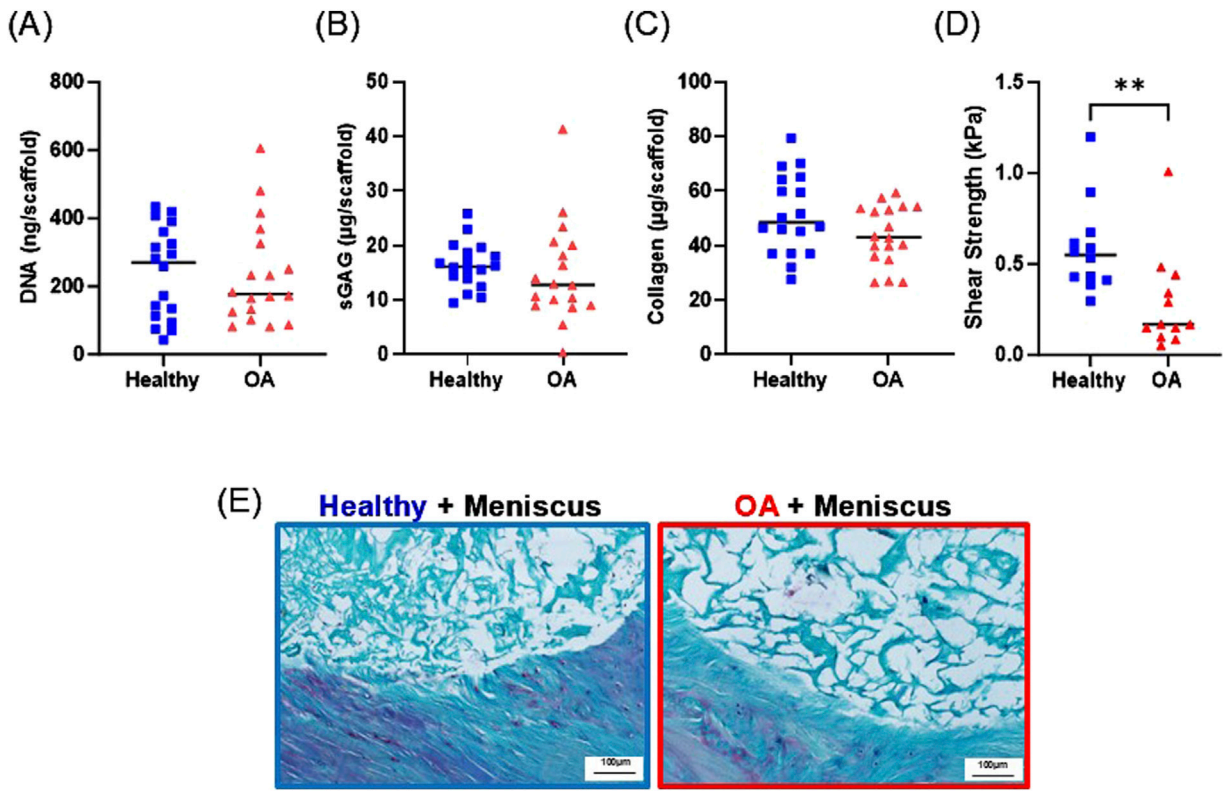

FIGURE 10
Day 28 **(A)** DNA, **(B)** sGAG, and **(C)** collagen content of healthy and OA scaffolds from the *ex vivo* meniscus defect model. **(D)** Shear strength of repair of the meniscus defect model. $^{**}p < 0.005$. The mean is indicated by a line for each group. **(E)** Representative histological staining of the interface of the meniscus defect model explants. Sections were stained with Safranin-O (red: proteoglycans), fast green (blue: collagen), and hematoxylin (black: nuclei).

tissue engineering strategy. Overall, we found that both healthy and OA scaffolds are biocompatible and promote cellular infiltration and growth. However, there was a significant difference in the functionality of the healthy and OA scaffolds based on the shear strength of repair, which quantifies the amount of healing between the meniscus tissue and the MDM scaffolds. Importantly, the shear strength of repair was reduced in meniscus defects containing OA scaffolds compared to healthy scaffolds, suggesting that the healthy scaffolds are promising for meniscus tissue engineering. In conclusion, we have shown that healthy human allograft tissue is a useful source for generating MDM scaffolds that can support cellular growth, ECM production, and *ex vivo* integrative repair of the meniscus, highlighting their suitability for future *in vivo* investigations.

In this study, we initially compared healthy and OA meniscus tissue. As expected (Pauli et al., 2011; Waldstein et al., 2016), OA tissue had higher gross grading scores than healthy tissue due to ECM disruption and meniscus tears. Furthermore, OA tissue contained regions of hypercellularity, which was consistent with the higher DNA content in the OA scaffolds prior to decellularization. Histologically, there were differences in Safranin-O staining in healthy *versus* OA tissue, but this difference was not statistically significant in the biochemical analysis of the MDM scaffolds. Much of the damage in the OA tissues was localized to the inner zone or resulted in the loss of the inner zone of the meniscus. Thus, due to the challenges of reproducibly identifying the inner zone and having enough remaining inner zone tissue for scaffold preparation, we used the whole meniscus to fabricate the scaffolds. It would be interesting to investigate the effects of zonal differences between healthy and OA scaffolds in the future.

The overall goal of this study was to compare healthy and OA scaffolds, but we were unable to remove age as a biological variable due to the patient populations. The OA tissues came from older donors than the healthy tissues. In this study, we cannot determine what differences in the scaffolds are specifically due to age-related changes *versus* osteoarthritis-related changes. Regardless, we were able to directly compare scaffolds generated from both healthy and OA meniscus tissues and show that there are functional differences between these scaffolds for meniscus tissue engineering applications.

To facilitate clinical translation of tissue engineering scaffolds, decellularization is necessary to reduce potential immunologic responses (Ahmed et al., 1983). The ideal decellularization is achieved when nucleic acid content is reduced, and the quantity and structure of ECM components are retained. In our prior work (Ruprecht et al., 2019; Lyons et al., 2019), we relied on loss of DNA content throughout cell culture; however, this prevents scaffolds from being implanted without prior culture. In this study, a new protocol was developed for the fabrication of decellularized MDM scaffolds from healthy and OA human menisci. Our decellularization method used a combined physical and enzymatic approach, which was effective at reducing the DNA content and retaining the majority of the major ECM components for both healthy and OA scaffolds. Following decellularization, on average each scaffold contained approximately 0.03 μg DNA/mg, which is a lower DNA concentration than several commercially available products used in patients, including MatriStem (1.56 μg/mg), which is a urinary bladder matrix, small intestinal submucosa (1.46 μg/mg), and XenMatrix (0.06 μg/mg), which is a dermis tissue (Huleihel et al., 2016). While the majority of sGAGs are preserved during our scaffold fabrication process, similar to prior studies (Rothrauff et al., 2017; Visser et al., 2015; Wu et al., 2015; Monibi and Cook, 2017), we experienced some loss of proteoglycans during our decellularization. Prior work has also revealed alterations in collagen content due to decellularization (Kasravi et al., 2023) but this was retained in both our healthy and OA MDM scaffolds.

Our *in vitro* results revealed that primary human meniscus cells attached, proliferated, were metabolically active, and retained ECM on both healthy and OA scaffolds for up to 14 days. Interestingly, the cellular responses were more promising on the OA scaffolds. Meniscus cells were able to spread into a fibroblastic morphology more quickly on the OA scaffolds compared to healthy scaffolds. This suggests that the OA scaffolds provide more adhesion sites and/or signaling cues for the cells, enhancing cell-biomaterial interactions (Goyal et al., 2017). Given that the cells were isolated from OA meniscus tissues, these cells may be primed for attachment to the adhesion sites in the OA scaffolds. Consistent with this difference in attachment, DNA content was higher in OA cell-seeded scaffolds throughout *in vitro* culture. Despite this observation, DNA content and CCK-8 measurements significantly increased over the 14 days in culture for both the healthy and OA scaffolds. In addition, there was high meniscus cell viability over time on both healthy and OA scaffolds. However, there was a decrease in the percent proliferative cells from day 4 to day 14 in both healthy and OA scaffolds. Notably, the proliferative cells were detected throughout the scaffolds on day 4; however, they were predominantly localized to the edges of the scaffolds on day 14. The change in location and number of proliferative cells over time is likely driven by cellular crowding within the interior of the scaffolds over time, resulting in reduced overall proliferation of the cells. Furthermore, ECM cues that drive proliferation (Sohrabi et al., 2023) may be less accessible at later times in culture. However, cellular growth and metabolic activity over time highlight the biocompatibility of the scaffolds. In future studies, it would be interesting to assess the gene expression profiles of meniscus cells on the scaffolds to understand transcriptomic changes in response to the healthy and OA scaffolds.

Both healthy and OA cell-seeded scaffolds produced similar amounts of sGAG throughout *in vitro* culture. However, there was an initial loss of GAG content that was likely due to leaching of the proteoglycans into the culture media from the scaffolds, which is similar to the phenomenon that is observed in meniscus explant culture (McNulty et al., 2010; Nishimuta and Levenston, 2012). Our prior work has shown that cross-linking of the MDM scaffolds can help to preserve the sGAG content (Lyons et al., 2019; Ruprecht et al., 2019) and may be useful to enhance retention of scaffold sGAGs in future studies. However, the sGAG content was trending towards an increase from days 7–14, indicating that the meniscus cells were able to synthesize new sGAGs that were incorporated into the scaffolds. These findings are similar to other work using PCL-meniscus ECM based hydrogel hybrid scaffolds or

PCL nanofibrous scaffolds seeded with bovine meniscus cells, which showed a gradual increase in sGAG content over 14 days (Chen et al., 2019; Xia et al., 2021). Most promising is that in both healthy and OA scaffolds, meniscus cells secreted sGAGs that were retained during culture, which is an important feature for meniscus repair and regeneration.

The collagen content of both the healthy and OA cell-seeded scaffolds remained stable over the 14 days in culture. This data is consistent with another study that evaluated collagen content in meniscus cell-seeded ECM-PCL nanofibrous scaffolds after 2 weeks (Xia et al., 2021). Overall, both heathy and OA scaffolds can support collagen maintenance and/or production during culture.

Healthy and OA scaffolds showed nearly equivalent biochemical content but vastly different integrative shear strength of repair between the scaffold and native meniscus tissue in the *ex vivo* meniscus defect model. In native meniscus tissue, the dense collagen network is a barrier for cell migration to sites of meniscus injury (Qu et al., 2019; Qu et al., 2018). In our previous work, we showed that fabrication of the scaffolds with MDM powder leads to a porous structure that facilitates meniscus cell migration into the MDM scaffolds from the porcine meniscus tissue (Ruprecht et al., 2019; Lyons et al., 2019). We took advantage of this successful approach to compare human meniscus cell responses to healthy and OA scaffolds in a human *ex vivo* meniscus defect model. Cells from the meniscus tissue were initially able to migrate into the OA scaffolds more rapidly than the healthy scaffolds, suggesting that the OA scaffolds provide more chemotactic factors and/or adhesion sites (Goyal et al., 2017) to attract and adhere native meniscus cells. However, in both scaffold types, meniscal cells were viable over the 4 weeks in culture and native cells migrating from the surrounding meniscus tissue filled the interface and scaffolds. In our previous work, the addition of exogenous cells and scaffold cross-linking were not necessary to promote meniscus tissue repair (Ruprecht et al., 2019); therefore, we employed a cell-free approach and used non cross-linked scaffolds in this study. In this human *ex vivo* model system, without exogenous growth factors, both healthy and OA scaffolds promoted cellular migration into the scaffolds. However, the shear strength of repair was significantly lower in defects containing the OA scaffolds compared to the healthy scaffolds. This reduced shear strength in the OA scaffolds may be due to tissue health and/or age-related changes in the matrix integrity and composition of these scaffolds. While biochemically the healthy and OA scaffolds appeared similar, grossly and histologically it is clear that the OA tissue was more degraded and contained less proteoglycans. Furthermore, there are likely alterations in many other biochemical components in the OA tissue and scaffolds that were not quantified in this study. Additionally, the healthy scaffolds in the meniscus defect model showed more collagenous matrix histologically, which likely contributed to improved repair strength. In the future, proteomic analyses will be necessary to assess the compositional differences between the healthy and OA MDM scaffolds to determine the biochemical changes that may affect the functionality of the scaffolds.

A higher shear strength of repair is desired to improve clinical meniscus repair, as this indicates that the repair tissue can withstand greater mechanical forces. The repair strength of the healthy human MDM scaffolds in the *ex vivo* meniscus defect model was lower than previously observed for porcine MDM scaffolds in an *ex vivo* porcine meniscus defect model after 28 days (Ruprecht et al., 2019). This finding may be due to the use of human meniscus tissue from older patients with end stage osteoarthritis in this study. This older, OA tissue is likely not very metabolically active or amenable to repair. On the other hand, in our porcine work the tissue was from 2 to 3 year old pigs without remarkable OA changes (Ruprecht et al., 2019). Therefore, it would be interesting to see if the repair responses were improved in non-OA, acutely injured human meniscus tissue, which would likely be more amenable to meniscus repair. Additionally, a longer time in culture may increase cellular numbers in the scaffolds and improve ECM synthesis by these migrated cells (Hennerbichler et al., 2007b; Ionescu and Mauck, 2013). Furthermore, infiltration of the scaffolds by exogenous stem cells (Mandal et al., 2011b), structural modification of the scaffolds using cell adhesion motifs (Xu et al., 2020), cross-linking (Lyons et al., 2019), or coating with polymers or nanoparticle solutions (Li et al., 2021b) may further enhance cell migration and ECM synthesis but may impede translatability for future clinical applications. Additional studies will be necessary to determine if any of these modifications can further improve tissue repair.

In this study, we compared healthy and OA human MDM scaffolds and revealed that while OA scaffolds showed slightly more favorable cellular growth *in vitro*, both scaffold types were biocompatible and can provide a supportive environment for meniscal cells to attach, proliferate, and migrate but only the healthy MDM scaffolds could facilitate repair with native meniscus tissue. Therefore, healthy human allograft tissue is a useful source for generating MDM scaffolds that can support cellular growth, ECM production, and *ex vivo* integrative repair of the meniscus. Our findings highlight the suitability of the healthy MDM scaffolds for future testing in *in vivo* preclinical models for meniscus repair.

Data availability statement

The original contributions presented in the study are included in the article/supplementary material, further inquiries can be directed to the corresponding author.

Ethics statement

The studies involving humans were approved by Duke University Health System Institutional Review Board. The studies were conducted in accordance with the local legislation and institutional requirements. The human samples used in this study were acquired from a by- product of routine care or industry. Written informed consent for participation was not required from the participants or the participants' legal guardians/next of kin in accordance with the national legislation and institutional requirements.

Author contributions

SF: Formal Analysis, Investigation, Methodology, Writing–original draft, Writing–review and editing. JL: Data curation, Formal Analysis, Investigation, Writing–review and editing. DC: Data curation, Formal Analysis, Investigation, Methodology, Writing–review and editing. DA: Resources, Writing–review and editing. SW: Resources, Writing–review and editing. AA: Resources, Writing–review and editing. AM: Conceptualization, Data curation, Formal Analysis, Funding acquisition, Methodology, Project administration, Resources, Supervision, Validation, Writing–original draft, Writing–review and editing.

Funding

The author(s) declare that financial support was received for the research, authorship, and/or publication of this article. Research funding for this project was provided in part by NIH grants AR078245 and AR073221.

Acknowledgments

We thank Drs. Michael Bolognesi and William Jiranek for providing OA meniscus tissue. This research was made possible by the donation of allograft tissue from JRF Ortho.

Conflict of interest

The authors declare that the research was conducted in the absence of any commercial or financial relationships that could be construed as a potential conflict of interest.

Publisher's note

All claims expressed in this article are solely those of the authors and do not necessarily represent those of their affiliated organizations, or those of the publisher, the editors and the reviewers. Any product that may be evaluated in this article, or claim that may be made by its manufacturer, is not guaranteed or endorsed by the publisher.

References

Ahmed, A., Burke, D., and Yu, A. (1983). *In-vitro* measurement of static pressure distribution in synovial joints—part II: retropatellar surface. *J. Biomech. Eng.* 105, 226–236. doi:10.1115/1.3138410

Ahn, G., Min, K.-H., Kim, C., Lee, J.-S., Kang, D., Won, J.-Y., et al. (2017). Precise stacking of decellularized extracellular matrix based 3D cell-laden constructs by a 3D cell printing system equipped with heating modules. *Sci. Rep.* 7, 8624. doi:10.1038/s41598-017-09201-5

An, Y. H., Kim, J. A., Yim, H. G., Han, W. J., Park, Y. B., Jin Park, H., et al. (2021). Meniscus regeneration with injectable Pluronic/PMMA-reinforced fibrin hydrogels in a rabbit segmental meniscectomy model. *J. Tissue Eng.* 12, 20417314211050141. doi:10.1177/20417314211050141

Andress, B. D., Irwin, R. M., Puranam, I., Hoffman, B. D., and McNulty, A. L. (2022). A tale of two loads: modulation of IL-1 induced inflammatory responses of meniscal cells in two models of dynamic physiologic loading. *Front. Bioeng. Biotechnol.* 10, 837619. doi:10.3389/fbioe.2022.837619

Andress, B., Kim, J. H., Cutcliffe, H. C., Amendola, A., Goode, A. P., Varghese, S., et al. (2021). Meniscus cell regional phenotypes: dedifferentiation and reversal by biomaterial embedding. *J. Orthop. Research®* 39, 2177–2186. doi:10.1002/jor.24954

Badlani, J. T., Borrero, C., Golla, S., Harner, C. D., and Irrgang, J. J. (2013). The effects of meniscus injury on the development of knee osteoarthritis: data from the osteoarthritis initiative. *Am. J. sports Med.* 41, 1238–1244. doi:10.1177/0363546513490276

Baek, J., Chen, X., Sovani, S., Jin, S., Grogan, S. P., and D'Lima, D. D. (2015). Meniscus tissue engineering using a novel combination of electrospun scaffolds and human meniscus cells embedded within an extracellular matrix hydrogel. *J. Orthop. Res.* 33, 572–583. doi:10.1002/jor.22802

Baek, J., Sovani, S., Glembotski, N. E., DU, J., Jin, S., Grogan, S. P., et al. (2016). Repair of avascular meniscus tears with electrospun collagen scaffolds seeded with human cells. *Tissue Eng. Part A* 22, 436–448. doi:10.1089/ten.tea.2015.0284

Bakarich, S. E., Gorkin, R., Het Panhuis, M., and Spinks, G. M. (2014). Three-dimensional printing fiber reinforced hydrogel composites. *ACS Appl. Mater. and interfaces* 6, 15998–16006. doi:10.1021/am503878d

Bansal, S., Floyd, E. R., A Kowalski, M., Aikman, E., Elrod, P., Burkey, K., et al. (2021). Meniscal repair: the current state and recent advances in augmentation. *J. Orthop. Research®* 39, 1368–1382. doi:10.1002/jor.25021

Blake, M. H., and Johnson, D. L. (2018). Knee meniscus injuries: common problems and solutions. *Clin. sports Med.* 37, 293–306. doi:10.1016/j.csm.2017.12.007

Carter, T. E., Taylor, K. A., Spritzer, C. E., Utturkar, G. M., Taylor, D. C., Moorman III, C. T., et al. (2015). *In vivo* cartilage strain increases following medial meniscal tear and correlates with synovial fluid matrix metalloproteinase activity. *J. biomechanics* 48, 1461–1468. doi:10.1016/j.jbiomech.2015.02.030

Chen, M., Feng, Z., Guo, W., Yang, D., Gao, S., Li, Y., et al. (2019). PCL-MECM-based hydrogel hybrid scaffolds and meniscal fibrochondrocytes promote whole meniscus regeneration in a rabbit meniscectomy model. *ACS Appl. Mater. and interfaces* 11, 41626–41639. doi:10.1021/acsami.9b13611

Chen, R., Zhao, H., Ai, L., Zhang, J., and Jiang, D. (2024). Inhibiting T-cell-mediated rejection of the porcine meniscus through freeze-thawing and downregulating porcine xenoreactive antigen genes. *Cell. Transpl.* 33, 9636897241273689. doi:10.1177/09636897241273689

Chevrier, A., Farr, J., Rodeo, S. A., and Buschmann, M. D. (2018). Augmentation techniques for meniscus repair. *J. knee Surg.* 31, 099–116. doi:10.1055/s-0037-1602247

Collins, A. T., Hatcher, C. C., Kim, S. Y., Ziemian, S. N., Spritzer, C. E., Guilak, F., et al. (2019). Selective enzymatic digestion of proteoglycans and collagens alters cartilage T1rho and T2 relaxation times. *Ann. Biomed. Eng.* 47, 190–201. doi:10.1007/s10439-018-02143-7

Englund, M., Guermazi, A., and Lohmander, S. L. (2009). The role of the meniscus in knee osteoarthritis: a cause or consequence? *Radiol. Clin.* 47, 703–712. doi:10.1016/j.rcl.2009.03.003

Farndale, R. W., Buttle, D. J., and Barrett, A. J. (1986). Improved quantitation and discrimination of sulphated glycosaminoglycans by use of dimethylmethylene blue. *Biochimica Biophysica Acta (BBA)-General Subj.* 883, 173–177. doi:10.1016/0304-4165(86)90306-5

Fox, A. J., Bedi, A., and Rodeo, S. A. (2012). The basic science of human knee menisci: structure, composition, and function. *Sports health* 4, 340–351. doi:10.1177/1941738111429419

Gao, S., Guo, W., Chen, M., Yuan, Z., Wang, M., Zhang, Y., et al. (2017). Fabrication and characterization of electrospun nanofibers composed of decellularized meniscus extracellular matrix and polycaprolactone for meniscus tissue engineering. *J. Mater. Chem. B* 5, 2273–2285. doi:10.1039/c6tb03299k

Gelse, K., Körber, L., Schöne, M., Raum, K., Koch, P., Pachowsky, M., et al. (2017). Transplantation of chemically processed decellularized meniscal allografts: a pilot sheep study. *Cartilage* 8, 180–190. doi:10.1177/1947603516646161

Goyal, R., Vega, M. E., Pastino, A. K., Singh, S., Guvendiren, M., Kohn, J., et al. (2017). Development of hybrid scaffolds with natural extracellular matrix deposited within synthetic polymeric fibers. *J. Biomed. Mater. Res. Part A* 105, 2162–2170. doi:10.1002/jbm.a.36078

Grogan, S. P., Chung, P. H., Soman, P., Chen, P., Lotz, M. K., Chen, S., et al. (2013). Digital micromirror device projection printing system for meniscus tissue engineering. *Acta biomater.* 9, 7218–7226. doi:10.1016/j.actbio.2013.03.020

Guo, W., Chen, M., Wang, Z., Tian, Y., Zheng, J., Gao, S., et al. (2021). 3D-printed cell-free PCL–MECM scaffold with biomimetic micro-structure and micro-environment to enhance *in situ* meniscus regeneration. *Bioact. Mater.* 6, 3620–3633. doi:10.1016/j.bioactmat.2021.02.019

Guo, W., Liu, S., Zhu, Y., Yu, C., Lu, S., Yuan, M., et al. (2015). Advances and prospects in tissue-engineered meniscal scaffolds for meniscus regeneration. *Stem Cells Int.* 2015, 1–13. doi:10.1155/2015/517520

Hatcher, C. C., Collins, A. T., Kim, S. Y., Michel, L. C., Mostertz III, W. C., Ziemian, S. N., et al. (2017). Relationship between T1rho magnetic resonance imaging, synovial fluid biomarkers, and the biochemical and biomechanical properties of cartilage. *J. biomechanics* 55, 18–26. doi:10.1016/j.jbiomech.2017.02.001

Hennerbichler, A., Moutos, F. T., Hennerbichler, D., Weinberg, J. B., and Guilak, F. (2007a). Interleukin-1 and tumor necrosis factor alpha inhibit repair of the porcine meniscus *in vitro*. *Osteoarthr. Cartil.* 15, 1053–1060. doi:10.1016/j.joca.2007.03.003

Hennerbichler, A., Moutos, F. T., Hennerbichler, D., Weinberg, J. B., and Guilak, F. (2007b). Repair response of the inner and outer regions of the porcine meniscus *in vitro*. *Am. J. sports Med.* 35, 754–762. doi:10.1177/0363546506296416

Huleihel, L., Hussey, G. S., Naranjo, J. D., Zhang, L., Dziki, J. L., Turner, N. J., et al. (2016). Matrix-bound nanovesicles within ECM bioscaffolds. *Sci. Adv.* 2, e1600502. doi:10.1126/sciadv.1600502

Hussey, G. S., Dziki, J. L., and Badylak, S. F. (2018). Extracellular matrix-based materials for regenerative medicine. *Nat. Rev. Mater.* 3, 159–173. doi:10.1038/s41578-018-0023-x

Ionescu, L. C., and Mauck, R. L. (2013). Porosity and cell preseeding influence electrospun scaffold maturation and meniscus integration *in vitro*. *Tissue Eng. Part A* 19, 538–547. doi:10.1089/ten.tea.2012.0052

Jiang, D., Zhang, Z.-Z., Zhao, F., Wang, S.-J., Qi, Y.-S., Zhao, L.-H., et al. (2018). The radiated deep-frozen xenogenic meniscal tissue regenerated the total meniscus with chondroprotection. *Sci. Rep.* 8, 9041. doi:10.1038/s41598-018-27016-w

Kasravi, M., Ahmadi, A., Babajani, A., Mazloomnejad, R., Hatamnejad, M. R., Shariatzadeh, S., et al. (2023). Immunogenicity of decellularized extracellular matrix scaffolds: a bottleneck in tissue engineering and regenerative medicine. *Biomaterials Res.* 27, 10–24. doi:10.1186/s40824-023-00348-z

Komatsu, D., Cabrera, A. R. E., Quevedo, B. V., Asami, J., Cristina Motta, A., DE Moraes, S. C., et al. (2024). Meniscal repair with additive manufacture of bioresorbable polymer: from physicochemical characterization to implantation of 3D printed poly (L-co-D, L lactide-co-trimethylene carbonate) with autologous stem cells in rabbits. *J. Biomater. Appl.* 39, 66–79. doi:10.1177/08853282241248517

Kremers, H. M., Larson, D. R., Crowson, C. S., Kremers, W. K., Washington, R. E., Steiner, C. A., et al. (2015). Prevalence of total hip and knee replacement in the United States. *J. bone Jt. Surg. Am. volume* 97, 1386–1397. doi:10.2106/jbjs.n.01141

Lian, L., Xie, M., Luo, Z., Zhang, Z., Maharjan, S., Mu, X., et al. (2024). Rapid volumetric bioprinting of decellularized extracellular matrix bioinks. *Adv. Mater* 36, e2304846. doi:10.1002/adma.202304846

Li, H., Wang, X., Liu, J., Liu, Z., Wang, H., Mo, X., et al. (2021a). Nanofiber configuration affects biological performance of decellularized meniscus extracellular matrix incorporated electrospun scaffolds. *Biomed. Mater* 16, 065013. doi:10.1088/1748-605x/ac28a5

Lin, D. D., Picardo, N. E., Adesida, A., and Khan, W. S. (2017). Clinical studies using biological and synthetic materials for meniscus replacement. *Curr. Stem Cell. Res. and Ther.* 12, 348–353. doi:10.2174/1574888x11666160429123110

Li, Y., Chen, M., Yan, J., Zhou, W., Gao, S., Liu, S., et al. (2021b). Tannic acid/Sr2+-coated silk/graphene oxide-based meniscus scaffold with anti-inflammatory and anti-ROS functions for cartilage protection and delaying osteoarthritis. *Acta Biomater.* 126, 119–131. doi:10.1016/j.actbio.2021.02.046

Lohmander, L. S., Englund, P. M., Dahl, L. L., and Roos, E. M. (2007). The long-term consequence of anterior cruciate ligament and meniscus injuries: osteoarthritis. *Am. J. sports Med.* 35, 1756–1769. doi:10.1177/0363546507307396

Luvsannyam, E., Jain, M. S., Leitao, A. R., Maikawa, N., and Leitao, A. E. (2022). Meniscus tear: pathology, incidence, and management. *Cureus* 14, e25121. doi:10.7759/cureus.25121

Lyons, L. P., Hidalgo Perea, S., Weinberg, J. B., Wittstein, J. R., and McNulty, A. L. (2019). Meniscus-derived matrix bioscaffolds: effects of concentration and cross-linking on meniscus cellular responses and tissue repair. *Int. J. Mol. Sci.* 21, 44. doi:10.3390/ijms21010044

Makris, E. A., Hadidi, P., and Athanasiou, K. A. (2011). The knee meniscus: structure–function, pathophysiology, current repair techniques, and prospects for regeneration. *Biomaterials* 32, 7411–7431. doi:10.1016/j.biomaterials.2011.06.037

Mandal, B. B., Park, S.-H., Gil, E. S., and Kaplan, D. L. (2011a). Multilayered silk scaffolds for meniscus tissue engineering. *Biomaterials* 32, 639–651. doi:10.1016/j.biomaterials.2010.08.115

Mandal, B. B., Park, S.-H., Gil, E. S., and Kaplan, D. L. (2011b). Stem cell-based meniscus tissue engineering. *Tissue Eng. Part A* 17, 2749–2761. doi:10.1089/ten.tea.2011.0031

Markolf, K. L., Bargar, W. L., Shoemaker, S. C., and Amstutz, H. C. (1981). The role of joint load in knee stability. *JBJS* 63, 570–585. doi:10.2106/00004623-198163040-00007

McNulty, A. L., Estes, B. T., Wilusz, R. E., Weinberg, J. B., and Guilak, F. (2010). Dynamic loading enhances integrative meniscal repair in the presence of interleukin-1. *Osteoarthr. Cartil.* 18, 830–838. doi:10.1016/j.joca.2010.02.009

McNulty, A. L., and Guilak, F. (2008). Integrative repair of the meniscus: lessons from *in vitro* studies. *Biorheology* 45, 487–500. doi:10.3233/bir-2008-0489

McNulty, A. L., Moutos, F. T., Weinberg, J. B., and Guilak, F. (2007). Enhanced integrative repair of the porcine meniscus *in vitro* by inhibition of interleukin-1 or tumor necrosis factor α. *Arthritis and Rheumatism Official J. Am. Coll. Rheumatology* 56, 3033–3043. doi:10.1002/art.22839

McNulty, A. L., Rothfusz, N. E., Leddy, H. A., and Guilak, F. (2013). Synovial fluid concentrations and relative potency of interleukin-1 alpha and beta in cartilage and meniscus degradation. *J. Orthop. Res.* 31, 1039–1045. doi:10.1002/jor.22334

McNulty, A. L., Weinberg, J. B., and Guilak, F. (2009). Inhibition of matrix metalloproteinases enhances *in vitro* repair of the meniscus. *Clin. Orthop. Relat. Research®* 467, 1557–1567. doi:10.1007/s11999-008-0596-6

Monibi, F. A., and Cook, J. L. (2017). Tissue-derived extracellular matrix bioscaffolds: emerging applications in cartilage and meniscus repair. *Tissue Eng. Part B Rev.* 23, 386–398. doi:10.1089/ten.teb.2016.0431

Nishimuta, J. F., and Levenston, M. E. (2012). Response of cartilage and meniscus tissue explants to *in vitro* compressive overload. *Osteoarthr. Cartil.* 20, 422–429. doi:10.1016/j.joca.2012.01.004

Orlando, G., Booth, C., Wang, Z., Totonelli, G., Ross, C. L., Moran, E., et al. (2013). Discarded human kidneys as a source of ECM scaffold for kidney regeneration technologies. *Biomaterials* 34, 5915–5925. doi:10.1016/j.biomaterials.2013.04.033

Pati, F., Jang, J., Ha, D.-H., Won Kim, S., Rhie, J.-W., Shim, J.-H., et al. (2014). Printing three-dimensional tissue analogues with decellularized extracellular matrix bioink. *Nat. Commun.* 5, 3935. doi:10.1038/ncomms4935

Pauli, C., Grogan, S., Patil, S., Otsuki, S., Hasegawa, A., Koziol, J., et al. (2011). Macroscopic and histopathologic analysis of human knee menisci in aging and osteoarthritis. *Osteoarthr. Cartil.* 19, 1132–1141. doi:10.1016/j.joca.2011.05.008

Qu, F., Guilak, F., and Mauck, R. L. (2019). Cell migration: implications for repair and regeneration in joint disease. *Nat. Rev. Rheumatol.* 15, 167–179. doi:10.1038/s41584-018-0151-0

Qu, F., Li, Q., Wang, X., Cao, X., Zgonis, M. H., Esterhai, J. L., et al. (2018). Maturation state and matrix microstructure regulate interstitial cell migration in dense connective tissues. *Sci. Rep.* 8, 3295. doi:10.1038/s41598-018-21212-4

Ray, L. (2024). Joint replacement surgery. *Am. Coll. Rheumatology*. Available at: https://rheumatology.org/patients/joint-replacement-surgery (Accessed October 27, 2024).

Reddy, G. K., and Enwemeka, C. S. (1996). A simplified method for the analysis of hydroxyproline in biological tissues. *Clin. Biochem.* 29, 225–229. doi:10.1016/0009-9120(96)00003-6

Riera, K. M., Rothfusz, N. E., Wilusz, R. E., Weinberg, J., Guilak, F., and McNulty, A. L. (2011). Interleukin-1, tumor necrosis factor-alpha, and transforming growth factor-beta 1 and integrative meniscal repair: influences on meniscal cell proliferation and migration. *Arthritis Res. and Ther.* 13 (6), R187. doi:10.1186/ar3515

Rothrauff, B. B., Shimomura, K., Gottardi, R., Alexander, P. G., and Tuan, R. S. (2017). Anatomical region-dependent enhancement of 3-dimensional chondrogenic differentiation of human mesenchymal stem cells by soluble meniscus extracellular matrix. *Acta biomater.* 49, 140–151. doi:10.1016/j.actbio.2016.11.046

Rowland, C. R., Colucci, L. A., and Guilak, F. (2016). Fabrication of anatomically-shaped cartilage constructs using decellularized cartilage-derived matrix scaffolds. *Biomaterials* 91, 57–72. doi:10.1016/j.biomaterials.2016.03.012

Rowland, C. R., Lennon, D. P., Caplan, A. I., and Guilak, F. (2013). The effects of crosslinking of scaffolds engineered from cartilage ECM on the chondrogenic differentiation of MSCs. *Biomaterials* 34, 5802–5812. doi:10.1016/j.biomaterials.2013.04.027

Ruprecht, J. C., Waanders, T. D., Rowland, C. R., Nishimuta, J. F., Glass, K. A., Stencel, J., et al. (2019). Meniscus-derived matrix scaffolds promote the integrative repair of meniscal defects. *Sci. Rep.* 9, 8719. doi:10.1038/s41598-019-44855-3

Salinas-Fernandez, S., Garcia, O., Kelly, D. J., and Buckley, C. T. (2024). The influence of pH and salt concentration on the microstructure and mechanical properties of meniscus extracellular matrix-derived implants. *J. Biomed. Mater Res. A* 112, 359–372. doi:10.1002/jbm.a.37634

Scotti, C., Hirschmann, M. T., Antinolfi, P., Martin, I., and Peretti, G. M. (2013). Meniscus repair and regeneration: review on current methods and research potential. *Eur. cells and Mater.* 26, 150–170. doi:10.22203/ecm.v026a11

Shimomura, K., Rothrauff, B. B., and Tuan, R. S. (2017). Region-specific effect of the decellularized meniscus extracellular matrix on mesenchymal stem cell–based meniscus tissue engineering. *Am. J. sports Med.* 45, 604–611. doi:10.1177/0363546516674184

Sohrabi, A., Lefebvre, A. E., Harrison, M. J., Condro, M. C., Sanazzaro, T. M., Safarians, G., et al. (2023). Microenvironmental stiffness induces metabolic reprogramming in glioblastoma. *Cell. Rep.* 42, 113175. doi:10.1016/j.celrep.2023.113175

Solchaga, L. A., Tognana, E., Penick, K., Baskaran, H., Goldberg, V. M., Caplan, A. I., et al. (2006). A rapid seeding technique for the assembly of large cell/scaffold composite constructs. *Tissue Eng.* 12, 1851–1863. doi:10.1089/ten.2006.12.1851

Stone, K. R., Walgenbach, A., and Galili, U. (2017). Induced remodeling of porcine tendons to human anterior cruciate ligaments by α-GAL epitope removal and partial cross-linking. *Tissue Eng. Part B Rev.* 23, 412–419. doi:10.1089/ten.teb.2016.0332

Terzidis, I. P., Christodoulou, A., Ploumis, A., Givissis, P., Natsis, K., and Koimtzis, M. (2006). Meniscal tear characteristics in young athletes with a stable knee: arthroscopic evaluation. *Am. J. sports Med.* 34, 1170–1175. doi:10.1177/0363546506287939

Van Der Straeten, C., Byttebier, P., Eeckhoudt, A., and Victor, J. (2016). Meniscal allograft transplantation does not prevent or delay progression of knee osteoarthritis. *PLoS One* 11, e0156183. doi:10.1371/journal.pone.0156183

Venugopal, E., Rajeswaran, N., Sahanand, K. S., Bhattacharyya, A., and Rajendran, S. (2018). *In vitro* evaluation of phytochemical loaded electrospun gelatin nanofibers for application in bone and cartilage tissue engineering. *Biomed. Mater.* 14, 015004. doi:10.1088/1748-605x/aae3ef

Vignes, H., Conzatti, G., Hua, G., and Benkirane-Jessel, N. (2022). Meniscus repair: from *in vitro* research to patients. *Organoids* 1, 116–134. doi:10.3390/organoids1020010

Visser, J., Levett, P. A., Te Moller, N. C., Besems, J., Boere, K. W., Van Rijen, M. H., et al. (2015). Crosslinkable hydrogels derived from cartilage, meniscus, and tendon tissue. *Tissue Eng. part A* 21, 1195–1206. doi:10.1089/ten.tea.2014.0362

Waldstein, W., Perino, G., Gilbert, S. L., Maher, S. A., Windhager, R., and Boettner, F. (2016). OARSI osteoarthritis cartilage histopathology assessment system: a biomechanical evaluation in the human knee. *J. Orthop. Res.* 34, 135–140. doi:10.1002/jor.23010

Wang, B., Barceló, X., VON Euw, S., and Kelly, D. J. (2023). 3D printing of mechanically functional meniscal tissue equivalents using high concentration extracellular matrix inks. *Mater Today Bio* 20, 100624. doi:10.1016/j.mtbio.2023.100624

Wang, H., Wu, J., Yang, L., Liu, S., Sui, X., Guo, Q., et al. (2024). Surgical therapy and tissue engineering for meniscal repair. *Tissue Eng. Part B Rev*. doi:10.1089/ten.teb.2024.0060

Wilusz, R. E., Weinberg, J. B., Guilak, F., and McNulty, A. L. (2008). Inhibition of integrative repair of the meniscus following acute exposure to interleukin-1 *in vitro*. *J. Orthop. Res.* 26, 504–512. doi:10.1002/jor.20538

Wojtys, E. M., and Chan, D. B. (2005). Meniscus structure and function. *Instr. course Lect.* 54, 323–330.

Wu, J., Ding, Q., Dutta, A., Wang, Y., Huang, Y.-H., Weng, H., et al. (2015). An injectable extracellular matrix derived hydrogel for meniscus repair and regeneration. *Acta biomater.* 16, 49–59. doi:10.1016/j.actbio.2015.01.027

Xia, B., Kim, D.-H., Bansal, S., Bae, Y., Mauck, R. L., and Heo, S.-J. (2021). Development of a decellularized meniscus matrix-based nanofibrous scaffold for meniscus tissue engineering. *Acta biomater.* 128, 175–185. doi:10.1016/j.actbio.2021.03.074

Xu, H., Dai, Z., Zou, X., Xia, P., Aboudi, M. A., Wang, J., et al. (2020). A novel full-reduced HMGB1 and kartogenin-containing bio-active scaffold for meniscus regeneration. *bioRxiv* 2020 (03. 26), 010108. doi:10.1101/2020.03.26.010108

Yang, Y., Chen, Z., Song, X., Zhang, Z., Zhang, J., Shung, K. K., et al. (2017). Biomimetic anisotropic reinforcement architectures by electrically assisted nanocomposite 3D printing. *Adv. Mater. Deerf. Beach, Fla.* 29. doi:10.1002/adma.201605750

Yuan, X., Wei, Y., Villasante, A., Ng, J. J., Arkonac, D. E., Chao, P.-H. G., et al. (2017). Stem cell delivery in tissue-specific hydrogel enabled meniscal repair in an orthotopic rat model. *Biomaterials* 132, 59–71. doi:10.1016/j.biomaterials.2017.04.004

Yu, Z., Lili, J., Tiezheng, Z., Li, S., Jianzhuang, W., Haichao, D., et al. (2019). Development of decellularized meniscus extracellular matrix and gelatin/chitosan scaffolds for meniscus tissue engineering. *Bio-medical Mater. Eng.* 30, 125–132. doi:10.3233/bme-191038

frontiers | Frontiers in Cell and Developmental Biology

TYPE Original Research
PUBLISHED 28 January 2025
DOI 10.3389/fcell.2024.1511908

Check for updates

OPEN ACCESS

EDITED BY
Elizabeth Vinod,
Christian Medical College and Hospital, India

REVIEWED BY
Sandeep P. Dumbali,
Moffitt Cancer Center, United States
Simon Tew,
University of Liverpool, United Kingdom

*CORRESPONDENCE
Ilyas M. Khan,
i.m.khan@swansea.ac.uk

RECEIVED 15 October 2024
ACCEPTED 04 December 2024
PUBLISHED 28 January 2025

CITATION
Anderson-Watters M and Khan IM (2025) BMP9 induces postnatal zonal stratification of immature articular cartilage through reconfiguration of the existing collagen framework.
Front. Cell Dev. Biol. 12:1511908.
doi: 10.3389/fcell.2024.1511908

COPYRIGHT
© 2025 Anderson-Watters and Khan. This is an open-access article distributed under the terms of the Creative Commons Attribution License (CC BY). The use, distribution or reproduction in other forums is permitted, provided the original author(s) and the copyright owner(s) are credited and that the original publication in this journal is cited, in accordance with accepted academic practice. No use, distribution or reproduction is permitted which does not comply with these terms.

BMP9 induces postnatal zonal stratification of immature articular cartilage through reconfiguration of the existing collagen framework

Miles Anderson-Watters and Ilyas M. Khan*

Faculty of Medicine, Health and Life Science, Swansea University, Swansea, United Kingdom

Articular cartilage lines bones in synovial joints, and its main structural element, collagen, has an arcade-like arrangement formed from an initially random network in a process called postnatal maturation. This reshaping of the extracellular matrix is similar across all species and is critical for the lifelong strength and durability of cartilage. Collagen remodelling during maturation is difficult to study because it spans a period of time between birth and puberty, and in larger animals this can be months or years. In this study, we show that growth factor bone morphogenetic protein-9 (BMP9) induces collagen remodelling in intact immature articular cartilage explants within 21 days, generating the characteristic arcade-like structure and zonal anisotropic architecture of adult cartilage. In explants exposed to BMP9, collagen fibrils underwent angular displacement from 19° to 78° with respect to the surface, cell density decreased 1.77-fold, and chondrons were significantly larger. The absence of labelling with anti-COL2¾m, a marker of collagen turnover, showed that the existing fibril network was restructured. We found that stromelysin-1 (metalloproteinase-3, MMP3) gene expression was consistently upregulated, whilst other MMP transcript levels were unchanged or reduced. Remodelling was dependent on proteoglycan turnover and could be inhibited using PD166973. These data suggest a possible mechanism whereby MMP3 induces proteoglycan turnover and depolymerises collagen fibrils enabling them to undergo spatial reorganisation. This process may be driven by tissue swelling, which generates directional strain to align fibrils into an arcade-like pattern. The ability to induce tissue maturation advances the potential for engineering durable and functional cartilage for patients requiring joint repair due to diseases such as osteoarthritis.

KEYWORDS

cartilage, postnatal maturation, collagen, BMP9/GDF2, Benninghoff arcades, zonal stratification

Introduction

Articular cartilage is a soft tissue that provides a smooth, frictionless surface at the ends of bones, allowing pain-free movement and cushioning loads by dissipating forces throughout the skeleton (Sophia Fox et al., 2009). It is made of a dense network of insoluble collagen fibrils that, in newborns, are randomly organised (Rieppo et al., 2009). As

animals mature into adulthood, their weight-bearing cartilage adapts to increased joint loading by undergoing a remarkable structural transformation, their collagen fibrils reorganise into an arcade-like pattern (Benninghoff, 1925). This spatial arrangement generates stratification of cartilage into a three-layer zonal architecture: superficial, middle, and deep zones, reflecting the new arrangement of collagen fibrils. This structure is mirrored by the distribution of cells, which are flattened at the surface, round and randomly distributed in the middle zone, and arranged in columns in the deep zone. Chondrocytes express the highly glycosylated proteoglycan, aggrecan (Maroudas, 1976), whose sulphated glycosaminoglycan carbohydrate chains generate a large osmotic pressure gradient that draws water into the extracellular matrix (ECM). The swelling pressure exerted by proteoglycans is restrained in deeper zones by columnar arrays of collagen fibrils, which increase cartilage's hydrostatic pressure, and this forms the basis of its resistance to dynamic compressive loading (van Turnhout et al., 2011). Postnatal changes in collagen fibril content and organisation directly influence tissue function (van Turnhout et al., 2011; Williamson et al., 2001).

The modification in collagen architecture in articular cartilage occurs as part of a coordinated postnatal maturational process seen in mice (Hughes et al., 2005), rabbits (Hunziker et al., 2007; Julkunen et al., 2010), pigs (Rieppo et al., 2009; Gannon et al., 2015), sheep (van Turnhout et al., 2010), horses (Hyttinen et al., 2009), and humans (Aspden and Hukins, 1981). Sensitive methods that detect collagen turnover in tissues, such as aspartate racemisation (Maroudas et al., 1992) and nuclear bomb pulse ^{14}C data (Heinemeier et al., 2016), strongly suggest that following maturation, collagen in joint cartilage remains fixed in place for the entire life of the individual (Eyre et al., 2006). There is no discernible repair or replacement of the collagen network following osteoarthritic disease, lending credence to the observation that joint cartilage 'once destroyed, is not repaired' (Hunter, 1743). Attempts to replace diseased or damaged cartilage with cartilage that approximates the correct zonal architecture using cell- or biomaterial-based techniques have yielded to little or no success. Therefore, understanding how articular cartilage undergoes postnatal maturational changes is critical to advancing our ability to create functional and durable tissue-engineered cartilage implants and, in a wider sense, to add to our knowledge of how collagen is patterned in tissues and organs during growth, development, and disease (Holmes et al., 2018; Musiime et al., 2021; Revell et al., 2021; Orgel et al., 2011).

Collagen remodelling from an isotropic network to one that is anisotropic and exhibiting zonal stratification in many animals occurs sometime between birth and puberty. In larger animals the latter time period can span months or years making studying this phenomenon difficult. As a result, the mechanisms driving changes in collagen orientation remain a matter of conjecture and debate (Hunziker, 2009). Bone morphogenetic protein-9 (BMP9) has diverse and pleiotropic developmental effects on cells and tissues, including chondrocytes and cartilage (Mostafa et al., 2019). Previously, we showed that BMP9 had the capacity to alter the trajectory of fibril growth in isolated chondrocytes grown as pellet cultures (Morgan et al., 2020); whether this property extends to intact cartilage is the subject of this study.

We show that the growth factor BMP9 rapidly induces collagen reorientation and columnar re-ordering of chondrocytes in intact immature bovine articular cartilage. Our analysis of this *in vitro* model of cartilage maturation found no significant collagen turnover, leading us to conclude that changes in fibril orientation are due to the reconfiguration of the existing network. We show that proteoglycan turnover is associated with collagen remodelling and that matrix metalloproteinase-3 (MMP3) expression levels rise whereas tissue inhibitor of metalloproteinase-1/2 expression decrease upon exposure to BMP9. Inhibition of MMP activity stops BMP9-induced collagen remodelling. The inter-relationship between collagen, proteoglycans, and water appears to control postnatal changes in fibril architecture, which is relevant to bioengineering tissues with architectures that specify their structural and functional competence (Revell et al., 2021).

Results

BMP9 induces collagen fibril remodelling in immature articular cartilage

When freshly isolated immature articular cartilage chondrocytes are induced to differentiate as high-density pellet cultures in the presence of 100 ngmL^{-1} BMP9, they exhibit collagen architectures that are reminiscent of adult mature articular cartilage (Morgan et al., 2020). Therefore, we tested the ability of BMP9 to induce postnatal maturational changes in intact articular cartilage over a 21-day (d) culture period using 4-mm diameter explants taken from the metacarpophalangeal joints of immature bovine steers. We also included a separate group of explants exposed to fibroblast growth factor-2 (100 ngmL^{-1} FGF2) and transforming growth factor-β1 (10 ngmL^{-1} TGFβ1), which show some key aspects of postnatal maturation of cartilage, such as epiphyseal cartilage resorption, pericellular matrix formation, and accumulation of mature crosslinking, but no interterritorial collagen remodelling (Khan et al., 2011; Khan et al., 2013). Explants were analysed at two timepoints: 10.5 d and 21 d, by histological staining using toluidine blue and picrosirius red to identify proteoglycan and collagen deposition, respectively (Figure 1). In 10.5 d picrosirius red (PSR)-stained sections of control explants, chondrons were flattened at the surface, and in deeper layers, they had an almost uniform size (Figure 1A) (Supplementary Figure S1—*for comparison with freshly isolated cartilage*). Viewing the latter sections under polarised light microscopy (PLM), the characteristic collagen organisation of immature cartilage was observed; at the surface, the fibrils exhibited a parallel arrangement with strong birefringence, which gradually decreased, indicating a random alignment in the deeper regions. FGF2–TGFβ1 10.5 d-cultured explants were more cellular, and under PLM, there was an increased birefringence signal localised to the pericellular zones of chondrocytes, which was clearer in the mid to deeper regions. In 10.5 d BMP9-cultured explants, PSR-stained sections show a radically different morphology; flattened cells were still apparent at the surface, but there is a distinct increase in the chondron size in the succeeding layers. In deeper zones, chondrons appear elongated and merge to stack upon one another (Figure 1A). PLM imaging of BMP9-cultured explants shows significant changes throughout the

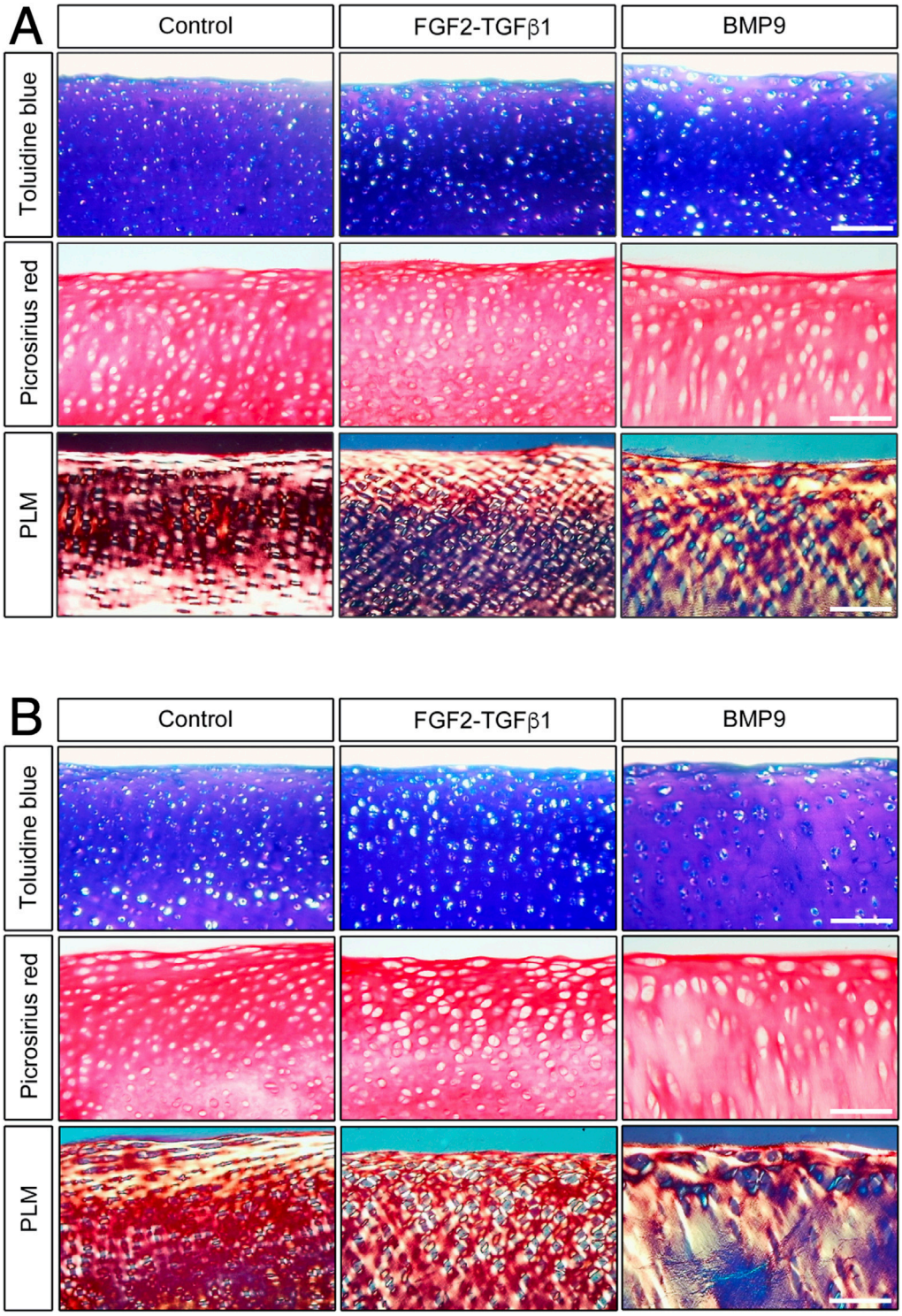

FIGURE 1
BMP9 induces postnatal maturational collagen remodelling in immature articular cartilage. Immature cartilage explants were cultured in serum-free medium, supplemented with FGF–TGFβ1 (100 ng mL^{-1} and 10 ng mL^{-1}) or BMP9 (100 ng mL^{-1}) for a total of 21 days. **(A)** Explants were removed from culture at 10.5 days for histological analysis using toluidine blue and picrosirius red staining. PSR sections were also visualised by polarised light microscopy. *Bar = 100 μm*. **(B)** Sectioned and stained explants visualised after 21 days in the culture. Data representative of explants taken from three or more individuals. *Bar = 100* μm.

tissue depth, particularly in the interterritorial matrix, where increasing birefringence deeper in the tissue signifies greater alignment of fibrils, providing evidence of significant remodelling of collagen. By 21 d, chondrocytes at the surface of control explants have slightly enlarged, but fibrils remain arrayed parallel to the surface with minimal angular displacement, below which there was

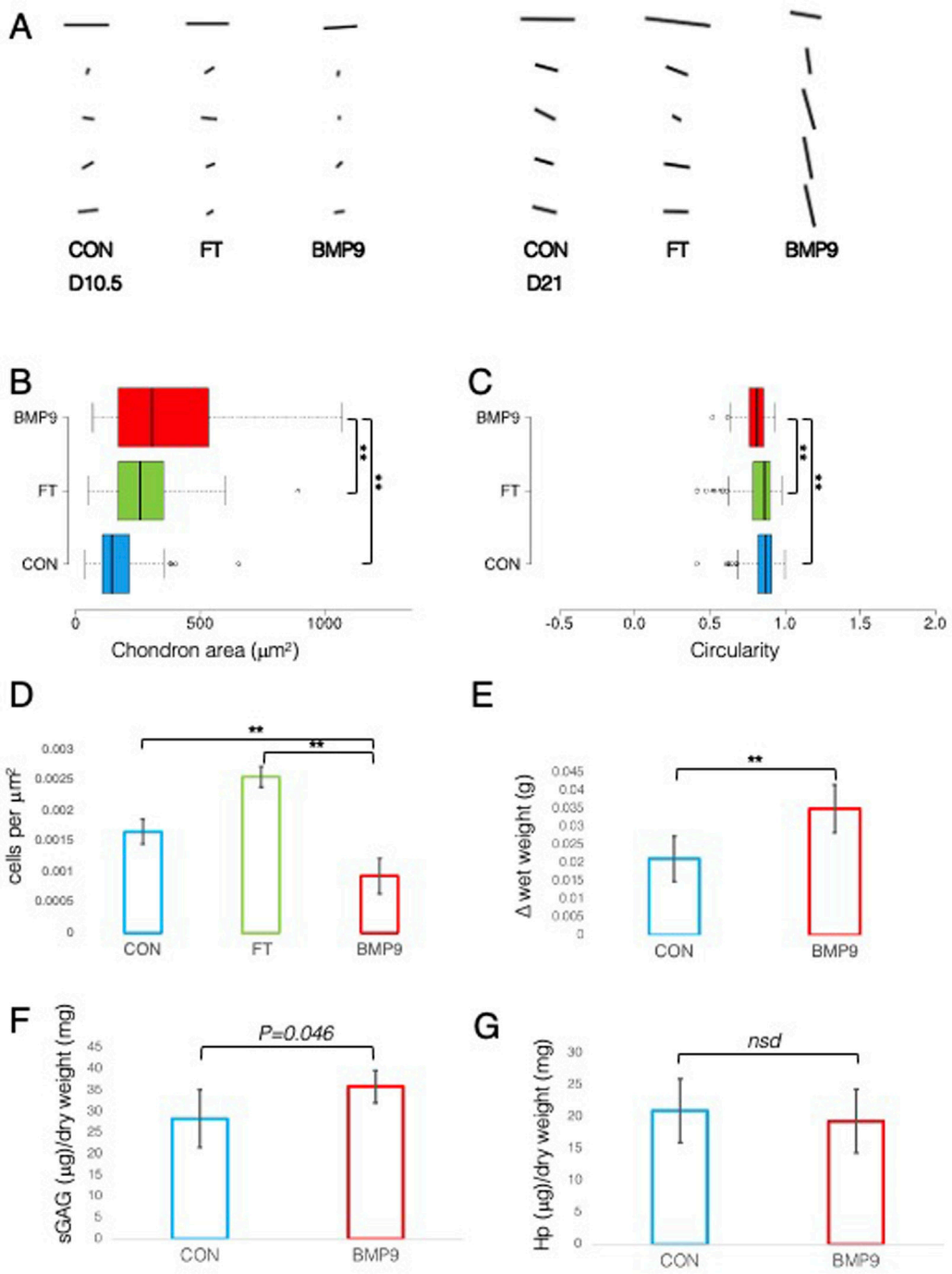

FIGURE 2
Collagen fibril alignment and cell-specific changes in BMP9-induced postnatal maturation of immature cartilage mirror those observed in adult cartilage. **(A)** FibrilTool collagen alignment analysis of picrosirius red-stained sections from 10.5- and 21-day explants. The length and direction of each bar are equal to the degree of anisotropy of fibrils and the angular displacement with respect to the surface (bars represent sequential sampled areas of 75 μm in height). **(B)** Box and whisker plots of chondron area, and **(C)** circularity index from PSR-stained sections of 21-day cultured explants measured using ImageJ (for both analyses, total cell counts were 113 (control), 162 (FGF2–TGFβ1), and 45 (BMP9), *ANOVA, post Tukey*). Data representative of explants taken from three individuals. **(D)** Histogram displaying the cell density in the surface remodelling zone of explants, expressed as cells per μm^2 (n = 3, 3 replicates per sample from different surface regions, total cell count per condition was 2411 (control), 3720 (FGF2–TGFβ1), and 1160 (BMP9), *ANOVA, post hoc Tukey*). Mean ± SD. **(E)** Change in wet weight of 21-day control and BMP9-cultured explants (n = 6, *ANOVA, post hoc Tukey*). Mean ± SD. **(F)** sGAG and **(G)** hydroxyproline (Hp) content of 21-day explants as a ratio of their dry weight (n = 6, *ANOVA, post hoc Tukey*). Mean ± SD.

little or no birefringence, again indicating random alignment of fibrils in deeper regions (Figure 1B). In FGF2–TGFβ1 explants, there was evidence of pericellular matrix remodelling, indicated by the presence of short orthogonal arrays of aligned collagen fibrils surrounding individual chondrocytes from the surface to deeper regions (Figure 1B). In contrast, BMP9-cultured explants under

PLM display extensive regions of highly birefringent perpendicularly aligned collagen fibrils with respect to the cartilage surface, a characteristic feature of mature articular cartilage (Figure 1B) (*also* Supplementary Figures S2, 3). Chondron size remained large in the middle zone, and columnar stacking of chondrocytes was evident in the succeeding cell layers (Figure 1B). The other notable features were a reduction in toluidine blue (metachromasia) and PSR staining in BMP9 compared to control and FGF2–TGFβ1-cultured explants, which were more evident after 21 days.

BMP9-cultured explants adopt the morphological characteristics of mature articular cartilage

A defining feature of mature articular cartilage are the Benninghoff arcades (Benninghoff, 1925), an arrangement of collagen fibrils in parallel orientation at the surface zone that appears to curve down in a perpendicular direction until they reach the calcified zone of the tissue. We used an ImageJ plugin, FibrilTool (Boudaoud et al., 2014), to provide a quantitative description of the overall direction of fibrils from PLM images of control and FGF2–TGFβ1- and BMP9-cultured explants (Figure 2A). The line length and angular direction for each analysed segment in Figure 2A correspond to the magnitude of anisotropy and the average orientation of fibrils with respect to (wrt) the cartilage surface, respectively. On 10.5 d, fibril alignment is the greatest at the surface zone, where parallel-orientated fibrils predominate. However, it is noteworthy that anisotropy (line length) decreases in BMP9 explants, indicating that a transition is occurring (Figure 2A). Despite the increase in birefringence in the latter sections, the collagen fibrils intersect and cancel each other out, resulting in a smaller measure of anisotropy. After 21 d, the orientation of mid and deep zone collagen fibrils in BMP9-cultured explants is slanted perpendicularly from the surface, whereas in control and FGF2–TGFβ1-cultured explants, anisotropy and angular displacement are only slightly increased (angular displacement for control, 19°; FGF2–TGFβ1, 20°; and BMP9, 78° wrt to the cartilage surface). Another feature of maturing cartilage is an increase in cell size (Decker et al., 2017), which in chondrocytes is demarcated by a thin layer of pericellular matrix forming the chondron (Poole, 1997), the unit cell structure of cartilage. Image analysis of chondron area of picrosirius red-stained sections showed that 21 d BMP9-cultured explants had a significantly larger area (383 ± 271 μm^2) (*ANOVA*, $p < 0.01$) than FGF2–TGFβ1 (221 ± 111 μm^2) or control explants (273 ± 135 μm^2) (Figure 2B). We analysed the circularity and aspect ratios of chondrons as decreases in the former and increases in the latter are also characteristic of the transition to the mature cartilage phenotype (Figure 2C). Average cell circularity was significantly reduced in 21 d BMP9-cultured explants, 0.78 ± 0.12 (*ANOVA*, $p < 0.01$), compared to 0.85 ± 0.11 and 0.87 ± 0.09 for FGF2–TGFβ1 and control explants, respectively; a perfect circle equals 1 (Figure 1C). The average aspect ratios of chondrocytes in 21 d BMP9-cultured explants of 1.79 ± 0.66 were significantly increased (*ANOVA*, $p < 0.01$) compared to FGF2–TGFβ (1.42 ± 0.31) and control (1.46 ± 0.35) explants. The sparsity of cells in articular cartilage is another characteristic property of adult articular cartilage, where there is a greater ratio of extracellular matrix to cell number (Jadin et al., 2005) (Figure 2D). Previous studies culturing immature explants with FGF2–TGFβ1 observed a pronounced proliferative response in chondrocytes (Khan et al., 2011), and this was reproduced in our experiments, where we observed an 1.54-fold increase in cell density (*ANOVA*, $p < 0.01$) compared to control explants. Cell density was significantly lower in 21 d BMP9-cultured explants by 1.77-fold than in both control and FGF2–TGFβ1-cultured explants ($p < 0.01$). BMP9-treated explants appeared more swollen at the end of the culture period, and this was more pronounced at the surface. The average wet weight of explants was 70.7 ± 0.006 mg for 21 d BMP9-treated explants and 57.2 ± 0.009 mg for control explants (*T-Test*, $p < 0.01$), representing a 1.23-fold increase on average. The difference between the start and end wet weights for both groups is shown in Figure 2E. Bulk biochemical content analysis of BMP9 explants showed a 1.26-fold increase in sGAG (*T-Test*, $p = 0.05$) over control explants, but no significant difference in collagen values was observed (Figures 2F, G).

BMP9-induced collagen fibril reorganisation does not occur through turnover of the existing fibril network

We next examined whether collagen reorganisation in BMP9-cultured explants is due to enzymatic turnover of the existing framework and synthesis of new fibrils with altered orientation. Anti-COL2¾m is a monoclonal antibody that recognises epitopes revealed by collagen denaturation (unwinding) caused by collagenase digestion (Hollander et al., 1994); therefore, the detection of epitopes at 10.5 d in BMP9-cultured explants, when collagen remodelling is highly active, would be indicative of enzymatic breakdown and resynthesis of a new network. Immunofluorescent analysis of antibody labelling of 10.5 d and 21 d BMP9-cultured explants showed no obvious enhancement of labelling in the surface zone, where collagen remodelling is most apparent, compared to that observed in control explants (Figure 3A). Epiphyseal cartilage in the deeper layers of immature articular cartilage is part of the growth plate, which is highly metabolic compared to the overlying hyaline cartilage and provides a natural internal control for collagenase activity. We found high levels of anti-COL2¾m labelling in the epiphyseal zone of all explants, with BMP9 10.5 d explants exhibiting the most intense labelling (Figure 3A). What, then, induces collagen reorganisation in explants? We earlier noted a decrease in toluidine blue staining, signifying proteoglycan depletion in the superficial zone of 10.5 d BMP9-cultured explants despite an overall increase in the bulk content. To confirm the presence of enzymatic activity leading to proteoglycan loss, we performed *in situ* zymography using a fluorogenic substrate, DQ gelatin, to reveal potential metalloproteinase (MMP) activity within 10.5 d frozen sections (Figure 3B). Explants cultured in FGF2–TGFβ1 were included in this assay as studies have shown that this combination of growth factors highly induces MMP activity in the deep zone of immature articular cartilage, leading to tissue resorption (Khan et al., 2011). Green fluorescent labelling indicative of MMP activity was found not only, as expected, in the

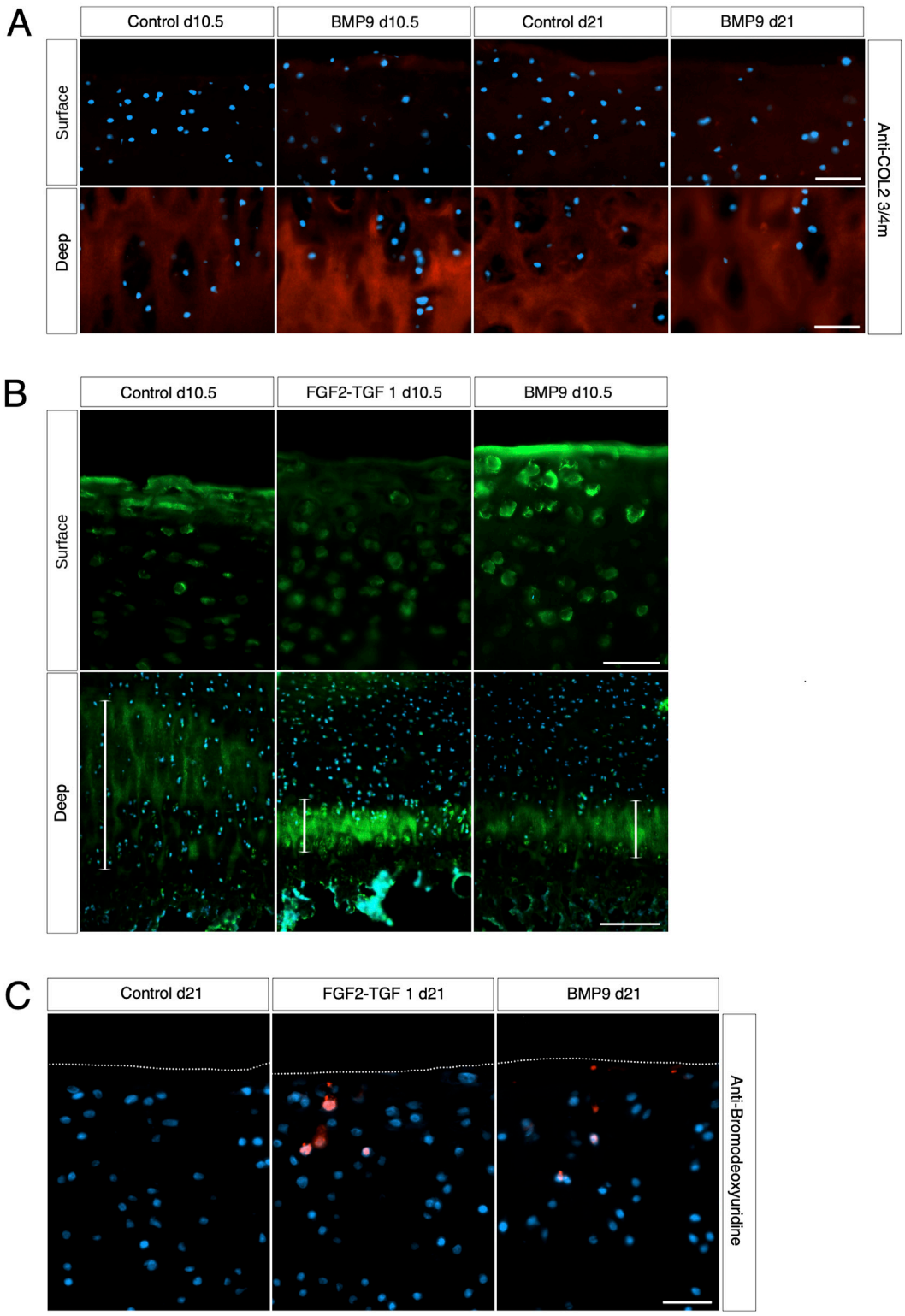

FIGURE 3
Collagen changes during BMP9-induced remodelling are not the result of fibril turnover. **(A)** Surface and deep zones of control and BMP9 of 10.5-day- and 21-day-treated explants are shown labelled with the antibody anti-COL2¾m. The secondary antibody used was anti-mouse IgG Alexa Fluor 594, and sections were counterstained with DAPI to visualise nuclei. *Bar = 50 μm*. **(B)** DQ gelatin labelling shows the surface (*upper panel*) and deep zones (*lower panel*) of 10.5-day control, FGF2–TGFβ1, and BMP9-cultured explants. The epiphyseal cartilage of the deep label with DQ gelatin in broader bands, and their extent is demarcated with a white line for each explant. *Upper panel bar = 50 μm* and *lower panel bar = 200 μm*. **(C)** BrdU labelling of 21-day-cultured explants. Secondary antibody, anti-mouse IgG Alexa Fluor 594; sections were counterstained with DAPI to visualise nuclei. *Bar = 50* μm.

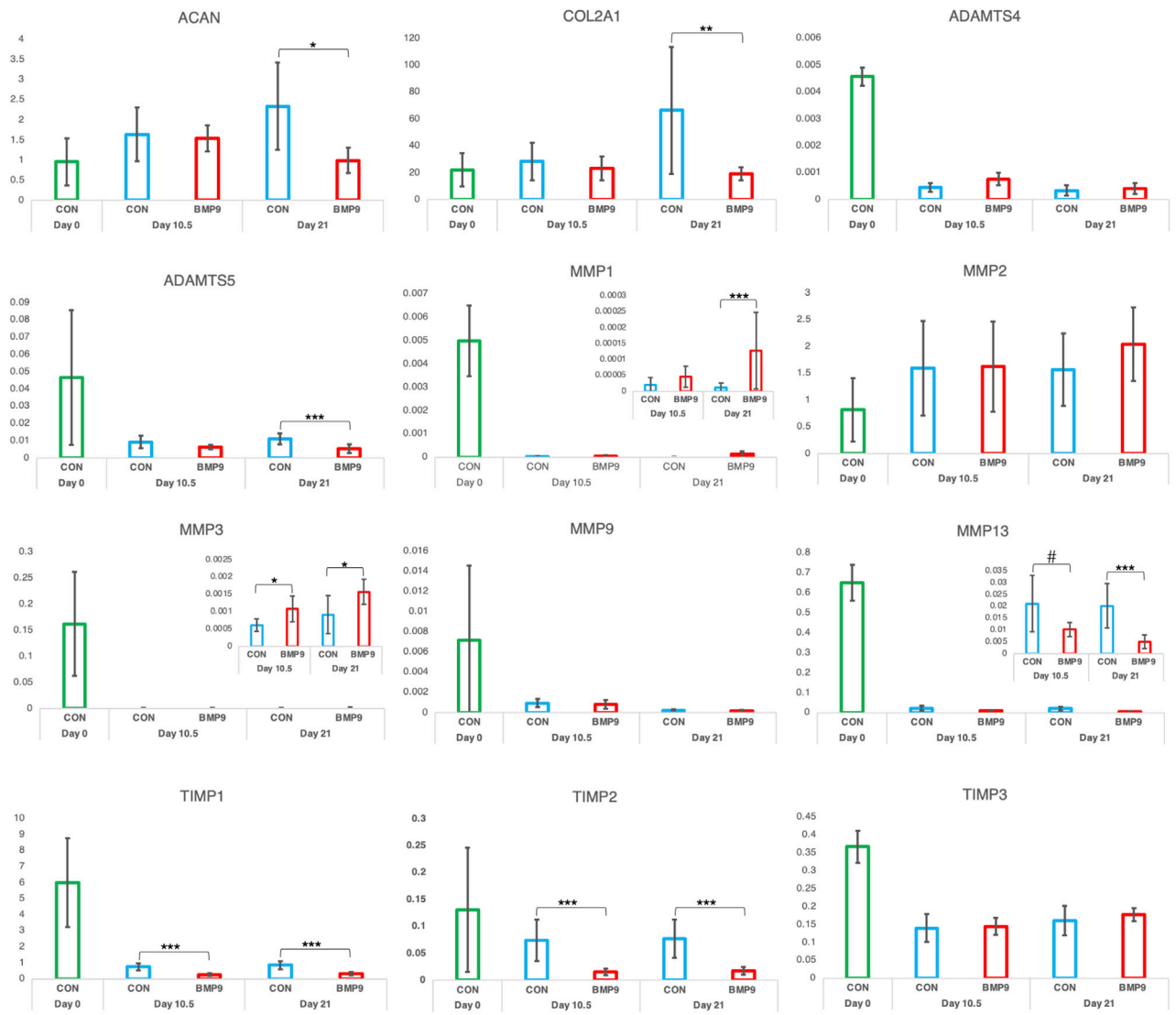

FIGURE 4
QPCR analysis of absolute gene expression levels of selected biomarkers during BMP9-induced postnatal maturation of immature articular cartilage explants. The *y*-axis of graphs denotes the ratio of transcript levels in ng of the gene of interest divided by the housekeeping in ng. Each panel also includes samples taken from freshly isolated explants (CON, Day 0, n = 3), which were included to provide some perspective on the effect of culture conditions on expression levels. (n = 6, per condition, parametric analysis, *ANOVA, post hoc Tukey*, non-parametric analysis *Kruskal–Wallis, and post hoc Conover/Holm*). # denotes $p = 0.07$. Mean ± SD.

deep zone of FGF2–TGFβ1 sections but also at lower levels in the deep zones of both control (wide band) and BMP9 (narrower band)-cultured explants (Figure 3B). In the superficial zone of explants, BMP9-cultured explants displayed intense pericellular and weaker extracellular matrix fluorescent labelling, contrasting with the relative lack of labelling observed in FGF2–TGFβ1 sections and weaker labelling in control sections (Figure 3B). PSR-stained sections of BMP9 explants show the rearrangement of cells into columns (Figure 1B and Supplementary Figure S3), and some studies have deduced that this is due to cellular proliferation (Hunziker et al., 2007; Kozhemyakina et al., 2015). Therefore, we also assayed 21 d explants for cell proliferation. Furthermore, we again used FGF2–TGFβ1-cultured explants for comparison as these growth factors have been shown to induce cellular proliferation in superficial zone cartilage (Figure 3C). Control explants showed no evidence of BrdU incorporation; we, however, observed sporadic BrdU incorporation across the surface of BMP9 explants, but there was no definitive pattern that could account for multiple columns of chondrocytes in the remodelling zone (Figure 3C). QPCR analysis of aggrecan (ACAN) gene expression showed a decrease of 2.36-fold (*ANOVA*, $p < 0.05$) at 21 d in BMP9-cultured explants compared to control explants, a pattern repeated for collagen type II (COL2A1) expression, where a decrease of 3.44-fold (*KW*, $p < 0.01$) was observed (Figure 4). There were no differences in expression between control and BMP9-cultured explants at the earlier timepoint (10.5 d) for either ACAN or COL2A1.

MMP3 gene expression is upregulated in BMP9-cultured explants

To identify which MMPs were being activated at the surface zone of 10.5 d BMP9-cultured explants, we performed targeted RT-qPCR of enzymes known to be active in articular cartilage during normal metabolism (Figure 4). For this analysis, we also included 21 d cultured explants. There was no change in the expression of aggrecanase ADAMTS4 at either timepoint, but a 0.49-fold decrease at 21 d in BMP9-treated explants for ADAMTS5 levels (*KW*, $p < 0.001$). Expression levels of gelatinases MMP2 and MMP9 were not altered over 21 d between explants. We identified a 10.7-fold increase in collagenase MMP1 expression in BMP9 explants (*KW*, $p < 0.001$); however, MMP1 transcript levels are 156-fold lower than MMP13, and therefore, this increase probably has little impact on collagen digestion. MMP13 expression levels in BMP9 explants decreased by 0.48- (*KW*, $p = 0.07$) and 0.25-fold ($p < 0.001$) at the two timepoints. The only protease that was consistently upregulated in BMP9 explants was MMP3, 1.78-fold at 10.5 d (*KW*, $p < 0.026$) and 1.72-fold at 21 d ($p < 0.001$). Tissue inhibitor of MMP-1/2 (TIMP) also showed consistent decreases over the two time periods in BMP9-treated explants compared to control explants (TIMP1 0.36- and 0.38-fold (*KW*, $p < 0.001$) and TIMP2 0.21- and 0.22-fold (*KW*, $p < 0.001$)).

Inhibition of MMP activity by PD166793 prevents collagen reorganisation in immature articular cartilage

MMP3 transcript levels are consistently elevated and TIMP1/2 decreased over the 3-week period in BMP9-cultured explants, and this occurs concurrently with an increase in gelatinase activity at the cartilage surface. Therefore, we hypothesised that it is proteoglycan turnover driven by MMP activity that initiates collagen reorganisation of the existing fibrillar network. First, we analysed proteoglycan loss over the 21 d culture period in cultured explants using the dimethylmethylene blue assay for sulphated glycosaminoglycan (sGAG) and observed a significant increase in sGAG release into the culture medium (*ANOVA*, $p < 0.01$) for BMP9-cultured explants, which released 1.4- and 1.8-fold more sGAG than either FGF2–TGFβ1 or control explants, respectively (Figure 5A). We then used an MMP3 inhibitor, PD166793 (IC_{50} values are similar for MMPs 2/3/13 but >750 higher for MMPs 1/7/9), to first determine the concentration at which it was able to inhibit sGAG release into the medium of BMP9-cultured explants (this was between 10 and 100 μM; Figure 5B). Next, we cultured immature cartilage explants for 21 d in the presence or absence of 10 or 100 μM PD166793 and BMP9. Histological analysis using toluidine blue staining and PLM of picrosirius-stained sections of control explants showed no overt changes when the culture medium was supplemented with either 10 μM or 100 μM PD166793 (Figure 5C). In BMP9-cultured explants, the loss of proteoglycan in BMP9 was visible through a marked reduction of toluidine blue staining, which is partially counteracted by the presence of 10 μM inhibitor and completely reversed by 100 μM inhibitor (Figure 5C). PLM imaging of corresponding picrosirius red-stained sections shows collagen remodelling, generating perpendicular arrays of fibrils, whose appearance is partially inhibited when explants are co-cultured with 10 μM PD166793 and completely inhibited with 100 μM PD166793.

BMP9 induces perpendicular alignment of collagen fibrils during pellet culture of immature and mature articular chondrocytes

A pressing question when engineering articular cartilage is whether chondrocytes have the intrinsic capacity to generate adult articular cartilage, including the correct orientation of collagen fibrils, which are essential for the long-term functional competence of the tissue. To test this, we cultured freshly isolated chondrocytes from both immature and mature articular cartilage as high-density pellets either in the standard chondrogenic medium with or without BMP9 (Figure 6A). Polarised light microscopy shows the radical change in fibril alignment when BMP9 is added to immature chondrocytes, with the orientation of fibrils being predominantly perpendicular to the surface of the pellet, compared to control pellets, where the birefringent signal is predominantly pericellular (Figure 1A). In mature control chondrocyte pellets, birefringent fibrils exhibited increased density in the interterritorial regions of the ECM, and their predominant direction was perpendicular to the surface. In BMP9-treated mature chondrocyte pellets, the interterritorial regions were expanded, forming a band of perpendicularly aligned birefringent collagen fibrils containing elongated chondrons, which in some cases housed multiple chondrocytes (Figure 6A). A notable feature, as with previous experiments with explants (Figures 1A, B), was the reduction in picrosirius red and toluidine blue staining intensity of pellets (Figure 6A). Culture with BMP9 caused a significant increase in volume in immature and mature-derived chondrocytes compared to that observed in control pellets (Figure 6B), and our calculations show that this increase is mainly due to the significant accumulation of water, with an 8.6-fold increase in immature (*ANOVA*, $p < 0.0001$) and a 3.2-fold increase in mature ($p < 0.0001$) cell pellets. Biochemical analyses of proteoglycan content (sGAG) showed no significant difference in deposition between pellets as a proportion of dry weight (*ANOVA*, $p = 0.205$) (Figure 6C; however, when normalised to wet weight, values of BMP9-cultured immature, 1.9-fold (*ANOVA*, $p < 0.01$), and mature, 1.6-fold ($p < 0.01$), chondrocytes were significantly increased (Figure 6C). These data imply that in BMP9-cultured cartilage pellets, the interactions between proteoglycan and water are somehow different; measuring the hydration of mature pellets showed a decreasing trend, 91.8% ± 0.88% *versus* 88.6% ± 0.85% water (*ANOVA*, $p = 0.06$) between control and BMP9-cultured pellets, mirroring the decrease in the water content of cartilage as it matures. When we measured collagen (hydroxyproline) content in pellets, we found that as a proportion of dry weight, there was an 11.2-fold (*ANOVA*, $p < 0.001$) and 3.4-fold ($p < 0.05$) decrease in deposition in BMP9-cultured immature and mature pellets compared to their control counterparts (Figure 6C). This difference persisted when the proportion of collagen to wet weight was calculated with a 7.0-fold (*ANOVA*, $p < 0.01$) and 2.4-fold ($p < 0.01$) decrease in BMP9 pellets (Figure 6C). Therefore, exposure of BMP9 to freshly isolated chondrocytes results in collagen deposition in a perpendicular orientation to the cartilage pellet surface, and

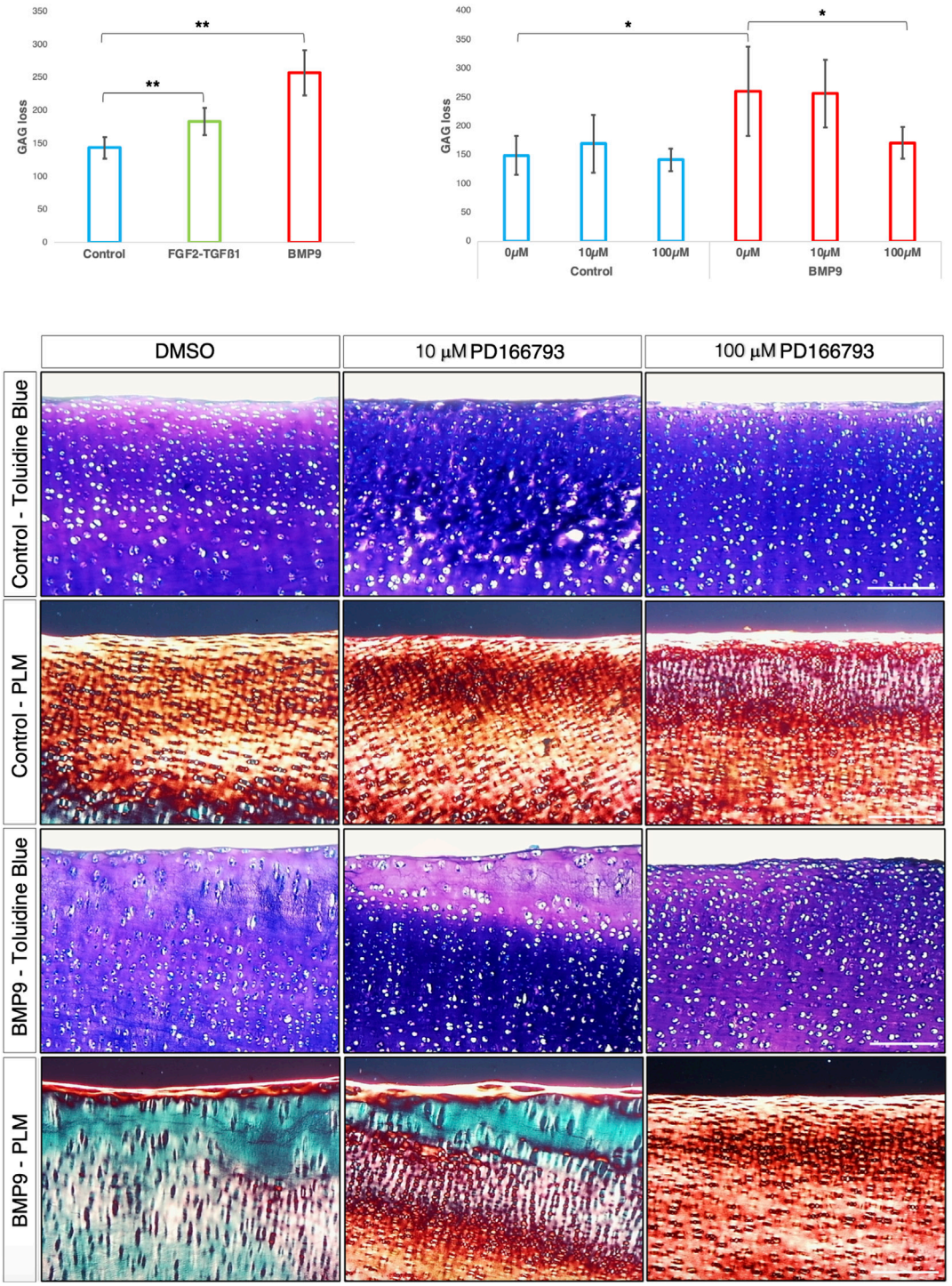

FIGURE 5
BMP9-induced collagen remodelling is repressed by the MMP inhibitor PD166793. **(A)** Histogram describing the total loss over 21 days of sGAG to the medium from explants (n = 6, *ANOVA, post hoc Tukey*). Mean ± SD. **(B)** Total sGAG loss to the medium over 21 days in control and BMP9 (100 ng mL^{-1})-cultured explants with or without 10 or 100 μM PD166793 (n = 6). Mean ± SD. **(C)** Toluidine blue staining, picrosirius red staining, and polarised light microscopy of control and BMP9-cultured explants cultured for 21 days with or without the stated concentrations of PD166793. *Bar = 200* μm. Data representative of explants extracted from three different donors. Note the failure of BMP9-cultured explants to partially and completely undergo collagen remodelling when exposed to PD166793; under PLM, collagen fibrils are aligned parallel to the surface, and toluidine staining indicates minimal proteoglycan loss.

when mature cells are employed, there is greater interterritorial alignment of fibrils, implying these differences are developmentally encoded. There are clear similarities between the decrease in picrosirius red and toluidine blue staining in the region of pellets, where significant collagen alignment was observed, and the zone of remodelling in BMP9-treated intact immature cartilage.

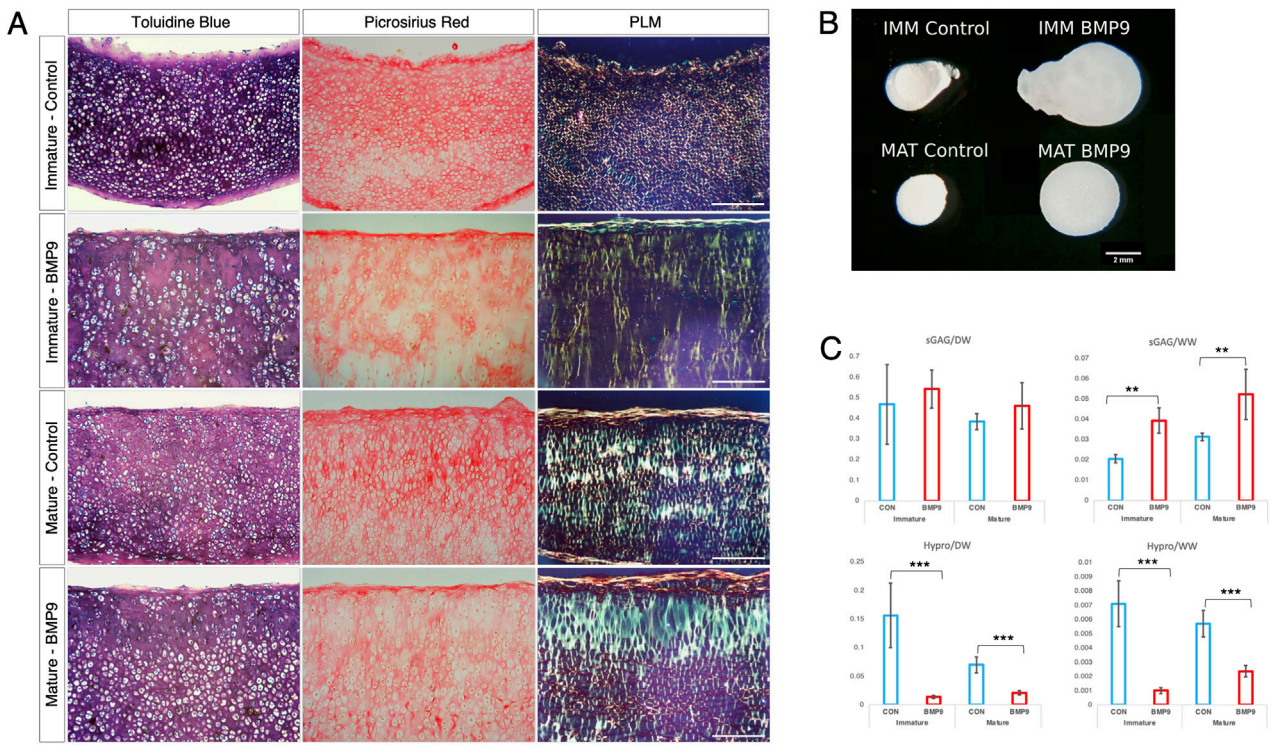

FIGURE 6
BMP9 induces postmaturational phenotype changes in isolated immature and mature chondrocytes during cartilage growth. **(A)** Toluidine blue staining, picrosirius red staining, and polarised light microscopy of wax sections of 21-day immature and mature chondrocyte pellet cultures. Data are representative of chondrocytes extracted from three different donors. Note the decreased staining for proteoglycan and collagen in BMP9-cultured explants. *Bar = 200 μm*. **(B)** Photographic image of formalin-fixed pellets following 21 days of culture. Bar = 2 mm. **(C)** Biochemical analyses of sGAG and hydroxyproline content (in μg) of pellets expressed as ratios of their dry and wet weights (in μg) (n = 6 per condition, *ANOVA, post hoc Tukey*). Mean ± SD.

Discussion

BMP9 stimulation of immature articular cartilage can model the postnatal transition of collagen architecture to generate the zonal stratification characteristic of mature adult tissue. We discovered that this transition involves a reconfiguration of the existing collagen network, and a contributory factor is proteoglycan turnover, which, if suppressed using a small molecule MMP inhibitor, stops matrix remodelling. QPCR analysis shows that MMP3 is consistently elevated in BMP9-treated cartilage explants, making it a likely candidate for initiating restructuring of the ECM to the mature configuration. We also show that chondrocytes isolated from immature and mature cartilage are phenotypically distinct when grown as pellet cultures with respect to the matrix they produce, but both generate perpendicularly aligned collagen fibrils characteristic of mature cartilage when stimulated with BMP9. Interestingly, the water content and volume of explants stimulated with BMP9 are significantly greater than controls, and we hypothesise that this is caused by MMP3-induced depolymerisation and hydration of collagen, expanding the tissue and generating a direction of principal strain, which acts to align collagen fibrils perpendicular to the tissue surface.

BMP9 is a member of the TGFβ superfamily of secreted factors and was originally discovered in foetal mouse livers, where it plays a role in tissue growth and homeostasis (Song et al., 1995). It is highly expressed by non-parenchymal cells (Miller et al., 2000) of the liver, where it enters the circulation accounting for 60 percent of serum BMP activity (Scharpfenecker et al., 2007). In serum, BMP9 acts as a vascular quiescence factor inhibiting endothelial cell sprouting through its high affinity receptor ALK1 and co-receptor endoglin (David et al., 2008) but in different contexts supports endothelial proliferation and angiogenesis (Suzuki et al., 2010). Intracellular BMP9 signalling occurs through the phosphorylation of receptor-regulated SMADs 1/5/8, which then form a complex with common mediator SMAD4, translocate to the nucleus where this heteromeric complex modulates gene expression. BMP9 appears to exert diverse and pleiotropic effects during postnatal growth and development of many tissues (Mostafa et al., 2019). In musculoskeletal cells and tissues, it is recognised as a potent osteogenic factor (Varady et al., 2001), stimulating robust and mature bone formation of intramuscularly implanted adenovirus-BMP9-infected osteoblast progenitors (Kang et al., 2004). BMP9 is a potent modulator of chondrogenic differentiation inducing precocious *in vitro* differentiation of articular and auricular chondroprogenitors and stimulating freshly isolated immature chondrocytes to increase matrix synthesis of collagen type II and aggrecan (Morgan et al., 2020; Blunk et al., 2003; Gardner et al., 2023; Hills et al., 2005). The overstimulation of chondrocytes with BMP9 *in vitro* can induce expression of markers of epiphyseal or calcifying cartilage such as alkaline phosphatase and collagen type X (Blunk et al., 2003; van

Caam et al., 2015), and it is hypothesised that in ageing tissues, an imbalance in the ratio of ALK5:ALK1 signalling through their respective ligands TGFβ1 and BMP9 promotes osteoarthritic changes in cartilage, an example of antagonistic pleiotropy (van der Kraan, 2014; Mitteldorf, 2019). It also exhibits morphogenetic properties; in pellet cultures of immature chondrocytes, exposure to BMP9 produces cartilage with collagen fibrils aligned perpendicularly to the tissue surface, whereas TGFβ1 induces concentric alignment (Morgan et al., 2020). Yu et al. found BMP9 expression in the interzone of developing mouse joints and, using a model of non-regenerative digit amputation, showed that when the stump is treated sequentially with beads soaked in BMP2 and BMP9 this induces joint regeneration and the formation of a distal skeletal element (Yu et al., 2019). Therefore, as with other tissues, BMP9 has many context-dependent functions that affect cartilage growth and development, significantly including modulation of collagen fibril growth (Morgan et al., 2020), leading us to hypothesise that it induces postnatal collagen network remodelling in intact immature articular cartilage.

In this study, we discovered that BMP9 induces perpendicular reorientation of collagen fibrils in immature cartilage explants within 21 days, although changes in cell shape and collagen fibril order are apparent as early as day 10.5. As remodelling of the ECM proceeds, collagen birefringence under polarised light microscopy increases, highlighting progressive fibril alignment. Simultaneously, the angular displacement of aligned fibrils in BMP9-cultured explants increases from ~20° in control explants to ~78°. These latter changes bring about the anisotropic zonal stratification of cells and tissue into distinct superficial, transitional, and radial zones as opposed to a thin surface layer and isotropically arranged cells in the subsequent deeper layer, as found in native immature cartilage (Jadin et al., 2005). Postnatal maturation of cartilage is associated with puberty (Hunziker et al., 2007; Hunziker, 2009), and this starts between months 10 and 12 in bulls, well beyond the post-parturition period (7–28 days) at which time we obtained immature bovine cartilage (Brito et al., 2007). Another quantitative measure of the anisotropy of cartilage upon postnatal maturation is cellular hypertrophy (enlargement, not epiphyseal chondrocyte differentiation) (Hunziker et al., 2007), where we observed an average increase in chondron size of 40% in BMP9-treated explants compared to control explants.

Chondrons are the structural, functional, and metabolic units of cartilage and are composed of one or more chondrocytes surrounded by a thin shell of the pericellular matrix (Poole, 1997). In native maturing cartilage, chondrons in the deep zone become elongated and multicellular, and their aspect ratio (AR, maximum length/width) increases (Youn et al., 2006). This change was also observed in BMP9-treated explants, where the average AR of chondrons increased by 20%. There were only sporadic incidences of incorporation of BrdU in chondrocyte nuclei throughout the cartilage depth of explants. The latter assay was conducted to exclude the possibility that maturational changes in cellular organisation were the result of proliferation, as previously described in rabbit (BrdU) (Hunziker et al., 2007) and mouse cartilage (PRG4 (GFP-CreERt2) cell fate tracking) (Kozhemyakina et al., 2015). Organisational changes in the ECM structure and chondrocyte localisation in cartilage during maturation may be driven by a process of appositional growth. An opposing view, one partially shared by us, is proposed by Decker et al. (2017), who found no significant evidence of appositional or interstitial postnatal cellular proliferation that can account for maturation of cartilage. By using cell tracking of R26-Confetti and GDF5-CreERt2 reporter mice, Decker *et al* found that anisotropic cellular organisation and articular cartilage tissue expansion occurred mainly through cell enlargement and the rearrangement of co-localised cells into columns, similar to integrin β1-dependent columnar chondrocyte formation in the growth plate (Aszodi et al., 2003), where relocated cells remodel the collagen fibril network. It is our contention, which we expand on below, that collagen remodelling precedes topographical cell rearrangement. In our model, we saw no evidence of epiphyseal cartilage resorption and associated tidemark formation, which are also important features of mature anisotropic tissue organisation and result from the formation of the calcified zone, a layer of crenellating tissue that connects the subchondral bone and overlying hyaline cartilage. Thus, BMP9 only induces postnatal maturational changes limited to hyaline cartilage, and this is not unexpected as epiphyseal growth and differentiation are controlled by many well-defined local and systemic regulatory factors (Karimian et al., 2011).

Is the activity of BMP9 in collagen remodelling contingent upon the prior formation of the immature cartilage ECM, or does it induce gene expression programmes that generate mature cartilage phenotypes? We answered this question by growing freshly isolated chondrocytes from immature and mature articular cartilage as pellet cultures in the presence or absence of BMP9. Histological analyses show that chondrocytes from either source are phenotypically distinct, depending on the ECM they generate; however, in both instances, when BMP9 is present, fibrils perpendicular to the surface are produced. The orientation of fibrils in mature chondrocyte pellets was predominantly perpendicular; however, exposure to BMP9 induced the appearance of a band of aligned fibrils in the interterritorial matrix, which became more prominent and formed a distinct lamina across the pellet. The differences between immature and mature pellet formation may be accounted by the fact that prior to and during puberty, joint cartilage is still expanding, whereas following growth plate closure, the matrix is in a process of consolidation. These tissue states are likely governed by distinct transcriptional profiles and biomechanical inputs. These experiments show that fully differentiated, developmentally mature chondrocytes can be used to rapidly tissue-engineer articular cartilage that mirrors the anisotropic structure and function of native tissues.

Therefore, BMP9-induced postnatal maturation of immature articular cartilage provides a tractable model system to investigate the mechanisms driving collagen network remodelling. We first questioned whether changes in fibril order were the result of collagen proteolytic turnover. To address this, we used the antibody anti-COL2¾m, which is capable of sensitively detecting *in situ* collagenase activity (Hollander et al., 1994). Upon digestion with collagenase, the collagen type II triple helix is cleaved between residues Gly^{775} and Gln^{779}, producing ¼ and ¾ fragments resulting in helix unwinding and revealing an epitope recognised by the antibody COL2¾m in the latter fragment (Billinghurst et al., 1997). We observed no significant anti-COL2¾m labelling in the

surface region of BMP9-treated cartilage, where collagen remodelling was occurring over and above what was present in control explants. Immature hyaline cartilage is continuous in the deeper layers with epiphyseal cartilage, and here, the tissue is dynamically being remodelled, consequently showing significant labelling in the interterritorial matrix with anti-COL2¾m is present at these sites, providing a useful internal control for antibody labelling. A gene expression screen found reduced levels of collagenase MMP13, but an increase in MMP1 was observed. MMP1 transcript levels were, however, extremely low, approximately 156-fold lower than MMP13. Additionally, they were not upregulated above baseline levels at the time (day 10.5) when remodelling was occurring; therefore, MMP1 probably has little or no effect on fibril remodelling. Thus, the absence of detectable collagenase activity strongly suggests that fibril remodelling occurs by restructuring or realignment rather than enzymatic breakdown and synthesis of a *de novo* network. The lack of evidence for appositional growth, the decrease in cell density, and, most significantly, no increase in COL2A1 gene expression over the remodelling timespan are additional supporting evidence that neoformation of the surface zone is a much less likely explanation for the acquisition of anisotropic organisation. Wu et al. (1991) previously suggested that selective proteolysis by stromelysin-1 can initiate remodelling, reorganisation, and growth without having to remove the existing collagen fibril network.

In toluidine blue-stained images of BMP9-treated explants, there was a perceptible decrease in staining and metachromasia in the surface region, indicating proteoglycan loss or turnover, further confirmed by increased labelling by fluorescein-conjugated substrate DQ gelatin, identifying *in situ* activity of MMPs such as gelatinases and stromelysin. We included FGF2–TGFβ1-treated explants in this assay as a useful positive control as a previous study had shown that these growth factors induce elevated levels of MMP activity in the epiphyseal zone, contributing to resorption of the ECM (Khan et al., 2011). A gene expression screen of proteases known to be active in the ECM of articular cartilage revealed a sustained increase in MMP3 (stromelysin-1) over 21 days. MMP3 cleaves aggrecan in its interglobular domain between amino acids Asn^{341} and Phe^{342}, releasing the entire glycosaminoglycan-containing portion of this protein (Fosang et al., 1991). Of similar significance is the sustained decrease in expression levels of MMP inhibitory proteins TIMP1 and TIMP2 in BMP9-treated explants, potentially accounting for further increased proteolytic activity. Analysis of DQ gelatin-assayed sections of BMP9-treated explants predicts that if TIMP activity falls in the deep zone, then the fluorescence signal should increase, but the zone of activity decreases compared to control explants, suggesting that reductions in TIMP1/2 expression may facilitate proteoglycan depletion in the upper zones of cartilage. The measurement of sGAG loss into the culture medium also confirmed proteolytic degradation of proteoglycan, and its return to baseline levels of turnover was used to determine the concentration of MMP inhibitor PD166793 to achieve this. The presence of 100 μM PD166793 inhibited collagen remodelling at the surface of BMP9-treated explants, implying that reorganisation of fibrils is conditional upon proteoglycan depletion or turnover.

Fibrillar collagens resist hydrodynamic, compressive, and tensile forces, and the amount and direction of strain positively correlate with the degree of collagen fibril alignment (Hapach et al., 2015). What, then, generates the internal tension within cartilage that aligns fibrils during BMP9 induced remodelling? Water (Cederlund and Aspden, 2022)? The loss of proteoglycan and depolymerisation of collagen not only free collagen to deform but also induce tissue swelling, and we suggest that water ingress generates the directional tensional stress to align fibrils. Proteoglycans within the cartilage ECM contribute to the fixed charge density and osmotic pressure, and this swelling pressure is counteracted by elastic forces within the collagen fibril network (Maroudas, 1976). With proteoglycan turnover, there is a reduction in swelling pressure, and consequently, the collagen matrix becomes less stiff (Maroudas et al., 1985), allowing it greater freedom to deform. The numerous glycosaminoglycan chains of the large aggregating proteoglycan aggrecan form electrostatic interactions with collagen, and this is suggested to occur through the axial d-periodic repeat gap of collagen, leading to the formation of an interlocked matrix exhibiting spatial organisation (Junqueira and Montes, 1983). Proteoglycans assemble with regularity along collagen type I fibrils in orthogonal arrays in tendon (Scott, 1991), and similar ordered associations between collagen type II and chondroitin sulphate containing proteoglycans have been confirmed using electron microscopy (Poole et al., 1982), low angle X-ray diffraction (Ronziere et al., 1985), and colloid force spectroscopy (Rojas et al., 2014). Therefore, proteoglycan turnover also has the effect of removing an imposed supramolecular order, further increasing the freedom of fibrils to be aligned under tension. Explants undergoing collagen remodelling significantly increase their water content during the culture period (~66%), mainly at the surface region; the cause is two-fold. First, MMP3 activation not only induces proteolytic depletion of cartilage proteoglycans but also collagen type IX. Collagen type IX is a fibril-associated collagen with interrupted helices (FACIT) that is covalently linked to the surface of collagen type II fibrils (van der Rest and Mayne, 1988). Its amino terminal non-collagenous domain (NC4) and adjacent collagenous domain (col3) project away from the fibril surface and are available to interact with other molecules in the ECM (van der Rest and Mayne, 1988). In articular cartilage, collagen type IX NC4 domains stabilise collagen type II interfibrillar interactions through covalent linkages to adjacent type II telopeptides and type IX NC4 domains (Wu et al., 1991; Wu et al., 1992). MMP3 proteolytically cleaves collagen type IX in its C-terminal NC2 domain, releasing NC4 and uncoupling it from the surface of type II fibrils (Wu et al., 1991), which together with its telopeptidase activity causes the depolymerisation of collagen type II fibril networks. Second, prior to the loss of proteoglycan, collagen is not fully hydrated as water molecules are drawn to glycosaminoglycan covalently bound to aggrecan; however, once glycosaminoglycan density is reduced by proteoglycan degradation, depolymerised collagen is free to hydrate. Collagen is highly hygroscopic, and as an extended molecule, it presents many donor and acceptor sites for hydrogen bonding. In its fully hydrated state, it contains three times as much water volumetrically as the collagen ground substance alone, leading to tissue swelling (Andriotis et al., 2018). Andriotis et al. have shown that fully hydrated collagen is subject to fewer intermolecular van der Waals and/or electrostatic forces, resulting in increased intrafibrillar distances. This change opens deformation pathways that were previously closed (Andriotis et al., 2018). There is direct

evidence of this mechanism in action in the developmentally regulated selective proteolysis of collagen type IX, which triggers corneal stroma matrix swelling (Fitch et al., 1988). Fitch et al found that when collagen type IX antibody reactivity in the stroma was lost, it coincided with matrix swelling. Type IX protein was found in soluble fractions of extracts, whereas collagen type II remained intact in the stroma and was found in insoluble fractions. Therefore, the ingress of water into the cartilage surface has the potential to hydrate a depolymerised collagen network and imposes a directional strain upon the tissue that is perpendicular to the surface. We hypothesise that the tensile stress directed to the surface as cartilage hydrates is sufficient to radially realign fibrils. If true, then in the absence of further collagen synthesis, the collagen density in this region should decrease as the tissue volume increases, and this should be reflected by a reduction in picrosirius red (collagen) staining, which is what we observed experimentally. The volumetric expansion of tissue, together with increased chondron size (Decker et al., 2017), accounts for the reduction in cellular density. In addition, proteoglycan composition as a fraction of dry weight should decrease as postnatal maturation proceeds as collagen remodelling is dependent on proteoglycan turnover, and when these analyses are performed, significant decreases ranging between 25% and 50% are observed in maturing cartilage (Gannon et al., 2015; Levin et al., 2005; Brama et al., 1999). Finally, collagen type IX has long or short, alternatively spliced isoforms that differ in the presence of the NC4 domain; their selective expression, along with collagen crosslinking lysyl oxidases (Zhang et al., 2017), which may underlie some of the phenotypic differences observed between immature and mature chondrocyte ECM growth during pellet development, as has been shown in the developing avian cornea (Fitch et al., 1995).

Collagen alignment can occur through direct or indirect physiological and non-physiological mechanisms (Revell et al., 2021). In tendons, fibril alignment is along the principal longitudinal axis of tension, and fibrils are assembled directionally from plasma membrane invaginations called fibropositors (Canty et al., 2004). These structures have not been detected in chondrocytes, and this is unsurprising as these cells are surrounded by a thin shell of the pericellular matrix, although chondrocytes are capable of directional polarisation through the orientation of mechanoresponsive primary cilia (Meier-Vismara et al., 1979; Poole et al., 1985). Another reason for disregarding the latter mechanism for remodelling in cartilage is our data strongly suggest an indirect mechanism of fibril alignment. Fibroblasts, using cell traction forces, are capable of long range (1.5 cm) deformation and remodelling of collagen gels to form aligned ligamentous straps between cell masses (Harris et al., 1981). The generation of tractional forces is a product of cell migration, which occurs through the formation of lamellipodia and filopodia over traction sites—features noticeably absent in chondrocytes from intact cartilage (Morales, 2007). Although we have shown bulk loss of proteoglycans, further analyses need to be conducted using antibodies that can detect aggrecan degradation products to precisely map the regions of increased turnover in the explant. Similarly, MMP3 expression localised by *in situ* hybridisation would provide further evidence of its role in collagen realignment.

In conclusion, this study has uncovered a possible mechanism governing collagen remodelling during postnatal articular cartilage maturation that generates Benninghoff arcade-like structures (Benninghoff, 1925). The central idea is that collagen–collagen and collagen–proteoglycan interactions provide spatial order in the ECM, but when enzymatic activity induces proteoglycan turnover and causes collagen depolymerisation, this allows fibrils the freedom to realign. Water hydrates depolymerised collagen fibrils, imparting further freedom whilst simultaneously inducing tissue expansion, which generates tensile stress to align fibrils along the direction of principal strain, in this case, perpendicular to the surface. This hypothesis can be tested in future studies in several ways to induce collagen reorganisation through, for example, specific enzymatic action or inhibiting the process by preventing tissue expansion. Furthermore, it will be instructive to know whether BMP9-treated cartilage is stiffer or whether further biochemical or biomechanical conditioning is required to fully mature the structure. Collagen is the most abundant protein in the human body and serves as the backbone of connective tissues, which form a myriad of specialised structures with tissue-specific three-dimensional organisations, including the cylindrical, calcified concentric lamellae of bone, the capsules that enclose tissues and organs, the circumferentially aligned fibres of arteries and veins, and the orthogonal lamellae of the cornea. Understanding precisely how these structures are made is important; only then can we engineer them to repair, replace, or regenerate tissues when they are damaged, diseased, or absent. The most successful method of replacing diseased cartilage is using donor transplants of pristine cartilage, not an economically viable solution for millions who suffer from osteoarthritis. The results of this study show that engineering durable cartilage implants with a mature anisotropic organisation may be closer to realisation.

Methods and materials

Articular cartilage explant culture: 7–28-day-old bovine feet were freshly obtained from local abattoirs, thoroughly washed, disinfected with 70% ethanol, and skin removed. Institutional ethical permission was granted for this study as the bovine feet are by-products of the human food chain, and their use complies with the Retained Animal By-Products Regulation (EC)1069/2009. In a sterile hood, metacarpophalangeal joints were opened using a size 23 scalpel, and cartilage explants from the inner aspects of the medial and lateral condyles were cored using a 4-mm biopsy punch. Explants were removed by cutting the inferior surface of the cores. These explants were placed in adjacent pairs or triplets in 24-well culture dishes (Corning, UK), with 1.5 mL of the chondrogenic medium consisting of Dulbecco's modified Eagle medium (DMEM) high glucose and GlutaMAX™, 1 x insulin–transferrin–selenium (ITS). In addition, 100 μg ml^{-1} L-ascorbic acid 2-phosphate sesquimagnesium salt hydrate, 10 mM HEPES (pH 7.5), and 50 μg mL^{-1} gentamicin were included, and the explants were allowed to equilibrate overnight. For treatments, control explants had their medium replaced, while growth factor additions included bone morphogenetic protein-9/growth and differentiation factor-2 (BMP9/gdf2, Peprotech Ltd., UK) at a concentration of 100 ng mL^{-1}, fibroblast growth factor-2 (FGF2, Peprotech Ltd., UK) at 100 ng mL^{-1}, and transforming growth factor-β1 (TGFβ1, Peprotech Ltd., UK) at 10 ng mL^{-1}. The culture medium was replaced every 4th day for

both 10.5- and 21-day cultured explants. For inhibitor studies, PD166793 (Tocris, UK), dissolved in dimethyl sulphoxide (DMSO), was added at a final concentration of either 10 μM or 100 μM to explant medium, with control explants receiving the same volume of DMSO. Inhibitor was replenished at medium changes.

Histological analysis: explants were fixed in 4% paraformaldehyde in phosphate-buffered saline (PBS) overnight at 4°C and then processed into wax, and 8 μm sections were cut. Dewaxed and rehydrated sections were either stained for proteoglycan using the metachromatic stain 1% (aq) toluidine blue for 60 s or collagen by picrosirius red for 60 min following treatment with 1% w/v hyaluronidase for 60 min at 37°C to remove proteoglycan. Polarised light microscopy was conducted using a Leica DMLP Microscope equipped with a circular stage where picrosirius red stained sections were orientated with the surface zone at 45° to the crossed polarising filters in order to detect birefringent light signal. Image analysis: the cell density of explants was quantified using ImageJ using fluorescent images of 4′,6-diamidino-2-phenylindole (DAPI)-stained histological sections. The image was converted to 16-bit greyscale and threshold adjusted to highlight cell nuclei, and the merged nuclei were separated using the watershed function and counted using the *Analyse Particles* function. The same technique was used to highlight chondrons in picrosirius red-stained sections and measure their circularity, aspect ratio, and area from spatially calibrated images (approximate dimensions 300 × 100 microns, l x w) using the *Analyse Particles* function. Analysis of collagen fibrils was performed using the ImageJ plugin FibrilTool (Boudaoud et al., 2014), which provides a quantitative description of the average orientation and anisotropy of fibrous arrays in tissues. Five sequential 75 μm × 75 μm areas from the surface of polarised light microscopy-imaged sections of explants were analysed for anisotropy and average orientation, and the outputs from the log file were re-plotted to lines (line length = anisotropy and line direction = average orientation).

Biochemical analysis: explants for cryosectioning or biochemical analysis were snap-frozen in beakers filled with n-hexane pre-cooled in a dry-ice and ethanol bath. Frozen explants were digested in 20 mM sodium phosphate (pH 6.8), 1 mM EDTA, 2 mM dithiothreitol, and 300 μg mL^{-1} papain at 60°C for 60 min. Proteoglycan in explants and explant culture medium was determined indirectly through the measurement of sulphated glycosaminoglycan (sGAG) content in papain-digested solutions using the dimethylmethylene blue assay and shark chondroitin sulphate to generate a standard curve (Farndale et al., 1986). Collagen content was determined indirectly through the quantification of hydroxyproline content of papain-digested solutions by alkali hydrolysis as described by Cissell et al. (2017).

Antibody labelling: cryosections, 5 μm, were cut and washed in Tris-buffered saline/0.1% (v/v) Tween-20 (TBST) to remove optimal cutting temperature cryomountant (OCT: RA Lamb), treated with 1% (w/v) hyaluronidase in TBST for 60 min at 37°C to remove proteoglycan, blocked with 10% goat serum in TBST for 30 min, and then incubated with 1 μg mL^{-1} of the primary antibody, mouse monoclonal IgG anti-COL2¾m in TBST, overnight at 4°C. Following several washes at room temperature with TBST, labelled epitopes were detected using 5 μg mL^{-1} of the secondary antibody, goat anti-mouse Alexa Fluor 594 (Thermo Fisher Scientific, UK) for 60 min, washed in TBST, overlaid with DAPI containing antifade mounting medium (VECTASHIELD, VectorLabs, UK), and imaged using an Axio Imager M1 Fluorescence Microscope (Zeiss, UK). For the *in situ* detection of bromodeoxyuridine (BrdU) incorporation in immature cartilage, 10 μg mL^{-1} BrdU was added to the medium for the final 3 days of cultures of 21-day explants, at the end of which explants were washed in DMEM, fixed in 4% paraformaldehyde in PBS overnight 4°C, and processed to generate 8-μm wax sections. Standard procedures for antibody labelling were performed, as described above, with the addition of an incubation step of 60 min in 0.2 M HCL to denature DNA, followed by incubation with 0.1 M sodium borate buffer (pH 8.5) to neutralise acid. In addition, 1 μg mL^{-1} mouse monoclonal antibody G3G4 (obtained from Development Studies Hybridoma Bank, U. Iowa, United States) was used to detect labelled DNA and goat anti-mouse Alexa Fluor 594 as a secondary antibody.

In situ zymography: frozen 5-μm sections were washed in TBST, then rinsed with wax, and overlaid with 100 μg mL^{-1} DQ gelatin (Thermo Fisher Scientific, UK) in 50 mM Tris-HCL (pH 7.6), 5 mM $CaCl_2$, and 150 mM NaCl for 60 min at 37°C in a humidified chamber. Sections were then washed three times for 5 min in TBST, overlaid with DAPI containing VECTASHIELD, and imaged using fluorescence microscopy.

Reverse transcription-quantitative polymerase chain reactions (RT-qPCR): all explants were snap-frozen in n-hexane, as described above, prior to processing for RNA extraction. Samples were placed in liquid nitrogen-frozen metal chambers containing 0.5 mL of TRIzol reagent (Merck, UK) and homogenised in a dismembrator at 2000 cycles per min for 120 s (Micro-dismembrator U, B. Braun Melsungen AG, Germany); the resulting powder was placed in an Eppendorf tube containing chloroform, vigorously mixed, and microcentrifuged for 15 min. The clear supernatant was then added to an equal volume of 70% ethanol. The mixture was transferred to a collection column from the RNeasy Plus Kit (QIAGEN, UK), and the supplier's protocol was followed to isolate total RNA. Complementary DNA was synthesised using 1 μg total RNA and M-MLV reverse transcriptase (Promega, UK) under the supplier's recommended conditions. QPCR was performed using the GoTaq SYBR Green Master Mix (Promega, UK), 0.3 μM forward and reverse primers, and 12.5 ng of cDNA. Reactions were run on a CFX96 programmable thermal cycler (Bio-Rad, UK) with the following program: at 95°C for 10 min, at 95°C for 30 s, at 60°C for 30 s, and at 72°C for 30 s for 40 cycles. Data are shown as absolute values in nanogrammes as a ratio of 18SrRNA for each sample. Primer sequences were obtained from previously published sources (Khan et al., 2011; Khan et al., 2013; Zhang et al., 2017).

High-density pellet culture: full-depth slices of cartilage were dissected from the metacarpophalangeal joints of immature (7–14-day old) and mature (18–23-month old) bovine steers under sterile conditions. The cartilage slices were temporarily placed in DMEM. Cartilage was finely diced and then incubated for 1 h at 37°C under constant agitation in DMEM high glucose and GlutaMAX™, supplemented with 10 mM HEPES (pH 7.5), 50 μg mL^{-1} gentamicin, and 0.1% (w/v) pronase (from *Streptomyces griseus*, Merck, UK). After the initial incubation, the pronase solution was replaced with 0.06% collagenase (from *Clostridium histolyticum*, Merck, UK) and 2.5% foetal bovine serum, and the cartilage was then digested for 12 h at 37°C under constant agitation. The extract was poured through a Falcon™ 40 μm cell strainer to produce a single-cell isolate. Cells were washed in the chondrogenic medium and re-suspended at a

concentration of 0.5×10^6 cells mL^{-1} in the chondrogenic medium, with or without 100 ng mL^{-1} BMP9, in 1.5 mL Eppendorf tubes. The tubes were spun at 500 x *g* for 5 min to generate cell pellets. Medium was replaced every 4th day. Pellets were cultured for 21 days, following which they were fixed in 4% paraformaldehyde in PBS for 12 h at 4°C. The fixed pellets were processed for wax embedding and sectioning.

Statistical analyses: the results are presented as the mean ± standard deviation (s.d.). All datasets involving multiple groups were assessed for normal distribution using the Shapiro–Wilk test and homogeneity of variances using Levene's test prior to parametric analysis of variance (one-way ANOVA with *post hoc* testing using the Tukey's method) or non-parametric analysis (the Kruskal–Wallis test with *post hoc* testing using the Conover/Holm method). For analysis of the averages of two groups, we used a two-tailed Student's t-test. Sample size, replicate descriptions, and details regarding the use of representative datasets are specified in each case in the figure legends. Significant differences are annotated in graphs using asterisks as follows: $p < 0.05$ (*), $p < 0.01$ (**), and $p < 0.001$ (***).

Data availability statement

The raw data supporting the conclusions of this article will be made available by the authors, without undue reservation.

Ethics statement

The animal studies were approved by the Faculty of Medicine, Health and Life Science, Swansea University. The studies were conducted in accordance with the local legislation and institutional requirements.

Author contributions

MA-W: conceptualization, investigation, methodology, writing–original draft, and writing–review and editing. IK: conceptualization, data curation, funding acquisition, investigation, methodology, project administration, supervision, writing–original draft, and writing–review and editing.

Funding

The author(s) declare that no financial support was received for the research, authorship, and/or publication of this article.

Acknowledgments

IK would like to acknowledge funding from the Medical Research Council United Kingdom (MR/V027670/1) and EPSRC (EP/S014306/1) for this study.

Conflict of interest

The authors declare that the research was conducted in the absence of any commercial or financial relationships that could be construed as a potential conflict of interest.

Generative AI statement

The author(s) declare that no Generative AI was used in the creation of this manuscript.

Publisher's note

All claims expressed in this article are solely those of the authors and do not necessarily represent those of their affiliated organizations, or those of the publisher, the editors and the reviewers. Any product that may be evaluated in this article, or claim that may be made by its manufacturer, is not guaranteed or endorsed by the publisher.

Supplementary material

The Supplementary Material for this article can be found online at: https://www.frontiersin.org/articles/10.3389/fcell.2024.1511908/full#supplementary-material

References

Andriotis, O. G., Desissaire, S., and Thurner, P. J. (2018). Collagen fibrils: nature's highly tunable nonlinear springs. *ACS Nano* 12, 3671–3680. doi:10.1021/acsnano.8b00837

Aspden, R. M., and Hukins, D. W. (1981). Collagen organization in articular cartilage, determined by X-ray diffraction, and its relationship to tissue function. *Proc. R. Soc. Lond B Biol. Sci.* 212, 299–304. doi:10.1098/rspb.1981.0040

Aszodi, A., Hunziker, E. B., Brakebusch, C., and Fassler, R. (2003). Beta1 integrins regulate chondrocyte rotation, G1 progression, and cytokinesis. *Genes Dev.* 17, 2465–2479. doi:10.1101/gad.277003

Benninghoff, A. (1925). Form und Bau der Gelenkknorpel in ihren Beziehungen zur Funktion. II. Der Aufbau des Gelenkknorpels in seinen Beziehungen zur Funktion. *Zeitschrift für Zellforschung mikroskopische Anatomie* 2, 783–862. doi:10.1007/bf00583443

Billinghurst, R. C., Dahlberg, L., Ionescu, M., Reiner, A., Bourne, R., Rorabeck, C., et al. (1997). Enhanced cleavage of type II collagen by collagenases in osteoarthritic articular cartilage. *J. Clin. Invest* 99, 1534–1545. doi:10.1172/JCI119316

Blunk, T., Sieminski, A. L., Appel, B., Croft, C., Courter, D. L., Chieh, J. J., et al. (2003). Bone morphogenetic protein 9: a potent modulator of cartilage development *in vitro*. *Growth factors.* 21, 71–77. doi:10.1080/0897719031000148822

Boudaoud, A., Burian, A., Borowska-Wykręt, D., Uyttewaal, M., Wrzalik, R., Kwiatkowska, D., et al. (2014). FibrilTool, an ImageJ plug-in to quantify fibrillar structures in raw microscopy images. *Nat. Protoc.* 9, 457–463. doi:10.1038/nprot.2014.024

Brama, P. A., Tekoppele, J. M., Bank, R. A., van Weeren, P. R., and Barneveld, A. (1999). Influence of different exercise levels and age on the biochemical characteristics of immature equine articular cartilage. *Equine Vet. J. Suppl.* 31, 55–61. doi:10.1111/j.2042-3306.1999.tb05314.x

Brito, L. F., Barth, A. D., Rawlings, N. C., Wilde, R. E., Crews, D. H., Boisclair, Y. R., et al. (2007). Effect of feed restriction during calfhood on serum concentrations of metabolic hormones, gonadotropins, testosterone, and on sexual development in bulls. *Reproduction* 134, 171–181. doi:10.1530/REP-06-0353

Canty, E. G., Lu, Y., Meadows, R. S., Shaw, M. K., Holmes, D. F., and Kadler, K. E. (2004). Coalignment of plasma membrane channels and protrusions (fibripositors)

specifies the parallelism of tendon. *J. Cell Biol.* 165, 553–563. doi:10.1083/jcb.200312071

Cederlund, A. A., and Aspden, R. M. (2022). Walking on water: revisiting the role of water in articular cartilage biomechanics in relation to tissue engineering and regenerative medicine. *J. R. Soc. Interface* 19, 20220364. doi:10.1098/rsif.2022.0364

Cissell, D. D., Link, J. M., Hu, J. C., and Athanasiou, K. A. (2017). A modified hydroxyproline assay based on hydrochloric acid in ehrlich's solution accurately measures tissue collagen content. *Tissue Eng. Part C Methods* 23, 243–250. doi:10.1089/ten.tec.2017.0018

David, L., Mallet, C., Keramidas, M., Lamandé, N., Gasc, J. M., Dupuis-Girod, S., et al. (2008). Bone morphogenetic protein-9 is a circulating vascular quiescence factor. *Circ. Res.* 102, 914–922. doi:10.1161/CIRCRESAHA.107.165530

Decker, R. S., Um, H. B., Dyment, N. A., Cottingham, N., Usami, Y., Enomoto-Iwamoto, M., et al. (2017). Cell origin, volume and arrangement are drivers of articular cartilage formation, morphogenesis and response to injury in mouse limbs. *Dev. Biol.* 426, 56–68. doi:10.1016/j.ydbio.2017.04.006

Eyre, D. R., Weis, M. A., and Wu, J. J. (2006). Articular cartilage collagen: an irreplaceable framework? *Eur. Cell Mater* 12, 57–63. doi:10.22203/ecm.v012a07

Farndale, R. W., Buttle, D. J., and Barrett, A. J. (1986). Improved quantitation and discrimination of sulphated glycosaminoglycans by use of dimethylmethylene blue. *Biochim. Biophys. Acta* 883, 173–177. doi:10.1016/0304-4165(86)90306-5

Fitch, J. M., Gordon, M. K., Gibney, E. P., and Linsenmayer, T. F. (1995). Analysis of transcriptional isoforms of collagen types IX, II, and I in the developing avian cornea by competitive polymerase chain reaction. *Dev. Dyn.* 202, 42–53. doi:10.1002/aja.1002020105

Fitch, J. M., Mentzer, A., Mayne, R., and Linsenmayer, T. F. (1988). Acquisition of type IX collagen by the developing avian primary corneal stroma and vitreous. *Dev. Biol.* 128, 396–405. doi:10.1016/0012-1606(88)90301-6

Fosang, A. J., Neame, P. J., Hardingham, T. E., Murphy, G., and Hamilton, J. A. (1991). Cleavage of cartilage proteoglycan between G1 and G2 domains by stromelysins. *J. Biol. Chem.* 266, 15579–15582. doi:10.1016/s0021-9258(18)98442-5

Gannon, A. R., Nagel, T., Bell, A. P., Avery, N. C., and Kelly, D. J. (2015). Postnatal changes to the mechanical properties of articular cartilage are driven by the evolution of its collagen network. *Eur. Cell Mater* 29, 105–121. doi:10.22203/ecm.v029a09

Gardner, O. F. W., Zhang, Y., and Khan, I. M. (2023). BMP9 is a potent inducer of chondrogenesis, volumetric expansion and collagen type II accumulation in bovine auricular cartilage chondroprogenitors. *PLoS One* 18, e0294761. doi:10.1371/journal.pone.0294761

Hapach, L. A., VanderBurgh, J. A., Miller, J. P., and Reinhart-King, C. A. (2015). Manipulation of *in vitro* collagen matrix architecture for scaffolds of improved physiological relevance. *Phys. Biol.* 12, 061002. doi:10.1088/1478-3975/12/6/061002

Harris, A. K., Stopak, D., and Wild, P. (1981). Fibroblast traction as a mechanism for collagen morphogenesis. *Nature* 290, 249–251. doi:10.1038/290249a0

Heinemeier, K. M., Schjerling, P., Heinemeier, J., Møller, M. B., Krogsgaard, M. R., Grum-Schwensen, T., et al. (2016). Radiocarbon dating reveals minimal collagen turnover in both healthy and osteoarthritic human cartilage. *Sci. Transl. Med.* 8, 346ra90. doi:10.1126/scitranslmed.aad8335

Hills, R. L., Belanger, L. M., and Morris, E. A. (2005). Bone morphogenetic protein 9 is a potent anabolic factor for juvenile bovine cartilage, but not adult cartilage. *J. Orthop. Res.* 23, 611–617. doi:10.1016/j.orthres.2004.12.009

Hollander, A. P., Heathfield, T. F., Webber, C., Iwata, Y., Bourne, R., Rorabeck, C., et al. (1994). Increased damage to type II collagen in osteoarthritic articular cartilage detected by a new immunoassay. *J. Clin. Invest* 93, 1722–1732. doi:10.1172/JCI117156

Holmes, D. F., Lu, Y., Starborg, T., and Kadler, K. E. (2018). Collagen fibril assembly and function. *Curr. Top. Dev. Biol.* 130, 107–142. doi:10.1016/bs.ctdb.2018.02.004

Hughes, L. C., Archer, C. W., and ap Gwynn, I. (2005). The ultrastructure of mouse articular cartilage: collagen orientation and implications for tissue functionality. A polarised light and scanning electron microscope study and review. *Eur. Cell Mater* 9, 68–84. doi:10.22203/ecm.v009a09

Hunter, W. (1743). Of the structure and diseases of articular cartilages. *Philosophical Trans. R. Soc. Lond.* 42, 514–521. doi:10.1098/rstl.1742.0079

Hunziker, E. B. (2009). The elusive path to cartilage regeneration. *Adv. Mater* 21, 3419–3424. doi:10.1002/adma.200801957

Hunziker, E. B., Kapfinger, E., and Geiss, J. (2007). The structural architecture of adult mammalian articular cartilage evolves by a synchronized process of tissue resorption and neoformation during postnatal development. *Osteoarthr. Cartil.* 15, 403–413. doi:10.1016/j.joca.2006.09.010

Hyttinen, M. M., Holopainen, J., van Weeren, P. R., Firth, E. C., Helminen, H. J., and Brama, P. A. J. (2009). Changes in collagen fibril network organization and proteoglycan distribution in equine articular cartilage during maturation and growth. *J. Anat.* 215, 584–591. doi:10.1111/j.1469-7580.2009.01140.x

Jadin, K. D., Wong, B. L., Bae, W. C., Li, K. W., Williamson, A. K., Schumacher, B. L., et al. (2005). Depth-varying density and organization of chondrocytes in immature and mature bovine articular cartilage assessed by 3d imaging and analysis. *J. Histochem Cytochem* 53, 1109–1119. doi:10.1369/jhc.4A6511.2005

Julkunen, P., Iivarinen, J., Brama, P. A., Arokoski, J., Jurvelin, J. S., and Helminen, H. J. (2010). Maturation of collagen fibril network structure in tibial and femoral cartilage of rabbits. *Osteoarthr. Cartil.* 18, 406–415. doi:10.1016/j.joca.2009.11.007

Junqueira, L. C., and Montes, G. S. (1983). Biology of collagen-proteoglycan interaction. *Arch. Histol. Jpn.* 46, 589–629. doi:10.1679/aohc.46.589

Kang, Q., Sun, M. H., Cheng, H., Peng, Y., Montag, A. G., Deyrup, A. T., et al. (2004). Characterization of the distinct orthotopic bone-forming activity of 14 BMPs using recombinant adenovirus-mediated gene delivery. *Gene Ther.* 11, 1312–1320. doi:10.1038/sj.gt.3302298

Karimian, E., Chagin, A. S., and Savendahl, L. (2011). Genetic regulation of the growth plate. *Front. Endocrinol. (Lausanne)* 2, 113. doi:10.3389/fendo.2011.00113

Khan, I. M., Evans, S. L., Young, R. D., Blain, E. J., Quantock, A. J., Avery, N., et al. (2011). Fibroblast growth factor 2 and transforming growth factor β1 induce precocious maturation of articular cartilage. *Arthritis Rheum.* 63, 3417–3427. doi:10.1002/art.30543

Khan, I. M., Francis, L., Theobald, P. S., Perni, S., Young, R. D., Prokopovich, P., et al. (2013). *In vitro* growth factor-induced bio engineering of mature articular cartilage. *Biomaterials* 34, 1478–1487. doi:10.1016/j.biomaterials.2012.09.076

Kozhemyakina, E., Zhang, M., Ionescu, A., Ayturk, U. M., Ono, N., Kobayashi, A., et al. (2015). Identification of a Prg4-expressing articular cartilage progenitor cell population in mice. *Arthritis Rheumatol.* 67, 1261–1273. doi:10.1002/art.39030

Levin, A. S., Chen, C. T., and Torzilli, P. A. (2005). Effect of tissue maturity on cell viability in load-injured articular cartilage explants. *Osteoarthr. Cartil.* 13, 488–496. doi:10.1016/j.joca.2005.01.006

Maroudas, A., Palla, G., and Gilav, E. (1992). Racemization of aspartic acid in human articular cartilage. *Connect. Tissue Res.* 28, 161–169. doi:10.3109/03008209209015033

Maroudas, A., Ziv, I., Weisman, N., and Venn, M. (1985). Studies of hydration and swelling pressure in normal and osteoarthritic cartilage. *Biorheology* 22, 159–169. doi:10.3233/bir-1985-22206

Maroudas, A. I. (1976). Balance between swelling pressure and collagen tension in normal and degenerate cartilage. *Nature* 260, 808–809. doi:10.1038/260808a0

Meier-Vismara, E., Walker, N., and Vogel, A. (1979). Single cilia in the articular cartilage of the cat. *Exp. Cell Biol.* 47, 161–171. doi:10.1159/000162933

Miller, A. F., Harvey, S. A., Thies, R. S., and Olson, M. S. (2000). Bone morphogenetic protein-9. An autocrine/paracrine cytokine in the liver. *J. Biol. Chem.* 275, 17937–17945. doi:10.1074/jbc.275.24.17937

Mitteldorf, J. (2019). What is antagonistic pleiotropy? *Biochem. (Mosc)* 84, 1458–1468. doi:10.1134/S0006297919120058

Morales, T. I. (2007). Chondrocyte moves: clever strategies? *Osteoarthr. Cartil.* 15, 861–871. doi:10.1016/j.joca.2007.02.022

Morgan, B. J., Bauza-Mayol, G., Gardner, O. F. W., Zhang, Y., Levato, R., Archer, C. W., et al. (2020). Bone morphogenetic protein-9 is a potent chondrogenic and morphogenic factor for articular cartilage chondroprogenitors. *Stem Cells Dev.* 29, 882–894. doi:10.1089/scd.2019.0209

Mostafa, S., Pakvasa, M., Coalson, E., Zhu, A., Alverdy, A., Castillo, H., et al. (2019). The wonders of BMP9: from mesenchymal stem cell differentiation, angiogenesis, neurogenesis, tumorigenesis, and metabolism to regenerative medicine. *Genes Dis.* 6, 201–223. doi:10.1016/j.gendis.2019.07.003

Musiime, M., Chang, J., Hansen, U., Kadler, K. E., Zeltz, C., and Gullberg, D. (2021). Collagen assembly at the cell surface: dogmas revisited. *Cells* 10, 662. doi:10.3390/cells10030662

Orgel, J. P., San Antonio, J. D., and Antipova, O. (2011). Molecular and structural mapping of collagen fibril interactions. *Connect. Tissue Res.* 52, 2–17. doi:10.3109/03008207.2010.511353

Poole, A. R., Pidoux, I., Reiner, A., and Rosenberg, L. (1982). An immunoelectron microscope study of the organization of proteoglycan monomer, link protein, and collagen in the matrix of articular cartilage. *J. Cell Biol.* 93, 921–937. doi:10.1083/jcb.93.3.921

Poole, C. A. (1997). Articular cartilage chondrons: form, function and failure. *J. Anat.* 191 (Pt 1), 1–13. doi:10.1046/j.1469-7580.1997.19110001.x

Poole, C. A., Flint, M. H., and Beaumont, B. W. (1985). Analysis of the morphology and function of primary cilia in connective tissues: a cellular cybernetic probe? *Cell Motil.* 5, 175–193. doi:10.1002/cm.970050302

Revell, C. K., Jensen, O. E., Shearer, T., Lu, Y., Holmes, D. F., and Kadler, K. E. (2021). Collagen fibril assembly: new approaches to unanswered questions. *Matrix Biol. Plus* 12, 100079. doi:10.1016/j.mbplus.2021.100079

Rieppo, J., Hyttinen, M. M., Halmesmaki, E., Ruotsalainen, H., Vasara, A., Kiviranta, I., et al. (2009). Changes in spatial collagen content and collagen network architecture in porcine articular cartilage during growth and maturation. *Osteoarthr. Cartil.* 17, 448–455. doi:10.1016/j.joca.2008.09.004

Rojas, F. P., Batista, M. A., Lindburg, C. A., Dean, D., Grodzinsky, A. J., Ortiz, C., et al. (2014). Molecular adhesion between cartilage extracellular matrix macromolecules. *Biomacromolecules* 15, 772–780. doi:10.1021/bm401611b

Ronziere, M. C., Berthet-Colominas, C., and Herbage, D. (1985). Low-angle X-ray diffraction analysis of the collagen-proteoglycan interactions in articular cartilage. *Biochim. Biophys. Acta* 842, 170–175. doi:10.1016/0304-4165(85)90199-0

Scharpfenecker, M., van Dinther, M., Liu, Z., van Bezooijen, R. L., Zhao, Q., Pukac, L., et al. (2007). BMP-9 signals via ALK1 and inhibits bFGF-induced endothelial cell proliferation and VEGF-stimulated angiogenesis. *J. Cell Sci.* 120, 964–972. doi:10.1242/jcs.002949

Scott, J. E. P. (1991). Proteoglycan: collagen interactions in connective tissues. Ultrastructural, biochemical, functional and evolutionary aspects. *Int. J. Biol. Macromol.* 13, 157–161. doi:10.1016/0141-8130(91)90041-r

Song, J. J., Celeste, A. J., Kong, F. M., Jirtle, R. L., Rosen, V., and Thies, R. S. (1995). Bone morphogenetic protein-9 binds to liver cells and stimulates proliferation. *Endocrinology* 136, 4293–4297. doi:10.1210/endo.136.10.7664647

Sophia Fox, A. J., Bedi, A., and Rodeo, S. A. (2009). The basic science of articular cartilage: structure, composition, and function. *Sports Health* 1, 461–468. doi:10.1177/1941738109350438

Suzuki, Y., Ohga, N., Morishita, Y., Hida, K., Miyazono, K., and Watabe, T. (2010). BMP-9 induces proliferation of multiple types of endothelial cells *in vitro* and *in vivo*. *J. Cell Sci.* 123, 1684–1692. doi:10.1242/jcs.061556

van Caam, A., Blaney Davidson, E., Garcia de Vinuesa, A., van Geffen, E., van den Berg, W., Goumans, M. J., et al. (2015). The high affinity ALK1-ligand BMP9 induces a hypertrophy-like state in chondrocytes that is antagonized by TGFβ1. *Osteoarthr. Cartil.* 23, 985–995. doi:10.1016/j.joca.2015.02.007[

van der Kraan, P. M. (2014). Age-related alterations in TGF beta signaling as a causal factor of cartilage degeneration in osteoarthritis. *Biomed. Mater Eng.* 24, 75–80. doi:10.3233/BME-140976

van der Rest, M., and Mayne, R. (1988). Type IX collagen proteoglycan from cartilage is covalently cross-linked to type II collagen. *J. Biol. Chem.* 263, 1615–1618. doi:10.1016/s0021-9258(19)77922-8

van Turnhout, M. C., Kranenbarg, S., and van Leeuwen, J. L. (2011). Contribution of postnatal collagen reorientation to depth-dependent mechanical properties of articular cartilage. *Biomech. Model Mechanobiol.* 10, 269–279. doi:10.1007/s10237-010-0233-7

van Turnhout, M. C., Schipper, H., van Lagen, B., Zuilhof, H., Kranenbarg, S., and van Leeuwen, J. L. (2010). Postnatal development of depth-dependent collagen density in ovine articular cartilage. *BMC Dev. Biol.* 10, 108. doi:10.1186/1471-213X-10-108

Varady, P., Li, J. Z., Cunningham, M., Beres, E. J., Das, S., Engh, J., et al. (2001). Morphologic analysis of BMP-9 gene therapy-induced osteogenesis. *Hum. Gene Ther.* 12, 697–710. doi:10.1089/104303401300057423

Williamson, A. K., Chen, A. C., and Sah, R. L. (2001). Compressive properties and function-composition relationships of developing bovine articular cartilage. *J. Orthop. Res.* 19, 1113–1121. doi:10.1016/S0736-0266(01)00052-3

Wu, J. J., Lark, M. W., Chun, L. E., and Eyre, D. R. (1991). Sites of stromelysin cleavage in collagen types II, IX, X, and XI of cartilage. *J. Biol. Chem.* 266, 5625–5628. doi:10.1016/s0021-9258(19)67640-4

Wu, J. J., Woods, P. E., and Eyre, D. R. (1992). Identification of cross-linking sites in bovine cartilage type IX collagen reveals an antiparallel type II-type IX molecular relationship and type IX to type IX bonding. *J. Biol. Chem.* 267, 23007–23014. doi:10.1016/s0021-9258(18)50048-x

Youn, I., Choi, J. B., Cao, L., Setton, L. A., and Guilak, F. (2006). Zonal variations in the three-dimensional morphology of the chondron measured *in situ* using confocal microscopy. *Osteoarthr. Cartil.* 14, 889–897. doi:10.1016/j.joca.2006.02.017

Yu, L., Dawson, L. A., Yan, M., Zimmel, K., Lin, Y. L., Dolan, C. P., et al. (2019). BMP9 stimulates joint regeneration at digit amputation wounds in mice. *Nat. Commun.* 10, 424. doi:10.1038/s41467-018-08278-4

Zhang, Y., Morgan, B. J., Smith, R., Fellows, C. R., Thornton, C., Snow, M., et al. (2017). Platelet-rich plasma induces post-natal maturation of immature articular cartilage and correlates with LOXL1 activation. *Sci. Rep.* 7, 3699. doi:10.1038/s41598-017-02297-9

frontiers | Frontiers in Cell and Developmental Biology

TYPE Original Research
PUBLISHED 27 February 2025
DOI 10.3389/fcell.2025.1533405

Check for updates

OPEN ACCESS

EDITED BY
Elizabeth Vinod,
Christian Medical College and Hospital, India

REVIEWED BY
Alessandra Pisciotta,
University of Modena and Reggio Emilia, Italy
Sven Geissler,
Berlin Institute of Health at
Charité – Universitätsmedizin Berlin, Center for Regenerative Therapies (BCRT), Germany
Ronaldo Jose Farias Correa Do Amaral,
Federal University of Rio de Janeiro, Brazil

*CORRESPONDENCE
Giovanna Desando,
giovanna.desando@ior.it

RECEIVED 23 November 2024
ACCEPTED 10 February 2025
PUBLISHED 27 February 2025

CITATION
Desando G, Tschon M, Martini L, Sartori M, Giavaresi G, Fini M, Cellamare A, Soranzo C, Longinotti C, D'Alessandro M, Roseti L and Grigolo B (2025) 3D connective micro-fragment enriched with stromal vascular fraction in osteoarthritis: chondroprotective evidence in a preclinical *in vivo* model. *Front. Cell Dev. Biol.* 13:1533405. doi: 10.3389/fcell.2025.1533405

COPYRIGHT
© 2025 Desando, Tschon, Martini, Sartori, Giavaresi, Fini, Cellamare, Soranzo, Longinotti, D'Alessandro, Roseti and Grigolo. This is an open-access article distributed under the terms of the Creative Commons Attribution License (CC BY). The use, distribution or reproduction in other forums is permitted, provided the original author(s) and the copyright owner(s) are credited and that the original publication in this journal is cited, in accordance with accepted academic practice. No use, distribution or reproduction is permitted which does not comply with these terms.

3D connective micro-fragment enriched with stromal vascular fraction in osteoarthritis: chondroprotective evidence in a preclinical *in vivo* model

Giovanna Desando[1]*, Matilde Tschon[2], Lucia Martini[2], Maria Sartori[2], Gianluca Giavaresi[2], Milena Fini[3], Antonella Cellamare[1], Carlo Soranzo[4], Cristina Longinotti[4], Martina D'Alessandro[1], Livia Roseti[1] and Brunella Grigolo[1]

[1]IRCCS Istituto Ortopedico Rizzoli, Laboratorio RAMSES, Bologna, Italy, [2]IRCCS Istituto Ortopedico Rizzoli, Scienze e Tecnologie Chirurgiche, Bologna, Italy, [3]IRCCS Istituto Ortopedico Rizzoli, Scientific Director, Bologna, Italy, [4]Fidia Farmaceutici S.p.A., Padova, Italy

Introduction: Adipose-derived cell therapies are one of the most common regenerative therapeutic options to alleviate the multi-component damage of osteoarthritis (OA). Adipose stromal vascular fraction (SVF) has gained scientific consensus for its ability to interact protectively with the joint microenvironment. Recently, the wide range of enzyme-free tissue processing systems has outperformed classical treatments, because of their ability to produce connective micrografts enriched with the SVF (mctSVF). This preclinical *in vivo* study evaluates the chondroprotective potential of a newly generated mctSVF compared with *in vitro* expanded adipose stromal cells (ASC) in OA.

Methods: A mild grade of OA was induced through bilateral anterior cruciate ligament transection (ACLT) surgery in 32 Specific Pathogen Free (SPF) Crl: KBL (NZW) male rabbits followed by the surgical excision of inguinal adipose tissue. After 2 months, OA joints were treated with an intra-articular (IA) injection of mctSVF or ASC. Local biodistribution analysis was used to determine migration patterns of PKH26-labelled cells in the knee joint after 1 month. Efficacy was assessed by gross analysis, histology and immunohistochemistry on the osteochondral unit, synovial membrane and meniscus.

Results: We elucidate the effectiveness of a one-step approach based on mechanical isolation of mctSVF. Through epifluorescence analysis, we found a similar pattern of cell distribution between cell treatments, mainly towards articular cartilage. Similar regenerative responses were observed in all experimental groups. These effects included: (i) osteochondral repair (promotion of typical anabolic markers and reduction of catabolic ones); (ii) reduction of synovial reactions (reduced synovial hypertrophy and inflammation, and change of macrophage phenotype to a more regenerative one); and (iii) reduction of degenerative changes in the meniscus (reduction of tears).

Discussion: Our study demonstrates the validity of a novel mechanical system for the generation of the mctSVF micrograft with chondroprotective potential in a preclinical model of moderate OA. The resulting final product can counteract inflammatory processes beyond the OA microenvironment and protect cartilage

through the colonization of its structure. The intact and active microanatomy of mctSVF makes it a suitable candidate for translational medicine to treat OA without the need for cell manipulation as with ASC.

KEYWORDS

adipose stromal cells, articular cartilage repair, cell-based therapies, preclinical *in vivo* study, osteoarthritis, stromal vascular fraction, connective tissue micrograft

1 Introduction

The multicomponent nature of osteoarthritis (OA) pathogenesis poses a major orthopaedic challenge because of the limited benefit of current clinical interventions (Vrouwe et al., 2021). In this context, cell-based therapeutics have attracted great attention for their pleiotropic wound-healing effects not only on cartilage but also on various joint tissues, affected during OA (Djouad et al., 2009; Filardo et al., 2013; Vinatier and Guicheux, 2016). While clinical studies on bone marrow and adipose tissue, the most common tissue sources for regenerative medical purposes (Zhang and Schon, 2022), have shown promising chondroprotective properties, it is still debated which of them will best counteract the hallmarks of OA (Beane et al., 2014; El-Badawy et al., 2016; Gun-II Im et al., 2005). However, the minimally invasive nature of adipose tissue harvesting, the wide range of isolation methods (Cicione et al., 2023; Gentile et al., 2019; Ossendorff et al., 2023), and the highest yield of mesenchymal stromal cells have led to its more prevalent use than bone marrow (Ibrahim et al., 2022; Oberbauer et al., 2015).

The classical enzymatic procedure, which includes treatment of the tissue with clinical-grade collagenases and/or dispases, permits the SVF first and then adipose stromal cells (ASC) isolation and subsequent culture expansion. Good clinical results have been reported using expanded ASC to improve joint pain and function (Perucca Orfei et al., 2023; Perdisa et al., 2015). Despite their benefits, the long-term cell culture and the need for two-step procedures make them time-consuming, increasing the risk of potential cell changes in apoptosis and senescence (Danisovic, 2017; Froelich et al., 2013) and the need for a GMP cleanroom (Si et al., 2019). On the other hand, the techniques available for mechanically disaggregating adipose tissue into fragments require various steps (centrifugation, filtration, and washing) (Greenwood et al., 2022; Aronowitz JA, 2014), by overcoming some of the limitations associated with the use of expanded cells. Typically, the final products from mechanical isolation may encompass clusters of free cells or fragmented adipose tissue, characterized by a structural connective tissue with its ASC-rich derivatives (mainly SVF) (Francesco et al., 2021). With a size range from micrometres to nanometers, which depends on the filtration system chosen, these components present a significant advantage: they are effectively retained in the OA knee joint, enhancing their therapeutic potential (Cicione et al., 2023; Gentile et al., 2019; Ossendorff et al., 2023). Of note, the various mechanical approaches available may be more advantageous than enzymatic isolation because they avoid the use of exogenous enzymes and preserve the native three-dimensional (3D) structure with intrinsic cues. However, they pose the need for rigorous preclinical studies to select the most promising clinical solutions (Francesco et al., 2021; Busato et al., 2021; Trivisonno et al., 2019; Aronowitz et al., 2015; Aronowitz et al., 2015). In this direction, several studies have compared enzymatic and mechanical isolation techniques using different systems (such as Cytori, Celution, Lipogems, etc.) to better understand their molecular signatures for clinical applications. While mechanical isolation techniques typically yield fewer nucleated cells than enzymatic methods, they are generally safe, cost-effective, and quick to process (Aronowitz et al., 2015). Despite common features, there are differences between filtration systems in terms of: (i) fragment size; (ii) cell population maintained; (iii) paracrine properties; (iv) differentiation potential; and (v) immunomodulatory properties (Gentile et al., 2017; Uguten et al., 2024). Our previous *in vitro* research demonstrated similar outcomes between mechanical and enzymatic isolation methods, showing that both systems contain functional cell populations capable of supporting osteochondral regeneration (Desando et al., 2021). Given the promising *in vitro* evidence, our focus was to validate *in vivo* the characteristics of the Hy-Tissue SVF system (Fidia Farmaceutici, Abano Terme), a CE-marked class IIa device for microfractionation of adipose tissue, and its potential to treat mild OA. This interest stems from the potential benefits that may arise from the use of mctSVF to overcome some of the ethical, regulatory and safety concerns that may be associated with expanded ASC (Desando et al., 2021). Herein, we aimed to test the therapeutic potential of connective tissue micro-fragments enriched with SVF (mctSVF), as an optional treatment for OA, in a validated rabbit model allowing good prediction of tissue repair and clinical translatability. It was hypothesized that the mctSVF encased in native connective tissue would stabilize at the articular site of the knee and have a greater ability to heal than ASC treatment. By characterizing the response to intra-articular (IA) administration of mctSVF, we can conclude that this approach is effective in restoring the osteochondral unit and reducing inflammation, with the potential for clinical translation in this clinical setting.

2 Materials and methods

2.1 Ethics committee approval and experimental design

All *in vivo* procedures were performed following the animal care and use guidelines in compliance with the Italian Law (Law by Decree no 26/2014) and according to the European Commission Recommendation on guidelines for the accommodation and care of animals used for experimental and other scientific purposes (2007/526/EC). The *in vivo* protocol was developed following the PREPARE guidelines (Planning Research and Experimental Procedures on Animals: Recommendations for Excellence); it was approved by the Animal Welfare Body of IRCCS-Istituto

Ortopedico Rizzoli (IOR) on 14th May 2019, authorized by the Italian Ministry of Health (Aut. n. 557/2019-PR on 23rd July 2019) and foresaw the efficacy testing of one-step and *in vitro* expanded cell-based and viscosupplementant products. To further improve the quality of this study, the *in vivo* research methodology has been reported according to criteria set in the Animal in Research: Reporting of *in Vivo* Experiments (ARRIVE 2.0) guidelines (Percie du Sert et al., 2020). The ARRIVE Essential checklist is provided in Supplementary Table 1. The sample size was calculated using the software G*Power v.3.1.9.2 (Franz Faul, Universität Kiel, Germany): by assuming that an effect $f \geq 0.63$ could be obtained for Laverty's histomorphometric score, in a one-way ANOVA model (type of treatment) with $\alpha = 0.05$ and $1\text{-}\beta = 0.80$, it was calculated that a minimum number of n = 8 animals per experimental group was required. Following the principle of the 3Rs, the sample size of the control groups, SHAM, and OA was reduced to n = 4 per group, considering previous studies (Desando et al., 2013; Grigolo et al., 2009) and literature efficacy studies (Mainil-Varlet et al., 2013) with the same animal model.

The present work reports data and results to compare ASC and mctSVF products in the treatment of rabbit knee OA versus the control groups. Animals received from the vendor with the same age were divided into 6 groups (OA (n = 4 + n = 9 from previous studies), SHAM (n = 4 + n = 7 from previous studies), ASC (n = 8), mctSVF (n = 8), PKH-26 ASC (n = 4), PKH26 mctSVF (n = 4)) and received the same stabling conditions. No randomization was applied to allocate animals to groups; however, outcome assessors (GD, AC) were blind to the allocation groups during the assessment and analysis of the data to minimize performance and detection biases. Animals in the same group receiving the same treatment were placed in closely spaced cages to minimise potential co-founders. No animal or data points were excluded before the final analysis. The primary outcome measure of this study was femoral and synovial histological analysis, supported by semi-quantitative scoring systems, to assess the efficacy of the 2 cell treatments.

2.2 Rabbit *in vivo* model and procedures

2.2.1 Surgical OA induction

Thirty-two SPF Crl: KBL (NZW) male rabbits (Charles River Laboratories, Italy), 2.7 ± 0.2 kg b. w., were used and housed in single cages in standard controlled conditions with free access to water and pellet diet and specific enrichments. A 10-day conditioning period with frequent animal handling was pursued to acclimate animals.

Surgical procedures were aseptically performed after a 10-day quarantine period and under general anaesthesia induced by premedication with i. m. injections of ketamine (44 mg/kg) and xylazine (0.3 mg/kg) and maintained with O_2/air and 2%–3% halogenate (isofluorane) in spontaneous breathing by a facial mask. A 2 cm surgical incision was bilaterally carried out in the lateral surface of the knee: after the articular capsule incision, the patellar bone was displayed medially, and the anterior cruciate ligament (ACL) was exposed and transected with the knee placed in full flexion. To avoid spontaneous healing, a small fragment of 2.5-mm length was removed. The articular capsule and skin were sutured by layers. In the SHAM group, skin and articular capsule incisions were performed, without ACL transection.

In the immediate post-op, i. m. injection of anaesthetics (3.75 mg of a solution 7.5 mg/mL of ropivacaine), applied locally to the surgical site, and 1/3 of a 50 μg/h/72 h fentanyl transdermal patch were used; in the following 5 days, analgesic (50 mg/kg/die) and antibiotic (10 mg/kg enrofloxacin) therapies were administered s. c. In the post-op, animals were clinically monitored daily in the first week and weekly thereafter, unless any complications occurred, by the control of the general conditions, weight measurements, major organ functions, and food and water consumption.

The following humane endpoints were set: loss of body weight greater than 20% of their physiological growth curve, severe limb lesions or irreversible alterations in major organic functions. Criteria for exclusion from analyses were severe intra-anaesthesiologic complications, knee infections or humane endpoint achievement.

2.2.2 Surgical harvest of adipose tissue, tissue processing and IA treatments

Under general anaesthesia and aseptic conditions, inguinal adipose tissue (AT) was surgically collected and processed, as described in detail in a previous article (Desando et al., 2021), for i) the generation of *in vitro* expanded ASC and ii) the production of mctSVF. For the expanded-ASC, inguinal AT was harvested 2 weeks before IA treatments and treated with 0.4 U/mL NB4 collagenase standard grade (Serva Electrophoresis, GmbH, Heidelberg, Germany, Cat. DS17454.01) for 30 min at 37°C to obtain the SVF and then kept a fortnight until passage 2 in α-MEM (Gibco, Carlsbad, CA, United States) medium containing 15% fetal bovine serum (FBS, Euroclone) and 0.05 g/mL penicillin G (Gibco). Cell count was evaluated at SVF isolation and expansion.

As for mctSVF, the inguinal AT was harvested on the same day of IA injection and processed in a single sterile disposable device Hy-Tissue SVF (Fidia Farmaceutici, Abano Terme, Italy). After collection, AT was minced with scissors, resuspended with saline, and then moved into a closed sterile bag to perform mechanical fragmentation. Duografter (Fidia Farmaceutici) subjected the filtered intermediate adipose product to centrifugation at 600 g for 10 min to generate the final product (Desando et al., 2021).

Eight weeks after OA induction, animals received IA injection of 2×10^6 ASC (n = 8) or mctSVF (n = 8) in each knee to assess their efficacy. For local biodistribution groups, 2×10^6 ASC and mctSVF were labelled with 2 μM PKH26 (Sigma-Aldrich, Cat. PKH26GL), and injected in each knee to monitor cell migration at 1 month from treatments. Live&Dead test (Thermo Fisher Scientific, Waltham, MA, United States, Cat. L10119) was performed on all adipose products for efficacy analyses before the IA treatment. Live (green staining) and dead (red staining) cells were evaluated with the DS-Ri2 microscope (Nikon, Tokyo, Japan), by using fluorescence channels: fluorescein isothiocyanate (FITC) and tetramethyl rhodamine isothiocyanate (TRITC). Trypan blue staining was used to assess the number of viable labelled cells in the cell suspension before IA injection for biodistribution analysis. The dye stains non-viable cells in blue, while it is excluded from living cells.

2.2.3 Experimental times and tissue explants

At the selected experimental times, rabbits were pharmacologically euthanized under deep general anaesthesia with intravenous administration of 1 mL of Tanax® (Hoechst AG, Frankfurt-am-Main, Germany). Animals allocated in the

local biodistribution groups were euthanized after 1 month from IA treatments: femoral condyles, tibial plateaus, menisci, synovial fluids and membranes and posterior cruciate and collateral ligaments were harvested for analysis through the assessment of the fluorescent cells with the DS-Ri2 microscope (Nikon, Tokyo, Japan). Briefly, biopsies were fixed with 10% neutral buffered formalin, decalcified when the bone component was present, paraffin-embedded, and microtome-cut. Dried cytospin preparations of synovial fluid were prepared after centrifugation for 10′ at 600 g in a cytocentrifuge (Thermo Fisher Scientific, Waltham, MA, United States). Then, cell nuclei of all samples were counterstained with 1 μg/mL 4′,6-diamidino-2-phenylindole (DAPI) (Sigma-Aldrich). Image analysis was performed with the NIS-Elements software, using the Hue/Saturation/Intensity (HSI) system, to quantify the percentage of positive cells at different specimen depths to better understand cell penetration within the tissues. Specifically, we presented a percentage of the stained cells over the total cells per tissue.

Animals allocated in the efficacy treatment groups were euthanized after 2 months from IA treatments: femoral condyles, meniscus and synovial membranes were explanted and processed for analyses.

2.3 Treatment efficacy on tissue samples: macroscopic and immunohistochemical analyses

Several methodologies were used to test the bio-functional properties of the osteochondral unit in the medial femoral condyle, synovial membrane and menisci in the control and experimental groups by two blinded investigators to the groups (GD and AC), according to the specific scores.

2.3.1 Macroscopic assessment on articular cartilage

Outerbridge score was used for macroscopic analysis of femoral condyles in the control and experimental groups. This method allows a first assessment of articular cartilage, discriminating early, mild and severe degrees of OA. Specifically, the Outerbridge score has a value from 0 (an indicator of healthy tissue) to 4 (severe OA grade) (Laverty et al., 2010).

2.3.2 Histological assessment on osteochondral, synovium and meniscus specimens

Next, histological examinations on different joint tissues were made to assess their architecture to ensure adequate function, using specific stainings with Safranin O/Fast green (Sigma Aldrich) for articular cartilage and meniscus and haematoxylin/eosin for synovial membrane. In general, seven sagittal sections per tissue, spaced 10 sections apart, were assessed to investigate the impact of cell treatments on cartilage and meniscus repair.

Specifically, we have used the Laverty score to provide a quantitative measurement of cartilage repair after treatments. This score has values ranging from 0 (healthy tissue) to 24 (severe OA) (Laverty et al., 2010). Parameters of this score, commonly associated with OA changes, include: (i) safranin-O staining to evaluate proteoglycan content; (ii) cartilage structure to assess extracellular matrix composition; (iii) chondrocyte density; and (iv) cluster formation.

As for subchondral bone, we have examined tissue architecture examining cellularity and bone marrow spaces using a semiquantitative score, which has a range from 0 (an indicator of healthy tissue) to 3 (an indicator of severe OA) (Aho et al., 2017).

Synovial specimens were stained with Hematoxylin/Eosin (Sigma Aldrich) to estimate their architectural appearance with a semi-quantitative analysis with Laverty score (Laverty et al., 2010). This score considers different parameters of synoviopathy, such as proliferation, hypertrophy, and inflammatory status, which affect tissue function.

As for the meniscus, with a pivotal role in knee biomechanics, a modified Pauli's score was included in the study to assess its histopathological features during OA, including tears. This score shows a range from 0 to 18, where 0 is an index of healthy tissue and 18 of severe OA (Chevrier et al., 2009; Pauli et al., 2011).

2.3.3 Immunohistochemical analysis on cartilage, bone, synovial and meniscus specimens

Further in-depth assessments were carried out on articular cartilage and synovial membrane using indirect colourimetric immunohistochemistry (IHC) with a dedicated panel of markers. Biotin-streptavidin (4plus Universal AP Detection; Biocare Medical) and the alkaline phosphatase detection system (Fast Red Substrate Kit; Biocare Medical) were used on biological replicates from the control and experimental groups. As for the articular cartilage, we used the following antibodies mouse monoclonal collagen type I (COL1) (2 μg/mL) (Sigma-Aldrich), mouse monoclonal collagen type II (COL2) (2 μg/mL) (Hybridoma Bank, Department of Biological Sciences, University of Iowa City, IA), mouse monoclonal matrix metalloproteinase (MMP)-3 (5 μg/mL) (Chemicon, Temecula, CA).

As for the subchondral bone, we tested osteocalcin (OC) (2 μg/mL) (Thermo Fisher Scientific, Waltham, MA, United States; Catalog #MA1-20788).

As for the synovial membrane, the protein expression of mouse monoclonal RAM-11 (1.5 μg/mL) (Dako) (macrophages found in inflammatory atherosclerotic plaques in rabbits), mouse monoclonal CD-163 (1 μg/mL) (Abcam) (macrophages with a regenerative phenotype) and MMP-3 (5 μg/mL) (Chemicon, CA) was performed to evaluate macrophage subtypes and catabolic processes, respectively.

As for the meniscus specimens, the protein expression of mouse monoclonal collagen type I (COL1) (2 μg/mL) (Sigma-Aldrich) and mouse monoclonal matrix metalloproteinase (MMP)-3 (5 μg/mL) (Chemicon, CA) was carried out.

The selection of markers has been made based on the anabolic and catabolic processes that are involved in joint degeneration in OA. Before incubation with the primary antibodies, specific unmasking procedures were done for articular cartilage with 1 mg/mL pronase (Sigma-Aldrich). Negative controls were run by omitting the primary antibodies or using an isotype-matching control.

Image analysis was performed on specimens immunostained to provide a quantitative assessment. Specifically, the Hue Saturation Intensity (HSI) system was adopted to define the threshold of positivity for each marker and establish a percentage value of positivity, ranging from 0 (no positivity) to 100 (highest positivity). All assessments were conducted by trained scientists (AC, GD) using a DS-Ri2 microscope (Nikon, Tokyo, Japan), blind to the type of treatment.

2.4 Statistical analysis

The Statistical Package for the Social Sciences (SPSS Inc., Chicago, IL, United States) software version 15.0 (SPSS Inc.) was used for statistical analyses. The presence of outliers was checked using the ROUT test (Q = 1%) before each test. If present, outliers were removed from each dataset. Kolmogorov-Smirnov (K-S) and Shapiro-Wilk tests were carried out to test the normality of data distribution. Datasets showing a Gaussian distribution were assayed by one-way ANOVA and general linear model (GLM) tests with the Sidak *post hoc* test for multiple comparisons. Specifically, a one-way ANOVA and Sidak tests were used to assess differences in cell biodistribution between ASC and mctSVF groups, which showed a normal distribution. Datasets from macroscopic and immunohistochemical assessments, that showed a normal distribution, were assayed the GLM with Sidak correction for multiple comparisons. In particular, the GLM with Tweedie/gamma distribution and log link function was used to analyse the parameters comprising the histological scores of cartilage, synovium, and meniscus (mPauli); the total score was the dependent variable and the cases were the fixed effects.

Datasets with no Gaussian distribution, as observed for the number of nucleated cells and cell viability were assayed with the Kruskall-Wallis and Dunn's *post hoc* test. The estimated expected values with Wald 95% confidence intervals were compared using contrasts versus OA and Sidak correction for multiple comparisons. The non-parametric Spearman's rank-order method was used to find correlations between viable cells of ASC and mctSVF treatments and (1) cartilage score; (2) synovium score; and (3) meniscus score. Data were considered significant at $P < 0.05$ (*), $P < 0.01$ (**), $P < 0.001$ (***), and $P < 0.0001$ (****).

3 Results

3.1 Report on adverse effects

No fractures, infections or changes in major organ functions were found in the post-op period. Some minor side effects mainly related to the type of surgery and the experimental model were found; in particular, 7/32 animals showed moderate joint effusion on the first post-op day, which resolved in 3–4 days, 10/32 animals developed lameness that resolved 1 week after surgery and 2/32 animals received analgesics for further 72 h. All cases were included in the data analysis. As detailed in the figure legends, for the SHAM and OA groups, we included additional cases from previous studies, conducted using the same surgical protocols and procedures, to increase the statistical power according to the principles of the 3Rs.

3.2 The mechanical process with Hy-tissue SVF produces viable cells

As a quality control, mctSVF cells were counted with the Turk stain and tested using the Live&Dead assay to monitor cell number and viability, respectively. The interval range of the mctSVF cells produced was from 3.5×10^4 to 3.5×10^5 nucleated cells/g of adipose tissue. Conversely, eSVF and ASC showed a higher amount of nucleated cells/g of adipose tissue, a mean value of 1.15×10^6 and 7.3×10^5, respectively (Figure 1A). Comparable values of cell viability among enzymatic SVF, expanded ASC and mctSVF were found, by reporting optimal percentages. The PKH26 staining had no effects on cell viability. According to the guidelines proposed by the International Federation for Adipose Therapeutics and Science (IFATS), all cell products showed good potential for clinical translation (Figure 1B) (Desando et al., 2021). We found a negative correlation between the cell viability of both cell groups and the cartilage, synovial, and meniscus scores (Supplementary Table 2). The highest levels of cell viability correlated with the lowest scores, reflecting better tissue repair. This suggests that higher levels of cell viability are associated with improved histological outcomes.

3.3 PKH26-ASC and mctSVF accumulate to a higher level in the cartilage at 1 month

Analysis of cell migration using a fluorescent dye, PKH26, was performed to track the distribution of ASC and mctSVF products to provide some mechanistic insights on their potential clinical translation in OA (Figures 1C, D). PKH26-ASC and PKH26-mctSVF showed a high tropism towards injured areas of articular cartilage (cell clones and fibrillated areas) after 1 month. In the ASC group, the cartilage tissue showed the highest percentage of labelled cells, displaying an increased percentage of 29.3%, 28.3%, 14.3%, and 27.7% than synovia, meniscus, ligaments, and synovial fluids, respectively. Both synovia and meniscus also showed the lowest migration pattern of 15% and 14% than the ligaments. ASC group reported a significantly higher percentage of cell distribution in cartilage than in the meniscus and ligaments. Similarly to ASC, the mctSVF group showed most cells migrating towards cartilage reporting higher values of the distribution pattern of 34%, 25.8%, 23%, and 26.7% than synovia, meniscus, ligaments, and synovial fluids, respectively. Labelled mctSVF showed a minor tropism to the synovial membrane, which displayed also reduced values than the meniscus. mctSVF group showed significantly higher mean values of distribution in cartilage than the meniscus and ligaments. Significant differences in the migration pattern between the two cell-treated groups were found only at the meniscal level, with a higher distribution pattern for mctSVF than the ASC group (Figure 1C) (Supplementary Tables 3, 4).

3.4 mctSVF treatment protects the cartilage from OA-related structural degradation

After 8 weeks from ACLT surgery, the femoral condyles of the OA group were analyzed to evaluate histopathological features (Figures 2A–D). The macroscopic assessment showed fibrillation areas and the presence of greater erosive zones in the medial femur. The IA treatment with ASC and mctSVF provided several benefits in reducing macroscopic OA features such as fibrillation and erosion in the articular cartilage. In particular, the Outerbridge score, a semi-quantitative measure of the macroscopic OA severity process, demonstrated a significant OA reduction especially after ASC-based therapy and to a lesser extent in the mtcSVF group (Figure 2A). As for the OA group, histochemical staining with Safranin-O/Fast green confirmed macroscopic assessments

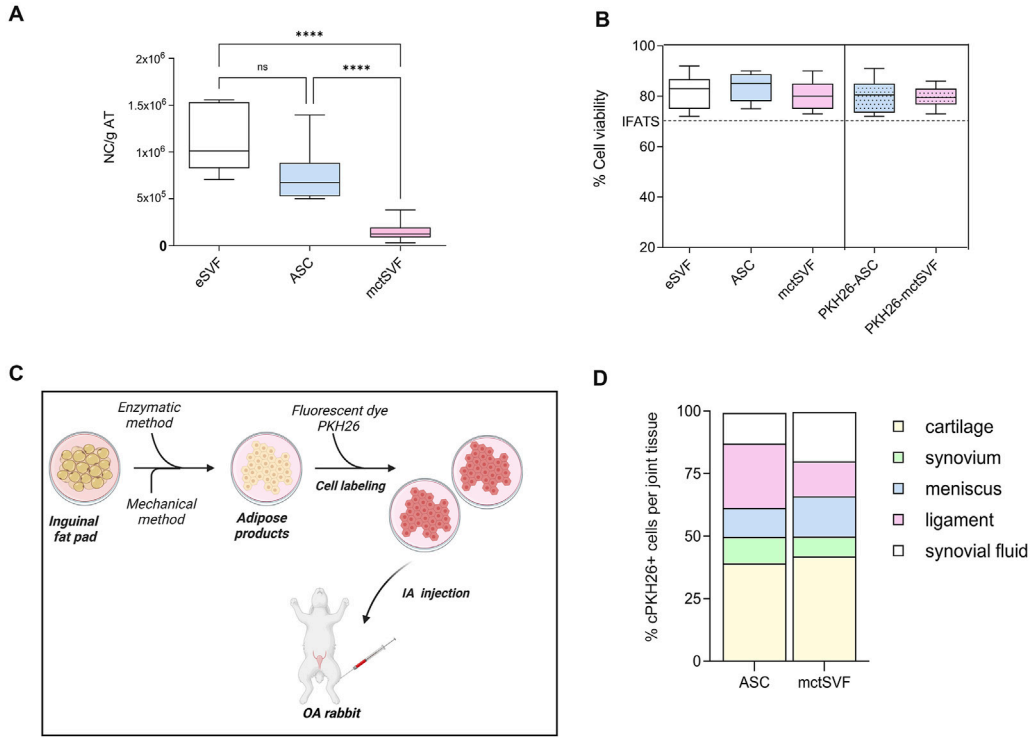

FIGURE 1
(A) Graphical representation of the number of nucleated cells (NC)/g of adipose tissue (AT) in enzymatic stromal vascular fraction (eSVF), ASC and mctSVF samples. **(B)** Graph of the percentage of cell viability, reported as mean, standard deviation and 95% confidence intervals, in eSVF, ASC, mctSVF after AT processing and PKH26-ASC and PKH26-mctSVF after labelling for local biodistribution assessment. The dotted line shows the 70% threshold suggested by the IFATS to consider a cell treatment clinically eligible. Results from the Kruskall-Wallis test and Dunn's test are reported (n = 8 samples/group). ****$P < 0.0001$ NC of ASC versus mctSVF; ****$P < 0.0001$ NC of eSVF versus mctSVF. **(C)** Schematic workflow of *in vitro* labelling of ASC and mctSVF before IA treatment with Biorender software http://Biorender.com/q879319. **(D)** Graphical representation of the percentage of local distribution of ASC (n = 8 articular joints: right and left hind limbs) and mctSVF (n = 8 articular joints: right and left hind limbs) in the entire articular joint. Percentage of cell positivity in synovial fluids, ligaments, menisci, synovia and articular cartilage at 1-month follow-up from the injection.

showing a rough articular surface, reduced articular thickness, irregular cell organization interspersing cell clones and empty areas, and reduced proteoglycan content (Figure 2B). On a 2-month follow-up after ASC and mctSVF treatments, several repair processes were evident in the femur which displayed a regular surface, proper cell distribution and density, and adequate proteoglycan content, similar to the SHAM group. Histochemical semi-quantification of the OA changes with Laverty's score showed a great ability of both cell therapies to counteract OA-related structural degradation (restoration of cell distribution and matrix organization), with a significantly lower score than the OA group (Figure 2B). Specifically, cartilage features related to safranin-o content, structure and cell clones, which are some of Laverty's parameters, were noticeably improved in both cell treatments. However, a significant improvement in cell density was only observed following the treatment with mctSVF (Supplementary Figure 4). IHC analyses showed the lowest percentage of COL2 positivity in the OA group, mainly confined in the deep cartilage layer, near the tidemark. Both ASC and mctSVF treatments contributed to a significantly increased positivity of this marker when compared to the OA group, mainly diffused in the extracellular matrix (ECM) in the superficial and the deep cartilage. (Figures 3A, B). Moreover, COL1 and MMP-3, specific markers associated with cartilage degeneration, were assessed (Figure 3). COL1 protein expression was highly observed at the cellular level in the OA group than in the SHAM group (Figures 3A, C). A significant reduction of COL1 expression was mainly observed after the IA treatment with ASC and mctSVF. As for MMP-3, the OA group displayed a strong cellular positivity mainly close to cell clones and fibrillated areas. The IA treatment with both ASC and mctSVF significantly reduced its expression by showing similar values to the SHAM group (Figures 3A, D).

3.5 IA administration of mctSVF improves subchondral bone architecture similar to ASC

To better understand the biological changes in the knee joint and how treatments differentially modulate them, specific IHC studies were performed in detail on trabecular bone and bone marrow. The baseline condition observed in the untreated group depicts a histological picture characterized by altered tidemark integrity, subchondral bone thickness, reduced number of trabecular bone and medullary spaces rich in adipose tissue, and low cell counts. Qualitative histological analysis of the ASC and mctSVF groups showed some regenerative processes, as evidenced by an increase in the number of trabecular bone and the cell number within the bone marrow spaces, similar to the SHAM group,

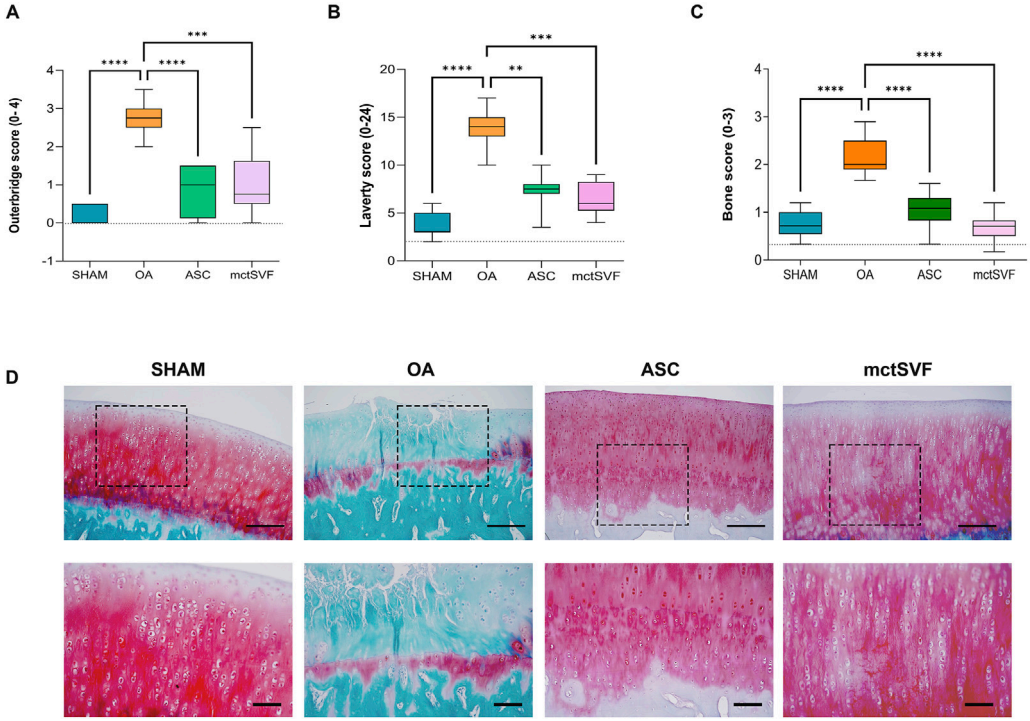

FIGURE 2
Graphical representation of Outerbridge score **(A)**, Laverty's score **(B)** and bone score **(C)**, reported as mean, standard deviation and 95% confidence intervals. **(D)** Representative histological images of medial femoral condyle with Safranin-O/Fast green staining in SHAM (n = 11), OA (n = 13), ASC (n = 8) and mctSVF (n = 8) groups at low (scale bar = 100 μm) (upper panel) and high magnification (scale bar = 50 μm) (lower panel). Red/pinkish staining: proteoglycan content; green staining: collagen content. The general linear model (GLM) with Sidak correction for multiple comparisons was used to assess the efficacy of ASC and mctSVF on all joint tissues. Outerbridge score: ****$P < 0.0001$ ASC vs. OA; ***$P < 0.001$ mctSVF vs. OA. Laverty's score: **$P < 0.01$ ASC vs. OA; ***$P < 0.001$ mctSVF vs. OA. Bone score: ****$P < 0.0001$ ASC vs. OA, and mctSVF vs. OA.

with a low number of osteoclasts, identified with haematoxylin/eosin staining for their typical multinucleated features. The scoring system used for examining the bone characteristics gave evidence of a better architecture in both treated groups reporting a significantly lower score, index of a better bone structure, than the OA group (Figure 2C). IHC analysis for the OC marker, one of the most abundant non-collagenous proteins in the bone matrix (Desando et al., 2021; Rodrigues et al., 2012), was examined to further assess bone repair after the IA treatments (Figure 4). The untreated OA and experimental groups showed different patterns of positivity for this marker between the medullary cavity and the bone compartment. Interestingly, the OA group showed positive staining in cells embedded in the bone matrix and located in the medullary cavities, whereas treated groups had mainly a marked positivity in the medullary cavities than the bone matrix (Figures 4A–C). Image analysis showed a significantly higher level of OC protein expression in the medullary cavities in both ASC/mctSVF treatments than in the OA group, and similar values to the SHAM group.

3.6 IA administration of ASC and mctSVF improves synovial architecture

Further analyses on the synovial architecture and synovial macrophage activity were performed to assess how they may be modulated after ASC and mctSVF treatments and how they may impact tissue repair in our ACLT model. As for the OA group, qualitative analyses with H/E staining showed hypertrophic and hyperplastic processes in the synovial lining layer, resulting in synovial thickness. In addition, some degenerative aspects with a vascular ECM and some inflammatory infiltrates were also observed in this group. Conversely, both ASC and mctSVF groups displayed a smooth surface with decreased hypertrophy and vascularization in the sub-synovium and a substantial lowering of OA characteristics. The semi-quantification with Laverty's score confirmed some benefits of both cell-based treatments, with significant evidence only from the mctSVF group (Figures 5A, B) (Supplementary Figure 2). Further analyses were focused on the evaluation of some markers beyond tissue catabolism and macrophage activation by IHC. As for the macrophage component, both treatments lowered the protein expression of RAM-11 in cells located in the lining layer, typically expressed by the inflammatory atherosclerotic plaques in rabbits. Conversely, both treatments increased protein expression for the CD-163 marker, typical of M2c-like macrophages (Figures 5C, D). The catabolic mediator MMP-3 was at its highest level in the OA group and mainly located in the lining layer. Interestingly, showing a similar pattern to the SHAM group, the IA delivery of both ASC and mctSVF significantly downregulated MMP-3 expression compared to the OA group (Figure 5E) (Supplementary Figure 3).

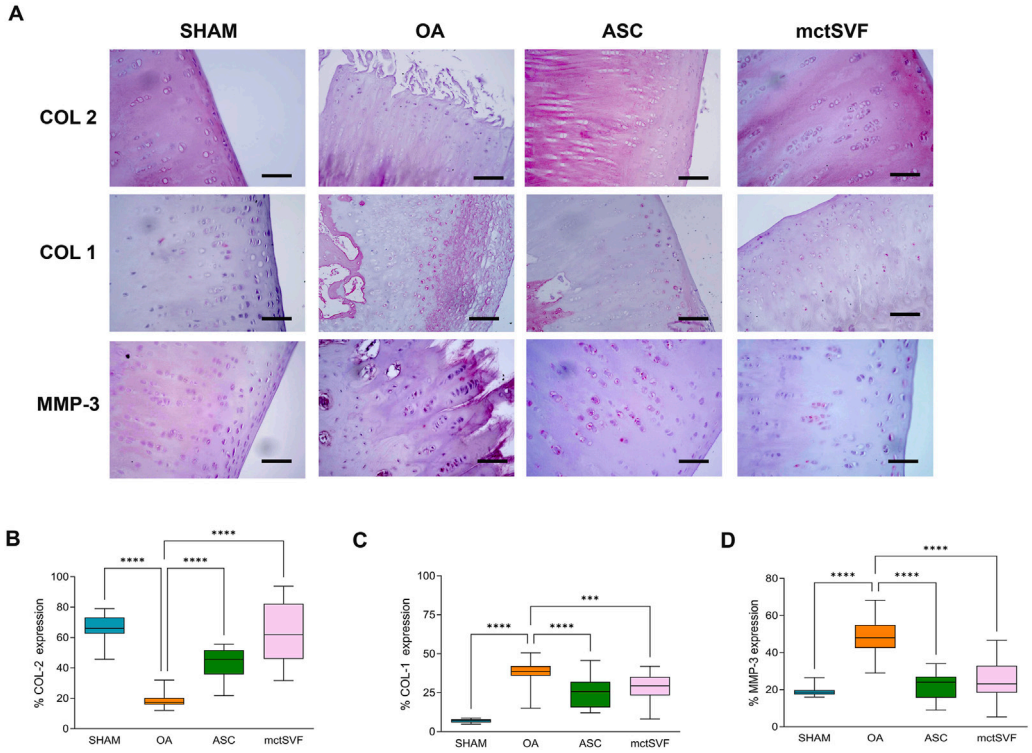

FIGURE 3
Representative immunohistochemical images of the medial femoral condyle in SHAM, OA, ASC and mctSVF-treated groups for COL2, COL1 and MMP-3 **(A)** (scale bar = 50 μm). Graphical representation of image analysis expressed as the percentage of positivity for COL2 **(B)**, COL1 **(C)** and MMP-3 **(D)**, reported as mean, standard deviation and 95% confidence intervals, in SHAM (n = 11), OA (n = 13), ASC (n = 8) and mctSVF (n = 8) groups. The general linear model (GLM) with Sidak correction for multiple comparisons was used to assess the efficacy of ASC and mctSVF for cartilage repair. COL2: ****$P < 0.0001$ ASC vs. OA and mctSVF vs. OA. COL1: ****$P < 0.0001$ ASC vs. OA; ***$P < 0.001$ mctSVF vs. OA. MMP-3: ****$P < 0.0001$ ASC vs. OA and mctSVF vs. OA.

3.7 ASC and mctSVF contribute to lower typical features of meniscus degeneration

Given that meniscal lesions can lead to knee biomechanical abnormalities with important implications for OA progression, specific histological evaluations have been performed for both anterior and posterior anatomical sites of the meniscus. During the qualitative analysis using Safranin-O/Fast Green staining, we observed an increase in tears, cell clones, and proteoglycans in the OA group in both the anterior and posterior zones. In contrast, both ASC and mtcSVF treatments played an active role in counteracting OA-related structural degradation through (i) the reduction of tears and cell clones, and (ii) the restoration of proteoglycan content and cell distribution in the ECM. Semi-quantitative analysis of histochemical OA changes with mPauli's score showed a worse histological scenario in the anterior rather than the posterior horn of the medial meniscus in the OA group. Interestingly, a significantly lower mPauli's score, an index of tissue repair, was observed following ASC and mtcSVF treatments compared to the OA group; however, no differences were found between the two treatments (Figure 6) (Supplementary Figures 4, 5). Immunohistochemical analyses confirmed regenerative processes after ASC and mctSVF therapies, reporting an increase of COL-1 and a reduction of MMP-3 in both the anterior and posterior horns of the medial meniscus (Figure 6).

4 Discussion

The search for alternative options to halt or delay the progression of OA and consequently joint replacement surgery has sparked great interest. Within the musculoskeletal field, an emerging trend is the development of biological approaches that process and maintain 3D tissue interactions as an alternative to other cell-based solutions. Point-of-care (POC) systems require minimal manipulation of biological samples to preserve the biophysical and biochemical cues of the native tissue microenvironment (Oberbauer et al., 2015; Greenwood et al., 2022; Aronowitz, 2014). With a focus on adipose-derived therapies (Ossendorff et al., 2023; Agarwal et al., 2021), this preclinical *in vivo* study aims to provide new bio-insights into the orthobiologic product mctSVF, obtained by the Hy-Tissue SVF system (Fidia Farmaceutici, Abano Terme) for OA treatment, compared to the ASC-based therapy (Agarwal et al., 2021). A preliminary *in vitro* study indicated that wrapping mctSVF in its native microenvironment ensures optimal cell viability and preserves phenotypic and functional properties (Desando et al., 2021). It has been proposed that the potential use of mctSVF in the treatment of OA may be explained by its ability to remain functionally active due to its spatial distribution and cell-matrix interaction. In particular, it was hypothesized that the IA delivery of mctSVF can exhibit greater stability at a joint injury site and superior

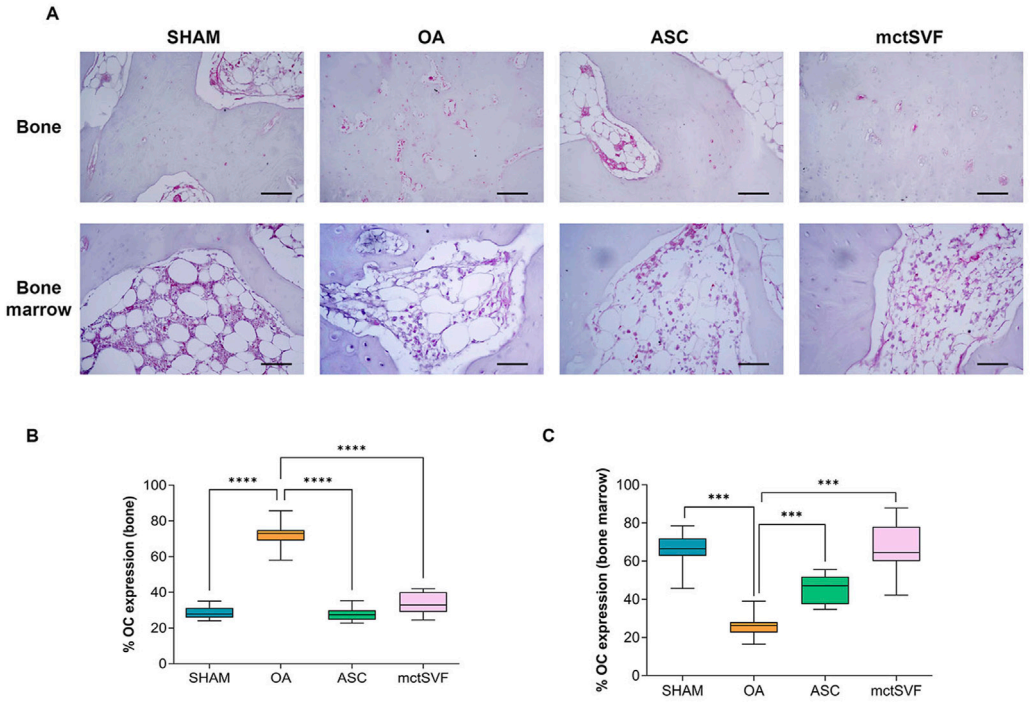

FIGURE 4
Representative immunohistochemical images of subchondral bone in medial femoral condyle in SHAM, OA, ASC and mctSVF-treated groups for osteocalcin (OC) in the bone matrix and medullary cavity (scale bar = 50 μm) **(A)**. Graphical representation of image analysis expressed as the percentage of positivity for OC in bone matrix **(B)** and medullary cavity **(C)**, reported as mean, standard deviation and 95% confidence intervals, in SHAM (n = 11), OA (n = 13), ASC (n = 8) and mctSVF (n = 8) groups. The general linear model (GLM) with Sidak correction for multiple comparisons was used to assess the efficacy of ASC and mctSVF for bone repair. OC (bone): ****$P < 0.0001$ ASC vs. OA and mctSVF vs. OA. OC (bone marrow): ***$P < 0.001$ ASC vs. OA and mctSVF vs. OA.

ability than ASC to attach to and penetrate joint tissue. This is based on the notion that the maintenance of the native tissue structure within mctSVF is crucial to preserve the stemness of tissue and to uphold native crosstalk with complex and multivalent signals (Gattazzo et al., 2014; Hynes, 2009). Given the multifaceted and multicompartmental nature of the OA phenotype (Mobasheri et al., 2019), various biological processes (inflammation, degradation, hypertrophy, and regeneration) need to be sufficiently characterized to assess the successful translation of mctSVF in clinics.

First, in line with the majority of studies on different SVF formulations (Boada-Pladellorens et al., 2022), this work highlighted the lack of adverse events and the efficacy of the current mctSVF micrograft product to improve preclinical outcomes in a post-traumatic OA model, similar to ASC. Interestingly, we found a correlation between cell viability and scoring systems, leading to the mechanistic conclusion that cell viability plays a relevant role in promoting tissue repair by ensuring a sufficient number of effective cells. IA delivery of ASC and mctSVF promoted comparable cell stabilization in the articular cartilage surface (Huang et al., 2022). We can speculate that similar cell migration may be the result of matrix degradation of mctSVF by enzymes in the *in vivo* microenvironment at 30 days, with the release of single cells, as occurs for ASC treatment. The lack of a short-term study, which is a limitation in evaluating local biodistribution, precludes providing information on the fate of cells following IA administration and early initiating events responsible for joint repair. This may help to better understand the mechanisms that go beyond tissue repair and to elucidate which are the first tissues to be involved in remodelling. Indeed, the lack of adverse effects on joint tissues and the cell engraftment observed at 2 months mainly to damaged areas of articular cartilage would indicate a tendency to promote cartilage repair by counteracting OA progression. To a lesser extent, the presence of cells in the adjacent joint tissues like the synovial membrane and meniscus provides indications of their potential role in modulating tissue remodelling in the articular joint. Moreover, the long-term assessment gives clues about cell integration into the articular cartilage, which may reflect the observed chondroprotective effects, similar to another study (Huang et al., 2022).

Second, the current study confirmed the repair potential of mctSVF to restore the hierarchical structure and functionality of the osteochondral tissue, crucial for facilitating metabolic exchange and joint biomechanics and restoring proper cellularity (Nukavarapu and Dorcemus, 2013). Although the cell yield of the mechanical procedure with Hy-tissue SVF is much lower than the enzymatic isolation, the tissue repair of mctSVF can have different interpretations. In particular, it may likely be the direct result of: (i) ASC (representing up to 10%), and (ii) cell complexes within its adipose-connective niche (ACN). ASC and ACN, the latter with a heterogenous reservoir of cells, could be active instructive players by: (1) fostering osteogenic and chondrogenic differentiation; and (2) modulating inflammatory and regenerative processes in the articular microenvironment thanks to their paracrine activity. A previous

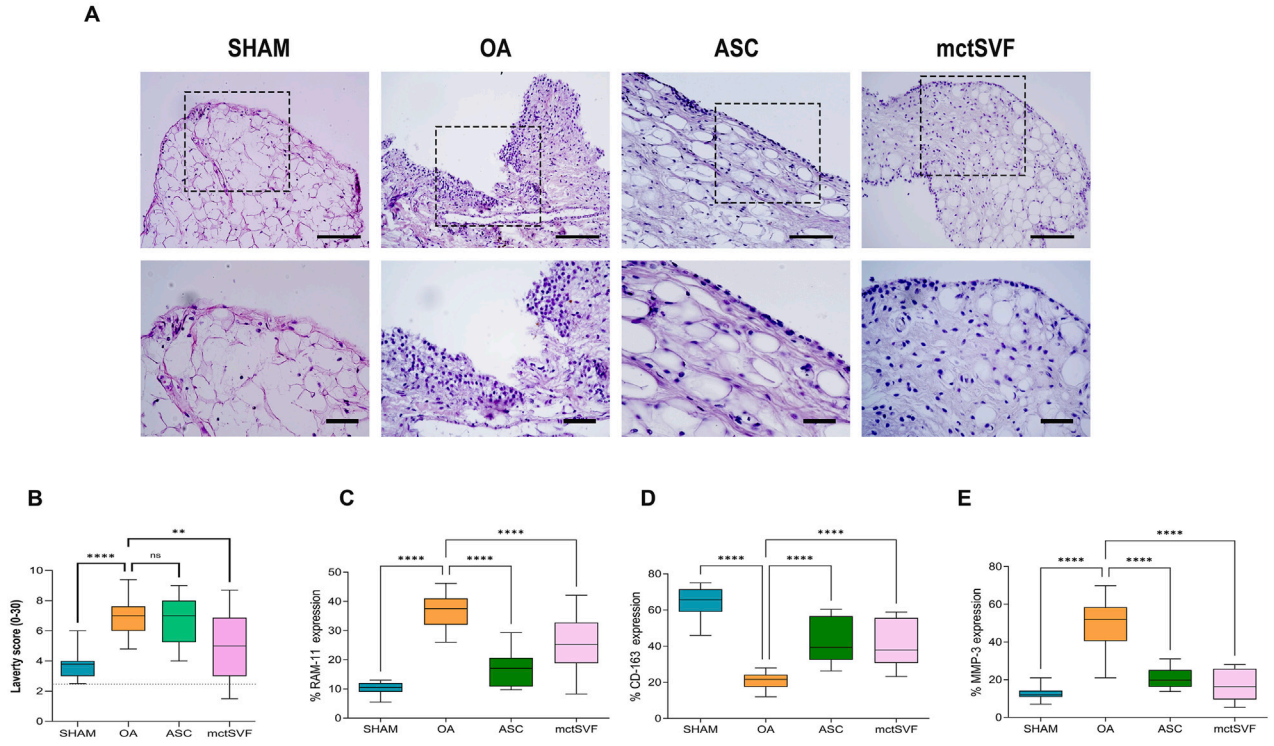

FIGURE 5
Representative histological images of the synovial membrane with hematoxylin/eosin staining in SHAM, OA, ASC and mctSVF groups at low (bar = 100 μm) (upper panel) and high magnification (lower panel) (scale bar = 50 μm) **(A)**. Graphical representation of Laverty's score **(B)** and image analysis for RAM-11 **(C)**, CD-163 **(D)** and MMP-3 **(E)**. in the synovial membrane reported as mean, standard deviation and 95% confidence intervals in SHAM (n = 11), OA (n = 13), ASC (n = 8) and mctSVF (n = 8) groups. The general linear model (GLM) with Sidak correction for multiple comparisons was used to study the impact of ASC and mctSVF on synovium tissue. Laverty's score: $^{**}P < 0.01$ mctSVF vs. OA. RAM-11, CD-163 and MMP-3: $^{****}P < 0.0001$ ASC vs. OA and mctSVF vs. OA.

in vitro study demonstrated the osteochondral potential of this micrograft and the release of some biomolecules, like VEGF and HGF, that may have clinical benefits in the osteochondral microenvironment (Desando et al., 2021; Traktuev et al., 2009). Despite the promising findings on such biomolecules, further studies aimed at investigating mechanisms beyond bone repair will require careful analysis of markers involved in bone resorption and deposition.

There has been a growing body of knowledge on the clinical significance of the correct interplay between bone and cartilage to protect cartilage, with bone nourishing articular cartilage and protecting it against degradative changes such as proteoglycan depletion (Nukavarapu and Dorcemus, 2013). Additionally, the enhanced proteoglycan content observed in the ECM of articular cartilage following cell-based treatments may be attributed to the secretion of HGF, reported *in vitro* for both ASC and mctSVF (Desando et al., 2021; Pak et al., 2014).

A major hurdle in cartilage repair, and the reason most treatments fail, is the formation of fibrocartilage. In particular, COL1 in articular cartilage is an indicator of ineffective cartilage repair, as the newly formed tissue, due to its fibrous profile, is unable to provide the correct biomechanical properties and joint loading. This study gives collective evidence towards the benefits of mctSVF treatment in counteracting fibrocartilage formation in favour of a hyalin-like phenotype, similar to ASC treatment. Similar to ASC, the mctSVF treatment effectively counteracts MMP-3 protein expression, a typical protease involved in COL2 cleavage. This is a further indication of its potential therapeutic value in inhibiting the reduction of this typical cartilage marker, which is often at low levels in OA conditions.

Third, tissue regeneration processes were also observed in the meniscus following ASC and mctSVF treatments, consistent with other studies focusing on this cell approach (Pak et al., 2014). Although at a low rate, the local biodistribution of ASC, and especially of mctSVF in the meniscus, could contribute to the reduction of several degenerative changes such as tearing (Pak et al., 2014). However, understanding this behaviour would require further analysis, which could open new insight into different orthopaedic contexts where meniscus lesions occur.

Fourth, attenuating the immune response at the injection site through immunomodulation may help to regenerate the host tissue. As natural components of the immune microenvironment of the joint, synovial macrophages are known to adopt either pathogenic or protective phenotypes in response to microenvironmental stimuli (Chen et al., 2020), and their role in OA pathogenesis is well established. By evaluating the macrophage profile in synovial samples after treatment, we found that both mctSVF and ASC effectively reduced fibrosis in terms of reduction of COL1 and drove the synovial macrophage subset towards a CD-163 phenotype, expressed by the M2 macrophage subset. Indeed, the

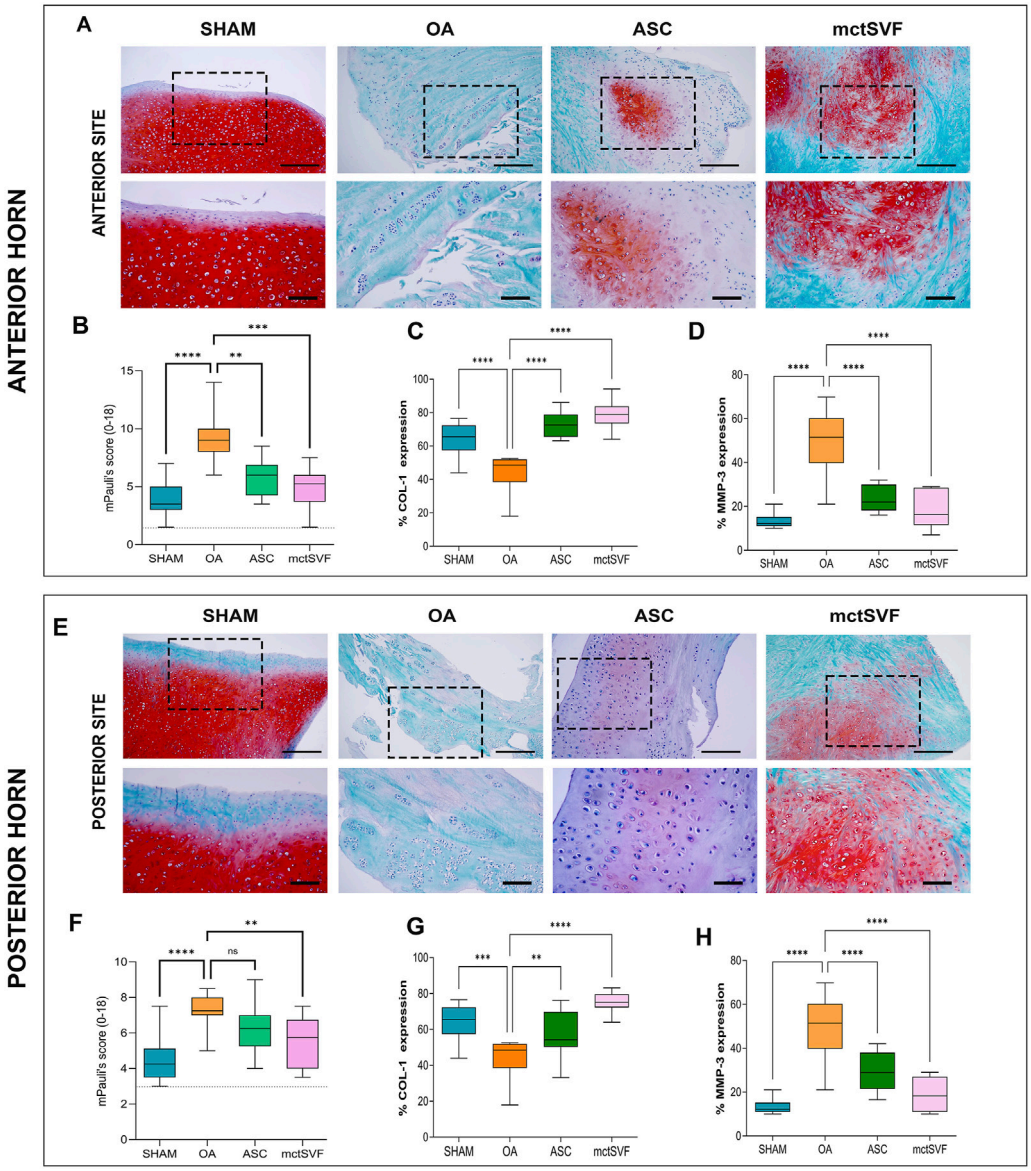

FIGURE 6
(A) Representative histological images of the medial meniscus with Safranin-O/Fast green in SHAM, OA, ASC and mctSVF groups at low (scale bar = 100 μm) and high magnification (scale bar = 50 μm) in the anterior horn (upper panel). **(B–D)** Graphical representation of mPauli's score, COL-1 and MMP-3 analyses in the anterior horn of the medial meniscus, reported as mean, standard deviation and 95% confidence intervals SHAM (n = 11), OA (n = 13), ASC (n = 8) and mctSVF (n = 8) groups. The general linear model (GLM) with Sidak correction for multiple comparisons was used to study the impact of ASC and mctSVF in the anterior horn of the medial meniscus. mPauli's score: ****$P < 0.0001$ SHAM vs. OA, **$P < 0.01$ ASC vs. OA, ***$P < 0.001$ mctSVF vs. OA; COL-1: ****$P < 0.0001$ SHAM vs. OA, ****$P < 0.0001$ ASC vs. OA; ****$P < 0.0001$ mctSVF vs. OA. **(E)** Representative histological images of the medial meniscus with Safranin-O/Fast green in SHAM, OA, ASC and mctSVF groups at low (scale bar = 100 μm) and high magnification (scale bar = 50 μm) in the posterior horn (lower panel). **(F–H)** Graphical representation of mPauli's score, COL-1 and MMP-3 analyses in the posterior horn of the medial meniscus, reported as mean, standard deviation and 95% confidence intervals SHAM (n = 11), OA (n = 13), ASC (n = 8) and mctSVF (n = 8) groups. The general linear model (GLM) with Sidak correction for multiple comparisons was used to study the impact of ASC and mctSVF on the posterior horn of the meniscus: mPauli's score: **$P < 0.01$ mctSVF vs. OA; COL-1: ***$P < 0.001$ SHAM vs. OA, **$P < 0.01$ ASC vs. OA, ****$P < 0.0001$ mctSVF vs. OA; MMP-3: ****$P < 0.0001$ SHAM vs. OA, ****$P < 0.0001$ ASC vs. OA, ****$P < 0.0001$ mctSVF vs. OA.

release of interleukin (IL)-10 found in a previous *in vitro* study characterizing mctSVF could reflect the change of macrophage phenotype from an inflammatory to a regenerative profile. However, to clarify this aspect and provide new insights into the role of potential immunomodulatory strategies for cartilage regeneration in OA (Kennedy et al., 2024), further research is needed. Specifically, modelling specific *in vitro* human culture systems with immunomodulatory molecules, such as anti-programmed death ligand (PDL1), an immune checkpoint whose blockade causes the development of OA in mice (Liu et al., 2019), might be a promising alternative to provide interesting insights in immune response attenuation.

A further suggestion for the mechanism of action underlying the use of ASC and mctSCF is the reduced expression of serum IL-10

and tumour necrosis factor (TNF)-α, which is characteristic of patients with post-traumatic OA, in favour of an inflammatory phenotype (Barker et al., 2021). The high level of IL-10 expression found in previous *in vitro* studies for the adipose cell-based strategies analyzed could re-establish an appropriate IL-10/TNF-α ratio, which is necessary to counteract some of the typical hallmarks of OA (i.e., inflammation, hypertrophy, fibrosis, etc.). Valuable insights into the factors and pathways involved in tissue regeneration could be gained from further *in vitro* studies modelling co-cultures and three-dimensional models between mctSVF and typical joint cells such as chondrocytes, osteoblasts and synoviocytes.

The lack of a comparative study between enzymatic and mechanical SVF using only expanded-ASC as a comparator group is a limitation of this study. Evidence for the safety and efficacy of enzymatic SVF as an injective intervention or augmentation of surgical procedures is available from various preclinical and clinical studies. However, they are often clinical case series with heterogeneous experimental designs. In general, it has been observed that the SVF has many advantages over the ASC being: 1) immediately available without the need for cell culture; 2) immediately available thanks to faster processing and direct delivery on the same day of the surgery. Mechanical processing alternatives have been proposed to overcome some of the concerns associated with enzymatic treatment. Although mechanical processing often provides a lower number of available cells, it ensures comparable and/or superior chondroprotective and immunomodulatory properties (Aletto et al., 2022).

Given these findings, tissue manipulation with the Hy-Tissue SVF system preserved the phenotypical and functional characteristics of the generated mctSVF without altering its regenerative potential, thus exerting disease-modifying effects on the joint tissue. Because of the similar profile of effectiveness between the 2 cell therapies, it would be more convenient to use mctSVF treatment by avoiding issues related to cell manipulation (enzymatic isolation, cell expansion, etc.) and the need for a GMP facility, by minimizing the costs. Indeed, a major clinical limitation of the mctSVF approach is the variability of cell precursors and bioactive molecules within the ACN, which does not guarantee similar clinical outcomes among OA patients. The patient's age, comorbidities (obesity, diabetes, etc.), lifestyle, site of aspiration of adipose tissue, and quality of adipose tissue are other key variables contributing to the variability in SVF yield and cell potency. In this context, a thorough evaluation of the harvested tissue's viability covers a relevant role in fostering tissue repair by ensuring an adequate amount of effective cells *in vivo*. Indeed, the development of standardized protocols for harvesting and processing SVF are another critical step, that might contribute to reducing the variability in SVF efficiency (Jeyaraman et al., 2024). In-depth studies aimed at evaluating a cohort of patients, considering age, gender, body mass index, and inflammation, may be a valuable tool for selecting patient groups having more advantageous benefits to receive this treatment, and to develop more personalized treatments.

Taken together, our results demonstrate that IA delivery of mctSVF is safe, effective and minimally invasive, accelerating cartilage repair and shifting the balance from cartilage destruction to chondroprotection with potential translatability to different orthopaedic clinical conditions.

Data availability statement

The original contributions presented in the study are included in the article/Supplementary Material, further inquiries can be directed to the corresponding author.

Ethics statement

The animal study was approved by the protocol was approved by the Animal Welfare Body of IRCCS-Istituto Ortopedico Rizzoli (IOR) on 14th May 2019, authorized by the Italian Ministry of Health (Aut. n. 557/2019-PR on 23rd July 2019). The study was conducted in accordance with the local legislation and institutional requirements.

Author contributions

GD: Data curation, Formal Analysis, Investigation, Methodology, Software, Visualization, Writing–original draft, Writing–review and editing. MT: Data curation, Formal Analysis, Investigation, Methodology, Writing–review and editing. LM: Data curation, Methodology, Writing–review and editing. MS: Formal Analysis, Investigation, Methodology, Writing–review and editing. GG: Data curation, Formal Analysis, Validation, Writing–review and editing. MF: Conceptualization, Supervision, Validation, Writing–review and editing. AC: Data curation, Formal Analysis, Investigation, Methodology, Writing–review and editing. CS: Methodology, Writing–review and editing. CL: Methodology, Writing–review and editing. MD'A: Investigation, Methodology, Writing–review and editing. LR: Data curation, Formal Analysis, Methodology, Writing–review and editing. BG: Conceptualization, Funding acquisition, Project administration, Supervision, Validation, Writing–original draft, Writing–review and editing.

Funding

The author(s) declare that financial support was received for the research, authorship, and/or publication of this article. This work was partially supported by Fidia Farmaceutici S.p.A company, which provided the Hy-Tissue SVF and Duografter II centrifuge to obtain mctSVF preparation. This research was partially supported by Italian Ministry of Health-5x1000 Anno 2022, redditi 2021; N° project: 5M-2022-23685320 "Ottimizzazione dei trattamenti attraverso l'integrazione di approcci innovativi e studio delle interazioni tissutali". CUP D33C23001460001.

Acknowledgments

The authors acknowledge the contribution of Elettra Pignotti for her help and advice on statistics, Katia Samoggia, Daniel Fota, Luca Fergnani, Salvatore Pellini, and Umberto Bonanno for their technical support at the Scienze e Tecnologie Chirurgiche.

Conflict of interest

CS and CL are employed by Fidia Farmaceutici S.p.A. GD declares a conflict of interest for having been paid as conference speaker for Fidia Farmaceutici.

The remaining authors declare that the research was conducted in the absence of any commercial or financial relationships that could be construed as a potential conflict of interest.

The authors declare that this study received funding from Fidia Farmaceutici S.p.A. The funder had the following involvement in the study: Fidia Farmaceutici S.p.A funded the in vivo study and IRCCS Istituto Ortopedico Rizzoli signed an agreement to conduct the investigation. Fidia Farmaceutici S.p.A had no role in the collection, analysis or interpretation of the data but was involved in the decision to submit it and approve the final version, as stated in the Author Contribution section.

The author(s) declared that they were an editorial board member of Frontiers, at the time of submission. This had no impact on the peer review process and the final decision.

Generative AI statement

The author(s) declare that no Generative AI was used in the creation of this manuscript.

Publisher's note

All claims expressed in this article are solely those of the authors and do not necessarily represent those of their affiliated organizations, or those of the publisher, the editors and the reviewers. Any product that may be evaluated in this article, or claim that may be made by its manufacturer, is not guaranteed or endorsed by the publisher.

Supplementary material

The Supplementary Material for this article can be found online at: https://www.frontiersin.org/articles/10.3389/fcell.2025.1533405/full#supplementary-material

References

Agarwal, N., Mak, C., Bojanic, C., To, K., and Khan, W. (2021). Meta-analysis of adipose tissue derived cell-based therapy for the treatment of knee osteoarthritis. *Cells* 10 (6), 1365. doi:10.3390/cells10061365

Aho, O. M., Finnila, M., Thevenot, J., Saarakkala, S., and Lehenkari, P. (2017). Subchondral bone histology and grading in osteoarthritis. *PLoS ONE* 12 (3), e0173726. doi:10.1371/journal.pone.0173726

Aletto, C., Francesco, O., and Maffulli, N. (2022). Knee intra-articular administration of stromal vascular fraction obtained from adipose tissue: a systematic review. *J. Clin. Orthop. Trauma* 25, 101773. doi:10.1016/j.jcot.2022.101773

Aronowitz, J. A., Lockhart, R. A., and Hakakian, C. S. (2015). Mechanical versus enzymatic isolation of stromal vascular fraction cells from adipose tissue. *SpringerPlus* 4, 713. doi:10.1186/s40064-015-1509-2

Aronowitz, J. A. E. J. D. (2014). Adipose stromal vascular fraction isolation: a head-to-head comparison of four commercial cell separation systems. *Plast. Reconstr. Surg.* 133 (6), 889e. doi:10.1097/prs.0000000000000188

Barker, T., Rogers, V. E., Henriksen, V. T., Trawick, R. H., Momberger, N. G., and Lynn Rasmussen, G. (2021). Circulating IL-10 is compromised in patients predisposed to developing and in patients with severe knee osteoarthritis. *Sci. Rep.* 11 (1), 1812–1910. doi:10.1038/s41598-021-81382-6

Beane, O. S., Fonseca, V. C., Cooper, L. L., Koren, G., and Darling, E. M. (2014). Impact of aging on the regenerative properties of bone marrow-muscle-and adipose-derived mesenchymal stem/stromal cells. *PLoS ONE* 9 (12), e115963. doi:10.1371/journal.pone.0115963

Boada-Pladellorens, A., Avellanet, M., Pages-Bolibar, E., and Veiga, A. (2022). Stromal vascular fraction therapy for knee osteoarthritis: a systematic review. *Ther. Adv. Musculoskelet. Dis.* 14, 1759720X221117879–15. doi:10.1177/1759720X221117879

Busato, A., De Francesco, F., Biswas, R., Mannucci, S., Conti, G., Fracasso, G., et al. (2021). Simple and rapid non-enzymatic procedure allows the isolation of structurally preserved connective tissue micro-fragments enriched with svf. *Cells* 10 (1), 36–14. doi:10.3390/cells10010036

Chen, Y., Jiang, W., Yong, H., He, M., Yang, Y., Deng, Z., et al. (2020). Macrophages in osteoarthritis: pathophysiology and therapeutics. *Am. J. Transl. Res.* 12 (1), 261–268.

Chevrier, A., Nelea, M., Hurtig, M. B., Hoemann, C. D., and Buschmann, M. D. (2009). Meniscus structure in human, sheep, and rabbit for animal models of meniscus repair. *J. Orthop. Res.* 27 (9), 1197–1203. doi:10.1002/jor.20869

Cicione, C., Vadalà, G., Di Giacomo, G., Tilotta, V., Ambrosio, L., Russo, F., et al. (2023). Micro-fragmented and nanofat adipose tissue derivatives: *in vitro* qualitative and quantitative analysis. *Front. Bioeng. Biotechnol.* 11 (January), 911600–911611. doi:10.3389/fbioe.2023.911600

Danisovic, L., Oravcova, L., Krajciova, L., Varchulova Novakova, Z., Bohac, M., Varga, I., et al. (2017). Effect of long-term culture on the biological and morphological characteristics of human adipose tissue-derived stem Cells. *J. Physiol. Pharmacol.* 1 (68), 149–158.

Desando, G., Bartolotti, I., Cattini, L., Tschon, M., Martini, L., Fini, M., et al. (2021). Prospects on the potential *in vitro* regenerative features of mechanically treated-adipose tissue for osteoarthritis care. *Stem Cell Rev. Rep.* 17 (4), 1362–1373. doi:10.1007/s12015-020-10099-2

Desando, G., Cavallo, C., Sartoni, F., Martini, L., Parrilli, A., Veronesi, F., et al. (2013). Intra-articular delivery of adipose derived stromal cells attenuates osteoarthritis progression in an experimental rabbit model. *Arthritis Res. Ther.* 15 (1), R22. doi:10.1186/ar4156

Djouad, F., Bouffi, C., Ghannam, S., Noël, D., and Jorgensen, C. (2009). Mesenchymal stem cells: innovative therapeutic tools for rheumatic diseases. *Nat. Rev. Rheumatol.*, 5, 392–399. doi:10.1038/nrrheum.2009.104

El-Badawy, A., Amer, M., Abdelbaset, R., Sherif, S. N., Abo-Elela, M., Gallagh, Y. H., et al. (2016). Adipose stem cells display higher regenerative capacities and more adaptable electro-kinetic properties compared to bone marrow-derived mesenchymal stromal cells. *Sci. Rep.* 6 (November), 37801–37811. doi:10.1038/srep37801

Filardo, G., Madry, H., Jelic, M., Roffi, A., Cucchiarini, M., and Kon, E. (2013). Mesenchymal stem cells for the treatment of cartilage lesions: from preclinical findings to clinical application in orthopaedics. *Knee Surg. Sports Traumatol. Arthrosc.* 21, 1717–1729. doi:10.1007/s00167-012-2329-3

Francesco, F.De, Gravina, P., Busato, A., Farinelli, L., Soranzo, C., Vidal, L., et al. (2021). Stem cells in autologous microfragmented adipose tissue: current perspectives in osteoarthritis disease. *Int. J. Mol. Sci.* 22, 10197. doi:10.3390/ijms221910197

Froelich, K., Mickler, J., Steusloff, G., Technau, A., Ramos Tirado, M., Scherzed, A., et al. (2013). Chromosomal aberrations and deoxyribonucleic acid single-strand breaks in adipose-derived stem cells during long-term expansion *in vitro*. *Cytotherapy* 15 (7), 767–781. doi:10.1016/j.jcyt.2012.12.009

Gattazzo, F., Urciuolo, A. B. P., and Bonaldo, P. (2014). Extracellular matrix: a dynamic microenvironment for stem cell niche. *Biochim. Biophys. Acta* 1840 (8), 2506–2519. doi:10.1016/j.bbagen.2014.01.010

Gentile, P., Calabrese, C., De Angelis, B., Pizzicannella, J., Kothari, A., and Garcovich, S. (2019). Impact of the different preparation methods to obtain human adipose-derived stromal vascular fraction cells (AD-SVFs) and human adipose-derived mesenchymal stem cells (AD-MSCs): enzymatic digestion versus mechanical centrifugation. *Int. J. Mol. Sci.* 20 (21), 5471–5526. doi:10.3390/ijms20215471

Gentile, P., Scioli, M. G., Bielli, A., Orlandi A, C. V., and Cervelli, V. (2017). Comparing different nanofat procedures on scars: role of the stromal vascular fraction and its clinical implications. *Regen. Med.* 12(8), 939–952. doi:10.2217/rme-2017-0076

Greenwood, V., Clausen, P., and Matuska, A. M. (2022). Micro - fragmented adipose tissue cellular composition varies by processing device and analytical method. *Sci. Rep.* 12, 16107–16108. doi:10.1038/s41598-022-20581-1

Grigolo, B., Lisignoli, G., Desando, G., Cavallo, C., Marconi, E., Tschon, M., et al. (2009). Osteoarthritis treated with mesenchymal stem cells on hyaluronan-based

scaffold in rabbit. *Tissue Eng. Part C. Methods* 15 (4), 647–658. doi:10.1089/ten.tec.2008.0569

Gun-II Im, M. D., Yong-Woon Shin, M. D. K.-B. L. M. D., and Lee, K. B. (2005). Do adipose tissue-derived mesenchymal stem cells have the same osteogenic and chondrogenic potential as bone marrow-derived cells. *Osteoarthr. Cartil.* 13, 845–853. doi:10.1016/j.joca.2005.05.005

Huang, H., Lou, Z., Zheng, S., Wu, J., Yao, Q., Chen, R., et al. (2022). Intra-articular drug delivery systems for osteoarthritis therapy: shifting from sustained release to enhancing penetration into cartilage. *Drug Deliv.* 29 (1), 767–791. doi:10.1080/10717544.2022.2048130

Hynes, R. O. (2009). The extracellular matrix: not just pretty fibrils. *Science* 326 (5957), 1216–1219. doi:10.1126/science.1176009

Ibrahim, A., Maurizio, D., and Hassan, Z. (2022). Minimally manipulated adipose derived mesenchymal stromal cells and osteoarthritis: a narrative review. *Acta Biomed.* 93, e2022135. doi:10.23750/abm.v93i1.11102

Jeyaraman, N., Shrivastava, S., Ravi, V. R., Nallakumarasamy, A., Pundkar, A., and Jeyaraman, M. (2024). Understanding and controlling the variables for stromal vascular fraction therapy. *World J. Stem Cells* 16 (8), 784–798. doi:10.4252/wjsc.v16.i8.784

Kennedy, O., Kitson, A., Okpara, C., Chow, L. W., and Gonzalez-Fernandez, T. (2024). Immunomodulatory strategies for cartilage regeneration in osteoarthritis. *Tissue Eng. - Part A* 30 (7–8), 259–271. doi:10.1089/ten.tea.2023.0255

Laverty, S., Girard, C. A., Williams, J. M., Hunziker, E. B., and Pritzker, K. P. H. (2010). The OARSI histopathology initiative - recommendations for histological assessments of osteoarthritis in the rabbit. *Osteoarthr. Cartil.* 18, 53–65. doi:10.1016/j.joca.2010.05.029

Liu, S., Mi, J., Liu, W., Xiao, S., and Gao, C. (2019). Blocking of checkpoint receptor PD-L1 aggravates osteoarthritis in macrophage-dependent manner in the mice model. *Int. J. Immunopathol. Pharmacol.* 33, 2058738418820760. doi:10.1177/2058738418820760

Mainil-Varlet, P., Schiavinato, A., and Ganster, M. M. (2013). Efficacy evaluation of a new hyaluronan derivative HYADD® 4-G to maintain cartilage integrity in a rabbit model of osteoarthritis. *Cartilage* 4 (1), 28–41. doi:10.1177/1947603512455193

Mobasheri, A., Saarakkala, S., Finnilä, M., Karsdal, M. A., and Spil, W. E. V. (2019). Recent advances in understanding the phenotypes of osteoarthritis [version 1; peer review: 2 approved]. *F1000Res* 8, 1–11. doi:10.12688/f1000research.20575.1

Nukavarapu, S. P., and Dorcemus, D. L. (2013). Osteochondral tissue engineering: current strategies and challenges. *Biotechnol. Adv.* 31 (5), 706–721. doi:10.1016/J.BIOTECHADV.2012.11.004

Oberbauer, E., Steffenhagen, C., Wurzer, C., Gabriel, C., Redl, H., and Wolbank, S. (2015). Enzymatic and non-enzymatic isolation systems for adipose tissue-derived cells: current state of the art. *Cell Regen.* 4, 7–14. doi:10.1186/s13619-015-0020-0

Ossendorff, R., Menon, A., Schildberg, F. A., Randelli, P. S., Scheidt, S., Burger, C., et al. (2023). A worldwide analysis of adipose-derived stem cells and stromal vascular fraction in orthopedics: current evidence and applications. *J. Clin. Med.* 12 (14), 4719. doi:10.3390/jcm12144719

Pak, J., Lee, J. H., and Lee, S. H. (2014). Regenerative repair of damaged meniscus with autologous adipose tissue-derived stem cells. *BioMed Res. Int.* 2014, 436029. doi:10.1155/2014/436029

Pauli, C., Grogan, S. P., Patil, S., Otsuki, S., Hasegawa, A., Koziol, J., et al. (2011). Macroscopic and histopathologic analysis of human knee menisci in aging and osteoarthritis. *Osteoarthr. Cartil.* 19 (9), 1132–1141. doi:10.1016/j.joca.2011.05.008

Percie du Sert, N., Ahluwalia, A., Alam, S., Avey, M. T., Baker, M., Browne, W. J., et al. (2020). Reporting animal research: explanation and elaboration for the arrive guidelines 2.0. *PLoS Biol.* 18 (Issue 7), e3000411. doi:10.1371/journal.pbio.3000411

Perdisa, F., Gostyńska, N., Roffi, A., Filardo, G., Marcacci, M., and Kon, E. (2015). Adipose-derived mesenchymal stem cells for the treatment of articular cartilage: a systematic review on preclinical and clinical evidence. *Stem Cells Int.* 2015, 597652. doi:10.1155/2015/597652

Perucca Orfei, C., Boffa, A., Sourugeon, Y., Laver, L., Magalon, J., Sánchez, M., et al. (2023). Cell-based therapies have disease-modifying effects on osteoarthritis in animal models. A systematic review by the ESSKA Orthobiologic Initiative. Part 1: adipose tissue-derived cell-based injectable therapies. *Knee Surg. Sports Traumatol. Arthrosc.* 31 (2), 641–655. doi:10.1007/s00167-022-07063-7

Rodrigues, A. M., Caetano-Lopes, J., Vale, A. C., Vidal, B., Lopes, A., Aleixo, I., et al. (2012). Low osteocalcin/collagen type I bone gene expression ratio is associated with hip fragility fractures. *Bone*, 51(6), 981–989. doi:10.1016/j.bone.2012.08.129

Si, Z., Wang, X., Sun, C., Kang, Y., Xu, J., Wang, X., et al. (2019). Adipose-derived stem cells: sources, potency, and implications for regenerative therapies. *Biomed. Pharmacother.* 114 (February), 108765. doi:10.1016/j.biopha.2019.108765

Traktuev, D. O., Prater, D. N., Merfeld-Clauss, S., Sanjeevaiah, A. R., Saadatzadeh, M. R., Murphy, M., et al. (2009). Robust functional vascular network formation *in vivo* by cooperation of adipose progenitor and endothelial cells. *Circulation Res.* 104 (12), 1410–1420. doi:10.1161/CIRCRESAHA.108.190926

Trivisonno, A., Alexander, R. W., Baldari, S., Cohen, S. R., Di Rocco, G., Gentile, P., et al. (2019). Intraoperative strategies for minimal manipulation of autologous adipose tissue for cell- and tissue- based therapies: concise review. *Stem Cell Traslational Med.* 8 (12), 1265–1271. doi:10.1002/sctm.19-0166

Uguten, M., van der Sluis, N., Vriend, L., Coert, J. H., Harmsen, M. C., van der Lei, B., et al. (2024). "Comparing mechanical and enzymatic isolation procedures to isolate adipose-derived stromal vascular fraction: a systematic review," in *Wound repair and regeneration* (John Wiley and Sons Inc). doi:10.1111/wrr.13228

Vinatier, C., and Guicheux, J. (2016). Cartilage tissue engineering: from biomaterials and stem cells to osteoarthritis treatments. *Ann. Phys. Rehabilitation Med.* 59 (3), 139–144. doi:10.1016/j.rehab.2016.03.002

Vrouwe, J. P. M., Burggraaf, J., Kloppenburg, M., and Stuurman, F. E. (2021). Challenges and opportunities of pharmacological interventions for osteoarthritis: a review of current clinical trials and developments. *Osteoarthr. Cartil. Open* 3 (4), 100212. doi:10.1016/j.ocarto.2021.100212

Zhang, Z., and Schon, L. (2022). The current status of clinical trials on biologics for cartilage repair and osteoarthritis treatment: an analysis of ClinicalTrials. gov data. *Cartilage* 13, 19476035221093065. doi:10.1177/19476035221093065

frontiers | Frontiers in Bioengineering and Biotechnology

TYPE Systematic Review
PUBLISHED 24 March 2025
DOI 10.3389/fbioe.2025.1545431

Check for updates

OPEN ACCESS

EDITED BY
Elizabeth Vinod,
Christian Medical College and Hospital, India

REVIEWED BY
Upasana Kachroo,
All India Institute of Medical Sciences Raipur, India
Secunda Rupert,
Stanley Medical College (SMC), India

*CORRESPONDENCE
Michael Silveira Santiago,
michaelquadril1308@gmail.com

RECEIVED 16 December 2024
ACCEPTED 10 March 2025
PUBLISHED 24 March 2025

CITATION
Santiago MS, Doria FM, Morais Sirqueira Neto J, Fontes FF, Porto ES, Aidar FJ, Silva MVVdMP, Cavalcante DVS, Akbarpoor F, Zamora FV, Souza DTd, Madruga RETTA, Díaz-de-Durana AL, Merino-Fernandez M and Cipolotti R (2025) Platelet-rich plasma with versus without hyaluronic acid for hip osteoarthritis: a systematic review and meta-analysis.
Front. Bioeng. Biotechnol. 13:1545431.
doi: 10.3389/fbioe.2025.1545431

COPYRIGHT
© 2025 Santiago, Doria, Morais Sirqueira Neto, Fontes, Porto, Aidar, Silva, Cavalcante, Akbarpoor, Zamora, Souza, Madruga, Díaz-de-Durana, Merino-Fernandez and Cipolotti. This is an open-access article distributed under the terms of the Creative Commons Attribution License (CC BY). The use, distribution or reproduction in other forums is permitted, provided the original author(s) and the copyright owner(s) are credited and that the original publication in this journal is cited, in accordance with accepted academic practice. No use, distribution or reproduction is permitted which does not comply with these terms.

Platelet-rich plasma with versus without hyaluronic acid for hip osteoarthritis: a systematic review and meta-analysis

Michael Silveira Santiago[1]*, Felipe Meireles Doria[2], José Morais Sirqueira Neto[3], Fabio França Fontes[3], Erick Sobral Porto[4], Felipe J. Aidar[3,5], Marcus Vinicius Vieira de Matos Pereira Silva[3], Deivyd Vieira Silva Cavalcante[6], Fatemeh Akbarpoor[7], Fernanda Valeriano Zamora[7,8], Davi Teixeira de Souza[2], Reuthemann Esequias Teixeira Tenorio Albuquerque Madruga[3,9], Alfonso López Díaz-de-Durana[10], María Merino-Fernandez[11] and Rosana Cipolotti[1,9]

[1]Health Sciences Graduate Program, Federal University of Sergipe, Aracaju, Brazil, [2]Department of Medicine, Tiradentes University, Aracaju, Brazil, [3]Department of Medicine, Federal University of Sergipe, São Cristóvão, Brazil, [4]Ribeirao Preto Medical School University of Sao Paulo, Ribeirao Preto, Brazil, [5]Department of Physical Education, Federal University of Sergipe, São Cristóvão, Brazil, [6]Department of Biology, Federal University of Maranhao, São Luís, Brazil, [7]Mohammed Bin Rashid University of Medicine and Health Sciences, Dubai, United Arab Emirates, [8]Department of Medicine, Rio de Janeiro State University, Rio de Janeiro, Brazil, [9]Department of Medicine, Federal University of Sergipe, Aracaju, Brazil, [10]Sports Department, Faculty of Physical Activity and Sports Science—INEF, Universidad Politécnica de Madrid, Madrid, Spain, [11]Facultad de Ciencias de la Salud, Universidad Francisco de Vitoria, Madrid, Spain

Background: The use of intra-articular orthobiologics in hip osteoarthritis (HOA) has been presented as a therapeutic option and to postpone arthroplasty. There is little scientific evidence on the clinical application of platelet-rich plasma (PRP) associated with hyaluronic acid as dual therapy. Thus, the aim of our systematic review is to compare the clinical improvement with the use of PRP with versus without hyaluronic acid (HA) in hip osteoarthritis.

Methods: We systematically searched Cochrane, PubMed, and Embase databases for studies evaluating patients with HOA who received PRP with vs. without HA. Pain and functional score were collected and pooled at 3-, 6-, and 12-months follow-up. Mean differences (MD) and 95% intervals were calculated, and heterogeneity was assessed using I^2 statistics. All statistical analysis was performed using R with the *meta* package.

Results: We included 2 randomized controlled trials (RCTs) and 1 cohort study, comprising 190 patients, of whom 88 received the PRP plus HA. Relative to PRP alone, dual therapy led to significantly higher pain scores at 3 months (SMD 0.35; 95% CI 0.06 to 0.64; $p < 0.01$; $I^2 = 0\%$) and at 12 months (MD 11.92 points; 95% CI 3.87 to 19.97; $p < 0.01$; $I^2 = 0\%$), translating into worsening of pain including HA. There was no difference between groups at any follow-up regarding functional score or pain at 6 months.

Conclusion: Joint infiltration in HOA with PRP combined to HA showed higher perception of pain scores. Our findings suggest that the addition of HA in PRP

treatment does not bring significant improvement and worsens patients' quality of life. However, more randomized trials with larger populations may increase robustness.

Systematic Review Registration: identifier, CRD42024581335

KEYWORDS

hip, osteoarthritis, platelet, PRP, hyaluronic acid, viscosupplementation

1 Introduction

Mobility issues directly impact the quality of life. Cartilage integrity plays a fundamental role in the movement. Established osteoarthritis is characterized by disrupted joint homeostasis, the development of osteophytes, subchondral bone sclerosis, and a decrease in joint space, as observed on radiographic assessment. Clinically, the painful symptoms and functional impairment are disabling. The hip is the second joint most affected by osteoarthritis, with femoro-acetabular impingement, previous traumatic events, osteonecrosis of the femoral head and rheumatic disease being the main predisposing pathological conditions. In this context, chondral damage is increased with mechanical overload in high-impact activities or with the aging process. Hip osteoarthritis (HOA) is a common condition affecting the joint, surrounding structures, leading to pain, stiffness, and often impairment of daily living (Sambe et al., 2023).

Approximately 10%–25% of people over 60 years of age are affected by HOA, with a slightly higher incidence in men, placing a worrying disease by the economic burden of expensive treatment. When there is resistance to clinical therapy, non-operative procedures have grown in importance in recent years, mainly because they do not imply a worsening of chondral damage and provide another option for controlling joint pain (Kravos and Jerman, 2012). Orthobiologics are most commonly used in knee osteoarthritis with promising results; they are increasingly important in HOA, particularly for delaying or postponing hip replacement surgery for younger patients or when patients refuse more aggressive procedures, such as hip replacement (Zhao et al., 2020).

Inside this complex degenerative disease, the balance between cartilage production and its destruction gained focus in the recent scientific literature. The intervention strategy involves approaching the early stages, slowing down the progression of cartilage damage and total hip arthroplasty for advanced cases. Non-surgical treatments, such as cell therapy using platelet-rich plasma (PRP) extracted from peripheral blood, have gained popularity primarily for the repair of tendon and ligament injuries. Due to the benefits generated at the extra-articular level, clinical articular application has been extended, delaying the need for joint replacement (Lim et al., 2023). PRP is theorized to aid cartilage repair by stimulating cell activity, reducing inflammation to relieve pain, and improving joint function. It may also enhance joint lubrication by increasing synovial fluid viscosity, potentially slowing disease progression. However, more robust clinical research is needed to confirm its effects on cartilage health. There are different PRP formulations available depending on the leukocyte concentration and centrifugation process of obtaining, which implies a greater catabolic effect of cytokines to the detriment of the repairing anabolic action on platelets (Lim et al., 2023).

PRP is a blood-derived product rich in growth factors, vascular and transforming factors, in addition to a high level of platelets. During the process of obtaining the final PRP product, there are two or more centrifugation phases with different speeds, which bring about satisfactory clinical results. However, the lack of a specific protocol, depending on the number and speed of centrifugation, results in uncertain and poorly reproducible results (Tjandra et al., 2024). With the increasing use of PRP for osteoarthritis, there is still no optimal formulation of PRP with platelet counts and attention has been focused on leukocyte concentrations in PRP. In the study by Filardo et al., side effects were observed in the treatment of osteoarthritis compared to pure PRP (P-PRP), which had a lower concentration of leukocytes, possibly due to the release of pro-inflammatory cytokines by leukocytes. Therefore, the best clinical response was found with the P-PRP formulation (Xu et al., 2017; Filardo et al., 2012). Their use can be added to HA to stimulate chondrogenesis and inhibit degenerative enzymes, in addition to its mechanical properties (Ye et al., 2018). Although there is insufficient scientific evidence to support the widespread application of PRP in osteoarthritis, and its stimulation of chondrogenesis is not well-established *in vivo* or *in vitro*, it has shown potential as a promising therapeutic alternative, particularly for improving pain control (Owaidah, 2024).

The synergistic action of these biological products in joint applications has been further investigated in knee osteoarthritis, with promising results. For HOA, results in agreement with knee osteoarthritis are expected when combining orthobiologics as we have HA with higher molecular weight (MW) concentrations and better standardization of the use of PRP (Gazendam et al., 2021). Depending on the MW of HA, there are different clinical responses and varying effects on osteoarthritis, with pain relief, improved function, and postponement of surgery. Considering the safety profile, viscosupplementation may be an effective option in the treatment of chondral damage, with emphasis on the use of HA with higher MW (Lu et al., 2023). Clinical improvement in short-term outcomes appears to be influenced by the cellular composition of intra-articular PRP and the severity of osteoarthritis. The interaction between these factors warrants further investigation by the scientific community (Filardo and Kon, 2016).

With an understanding of the biochemical actions of HA for joint health in promoting improved viscosity, adhesion capacity and anti-inflammatory and analgesic effects, it is considered a biological product for use in joint diseases, playing a crucial role in maintaining joint stability and facilitating movement. Once osteoarthritis is diagnosed, we notice a 33%–50% decrease in the concentration levels of this natural orthobiological product and an increase in infiltrations, which disrupts the homeostasis of the joint environment. With the ease of access to ultrasound-guided procedures for hip infiltrations, we have seen greater use of HA,

but the number of studies evaluating improvements in pain and joint function is still limited. Regardless of the joint being treated by HA, the physiological environment of an osteoarthritic joint improves by restoring protective viscoelasticity, reducing friction, and enhancing mobility (Leite and Buehler, 2018). In the search for an addition of anabolic effects with a reduction in inflammatory cytokines, dual therapy has been used, combining two orthobiologics.

The combination of PRP and HA in osteoarthritis was initially studied in the knee joint following promising results in laboratory animal models. This combination exhibits a synergistic biochemical action through independent mechanisms, facilitating cell signaling by releasing inflammatory molecules, catabolic enzymes, cytokines, and growth factors. The repair of degenerated cartilage is mediated by orthobiologics, which modulate the role of inflammatory cytokines in chondrocyte destruction through specific mediators such as CD44 and TGF-β. These actions theoretically inhibit the inflammatory response and slow the progression of osteoarthritis (Leite and Buehler, 2018; Chen et al., 2014; Andia and Abate, 2014). However, this association has been minimally investigated in hip osteoarthritis as it requires the use of ultrasound to guide the procedure (Zahir et al., 2021).

To avoid heterogeneity of the sample, recent systematic reviews have focused on comparing PRP plus HA versus PRP alone, particularly on knee degeneration, showing promising results when some outcomes were evaluated (Ivander and Anggono, 2024; Baria et al., 2022). The present meta-analysis aims to evaluate the influence of HA in combination with PRP compared to PRP alone in the therapeutic management of HOA in different follow-ups, considering pain and functional score outcomes.

2 Materials and methods

This systematic review and pairwise meta-analysis were conducted in accordance with the Cochrane Collaboration recommendations and Preferred Reporting Items for Systematic Reviews and Meta-Analyses guidelines and Protocols checklist (available in the online version of this article (Belk et al., 2022; Sterne et al., 2016). As such, its protocol was prospectively registered in PROSPERO database under the protocol CRD42024581335.

2.1 Eligibility criteria

In the study selection process, we started with deduplication and independently screened all potentially eligible studies. Four independent reviewers (FJA; FVZ; FMD; MCVF) and one validator (MSS) collaborated in combining outcomes from three databases and evaluated the studies for inclusion. Initially, they were excluded based on title and abstract if they did not pertain to the subject of interest. The remaining studies were then reviewed in full to verify eligibility. According to the inclusion criteria, two PRP centrifugation processes were accepted and we did not discriminate the leukocyte content of the final product to be infiltrated into the joint. We excluded trials not concluded, technical reports, editor responses, narrative reviews, systematic reviews, meta-analyses, non-comparative research, scientific posters, study protocols, conference abstracts not published as well as any pre-clinical studies or those not published in English. Unrelated papers not addressing the application of orthobiologics to treat hip osteoarthritis were also excluded.

We finished with a full independent reading of the papers by two authors, and we emphasized the presence of the following points: 1) peer-reviewed articles; 2) compared PRP in association with HA to PRP alone. Studies were excluded if they (1) were ongoing trials, not concluded; (2) were basic science research; (3) did not provide data on HOA patients; or (4) were case reports. We made no exclusions related to the publication date. Data extraction was manually performed.

Discrepancies were resolved through consensus between the reviewers and a third author (FJA) made the final decision in the event divergence was reached.

2.2 Search strategy

A comprehensive search was conducted across MEDLINE (via PUBMED), EMBASE (via OVID), and Cochrane databases from their inception until August 2024. No language restrictions were applied, and our search terms were a combination of Medical Subject Headings terms and keywords relating to "hip," "osteoarthritis," "platelet-rich plasma," and "hyaluronic acid." References from eligible studies and systematic reviews were also examined for additional relevant research. The specific search strategies for each database are available in Supplementary Table S1.

2.3 Clinical analysis tools

The data were extracted from eligible studies: study details—title, authors, publication year, study design, study definition, and inclusion/exclusion criteria; participant information—sample size, mean age, sex ratio, and HOA severity according to the Kellgren-Lawrence radiographic classification (K-L scale), which ranges from grade I (doubtful), grade II (mild), grade III (moderate), and grade IV (severe).

When extracting clinical data from articles, we choose outcomes compatible with *PICOTT* (population - HOA, intervention - Dual therapy, outcomes, control group- PRP alone, type of study- therapeutic, no restriction time) as main outcomes: pain, functional impairment. We used the numerical rating scale (NRS) ranging from 0 to 10 (or 100) mm as the data is reported, and functional questionnaires applied for general osteoarthritis, as the Western Ontario and McMaster Universities Osteoarthritis Index (WOMAC) score (from 0 to 100, in which 0 denotes the lowest degree of OA and 100 denotes the highest degree of OA) and in the hip joint, it was considered HARRIS HIP SCORE (HHS), ranging <70 is a poor result, 70–80 is fair, 80–90 is good, and a score of 90–100 is excellent. The final score of the functional questionnaires represented the current clinical condition. As the clinical improvement based on the final score in each questionnaire is with the inversion of the values upwards (increasing - HHS) and downwards (WOMAC), the tabulation was changed to a negative sign in the spreadsheet for the correct interpretation of the final data in the analysis in the statistical program. After treatment with each orthobiologic, final scores from these questionnaires were recorded.

2.4 Group analysis

Data extracted from studies included: 1) study details such as authors, sample size, intervention groups, and follow-up duration; 2) patient information including mean age, standard deviation, gender, and K-L scale (Kohn et al., 2016); 3) outcomes for pain and functional at 3, 6, and 12- months.

Due to the restricted number of studies at the end of the selection process and the availability of data, we choose a minimum of 2 studies for analysis according to the follow-up. Pain and functional scores outcomes were evaluated at 3-, 6- and 12- month follow-ups. In the 3-month pain outcome, all articles were included because they made *PICOOT* data available. In the functional score outcome, we only restricted the analysis to 2 articles in the 6-month follow-up due to lack of data.

In the intervention group of studies, we restricted the analysis to those who received the combination of PRP and hyaluronic acid. While in the control group, only in Palco et al. did the participants in the control group receive leukocyte-poor PRP (Palco et al., 2021).

2.5 Quality of evidence

In line with Cochrane guidelines, we employed the revised Cochrane risk-of-bias tool for non-randomized studies (ROBINS-I) to assess observational studies. The Cochrane risk-of-bias tool for randomized trials (ROB-2) was used to evaluate RCTs (Moher et al., 2009; Sterne et al., 2019). Pain was the primary outcome assessed using both ROBINS-I and ROB-2. Disagreements were resolved through consensus after discussion between the authors (MS and FV).

Considering that the level of evidence represents confidence in the information provided, the GRADE (Grading of Recommendation, Assessment, Development, and Evaluation) system was used, which assesses the quality of evidence for each available outcome. GRADE was a tool applied to assess the certainty of evidence in this Systematic Review, with four levels of classification: high, moderate, low and very low. Study design, publication bias, effect magnitude, dose-response gradient, and residual confounding factors were the main factors considered to determine the level of evidence.

2.6 Assessment of publication bias

Two review authors (FVZ; DVSC) assessed the risk of bias in each study by using the revised Cochrane risk of bias (RoB2/ROBINS-I tools). The examination domains included biases arising from the randomization process, deviations from intended interventions, missing outcome data, measurement of the outcome, and selection of the reported result. After responding to the signaling questions, one of three types of bias judgments was selected, namely "low," "high," and "some concerns." In the case of conflicts, a third author (DTS) was contacted as an unbiased arbitrator. The limited number of studies (fewer than ten) precluded a quantitative analysis for small study effects or publication bias (Sterne et al., 2016).

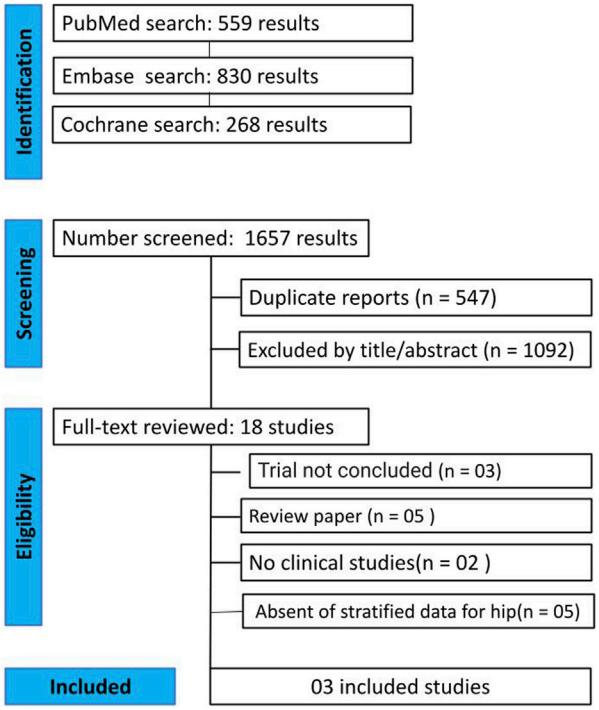

FIGURE 1
PRISMA (Preferred Reporting Items for Systematic Reviews and Meta-Analyses) Flow diagram of study screening and selection to the studies identified with the search strategy.

2.7 Statistical analysis

Mean differences (MD) with 95% confidence intervals (CIs) were used as the measure of association when units were consistent; otherwise, standardized mean differences (SMD) were calculated when the measurements were reported in a non-identical way in each study, either with regard to the pain scale or the functional questionnaire (WOMAC/HHS) with individual interpretation for each final score. A restricted maximum likelihood (REML) random-effects model was applied using the inverse variance method (Schwarzer et al., 2019). As there were 03 studies in the systematic review, we limited the meta-analysis by comparing the means at different times, without using other statistical studies.

Statistical analyses were conducted with R software (version 4.3.0; R Foundation for Statistical Computing, Vienna, Austria). Heterogeneity was assessed using Higgins and Thompson's I^2 statistics. P-values less than 0.05 were considered statistically significant. Heterogeneity was categorized as high ($I^2 \geq 50\%$), moderate (I^2 25%–50%), or low ($I^2 < 25\%$) (Deeks et al., 2019).

3 Results

3.1 Study selection and characteristics

As shown in Figure 1, the initial search yielded 1,657 results. After a meticulous review of titles, abstracts, and full texts, we eliminated 547 duplicate entries, and 1,092 studies that did not meet the criteria

TABLE 1 Baseline characteristics of the included studies.

Author and year	Study design	K-L1(n)	K-L2(n)	K-L3 (n)	K-L4(n)	Hips	Follow-up (months)	Molecular weight (HA)kDa	Group	Sample size	Age (years)	Female
Dallari et al. (2016)	RCT	22	18	24	16	80	12	1,500–3,200	PRP + HA	31	MD	19
									PRP	44		24
Nouri et al. (2022)	RCT	0	33	30	0	63	6	2,500–3,200	PRP + HA	31	60.29	23
									PRP	32	58.22	22
Palco et al. (2021)	Cohort	0	24	28	0	52	12	MD	PRP + HA	26	64.81	14
									PRP	26	50.62	10

Abbreviations: RCT, Randomized Clinical Trial; K-L, Kellgren-Lawrence scale; PRP, Platelet Rich Plasma; HA, Hyaluronic Acid; MD, Missing Data.

were excluded. At final selection, 18 studies remained for evaluation based on predetermined inclusion standards. From these, 3 studies were selected: 2 RCTs and 1 cohort study. These studies involved 190 participants, with 88 individuals receiving dual therapy.

There was a similar distribution by gender in both the control group (PRP treatment alone or leukocyte-poor PRP) and the intervention group (dual therapy), with a mean age of 50.62–64.9 years, considering the lack of data available in Dallari et al. (Dallari et al., 2016; Nouri et al., 2022). Patients were included based on both the clinical criteria and a radiological grading system, using the K-L scale. 2 studies included patients with K-L grades 2 and 3, while the last study split the sample to all grades. The molecular weight of HA was reported in 2 studies and ranged from 1,500 to 3,200 kDa. The studies' characteristics are presented in Table 1.

3.2 Pooled analysis

3.2.1 Pain at 3, 6, and 12 months

Compared with PRP injections alone, combined PRP and HA injections resulted in significantly higher pain at 3 months (MD 0.35; 95% CI: 0.06–0.64; $p = 0.02$; $I^2 = 0\%$; Figure 2A) and 12 months (MD 11.92; 95% CI: 3.87–19.97; $p < 0.01$; $I^2 = 65\%$; Figure 2B). Nevertheless, the 6-month assessment showed comparable results between the approaches (MD 0.30; 95% CI: −0.28–0.88; $p = 0.31$; $I^2 = 66\%$; Figure 2C).

3.2.2 Functional score at 3, 6, and 12 months

The analysis revealed no statistically significant variations in functional outcomes between groups at 3-, 6-, 12- months. The results were as follows: (MD -0.35; 95% CI: −0.85–0.15; $p = 0.17$; $I^2 = 66\%$; Figure 3A), (MD -6.36; 95% CI: −18.72–6.00; $p = 0.31$; $I^2 = 88\%$; Figure 3B), and (MD -0.27; 95% CI: −0.61–0.07; $p = 0.12$; $I^2 = 0\%$; Figure 3C), respectively. All three studies show no improvement in functional scores, likely due to greater joint damage as classified by the Kellgren-Lawrence scale. This damage, particularly the reduced femoro-acetabular joint space, may result in mechanical blockage, limiting the potential impact of the synergistic effect of orthobiological combined treatments. In the study by Dallari et al., patients are distributed across the four K-L grades, while in the other studies, they are distributed across K-L grades 2–3, which justifies a population sample with more advanced joint degeneration (Palco et al., 2021; Dallari et al., 2016; Nouri et al., 2022).

Interpretation of findings about NRS and functional outcomes showed no significant differences, but the confidence intervals are wide, suggesting low statistical power.

3.3 Risk of bias evaluation

As shown in Supplementary Figure S1A, the two RCTs exhibited some concerns about this confounding factor. Both were unable to blind the patients given the need to collect blood samples to prepare PRP before its administration. However, given that this was the only point of deviation in the direction of bias - and inherent to the type of intervention - we maintained the level of bias as "some concerns." Additionally, Supplementary Figure S1B reveals that Palco et al., had some concerns in the ROBINS-I evaluation. These concerns

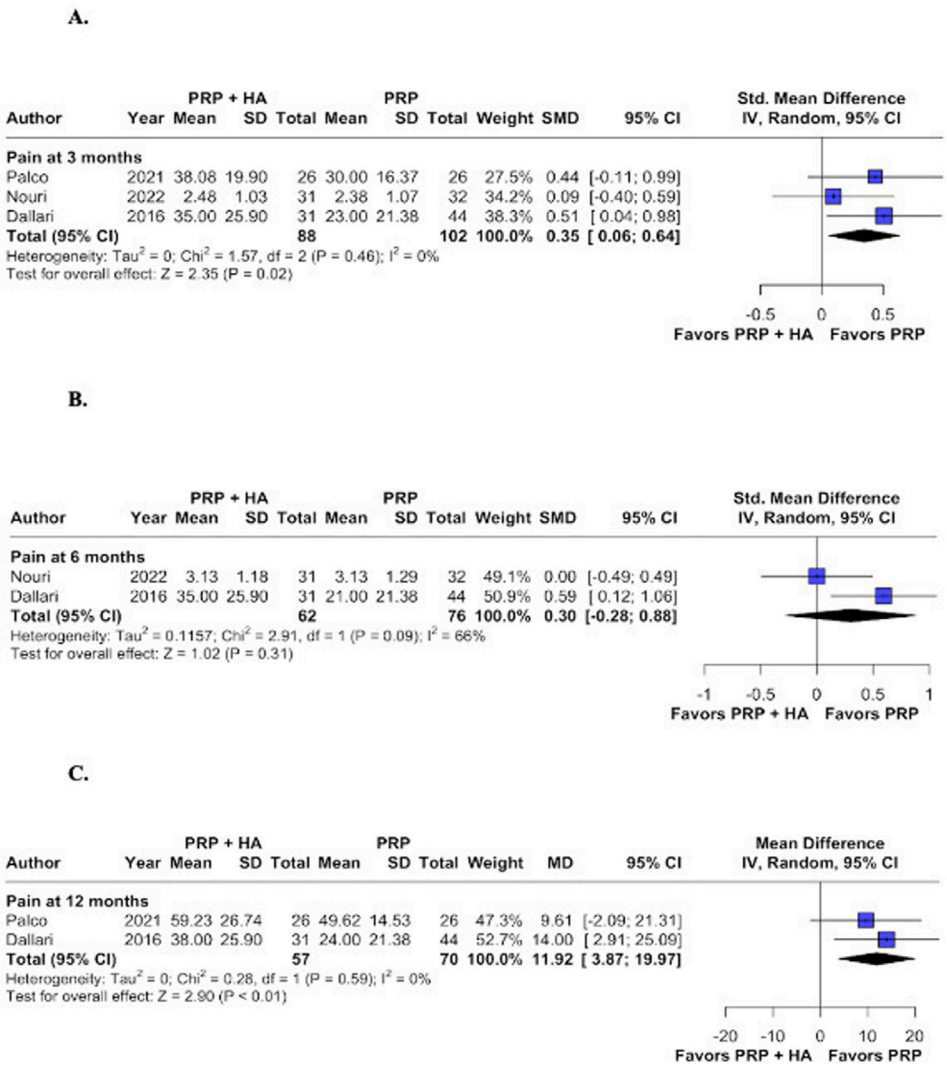

FIGURE 2
Forest plots for the following endpoints: **(A)** Pain at 3 months; **(B)** Pain at 6 months; **(C)** Pain at 12 months.

primarily arose from issues related to confounding and participant selection (Sterne et al., 2016; Palco et al., 2021; McGuinness and Higgins, 2021). This figure shows overall concerns, primarily due to confounding issues.

3.4 Quality assessment

The GRADE quality assessment revealed very low confidence in pain at 3 months and functional score at 12 months, moderate confidence in both outcomes at 6 months, and high confidence in pain outcome at 12 months. The very low and low confidence ratings were due to serious concerns about inconsistency and imprecision in the studies. Consequently, the actual effects may differ from the estimated effects, as depicted in Supplementary Figure S2. The GRADE assessment was performed using GRADEpro GDT (GRADE pro Guideline Development Tool, McMaster University and Evidence Prime, 2024) (Guyatt et al., 2011).

The GRADE quality assessment indicated very low confidence in the functional score outcome at 3 months, low confidence in both pain at 3 months and functional score at 12 months, moderate confidence in pain and functional score at 6 months, and high confidence in pain at 12 months.

4 Discussion

With the inclusion of 3 studies, representing 190 patients, we evaluated the comparative efficacy of intra-articular PRP with versus without HA for managing pain in patients with HOA in any K-L scale awaiting arthroplasty. Our findings revealed: 1) a statistically significant reduction in NRS at 3 and 12 months favoring the PRP group, and 2) no significant improvement in functional scores at any follow-up or in NRS at 6 months. In addition, no significant improvement in pain was noted at 6 months and in functional outcome at any follow-up.

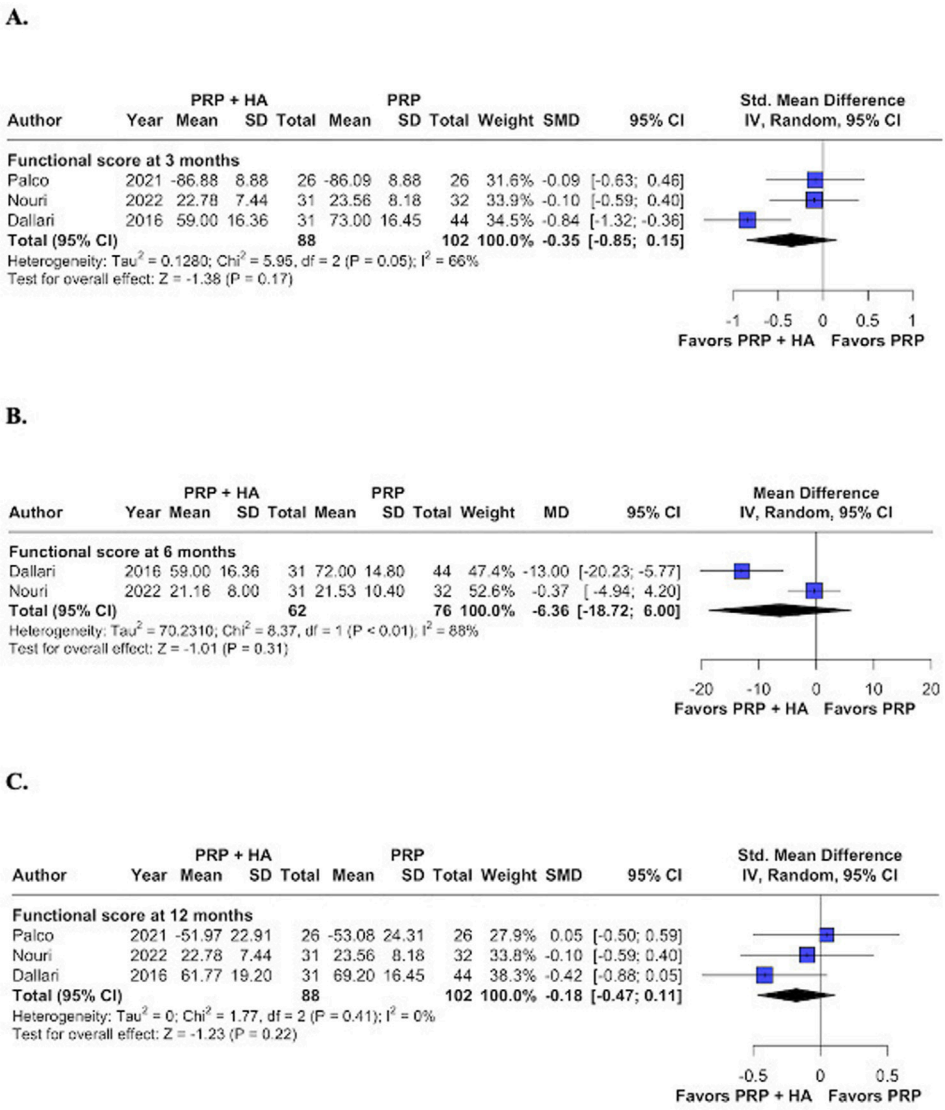

FIGURE 3
Forest plots for the following endpoints: **(A)** Functional score at 3 months; **(B)** Functional score at 6 months; **(C)** Functional score at 12 months.

In chronic joint inflammatory processes, there is a reduction in the MW and concentration of HA. When considering viscosupplementation in hip osteoarthritis, studies have shown better clinical response with the use of high molecular weight and severity according to the K-L scale up to 6 months. In this systematic review, we observed that even the use of medium MW (1,500–3,200 kDa) HA was related to a reduction in pain levels for up to 12 months (Schünemann et al., 2013; Wu et al., 2021). However, we observed a lack of standardization in both the molecular weight of HA and the preparation of PRP, which makes a more accurate analysis of the results difficult. A beneficial clinical response is observed when comparing PRP alone with corticosteroids in hip or Knee osteoarthritis in longer follow-ups. In addition to the short duration of pain relief with corticosteroids, it also brings adverse effects that limit their use (Zhao et al., 2020; Freire et al., 2020). However, the use of PRP alone as a regenerative therapy has been more studied, with less than encouraging results, despite knowing its biological properties and safety of use in hip osteoarthritis during a similar period (Pogliacomi et al., 2018).

Regarding knee osteoarthritis of mild and moderate severity, the benefit of dual therapy has been observed in pain control for up to 1 year, while functional improvement is maintained only for the first 3 months (Medina-Porqueres et al., 2021). Given the larger number of studies with bigger sample sizes on the use of orthobiologicals in knee osteoarthritis, we applied this understanding to the hip. It is noted that in knee osteoarthritis, there are better results in pain control and joint function with the addition of HA to PRP than with PRP alone, up to 1 year of administration follow-up. However, combined therapy proved to be superior in long-term follow-up at 2 years. Otherwise, the Gao et al. study shows superiority of the therapy compared to

monotherapy, HA, or PRP alone. Still considering this segment, conflicting results have been reported with PRP monotherapy vs. PRP plus HA because there is no standardized procedure for preparation and specific dosage of PRP (Gao et al., 2024; Lana et al., 2016; Howlader et al., 2023; Cole et al., 2017).

Nevertheless, although the basic scientific rationale for adding HA is convincing due to its rheological properties, randomized clinical studies have shown no statistical significance in knee osteoarthritis. It confirmed the benefit in the clinical parameters of pain and function and the improvement both with the isolated use of PRP and with dual therapy using HA of different MW. Even with the comparison between groups, there was no superiority of any intervention (Garcia et al., 2020; Gormeli et al., 2017). The non-discrimination of MW in one of the studies included in our systematic review did not allow the analysis of the results according to this variable since HA with a MW < 3,200 kDa was used. But even so, we observed that regardless of the molecular weight of HA, there was no contribution to pain improvement when associated with PRP. This differs from other studies, corroborating the positive effect of high MW infiltrations in hip joint osteoarthritis (Safali et al., 2024).

This study is the first systematic evaluation of the clinical response of dual therapy (PRP + HA) versus PRP alone for HOA. Considering the paucity of studies in HOA, our results regarding pain outcomes in monotherapy with PRP are similar to the Baria et al. (2022), which saw similar results in knee osteoarthritis (Baria et al., 2022). However, no significant improvement in functional score was found in dual therapy at any follow-up when compared with the PRP group (Filardo et al., 2021). When analyzing the clinical results in younger patients and those with less structural cartilage damage, a better response is seen with the use of PRP alone, but even so there are few studies that support this statement in both knee and hip osteoarthritis. In this way, the results of the functional score using orthobiologics in HOA demonstrate a reduction in pain about specific domains, but considering the final score, no improvement was found (Jacob et al., 2017). However, it is important to notice that this outcome involves many variables, especially within the biopsychosocial context, which may influence these findings (Bennell et al., 2017). While the response to PRP monotherapy in HOA is beneficial for up to 1 year, there is no significant improvement when compared to HA in the same period, when considering intra-articular hip pathologies and any MW of HA (Zaffagnini et al., 2022).

In regulatory and ethical considerations on the use of combined therapy, we have seen that PRP is considered a biological product and may be subject to different regulatory frameworks depending on the country and must be prepared from fresh blood and used during the same medical session and in the same room. HA, on the other hand, is often classified as a medical device or a drug. Given the lack of specific guidelines, it is advisable to consult local regulatory authorities before mixing PRP with HA *ex vivo*. Ensuring compliance with general standards for autologous product preparation and medical device use is crucial. Transparency with patients regarding risks and benefits were essential in all studies. There are ethical concerns and the patients must be appropriately consented in each study.

This study has limitations. The number of published trials available on databases was a significant impediment in formulating this systematic review, with many of the included studies of low confidence ratings not in accordance with the Consolidated Standards of Reporting of Trials (CONSORT) (The CONSORT Statement, 2022), which may limit the reliability of the conclusions. As one of the studies was a retrospective cohort with a reduced sample size, it also represents a factor that prevents a more accurate inference from the general population. Second, the relatively small sample size of 102 patients in the PRP group and 88 patients in the PRP + HA group in the final analysis of the selected studies could affect the generalizability of the results. Third, the variability in study design (including two RCTs and one cohort study) and follow-up duration may introduce methodological and statistical heterogeneity. Considering the different PRP preparation techniques, the MW of HA and the frequency of joint infiltrations that show variation in results also contribute to high heterogeneity. Fourth, the scales used to analyze pain and functional deficit of the hip differed across studies, and this is one more factor that introduces bias in the outcomes. The lack of significant improvement in functional scores suggests that while pain management might be enhanced, the overall clinical benefit remains unclear. These limitations can be addressed by using orthobiologicals with standardized PRP preparation methods and higher molecular weight HA in patients with similar degrees of hip osteoarthritis. This approach could improve the measurement of outcomes, aiming to enhance clinical applications and provide greater benefits to patients.

5 Conclusion

The outcomes analyzed in this meta-analysis suggest that the utilization of dual therapy versus PRP in the context of HOA confers a significant reduction in pain. However, this does not apply to the improvement in quality of life-related to the application of functional questionnaires at any follow-up time without statistical significance. The addition of HA did not influence the improvement in clinical response to pain and function outcomes. Finally, we found a significant reduction in pain at 3- and 12- months, favoring joint infiltration with PRP alone, relative to HA plus PRP, which leads to maintenance of clinical improvement for a longer period, even considering it is a chronic degenerative disease. Although our results showed promising results favoring the use of orthobiologics, we understand that the low number of trials and sample size limits make our conclusions preliminary warranting more trials with larger population samples. Nevertheless, large sample sizes are also warranted to validate our findings about the benefit of HA plus PRP in HOA before these results are implemented in clinical practice. We recognize that standardized PRP/HA protocols are needed before strong clinical recommendations can be made that provide a more balanced interpretation. Therefore, high-quality RCTs and longer follow-up periods (>12 months). Are warranted to understand the clinical benefit of HA plus PRP in HOA.

Data availability statement

The original contributions presented in the study are included in the article/Supplementary Material, further inquiries can be directed to the corresponding author.

Author contributions

MS: Conceptualization, Writing–original draft, Writing–review and editing. FD: Project administration, Writing–review and editing. JM: Data curation, Writing–review and editing. FF: Visualization, Writing–review and editing. EP: Data curation, Writing–review and editing. FJA: Formal Analysis, Writing–review and editing. MS: Investigation, Writing–review and editing. DC: Methodology, Writing–review and editing. FA: Visualization, Writing–review and editing. FZ: Methodology, Writing–review and editing. DS: Visualization, Writing–review and editing. RM: Investigation, Writing–review and editing. AD-dD: Project administration, Writing–review and editing. MM-F: Formal Analysis, Writing–review and editing. RC: Supervision, Writing–original draft, Writing–review and editing.

Funding

The author(s) declare that no financial support was received for the research and/or publication of this article.

Acknowledgments

The authors would like to thank the research sector of the health sciences program at the Federal University of Sergipe for providing access to the databases for literature review. We also recognize the important role of the senior advisor, Rosana Cipolotti, in the final evaluation of the manuscript.

Conflict of interest

The authors declare that the research was conducted in the absence of any commercial or financial relationships that could be construed as a potential conflict of interest.

Generative AI statement

The author(s) declare that no Generative AI was used in the creation of this manuscript.

Publisher's note

All claims expressed in this article are solely those of the authors and do not necessarily represent those of their affiliated organizations, or those of the publisher, the editors and the reviewers. Any product that may be evaluated in this article, or claim that may be made by its manufacturer, is not guaranteed or endorsed by the publisher.

Supplementary material

The Supplementary Material for this article can be found online at: https://www.frontiersin.org/articles/10.3389/fbioe.2025.1545431/full#supplementary-material

References

Andia, I., and Abate, M. (2014). Knee osteoarthritis: hyaluronic acid, platelet-rich plasma or both in association? *Expert Opin. Biol. Ther.* 14, 635–649. doi:10.1517/14712598.2014.889677

Baria, M. R., Vasileff, W. K., Borchers, J., DiBartola, A., Flanigan, D. C., Plunkett, E., et al. (2022). Treating knee osteoarthritis with platelet-rich plasma and hyaluronic acid combination therapy: a systematic review. *Am. J. Sports Med.* 50 (1), 273–281. doi:10.1177/0363546521998010

Belk, J. W., Houki, D. A., Littlefield, C., Kraeutler, M. J., Potyk, A. G., Dragoo, J. L., et al. (2022). Platelet-rich plasma versus hyaluronic acid for hip osteoarthritis yields similarly beneficial short-term clinical outcomes: a systematic review and meta-analysis of level I and II randomized controlled trials. *Arthroscopy* 38, 2035–2046. doi:10.1016/j.arthro.2021.11.005

Bennell, K. L., Hunter, D. J., and Paterson, K. L. (2017). Platelet-rich plasma for the management of hip and knee osteoarthritis. *Curr. Rheumatol. Rep.* 19 (5), 24. doi:10.1007/s11926-017-0652-x

Chen, W. H., Lo, W. C., Hsu, W. C., Wei, H. J., Liu, H. Y., Lee, C. H., et al. (2014). Synergistic anabolic actions of hyaluronic acid and platelet-rich plasma on cartilage regeneration in osteoarthritis therapy. *Biomaterials* 35 (36), 9599–9607. doi:10.1016/j.biomaterials.2014.07.058

Cole, B. J., Karas, V., Hussey, K., Pilz, K., and Fortier, L. A. (2017). Hyaluronic acid versus platelet-rich plasma: a prospective, double-blind randomized controlled trial comparing clinical outcomes and effects on intra-articular biology for the treatment of knee osteoarthritis. *Am. J. Sports Med.* 45 (2), 339–346. doi:10.1177/0363546516665809

Dallari, D., Stagni, C., Rani, N., Sabbioni, G., Pelotti, P., Torricelli, P., et al. (2016). Ultrasound-guided injection of platelet-rich plasma and hyaluronic acid, separately and in combination, for hip osteoarthritis: a randomized controlled study. *Am. J. Sports Med.* 44 (3), 664–671. doi:10.1177/0363546515620383

Deeks, J. J., Higgins, J. P. T., and Altman, D. G. (2019). Chapter 10: analyzing data and undertaking meta-analyses. *Cochrane Handb. Syst. Rev. Interventions.* doi:10.1002/9781119536604.ch10

Filardo, G., and Kon, E. (2016). PRP: product rich in placebo? *Knee Surg. Sports Traumatol. Arthrosc.* 24 (12), 3702–3703. doi:10.1007/s00167-015-3778-2

Filardo, G., Previtali, D., Napoli, F., Candrian, C., Stefano Zaffagnini, S., and Grass, A. (2021). PRP injections for the treatment ofKnee osteoarthritis: a meta-analysis of randomized controlled trials. *Cartilage* 13, 364–375. doi:10.1177/1947603520931170

Filardo, G. K., Ruiz, M. T. P., Vaccaro, F., Guitaldi, R., Martino, A., Cenacchi, A., et al. (2012). Platelet-rich plasma intra-articular injections for cartilage degeneration and osteoarthritis: single-versus double spinning approach. *Knee Surg. Sports Traumatol. Arthrosc.* 20, 2082–2091. doi:10.1007/s00167-011-1837-x

Freire, M. R. M., Silva, P. M. C., Azevedo, A. R., Silva, D. S., Silva, R. B. B., and Cardoso, J. C. (2020). Comparative effect between infiltration of platelet-rich plasma and the use of corticosteroids in the treatment of knee osteoarthritis: a prospective and randomized clinical trial. *Rev. Bras. Ortop. (Sao Paulo)* 55 (5), 551–556. doi:10.1016/j.rbo.2018.01.001

Gao, J., Ma, Y., Tang, J., Zhang, J., and Zuo, J. (2024). Efficacy and safety of platelet-rich plasma and hyaluronic acid combination therapy for knee osteoarthritis: a systematic review and meta-analysis. *Arch. Orthop. Trauma Surg.* 144, 3947–3967. doi:10.1007/s00402-024-05442-y

Garcia, F. L., Williams, B. T., Polce, E. M., Heller, D. B., Aman, Z. S., Nwachukwu, B. U., et al. (2020). Preparation methods and clinical outcomes of platelet-rich plasma for intra-articular hip disorders: a systematic review and meta-analysis of randomized clinical trials. *Orthop. J. Sports Med.* 8 (10), 2325967120960414. doi:10.1177/2325967120960414

Gazendam, A., Ekhtiari, S., Bozzo, A., Phillips, M., and Bhandari, M. (2021). Intra-articular saline injection is as effective as corticosteroids, platelet-rich plasma and hyaluronic acid for hip osteoarthritis pain: a systematic review and network meta-analysis of randomised controlled trials. *Br. J. Sports Med.* 55 (5), 256–261. doi:10.1136/bjsports-2020-102179

Gormeli, G., Gormeli, C. A., Ataoglu, B., Çolak, C., Aslanturk, O., and Ertem, K. (2017). Multiple PRP injections are more effective than single injections and hyaluronic acid in knees with early osteoarthritis: a randomized, double-blind, placebo-controlled trial. *Knee Surg. Sports Traumatol. Arthrosc.* 25, 958–965. doi:10.1007/s00167-015-3705-6

Guyatt, G. H., Oxman, A. D., Vist, G., Kunz, R., Brozek, J., Alonso-Coello, P., et al. (2011). GRADE guidelines: 4. Rating the quality of evidence--study limitations (risk of bias). *J. Clin. Epidemiol.* 64 (4), 407–415. doi:10.1016/j.jclinepi.2010.07.017

Howlader, M. A. A., Almigdad, A., Urmi, J. F., and Ibrahim, H. (2023). Efficacy and safety of hyaluronic acid and platelet-rich plasma combination therapy versus platelet-rich plasma alone in treating knee osteoarthritis: a systematic review. *Cureus* 15 (10), e47256. doi:10.7759/cureus.47256

Ivander, G., and Anggono, Y. (2024). A comparison of intra-articular hyaluronic acid and platelet-rich plasma for knee osteoarthritis: a systematic review. *Orthop. Rev. (Pavia).* 16, 94236. doi:10.52965/001c.94236

Jacob, G., Shetty, V., and Shetty, S. (2017). A study assessing intra-articular PRP vs PRP with HMW HA vs PRP with LMW HA in early knee osteoarthritis. *J. Arthrosc. Jt. Surg.* 4, 65–71. doi:10.1016/j.jajs.2017.08.008

Kohn, M. D., Sassoon, A. A., and Fernando, N. D. (2016). Classifications in brief: kellgren-lawrence classification of osteoarthritis. *Clin. Orthop. Relat. Res.* 474 (8), 1886–1893. doi:10.1007/s11999-016-4732-4

Kravos, A., and Jerman, M. (2012). Impact of hip and/or knee osteoarthrosis on quality of life. *ACTA MEDICO–BIOTECHNICA* 5, 47–57. doi:10.18690/actabiomed.75

Lana, J. F. W. A., Sampson, S. E., Vicente, E. F., Huber, S. C., Souza, C. V., Ambach, M. A., et al. (2016). Randomized controlled trial comparing hyaluronic acid, platelet-rich plasma and the combination of both in the treatment of mild and moderate osteoarthritis of the knee. *J. Stem Cells Regen. Med.* 12, 69–78. doi:10.46582/jsrm.1202011

Leite, V. F. A. ; J. E. D., and Buehler, A. M. (2018). Viscosupplementation for hip osteoarthritis: a systematic review and meta-analysis of the efficacy on pain and disability, and the occurrence of adverse events. *Arch. Phys. Med. Rehabil.* 99, 574–583.e1. doi:10.1016/j.apmr.2017.07.010

Lim, A., Zhu, J. B., and Khanduja, V. (2023). The use of intra-articular platelet-rich plasma as a therapeutic intervention for hip osteoarthritis: a systematic review and meta-analysis. *Am. J. Sports Med.* 51, 2487–2497. doi:10.1177/03635465221095563

Lu, K., Lu, P. W., Lin, C., Lu, E. W., and Yang, S. (2023). Different molecular weights of hyaluronan research in knee osteoarthritis: a state-of-the-art review. *Matrix Biol.* 117, 46–71. doi:10.1016/j.matbio.2023.02.006

McGuinness, L. A., and Higgins, J. P. T. (2021). Risk-of-bias VISualization (robvis): an R package and Shiny web app for visualizing risk-of-bias assessments. *Res. Synth. Methods* 12 (1), 55–61. doi:10.1002/jrsm.1411

Medina-Porqueres, I., Ortega-Castillo, M., and Muriel-Garcia, A. (2021). Effectiveness of platelet-rich plasma in the management of hip osteoarthritis: a systematic review and meta-analysis. *Clin. Rheumatol.* 40 (1), 53–64. doi:10.1007/s10067-020-05241-x

Moher, D., Liberati, A., Tetzlaff, J., and Altman, D. G. (2009). Preferred reporting items for systematic reviews and meta-analyses: the PRISMA statement. *PLoS Med.* 6 (7), e1000097. doi:10.1371/journal.pmed.1000097

Nouri, F., Babaee, M., Peydayesh, P., Esmaily, H., and Raeissadat, S. A. (2022). Comparison between the effects of ultrasound guided intra-articular injections of platelet-rich plasma (PRP), high molecular weight hyaluronic acid, and their combination in hip osteoarthritis: a randomized clinical trial. *BMC Musculoskelet. Disord.* 23 (1), 856. doi:10.1186/s12891-022-05787-8

Owaidah, A. Y. (2024). Induced pluripotent stem cells in cartilage tissue engineering: a literature review. *Biosci. Rep.* 44 (5). doi:10.1042/bsr20232102

Palco, M., Rizzo, P., Basile, G. C., Alito, A., Bruschetta, D., Accorinti, M., et al. (2021). Short- and midterm comparison of platelet-rich plasma with hyaluronic acid versus leucocyte and platelet-rich plasma on pain and function to treat hip osteoarthritis. A retrospective study. *Gels* 7 (4), 222. doi:10.3390/gels7040222

Pogliacomi, F., Schiavi, P., Paraskevopoulos, A., Leigheb, M., Pedrazzini, A., Ceccarelli, F., et al. (2018). When is indicated viscosupplementation in hip osteoarthritis? *Acta Biomed.* 90 (1-S), 67–74. doi:10.23750/abm.v90i1-S.8000

Safali, S., Ertas, E. S., Ozdemir, A., and Catakli, D. (2024). Evaluation of single and multiple hyaluronic acid injections at different concentrations with high molecular weight in the treatment of knee osteoarthritis. *BMC Musculoskelet. Disord.* 25 (1), 164. doi:10.1186/s12891-024-07200-y

Sambe, H. G., Yasir, M., Man, R. K., Gogikar, A., Nanda, A., Janga, L. S. N., et al. (2023). Comparing intra-articular platelet-rich plasma with hyaluronic acid for the treatment of hip osteoarthritis: a systematic review and meta-analysis. *Cureus* 15 (10), e47919. doi:10.7759/cureus.47919

Schünemann, H., Oxman, A.D., Brozek, J., Glasziou, P., Jaeschke, R., and Vist, G.E. (2008). GRADE Working Group. Grading quality of evidence and strength of recommendations for diagnostic tests and strategies. *BMJ.* 336 (7653), 1106–10. doi:10.1136/bmj.39500.677199.AE

Schwarzer, G., Chemaitelly, H., Abu-Raddad, L. J., and Rucker, G. (2019). Seriously misleading results using inverse of Freeman-Tukey double arcsine transformation in meta-analysis of single proportions. *Res. Synth. Methods* 10 (3), 476–483. doi:10.1002/jrsm.1348

Sterne, J. A., Hernan, M. A., Reeves, B. C., Savovic, J., Berkman, N. D., Viswanathan, M., et al. (2016). ROBINS-I: a tool for assessing risk of bias in non-randomised studies of interventions. *S. BMJ* 355, i4919. doi:10.1136/bmj.i4919

Sterne, J. A. C., Savovic, J., Page, M. J., Elbers, R. G., Blencowe, N. S., Boutron, I., et al. (2019). RoB 2: a revised tool for assessing risk of bias in randomised trials. *BMJ* 366, l4898. doi:10.1136/bmj.l4898

Tjandra, K. C., Novriansyah, R., Sudiasa, I. N. S., Ar, A., Rahmawati, N. A. D., and Dilogo, I. H. (2024). Modified Mesenchymal stem cell, platelet-rich plasma, and hyaluronic acid intervention in early stage osteoarthritis: a systematic review, meta-analysis, and meta-regression of arthroscopic-guided intra-articular approaches. *PLoS One* 19 (3), e0295876. doi:10.1371/journal.pone.0295876

Wu, Y., Huang, H., Ho, C., Shih, C., Chen, C., Cheng, T., et al. (2021). Molecular weight of hyaluronic acid has major influence on its efficacy and safety for viscosupplementation in hip osteoarthritis: a systematic review and meta-analysis. *Cartilage* 13, 169S–184S. doi:10.1177/19476035211021903

Xu, Z., Yin, W., Zhang, Y., Qi, X., Chen, Y., Xie, X., et al. (2017). Comparative evaluation of leukocyte- and platelet-rich plasma and pure platelet-rich plasma for cartilage regeneration. *Sci. Rep.* 7, 43301. doi:10.1038/srep43301

Ye, Y., Zhou, X., Mao, S., Zhang, J., and Lin, B. (2018). Platelet rich plasma versus hyaluronic acid in patients with hip osteoarthritis: a meta-analysis of randomized controlled trials. *Int. J. Surg.* 53, 279–287. doi:10.1016/j.ijsu.2018.03.078

Zaffagnini, M., Boffa, A., Andriolo, L., Raggi, F., Zaffagnini, S., and Filardo, G. (2022). Orthobiologic injections for the treatment of hip osteoarthritis: a systematic review. *J. Clin. Med.* 11 (22), 6663. doi:10.3390/jcm11226663

Zahir, H., Dehghani, B., Yuan, X., Chinenov, Y., Kim, C., Burge, A., et al. (2021). *In vitro* responses to platelet-rich-plasma are associated with variable clinical outcomes in patients with knee osteoarthritis. *Sci. Rep.* 11 (1), 11493. doi:10.1038/s41598-021-90174-x

Zhao, Z., Ma, J. X., and Ma, X. L. (2020). Different intra-articular injections as therapy for hip osteoarthritis: a systematic review and network meta-analysis. *Arthroscopy* 36 (5), 1452–1464 e2. doi:10.1016/j.arthro.2019.09.043

frontiers | Frontiers in Cell and Developmental Biology

TYPE Original Research
PUBLISHED 26 March 2025
DOI 10.3389/fcell.2025.1521437

Check for updates

OPEN ACCESS

EDITED BY
Elizabeth Vinod,
Christian Medical College and Hospital, India

REVIEWED BY
Kefei Li,
Cornell University, United States
Jeya Lisha J,
Christian Medical College and Hospital, India

*CORRESPONDENCE
J. Mary Murphy,
mary.murphy@universityofgalway.ie

RECEIVED 01 November 2024
ACCEPTED 12 February 2025
PUBLISHED 26 March 2025

CITATION
Ivanovska A, Mancuso P, Burke A, Hennessy C, Raman S, Dooley C, McLoughlin S, Shaw G, Mukeria E, Reilly J, O'Brien A, Ritter T, Ryan AE, Kamath R, Levesque MC, Riet DV, English K, Hawthorne I, Johnstone B, Morris DW, Barry F and Murphy JM (2025) Identification of disease-stage therapeutic responses of mesenchymal stromal cells retrieved from murine osteoarthritic joints.
Front. Cell Dev. Biol. 13:1521437.
doi: 10.3389/fcell.2025.1521437

COPYRIGHT
© 2025 Ivanovska, Mancuso, Burke, Hennessy, Raman, Dooley, McLoughlin, Shaw, Mukeria, Reilly, O'Brien, Ritter, Ryan, Kamath, Levesque, Riet, English, Hawthorne, Johnstone, Morris, Barry and Murphy. This is an open-access article distributed under the terms of the Creative Commons Attribution License (CC BY). The use, distribution or reproduction in other forums is permitted, provided the original author(s) and the copyright owner(s) are credited and that the original publication in this journal is cited, in accordance with accepted academic practice. No use, distribution or reproduction is permitted which does not comply with these terms.

Identification of disease-stage therapeutic responses of mesenchymal stromal cells retrieved from murine osteoarthritic joints

Ana Ivanovska[1,2], Patrizio Mancuso[1,2], Amy Burke[1,2], Conor Hennessy[1,2], Swarna Raman[1,2], Claire Dooley[1,2], Steven McLoughlin[1,2], Georgina Shaw[1], Eka Mukeria[1,2], Jamie Reilly[1], Aisling O'Brien[1], Thomas Ritter[1,2], Aideen E. Ryan[1,2], Raj Kamath[3], Marc C. Levesque[3], Deborah Van Riet[3], Karen English[4], Ian Hawthorne[4], Brian Johnstone[5], Derek W. Morris[6], Frank Barry[1,2] and J. Mary Murphy[1,2]*

[1]School of Medicine, Regenerative Medicine Institute (REMEDI), University of Galway, Galway, Ireland, [2]Centre for Research in Medical Devices (CÚRAM), University of Galway, Galway, Ireland, [3]AbbVie Bioresearch Center, Worcester, MA, United States, [4]Cellular Immunology Lab, Department of Biology, Kathleen Lonsdale Institute for Human Health Research, Maynooth University, Maynooth, Ireland, [5]Department of Orthopaedics and Rehabilitation, Oregon Health & Science University, Portland, OR, United States, [6]Discipline of Biochemistry, Center for Neuroimaging, Cognition and Genomics (NICOG), University of Galway, Galway, Ireland

Objective: Osteoarthritis (OA) is a widespread and debilitating joint disease characterized by synovial inflammation, cartilage degeneration, and chronic joint pain. Mesenchymal stromal cells (MSCs) have shown therapeutic efficacy for many diseases with a strong inflammatory profile, including OA. However, the disease-specific mechanisms of action underpinning the effects of post-local MSC delivery remain unaddressed. In this study, we aimed to characterize the disease-induced profile of MSCs following exposure to the *in vivo* osteoarthritis environment.

Methods: Murine syngeneic GFP + bone marrow-derived MSCs (BM-MSCs) were delivered *via* intra-articular injection in a mouse collagenase-induced osteoarthritis (CIOA) model (n = 8). BM-MSCs were retrieved by cell sorting on days 14 and 56, following whole mouse knee digestions. The retrieved cells were expanded in culture and characterized based on their phenotype, immunomodulatory effects on lymphocytes and macrophages, and transcriptomic profile.

Results: Retrieved BM-MSCs (1.33%) had minimal effects on lymphocyte proliferation but induced macrophage anti-inflammatory activity. Surviving retrieved BM-MSCs activated various pathways, with their secretome impacting immune system regulation and extracellular matrix organization, correlating with the disease stage. Data comparing the transcriptomic profiles of retrieved and *in vitro*-licensed BM-MSCs suggested a chondroprogenitor profile and identified BRINP3 as a novel factor in MSC function for potential OA modulation.

Conclusion: The beneficial effects of BM-MSCs in OA post-local delivery could be attributed to a specific subset of cells able to resist the micro-inflammatory milieu and contribute to cartilage healing and suppression of associated synovial inflammation. Furthermore, data suggest a paradigm of environmentally guided plasticity associated with MSCs upon local delivery in both early and late OA.

KEYWORDS

mesenchymal stromal cells, osteoarthritis, murine model, disease-stage response, chondroprogenitor cells

1 Introduction

Osteoarthritis (OA) is a widespread, debilitating, and chronic joint disease characterized by inflammation and degradation of articular cartilage (AC). It is a major global contributor to disability, becoming more prevalent in aging populations with a severe impact on the quality of life (Das and Farooqi, 2008; Yucesoy et al., 2015). It also represents a significant economic burden in terms of loss of income and healthcare delivery (Xie et al., 2016). Despite the global burden, OA is still an untreatable disease with no pharmacological, biological, or medical intervention that reverses the degradative course. As such, there is a clear need for disease-modifying interventions that can slow progressive joint destruction, reduce pain, restore function, and delay or eliminate the need for joint replacement.

AC injuries are difficult to treat with slow cellular turnover, contributing to limited intrinsic reparative capacity (Sophia Fox et al., 2009). Endogenous mesenchymal stem/stromal cells (MSCs), localizing to synovium, synovial fluid, fat pad, the superficial zone of AC, perichondral groove of Ranvier, and meniscal red zone, can be recruited in response to OA, traumatic injuries, and aging. However, due to age-related and disease-induced changes, the capacity of endogenous MSCs to induce significant disease amelioration is limited (Mantripragada et al., 2019). The ability of MSCs to respond to the injured joint environment *in vivo* by secreting reparative factors was first shown in a caprine model of OA. In this model, cells injected into joints subjected to meniscectomy and anterior cruciate ligament destabilization engrafted onto the synovium and the surface of the regenerated, host cell-derived medial meniscus (Murphy et al., 2003). Although engrafted MSCs survived for at least 6 weeks post intra-articular (IA) injection, they did not differentiate into chondrocytes *in vivo* but significantly impeded the progression of osteoarthritic symptoms. In addition, IA administration of murine MSCs resulted in minimal engraftment in arthritic knee joints in multiple studies (8) with a decreased expression of inflammatory mediators in the synovium described in the collagenase-induced OA model (CIOA) in mice (Ter Huurne et al., 2012; Schelbergen et al., 2014). Associations between apoptosis and MSC-based immunosuppressive effects were first shown in a graft-versus-host disease model, where intravenously introduced MSCs underwent apoptosis; apoptotic cells were phagocytosed by macrophages with induced release of indoleamine-pyrrole 2,3-dioxygenase (IDO), promoting the resolution of inflammation (Galleu et al., 2017).

We hypothesized that MSC-induced OA modulation following local delivery is initially associated with apoptosis-mediated immune reprogramming through phagocytosis by synovial lining macrophages, and surviving MSCs were licensed through exposure to the inflamed OA joint environment, enabling them to respond by molecular reprogramming specific to the "injured" environment. To investigate the fate and molecular mechanisms underpinning MSC therapeutic effects in OA, syngeneic eGFP BM-MSCs were retrieved from whole joint digests using fluorescence-activated cell sorting (FACS) after local IA delivery in a murine OA model induced by collagenase type VII. Molecular and phenotypic characterization of the surviving implanted cells was performed to identify mechanisms underpinning 1) the MSC therapeutic response after joint injury and 2) the molecular response to the established OA environment.

2 Materials and methods

2.1 Isolation of murine BM-MSCs

Wild-type (wt) BM-MSCs were isolated from C57BL/6 mice (Charles River Laboratories, Margate, Kent, United Kingdom). GFP + BM-MSCs were isolated from C57BL/6-Tg (UBC-GFP) 30Scha/J mice (Jackson Laboratory, Bar Harbor, ME, United States) (Da Silva Meirelles and Nardi, 2003). All animals (male, 8–12 weeks) were maintained on a 12-h light/dark cycle with *ad libitum* access to standard laboratory chow and water. All procedures were approved by the Animal Care and Research Ethics Committee (ACREC) of the National University of Ireland, Galway, and conducted under licenses issued by the Health Products Regulatory Authority (HPRA), Dublin, Ireland.

Following euthanasia, femurs and tibias were dissected, and the flushed BM was filtered using a 40-μm cell strainer and centrifuged at 400x g for 10 min. The obtained pellet was stained with trypan blue (Sigma-Aldrich), and the cells were cultured at a density of $2 \times 10^6/cm^2$ in a humidified 5% CO_2 incubator at 37°C for 3–5 days. The medium was changed to remove non-adherent cells, and BM-MSCs were fed every 3–4 days until they reached ~80% confluence. At this point, they were detached using trypsin/EDTA (ethylenediaminetetraacetic acid) (Gibco, Thermo Fisher Scientific) and re-plated at a density of $5 \times 10^3/cm^2$.

2.2 Intra-articular injection

Experimental CIOA was initiated bilaterally in the knee joints of C57BL/6 mice by IA injection of 1 unit of purified bacterial type VII collagenase (Sigma-Aldrich) in 7 μL of physiological saline. The control group (sham) received saline only, with n = 6 mice per each group. IA injections were performed under isoflurane-induced

anesthesia using a 10-μL syringe (Hamilton Company, Nevada, United States) with a 27G needle inserted laterally to prevent patellar ligament damage. Two collagenase treatments were carried out on days 0 and 2. On day 7, the mice received an IA injection of 2×10^5 GFP + BM-MSCs suspended in 7 μL of α-MEM (Gibco, Thermo Fisher Scientific). All animals were included in the analysis.

2.3 Digestion of whole mouse knees

C57BL/6 mice were euthanized 12 h and 72 h post-BM-MSC delivery by CO_2 overdose, followed by cervical dislocation. Whole limbs were removed and cleaned of muscle tissue while preserving the synovium. The AC was exposed by the dissection of the synovial membrane along with the frontal cruciate ligament. The exposed tissue was incubated with 100 μL of 1 mg/mL collagenase type I (*Clostridium histolyticum*, Sigma-Aldrich C0130). After 3 h, the released cell suspension was collected, and fresh collagenase was added for an additional 3 h. Knee digests from the same experimental groups were pooled.

2.4 Cell sorting

For FACS-coupled cell sorting of the retrieved BM-MSCs, the cell suspensions were washed in FACS buffer (PBS, 1% FBS, 2 mM EDTA, and 25 mM HEPES) and sorted using FACS Aria (BD Biosciences). Controls for establishing gating included a non-injected knee digest and a knee digest spiked with 1×10^5 GFP-MSCs. DRAQ7 viability dye was used to exclude dead cells. Receiving tubes were pre-coated with FBS and filled with 1 mL of the MSC culture medium. Retrieved BM-MSCs were cultured in this medium, fed every 3–4 days, and passaged at approximately 80% confluence until passage 2. Cell-conditioned medium (CM) was collected at after 48 h of passage 2 culture, and cell debris was removed by centrifugation.

2.5 Immunophenotyping of naïve and retrieved BM-MSCs

For immunophenotyping, cells were stained using antibodies (Supplementary Table S1) targeting CD105, CD106, CD146, CD44, and Ly-6A/E (Sca-1) (BioLegend); CD140b and CD29 (eBioscience); and CD90.2, CD11b, and CD45 (BD Pharmingen) in FACS buffer (PBS with 2% FBS and 0.05% sodium azide (NaN3) at 4°C in the dark for 30 min. Isotype controls were used to differentiate non-specific background signals. All samples were analyzed on a FACS Canto A (BD Biosciences) using FACS Diva software (BD Biosciences).

2.6 ELISA assays for cytokine quantification

Next, we investigated the immunomodulatory ability of retrieved cells from SHAM and CIOA joints (Section 1.2 of Supplementary Material and Methods). Commercially available ELISA kits were used to determine the concentration of soluble cytokines in MSC and BMDM culture media, as per the manufacturer's instructions. For IL-10, IL-12 p70, and TNF-α, DuoSet ELISAs (R&D systems DY417, DY419, and DY410) were used with minor modifications to the manufacturer's protocol. These cytokines have been previously identified in the osteoarthritic synovial fluid of human patients with knee OA (Sohn et al., 2012) and validated in a preliminary study aimed at identifying the *in vivo* inflammatory profile of the CIOA model (Section 1.3 of Supplementary Material and Methods; Supplementary Table S5). In brief, 96-well flat-bottom plates were coated with rat anti-mouse IL-10/IL-12 p70/TNF-α capture antibodies, diluted in PBS, and incubated overnight at RT. Following sample incubation, plates were washed, and biotinylated goat anti-mouse IL-10/IL-12 p70/TNF-α detection antibodies diluted in reagent diluent were added. After incubation, plates were washed, and streptavidin-horseradish peroxidase (1:200 dilution) was added. Plates were incubated and washed, and the TMB/E substrate solution (Merck Millipore) was added, followed by a stop solution (2N H2SO4). Optical density was determined using a Wallac 1420 Victor 3 plate reader set to 540/450 nm. For PGE2 quantification, the Parameter Assay Kit (R&D systems KGE004) was used.

2.7 Nitric oxide assay

The amount of nitric oxide (NO) present in cell culture supernatants was measured using Griess assays. In brief, Griess reagent, consisting of H_2O, 1% sulphanilamde, 0.1% naphthylethylene diamine, and 5% phosphoric acid, was added in a 1:1 ratio to samples or standards (sodium nitrite, $NaNO_2$, 1,000 to 15.625 μM in culture medium), and incubated for 10 min at RT in the dark. Optical density was determined using a Wallac 1420 Victor 3 plate reader set to 540 nm.

2.8 Retrieval and molecular analysis of BM-MSCs

GFP + BM-MSCs from sham or CIOA knee joints were sorted directly into ice-cold PBS, snap-frozen, and stored at −80°C. Control, non-injected GFP-MSCs (5×10^3) treated with 50 ng/mL of IL6 or a combination of 50 ng/mL IL6, IFN-γ, and monocyte chemoattractant protein-1 (MCP-1) (triple licensing cocktail) were also included for analysis. RNA was isolated from all samples using the RNeasy® Micro RNA Isolation Kit (QIAGEN), following the manufacturer's instructions and making the following adjustments due to the low cell numbers available. RNA was quantified using the RNA 6000 Pico Kit and analyzed using the Bioanalyzer 2100 (both from Agilent Technologies). First-strand cDNA synthesis was performed using the SMART-Seq® v4 Ultra® Low Input RNA Kit (TaKaRa Bio USA, INC.), and cDNA quality was determined using bioanalyzer high-sensitivity DNA chips. Following quality control using the bioanalyzer, tagmentation was performed using the Nextera XT DNA Sample Preparation Kit and Nextera XT DNA Index Kit (both from Illumina). Once tagged, samples were normalized and pooled. Sample quality control was performed prior to sequencing at the Genomics Core Technology Unit (Queen's University Belfast, Northern Ireland),

and FASTQ files were generated for further bioinformatics analysis (Section 1.5 of Supplementary Materials and Methods).

2.9 Immunofluorescence staining validation

Murine joints were dissected, fixed in 10% formalin for 1 h, and decalcified in 10% EDTA in PBS for 2 weeks at 4°C. E14–E15 embryonic mouse limb sections (Murphy et al., 1999) and chondrogenic pellets from human BM-MSCs and articular cartilage progenitor cells (ACPs) (Anderson et al., 2018) were analyzed. For the latter, 1×10^5 cells/pellet were processed for chondrogenic differentiation induced by 10 ng/mL TGF-β3 (Peprotech) and 100 ng/mL BMP-2 (Peprotech) at 2% O_2 and 5% CO_2 for 28 days. The pellets and decalcified mouse joints were washed, fixed in 10% formalin, dehydrated (Leica ASP300 S), paraffin embedded, sectioned, and mounted for IF staining. Fixed or fixed and decalcified sections were heated at 60°C for 1 h and rehydrated in graded ethanol (100%–75%) before antigen retrieval using 1 mg/mL pronase in PBS for 5–10 min and blocked with 10% goat serum for 1 h at room temperature. The primary antibodies anti-FAM5C (ab254837, Abcam), anti-lubricin/MSF (ab254937), and anti-Collagen II (ab185430) were applied overnight (1:100–1:200) at 4°C, and the signal was visualized post 1 h incubation with the corresponding secondary fluorochrome-conjugated antibodies (Anti-rabbit IgG (H + L), F (ab') 2 Fragment–Alexa Fluor 488, Alexa Fluor 555; and Anti-mouse IgG (H + L), F (ab') 2 Fragment–Alexa Fluor 555, Cell Signaling Technology) at room temperature with DAPI-mounting medium used for nuclei staining. BRINP3 antibody specificity was validated in human teratomas (Supplementary Figure S11) and rabbit isotype control IgG (ab37415, Abcam) was used in tested samples to confirm BRINP3 signal specificity. Confocal microscopy images were taken using the Olympus Fluoview FV3000 Microscope (FV31S-SW software).

2.10 Statistical analyses

Statistical analysis was performed using GraphPad Prism version 5. Significance was assessed using one-way or two-way ANOVA, followed by a Tukey test. Error bars represent the mean ± standard error of the mean (SEM) of biological replicates, and p-values ≤0.05 were considered statistically significant. Statistical significance was assessed. When the sample number was n ≤ 3, data were considered biological replicates (different donor), and where biological replicates were not available (n = 1), the mean ± SEM of technical triplicates is shown without statistical analysis.

3 Results

3.1 Characterization of retrieved vs. naïve BM-MSCs

QDot-labeled syngeneic MSCs (2×10^5) were delivered to CIOA mouse joints by IA injection to quantify cell survival using Cryoviz imaging (Supplementary Figure S1). A single cluster of cells was detected in the joint 1 h post-delivery, with 1.4% of injected cells surviving at 72 h, indicating rapid clearance of the majority of delivered cells. Similarly, retrieval optimization experiments performed in healthy mice (n = 4; 8 knee joints) with 2×10^5 GFP + BM-MSCs delivered *via* bilateral IA injection recovered only 1.627% of the injected cells (Supplementary Figure S2). When these transplanted, retrieved, and sorted GFP + BM-MSCs were cultured, they proliferated with growth kinetics and morphology similar to the control (untransplanted) population. Retrieved cells showed increased clonogenicity as measured by CFU-F activity and demonstrated greater osteogenic and chondrogenic propensity compared to control cells (Supplementary Figure S3). Data indicated the retrieval of a small population of engrafted cells that retained overt characteristics of BM-MSCs.

Experiments (n = 3) involving the delivery and retrieval of GFP-MSCs in CIOA joints were then assessed. In brief, 2×10^5 BM-MSCs were delivered bilaterally via IA injection to knees previously treated with collagenase Type VII to induce CIOA or saline as a control (sham) (n = 6; 12 knee joints). Three days post-administration, whole joints from both groups were exposed and digested to generate single-cell suspensions. GFP^+ cells were separated from the suspension by fluorescent cell sorting. Yields varied between 0.01% and 0.332% of 2×10^5 cells injected (Supplementary Table S2). The mean quantitative recovery of cells from OA joints (0.134% of injected cells) was consistently higher than that from sham joints (0.02% of injected cells), suggesting greater persistence of engrafted cells in the OA environment. Retrieved GFP + BM-MSCs formed characteristic colonies in cultures with comparable morphology and proliferation rates to control non-injected MSCs. Control GFP + BM-MSCs (CTRL) and retrieved sham- and CIOA-injected cells were negative for CD45, CD31, and CD11b, with Sca-1, CD29, and CD140b highly expressed. CD105 and CD90 were minimally detected in both cell populations (Figure 1).

3.2 Retrieved MSCs exhibit an immunomodulatory effect on T cells and bone marrow-derived macrophages

The assessment of immunomodulation by non-injected (Ctrl), sham, and CIOA-retrieved BM-MSCs revealed that MSC populations were unable to inhibit T-cell proliferation in co-culture experiments, except for the inhibition of CD8-positive cells by sham-retrieved BM-MSCs (Figure 2).

Bone marrow derived macrophages (BMDMs) were cultured with CM from control, sham, and CIOA-retrieved BM-MSCs. BMDMs released anti-inflammatory IL-10 in response to LPS-mediated activation; while naive MSC-CM induced low IL-10 levels, CM from SHAM- and CIOA-challenged MSC upregulated IL-10 compared to both macrophages alone and the CTRL-MSC-treated sample. Macrophages exposed to the CIOA environment produced IL10 at levels significantly higher than sham and control BM-MSCs. Immunosuppressive effects of BM-MSCs were supported by decreased, although not significant, TNF-α levels. PGE2 was detected at similar levels in all BM-MSC supernatants, whereas activated and resting BMDMs released PGE2 at comparable levels. Low levels of IL-12 p70 were produced by MSCs, while BMDMs showed high secretion in all groups (Figure 2).

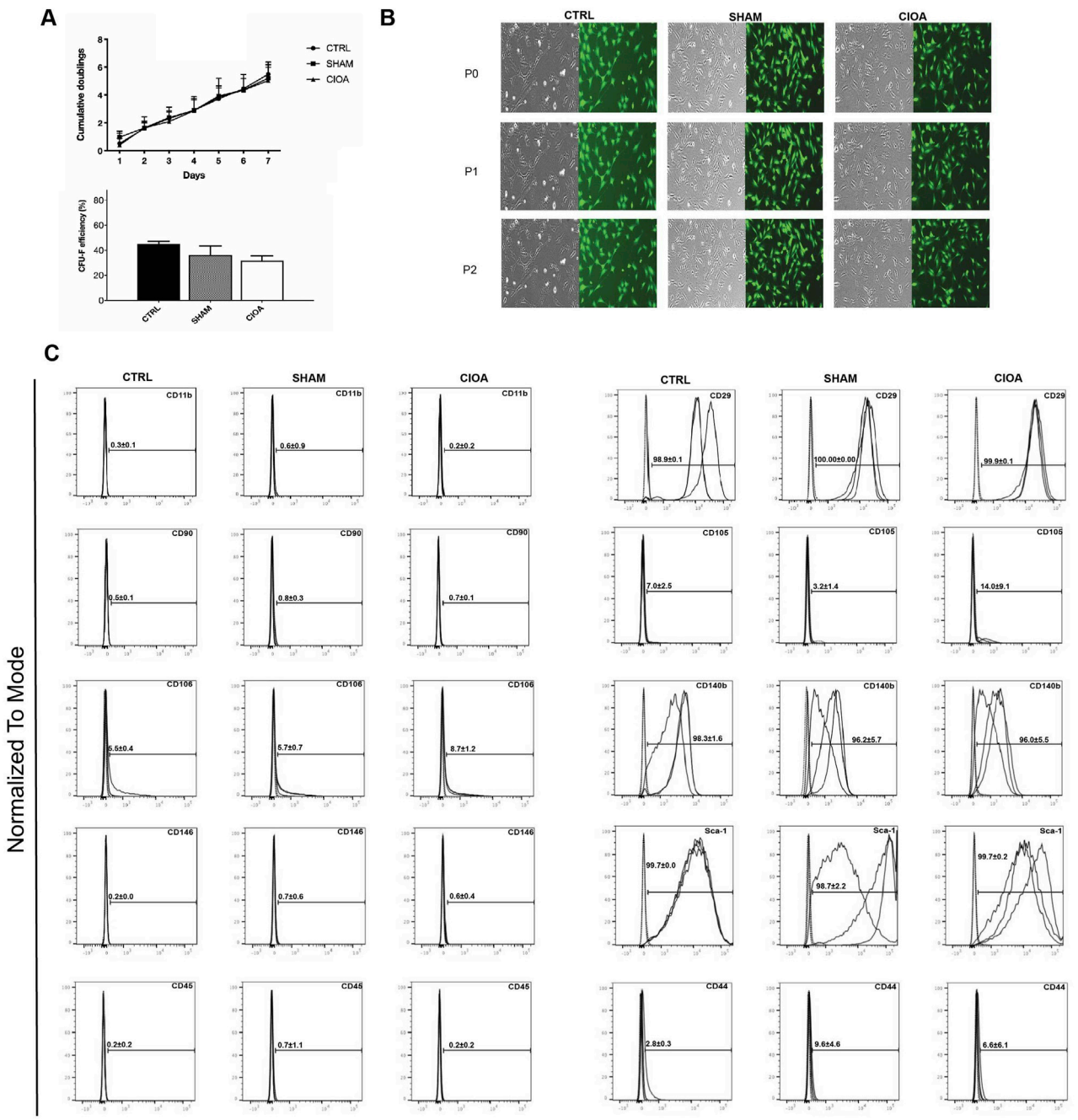

FIGURE 1
Characterization of BM-MSCs retrieved from the CIOA joint. **(A)** Proliferation of retrieved BM-MSCs and CFU-F efficiency at passage 2 post-retrieval; mean + SEM (n = 3). **(B)** Representative images of sorted cells; bright field (left) and FITC (right); scale bar, 100 μm. **(C)**: Surface marker expression of retrieved MSCs.

3.3 Establishment of the molecular therapeutic phenotype of MSCs in osteoarthritis

Optimal times for cell retrieval to define molecular changes were selected by defining the inflammatory environment in mouse joints and local and systemic macrophage profiles (Supplementary Figure S4). A mouse cytokine panel was designed based on the expression of inflammatory cytokines in the human OA synovial fluid (Sohn et al., 2012) and joint cytokine levels in CIOA, determined 7 to 56 after the first injection of collagenase type VII or saline. Relative levels of selected factors in CIOA versus sham joints demonstrated a pattern of expression where MCP-1, IFNγ, IL-6, RANTES (CCL5 (Chemokine (C-C motif) ligand 5), IL-13, and TNFα showed peak of expression (Supplementary Figure S5). Days 14 and 56 were chosen as selected time points for the injection of MSCs (Ferrao Blanco et al., 2022) for retrieval 12 h and 3 days post-injection to generate the MSC therapeutic signature in OA. For this purpose, additional

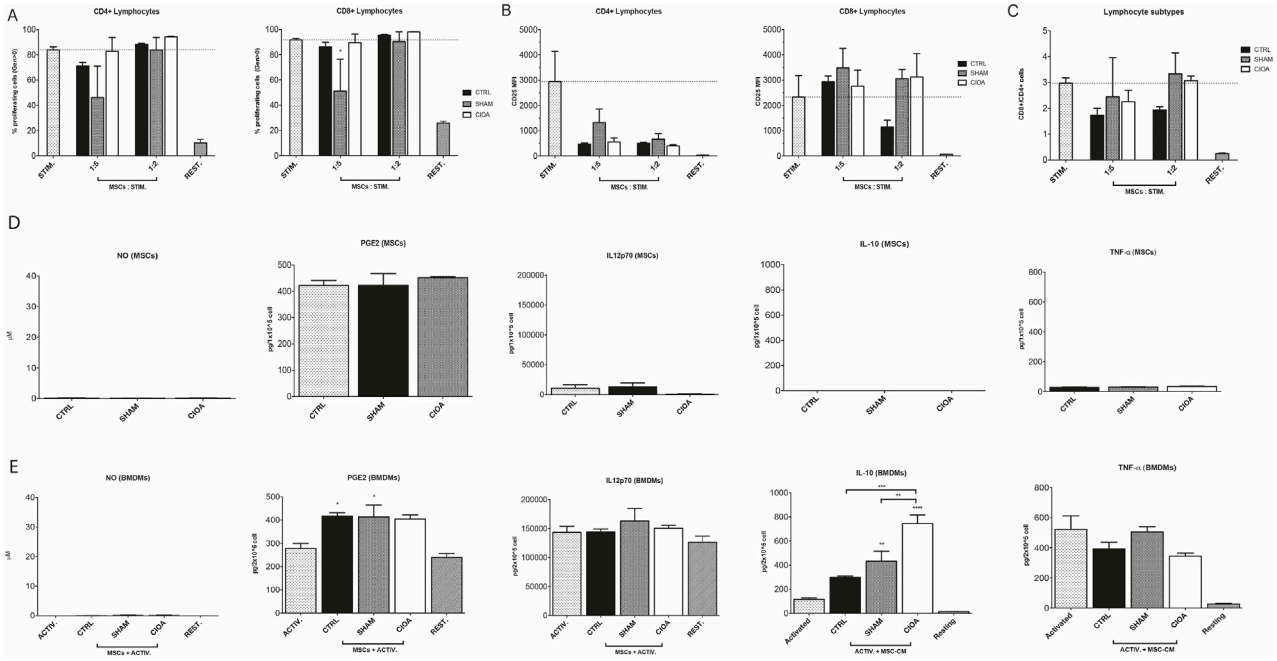

FIGURE 2
Immunomodulatory potential of retrieved BM-MSCs. **(A)** Proliferation of CD4⁺ and CD8⁺ T cells after the third generation, quantified by CTV staining. **(B)** Expression of CD25 by CD4⁺ and CD8⁺ T cells. **(C)** CD4+/CD8+ T cell relative quantity. Secretion of NO, PGE2, IL12p70, IL-10, and TNF-alpha from **(D)** naïve (CTRL) or retrieved BM-MSCs from the sham and CIOA experimental groups and from **(E)** BMDMs in activated or resting state and/or treated with conditioned media from control, sham, and CIOA BM-MSCs (data were shown as the mean ± SEM (n = 3). *P ≤ 0.05; **P ≤ 0.01; ***P ≤ 0.001; ****P ≤ 0.0001. Statistical significance compared to activated macrophages (ACTIV) as positive control, unless indicated by brackets.

retrieval experiments were conducted. Supplementary Figure S6, summarizing the numbers of retrieved MSC populations from n = 8 mice (16 knee joints)/per group and timepoint, indicates that significantly more MSCs survived and engrafted in CIOA compared to sham-injected joints, with increased fold recoveries ranging from 1.9 (56 days CIOA, 3-day) to 4.4 fold (14 days CIOA, 0.5-day).

An initial heat map assessment of the RNAseq analysis indicated the extensive gene upregulation and activation of multiple pathways at the 12-h retrieval time point for both early and late CIOA (days 14 and 56, respectively) (Supplementary Figure S7). The 3-day retrieval time point was, therefore, used to identify therapeutic mechanisms. On days 14 and 56, respectively, 878 and 1,606 differentially expressed genes (DEGs) were identified between BM-MSCs retrieved from CIOA and SHAM knee joints. The top 100 upregulated and downregulated genes are listed in Supplementary Tables S6–S9. Figure 3A shows the 10 most significantly upregulated and downregulated genes in each group. Upregulated genes in early OA retrieved cells were associated with promoting cell survival and proliferation, repression of apoptosis through Akt signaling (*PROKR1*), TGF-beta/SMAD activation (*MEGF6*), and autophagy (ATP6V0D2), indicating an association between autophagy and cell survival.

BM-MSCs retrieved at the later OA stage play an immunomodulatory role, interacting with local immune cells through the complement cascade (*C1QB* and *C1QC*), secretion of cytokines and adipokines (*LCN2* and *CXCL3*), growth factors (*PGF*), and cells expressing M2 macrophage markers (*ARG1*).

All DEGs were analyzed to generate canonical pathways associated with early and late OA retrieved cells using ingenuity pathway analysis (IPA) (Figure 3B). In 14D retrieved cells, "leukocyte extravasation signaling" was associated with the highest activation, while "inhibition of matrix metalloproteinases" and "EIF2 signaling" had the lowest activation z-scores. The highest activated pathways in 56D retrieved cells were "TREM1 signaling," "dendritic cell maturation," "role of pattern recognition receptors in recognition of bacteria and viruses," "complement system," and "apelin cardiomyocite signaling pathway,", while "role of NFAT in cardiac hypertrophy" had a negative activation z-score (Figure 3B). The cellular molecular fingerprint predicted upstream regulators at both time points. For early OA-retrieved MSCs, IL-1 beta, IFN-gamma, NF-kB, and HIF-1 alpha were the most activated upstream regulators, with TCL1A, STAT3, IL-1 beta, OSM, and CCR3 associated with 56D cells (Supplementary Table S10).

An analysis of DEGs identified in early and late OA-retrieved MSCs identified 156 common elements (Figure 3C), and for these, the top five canonical pathways were identified in IPA (Figure 3D). "Role ofmacrophages, fibroblasts, and endothelial cells in rheumatoid arthritis" showed the highest *p*-value and gene overlap score, indicating a potential immunomodulatory role in cells retrieved from both time points.

All differentially expressed genes were further analyzed for Gene Ontology (GO) enrichment annotations for biological processes, molecular functions, and cellular components. Supplementary Table S11 lists the top five most enriched terms for each ontology in both datasets.

In 14D-retrieved BM-MSCs, the five most enriched GO biological processes were associated with ECM metabolism, regulation of cell migration, and establishment of apical–basal

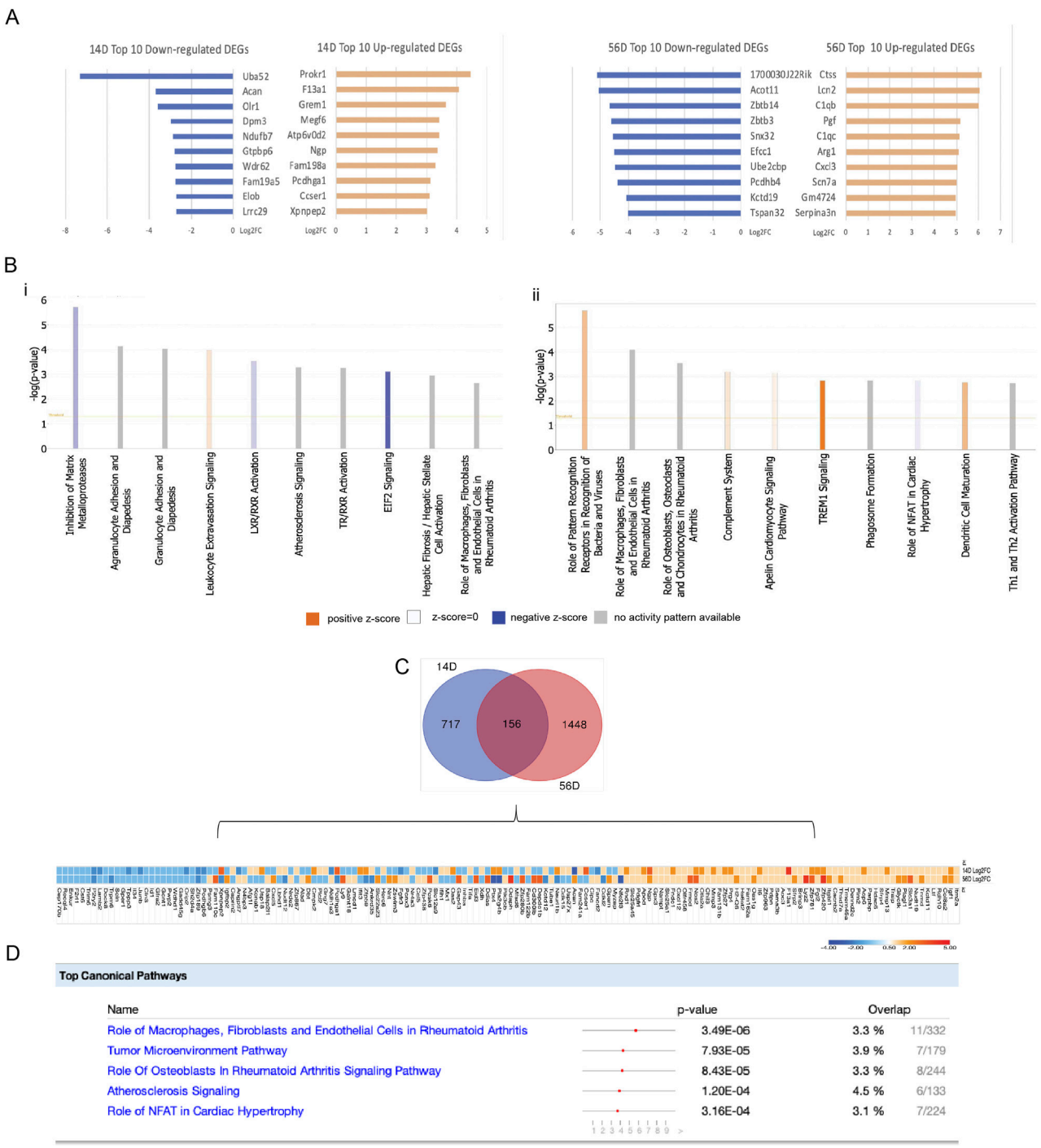

FIGURE 3
Identification and bioinformatics analysis of DEGs in day 14- and day 56-retrieved cells. **(A)** Top 10 upregulated and downregulated DEGs in 14D and 56D, expressed as $\log_2$fold change. **(B)** Top 10 canonical pathways identified with the ingenuity pathway analysis on 14D and 56D. **(C)** Overlap of DEGs between 14D and 56D with a representative heatmap of similarly and differently expressed genes. **(D)** Canonical pathways associated with the common DEGs between 14D- and 56D-retrieved BM-MSCs, ranked based on their p-value. For each pathway, the gene overlap compared to the IPA database is shown as numerical value and percentage.

polarity. These terms suggest that MSCs are directly involved in the maintenance of ECM structural integrity, with increased migratory abilities toward injury sites. In 56D-retrieved BM-MSCs, the five most enriched GO biological processes were related to immune processes involving leukocyte aggregation, macrophage differentiation, and T-helper cell differentiation, as well as transport of amino acids. These may suggest that MSCs injected and retrieved in the later CIOA stage exhibit strong immunomodulatory activities through a synergy of mechanisms involved in CD4-positive T-cell and macrophage differentiation.

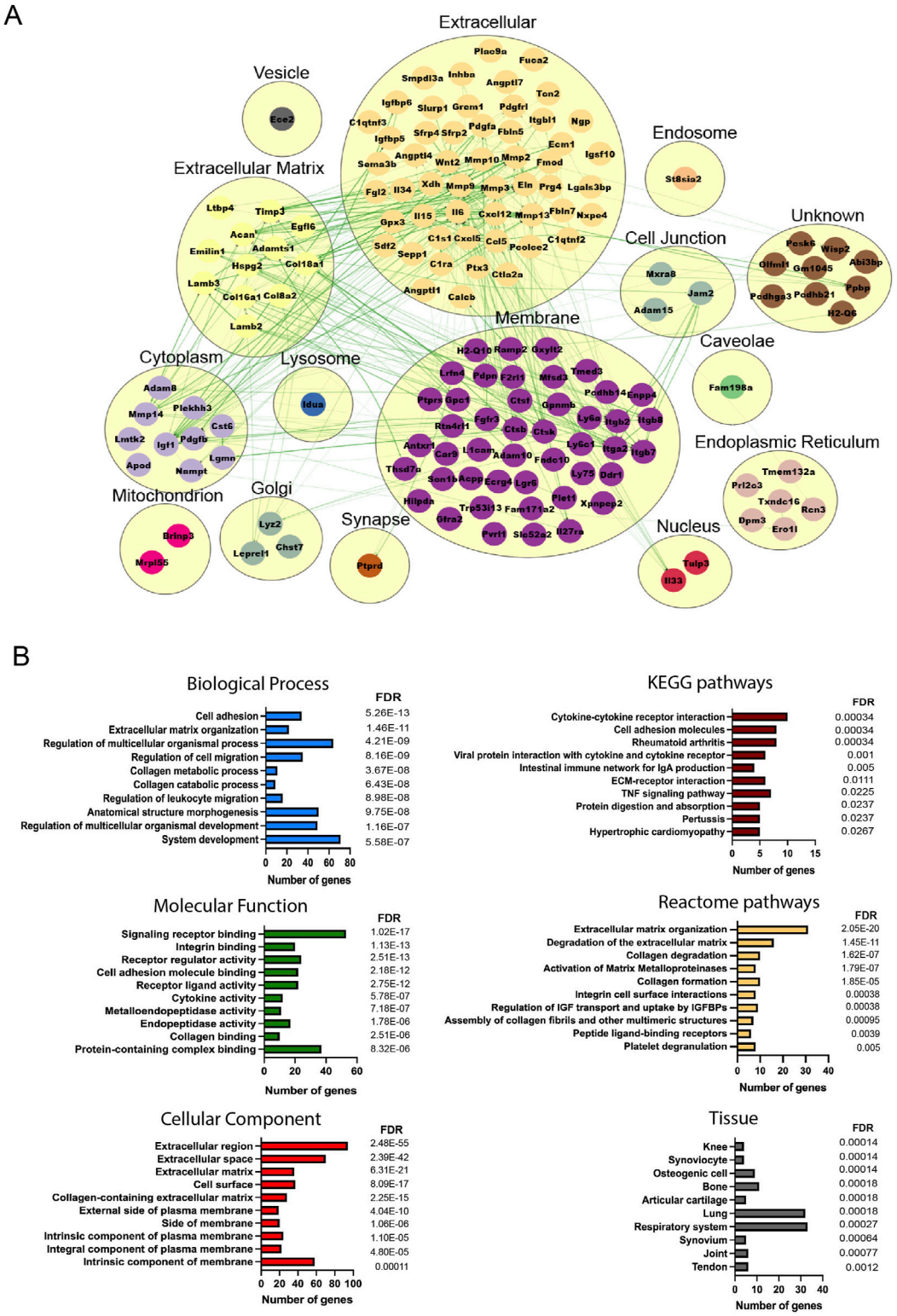

FIGURE 4
Analysis of the predicted secretome in 14D-retrieved cells. **(A)** Protein–protein interaction (PPI) network visualizing clustering results, where each cluster represents a cellular compartment. Unknown clusters contain elements not mapped to any specific cell location. Green lines represent STRING interaction lines (Zeng et al., 2022). **(B)** Representative enrichment results, including Gene Ontology elements, pathways, and tissues corresponding to the PPI network. Terms are ranked based on the FDR value, and for each term, the number of corresponding genes is represented.

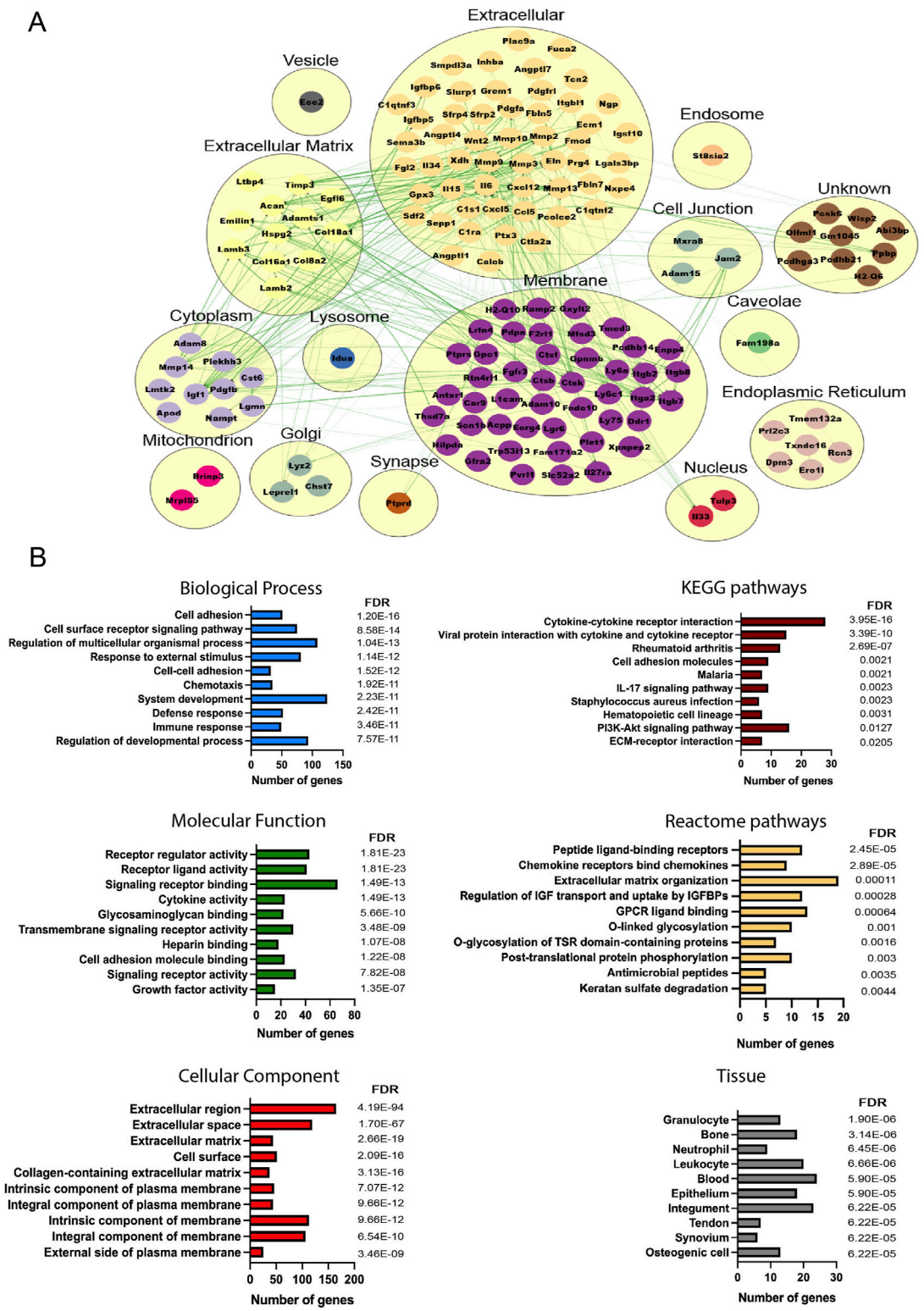

FIGURE 5
Analysis of the predicted secretome in 56D-retrieved cells. **(A)** PPI network visualizing clustering results, where each cluster represents a cellular compartment. Unknown clusters contain elements not mapped to any specific cell location. Green lines represent STRING interaction lines, and the red lines are generated based on the published literature (Zeng et al., 2022). **(B)** Representative enrichment results including Gene Ontology elements, pathways, and tissues corresponding to the PPI network. Terms are ranked based on the FDR value, and for each term, the number of corresponding genes is represented.

This finding was also supported by the expression of chemokine receptors, promoting interactions with chemokines secreted by the microenvironment. A possible mechanism to counterbalance autophagy-mediated deprivation of essential molecules might be mediated by the upregulation of transport complexes and the enrichment of extracellular amino acid uptake (Zhang et al., 2018).

3.4 Disease-related differences in the secretome profile of early and late OA-retrieved MSCs

To understand the molecular cross-talk between MSCs and the OA microenvironment, the predicted secretome in day 14- and day 56-retrieved cells was investigated, identifying 157 and 278 predicted secreted genes, respectively (39 common elements) (Supplementary Figure S8). More secreted elements were found in the late retrieved MSCs, indicating that at this disease stage, with overt OA changes to cartilage and synovium, a stronger MSC–OA interaction may be present. Clusters were generated to mimic the cellular structure, and interaction networks were organized based on subcellular components (Zhu et al., 2015). In both time points, the highest number of elements were located in the membrane and extracellular components, in line with the top KEGG pathways corresponding to cytokine–cytokine interactions and cell adhesion molecules (Figures 4, 5). Enrichment analysis showed functional differences between the time points, indicating that the disease stage influences the nature of the cellular secretome. Based on enriched biological processes (BPs), on 14D, the network of proteins seemed to be mainly involved in ECM organization and collagen metabolism, whereas on 56D, these were concentrated on chemotaxis and immune responses. Similarly, these differences were further observed in the identified reactome pathways, where catabolic and anabolic processes correlated with the extracellular matrix and collagen were enhanced on 14D, while chemotactic receptors and their activation were upregulated on 56D. Mapping the elements to various tissue sources resulted in the identification of similarities between the retrieved cells and certain cell types. These followed the same time-point-related pattern since 14D-retrieved cells seem to be similar to synoviocytes and articular chondrocytes, whereas 56D-retrieved cells had similarities with granulocytes, neutrophils, and blood cells, potentially indicating a role in the immune response.

3.5 Validation of BRINP3 as a therapeutic target: protein expression and licensing effects on mesenchymal stromal cells

To further analyze the predicted secretome of retrieved cells as therapeutically licensed by the OA environment, we compared 14D and 56D datasets with the predicted secretome of control groups: *in vitro*-licensed MSCs with IL-6 alone or IL-6, MCP-1, and IFN-gamma combined (Supplementary Figure S9). *BRINP3*, identified as a novel predicted secreted gene expressed by BM-MSCs in all groups, was selected for further validation. The possible role of BRINP3 in synovial joint development in mouse embryo histological sections was assessed in tissues corresponding to gestational age E14–E15 (Martin, 1990), enabling the assessment of involvement in synovial joint cavitation and cartilage differentiation confirmed by the positive expression of PRG4 (Rhee et al., 2005). BRINP3 and PRG4 were detected at the superficial layer of the distal end of the digit and in the interdigital tissue. Both signals were detected in specific joint-forming locations comprised of cells undergoing active proliferation and differentiation, such as the remnant element of the joint interzone transiting toward cavitation. Chondrocytes located near the proximal and distal regions stained positive; however, signal intensity seemed to be reduced in cells, assuming a hypertrophic phenotype, and no signal was detected in the developing bone subchondral plate (Figure 6A). Given the premise that BRINP3 protein is highly conserved among vertebrates (Kawano et al., 2004) and to further assess its role in cartilage development, expressions of chondrogenically induced human MSCs and AC progenitor cells (ACPs) were assessed (Anderson et al., 2018). BRINP3 expression was identified in both cell types at D28 (Figures 6B, C), with higher magnification (×60) images revealing a diverse pattern of the BRINP3 signal. Expression in MSC pellets was identified in the cell cytoplasm and ECM as positive for collagen II staining, as well as in the external pellet layer, suggesting that MSCs under these conditions might synthesize and secrete BRINP3. ACPs also formed chondrogenic pellets, as confirmed by Safranin-O staining, containing fibroblast-like cells that generated a dense ECM, where the BRINP3 signal was detected in cells and the pericellular matrix surrounding the cells.

The expression of BRINP3 was further assessed in animal-induced OA models to examine its possible role in cartilage degradation. In murine CIOA and surgical destabilization of the medial meniscus (DMM) models (Farrell et al., 2016; Figures 6D, E), the BRINP3 signal was detected in a monolateral pattern on the meniscal and articular cartilage surface, corresponding to the healthy section of the joint. The lack of proteoglycans evidenced with Safranin-O staining was evidenced at the contralateral joint structures in both models, suggesting that BRINP3 expression might be lost during the pathophysiological process affecting the OA joint.

From a functional perspective, licensing with recombinant BRINP3 contributed to the maintenance of a normal fibroblast-like morphology in human MSCs. In terms of immunomodulatory effects, there was an absence of IDO secretion and increased gene expression of PTGS-2, hence potentially affecting the secretion of PGE2, a known modulator of anabolic and catabolic processes in OA (Goldring and Berenbaum, 2004). This finding suggests a possible role in the immunomodulation in OA (Supplementary Figure S10).

4 Discussion

The successful translation of MSC-based therapies from bench to bedside is still a persistent challenge in clinical practice. The missing link correlating mechanistic insights and clinical efficiency is an important barrier to the design of disease-relevant potency assays and effective clinical decision-making. To address the issue, we describe a strategy to characterize therapeutic mechanisms underpinning local MSC effects, whether delivered as a therapy to prevent the development of the disease post-joint injury or used to treat established OA. BM-MSCs were introduced *via* IA injection in a syngeneic murine CIOA model, mimicking autologous BM-MSC-based treatments, and surviving BM-MSCs were retrieved for analysis.

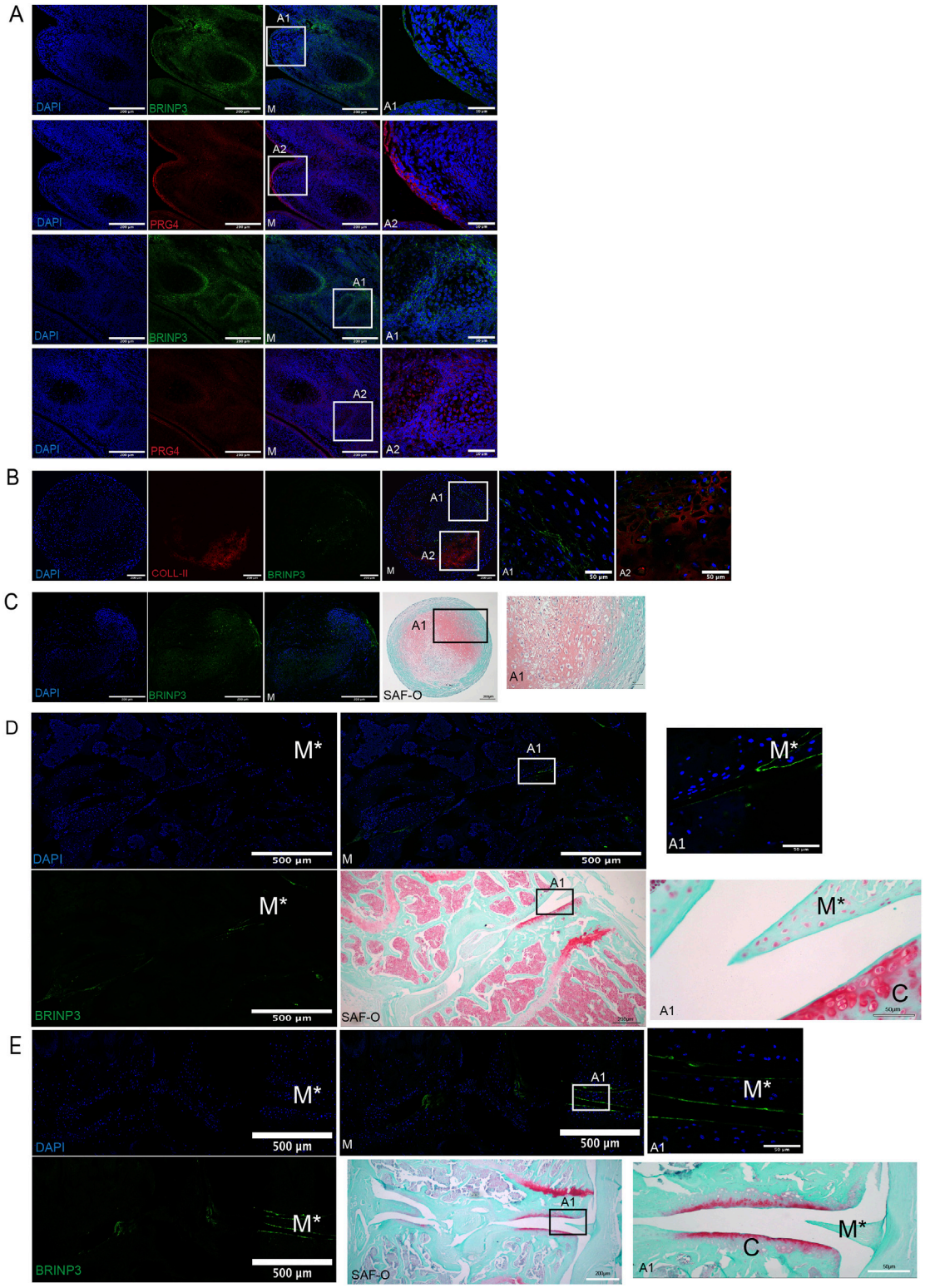

FIGURE 6
Validation of BRINP3 protein expression by immunofluorescence detection. **(A)** BRINP3 and PRG4 expression in developing digits of mouse embryos (E14–E15). **(B)** Co-expression of BRINP3 and collagen-II in the extracellular matrix in 28-day chondrogenically differentiated human BM-MSCs. **(C)** Expression of BRINP3 in the extra-cellular matrix and histological evidence of chondrogenic differentiation with Safranin-O staining in 28-day chondrogenically differentiated human ACPs (D/E). Immunofluorescent detection of BRINP3 in articular cartilage and meniscus in a murine CIOA **(D)** and DMM **(E)** model. For reference of anatomical structures, Safranin-staining of consecutive sections has been included for the CIOA and DMM models.

The results demonstrated that (1) the majority of cells do not survive 3-day post-delivery with impaired cell survival more evident in sham-injected mice, suggesting that the inflammatory milieu induces a survival stimulus; (2) retrieved BM-MSCs can secrete trophic factors capable of polarizing macrophages to an anti-inflammatory IL-10-producing phenotype; and (3) the transcription profile differs between cells retrieved in early and late-stage OA, indicating the important role of host environments in coordinating therapeutic outcomes.

This indicates that MSCs act *via* a hit-and-run mechanism characterized by short interactions with the inflammatory-diseased microenvironment, cell death, and lack of significant cell engraftment (Cheung et al., 2019) that does not, however, hinder their therapeutic efficacy (Murphy et al., 2003).

To assess the subsequent therapeutic effects, we investigated the immunomodulatory abilities of sham- and CIOA-retrieved BM-MSCs. Conditioned medium from retrieved cells could alternatively polarize *in vitro*-activated BMDMs, resulting in the lower surface expression of MHC-II and CD86 and increased expression of IL-10 known to be secreted by anti-inflammatory macrophages (Melief et al., 2013a; Melief et al., 2013b). This is in line with increasing evidence on immunomodulatory interactions between apoptotic MSCs and local microenvironments through the release of membrane particles and direct interaction with host monocytes and macrophages, resulting in the secretion of IL-10, TGF- β, IDO, and PGE2 (Antonio et al., 2017; Morrison et al., 2017; Masterson et al., 2019; Giacomini et al., 2023; Schrodt et al., 2023).

In this study, retrieved- and naïve *in vitro*-expanded BM-MSCs were similar in their morphology and cell surface marker expression, although transcriptomic analysis revealed differences associated with gene patterns and pathways involved in OA modulation and the chondrogenic phenotype. This confirms the hypothesis that upon transplantation, cell differentiation pathways can be activated or arrested, which could explain the observed differences in the retrieved cell data (Friedenstein et al., 1966). Our results imply that certain cell populations have an intrinsic enhanced ability to survive or that the inflammatory milieu induces transcriptional changes, promoting survival in responding cells. Differences in early- and late-CIOA-retrieved BM-MSCs reflect a direct cell response to OA disease status. Early stages are characterized by structural matrix-associated anabolic- and catabolic-driven changes; data revealed a distinct mapping profile related to the restoration of ECM organization and cell migration in early CIOA-retrieved BM-MSCs, a possible response to stimuli that accompany initial stages of joint synovitis with ECM degradation (Seol et al., 2014), aiming to resurface the joint and provide chondroprotection. Surviving cells in established OA, characterized by chronic inflammation and significant structural changes, were enriched for immune response regulation pathways known to counteract and modulate disease progression (Leijs et al., 2012). The inflammatory milieu may activate mechanistic cascades controlling cell death and differentiation, paracrine signaling, and immunomodulation, underlining the importance of injury and the local inflammatory status for successful cell treatments. The database of secretory gene expression generated represents a valuable catalog of the *in vivo* profile of BM-MSCs in the context of experimental osteoarthritis. However, future work needs to elucidate whether these mechanisms and associated pathways can be activated after cell transplantation in naturally occurring OA in both human and veterinary patients.

Although different expression profiles were observed between early- and late-retrieved BM-MSCs, progenitor cell markers active during limb development were characteristic of surviving BM-MSCs.

Differential expressions of genes with fundamental roles in synovial joint organogenesis were identified (PRG4 and GREM-1), suggesting the involvement of embryonic and fetal development pathways in surviving BM-MSCs. The potential therapeutic cell capacity can be correlated with the ability of putative chondroprogenitor PRG4+ cells to restore the AC surface in an *in vivo* cartilage wound model (Massengale et al., 2023). These cells express a pattern of unique chondrocyte-like markers, distinguishing naïve MSCs from mature chondrocytes, similar to what we identified in our study.

The BRINP3 signal was observed for the first time on the surface of AC and meniscus in a mouse OA model. BRINP3/FAM5C is diversely methylated in human OA being hypomethylated in cartilage (Fernández-Tajes et al., 2014) and hypermethylated in subchondral bone in intermediate-late disease phases (Zhang et al., 2016). However, it is unknown whether its methylation status contributes to OA onset and progression or is merely a consequence of joint tissue changes in response to synovial inflammation, potentially driven by the upregulation of pro-inflammatory cytokines such as TNF-α, IL-6, IL-1β, and LPS (Sato et al., 2014). Here, BRINP3 was tested as a licensing factor in human BM-MSCs and showed the ability to regulate the gene expression of key inflammatory mediators in OA, resulting in the upregulation of PTGS-2, associated with MSC-mediated immunosuppression (Paradiso et al., 2022) and the downregulation of TSG-6, one of the most highly upregulated genes in OA associated with cartilage degradation (Chou et al., 2018). Further studies are needed to fully elucidate the effect of BRINP3 and, in addition, the cumulative effect of multiple cytokines and immune cell populations present in the OA synovial fluid.

BRINP3 is involved in bat short digit development (Wang et al., 2014), and it is also expressed in human embryonic stem cells and derived chondrogenic progenitors (Griffiths et al., 2020). The current literature, along with this study's findings, indicate that BRINP3, involved in human limb development, could be a novel factor expressed by surviving BM-MSCs in response to the OA inflammatory milieu. Molecular analysis data of retrieved cells also contribute to the premise that (1) BM-MSCs exposed to the joint inflammatory milieu may assume a cartilage-derived progenitor/stem cell-like phenotype or (2) a specific subpopulation of adult MSCs, known to express transcripts of embryonic cell types, survive as progenitor-like cells with enhanced capacity to engraft, survive, and mediate tissue repair and/or joint protection.

The limitations to our study include the number of pooled retrieved cells because the size of the mouse joint and larger animal models would be able to yield a higher number of cells, allowing a more comprehensive validation of the predicted secretome. Performing an additional analysis of the *in vivo* apoptotic profile of IA-injected BM-MSCs would enable the elucidation of the mechanisms involved in cell death and correlate them with desired therapeutic outcomes.

Our data highlight species-related differences in skeletal regulatory pathways between mice and humans, which must be considered for the translational value of this work. The database of secretory gene expression generated represents a valuable catalog of the *in vivo* profile of BM-MSCs in the context of experimental osteoarthritis. Furthermore, the relevance of this secretory gene

expression profile needs to be considered for the design of potency assays, the evaluation of quality control of MSC or MSC-derived therapeutic products, and the development of new clinical strategies for OA. Addressing these gaps will be beneficial for understanding and optimizing clinical applications of the cells and defining pharmacokinetic and pharmacodynamic parameters necessary for any medicinal product used in the clinical setting.

Data availability statement

The raw data supporting the conclusions of this article will be made available by the authors, without undue reservation.

Ethics statement

All pre-clinical studies were approved by the Animal Care and Research Ethics Committee, National University of Ireland Galway and conducted in accordance with local legislation and institutional requirements. Human MSCs were harvested from healthy donors under the approval of the Research Ethics Committee, National University of Ireland Galway. Human ACPs were isolated at Oregon Health and Science University, USA from surgical waste from deceased donors who were completely de-identified prior to the study.

Author contributions

AI: Investigation, Methodology, Validation, Visualization, Writing–original draft, and Writing–review and editing. PM: Investigation, Methodology, Validation, Visualization, Writing–original draft. AB: Investigation, Validation and Writing–review and editing. CH: Investigation, Validation and Writing–review and editing. SR: Resources, Validation, and Writing–original draft. CD: Validation, and Writing–review and editing. SM: Investigation, Validation, Visualization, GS: Resources, Validation, Writing–review and editing. EM: Investigation, Validation and Writing–review and editing. JR: Validation, Visualization, Writing–original draft and Writing–review and editing. AO: Resources, Validation and Writing–review and editing. TR: Methodology, Writing–review and editing AR: Methodology, Writing–review and editing. RK: Conceptualization and Writing–review and editing. ML: Conceptualization and Writing–review and editing. DR: Conceptualization and Writing–review and editing. KE: Resources, Visualization, and Writing–review and editing. IH: Resources, Visualization, and Writing–review and editing. BJ: Resources and writing–review and editing. DM: Resources and writing–review and editing. FB: Conceptualization, Funding acquisition, Methodology, Supervision, Visualization, and writing–review and editing. JM: Conceptualization, Funding acquisition, Methodology, Supervision, Writing original draft and Writing–review and editing.

Funding

The author(s) declare that financial support was received for the research, authorship, and/or publication of this article. This study was funded by Science Foundation Ireland (SFI) and the European Regional Development Fund (Grant Number 13/RC/2073). The authors acknowledge funding and scientific input from AbbVie.

Acknowledgments

All flow cytometry experiments were performed in the UoG Flow Cytometry Core Facility, which is supported by funds from the University of Galway (UoG), Science Foundation Ireland, the Irish Government's Programme for Research in Third Level Institutions, Cycle 5, and the European Regional Development Fund. Technical and consultative support for flow cytometry experiments were provided by Shirley Hanley of the UoG Flow Cytometry Core Facility. The authors thank the BRU (Bio-Resources Unit) technical, veterinary, and administrative staff in UoG for facilitating *in vivo* studies and for their ongoing assistance, advice, and support in animal procedures, husbandry, care, and welfare. The authors also acknowledge the support and work of Sara Montagna.

Conflict of interest

Authors RK, ML and DR were employed by company AbbVie.

The remaining authors declare that the research was conducted in the absence of any commercial or financial relationships that could be construed as a potential conflict of interest.

The authors declare that this study received funding from the Abbvie Bioresearch Centre through Science Foundation Ireland, Centre for Research in Medical Devices (CÚRAM) (Grant No. 13/RC/2073). The funder was advised on the overall study design and received progress reports. However, data collection and analysis, the decision to publish or the preparation of the manuscript was the remit of lead author.

The author(s) declared that they were an editorial board member of Frontiers, at the time of submission. This had no impact on the peer review process and the final decision.

Generative AI statement

The author(s) declare that no Generative AI was used in the creation of this manuscript.

Publisher's note

All claims expressed in this article are solely those of the authors and do not necessarily represent those of their affiliated organizations, or those of the publisher, the editors and the reviewers. Any product that may be evaluated in this article, or claim that may be made by its manufacturer, is not guaranteed or endorsed by the publisher.

Supplementary material

The Supplementary Material for this article can be found online at: https://www.frontiersin.org/articles/10.3389/fcell.2025.1521437/full#supplementary-material

References

Anderson, D. E., Markway, B. D., Weekes, K. J., McCarthy, H. E., and Johnstone, B. (2018). Physioxia promotes the articular chondrocyte-like phenotype in human chondroprogenitor-derived self-organized tissue. *Tissue Eng. Part A* 24, 264–274. doi:10.1089/ten.tea.2016.0510

Antonio, G., Yanira, R.-V., Cristina, T., Cara, L., Luigi, D., Tik, C. S., et al. (2017). Apoptosis in mesenchymal stromal cells induces *in vivo* recipient-mediated immunomodulation. *Sci. Transl. Med.* 9, eaam7828. doi:10.1126/scitranslmed.aam7828

Cheung, T. S., Galleu, A., von Bonin, M., Bornhauser, M., and Dazzi, F. (2019). Apoptotic mesenchymal stromal cells induce prostaglandin E2 in monocytes: implications for the monitoring of mesenchymal stromal cell activity. *hematologica* 104, 438–441. doi:10.3324/haematol.2018.214767

Chou, C. H., Attarian, D. E., Wisniewski, H. G., Band, P. A., and Kraus, V. B. (2018). TSG-6 – a double-edged sword for osteoarthritis (OA). *Osteoarthr. Cartil.* 26, 245–254. doi:10.1016/j.joca.2017.10.019

Das, S. K., and Farooqi, A. (2008). Osteoarthritis. *Best. Pract. Res. Clin. Rheumatol.* 22, 657–675. doi:10.1016/j.berh.2008.07.002

Da Silva Meirelles, L., and Nardi, N. B. (2003). Murine marrow-derived mesenchymal stem cell: isolation, *in vitro* expansion, and characterization. *Br. J. Haematol.* 123, 702–711. doi:10.1046/j.1365-2141.2003.04669.x

Farrell, E., Fahy, N., Ryan, A. E., Flatharta, C. O., O'Flynn, L., Ritter, T., et al. (2016). VIL-10-overexpressing human MSCs modulate naïve and activated T lymphocytes following induction of collagenase-induced osteoarthritis. *Stem Cell Res. Ther.* 7, 74–11. doi:10.1186/s13287-016-0331-2

Fernández-Tajes, J., Soto-Hermida, A., Vázquez-Mosquera, M. E., Cortés-Pereira, E., Mosquera, A., Fernández-Moreno, M., et al. (2014). Genome-wide DNA methylation analysis of articular chondrocytes reveals a cluster of osteoarthritic patients. *Ann. Rheum. Dis.* 73, 668–677. doi:10.1136/annrheumdis-2012-202783

Ferrao Blanco, M. N., Bastiaansen Jenniskens, Y. M., Kops, N., Chavli, A., Narcisi, R., Botter, S. M., et al. (2022). Intra-articular injection of triamcinolone acetonide sustains macrophage levels and aggravates osteophytosis during degenerative joint disease in mice. *Br. J. Pharmacol.* 179, 2771–2784. doi:10.1111/bph.15780

Friedenstein, A. J., Piatetzky-Shapiro, I. I., and Petrakova, K. V. (1966). Osteogenesis in transplants of bone marrow cells. *J. Embryol. Exp. Morphol.* 16, 381–390. doi:10.1242/dev.16.3.381

Galleu, A., Riffo-Vasquez, Y., Trento, C., Lomas, C., Dolcetti, L., Cheung, T. S., et al. (2017). Apoptosis in mesenchymal stromal cells induces *in vivo* recipient-mediated immunomodulation. *Sci. Transl. Med.* 9, eaam7828. doi:10.1126/scitranslmed.aam7828

Giacomini, C., Granéli, C., Hicks, R., and Dazzi, F. (2023). The critical role of apoptosis in mesenchymal stromal cell therapeutics and implications in homeostasis and normal tissue repair. *Cell Mol. Immunol.* 20, 570–582. doi:10.1038/s41423-023-01018-9

Goldring, M. B., and Berenbaum, F. (2004). The regulation of chondrocyte function by proinflammatory mediators: prostaglandins and nitric oxide. *Clin. Orthop. Relat. Res.* 427, S37–S46. (Lippincott Williams and Wilkins). doi:10.1097/01.blo.0000144484.69656.e4

Griffiths, R., Woods, S., Cheng, A., Wang, P., Griffiths-Jones, S., Ronshaugen, M., et al. (2020). The transcription factor-microRNA regulatory network during hESC-chondrogenesis. *Sci. Rep.* 10, 4744–4816. doi:10.1038/s41598-020-61734-4

Kawano, H., Nakatani, T., Mori, T., Ueno, S., Fukaya, M., Abe, A., et al. (2004). Identification and characterization of novel developmentally regulated neural-specific proteins, BRINP family. *Mol. Brain Res.* 125, 60–75. doi:10.1016/j.molbrainres.2004.04.001

Leijs, M. J. C., van Buul, G. M., Lubberts, E., Bos, P. K., Verhaar, J. A. N., Hoogduijn, M. J., et al. (2012). Effect of arthritic synovial fluids on the expression of immunomodulatory factors by mesenchymal stem cells: an explorative *in vitro* study. *Front. Immunol.* 3, 231–237. doi:10.3389/fimmu.2012.00231

Mantripragada, V. P., Bova, W. A., Piuzzi, N. S., Boehm, C., Obuchowski, N. A., Midura, R. J., et al. (2019). Native-osteoarthritic joint resident stem and progenitor cells for cartilage cell-based therapies: a quantitative comparison with respect to concentration and biological performance. *Am. J. Sports Med.* 47, 3521–3530. doi:10.1177/0363546519880905

Martin, P. (1990). Tissue patterning in the developing mouse limb. *Int. J. Dev. Biol.* 34, 323–336. doi:10.1387/ijdb.1702679

Massengale, M., Massengale, J. L., Benson, C. R., Barywano, N., Oki, T., Steinhauser, M. L., et al. (2023). Adult Prg4+ progenitors repair long-term articular cartilage wounds *in vivo*. *JCI Insight* 8, e167858. doi:10.1172/jci.insight.167858

Masterson, C. H., Curley, G. F., and Laffey, J. G. (2019). Modulating the distribution and fate of exogenously delivered MSCs to enhance therapeutic potential: knowns and unknowns. *Intensive Care Med. Exp.* 7, 41. doi:10.1186/s40635-019-0235-4

Melief, S. M., Geutskens, S. B., Fibbe, W. E., and Roelofs, H. (2013a). Multipotent stromal cells skew monocytes towards an anti-inflammatory interleukin-10-producing phenotype by production of interleukin-6. *Haematologica* 98, 888–895. doi:10.3324/haematol.2012.078055

Melief, S. M., Schrama, E., Brugman, M. H., Tiemessen, M. M., Hoogduijn, M. J., Fibbe, W. E., et al. (2013b). Multipotent stromal cells induce human regulatory T cells through a novel pathway involving skewing of monocytes toward anti-inflammatory macrophages. *Stem Cells* 31, 1980–1991. doi:10.1002/stem.1432

Morrison, T. J., Jackson, M. V., Cunningham, E. K., Kissenpfennig, A., McAuley, D. F., O'Kane, C. M., et al. (2017). Mesenchymal stromal cells modulate macrophages in clinically relevant lung injury models by extracellular vesicle mitochondrial transfer. *Am. J. Respir. Crit. Care Med.* 196, 1275–1286. doi:10.1164/rccm.201701-0170OC

Murphy, J. M., Fink, D. J., Hunziker, E. B., and Barry, F. P. (2003). Stem cell therapy in a caprine model of osteoarthritis. *Arthritis Rheum.* 48, 3464–3474. doi:10.1002/art.11365

Murphy, J. M., Heinegård, D., McIntosh, A., Sterchi, D., and Barry, F. P. (1999). Distribution of cartilage molecules in the developing mouse joint. *Matrix Biol.* 18, 487–497. doi:10.1016/S0945-053X(99)00042-6

Paradiso, F., Lenna, S., Isbell, R., Garcia Garza, M. F., Williams, M., Varner, C., et al. (2022). Immunosuppressive potential evaluation of synovial fluid mesenchymal stem cells grown on 3D scaffolds as an alternative source of MSCs for osteoarthritis cartilage studies. *Front. Biomaterials Sci.* 1. doi:10.3389/fbiom.2022.989708

Rhee, D. K., Marcelino, J., Baker, M., Gong, Y., Smits, P., Lefebvre, V., et al. (2005). The secreted glycoprotein lubricin protects cartilage surfaces and inhibits synovial cell overgrowth. *J. Clin. Investigation* 115, 622–631. doi:10.1172/JCI22263

Sato, J., Kinugasa, M., Satomi-Kobayashi, S., Hatakeyama, K., Knox, A. J., Asada, Y., et al. (2014). Family with sequence similarity 5, member C (FAM5C) increases leukocyte adhesion molecules in vascular endothelial cells: implication in vascular inflammation. *PLoS One* 9, e107236. doi:10.1371/journal.pone.0107236

Schelbergen, R. F., van Dalen, S., ter Huurne, M., Roth, J., Vogl, T., Noël, D., et al. (2014). Treatment efficacy of adipose-derived stem cells in experimental osteoarthritis is driven by high synovial activation and reflected by S100A8/A9 serum levels. *Osteoarthr. Cartil.* 22, 1158–1166. doi:10.1016/j.joca.2014.05.022

Schrodt, M. V., Behan-Bush, R. M., Liszewski, J. N., Humpal-Pash, M. E., Boland, L. K., Scroggins, S. M., et al. (2023). Efferocytosis of viable versus heat-inactivated MSC induces human monocytes to distinct immunosuppressive phenotypes. *Stem Cell Res. Ther.* 14, 206. doi:10.1186/s13287-023-03443-z

Seol, D., Yu, Y., Choe, H., Jang, K., Brouillette, M., Zheng, H., et al. (2014). Effect of short-term enzymatic treatment on cell migration and cartilage regeneration: *in vitro* organ culture of bovine articular cartilage. *Tissue Eng. Part A* 20, 1807–1814. doi:10.1089/ten.tea.2013.0444

Sohn, D. H., Sokolove, J., Sharpe, O., Erhart, J. C., Chandra, P. E., Lahey, L. J., et al. (2012). Plasma proteins present in osteoarthritic synovial fluid can stimulate cytokine production via Toll-like receptor 4. *Arthritis Res. Ther.* 14, R7. doi:10.1186/ar3555

Sophia Fox, A. J., Bedi, A., and Rodeo, S. A. (2009). The basic science of articular cartilage: structure, composition, and function. *Sports Health* 1, 461–468. doi:10.1177/1941738109350438

Ter Huurne, M., Schelbergen, R., Blattes, R., Blom, A., De Munter, W., Grevers, L. C., et al. (2012). Antiinflammatory and chondroprotective effects of intraarticular injection of adipose-derived stem cells in experimental osteoarthritis. *Arthritis Rheum.* 64, 3604–3613. doi:10.1002/art.34626

Wang, Z., Dai, M., Wang, Y., Cooper, K. L., Zhu, T., Dong, D., et al. (2014). Unique expression patterns of multiple key genes associated with the evolution of mammalian flight. *Proc. R. Soc. B Biol. Sci.* 281, 20133133. doi:10.1098/rspb.2013.3133

Xie, F., Kovic, B., Jin, X., He, X., Wang, M., and Silvestre, C. (2016). Economic and humanistic burden of osteoarthritis: a systematic review of large sample studies. *Pharmacoeconomics* 34, 1087–1100. doi:10.1007/s40273-016-0424-x

Yucesoy, B., Charles, L. E., Baker, B., and Burchfiel, C. (2015). Occupational and genetic risk factors for osteoarthritis: a review. *Work* 50, 261–273. doi:10.3233/WOR-131739

Zeng, W., Xu, H., Wei, T., Liang, H., Ma, X., and Wang, F. (2022). Overexpression of BRINP3 predicts poor prognosis and promotes cancer cell proliferation and migration via MAP4 in osteosarcoma. *Dis. Markers* 2022, 2698869. doi:10.1155/2022/2698869

Zhang, Y., Fukui, N., Yahata, M., Katsuragawa, Y., Tashiro, T., Ikegawa, S., et al. (2016). Identification of DNA methylation changes associated with disease progression in subchondral bone with site-matched cartilage in knee osteoarthritis. *Sci. Rep.* 6, 34460–34513. doi:10.1038/srep34460

Zhang, Y., Whaley-Connell, A. T., Sowers, J. R., and Ren, J. (2018). Autophagy as an emerging target in cardiorenal metabolic disease: from pathophysiology to management. *Pharmacol. Ther.* 191, 1–22. doi:10.1016/j.pharmthera.2018.06.004

Zhu, L., Malatras, A., Thorley, M., Aghoghogbe, I., Mer, A., Duguez, S., et al. (2015). CellWhere: Graphical display of interaction networks organized on subcellular localizations. *Nucleic Acids Res.* 43, W571–W575. doi:10.1093/nar/gkv354

frontiers | Frontiers in Cell and Developmental Biology

TYPE Original Research
PUBLISHED 08 April 2025
DOI 10.3389/fcell.2025.1559155

Check for updates

OPEN ACCESS

EDITED BY
Elizabeth Vinod,
Christian Medical College and Hospital, India

REVIEWED BY
Mildred Embree,
Columbia University, United States
Roland Adam Takacs,
University of Debrecen, Hungary

*CORRESPONDENCE
Christopher Kim,
christopher.kim@uhn.ca

†These authors have contributed equally to this work and share first authorship

RECEIVED 11 January 2025
ACCEPTED 24 March 2025
PUBLISHED 08 April 2025

CITATION
Kim C, Li B, Nakamura S, Neely EJ, Rockel JS, Oussenko T, Zhang P, Kapoor M and Nagy A (2025) Engineered mesenchymal stromal cells with interleukin-1beta sticky-trap attenuate osteoarthritis in knee joints.
Front. Cell Dev. Biol. 13:1559155.
doi: 10.3389/fcell.2025.1559155

COPYRIGHT
© 2025 Kim, Li, Nakamura, Neely, Rockel, Oussenko, Zhang, Kapoor and Nagy. This is an open-access article distributed under the terms of the Creative Commons Attribution License (CC BY). The use, distribution or reproduction in other forums is permitted, provided the original author(s) and the copyright owner(s) are credited and that the original publication in this journal is cited, in accordance with accepted academic practice. No use, distribution or reproduction is permitted which does not comply with these terms.

Engineered mesenchymal stromal cells with interleukin-1beta sticky-trap attenuate osteoarthritis in knee joints

Christopher Kim[1,2]*†, Biao Li[1,2†], Sayaka Nakamura[2], Eric J. Neely[1], Jason S. Rockel[2], Tatiana Oussenko[1], Puzheng Zhang[1], Mohit Kapoor[2] and Andras Nagy[1,3,4]

[1]Lunenfeld Tanenbaum Research Institute, Sinai Health System, Toronto, ON, Canada, [2]Schroeder Arthritis Institute, Krembil Research Institute, University Health Network, Toronto, ON, Canada, [3]Department of Obstetrics and Gynaecology and Institute of Medical Science, University of Toronto, Toronto, ON, Canada, [4]Australian Regenerative Medicine Institute, Monash University, Melbourne, VIC, Australia

Osteoarthritis (OA) is a common chronic inflammatory joint disease, in which innate immunity plays a pivotal role in pathogenesis. Anti-interleukin-1(IL-1) therapies have shown inconsistent results in clinical trials, potentially due to a mismatch in the spatial and temporal dynamics of interleukin-1beta (IL-1β) production and therapeutic interventions. To address this issue, we developed a novel IL-1β "sticky-trap" utilizing cell and gene-based technologies from our lab and evaluated its efficacy in reducing osteoarthritis progression using a murine destabilization of the medial meniscus (DMM) OA model and a compact bone-derived mesenchymal stromal cell (MSC)-based gene expression system. The extracellular domain of interleukin-1 receptor 2 (IL1R2) was employed to design the sticky IL1R2 trap (stkIL1R2). A murine compact bone-derived MSC line was engineered for gene delivery. Although stkIL1R2 was undetectable in the engineered MSC supernatants by enzyme-linked immunosorbent assay (ELISA) and Western blot, it was localized on the cell surface and extracellular matrix (ECM) and demonstrated specific binding to IL-1β using a fluorescent protein-fused binding assay. Doxycycline (Dox)-induced expression of stkIL1R2 significantly inhibited lipocalin-2 (LCN2) expression which is a biomarker of IL-1β activity. For *in vivo* experiments, 5×10^4 Dox-inducible stkIL1R2f expressing MSCs were injected into the knee joints of DMM mice. Bioluminescence imaging revealed MSC survival in the knee joints for up to 7 weeks post-injection. Histological analyses at 10 weeks post-injection, including Safranin-O and Masson trichrome staining, showed that stkIL1R2 treated joints exhibited significantly less cartilage degradation and synovitis compared to controls, as assessed by Osteoarthritis Research Society International (OARSI) scoring of the femur, tibia, and synovium. Moreover, stkIL1R2 treatment reduced matrix metalloproteinases-13 (MMP-13) positive cells and collagen type II degradation in the affected joints. In conclusion, we developed a MSC line expressing an inducible IL1 sticky-trap, which localized to the cell surface and ECM and specifically bound IL-1β. These engineered MSCs survived in normal and DMM knee joints for up to 7 weeks and significantly delayed OA progression and inflammation in the murine

model. This study introduces a promising therapeutic approach to combat OA progression.

KEYWORDS

osteoarthritis, sticky biologics, cell-based gene therapy, interleukin-1beta, interleukin-1 receptor 2, mesenchymal stromal cell

1 Introduction

Osteoarthritis (OA) is a chronic, degenerative, whole-joint disease characterized by the breakdown of articular cartilage, osteophyte formation, remodeling of subchondral bone, and inflammation of the synovial membrane (Pelletier et al., 2001). An imbalance of chondrocyte homeostasis leads to the progressive degradation of cartilage extracellular matrix, involving pro-inflammatory cytokines and matrix metalloproteinases (MMPs) (Pelletier et al., 2001). OA stands as a leading cause of disability, pain, loss of function and decreased quality of life (QOL) in the elderly (Hunter et al., 2014).

Increasing evidence suggests that OA is a low-grade inflammatory condition of the joint (Robinson et al., 2016; Scanzello, 2017a). Notably, the interaction between cartilage and the synovial membrane is critical in sustaining this chronic low-grade inflammation (Chou et al., 2020; Hamasaki et al., 2021; Sanchez-Lopez et al., 2022; Scanzello and Goldring, 2012). The term "low-grade inflammation" distinguishes OA from inflammatory arthritis like rheumatoid arthritis (RA). Unlike RA, where inflammation primarily arises from adaptive immunity, OA's inflammation stems from innate immunity, either systemic or local (Knights et al., 2023; Roover et al., 2023). The pro-inflammatory cytokine interleukin-1beta (IL-1β) plays a key role in innate immunity (Hoseini et al., 2018; Im and Ammit, 2014; Keyel, 2014) and has been implicated in both preclinical and clinical OA conditions (Krenytska et al., 2023; Panina et al., 2017; Wang et al., 2019). However, anti-interleukin-1 (IL-1) therapies adapted from RA treatments have shown limited success in OA (Chevalier et al., 2009; Cohen et al., 2011; Fleischmann et al., 2019; Kloppenburg et al., 2018; 2019), with debates surrounding IL-1β′s role in OA (Chevalier et al., 2009; Cohen et al., 2011; Fleischmann et al., 2019; Kloppenburg et al., 2018; 2019). These debates were clarified by the Canakinumab Antiinflammatory Thrombosis Outcome Study (CANTOS), where IL-1β inhibition significantly reduced the need for hip or knee replacements (Ridker et al., 2017; Schieker et al., 2020). The variability in preclinical and clinical outcomes can be attributed to OA's inflammatory heterogeneity, its diverse phenotypes and endotypes (Bosch et al., 2024; Chevalier et al., 2013), and the short half-life of IL-1β in serum (Kudo et al., 1990; REIMERS et al., 1991). This underscores the need for precise timing and delivery strategies for anti-IL-1 therapies.

Presently, OA remains incurable and no approved medications, biological therapy, or procedure cures or prevents the progressive destruction of the joint. Present treatment options primarily offer symptomatic relief rather than preventative or regenerative results. There is an urgent call to innovate, validate, and explore new biological therapeutics. Among these, cell-based therapies involving the injection of MSCs to the osteoarthritic knee joint have surfaced as a promising solution to address this clinical challenge.

Our lab has pioneered a novel approach to express local-acting biologics, termed "sticky-trap" technology, which was previously successful in trapping vascular endothelial growth factor (VEGF) in the eye (Michael et al., 2014). Building on this success, we developed a IL-1β sticky-trap using the extracellular domain of IL-1 receptor 2 (IL1R2) and employed isogenic mouse compact bone-derived MSCs as carriers. This study explores whether this cell-based therapy can mitigate inflammation and slow OA progression in a murine DMM model. Our hypothesis is that intraarticular injection of local acting IL-1β sticky trap expressing MSCs could reduce inflammation and attenuate the progression of OA.

2 Methods

2.1 Mouse studies

Mouse studies were conducted following a protocol approved by the Institutional Animal Care and Use Committee of The Toronto Phenogenomics (TCP, Toronto)(AUP #25–0308H). Mice were housed in a room with controlled temperature (21°C–23°C), humidity (40%–60%), and a light cycle consisting of 12 h of light (starting at 07:00) and 12 h of dark (starting at 19:00). Mice were kept in individual ventilated cages (Techniplast Greenline GM500 cage, LABEX Inc., MA, United States) and provided with quality water via an automated watering system (Avidity Science, WI, United States) with a sterile quick-disconnect Avidity Science water valve. They were fed with extruded pellets from Envigo (Inotiv Inc., WI, United States). C57BL/6J mice were purchased from TCP and maintained in the mouse room.

2.2 MSC isolation and culture

MSCs were isolated from compact bone as per Zhu et al. (2010). Briefly, a 3-week-old C57BL/6J mouse was euthanized by cervical dislocation. The carcass was rinsed in 70% ethanol for 3 min, and femurs were dissected in a sterile 100-mm dish. Bone marrow was flushed out using 5 mL of α-MEM (Gibco, Thermo Fisher, cat. no. 12571063), supplemented with 0.1% penicillin/streptomycin (P/S) and 2% FBS (Multicell, Wisent Inc., cat. no. 080150) until the bones became clear. The femurs were then chopped into 1–3 mm^3 pieces using scissors. Bone chips were digested in 3 mL of α-MEM containing 10% FBS and 1 mg/mL collagenase II (Sigma, cat. no. C6885) and incubated at 37°C with shaking (200 rpm) for 2 h. The bone chips were washed three times with 5 mL of α-MEM and seeded into a 100-mm sterile dish with 10 mL of DMEM/F12 medium (Gibco, Thermo Fisher, cat. no. 11330-032) supplemented with 10% FBS, 1% P/S, and 10 ng/mL bFGF (PeproTech, cat. no. 100-18B). Cells were incubated at 37°C in a 5% CO_2 incubator for 3 days

without disturbance. The medium was changed every 3 days until confluence. These cells were defined as passage 0 (P0). MSCs were cultured in DMEM/F12 with 10% FBS, 10 ng/mL bFGF, and 1% P/S. Cells were passaged with 0.25% trypsin-EDTA and cryopreserved at −80°C for 1 day before being transferred to liquid nitrogen.

2.3 FACS sorting

Cells were harvested by trypsin digestion, washed twice with cold PBS, and incubated with antibodies on ice for 10 min. After washing, cells were filtered and analyzed by flow cytometry using a Beckman Coulter Gallios and BD Fortessa X-20 flow cytometer. Data were analyzed using Beckman Coulter Kaluza and FlowJo software (BD Biosciences, ver. 10.10.0). Antibodies used for flow analysis were listed in Supplementary Table S1.

2.4 Quantitative PCR

Freshly harvested cells were used for total RNA purification with Trizol regent (cat. no. 15596-026, Invitrogen). The purified RNA was dissolved in DEPC-treated water (Diethyl pyrocarbonate) (cat. no. D5758-25 mL, sigma). RNA concentration was quantified by Nanodrop 1000 spectrophotometer (Thermo Scientific). A total of 1 μ g of RNA was reverse transcribed to cDNA using the iScript cDNA Synthesis Kit (cat. no. 1708891, Bio-Rad) following the manufacturer's instructions. For amplification, 1 μ l of 1:100 diluted cDNA sample was applied in the SsoAdvanced Universal SYBR green supermix (cat. no. 1725271, Bio-Rad) in a total reaction volume of 5 μ l, prepared in a 384-well plate (cat. no. HSP3805, Bio-Rad). The reactions were were run on a DNA amplifier (CFX384 Real-Time system, C1000 Thermal cycler, Bio-Rad). All samples were analyzed in duplicate. Relative quantification of gene expression was calculated using the comparative Ct method (Schmittgen and Livak, 2008). The ΔCt value was determined by subtracting the Ct value of the house keeping gene from respective respective target gene Ct value for each sample. Relative expression levels were calculated as $2^{-\Delta Ct}$, and incremental changes in target gene expression were determined as $2^{-\Delta\Delta Ct}$. Primers used in this study are listed in the Supplementary Table S2.

2.5 Generation of enhanced luciferase expression cell line

The PB-CAG-e-Luciferase-IRES-eGFP plasmid was generated in our lab and used to transfect mouse MSCs. MSCs (2×10^6) were plated in a 100-mm plate and incubated overnight at 37°C in 5% CO_2. When cells reached 70%–90% confluence, they were transfected using jetPRIME transfection reagent (Poly-Plus Transfection, France, cat. no. #114-15) according to the manufacturer's instructions. Briefly, 10 μg of DNA was diluted in 500 μL jetPRIME buffer, mixed with 20 μL jetPRIME reagent, and incubated at room temperature for 10 min. The mixture was then added to the cells. The plate was incubated at 37°C in 5% CO_2 for 24–48 h. Gene expression was confirmed by the GFP signal observed under fluorescence microscopy.

2.6 Cell differentiation

MSC differentiation reagents were purchased from LONZA (www.lonza.com). Adipocyte, chondrocyte, and osteocyte differentiation protocols were followed as recommended by the manufacturer. For each differentiation protocol, the same number of cells were cultured in standard MSC medium for the same duration as the control group.

2.7 Bioluminescence imaging (BLI)

Bioluminescent signals from e-luciferase and luciferin reactions in cells were acquired using the IVIS Lumina III BLI System (PerkinElmer, Guelph, Canada; Part No. CLS136334). Mice were injected with 200 μg of luciferin (Promega, Madison, United States, cat. no. P1043) in 100 μL PBS via intraperitoneal injection, anesthetized with isoflurane USP (Piramal Critical Care Inc., Bethlehem, United States, cat. no. DVM-102190), and imaged. Care was taken to remove hair from the knees of the mice before imaging.

2.8 Generation of inducible gene expression plasmids

The extracellular domain cDNA sequence, including the signal peptide of murine IL1R2 (nt1-1065), was used for constructing the short trap IL1R2 (sIL1R2) and sticky trap IL1R2 (stkIL1R2) plasmids. Additional domains included a GS linker, IgG1-CH3 domain, heparin-binding domain (exons 6 and 8), a Flag tag, and an His tag (x8). Inducible expression plasmids for stkIL1R2 and sIL1R2 were generated using Invitrogen Gateway Technology. The target gene cDNA sequences were flanked by att-B and att-P sequences (Eurofins Genomics, Toronto, Canada). Synthesized DNAs were subcloned into a pDNOR221 plasmid via BP reaction, then transformed into One Shot TOP10 chemically competent *E. coli* (Invitrogen, cat. no. 4040-10). After enzyme digestion, the targeted plasmid was confirmed by DNA sequencing (ACGT Corp., Toronto, Canada). The confirmed plasmid was then used for an LR reaction with the final targeting plasmid (PB-teto-GW-IRES-GFP/mCherry). The plasmids were transformed into *E. coli*, and the final plasmids were confirmed by enzyme digestion. Colonies were maxi-prepped (Qiagen, Hilden, Germany) for high-quality DNA. This protocol was also used for other expression plasmids in this study. IgG and stk plasmid controls in protein generation studies using HEK293 cells were kindly donated by coauthor, Dr. Eric Neely.

2.9 Western blot analysis

Tissues and cells were lysed in RIPA buffer (50 mM Tris-HCl, pH 7.4, 150 mM NaCl, 1% Triton X-100, 1% sodium deoxycholate, 0.1% SDS, 1 mM EDTA) with protease inhibitor mix (Sigma). Homogenization was performed using a TissueLyser (Bio-Rad), followed by centrifugation at 13,200 rpm for 15 min at 4°C. The supernatant was collected for protein analysis. Protein concentration was measured by the Pierce BCA protein assay kit (Thermo Scientific, cat. no. 23225).

20 μg of protein was resolved on a NuPAGE 4%–12% Bis-Tris SDS-PAGE gel (Thermo Scientific, cat. no. NP0336) and transferred to a PVDF membrane using an iBlot 2 PVDF mini stack transfer kit (Thermo Scientific, cat. no. IB24002). After blocking with 5% non-fat milk, the membrane was incubated with primary antibody overnight at 4°C, followed by incubation with HRP-conjugated secondary antibody. Proteins were detected using the Amersham ECL prime Western blotting detection reagent (GE Healthcare Life Sciences, cat. no. RPN2232). Images were acquired and processed using a ChemiDoc XRS + system (Bio-Rad).

Antibodies used: rabbit monoclonal to lipocalin-2 (LCN2) (Abcam, cat. no. 216462), goat anti-rabbit IgG H&L HRP secondary antibody (Abcam, cat. no. ab7090), and mouse monoclonal anti-β-Actin antibody (Sigma, cat. no. A3854).

2.10 ELISA

To assess IL1R2 expression, 5×10^5 inducible sIL1R2 and stkIL1R2 expressing MSCs were plated into a 6-well plate, with Dox either present or absent. The cells were cultured at 37°C in 5% CO_2 for 72 h, and the supernatants were collected for ELISA analysis. Mouse IL1R2 was quantified using the mouse IL1R2 ELISA kit (cat. no. RD-IL1R2-mu, RedDot Biotech Inc., Kelowna, Canada) following the manufacturer's protocol. Briefly, samples were diluted according to the kit's instructions using calibrator diluent and incubated for 2 h at room temperature (RT) with the primary antibody-coated 96-well strips. After four washes with washing buffer, the samples were incubated with the HRP-conjugated secondary antibody for 2 h at RT. Following an additional four washes, substrate solution was added for 30 min, and the reaction was stopped with the provided stop solution. Optical density (OD) was measured at 450 nm and 540 nm using an EnSpire 2300 multilabel reader (PerkinElmer, ON, CA). A standard curve was constructed using the provided mouse LCN2 standard, and OD values were corrected by subtracting OD540 from OD450. The corrected OD values were then used to calculate IL1R2 concentration based on the standard curve.

2.11 Protein generation

HEK-293F cells were used for protein production. The cells were cultured in Freestyle 293 medium (cat. no. 12338-018, Gibco) supplemented with 2.5 mM sodium butyrate (cat. no. 303410, Sigma) at 37°C and 5% CO_2, shaking at 1.5 mm/s for 3 days. pH and glucose levels were monitored daily to maintain a pH of 6.8 and glucose concentration between 18 and 27 mmol/L. After 3 days, the cells were spun down, and the supernatant was collected and stored at 4°C. The cells were then resuspended in fresh medium without sodium butyrate and cultured for another 3 days. The supernatants from both collections were combined for protein purification. To remove cellular debris, the supernatants were filtered through a 0.45 μm Nalgen filter (cat. no. 166-0045, Thermo Scientific), then incubated with Heparin Sepharose 6 Fast Flow beads (cat. no. 17-0998-01, Qiagen) at 4°C overnight. The beads were packed into a column the following day, eluted with NaCl, and the eluates were bound to a Ni-NTA column (cat. no. 30410, Qiagen) and eluted with imidazole (cat. no. 15513–25 g, Sigma). The eluates were concentrated to 2–3 mL using an Amicon Ultra-15 centrifugal filter (EMD Millipore, United States) and desalted with a PD10 column (cat. no. 17-0851-01, GE Healthcare Life Sciences). Finally, proteins were eluted from the PD10 column with 3 mL storage buffer (5% D-Mannitol, 5% D-Trehalose dihydrate in PBS) (Sigma). Protein concentration was determined using Bradford reagent (cat. no. 15513, Bio-Rad).

2.12 Protein binding assay

To generate the IL-1β sticky-trap, we constructed two plasmids: PB-tetO-stkIL1R2-mCherry-IRES-puromycin (which expresses stkIL1R2-mCherry under Dox induction) and PB-tetO-IL-1β-GFP-IRES-puromycin (which expresses IL-1β-GFP under Dox induction) (Figure 3A). The stkIL1R2-mCherry plasmid was transfected into R61MSC and HEK-293F cells, and protein expression was induced by Dox. Fluorescent signals were monitored using a fluorescent microscope. The IL-1β-GFP plasmid was transfected into HEK-293F cells, and the supernatant was collected for IL-1β-GFP protein purification.

For the sticky-trap assay, 7.5×10^4 cells expressing IL-1β sticky-trap were plated onto coverslips in a 6-well plate and incubated with Dox (1.5 μg/mL) for 48 h. The medium was removed, and the cells were washed three times with PBS, then fixed with 4% paraformaldehyde (PFA) (cat. no. J61899, Alfa Aesar) in PBS (unpermeabilized) for 10 min at RT. After fixation, cells were washed three times with PBS and blocked for 1 h at RT using blocking buffer (2% BSA in PBS). The cells were washed three times with PBS and incubated with IL1β-GFP protein (5 ng/mL) for 1 h at RT. After washing, coverslips were mounted with VECTASHIELD Antifade Mounting Medium with DAPI (cat. no. H-1200-10, Vector Laboratories) and imaged using a Carl Zeiss LSM 780 confocal microscope.

2.13 DMM mouse knee OA model

The DMM model was used to induce OA in male C57BL/6J mice (10 weeks old). The procedure followed Glasson et al. (2007). Mice were anesthetized with isoflurane and the right hind leg was disinfected with 70% ethanol. A 3 mm longitudinal incision was made over the distal patella to the proximal tibial plateau. The joint capsule medial to the patella tendon was opened with micro-iris scissors, and the medial meniscotibial ligament (MMTL) and medial meniscus (MM) were visualized and transected with micro-iris scissors. Transection was confirmed by lifting the medial meniscus from the tibial plateau. The joint capsule and skin were sutured closed. Sham surgeries were performed with identical aseptic technique, but without ligament transection. DMM and sham surgeries were performed by the same surgeon. Depending on the experimental group, mice were administered Dox chow (Envigo, green) post-surgery.

2.14 Histology

Following euthanasia, freshly dissected mouse hind limbs without skin were fixed overnight in 4% paraformaldehyde/PBS (cat. no.

J61899, Alfa Aesar). Tissues were then decalcified in 10% EDTA for 1 week, embedded in paraffin, sectioned sagittally, and stained with H&E, Safranin-O, Fast Green, and Masson's Trichrome. For Immunohistochemistry (IHC), paraffin slides were deparaffinized in xylene, followed by alcohol treatment. Antigen retrieval was performed using 10 mM citrate buffer (pH 6.0). Slides were blocked with Dako protein block for 10 min at RT, then incubated overnight at 4°C with primary antibodies. After washing with PBS-T, slides were incubated with HRP-conjugated secondary antibody for 1 h at RT. Following washes, slides were developed using 3,3′-diaminobenzidine (DAB), and counterstained with H&E. OARSI score was used to quantify the pathological changes in femur, tibia and synovial membrane. OARSI scoring was performed by two independent researchers using the OARSI semi-quantitative scoring system (Glasson et al., 2010). Both scorers were blinded to the experimental groups.

2.15 Statistical analysis

Data were presented as mean ± SEM. Data were first analyzed using an F-test to determine if the variances were significantly different or not. Then, a two-tailed unpaired Student's t-test, accounting for equal or unequal variance, was performed to compare two independent groups, $p < 0.05$ was recognized as a significant difference, with all analyses performed in Microsoft Excel and Prism 10 (GraphPad Software Inc). Figures were generated using Prism 10.

3 Results

3.1 Isolation and primary culture of compact bone derived MSC cell line

MSCs are a heterogeneous population of cells with self-renewal properties and the multipotential ability to differentiate into mesodermal cells, such as adipocytes, chondrocytes, and osteocytes (Pittenger et al., 1999). Injection of MSCs to the OA knee joint have surfaced as a promising cell-based therapy (Harrell et al., 2019). To establish a joint-friendly MSC cell line, we followed Zhu's protocol to generate a cell line from mouse compact bones (Zhu et al., 2010). This resulted in a heterogeneous population of cells with various morphologies, such as spindle, stellate, and polygonal shapes (Figure 1A, P0, P2).

To make the cell population more homogeneous and enriched with proliferative and active cells, we further sorted the cells against negative MSC markers CD45 and TER119, then further sorted $CD45^{-}TER119^{-}$ cells by their expression of PDGFRα and Sca-1, finally, we collected the $CD45^{-}TER119^{-}PDGFR\alpha^{+}Sca\text{-}1^{+}$ populations (Morikawa et al., 2009) (Figure 1B). After sorting, the cells appeared much more homogeneous (Figure 1C). To investigate whether MSC marker expression changed after multiple passages, we characterized MSC marker expression in passage 8, 15, and 30, and compared them with unsorted passage 1 cells, using bone marrow cells as a control (Figure 1D). Most of the MSC markers were stably expressed even up to passage 30.

To observe the morphological changes of the cells and track them after injection into mouse knees, we generated a *PiggyBac*-based e-Luciferase expression plasmid tagged with eGFP to transfect the MSCs. The engineered MSCs (transfected MSCs) were bulk sorted based on eGFP expression (Figure 1E). We then further tested the multilineage differentiation ability of these eLuciferase-eGFP engineered MSCs by differentiating them into chondrocytes, adipocytes, and osteocytes (Figures 1F–H). For chondrocyte differentiation, pellets were collected at day 28 following the protocol provided by the manufacturer and H&E and Alcian blue stains were used to confirm the presence of chondrocytes (Figure F). For adipocyte differentiation, engineered cells at 100% confluence were cultured with 3 cycles of induction/maintenance medium, while control cells were cultured in normal MSC culture medium. Cells were stained with Oil Red and numerous lipid droplets were observed in the differentiation group (Figure 1G). For osteocyte differentiation, induction medium was used for the entire differentiation protocol, while control cells were maintained in normal MSC culture medium. By day 21, Alizarin red staining was used and revealed the morphology of osteocytes (Figure 1H).

To explore how long MSCs can survive in the mouse knees, we injected 5×10^4 MSCs into mouse knees and tracked the cells by intraperitoneal injection of luciferin, monitoring the local signal using BLI (Figure 1I). Interestingly, most of the injected cells survived in the knee joint for up to 7 weeks, with the longest survival reaching up to 72 days. Injected cells were not observed in other body parts of the mouse.

MSCs, which serve as precursors to chondrocytes, play a pivotal role in the initiation and progression of OA. To investigate how compact bone-derived MSCs respond to pro-inflammatory cytokines, we stimulated them with IL-1β at a concentration of 100 pg/mL and compared their responses to those induced by interleukin-6 (IL-6) and tumor necrosis factor-alpha (TNF-α) at the same dosage (Figure 2). IL-1β significantly increased the expression of tissue matrix metalloproteinases (MMPs), including MMP13, MMP3, and MMP10, while notably reducing the expression of MMP inhibitors such as tissue inhibitor of metalloproteinase 1 (TIMP1), TIMP2, and TIMP3. Additionally, it suppressed MMP2, A disintegrin and metalloproteinase with thrombospondin motifs 1 (ADAMTS1), ADAMTS5, and collagen type II alpha 1 (COL2A1). Collectively, these changes promote catabolic processes associated with OA progression. Interestingly, IL-1β also significantly elevated the levels of Lipocalin 2 (LCN2) and monocyte chemoattractant protein 1 (MCP-1). The relevance of the LCN2 increase is further explored in our other paper (Biao Li et al., submitted for publication).

3.2 Generation of soluble IL1R2 trap (sIL1R2) and sticky IL1R2 trap (stkIL1R2)

IL1R2 is a transmembrane protein that consists of three key domains: an intracellular domain (spanning residues R382 to N410), a transmembrane domain (residues V356 to M381), and an extracellular domain (residues M1 to E355) (Figure 3A). The extracellular domain includes three Ig-C2 motifs responsible for ligand binding. To generate a sIL1R2 while maintaining optimal binding efficiency to its ligands, we truncated the extracellular domain at the E355-V356 boundary, using the soluble fragment from M1 to E355 to develop our biologic.

The final sIL1R2 biologic comprises the IgG1-CH3 domain, a FLAG tag, and eight His tags, all connected by GS linkers

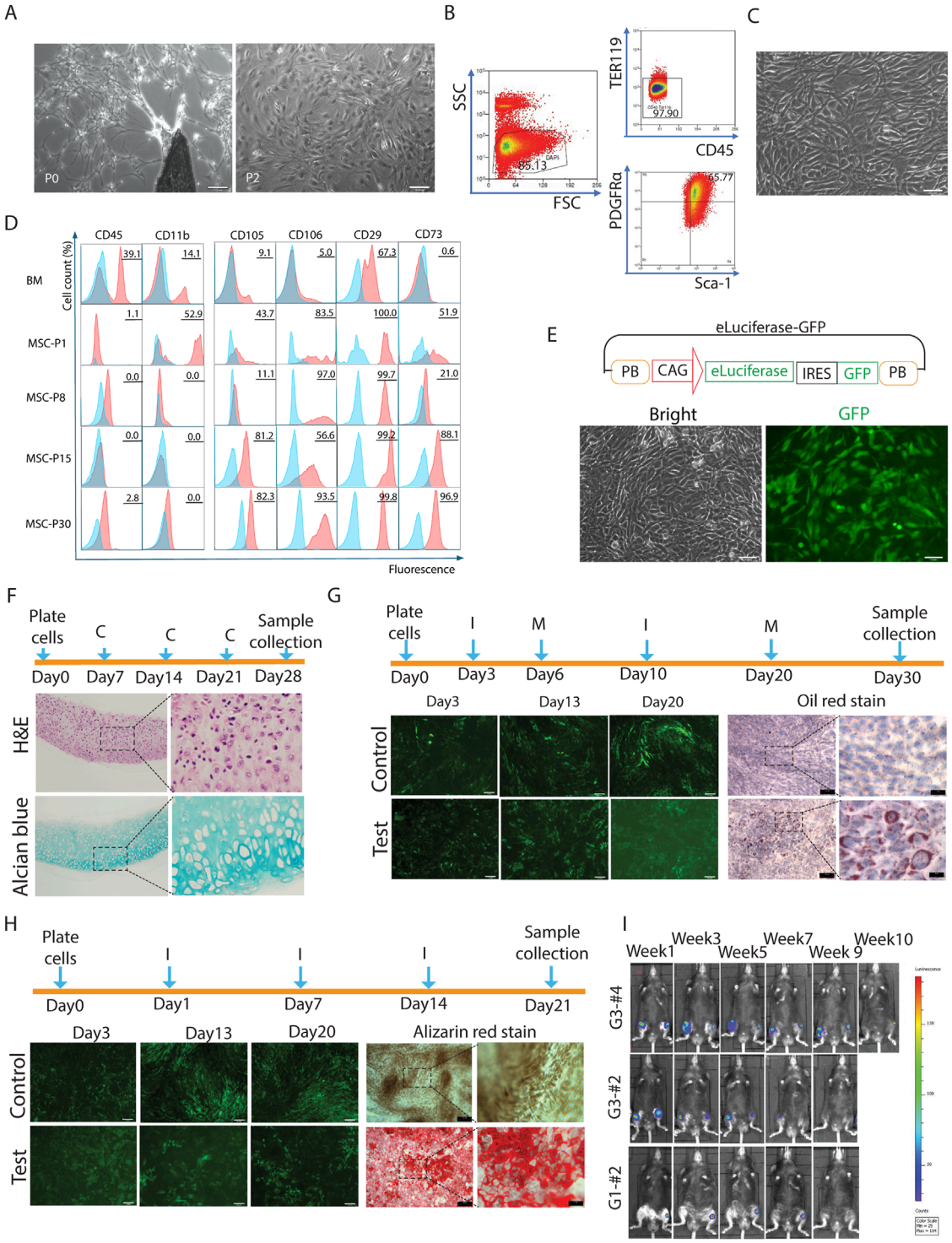

FIGURE 1
The generation of a mesenchymal stromal cell line. **(A)** Bone chips were seeded in the plate, and several days later, cells grew out from the bone chip (P0, magnification ×5), the cells were a heterogenous population (P2, magnification ×10); **(B)** Primary cultured cells were bunk sorted according to the expression of negative markers TER119 and CD45, and both PDGFRα and Scal-1 positive, the sorting gate was defined by isotype antibody controls; **(C)** The sorted cells looked more homogenous (magnification ×10); **(D)** The MSC negative and positive marker expressions on MSCs with different passages; **(E)** The components of e-Luciferase expression plasmid based on PB transposon system, which contained a GFP tag, the e-luciferase-GFP transfected MSC still kept the spindle morphology (magnification ×10); **(F)** The e-luciferase-GFP transfected MSCs were differentiated to chondrocytes (stained by Alcian blue) (magnification ×5), C-complete medium; **(G)** The e-luciferase-GFP transfected MSCs were differentiated to adipocytes (stained by Oil red) (magnification ×5), I-induction medium, M-maintenance medium; **(H)** The e-luciferase-GFP transfected MSCs were differentiated to osteocytes (stained by Alizarin red) (magnification ×5), I-induction medium; **(I)** 5 × 10^4 of e-luciferase-GFP transfected MSCs were injected into C57BL6/J mouse joints, and monitored by luciferase-Luciferin reaction using BLI.

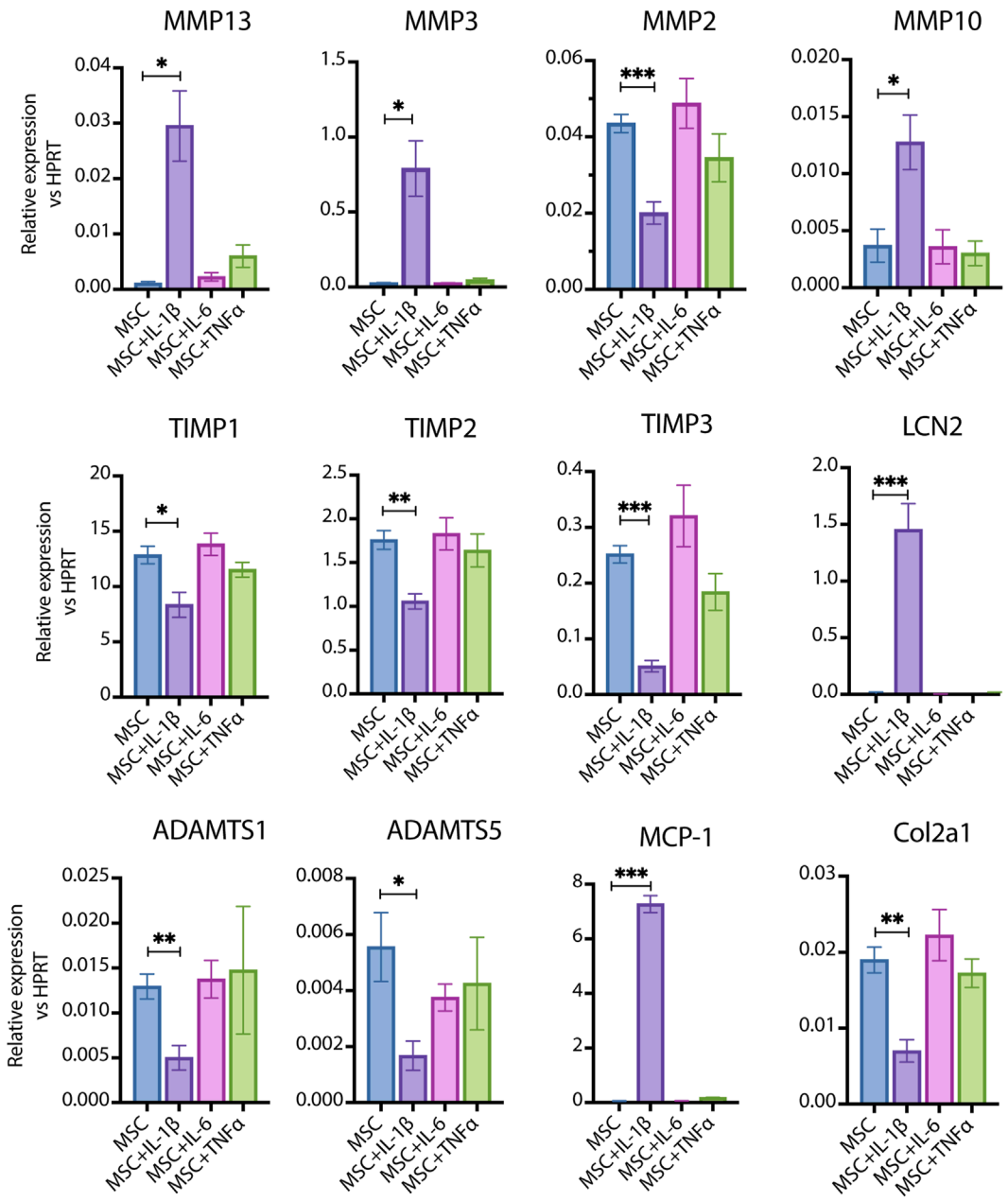

FIGURE 2
The response of primary cultured MSCs to pro-inflammatory cytokines. 100 pg/mL of IL-1β, IL-6 and TNF-α were used to stimulate MSCs respectively. IL-1β significantly induced the expression of MMP13, MMP3, MMP10, LCN2 and MCP-1 (IL-1β vs. Control, $p < 0.05–0.001$, n = 4–6); IL-1β significantly inhibited the expression of MMP2, TIMP1, TIMP2, TIMP3, ADAMTS1, ADAMTS5 and Col2a1(IL-1β vs. Control, $p < 0.05–0.001$, n = 4–6); while the same dosage of IL-6 and TNF-α did not induce significant changes. Data are expressed as mean ± SEM,*$p < 0.05$;**$p < 0.01$;***$p < 0.001$.

(Figure 3A). In comparison, the stkIL1R2 contains an additional cassette, including a heparin-binding domain (HBD) encoded by VEGF-A exon 6 and a non-HBD encoded by VEGF-A exon 8 (Michael et al., 2014). This additional domain is flanked by GS linkers and inserted between the IgG1-CH3 domain and the FLAG tag of sIL1R2 (Figure 3A).

A Dox-inducible gene expression cassette, utilizing the Tet-ON system, was employed to enable inducible expression (Das et al., 2016). The plasmids for inducible expression were constructed using the *PiggyBac* (PB) transposon system. In this system, the upstream promoter cassette, TetO, is activated following the binding of rtTA in the presence of Dox, it triggers the downstream fluorescence signal, with mCherry used for sIL1R2 and GFP for stkIL1R2 (Figure 3B).

To create MSC lines for injection, an inducible stkIL1R2 engineered MSC line was generated by co-transfecting PB-TetO-stkIL1R2-IRES-eGFP and PB-CAG-eLuc-IRES-mCherry plasmids into MSCs. An sIL1R2 MSC line was also generated as a control (Figure 3C). For cells stably expressing sIL1R2 or stkIL1R2, supernatants were collected and analyzed using an ELISA kit designed to detect the extracellular domain of IL1R2. With

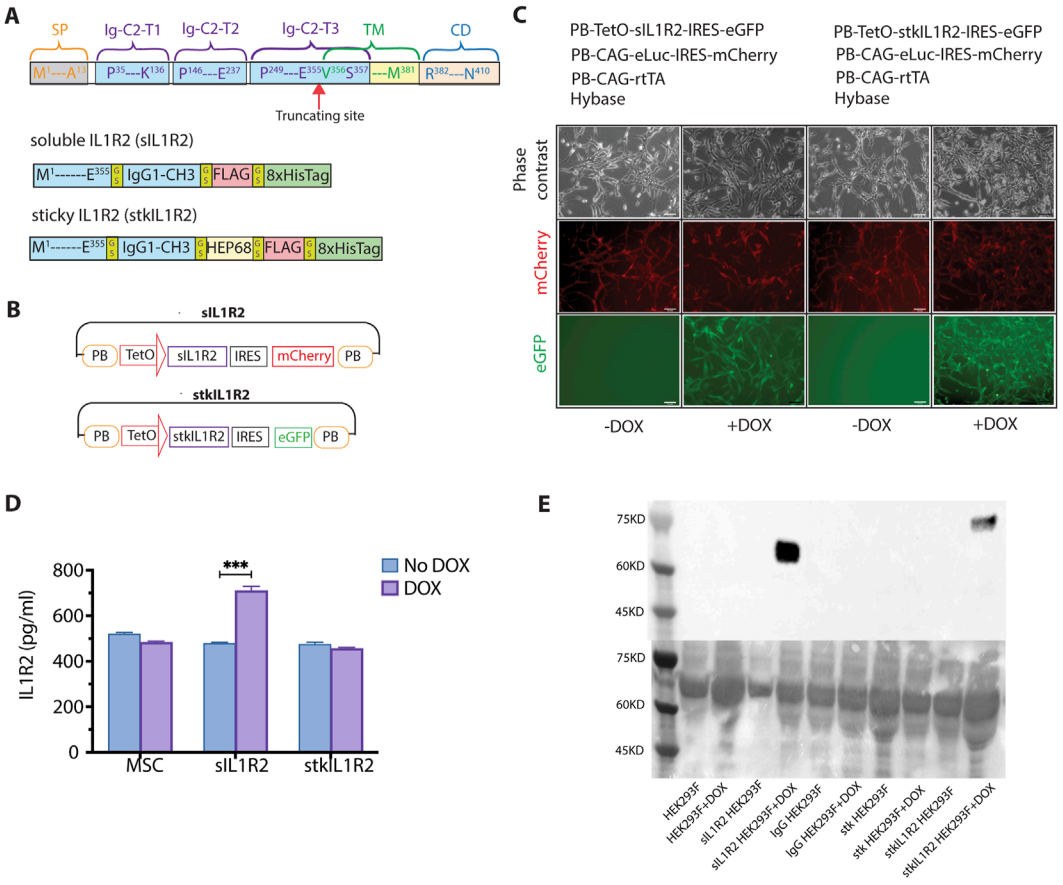

FIGURE 3
The generation of sticky IL-1 receptor 2 (stkILR2) biologics and stable expression cell lines. **(A)** The strategy and the primary components of ILR2, sIL1R2 and stkIL1R2; **(B)** The expression plasmids of sIL1R2 and stkIL1R2 based on PB transposon system, which included a TetO operator; **(C)** sIL1R2 and stkIL1R2 plasmids were transfected into MSCs, the expression of sIL1R2 and stkIL1R2 were under the control of Dox (magnification ×5); **(D)** In the presence of Dox, there was a significant increase of sIL1R2 in the supernatant quantified by ELISA (No Dox vs. Dox, $p < 0.001$, $n = 3$), while there was significant expression of stkIL1R2 in the supernatant; **(E)** Forced expression of sIL1R2 and stkIL1R2 in HEK293 cells detected by Western blot assay, the protein samples were from the supernatants in the presence of Dox. Data are expressed as mean ± SEM, $^{***}p < 0.001$.

Dox induction, ELISA detected the expression of sIL1R2 in the engineered MSC supernatant and did not detect the expression of stkIL1R2 in the supernatant (Figure 3D).

As we did not detect the expression of stkIL1R2 in the transgenic MSC supernatant (Figure 3D), and we wanted to confirm the presence of stkIL1R2 protein, we resorted to the protein generation platform HEK293 cells. sIL1R2 and stkIL1R2 expression plasmids were transfected into the HEK293F protein production cell line to force the production of proteins. IgG and stk plasmids were used and served as controls. The collected supernatants were analyzed by Western blot to detect the protein forms (Figure 3E). We can see there were clear protein expression of sIL1R2 and stkIL1r2 proteins, which means our transgenes did generate proteins.

3.3 *In vitro* functional test of stkIL1R2

To visualize the binding ability of stkIL1R2 with IL-1β and demonstrate that stkIL1R2 protein adheres to the cell surface and ECM, we developed a novel binding test platform. First, we generated a fusion protein IL-1β-GFP gene expression plasmid (PB-CAG-IL-1β-GFP-IRES-puro-PB) and an inducible fusion protein stkIL1R2-mCherry gene expression plasmid (PB-TetO-stkIL1R2-mCherry-IRES-puro-PB) (Figure 4A).

Both plasmids were transfected into MSCs, and after puromycin selection, most MSCs expressed the target proteins. Interestingly, the IL-1β-GFP protein exhibited an even distribution of GFP signal within the cells (Figure 4B), whereas the stkIL1R2-mCherry protein displayed an entirely different distribution pattern. It appeared as variably sized dots randomly scattered throughout the cell surface and ECM (Figure 4C).

To produce IL-1β-GFP fusion protein, the IL-1β-GFP plasmid was transfected into HEK293F cells, and the IL-1β-GFP fusion protein was isolated from the supernatant. Functionally, the IL-1β-GFP fusion protein was comparable to commercial IL-1β in inducing LCN2 expression in MSCs (Figure 4D). Subsequently, the stkIL1R2-mCherry plasmid was transfected into both HEK293F cells and MSCs (Figure 4E). Following Dox induction, stkIL1R2-mCherry expression appeared as random nuclear and cytoplasmic dots in the cells. The cells were fixed without permeabilization

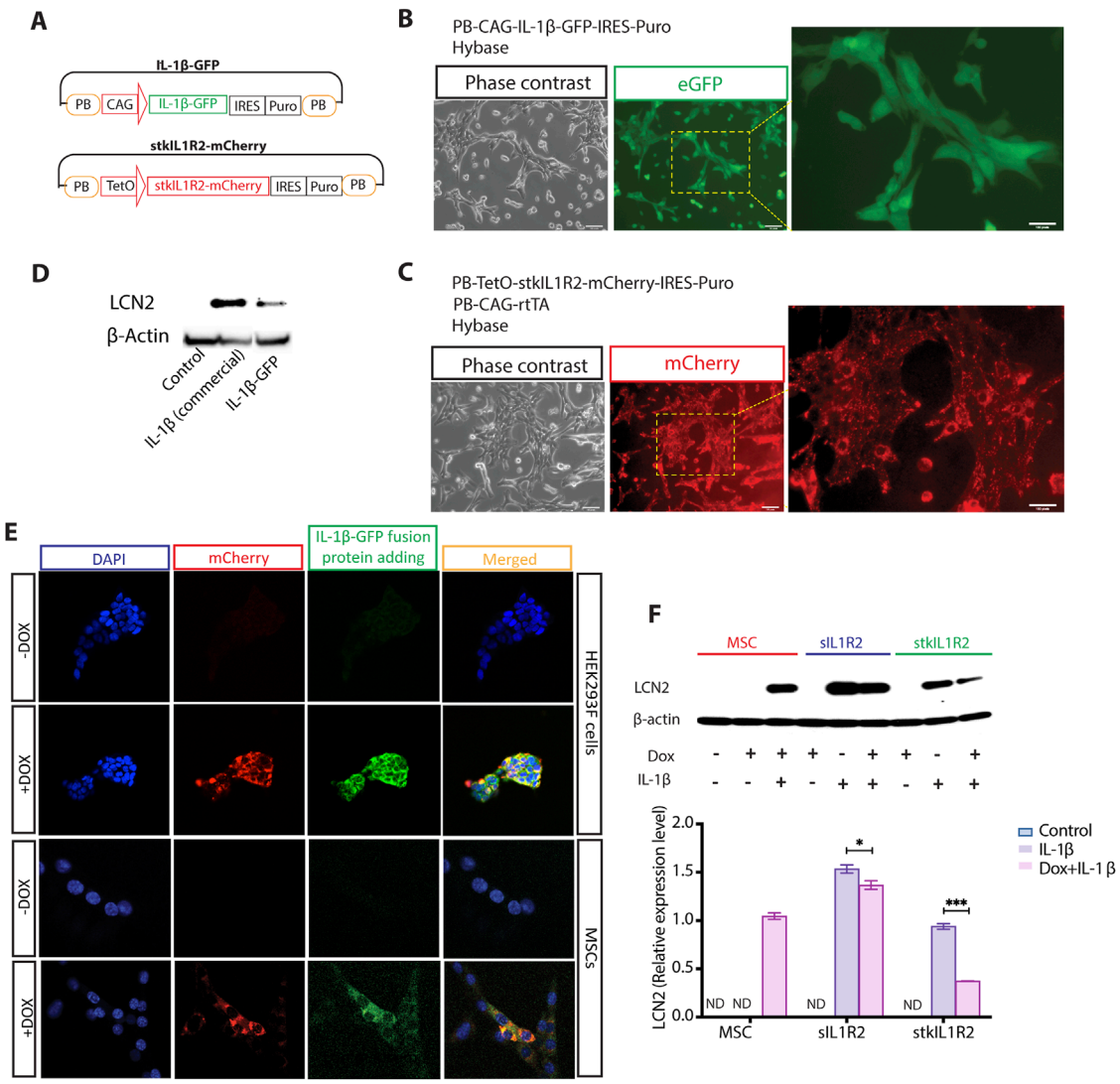

FIGURE 4
In vitro functional test of stkIL1R2. **(A)** The components of IL-1β-GFP fusion protein gene and stkIL1R2-mCherry fusion protein gene expression plasmids based on PB transposon system; **(B)** The expression of IL-1β-GFP fusion protein in MSCs, which showed an evenly distribution in the cytoplasm (magnification ×10); **(C)** The expression stkIL1R2-mCherry fusion protein in MSCs looked like clumps in the cells, which was obviously different from the expression pattern of IL-1β-GFP fusion protein (magnification ×10); **(D)** The home-made IL-1β-GFP fusion protein had similar function the commercial IL-1β in inducing LCN2 expression, which is a specific biomarker of IL-1β; **(E)** stkIL1R2-mCherry fusion gene transfected HEK293F cells and MSCs were plated on slides with and without Dox respectively, cells were fixed without perforated regents, then IL-1β-GFP fusion protein were added to each, then washed out with PBS, the binding of IL-1β-GFP fusion protein on the cell membrane and co-localized with mCherry signal clearly demonstrated that stkIL1R2 was on the cell membrane and ECM (magnification ×5); **(F)** Western blotting of IL-1β biomarker LCN2 expression in MSCs showed that both sIL1R2 and stkIL1R2 significantly blocked the function of 100 pg/mL of IL-1β (For sIL1R2, Dox + vs. Dox-, $p = 0.0198$, $n = 3$; For stkIL1R2, Dox + vs. Dox-, $p = 0.0004$, $n = 3$). Data are expressed as mean ± SEM,*$p < 0.05$;***$p < 0.001$.

reagents, and purified IL-1β-GFP fusion protein was added to the surface of fixed cells. In the absence of Dox induction, there was little to none binding of IL-1β-GFP fusion protein to the cells. However, when Dox was present, there was significant binding of IL-1β-GFP fusion protein to the cells, with GFP signals co-localizing strongly with mCherry signals. This strategy clearly demonstrated that stkIL1R2 adhered to the cell membrane and extracellular matrix (ECM) and effectively bound to IL-1β.

To further confirm the binding ability and function of stkIL1R2, we evaluated the response of stkIL1R2-transfected MSCs to IL-1β stimulation. Unstimulated MSCs and Dox added MSC were served as negative controls, while MSCs stimulated with 100 pg/mL of IL-1β served as positive controls. For both sIL1R2 and stkIL1R2, IL-1β induced a notable expression of LCN2 compared to positive control, while under the induction of Dox, sIL1R2 expression significantly reduced the expression of LCN2 induced by IL-1β (No Dox vs. Dox, $p < 0.05$, $n = 3$); Dox induced expression of stkIL1R2 also significantly reduced the expression of LCN2 induced by IL-1b (No Dox vs. Dox, $p < 0.001$, $n = 3$) (Figure 4F).

3.4 *In vivo* evaluation of stkIL1R2

To examine the efficiency of the stkIL1R2 trap in slowing the progression of OA, we utilized the destabilization of the murine DMM model, a well-established post-traumatic OA (PTOA) model. The study groups were as follows: 1) Sham + PBS + Dox; 2) Sham + MSC + Dox; 3) Sham + stkIL1R2 MSC–Dox; 4) Sham + stkIL1R2 MSC + Dox; 5) DMM + PBS + Dox; 6) DMM + MSC + Dox; 7) DMM + stkIL1R2 MSC–Dox; 8) DMM + stkIL1R2 MSC + Dox. One week after surgery, phosphate-buffered saline (PBS), 5×10^4 MSCs, or stkIL1R2 expressing MSCs were injected intra-articular into the right knees of mice. Dox chow was administered to the Dox + groups. At 10 weeks post-surgery, all mice were sacrificed, and their knees were collected for analysis (Figure 5A).

BLI of luminescent signals from luciferin-luciferase reaction in groups 3, 4, 7, and 8 was monitored for up to 7 weeks (Figure 5B). Representative images of safranin-O-stained sections from sham-only and DMM-only groups were analyzed (Supplementary Figure S1). Compared to sham-only sections (Supplementary Figures 1A1–5), DMM-only sections (Supplementary Figures 1B1–5) exhibited loss of safranin-O staining, cartilage erosion, vertical clefts, and lesions extending to the calcified layer, affecting 25%–50% of the articular cartilage. Moderate to severe synovitis was also observed (Supplementary Figures 1B1–4). OARSI scoring for the femur, tibia, and synovium confirmed that the DMM-only group had significantly higher scores for OA damage and synovitis compared to the sham-only group (Supplementary Figures 1C–E), validating the OA changes induced in the DMM group.

Next, we assessed the efficacy of the stkIL1R2 trap in slowing OA progression in the DMM model. No significant differences were observed in the severity of cartilage degeneration or synovitis among the sham groups (Figures 5C,D, Sham), which was confirmed by the quantification using OARSI score (Figures 5E–G, Sham). On the other side, in both of the femur and tibia of DMM groups (Figures 5E,F, 5DMM), DMM + stkIL1R2 MSC + Dox significantly attenuated DMM-induced cartilage degeneration as quantified by OARSI scoring, compared to the DMM + stkIL1R2 MSC–Dox and DMM + MSC + Dox groups. Synovitis was also significantly reduced in the DMM + stkIL1R2 MSC + Dox group compared to all other DMM groups (Figures 5G,DMM).

To confirm the effectiveness of our new biologics in OA treatment, we evaluated cartilage breakdown markers: MMP-13 and collagen type I/II cleavage neoepitope (C1,2C). Immunohistochemical stained sections for MMP-13 (Figures 5H,I) and C1,2C (Figure 5J) showed a significant decrease in the percentage of MMP-13-positive cells and C1,2C expression in the DMM + stkIL1R2 MSC + Dox group compared to the DMM + stkIL1R2 MSC–Dox and DMM + MSC + Dox groups.

4 Discussion

In this study, we developed an inducible, locally acting IL-1β sticky-trap (stkIL1R2) plasmid based on the PiggyBac transposon system and transfected it into murine MSCs derived from compact bone. This approach established a cell-based gene expression therapeutic platform, which was tested for its efficacy using the murine DMM model. Our findings demonstrated that the IL-1β sticky-trap effectively delayed OA progression and reduced synovitis in the DMM model.

OA is increasingly recognized as a low-grade inflammatory whole-joint disease, with innate immunity playing a central role in its inflammatory pathology (Knights et al., 2023; Robinson et al., 2016; Roover et al., 2023; Scanzello, 2017b). Among pro-inflammatory cytokines, IL-1β has been well-documented to contribute to OA pathogenesis (Krenytska et al., 2023; Panina et al., 2017; Wang et al., 2019). However, anti-IL-1 strategies have produced inconsistent results. Given that IL-1β is a small molecule with activity in the picogram range (Gentile et al., 2013) and a short serum half-life, these challenges are likely due to spatial and temporal mismatches between IL-1β activity and the administered therapeutic agents (Kudo et al., 1990; REIMERS et al., 1991). To overcome this limitation, we employed a cell-based, locally expressed sticky biologics technology, generating MSCs that inducibly express stkIL1R2 biologics.

IL-1R2 is a decoy receptor with high binding affinity for both interleukin-1alpha (IL-1α) and IL-1β, surpassing that of IL-1 receptor type 1 (IL-1R1) (Mantovani et al., 1998). We harnessed this strong binding capacity, integrating IL-1R2 with the sticky-trap technology previously developed in our lab (Michael et al., 2014) to create the novel biologic stkIL1R2. This construct was introduced into compact bone-derived MSCs via an inducible expression plasmid. Fluorescent protein tagging confirmed that stkIL1R2 was expressed on the cell membrane and could bind IL-1β. Functional assays further demonstrated that MSCs expressing stkIL1R2 effectively blocked 50 pg/mL of IL-1β induced LCN2 expression.

To assess the therapeutic efficacy of stkIL1R2, we utilized the classical surgical OA model through the DMM, which mimics PTOA. In this model, transection of the medial meniscotibial ligament destabilizes the medial meniscus, leading to cartilage damage and subsequent OA (Glasson et al., 2007). At 10 weeks post-surgery, histological analysis of DMM joints revealed three key pathological changes: loss of cartilage integrity between the femur and tibia, thinning of subchondral bone, and significant inflammatory cell infiltration at the joint periphery. These findings were quantified using OARSI scores for the femur, tibia, and synovium, confirming the successful induction of moderate to severe OA, consistent with previous studies (Glasson et al., 2010).

In this study, we administered 5×10^4 MSCs per injection into the murine knee joint. The survival of injected cells was monitored via BLI, revealing cell viability for up to 7 weeks. Histological analyses at 10 weeks post-surgery showed that the IL-1β sticky trap significantly reduced joint OA and synovitis compared to sham and other DMM control groups. These findings were corroborated by decreased expression of cartilage breakdown markers MMP-13 and collagen cleavage neoepitope C1,2C in the stkIL1R2 treated groups.

Despite these promising results, the study has some limitations. First, the compact bone-derived MSCs used were sorted in bulk, resulting in a heterogeneous cell population with variable reproducibility and biologic productivity. Second, the luciferase-luciferin tracking system has its limitations for monitoring injected cells in the knee joints as luciferin delivery to the cells may be low due to post traumatic changes to the knee joint and limited blood supply to the joint cavity, cartilage and parts of the meniscus. Also, the strength of the luminescence may need to be a stronger luciferase

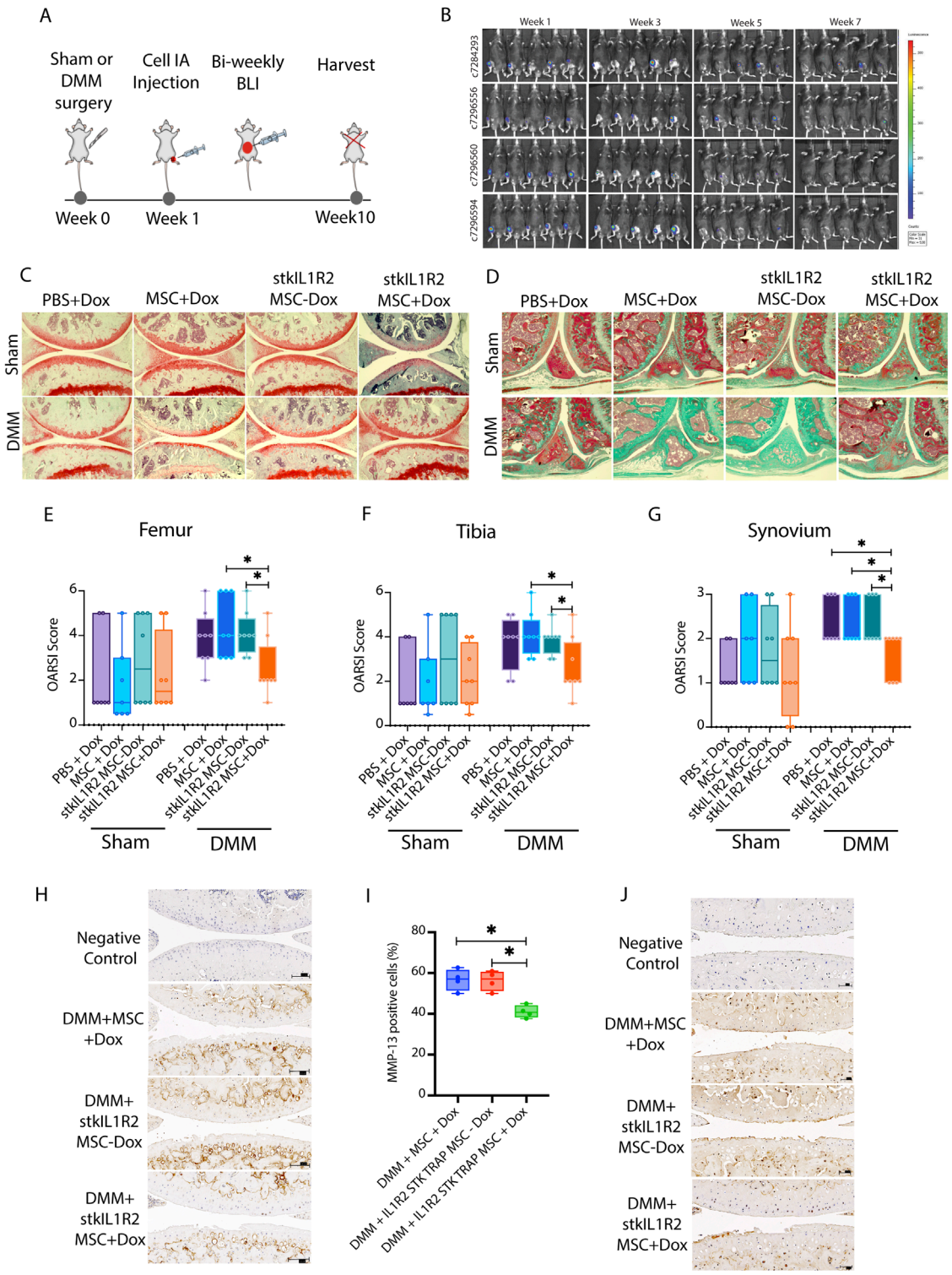

FIGURE 5
MSC expressed stkIL1R2 attenuated the progression of OA in DMM. **(A)** The study design of *in vivo* test of stkIL-1R2; **(B)** The BLI monitoring results from stkIL-1R2 expression MSCs injected into the joint cavities; **(C)** The histological results of femur and tibia from Sham and DMM groups after 10 weeks (magnification ×10); **(D)** The histological results of synovium from Sham and DMM groups after 10 weeks (magnification ×10); **(E)** Quantification of the pathological changes by OARSI score on femur, stkIL1R2 expression significantly reduced the OARSI scores in femur from DMM group (stkIL1R2 MSC + Dox vs. MSC + Dox and stkIL1R2 MSC-Dox, $p < 0.05$, n = 8 for each); **(F)** Quantification of the pathological changes by OARSI score on tibia, stkIL1R2 expression significantly reduced the OARSI scores in tibia from DMM group (stkIL1R2 MSC + Dox vs. MSC + Dox and stkIL1R2 MSC-Dox, $p < 0.05$, n = 8 for each); **(G)** Quantification of the pathological changes by OARSI score on synovium, stkIL1R2 expression significantly reduced the OARSI score in synovium (stkIL1R2 MSC + Dox vs. PBS + Dox, MSC + Dox and stkIL1R2 MSC-Dox respectively, $p < 0.05$, n = 8 for each); **(H)** IHC staining of the expression of MMP-13 on femur and tibia (magnification ×10); **(I)** Quantification of MMP-13 expression cells on both femur and tibia of DMM groups, stkIL1R2 significantly reduced the expression of MMP-13 (stkIL1R2 MSC + Dox vs. MSC + Dox and stkIL1R2 MSC-Dox, $p < 0.05$, n = 4 for each); **(J)** IHC staining of C1,C2 expression on femur and tibia of DMM groups (magnification ×10). Data are expressed as mean ± SDM,*$p < 0.05$. IA: Intraarticular.

variant to detect and improve cell tracking in the knee joint. Lastly, the efficacy of stkIL1R2 was evaluated using a PTOA model, which may not fully represent other forms of OA. Future studies should explore its performance in chemically induced OA models or other relevant systems.

In conclusion, this study developed a novel, locally acting IL-1β sticky-trap (stkIL1R2) expressed in compact bone-derived MSCs. We demonstrated its binding ability to IL-1β and its therapeutic efficacy in preventing OA progression using the murine DMM model. The stkIL1R2 biologic shows strong potential as a stand-alone treatment or in combination with other therapeutic strategies for OA. These findings provide a foundation for new approaches to combat OA.

Data availability statement

The raw data supporting the conclusions of this article will be made available by the authors, without undue reservation.

Ethics statement

The animal study was approved by the Institutional Animal Care and Use Committee of The Toronto Phenogenomics (TCP, Toronto). The study was conducted in accordance with the local legislation and institutional requirements.

Author contributions

CK: Conceptualization, Data curation, Formal Analysis, Investigation, Methodology, Project administration, Resources, Software, Validation, Visualization, Writing – original draft, Writing – review and editing. BL: Conceptualization, Data curation, Formal Analysis, Investigation, Methodology, Project administration, Resources, Software, Validation, Visualization, Writing – original draft, Writing – review and editing. SN: Methodology, Writing – review and editing. EN: Data curation, Writing – review and editing. JR: Data curation, Methodology, Writing – review and editing. TO: Data curation, Methodology, Writing – review and editing. PZ: Data curation, Writing – review and editing. MK: Methodology, Supervision, Writing – review and editing. AN: Conceptualization, Funding acquisition, Project administration, Supervision, Writing – review and editing.

Funding

The author(s) declare that financial support was received for the research and/or publication of this article. This research received support from the Canadian Institute of Health Research Foundation Grant (143231), Canada Research Chairs Program Stem cells and Regeneration Tier 1, Ontario Research Fund - Research Excellence Round 11-ORF-RE011-066 to AN.

Acknowledgments

We thank, Annie Bang for her assistance with MSC FACS sorting. We thank, You Li, MD candidate on creating Figure 5A and writing review and editing.

Conflict of interest

The authors declare that the research was conducted in the absence of any commercial or financial relationships that could be construed as a potential conflict of interest.

Generative AI statement

The author(s) declare that no Gen AI was used in the creation of this manuscript.

Publisher's note

All claims expressed in this article are solely those of the authors and do not necessarily represent those of their affiliated organizations, or those of the publisher, the editors and the reviewers. Any product that may be evaluated in this article, or claim that may be made by its manufacturer, is not guaranteed or endorsed by the publisher.

Supplementary material

The Supplementary Material for this article can be found online at: https://www.frontiersin.org/articles/10.3389/fcell.2025.1559155/full#supplementary-material

SUPPLEMENTARY FIGURE S1
Generation of murine DMM OA model. **(A)** Sham mouse joint histology, 1–4 are 4 corners of the joint to show synovial membranes, 5 is the Zoom in figure of femur and tibia; **(B)** DMM mouse joint histology, 1–4 are 4 corners of the joint to show synovial membranes, 5 is the Zoom in figure of femur and tibia; **(C)** OARSI score was used to evaluate the histological changes after 10 weeks of surgery, DMM group OARSI score of femur was significantly higher than Sham groups (Sham vs. DMM, $p < 0.05$, n = 6,5); **(D)** DMM group OARSI score of tibia was significantly higher than Sham groups (Sham vs. DMM, $p < 0.05$, n = 6,5); **(E)** DMM group OARSI score of synovial membrane was significantly higher than Sham groups (Sham vs. DMM, $p < 0.05$, n = 6,5). Data are expressed as mean ± SEM, $^{*}p < 0.05$; $^{**}p < 0.01$; $^{***}p < 0.001$.

References

Bosch, M. H. J. van den, Blom, A. B., and Kraan, P. M. van der. (2024). Inflammation in osteoarthritis: our view on its presence and involvement in disease development over the years. *Osteoarthr. Cartil.* 32, 355–364. doi:10.1016/j.joca.2023.12.005

Chevalier, X., Eymard, F., and Richette, P. (2013). Biologic agents in osteoarthritis: hopes and disappointments. *Nat. Rev. Rheumatol.* 9, 400–410. doi:10.1038/nrrheum.2013.44

Chevalier, X., Goupille, P., Beaulieu, A. D., Burch, F. X., Bensen, W. G., Conrozier, T., et al. (2009). Intraarticular injection of anakinra in osteoarthritis of the knee: a multicenter, randomized, double-blind, placebo-controlled study. *Arthritis Rheumatism* 61, 344–352. doi:10.1002/art.24096

Chou, C.-H., Jain, V., Gibson, J., Attarian, D. E., Haraden, C. A., Yohn, C. B., et al. (2020). Synovial cell cross-talk with cartilage plays a major role in the pathogenesis of osteoarthritis. *Sci. Rep.* 10 (1), 10868. doi:10.1038/s41598-020-67730-y

Cohen, S. B., Proudman, S., Kivitz, A. J., Burch, F. X., Donohue, J. P., Burstein, D., et al. (2011). A randomized, double-blind study of AMG 108 (a fully human monoclonal antibody to IL-1R1) in patients with osteoarthritis of the knee. *Arthritis Res. and Ther.* 13 (4), R125. doi:10.1186/ar3430

Das, A. T., Tenenbaum, L., and Berkhout, B. (2016). Tet-On Systems For Doxycycline-inducible Gene Expression. *Current Gene Therapy* 16 (3), 156–167. doi:10.2174/1566523216666160524144041

Fleischmann, R. M., Bliddal, H., Blanco, F. J., Schnitzer, T. J., Peterfy, C., Chen, S., et al. (2019). A phase II trial of lutikizumab, an anti–interleukin-1α/β dual variable domain immunoglobulin, in knee osteoarthritis patients with synovitis. *Arthritis and Rheumatology* 71 (7), 1056–1069. doi:10.1002/art.40840

Gentile, L. F., Cuenca, A. G., Vanzant, E. L., Efron, P. A., McKinley, B., Moore, F., et al. (2013). Is there value in plasma cytokine measurements in patients with severe trauma and sepsis? *Methods* 61, 3–9. doi:10.1016/j.ymeth.2013.04.024

Glasson, S. S., Blanchet, T. J., and Morris, E. A. (2007). The surgical destabilization of the medial meniscus (DMM) model of osteoarthritis in the 129/SvEv mouse. *Osteoarthr. Cartil.* 15 (9), 1061–1069. doi:10.1016/j.joca.2007.03.006

Glasson, S. S., Chambers, M. G., Berg, W. B. V. D., and Little, C. B. (2010). The OARSI histopathology initiative – recommendations for histological assessments of osteoarthritis in the mouse. *Osteoarthr. Cartil.* 18, S17–S23. doi:10.1016/j.joca.2010.05.025

Hamasaki, M., Terkawi, M. A., Onodera, T., Homan, K., and Iwasaki, N. (2021). A novel cartilage fragments stimulation model revealed that macrophage inflammatory response causes an upregulation of catabolic factors of chondrocytes *in vitro*. *CARTILAGE* 12 (3), 354–361. doi:10.1177/1947603519828426

Harrell, C. R., Markovic, B. S., Fellabaum, C., Arsenijevic, A., and Volarevic, V. (2019). Mesenchymal stem cell-based therapy of osteoarthritis: current knowledge and future perspectives. *Biomed. and Pharmacother.* 109, 2318–2326. doi:10.1016/j.biopha.2018.11.099

Hoseini, Z., Sepahvand, F., Rashidi, B., Sahebkar, A., Masoudifar, A., and Mirzaei, H. (2018). NLRP3 inflammasome: its regulation and involvement in atherosclerosis. *J. Cell. Physiology* 233 (3), 2116–2132. doi:10.1002/jcp.25930

Hunter, D. J., Schofield, D., and Callander, E. (2014). The individual and socioeconomic impact of osteoarthritis. *Nat. Rev. Rheumatol.* 10 (7), 437–441. doi:10.1038/nrrheum.2014.44

Im, H., and Ammit, A. J. (2014). The NLRP3 inflammasome: role in airway inflammation. *Clin. and Exp. Allergy* 44 (2), 160–172. doi:10.1111/cea.12206

Keyel, P. A. (2014). How is inflammation initiated? Individual influences of IL-1, IL-18 and HMGB1. *Cytokine* 69, 136–145. doi:10.1016/j.cyto.2014.03.007

Kloppenburg, M., Peterfy, C., Haugen, I. K., Kroon, F., Chen, S., Wang, L., et al. (2019). Phase IIa, placebo-controlled, randomised study of lutikizumab, an anti-interleukin-1α and anti-interleukin-1β dual variable domain immunoglobulin, in patients with erosive hand osteoarthritis. *Ann. Rheumatic Dis.* 78 (3), 413–420. doi:10.1136/annrheumdis-2018-213336

Kloppenburg, M., Ramonda, R., Bobacz, K., Kwok, W.-Y., Elewaut, D., Huizinga, T. W. J., et al. (2018). Etanercept in patients with inflammatory hand osteoarthritis (EHOA): a multicentre, randomised, double-blind, placebo-controlled trial. *Ann. Rheumatic Dis.* 77, 1757–1764. doi:10.1136/annrheumdis-2018-213202

Knights, A. J., Redding, S. J., and Maerz, T. (2023). Inflammation in osteoarthritis: the latest progress and ongoing challenges. *Curr. Opin. Rheumatology* 35 (2), 128–134. doi:10.1097/bor.0000000000000923

Krenytska, D., Strubchevska, K., Kozyk, M., Vovk, T., Halenova, T., Kot, L., et al. (2023). Circulating levels of inflammatory cytokines and angiogenesis-related growth factors in patients with osteoarthritis after COVID-19. *Front. Med.* 10, 1168487. doi:10.3389/fmed.2023.1168487

Kudo, S., Mizuno, K., Hirai, Y., and Shimizu, T. (1990). Clearance and tissue distribution of recombinant human interleukin 1 beta in rats. *Cancer Res.* 50, 5751–5755.

Mantovani, A., Muzio, M., Ghezzi, P., Colotta, C., and Introna, M. (1998). Regulation of inhibitory pathways of the interleukin-1 system. *Ann. N. Y. Acad. Sci.* 840, 338–351. doi:10.1111/j.1749-6632.1998.tb09573.x

Michael, I. P., Westenskow, P. D., Hacibekiroglu, S., Greenwald, A. C., Ballios, B. G., Kurihara, T., et al. (2014). Local acting Sticky-trap inhibits vascular endothelial growth factor dependent pathological angiogenesis in the eye. *EMBO Mol. Med.* 6 (5), 604–623. doi:10.1002/emmm.201303708

Morikawa, S., Mabuchi, Y., Kubota, Y., Nagai, Y., Niibe, K., Hiratsu, E., et al. (2009). Prospective identification, isolation, and systemic transplantation of multipotent mesenchymal stem cells in murine bone marrow. *J. Exp. Med.* 206 (11), 2483–2496. doi:10.1084/jem.20091046

Panina, S. B., Krolevets, I. V., Milyutina, N. P., Sagakyants, A. B., Kornienko, I. V., Ananyan, A. A., et al. (2017). Circulating levels of proinflammatory mediators as potential biomarkers of post-traumatic knee osteoarthritis development. *J. Orthop. Traumatology* 18 (4), 349–357. doi:10.1007/s10195-017-0473-8

Pelletier, J. P., Martel-Pelletier, J., and Abramson, S. B. (2001). Osteoarthritis, an inflammatory disease: potential implication for the selection of new therapeutic targets. *Arthritis Rheumatism* 44, 1237–1247. doi:10.1002/1529-0131(200106)44:6<1237::aid-art214>3.0.co;2-f

Pittenger, M. F., Mackay, A. M., Beck, S. C., Jaiswal, R. K., Douglas, R., Mosca, J. D., et al. (1999). Multilineage potential of adult human mesenchymal stem cells. *Science* 284 (5411), 143–147. doi:10.1126/science.284.5411.143

Reimers, J., Wogensen, L. D., Nerup, J., Hejnæs, K. R., Poulsen, S. S., Nilsson, P., et al. (1991). The pharmacokinetics, distribution and degradation of human recombinant interleukin 1β in normal rats. *Scand. J. Immunol.* 34, 597–617. doi:10.1111/j.1365-3083.1991.tb01583.x

Ridker, P. M., Everett, B. M., Thuren, T., MacFadyen, J. G., Chang, W. H., Ballantyne, C., et al. (2017). Antiinflammatory therapy with Canakinumab for atherosclerotic disease. *N. Engl. J. Med.* 377 (12), 1119–1131. doi:10.1056/nejmoa1707914

Robinson, W. H., Lepus, C. M., Wang, Q., Raghu, H., Mao, R., Lindstrom, T. M., et al. (2016). Low-grade inflammation as a key mediator of the pathogenesis of osteoarthritis. *Nat. Rev. Rheumatol.* 12 (10), 580–592. doi:10.1038/nrrheum.2016.136

Roover, A. D., Escribano-Núñez, A., Monteagudo, S., and Lories, R. (2023). Fundamentals of osteoarthritis: inflammatory mediators in osteoarthritis. *Osteoarthr. Cartil.* 31 (10), 1303–1311. doi:10.1016/j.joca.2023.06.005

Sanchez-Lopez, E., Coras, R., Torres, A., Lane, N. E., and Guma, M. (2022). Synovial inflammation in osteoarthritis progression. *Nat. Rev. Rheumatol.* 18 (5), 258–275. doi:10.1038/s41584-022-00749-9

Scanzello, C. R. (2017a). Chemokines and inflammation in osteoarthritis: insights from patients and animal models. *J. Orthop. Res.* 35 (4), 735–739. doi:10.1002/jor.23471

Scanzello, C. R. (2017b). Role of low-grade inflammation in osteoarthritis. *Curr. Opin. Rheumatology* 29 (1), 79–85. doi:10.1097/bor.0000000000000353

Scanzello, C. R., and Goldring, S. R. (2012). The role of synovitis in osteoarthritis pathogenesis. *Bone* 51 (2), 249–257. doi:10.1016/j.bone.2012.02.012

Schieker, M., Conaghan, P. G., Mindeholm, L., Praestgaard, J., Solomon, D. H., Scotti, C., et al. (2020). Effects of interleukin-1β inhibition on incident hip and knee replacement: exploratory analyses from a randomized, double-blind, placebo-controlled trial. *Ann. Intern. Med.* 173 (7), 509–515. doi:10.7326/m20-0527

Schmittgen, T. D., and Livak, K. J. (2008). Analyzing real-time PCR data by the comparative C(T) method. *Nat. Protoc.* 3 (6), 1101–1108. doi:10.1038/nprot.2008.73

Wang, Z.-W., Chen, L., Hao, X.-R., Qu, Z.-A., Huang, S.-B., Ma, X.-J., et al. (2019). Elevated levels of interleukin-1β, interleukin-6, tumor necrosis factor-α and vascular endothelial growth factor in patients with knee articular cartilage injury. *World J. Clin. Cases* 7, 1262–1269. doi:10.12998/wjcc.v7.i11.1262

Zhu, H., Guo, Z.-K., Jiang, X.-X., Li, H., Wang, X.-Y., Yao, H.-Y., et al. (2010). A protocol for isolation and culture of mesenchymal stem cells from mouse compact bone. *Nat. Protoc.* 5 (3), 550–560. doi:10.1038/nprot.2009.238

frontiers | Frontiers in Cell and Developmental Biology

TYPE Original Research
PUBLISHED 13 May 2025
DOI 10.3389/fcell.2025.1582083

Check for updates

OPEN ACCESS

EDITED BY
Csaba Matta,
University of Debrecen, Hungary

REVIEWED BY
Marco Tatullo,
University of Bari Medical School, Italy
Kursad Turksen,
Independent Researcher, United States

*CORRESPONDENCE
Francesco De Francesco,
francesco.defrancesco@ospedaliriuniti.marche.it

‡These authors have contributed equally to this work and share first authorship

§These authors share senior authorship

RECEIVED 23 February 2025
ACCEPTED 14 April 2025
PUBLISHED 13 May 2025

CITATION
Ossanna R, Quintero Sierra LA, Ghazanfar Tehrani S, Jha V, Curatola C, Busato A, Conti A, Conti G, Zingaretti N, Parodi PC, De Francesco F, Riccio M and Sbarbati A (2025) Revolutionizing bone regeneration and wound healing: Mechanical stromal vascular fraction and hyaluronic acid in a mouse calvarial defect model.
Front. Cell Dev. Biol. 13:1582083.
doi: 10.3389/fcell.2025.1582083

COPYRIGHT
© 2025 Ossanna, Quintero Sierra, Ghazanfar Tehrani, Jha, Curatola, Busato, Conti, Conti, Zingaretti, Parodi, De Francesco, Riccio and Sbarbati. This is an open-access article distributed under the terms of the Creative Commons Attribution License (CC BY). The use, distribution or reproduction in other forums is permitted, provided the original author(s) and the copyright owner(s) are credited and that the original publication in this journal is cited, in accordance with accepted academic practice. No use, distribution or reproduction is permitted which does not comply with these terms.

Revolutionizing bone regeneration and wound healing: Mechanical stromal vascular fraction and hyaluronic acid in a mouse calvarial defect model

Riccardo Ossanna[1‡], Lindsey Alejandra Quintero Sierra[1‡], Sara Ghazanfar Tehrani[1‡], Vivekanand Jha[1], Chiara Curatola[1], Alice Busato[2], Anita Conti[1], Giamaica Conti[1], Nicola Zingaretti[3], Pier Camillo Parodi[3], Francesco De Francesco[4*§], Michele Riccio[4§] and Andrea Sbarbati[1§]

[1]Department of Neuroscience, Biomedicine, and Movement, Section of Anatomy and Histology, University of Verona, Verona, Italy, [2]Aptuit and Evotec Company, Safety and Assessment Department, Verona, Italy, [3]Clinic of Plastic and Reconstructive Surgery, Academic Hospital of Udine, Department of Medical Area (DAME), University of Udine, Udine, Italy, [4]Department of General and Specialties Surgery, SOD of Reconstructive Surgery and Hand Surgery, Azienda Ospedaliera Universitaria Delle Marche, Ancona, Italy

Introduction: The stromal vascular fraction (SVF) is a complex and heterogeneous suspension derived from adipose tissue, containing both cellular and noncellular components. Its cellular fraction includes adipose-derived stem cells (ASCs), endothelial precursor cells, pericytes, macrophages, lymphocytes, and smooth muscle cells. The acellular "secretome" of SVF includes bioactive molecules such as growth factors, cytokines, chemokines, extracellular vesicles, and fragments of extracellular matrix (ECM), which contribute to its regenerative potential. Bone defeatures can be stimulated by mesenchymal stem cells (MSCs) that differentiate into osteoblast to support the healing and repair process. In addition to its cell content, the SVF is rich in growth factors, cytokines and chemokines, extracellular vesicles, and extracellular matrix components, which could stimulate regenerative processes through a trophic effect. Studies showed that hyaluronic acids are usually involved in healing processes. This study was focused on the healing potency of stromal stem cells isolated from adipose tissues by mechanical digestion, and the role of low-molecular-weight hyaluronic acid (LMW-HA, ACP) in the healing process was tested in calvarial defeatures in a mouse model, in comparison with the enzymatic digestion method.

Methods: The bone healing and remodeling process was evaluated *in vivo* using magnetic resonance imaging (MRI) up to 15 days post-treatment, and differences in the quality of bone regeneration were assessed by *ex vivo* histological analysis, immunofluorescences, and ultrastructural analysis. The bone matrix formed after treatment with mechanically digested

Hy tissue stromal vascular fraction + hyaluronic acid (HT-SVF + ACP) was compared to that formed with enzymatically digested stromal vascular fraction + hyaluronic acid (ED-SVF + ACP), with the saline group serving as the control group.

Results: In this study, we explore a groundbreaking approach using HT-SVF combined with ACP to promote bone regeneration. Through comparative analysis with ED-SVF in a calvarial defect mouse model, we demonstrate the superior efficacy of HT-SVF + ACP in enhancing bone healing, reducing fibrotic tissue, and improving bone matrix maturity.

Discussion: The findings establish the potential of HT-SVF as a cost-effective and efficient method for bone regenerative therapy.

KEYWORDS

bone repair, stromal vascular fraction, calvarial bone defects, hyaluronic acid, adipose-derived stem cell

Introduction

Bone is a dynamic tissue with a highly vascularized dense structure that enables its unique capacity to leave no scars after the healing and remodeling processes (Simunovic and Finkenzeller, 2021). The stress and biological environment are relevant to bone function and structure formation (Rubin et al., 2001). New bone development is thought to occur under low oxygen tension (Brighton and Krebs, 1972), allowing the expression of specific genes that increase cell survival under hypoxic conditions and re-establish the vasculature for oxygen delivery (Semenza, 2000). In addition, hypoxia induces the production of chemotactic factors implicated in cell migration, differentiation, and new bone formation.

During the natural healing process of bone, the reparative cascade is activated. Platelets, inflammatory cells, and stem cells arrive at the site of injury, secreting cytokines and growth factors, including IL-1 to IL-6, platelet-derived growth factor (PDGF), vascular endothelial growth factor (VEGF), and bone morphogenetic protein (BMP) (Rui et al., 2012). This cellular response leads to the invasion of mesenchymal stem cells (MSCs), which differentiate into osteoblasts and chondrocytes to complete the repair (Schindeler et al., 2008). Numerous studies have confirmed that MSCs form bone by differentiating into osteoblasts (Bruder et al., 1998; Gu et al., 2012; Zhu et al., 2012). In addition, many other studies have confirmed that the recruitment of factors with an adequate amount of MSCs and the micro-environment around the fracture are effective for fracture repair (Tsai et al., 2012; Zhi et al., 2011; Zuo et al., 2013).

Bone defects often arise from trauma, tumor resection, reconstructive surgery, congenital malformations, infections, and orthopedic or maxillofacial surgery procedures, and promoting bone regeneration is a unique challenge for both clinicians and scientists. Based on these observations, the regenerative medicine could be considered one of the major promises for all the patients suffering from bone problems, which has a huge detrimental effect on patient's lives and society (Majidinia et al., 2018). Unlike in other tissues, most bone injuries (fractures) heal without forming scar tissue, and bone is regenerated with its preexisting properties (Einhorn, 1998). However, there are complex clinical conditions in which a large amount of bone regeneration is required, such as skeletal reconstruction of extensive bone defects created by trauma, infection, tumor resection, skeletal abnormalities, or cases in which the regenerative process is compromised, such as vascular necrosis and osteoporosis (Dimitriou et al., 2011). In fields such as oral and maxillofacial surgery, several treatment methods are currently available, which can be used either alone or in combination for the enhancement or management of these complex clinical situations (Dimitriou et al., 2011). Standard approaches clinically applied to stimulate or augment bone regeneration included distraction osteogenesis and bone transplantation (Aronson, 1997; Green et al., 1992), but there are also other several bone-grafting methods, such as autologous bone grafts, allografts, and bone-graft substitutes or growth factors (Giannoudis et al., 2005; Giannoudis and Einhorn, 2009). Furthermore, bone grafting is commonly performed in orthopedic and maxillofacial surgery as a "gold standard" approach (Bauer and Muschler, 2000) because it is the patient's own tissue; autologous bone is histocompatible and non-immunogenic, reducing the likelihood of immunoreactions and transmission of infections to a minimum. Nevertheless, harvesting requires an additional surgical procedure, with well-documented complications and discomfort for the patient (Ahlmann et al., 2002). In this direction, wide progress has been made in cellular and molecular biology, allowing detailed histological analyses, *in vitro* and *in vivo* characterization of bone-forming cells, and identification of transcriptional and translational profiles of the genes and proteins involved in the process of bone regeneration and fracture repair (Komatsu and Warden, 2010). With an improved understanding of fracture healing and bone regeneration at the molecular level (Dimitriou et al., 2005), a number of key molecules that regulate this complex physiological process have been identified and are already in clinical use or under investigation to enhance bone repair. Among these molecules, bone morphogenic proteins (BMPs) have been the most extensively studied as they are potent osteo-inductive factors.

However, there are several issues with their use, including safety (because of the supraphysiological concentrations of growth factors needed to obtain the desired osteo-inductive effects), the high cost

of treatment, and, more importantly, the potential for ectopic bone formation (Argintar et al., 2011).

MSCs or stromal stem cells are adult cells isolated from mesenchymal tissues. They have the property of being able to differentiate into many other cell types (Quintero Sierra et al., 2023; Wakao et al., 2011; Kuroda et al., 2013). The application of stem cells in cell-based therapy promotes the repair response of diseased, dysfunctional, or injured tissue. This is obtained by using both the stem cell progenitor, which *in vitro* differentiates into tissue-specific cells, and their derivative (a subpopulation of mature cells derived from stem cell differentiation *in vitro*) (Kuroda et al., 2013). In humans, MSC sources include bone marrow, adipose tissue, umbilical cord tissue, dermis, and peripheral blood (Sato et al., 2020). The fact that these MSCs are adipose tissue-resident cells makes them potentially attractive as they could be extracted and isolated from easily harvested fat by liposuction (Wakao et al., 2011; Wakao et al., 2014; Dai Prè et al., 2020). The application of MSCs in regenerative medicine presents two key advantages: first, a low risk of tumorigenesis, and second, a high differentiation capacity, which permits their application to the restoration of various pathological cell loss conditions (Wakao et al., 2011; Wakao et al., 2014; Rigotti et al., 2009; Heneidi et al., 2013).

Moreover, due to their origin from mesodermal lineage, they are able to differentiate into cells such as osteocytes, chondrocytes, adipocytes, skeletal muscle cells, endothelial cells, and cardiomyocytes. Therefore, they can find numerous applications in regenerative therapy studies (De Francesco et al., 2021a; Ogura et al., 2014; Ossanna et al., 2024).

Another alternative cellular source is the stromal vascular fraction (SVF). The SVF consists of adipose-derived stem cells (ASCs), endothelial precursor cells, macrophages, smooth muscle cells, lymphocytes, pericytes, and pre-adipocytes (Grünherz et al., 2019; Lo Furno et al., 2017; Capuzzo et al., 2023). Moreover, the SVF secretum consists of proliferative, pro-angiogenic, pro-differentiative, and pro-antiapoptotic factors, along with extracellular matrix components (Quintero Sierra et al., 2023; Simonacci et al., 2017; De Francesco et al., 2021b; Kachgal and Putnam, 2011). Altogether, the SVF contains a milieu of cells that constitute the functional cellular niche for regenerative processes (Xue et al., 2020; Rosa et al., 2021). Interestingly, adipose tissue contains a higher number of stem cells than bone marrow (Doornaert et al., 2019), making it a more effective source (500 times greater when counted per unit volume than bone marrow) with no ethical concerns regarding its procurement (Deptuła et al., 2021). The ASC content within the SVF of lipoaspirate samples is well known, and consequently, the SVF is used in several therapies and in a wide range of human regenerative medicine approaches (De Francesco et al., 2024). The contents of SVF can promote revascularization, activate local stem cell niches, modulate immune responses *via* paracrine secretion of numerous bioactive molecules, promote wound healing, exhibit anti-inflammatory activity, and promote angiogenesis. These regenerative effects could be partially due to the MSC content of the SVF (Capuzzo et al., 2023; Bora and Majumdar, 2017; Luck et al., 2018).

The SVF can be obtained from adipose tissue either through enzymatic methods by using collagenase enzyme that allows to separation the contents into two distinct phases: the floating mature adipocyte fraction and the cellular components in the lower aqueous fraction (Matsumoto et al., 2006; Zuk et al., 2001), resulting in an MSC-rich product, or non-enzymatic techniques, in which their mechanical strategies help desegregate adipose tissue, with cellular yield lower than enzymatic methods but with highly preserved micro-fragments of connective tissue (Quintero Sierra et al., 2023). Altogether, the SVF contains a milieu of cells that constitute the functional cellular niche for regenerative processes (De Francesco et al., 2009; Ferraro et al., 2013).

Hyaluronic acid, a critical component of the extracellular matrix, is a good example of natural molecule that has been applied in regenerative medicine with good results (Valachová and Šoltés, 2021; Carton and Malatesta, 2024). In the last decade, it has become clear that, in addition to their scaffolding properties, low-molecular-weight hyaluronic acid (LMW-HA) molecules can also contribute to other mechanisms like in the processing of injury and healing (Marinho et al., 2021).

In this work, we aim to evaluate the regenerative potential of SVF, containing the stem cell niches activated by mechanical processes (HT-SVF) and mixed with a low molecular weight hyaluronic acid (ACP) as a scaffold, in order to maintain the pro-regenerative product in the calvarial defect locus during the reparative process, and comparing the obtained product by enzymatic digestion mixed with ACP, along with control groups (ACP and saline). In particular, our goal was to investigate the ability of wound healing and tissue repairing, specifically in the case of hard tissues like bone, which was promoted by a new mechanical stromal vascular fraction in a calvarial defect model.

Materials and methods

Fat harvesting

The adipose tissue was harvested from women (n = 3) subjected to ambulatory liposuction, aged between 41 and 69 years. Informed consent was signed by patients prior to tissue harvesting, and all processes were carried out according to the ethical guidelines established by the review committee for human studies of AOU "delle Marche," Ancona, Italy (Micro-adipose graft_01, 18 May 2017). In brief, the Klein solution was injected (2% lidocaine solution: 0.08% w/v; adrenaline 1 mg/mL solution: 0.1% v/v in 0.9% saline) and left to rest for 8–10 min before starting the liposuction. The cannula and the 20-mL Vac-Lock syringe provided in the kit were used (11G, six holes) to lipoaspirate 20 mL of fat from each donor. Moreover, harvested fat was received and used in experimental protocols, from the University of Verona Laboratory, following the guidelines of the Human Research Approval Committee protocol number 2/2019.

ED-SVF and HT-SVF productions

The extraction of the SVF was performed following the methodologies already proven in the laboratory, with the enzymatic and mechanic digestion systems. In summary, 20 mL of adipose tissue from each healthy informed donor (n = 3) was divided into two portions. The first portion (10 mL) was processed enzymatically using collagenase type I (Gibco; lot number: 17100017), following

the study reported by Busato et al. (2020). The cells extracted using this method were named ED-SVF. The second portion (10 mL) was treated mechanically using a Hy-tissue-SVF kit (Fidia Farmaceutici, Abano Terme, Italy). The method consists of a sterile, single-use double bag, containing an inner filter bag with a mesh size of 120 μm. A volume of 10 mL of lipoaspirate was introduced into the inner porous bag using an upper syringe. The adipose tissue was manually processed for 5 min with the plastic rod located within the microporous bag. The micro-fragmented tissue was then collected through a syringe in the lower part of the outer bag and centrifuged at 1,200 × g for 10 min. The cellular pellet obtained was named HT-SVF. All SVF preparations were obtained freshly from individual donor samples and processed within the same experimental session to minimize inter-sample variability. The use of three biological replicates (n = 3 donors) allowed comparative analysis across treatment groups. No cryopreservation or storage was applied; thus, all samples were used immediately after isolation. Based on current protocols and previous experience in our laboratory, mechanical processing tends to yield SVF products with a lower but more consistent cell count and preserved ECM components, whereas enzymatic digestion results in a higher cellular yield but increased variability depending on the enzyme batch and exposure time.

ACP preparation and characterization

The ACP used in this study was manufactured by FIDIA Farmaceutici S.P.A. (Abano Terme, Padova, Italy). The ACP formulation has a molecular weight of approximately 200 kDa and undergoes a proprietary auto-crosslinking post-modification process. It was supplied as a sterile, ready-to-use injectable solution and used without further modification. This crosslinking is designed to increase the residence time of the product at the injection site, enhancing the local availability of the bioactive compound during the early regenerative phases. The selection of LMW-HA is based on its known bioactivity in promoting cell migration and proliferation in regenerative contexts. Prior to *in vivo* application, its physicochemical properties (viscosity and molecular weight distribution) were confirmed using gel permeation chromatography and rheological analysis according to the manufacturer's certificate of analysis. Its selection was based on its known regenerative and scaffold-supportive roles in wound- and bone-healing environments.

Animal model

Ten-week old, homozygote male nude mice (n = 12) were purchased from Envigo (Milan, Italy). Animals were housed in each cage, with controlled temperature and humidity. They had free access to chops and water. After 1 week of adaptation, animals were housed individually in each cage. To evaluate the potential effect of cellular treatment in bone regeneration, an *in vivo* cranial damage model, known as "Calvaria defect mouse model," was designed in homozygote nude mice. The animals were randomly divided into four groups: HT-SVF + ACP (n = 3), ED-SVF + ACP (n = 3), ACP (n = 3), and saline solution as the control group (n = 3). Each lipoaspirate (n = 3) was equally used for a single series of experimental groups in order to confront the effect of single-donor lipoaspirates between all the tested conditions.

To perform the cranial defect, animals were first anesthetized with isoflurane (Ugo Basile S.R.L, Varese, Italy). Furthermore, an incision was made using a scalpel, cutting through both dermal layers and the periosteum, to expose the cranial bone. Damage was created bilaterally in the parietal cortex using a mini-drill with a 2-mm-diameter tip.

The created non-trespassing holes (approximately 0.5 mm depth) were filled with 50 μL of ACP mixed with the respective treatment (ED-SVF or HT-SVF), or 50 μL ACP or 50 μL saline. To avoid any leakage of the evaluated treatments, a 2.5-mm-diameter dish of Attiva film (sterile transparent polyurethane adhesive dressing, Svas Biosana S.p.A.) was used to cover the injured cranial bone and then fixed with a drop of tissue glue (3M Vetbond Tissue Adhesive). The superficial skin of the animal was finally sutured with resorbable stitches (737H silk sutures, ETHICON 3-0). In order to ameliorate the animal during postoperative recovery, animals were treated subcutaneously with an analgesic (carprofen, Rimadyl®, 1 mL/kg, 1:10; Pfizer, Roma, Italy) and a wide-spectrum antibiotic (enrofloxacin, Baytril®, 10 mL/kg, 1:50, Bayer S.p.a., Milano, Italy) every other day, for 5 days.

To ensure humane treatment of the animals, euthanasia was performed using an overdose of sodium pentobarbital, administered intraperitoneally at a dose of 150 mg/kg. This method was chosen for its rapid effectiveness and to minimize animal discomfort. All the procedures involving animals were approved by the Italian NHI, authorization 56DC9.79. All procedures were conducted in full compliance with the ARRIVE guidelines, and all methods were carried out in accordance with relevant guidelines and regulations.

Immunophenotyping

Cells from ED-SVF and HT-SVF were characterized by flow cytometry. For this purpose, both SVF products were passed through a 45-μm cells strainer to remove cellular aggregates; then, the cell pellet was incubated with 1 mL of erythrocyte lysis buffer 1X (Macs Miltenyi Biotec, Milan, Italy) for 10 min and filtered through a 70-μm cell strainer. Next, cells were collected and counted with trypan blue exclusion assay using a CytoSMART counter (Automated Image-Based Cell Counter, version 1.5.0.16380; CytoSMART Technologies B.V, Eindhoven, Netherlands), and 20,000 cells were washed with PBS (1X) and incubated with a specific monoclonal antibody on ice for 30 min. After incubation, the pellets were centrifuged (5,000 rpm, 7 min) and resuspended in 100 μL of PBS (1X).

The following antibodies were used: CD73 V-450A conjugate (1:5 dilution), CD34 PE-A conjugate (1:20 dilution), and CD105 PerPC-Cy-5-5-A conjugate (1:5 dilution). For cell viability, propidium iodide was used. All antibodies were purchased from BD Biosciences (Becton Dickinson Italy S.P.A., Milano, Italy). Immunophenotyping was performed through a chant II FACS (BD, Becton Dickinson, Milano, Italy).

Magnetic resonance imaging

The animals were monitored at 5 and 15 days after the surgery through magnetic resonance imaging (MRI) by performing T2_turboRARE_highres analysis (Bruker, Karlsruhe, Germany) equipped with a 7 T (T), 33-cm bore horizontal magnet (Oxford Ltd., Oxford, United Kingdom).

Given that bone is not directly visualized in magnetic resonance, this technique allows to observe the organization and integrity of structures such as the meninges, periosteum, and skin. In addition, the MRI technique provides information regarding the different degree of wound healing by assessing the integrity of tissues adjacent to the point of damage.

Sample fixation and histological analysis

At 15 dpi, the animals were sacrificed, and the crania were collected for subsequent analysis. The parietal area of the skull was fixed in 4% paraformaldehyde (PFA) for 48 h, decalcified for 24 h using Biodec R (Bio-Optica, Milan, Italy), and then washed with 0.1 M phosphate buffer (pH 7.4). The damage in the right hemisphere of each animal was embedded in OCT and frozen at −20°C. Successively, the samples were cryosectioned at a thickness of 15 μm. For each experimental group, the following histological stainings were performed: hematoxylin/eosin for a morphological evaluation, fibrosis, and inflammatory infiltrates; Alcian blue/Fast red to evaluate the extracellular matrix component formation; Alizarin red/hematoxylin to check the presence of calcium at the site of injury across all the samples. Three slices from each animal were collected for each histological staining. Slides were first washed with PBS 1X for 5 min, stained with Meyer's hematoxylin (H&E, Bio-Optica, Milan, Italy) for 30 s, washed in running water, stained with 1/10 eosin (H&E, Bio-Optica) for 10 s, and washed with distilled water. Second, slices were washed with PBS 1X, stained with Alcian blue (Merck KGaA, Darmstadt, Germany) for 30 min, washed with distilled water, stained with Fast red solution (Bio-Optica) for 20 min, and washed with distilled water. For the last staining, slices were washed with PBS 1X, stained with Alizarin red (Bio-Optica) for 30 min, washed with distilled water, stained with Meyer's hematoxylin (H&E, Bio-Optica, Milan, Italy) for 20 min, and washed with distilled water.

Slides were dehydrated with increasing concentrations of alcohol (60, 80, 95, and 100%, each for 10 min), ending with a double wash in xylene for 10 min. Finally, slides were mounted with Entellan (Merck KGaA), dried, and gently cleaned with ethanol. Slides were examined by light microscopy using an Olympus BX-51 microscope (Olympus, Tokyo, Japan) equipped with a JVC DKY-F58 CCD digital camera (Yokohama, Japan).

Immunofluorescence analysis

Cranial slices were defrosted at room temperature for 10 min and then washed in PBS 1X solution for 10 min and incubated for 30 min in blocking solution (0.25% Triton X-100, 2% bovine serum albumin in PBS 1X). Slices were then incubated overnight at 4°C with a solution containing the selected primary antibody (anti-mouse HLA with human reactivity, Abcam, ab70328; anti-rabbit osteopontin with mouse reactivity, Abcam, ab63856), diluted in blocking solution (1:200). The next day, slices were washed six times for 5 min, each with the blocking solution, and incubated at room temperature under dark condition for 4 h in the secondary antibody solution (anti-mouse ab150113 Abcam, 488; anti-rabbit ab175471 Abcam in 568, respectively), composed by specific secondary antibodies diluted in the blocking solution (1:500). After this step, slices were washed thrice for 5 min, each with the blocking solution, and then washed again thrice for 5 min, each with PBS 1X. Slices were then incubated for 10 min with a solution containing 4,6-diamino-2-phenylindole dihydrochloride (DAPI, Molecular Probes-Thermo Fisher Scientific, 1:2,000) diluted in PBS 1X for the nuclei staining. Finally, slices were washed with PBS 1X, and cover slides were mounted using 1,4-diazabicyclo [2.2.2] octane (DABCO, Sigma-Aldrich).

Scanning electron microscopy

The damage in the left parietal cortex was processed for scanning electron microscopy (SEM). The samples were post-fixed in 1% osmium tetroxide (OsO4) diluted in 0.1M phosphate buffer for 1 h. Subsequently, the samples were dehydrated by increasing concentrations of ethanol and finally using the critical point dryer (CPD 030, Balzers, Vaduz, Liechtenstein). They were then metallized with gold using an MED 010 coater (Balzers) and were viewed using an FEI XL30 scanning electron microscope (FEI Company, Eindhoven, Netherlands). The images were acquired in transversal cross-section.

Results

Characterization of the stromal vascular fraction

FACS analysis displayed high cell viability in both ED and HT-SVF. Moreover, HT-SVF and ED-SVF cytofluorimetric analysis showed that $CD34^+$ cell population (endothelial, pericytes, and adipose-derived stem cells) was 9.9% ± 1.5% and 3.7% ± 1.3%, respectively. Additionally, the frequency of cells positive for CD73 and CD105 (mesenchymal stem cells) was analyzed. The percentages of expression in HT-SVF were 7.61% ± 2.59% and 6.28% ± 2.40% for CD73 and CD105, respectively, not thus far from the percentage of expression obtained for the same antibody with ED-SVF (10.14% ± 2.91% and 9.98% ± 1.49%, respectively), as presented in Figure 1.

Visual evaluation of wound healing

As a follow-up post-surgery procedure, different experimental groups were systematically monitored and evaluated. After the surgery, the degree of wound scarring was assessed at 15 dpi in the different experimental groups through visual evaluation. As shown in Figure 2, the wounds of animals treated with HT-SVF + ACP appeared to be completely healed after 15 days of study, compared to the other experimental groups, which still showed large scars and open wounds.

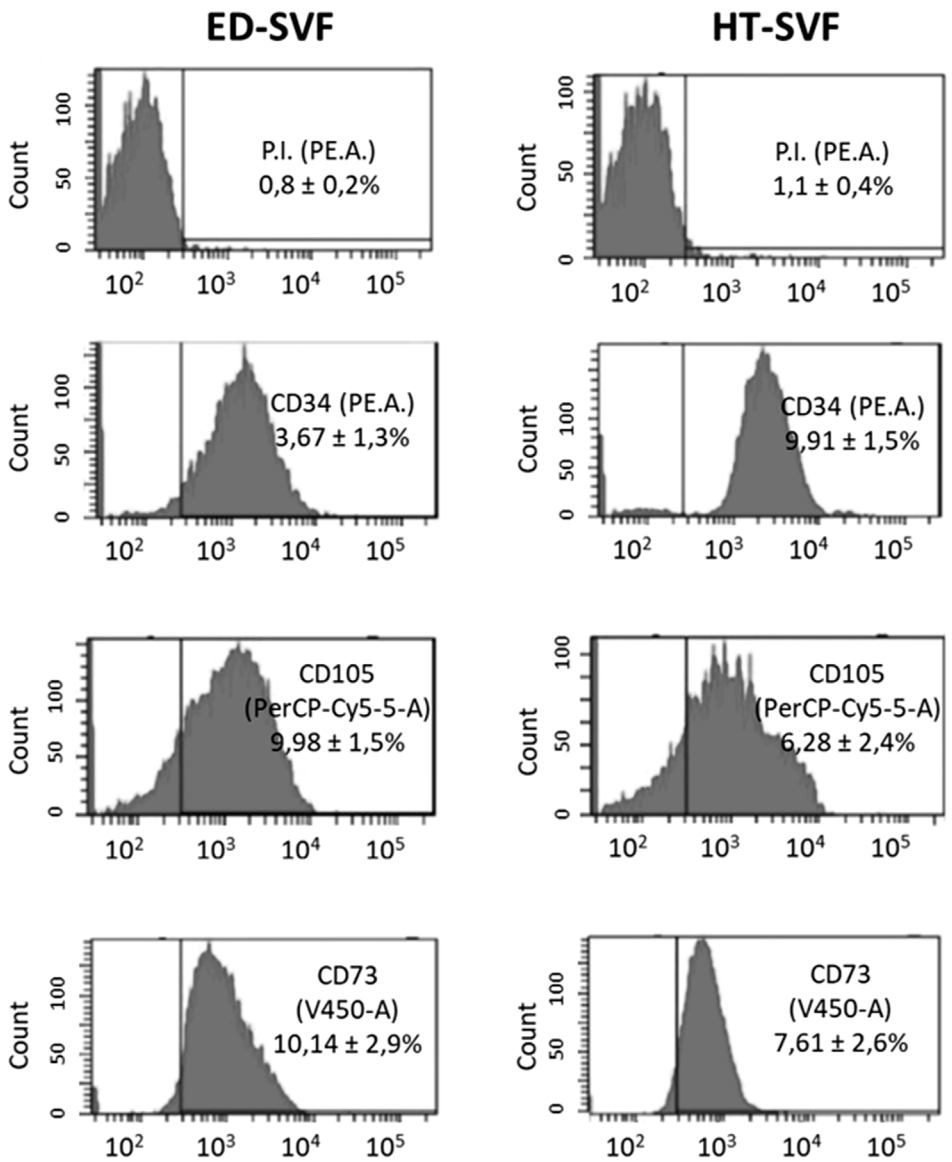

FIGURE 1
The cell viability and population of ED-SVF and HT-SVF were characterized by flow cytometry by using the P.I., CD34, CD105, and CD73 markers. Data are expressed in percentage of positive cells ±SEM.

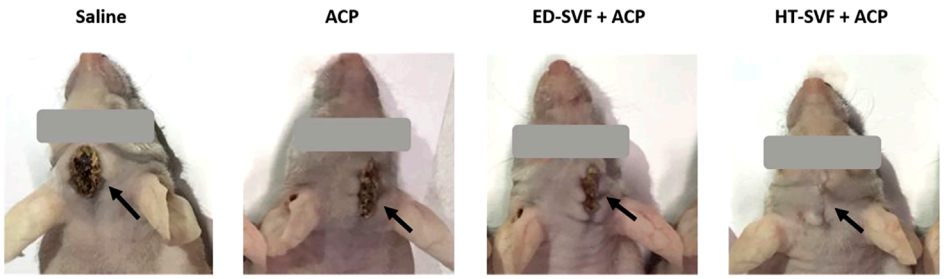

FIGURE 2
Visual observation of the wound after 15 days post-surgery. The black arrows indicate the wounds. All the experimental groups are presented, including controls (saline and ACP) and treatments (HT-SVF and ED-SVF).

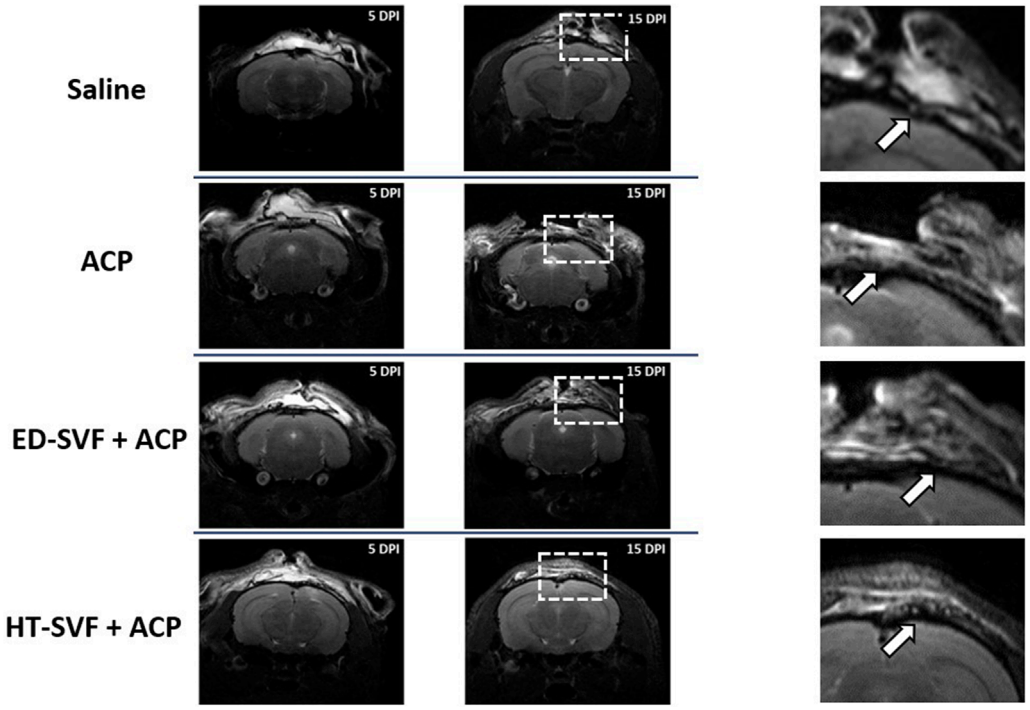

FIGURE 3
Representative MRI of the wound healing process at 5 and 15 days after the operation. The squares are representative for the magnifications, and the white arrows indicate the injury sites. All the experimental groups are presented, including controls (saline and ACP) and treatments (HT-SVF and ED-SVF).

In vivo monitoring with MRI

After inducing the bone injury, mice were monitored by magnetic resonance at 5 and 15 days after the surgery. The MRI images allowed to control if the defect was performed satisfactorily by supervising that the surrounding structures underlying the cranial bone do not appear compromised.

MRI images (Figure 3) show that treatment with HT-SVF + ACP promotes greater integrity of the skin tissue that covers the cranial bone, unlike all other treatments. In fact, it can be observed how the meninges, periosteum, and skin in the case of treatment with HT-SVF + ACP are structurally more organized and intact, if compared with all the other experimental groups. Moreover, animals that received ED + ACP and ACP showed partial integrity of the observed structures compared to those that received saline treatment. The latter showed a lower integrity of the damaged skin tissues than the other experimental groups.

Histological analysis

After 15 days of surgery, the treated site of the bone-injured area had been removed to proceed with the different histological analysis. The skulls have been cryo-sectioned and stained with different methodologies that allow us to evaluate different parameters related to the possible regeneration of the damaged bone.

Hematoxylin and eosin

The hematoxylin and eosin staining analysis had been used on the cross-sectioned calvarial bone in order to study tissue regeneration and their cellular components. As shown in Figure 4, skulls derived from animals treated with saline and ACP have a greater amount of scar material at the site of bone damage than skulls derived from animals treated with HT-SVF + ACP and ED-SVF + ACP, where a lower amount of scar tissue was found. Moreover, the gap in the injured site was reduced, as represented in Figure 4. In fact, the holes of animals that received cellular treatments appeared to have a smaller diameter than those of animals in the controls. However, in Figure 4, on the right, it can also be seen that the bone damage site in HT-SVF + ACP and ED-SVF + ACP treatments had a greater amount of newly formed bone tissue than the bone damage site in saline and ACP controls.

Alcian blue and Fast red

As fracture bone healing is associated with transient cartilage formation, we proceeded to investigate the association between cartilage and the bone defects. Therefore, Alcian blue staining identifies the extracellular matrix components, which are essential precursors of bone regeneration, and Fast red stains cell nuclei red. As shown in Figure 5, the skull treated with HT-SVF + ACP shows a greater blue staining intensity degree than that treated with ED-SVF + ACP, which has a high amount of these bone precursor components. In contrast, saline and ACP control groups display poor blue staining at the site of bone injury. The greater blue staining at the site of cranial damage that can be observed in the cellular

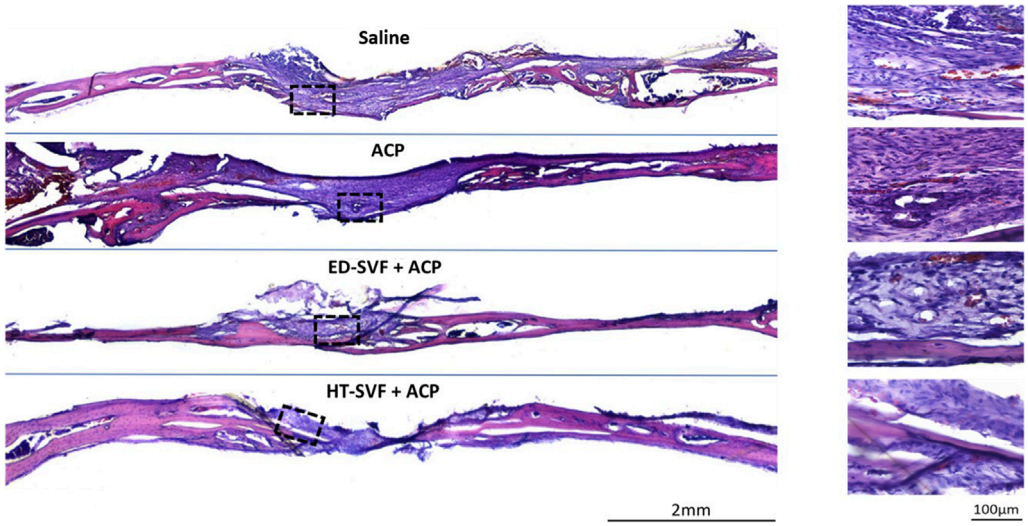

FIGURE 4
Morphological evaluation with hematoxylin/eosin staining. The squares represent the magnifications in the right column, the black lines represent the initial hole diameter, and the dotted lines represent the newly formed bone area and scar tissue. All the experimental groups are presented, including controls (saline and ACP) and treatments (HT-SVF and ED-SVF).

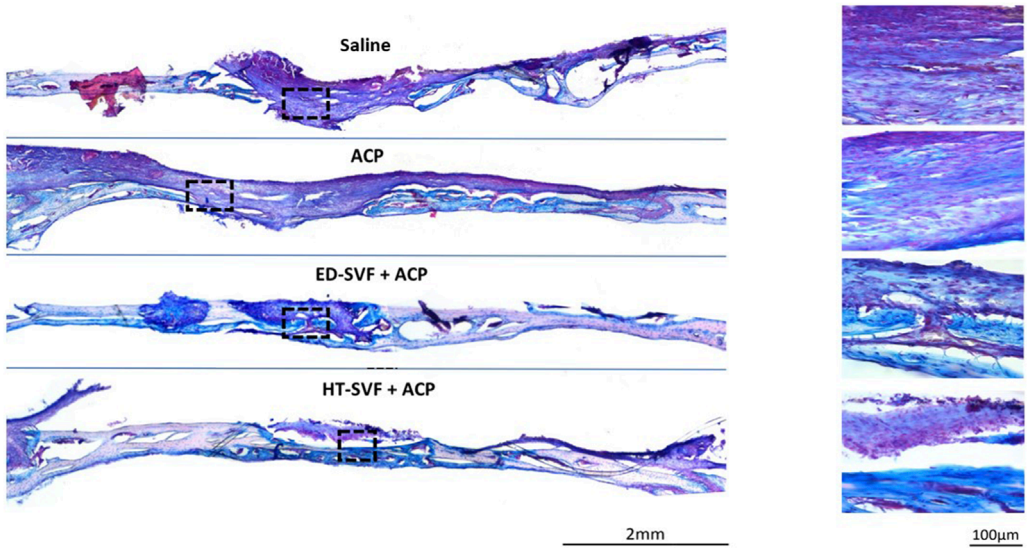

FIGURE 5
Glycosaminoglycan evaluation with Alcian blue/Fast red staining. The squares represent the magnifications in the right column, the black lines represent the initial hole diameter, and the dotted lines represent the newly formed bone area. All the experimental groups are presented, including controls (saline and ACP) and treatments (HT-SVF and ED-SVF).

treatments (HT-SVF + ACP and ED-SVF + ACP) highlights a greater amount of glycosaminoglycan bone precursors, which result in a greater bone regeneration capacity. In particular, HT-SVF + ACP treatment shows a greater thickness of newly formed bone than treatment with ED-SVF + ACP, ACP, and saline controls.

Alizarin red and hematoxylin

For further confirmation of bone maturation, Alizarin red has been used to mark calcium deposits, which is the main and essential precursor for the bone regeneration process. As shown in Figure 6, the damage area treated with HT-SVF + ACP shows a greater intensity of red coloration than that treated with ED-SVF + ACP. However, the saline and ACP controls display less staining intensity, as can be seen from the damaged zone magnification in Figure 6. In addition, as observed in the other staining analyses, the HT-SVF + ACP and ED-SVF + ACP treatments show a reduction in the cranial hole diameter. The greater intensity of staining at the cranial damage site that can be observed in cellular treatments is linked to

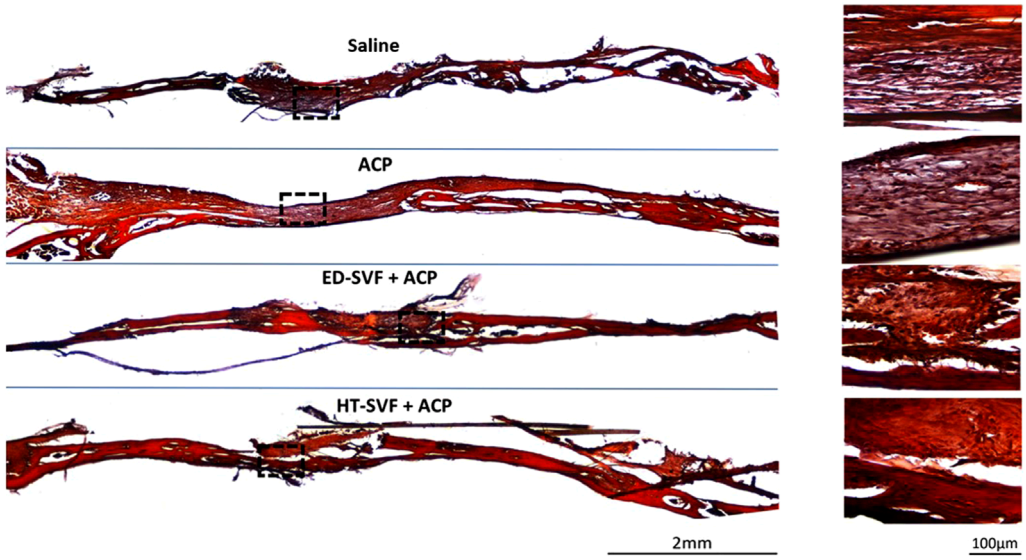

FIGURE 6
Calcium deposit evaluation with Alizarin red and hematoxylin. The squares represent the magnifications in the right column, the black lines represent the initial hole diameter, and the dotted lines represent the magnification zone of the newly formed area. All the experimental groups are presented, including controls (saline and ACP) and treatments (HT-SVF and ED-SVF).

a greater amount of calcium deposits, which is one of the essential components of bone neoformation.

Immunofluorescence analysis

Human cell analysis

The immunofluorescence technique was carried out to assess the presence of human cells 15 days after the treatment in the cranial region of injury. Positive control is represented by a human capsular contracture. As shown in Figure 7, the first row in the panel shows the immunofluorescent staining related to DAPI, which marks the cell nuclei in blue; the second row depicts the channel related to the immunofluorescent staining of the human leukocyte antigen (HLA) marker, which is in green; and the third row defines the co-localization of the two channels. As shown in Figure 7, after 15 days, cellular treatments present some positivity of HLA^+ human cells on the calvarial defect scar surface for the presence of human cells in the HT-SVF + ACP and ED-SVF + ACP treatment groups, whereas there was no positivity in the other experimental groups.

New bone formation analysis with osteopontin

Anti-OPN analysis revealed that the newly formed tissue derived from cellular treatments presents some positivity for the osteopontin marker, which is a neoformation bone marker. As shown in Figure 8, the first row shows the immunofluorescent staining related to DAPI, which marks the cell nuclei in blue; the second row depicts the channel related to the immunofluorescent staining of the osteopontin marker; and the third row defines the co-localization of the two channels. It can be seen from the panel that there is higher positivity of the osteopontin marker in HT-SVF + ACP than in ED-SVF + ACP, whereas weak signal was observed in the other experimental groups (saline and ACP).

Ultrastructural analysis: scanning electron microscopy

SEM is a useful technique to analyze the microstructural organization of the sample's surface. As shown in Figure 9, the newly formed tissue in HT-SVF + ACP and ED-SVF + ACP treatments have a more defined, compact, and organized structure in the cranial damaged region. In contrast, ACP and saline controls show a poorly organized structure, with cracks and breaks in the newly formed material. In addition, both the cellular treatments appear to promote greater bone-like morphology of the newly formed tissue.

Discussion

Regenerative medicine has profoundly transformed the landscape of bone repair, offering innovative solutions through the integration of stem cell-based therapies and bioactive scaffolds (De Francesco et al., 2023). These approaches address long-standing challenges in treating extensive and complex bone defects, particularly where traditional methods, such as grafting or mechanical fixation, have shown limited efficacy. By leveraging the body's intrinsic healing mechanisms, cell-based therapies, especially autologous approaches, minimize immunogenic risks and enhance biocompatibility, making them a cornerstone in modern bone regeneration strategies.

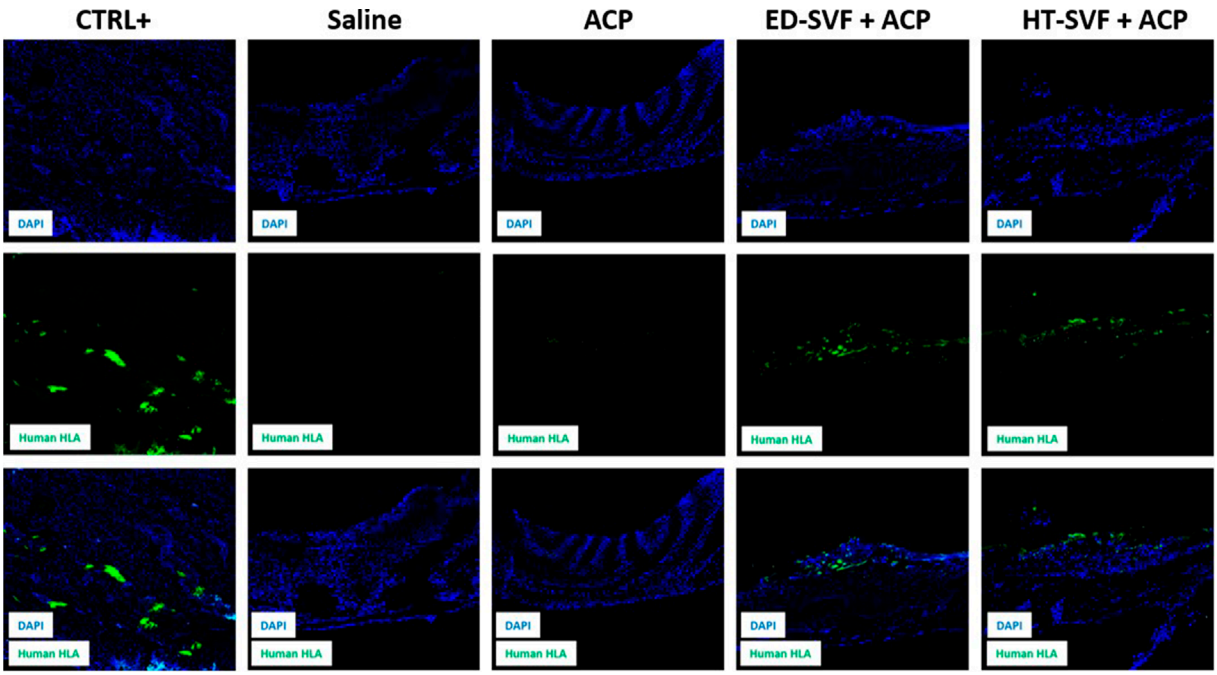

FIGURE 7
Immunofluorescence analysis of HLA^{+} human cells. The columns consist of different experimental groups (CTRL+, saline, ACP, ED-SVF + ACP, and HT-SVF + ACP). Each row represents different markers, including nuclei marker (DAPI, blue), human leukocyte antigen marker (HLA, green), and composite of markers. All the images were acquired with a ×20 magnification objective.

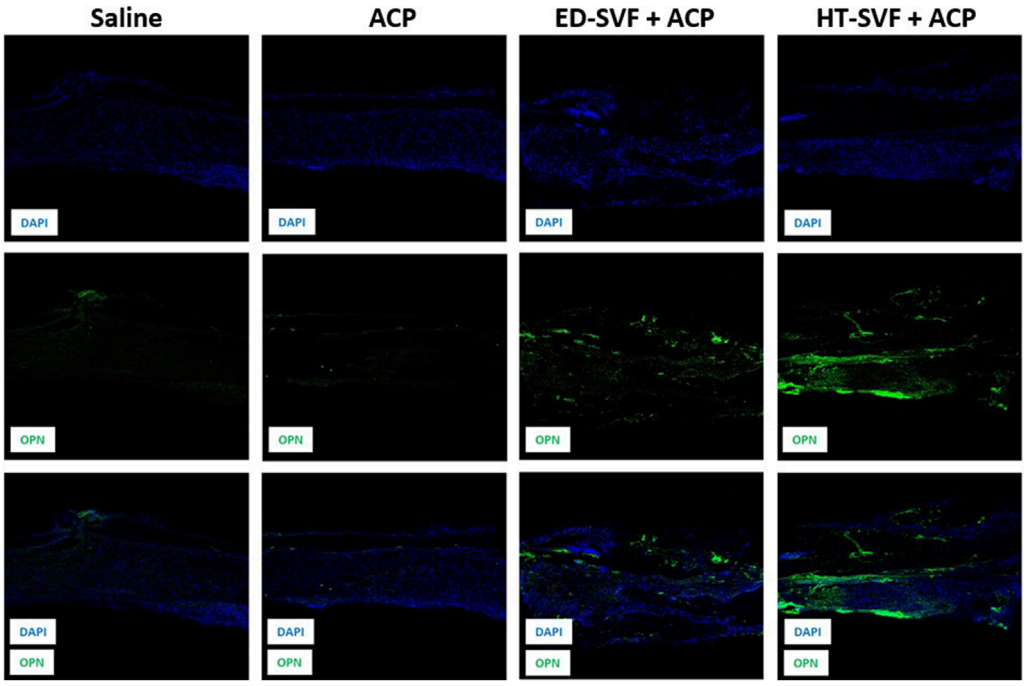

FIGURE 8
Immunofluorescence analysis of the newly formed bone marker. The columns consist of different experimental groups (CTRL+, saline, ACP, ED-SVF + ACP, and HT-SVF + ACP). Each row represents different markers, including nuclei marker (DAPI, blue), bone neoformation marker (OPN, green), and composite of markers. All the images were acquired with a ×20 magnification objective.

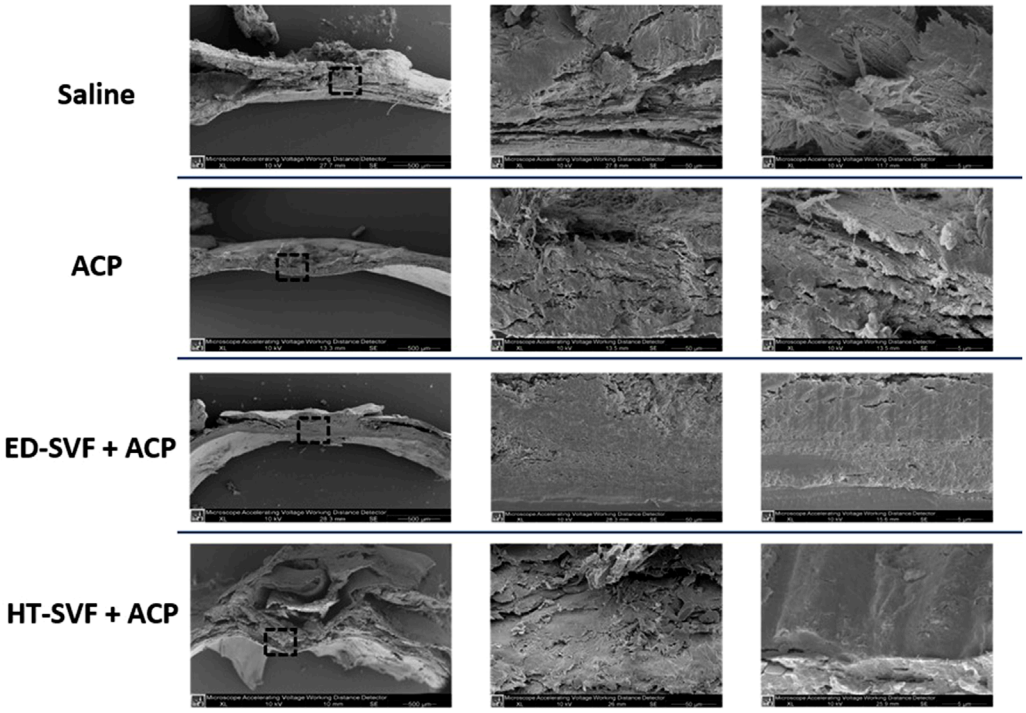

FIGURE 9
Ultrastructural analysis using scanning electron microscopy (SEM). The squares represent the magnification areas, and the right column represents its further magnification. All the experimental groups are presented, including controls (saline and ACP) and treatments (HT-SVF and ED-SVF).

In our study, both HT-SVF and ED-SVF demonstrated comparable cell viability and ADSC content, highlighting their potential as regenerative tools. However, HT-SVF emerged as a superior alternative, owing to its ability to preserve the extracellular matrix and secretory factors. This preservation is pivotal, as the extracellular matrix not only provides structural support but also serves as a reservoir for pro-regenerative cytokines, growth factors, and chemokines. These elements collectively create a conducive microenvironment for cellular migration, proliferation, and differentiation, accelerating wound healing and osteogenesis.

The combination of HT-SVF with ACP further amplified its therapeutic efficacy. ACP acts as both a scaffold and a bioactive agent, facilitating the retention and gradual release of regenerative factors while supporting cellular adhesion and tissue integration. Our histological analyses revealed that the HT-SVF + ACP treatment significantly enhanced osteogenesis, as evidenced by the presence of mature bone and enhanced expression of bone precursor markers. These findings underscore the synergy between HT-SVF and ACP in promoting rapid and robust bone regeneration, reducing fibrotic tissue formation, and improving the structural and functional quality of the newly formed bone matrix.

Although ED-SVF + ACP also demonstrated regenerative potential, the differences in outcomes highlight the advantages of mechanical processing. Mechanical digestion methods, as used for HT-SVF, retain micro-fragments of connective tissue and associated vascular niches, which are often disrupted in enzymatic digestion. This retention may explain the superior regenerative outcomes observed with HT-SVF + ACP as these niches are critical for maintaining cellular viability and functionality. Although this study focused on calvarial bone regeneration, the biological features of SVF, including its multi-lineage differentiation capacity and secretory profile, make it a promising candidate for applications in other tissues. The preservation of stromal architecture in HT-SVF further supports its potential translational use across various regenerative medicine fields.

Despite the promising results, there are limitations to be considered. The reliance on a murine model introduces challenges in extrapolating findings to human clinical scenarios. Murine physiology, particularly in bone remodeling and healing dynamics, differs significantly from that of humans. Additionally, the relatively short follow-up period in this study limits the ability to assess long-term outcomes, such as the durability and integration of the regenerated bone under physiological stress. It is important to acknowledge that the present study is limited to the use of a murine calvarial defect model, which, although valuable for initial proof-of-concept data, does not fully replicate the complex biomechanical and physiological environment of human bone tissue. Moreover, the 15-day follow-up period, although sufficient to evaluate early stages of healing and bone matrix formation, precludes assessment of long-term outcomes such as structural remodeling, integration, and mechanical strength. Future studies should consider larger animal models and extended monitoring periods to validate the translational potential of HT-SVF + ACP therapy.

Future research should address these gaps by extending the duration of studies and incorporating larger animal models that better mimic human bone physiology. Translational studies

focusing on the scalability, safety, and efficacy of HT-SVF + ACP in clinical settings are crucial. Moreover, exploring the potential of combining HT-SVF with other bioactive molecules or advanced scaffold designs could further enhance its regenerative capabilities. Investigating its application in more complex defect models, such as those involving load-bearing bones or multi-tissue interfaces, would also provide valuable insights into its clinical utility.

In conclusion, the findings from this study establish HT-SVF as a transformative approach in bone regenerative medicine. Its cost-effectiveness, simplicity, and superior regenerative outcomes position it as a viable alternative to enzymatic methods. When combined with bioactive scaffolds like ACP, HT-SVF holds the potential to address a wide range of clinical challenges in bone repair, paving the way for innovative, patient-specific therapies that restore both form and function in severe and complex bone injuries.

Conclusion

In this study, we demonstrate that HT-SVF significantly enhances the healing process of bone defects, outperforming conventional methods. Cranial bone regeneration was characterized by early connective tissue formation in the cortical bone region, followed by accelerated remodeling and maturation. The rapid healing observed with HT-SVF + ACP can be attributed to its enriched regenerative compounds and the synergistic effect of ACP, which together provide a robust scaffold for bone growth.

Our findings underscore the pivotal role of SVF, not only in delivering stem cells essential for bone repair but also in leveraging the trophic effects of the extracellular matrix and associated regenerative niches preserved through mechanical purification. Moreover, HT-SVF presents a simplified, cost-effective alternative to enzymatic methods, making it a viable option for clinical application.

In conclusion, these results establish the efficacy of SVF supplementation as a transformative approach for severe bone injuries. The insights gained pave the way for combining SVF with other bioactive molecules, such as hyaluronic acid, to develop innovative, highly effective strategies for enhancing bone regeneration and repair in complex clinical scenarios.

Data availability statement

The raw data supporting the conclusions of this article will be made available by the authors, without undue reservation.

Ethics statement

The studies involving humans were approved following the guidelines of the Human Research Approval committee of Verona University aut.n 2/2019, and all the procedures involving animals were approved by the Italian NHI, n. 685/2021-PR. The studies were conducted in accordance with the local legislation and institutional requirements. The participants provided their written informed consent to participate in this study.

Author contributions

RO: Conceptualization, Data curation, Formal analysis, Investigation, Methodology, Software, Validation, Visualization, Writing – original draft, and Writing – review and editing. LQ: Conceptualization, Data curation, Investigation, Methodology, Software, and Writing – original draft. SG: Conceptualization, Formal analysis, Investigation, Methodology, Software, Validation, Writing – original draft, and Writing – review and editing. VJ: Writing – original draft and Writing – review and editing. CC: Software and Writing – original draft. AB: Data curation and Writing – original draft. AC: Methodology and Writing – original draft. GC: Conceptualization, investigation, supervision, validation, and writing – review and editing. NZ: Conceptualization, Supervision, and Writing – review and editing. PP: Conceptualization, Supervision, and Writing – review and editing. FD: Conceptualization, Supervision, and Writing – review and editing. MR: Funding acquisition, Project administration, Supervision, Validation, and Writing – original draft. AS: Project administration, Supervision, and Writing – review and editing.

Funding

The author(s) declare that no financial support was received for the research and/or publication of this article.

Conflict of interest

Author AB was employed by Aptuit and Evotec company and this company is not involved in this study.

The remaining authors declare that the research was conducted in the absence of any commercial or financial relationships that could be construed as a potential conflict of interest.

Generative AI statement

The authors declare that no Generative AI was used in the creation of this manuscript.

Publisher's note

All claims expressed in this article are solely those of the authors and do not necessarily represent those of their affiliated organizations, or those of the publisher, the editors and the reviewers. Any product that may be evaluated in this article, or claim that may be made by its manufacturer, is not guaranteed or endorsed by the publisher.

References

Ahlmann, E., Patzakis, M., Roidis, N., Shepherd, L., and Holtom, P. (2002). Comparison of anterior and posterior iliac crest bone grafts in terms of harvest-site morbidity and functional outcomes. *J. Bone Jt. Surg. Am.* 84, 716–720. doi:10.2106/00004623-200205000-00003

Argintar, E., Edwards, S., and Delahay, J. (2011). Bone morphogenetic proteins in orthopaedic trauma surgery. *Injury* 42, 730–734. doi:10.1016/j.injury.2010.11.016

Aronson, J. (1997). Limb-lengthening, skeletal reconstruction, and bone transport with the Ilizarov method. *J. Bone Jt. Surg. Am.* 79, 1243–1258. doi:10.2106/00004623-199708000-00019

Bauer, T. W., and Muschler, G. F. (2000). Bone graft materials: an overview of the basic science. *Clin. Orthop. Relat. Res.* 371, 10–27. doi:10.1097/00003086-200002000-00003

Bora, P., and Majumdar, A. S. (2017). Adipose tissue-derived stromal vascular fraction in regenerative medicine: a brief review on biology and translation. *Stem Cell Res. Ther.* 8, 145. doi:10.1186/s13287-017-0598-y

Brighton, C. T., and Krebs, A. G. (1972). Oxygen tension of healing fractures in the rabbit. *J. Bone Jt. Surg. Am.* 54, 323–332. doi:10.2106/00004623-197254020-00010

Bruder, S. P., Kurth, A. A., Shea, M., Hayes, W. C., Jaiswal, N., and Kadiyala, S. (1998). Bone regeneration by implantation of purified, culture-expanded human mesenchymal stem cells. *J. Orthop. Res.* 16, 155–162. doi:10.1002/jor.1100160202

Busato, A., De Francesco, F., Biswas, R., Mannucci, S., Conti, G., Fracasso, G., et al. (2020). Simple and rapid non-enzymatic procedure allows the isolation of structurally preserved connective tissue micro-fragments enriched with SVF. *Cells* 10, 36. doi:10.3390/cells10010036

Capuzzo, M. A., Ossanna, R., Quintero Sierra, L. A., Virla, F., Negri, A., Conti, A., et al. (2023). From the classification of stem cells to the release of potential in cell therapies: limits, considerations and future aspects in regenerative medicine. *Possibilities limitations Curr. Transl. stem cell Res.* 44, 1–17. doi:10.5772/intechopen.110572

Carton, F., and Malatesta, M. (2024). Nanotechnological research for regenerative medicine: the role of hyaluronic acid. *Int. J. Mol. Sci.* 25, 3975. doi:10.3390/ijms25073975

Dai Prè, E., Busato, A., Mannucci, S., Vurro, F., De Francesco, F., Riccio, V., et al. (2020). *In vitro* characterization of adipose stem cells non-enzymatically extracted from the thigh and abdomen. *Int. J. Mol. Sci.* 21, 3081. doi:10.3390/ijms21093081

De Francesco, F., Gravina, P., Busato, A., Farinelli, L., Soranzo, C., Vidal, L., et al. (2021a). Stem cells in autologous microfragmented adipose tissue: current perspectives in osteoarthritis disease. *Int. J. Mol. Sci.* 22, 10197. doi:10.3390/ijms221910197

De Francesco, F., Matta, C., Riccio, M., Sbarbati, A., and Mobasheri, A. (2021b). Reevolution of tissue regeneration: from recent advances in adipose stem cells to novel therapeutic approaches. *Stem Cells Inter* 2021, 2179429. doi:10.1155/2021/2179429

De Francesco, F., Sbarbati, A., Quintero Sierra, L. A., Zingaretti, N., Sarmadian, Z., Parodi, P. C., et al. (2024). Anatomy, Histology, and Embryonic origin of Adipose tissue: insights to understand adipose tissue homofunctionality in regeneration and therapies. *Adv. Exp. Med. Biol.* 1474, 53–78. doi:10.1007/5584_2024_801

De Francesco, F., Tirino, V., Desiderio, V., Ferraro, G., D'Andrea, F., Giuliano, M., et al. (2009). Human CD34/CD90 ASCs are capable of growing as sphere clusters, producing high levels of VEGF and forming capillaries. *PLoS One* 4, e6537. doi:10.1371/journal.pone.0006537

De Francesco, F., Zingaretti, N., Parodi, P. C., and Riccio, M. (2023). The evolution of current concept of the reconstructive ladder in plastic surgery: the emerging role of translational medicine. *Cells* 12, 2567. doi:10.3390/cells12212567

Deptuła, M., Brzezicka, A., Skoniecka, A., Zieliński, J., and Pikuła, M. (2021). Adipose-derived stromal cells for nonhealing wounds: emerging opportunities and challenges. *Med. Res. Rev.* 41, 2130–2171. doi:10.1002/med.21789

Dimitriou, R., Jones, E., McGonagle, D., and Giannoudis, P. V. (2011). Bone regeneration: current concepts and future directions. *BMC Med.* 9, 66. doi:10.1186/1741-7015-9-66

Dimitriou, R., Tsiridis, E., and Giannoudis, P. V. (2005). Current concepts of molecular aspects of bone healing. *Injury* 36, 1392–1404. doi:10.1016/j.injury.2005.07.019

Doornaert, M., Colle, J., De Maere, E., Declercq, H., and Blondeel, P. (2019). Autologous fat grafting: latest insights. *Ann. Med. Surg. (Lond)* 16, 47–53. doi:10.1016/j.amsu.2018.10.016

Einhorn, T. A. (1998). The cell and molecular biology of fracture healing. *Clin. Orthop. Relat. Res.* 355 (Suppl. l), S7–S21. doi:10.1097/00003086-199810001-00003

Ferraro, G. A., De Francesco, F., Nicoletti, G., Paino, F., Desiderio, V., Tirino, V., et al. (2013). Human adipose CD34+ CD90+ stem cells and collagen scaffold constructs grafted *in vivo* fabricate loose connective and adipose tissues. *J. Cell Biochem.* 114, 1039–1049. doi:10.1002/jcb.24443

Giannoudis, P. V., Dinopoulos, H., and Tsiridis, E. (2005). Bone substitutes: an update. *Injury* 36 (Suppl. 3), S20–S27. doi:10.1016/j.injury.2005.07.029

Giannoudis, P. V., and Einhorn, T. A. (2009). Bone morphogenetic proteins in musculoskeletal medicine. *Injury* 40 (Suppl. 3), S1–S3. doi:10.1016/S0020-1383(09)00642-1

Green, S. A., Jackson, J. M., Wall, D. M., Marinow, H., and Ishkanian, J. (1992). Management of segmental defects by the Ilizarov intercalary bone transport method. *Clin. Orthop. Relat. Res.* 280, 136–142. doi:10.1097/00003086-199207000-00016

Grünherz, L., Sanchez-Macedo, N., Frueh, F. S., McLuckie, M., and Lindenblatt, N. (2019). Nanofat applications: from clinical esthetics to regenerative research. *Curr. Opin. Biomed. Eng.* 10, 174–180. doi:10.1016/j.cobme.2019.07.002

Gu, Q., Cai, Y., Huang, C., Shi, Q., and Yang, H. (2012). Curcumin increases rat mesenchymal stem cell osteoblast differentiation but inhibits adipocyte differentiation. *Pharmacogn. Mag.* 8, 202–208. doi:10.4103/0973-1296.99285

Heneidi, S., Simerman, A. A., Keller, E., Singh, P., Li, X., Dumesic, D. A., et al. (2013). Awakened by cellular stress: isolation and characterization of a novel population of pluripotent stem cells derived from human adipose tissue. *PloS One* 8, e64752. doi:10.1371/journal.pone.0064752

Kachgal, S., and Putnam, A. J. (2011). Mesenchymal stem cells from adipose and bone marrow promote angiogenesis via distinct cytokine and protease expression mechanisms. *Angiogenesis* 14, 47–59. doi:10.1007/s10456-010-9194-9

Komatsu, D. E., and Warden, S. J. (2010). The control of fracture healing and its therapeutic targeting: improving upon nature. *J. Cell Biochem.* 109, 302–311. doi:10.1002/jcb.22418

Kuroda, Y., Wakao, S., Kitada, M., Murakami, T., Nojima, M., and Dezawa, M. (2013). Isolation, culture and evaluation of multilineage-differentiating stress-enduring (Muse) cells. *Nat. Protoc.* 8, 1391–1415. doi:10.1038/nprot.2013.076

Lo Furno, D., Tamburino, S., Mannino, G., Gili, E., Lombardo, G., Tarico, M. S., et al. (2017). Nanofat 2.0: experimental evidence for a fat grafting rich in mesenchymal stem cells. *Physiol. Res.* 66, 663–671. doi:10.33549/physiolres.933451

Luck, J., Smith, O. J., Malik, D., and Mosahebi, A. (2018). Protocol for a systematic review of autologous fat grafting for wound healing. *Syst. Rev.* 7, 99. doi:10.1186/s13643-018-0769-7

Majidinia, M., Sadeghpour, A., and Yousefi, B. (2018). The roles of signaling pathways in bone repair and regeneration. *J. Cell Physiol.* 233, 2937–2948. doi:10.1002/jcp.26042

Marinho, A., Nunes, C., and Reis, S. (2021). Hyaluronic acid: a key ingredient in the therapy of inflammation. *Biomolecules* 11, 1518. doi:10.3390/biom11101518

Matsumoto, D., Sato, K., Gonda, K., Takaki, Y., Shigeura, T., Sato, T., et al. (2006). Cell-assisted lipotransfer: supportive use of human adipose-derived cells for soft tissue augmentation with lipoinjection. *Tissue Eng.* 12, 3375–3382. doi:10.1089/ten.2006.12.3375

Ogura, F., Wakao, S., Kuroda, Y., Tsuchiyama, K., Bagheri, M., Heneidi, S., et al. (2014). Human adipose tissue possesses a unique population of pluripotent stem cells with nontumorigenic and low telomerase activities: potential implications in regenerative medicine. *Stem Cells Dev.* 23, 717–728. doi:10.1089/scd.2013.0473

Ossanna, R., Ghazanfar Tehrani, S., Dallatana, A., Khabouri, S., Veronese, S., Sbarbati, A., et al. (2024). Innovative non-surgical plastic technique for saddle nose correction: a study on 97 patients. *J. Clin. Med.* 13, 2387. doi:10.3390/jcm13082387

Quintero Sierra, L. A., Biswas, R., Conti, A., Busato, A., Ossanna, R., Zingaretti, N., et al. (2023). Highly pluripotent adipose-derived stem cell–enriched nanofat: a novel translational system in stem cell therapy. *Cell Transpl.* 32, 9636897231175968. doi:10.1177/09636897231175968

Rigotti, G., Marchi, A., and Sbarbati, A. (2009). Adipose-derived mesenchymal stem cells: past, present, and future. *Aesthetic Plast. Surg.* 33, 271–273. doi:10.1007/s00266-009-9339-7

Rosa, I., Romano, E., Fioretto, B. S., Matucci-Cerinic, M., and Manetti, M. (2021). Adipose-derived stem cells: pathophysiologic implications vs therapeutic potential in systemic sclerosis. *World J. Stem Cells* 13, 30–48. doi:10.4252/wjsc.v13.i1.30

Rubin, C., Turner, A. S., Bain, S., Mallinckrodt, C., and McLeod, K. (2001). Anabolism. Low mechanical signals strengthen long bones. *Nature* 412, 603–604. doi:10.1038/35088122

Rui, Y. F., Lui, P. P. Y., Lee, Y. W., and Chan, K. M. (2012). Higher BMP receptor expression and BMP-2-induced osteogenic differentiation in tendon-derived stem cells compared with bone-marrow-derived mesenchymal stem cells. *Int. Orthop.* 36, 1099–1107. doi:10.1007/s00264-011-1417-1

Sato, T., Wakao, S., Kushida, Y., Tatsumi, K., Kitada, M., Abe, T., et al. (2020). A novel type of stem cells double-positive for SSEA-3 and CD45 in human peripheral blood. *Cell Transpl.* 29, 963689720923574. doi:10.1177/0963689720923574

Schindeler, A., McDonald, M. M., Bokko, P., and Little, D. G. (2008). Bone remodeling during fracture repair: the cellular picture. *Semin. Cell Dev. Biol.* 19, 459–466. doi:10.1016/j.semcdb.2008.07.004

Semenza, G. L. (2000). HIF-1: mediator of physiological and pathophysiological responses to hypoxia. *J. Appl. Physiol.* 88, 1474–1480. doi:10.1152/jappl.2000.88.4.1474

Simonacci, F., Bertozzi, N., Grieco, M. P., Grignaffini, E., and Raposio, E. (2017). Procedure, applications, and outcomes of autologous fat grafting. *Ann. Med. Surg.* 20, 49–60. doi:10.1016/j.amsu.2017.06.059

Simunovic, F., and Finkenzeller, G. (2021). Vascularization strategies in bone tissue engineering. *Cells* 10, 1749. doi:10.3390/cells10071749

Tsai, M. T., Lin, D. J., Huang, S., Lin, H. T., and Chang, W. H. (2012). Osteogenic differentiation is synergistically influenced by osteoinductive treatment and direct cell–cell contact between murine osteoblasts and mesenchymal stem cells. *Int. Orthop.* 36, 199–205. doi:10.1007/s00264-011-1259-x

Valachová, K., and Šoltés, L. (2021). Hyaluronan as a prominent biomolecule with numerous applications in medicine. *Int. J. Mol. Sci.* 22, 7077. doi:10.3390/ijms22137077

Wakao, S., Akashi, H., Kushida, Y., and Dezawa, M. (2014). Muse cells, newly found non-tumorigenic pluripotent stem cells, reside in human mesenchymal tissues. *Pathol. Int.* 64, 1–9. doi:10.1111/pin.12129

Wakao, S., Kitada, M., Kuroda, Y., Shigemoto, T., Matsuse, D., Akashi, H., et al. (2011). Multilineage-differentiating stress-enduring (Muse) cells are a primary source of induced pluripotent stem cells in human fibroblasts. *Proc. Natl. Acad. Sci. U. S. A.* 108, 9875–9880. doi:10.1073/pnas.1100816108

Xue, E. Y., Narvaez, L., Chu, C. K., and Hanson, S. E. (2020). Fat processing techniques. *Semin. Plast. Surg.* 34, 11–16. doi:10.1055/s-0039-3402052

Zhi, L., Chen, C., Pang, X., Uludag, H., and Jiang, H. (2011). Synergistic effect of recombinant human bone morphogenic protein-7 and osteogenic differentiation medium on human bone-marrow-derived mesenchymal stem cells *in vitro*. *Int. Orthop.* 35, 1889–1895. doi:10.1007/s00264-011-1247-1

Zhu, H., Liu, Y. L., Chen, J. D., Li, H., Liu, Y. X., Xu, F. F., et al. (2012). Effect of osteogenically and adipogenically differentiated bone mesenchymal stem cells from mouse on osteoclast formation. *Zhongguo Shi Yan Xue Ye Xue Za Zhi* 20, 1187–1190.

Zuk, P. A., Zhu, M., Mizuno, H., Huang, J., Futrell, J. W., Katz, A. J., et al. (2001). Multilineage cells from human adipose tissue: implications for cell-based therapies. *Tissue Eng.* 7, 211–228. doi:10.1089/107632701300062859

Zuo, Q., Cui, W., Liu, F., Wang, Q., Chen, Z., and Fan, W. (2013). Co-cultivated mesenchymal stem cells support chondrocytic differentiation of articular chondrocytes. *Int. Orthop.* 37, 747–752. doi:10.1007/s00264-013-1782-z

frontiers | Frontiers in Bioengineering and Biotechnology

TYPE Original Research
PUBLISHED 31 July 2025
DOI 10.3389/fbioe.2025.1574145

Check for updates

OPEN ACCESS

EDITED BY
Elizabeth Vinod,
Christian Medical College and Hospital, India

REVIEWED BY
Yuanming Ouyang,
Shanghai Jiao Tong University, China
Roberta Costa,
University of Bologna, Italy
Tao Yang,
Sun Yat-sen University, China

*CORRESPONDENCE
Chengqi Lyu,
loner_lcq@sjtu.edu.cn
Jiayu Lu,
angelinelu@sjtu.edu.cn

RECEIVED 10 February 2025
ACCEPTED 21 July 2025
PUBLISHED 31 July 2025

CITATION
Chen Y, Zhu Z, Shen Y, Liu X, He Y, Lyu C and Lu J (2025) Evaluating the potential of graphene oxide to promote skeletal muscle complex regeneration.
Front. Bioeng. Biotechnol. 13:1574145.
doi: 10.3389/fbioe.2025.1574145

COPYRIGHT
© 2025 Chen, Zhu, Shen, Liu, He, Lyu and Lu. This is an open-access article distributed under the terms of the Creative Commons Attribution License (CC BY). The use, distribution or reproduction in other forums is permitted, provided the original author(s) and the copyright owner(s) are credited and that the original publication in this journal is cited, in accordance with accepted academic practice. No use, distribution or reproduction is permitted which does not comply with these terms.

Evaluating the potential of graphene oxide to promote skeletal muscle complex regeneration

Yulu Chen[1], Zeyu Zhu[1], Yian Shen[1], Xuling Liu[1], Yushi He[2], Chengqi Lyu[1]* and Jiayu Lu[1]*

[1]Department of Stomatology, Shanghai Sixth People's Hospital Affiliated to Shanghai Jiao Tong University School of Medicine, Shanghai, China, [2]Shanghai Electrochemical Energy Devices Research Center, School of Chemistry and Chemical Engineering, Shanghai Jiao Tong University, Shanghai, China

Background: Repair and regeneration of the musculoskeletal system are critical for maintaining mobility, physical function, and overall quality of life. This study aimed to optimize the size and concentration of graphene oxide (GO) to achieve a balance that enhances the proliferation and myogenic differentiation of C2C12 cells and investigate the underlying mechanisms, including the activation of key myogenic genes and signaling pathways. Additionally, the effects of exosomes derived from GO-treated C2C12 myoblasts on osteoblasts were explored.

Methods: C2C12 cells were cultured with different concentrations (0.1, 0.5, 2.5, 12.5, and 62.5 μg/mL) and particle sizes (>500 and <500 nm) of GO. Thereafter, cell viability, proliferation, cycle, and migration were evaluated via fluorescence staining, CCK-8, flow cytometry, and scratch assays, respectively. Immunofluorescence, polymerase chain reaction, and RNA sequencing (RNA-seq) were used to detect the effects of GO on C2C12 cell differentiation and explore the related molecular mechanisms. Furthermore, RNA-seq analysis was performed to investigate the impact of exosomes derived from GO-treated C2C12 myoblasts on MC3T3-E1 cells.

Results: GO with particle sizes of >500 nm at a concentration of 2.5 μg/mL significantly enhanced C2C12 cell proliferation and myogenic differentiation. Increased GO conductivity played a crucial role in supporting *MyoD* expression and promoting myocyte differentiation, likely by modulating membrane electrical activity and facilitating intercellular signaling. These effects were associated with the activation of the PI3K-Akt signaling pathway and the upregulation of the *NFATc1* gene, further highlighting the role of GO's conductive properties in regulating myogenic differentiation. Exosomes derived from GO-treated myoblasts upregulated genes such as *PDGFRB*, *COL12A1*, and *TBX2* while downregulating inflammation-related genes such as *C3*, thereby demonstrating the crosstalk between muscle and bone cells.

Conclusion: The conductive properties and surface roughness of GO significantly enhanced interactions between muscle and bone tissues, consequently facilitating effective musculoskeletal repair. This study suggests that GO can serve as a promising material for integrated approaches in musculoskeletal tissue engineering by promoting both myogenic

differentiation and osteoblastic activity. Our findings highlight the potential utility of GO in regenerative medicine, offering a novel strategy for musculoskeletal regeneration.

KEYWORDS

graphene, exosome, myogenic differentiation, musculoskeletal repair, C2C12

1 Introduction

Skeletal muscles, which account for 40%–50% of adult body weight, are essential for movement, posture, breathing, and heat production (Laumonier and Menetrey, 2016). Muscle damage caused by trauma, overuse, or degenerative conditions such as Duchenne muscular dystrophy, facioscapulohumeral muscular dystrophy (FSHD), and myotonic dystrophy type 1 (DM1) can lead to severe pain, loss of mobility, and a markedly reduced quality of life (Duan et al., 2021; Papaefthymiou et al., 2022; Dumont et al., 2015). Over the past 3 decades, musculoskeletal disorders have increased by 30% (Global, 2019; Safiri et al., 2021). Muscle repair relies on satellite cells, which are activated by signals from the damaged environment to migrate to the injury site, proliferate, and regenerate muscle tissue (Liu et al., 2018). However, this regenerative capacity is limited, allowing compensation for up to 20% of muscle mass loss; beyond this point, its adaptive and regenerative potential becomes inadequate (Liu et al., 2018; Corona et al., 2015). Repair is further complicated by challenges such as incomplete regeneration, scar tissue formation, chronic inflammation, and limited vascularization, hindering effective healing. This regenerative ability is impaired in conditions such as muscular dystrophy, leading to muscle dysfunction. Furthermore, aging and poor integration with surrounding tissues impede recovery, highlighting the urgent need for novel therapies that enhance muscle regeneration and address these challenges to effectively restore muscle function (Moiseeva et al., 2023).

The musculoskeletal system comprises bones, muscles, tendons, ligaments, and other connective tissues that work together to support the body structure, enable movement, and maintain stability. Bone and muscle tissues interact in a dynamic manner, with muscle contraction exerting forces on bones through tendons, allowing joint movement. This interaction is essential for mobility, posture, and overall function. Furthermore, skeletal muscles and bones are influenced by shared biochemical and biomechanical signals that regulate their development, maintenance, and response to injury (Herrmann et al., 2020). Disruption in the interaction between muscles and bones, often observed in conditions such as osteoporosis, muscular dystrophies, and age-related degeneration, can impair the ability of the musculoskeletal system to maintain function and stability (He et al., 2020; Catalano et al., 2022; Chagarlamudi et al., 2017; Gielen et al., 2023; Lu et al., 2018).

Current repair strategies for the musculoskeletal system primarily focus on addressing bone and muscle injuries independently. For bone repair, these strategies include the use of bone grafts, synthetic scaffolds, and osteogenic growth factors to promote healing (Safari et al., 2021; Stamnitz and Klimczak, 2021). Meanwhile, muscle repair is typically approached through the activation of satellite cells, myoblast transplantation, and the use of biomaterials to stimulate myogenic differentiation (Sousa-Victor et al., 2022; Nuge et al., 2021). Although these approaches have shown some success, they often fail to address the complex interconnected nature of muscle–bone interactions. For example, bone repair strategies often overlook the role of muscle strength and function in maintaining bone health, whereas muscle repair techniques do not sufficiently account for the influence of bones on muscle regeneration. Furthermore, numerous existing therapies do not fully restore function, particularly in degenerative conditions such as muscular dystrophies or age-related sarcopenia, wherein both muscles and bones are compromised. The complexity of these interactions presents challenges in developing therapies that target both systems simultaneously, and more research is necessary to optimize such integrated approaches.

Graphene oxide (GO) exhibits exceptional physical properties, including higher hardness than diamond, an elastic modulus of up to 1 TPa, and a tensile strength of ~130 MPa (Lee et al., 2008). These properties render GO ideal for simulating the mechanical strength and elasticity of skeletal muscles. Furthermore, its nanoscale roughness effectively mimics that of natural extracellular matrix (ECM), which can promote protein adsorption and cell adhesion (Bacakova et al., 2011). The π–π interactions and the presence of oxygen-containing functional groups on GO enhance its ability to bind proteins, further facilitating muscle cell adhesion and differentiation (Kenry et al., 2018; Luong-Van et al., 2020). Skeletal muscles are highly responsive to electrical signals, and processes such as cell communication, proliferation, differentiation, and contraction depend on these stimuli. The excellent electrical conductivity of GO, resulting from its sp^2 hybridized carbon structure and free-moving π electrons, can influence gene expression, thereby enhancing muscle cell adhesion, proliferation, and differentiation (Jung et al., 2008; Dong et al., 2020; Han et al., 2023; Chen et al., 2013).

In addition to its effects on muscle cells, GO has demonstrated considerable potential in bone regeneration. International studies have reported that GO enhances osteoblast proliferation and differentiation, thereby improving bone mineralization and accelerating bone repair processes (Bahrami et al., 2021; Berrio et al., 2021; Wong et al., 2020; Ş et al., 2022). MC3T3-E1 cells are osteoblastic precursor cells derived from mouse calvaria that can differentiate into mature osteoblasts to form a mineralized bone matrix under appropriate conditions. These cells are extensively used in bone biology research because of their relevance in osteogenesis and bone tissue repair (Izumiya et al., 2021; Seo et al., 2010; Fukuda et al., 2013).

Abbreviations: AFM, Atomic force microscopy; BSA, Bovine serum albumin; DEG, Differentially expressed genes; DMEM, Dulbecco's Modified Eagle Medium; ECM, Extracellular matrix; GO, Graphene oxide; PBS, Phosphate-buffered saline; HBSS, Hank's Balanced Salt Solution; PCR, Polymerase chain reaction; PI, Propidium iodide; SEM, Scanning electron microscopy.

To investigate the impact of GO on skeletal muscle proliferation and differentiation and the effects of the interplay between muscles and bones (musculoskeletal crosstalk), this study evaluated the effects of GO on C2C12 cells, examining how different GO concentrations and sizes influence cell viability, migration, and differentiation. GO was found to promote the intracellular flow of calcium ions through its electrical conductivity, in turn activating the NFATc1 signaling pathway, which leads to the upregulation of MyoD and promotes myogenic differentiation. Furthermore, we explored the effects of exosomes derived from GO-treated C2C12 cells on MC3T3-E1 cells, highlighting GO's potential for comprehensive musculoskeletal regeneration. This dual focus emphasizes the interconnectedness of muscle and bone regeneration and highlights potential pathways through which GO can promote comprehensive musculoskeletal repair, thereby offering a holistic approach to addressing musculoskeletal disorders.

2 Methods

2.1 Characterization and conductivity

The GO used in this research was purchased from Nano Xianfeng Company, China. We observed the shape and size of GO using scanning electron microscopy (SEM) (Tescan MIRA, Czech Republic) and measured its surface roughness using atomic force microscopy (AFM) (PARK NX-Hivac, Korea).

The samples with particle sizes greater and less than 500 nm were diluted to concentrations of 0.1, 0.5, 2.5, 12.5, and 62.5 μg/mL, respectively, following a concentration gradient. The conductivity of each dilution was subsequently measured using a conductivity detector (HANNA HI8733, Italy).

2.2 Cell culture

The C2C12 cell line was purchased from Procell (CL-0044, China) and cultured in Dulbecco's Modified Eagle Medium (DMEM) (HyClone, United States) supplemented with 10% fetal bovine serum (HyClone) and 1% penicillin–streptomycin (HyClone). The cells were maintained at 37°C in a humidified incubator containing 5% CO_2 (Zhang et al., 2023). The medium was replaced every 2–3 days to ensure optimal growth conditions. The cells were passaged when they reached approximately 80%–90% confluence. All subsequent cell culture experiments were performed with at least three biological replicates (n = 3) to ensure reproducibility.

2.3 Cell viability assay

To evaluate the effects of different concentrations and sizes of GO on the viability of C2C12 cells, these cells were seeded in 96-well plates (NEST, United States) at a density of 1×10^4 cells per well. The cells were allowed to adhere for 12 h and then treated with two types of GO differing in sheet size: one with diameters of >500 nm and the other with diameters of <500 nm. The treatments were administered at concentrations of 0, 0.1, 0.5, 2.5, 12.5, and 62.5 μg/mL. On days 1, 3, and 5 after treatment, 10 μL of the CCK-8 reagent (Beyotime Biotechnology, China) was added to each well containing cells in a 96-well plate. The cells were then incubated with the reagent for 2 h. The absorbance measured by the microplate reader was recorded for further analysis to assess the effects of both types of GO on cells over time.

The C2C12 cells were seeded into 24-well plates (NEST) at a density of 2×10^4 cells per well and allowed to adhere. Following cell attachment, the cells were treated with two types of GO (diameters >500 nm and diameters <500 nm) at concentrations of 0, 0.1, 0.5, 2.5, 12.5, and 62.5 μg/mL with particle sizes of either >500 nm or <500 nm. The cells were incubated for 24 h, following which they were washed with phosphate-buffered saline (PBS). Subsequently, the cells were stained using a live/dead cell staining kit (ScienCell, United States) and photographed with a fluorescence microscope (Olympus CKX53, Japan).

2.4 Flow cytometric analysis

The C2C12 cells were seeded in six-well plates at a density of 1×10^5 cells per well. They were treated with different concentrations of GO, particularly 0.1, 0.5, 2.5, and 62.5 μg/mL, with particle sizes of either >500 nm or <500 nm. Following a 24-h incubation period, the cells were harvested, fixed in 70% ethanol, and stained with propidium iodide (PI) to label DNA. Flow cytometric analysis was performed to determine the percentage of cells in each phase of the cell cycle—G0/G1, S, and G2/M.

The C2C12 cells were seeded into six-well plates at a density of 1×10^5 cells per well. Upon reaching 70%–80% confluence, the cells were treated with varying concentrations of GO (0.5 and 2.5 μg/mL) and particle sizes of >500 and <500 nm. After 48 h of treatment, the cells were washed thrice with Hank's balanced salt solution (HBSS, Siwega) and then incubated with Fluo-4 AM working solution (YEASEN, China). After incubation, the cells were washed thrice with HBSS and then further incubated in HBSS at 37°C for an additional 30 min to allow the complete uptake of Fluo-4 AM. Subsequently, the adherent cells from each treatment group were trypsinized, suspended in a medium, and centrifuged at 1,000 rpm for 5 min. The supernatant was discarded, and the cells were resuspended in PBS. The suspension was centrifuged again at 1,000 rpm for 5 min. This washing step was repeated 1 to 2 times. Finally, the cells were transferred to flow cytometry tubes for detection.

2.5 Cell migration

The C2C12 cells were cultured in six-well plates until they reached ~90% confluence. A sterile 200-μL pipette tip was then used to create a straight scratch in each well to simulate a wound. The cells were gently washed with PBS to remove detached cells and debris, and fresh culture medium was added, followed by treatment with two types of GO with different sheet sizes (diameters >500 nm and diameters <500 nm) at concentrations of 0.5 and 2.5. Images were captured using a Nikon DS-Qi2 optical microscope immediately after scratching and 24 h after scratching. To assess the scratch width at 0 and 24 h, six measurement points in the image were selected using ImageJ software. The cell migration rate was then calculated using the following formula: migration rate (%) = [(Scratch width at 0 h − Scratch width at 24 h)/Scratch width at 0 h] × 100%.

2.6 F-actin staining

The C2C12 cells were seeded in a 12-well plate (NEST, United States) with round coverslips (Biosharp, China) at a density of 1×10^5 cells per well. Subsequently, the cells were treated with two types of GO with different sheet sizes at concentrations of 0.5 and 2.5 μg/mL until they reached 70% confluence. The cells were fixed with 4% paraformaldehyde in PBS for 10 min at room temperature (24°C). Then, the cells were permeabilized with 0.1% Triton X-100 (BioFroxx, Germany) in PBS for 5 min. After permeabilization, the cells were incubated with a blocking solution of 3% bovine serum albumin (BSA) (Beyotime, China) in PBS for 30 min to prevent nonspecific binding. Actin-Tracker Red (Beyotime, China) was then diluted with secondary antibody diluent at a ratio of 1:150, and 200 μL of the solution was added to each sample. The mixture was then incubated for 60 min at room temperature in the dark. The cells were subsequently washed with PBS and counterstained with 4′,6-diamidino-2-phenylindole (DAPI) to visualize the nuclei. Images were captured using a fluorescence microscope (Zeiss Axio Imager A2, Germany). From the obtained fluorescence images, cell width, length, and aspect ratio data were analyzed using ImageJ. The aspect ratio was calculated as follows: Aspect Ratio = Cell Length/Cell Width.

2.7 Cell differentiation

The cell viability assay results indicated that GO at concentrations of ≤2.5 μg/mL exhibited good biocompatibility. The C2C12 cells were differentiated in DMEM containing 2% horse serum (Procell, China) and 1% penicillin–streptomycin. The experimental groups were treated with GO having diameters of >500 nm and <500 nm at concentrations of 0.1, 0.5, and 2.5 μg/mL, with a control group lacking GO. Medium changes were performed every 2–3 days.

2.7.1 Real-time polymerase chain reaction

Based on the biocompatibility assessments results, 5 days after the C2C12 cells were treated with two types of GO with different sheet sizes (diameters >500 nm and diameters <500 nm) at concentrations of 0.5 and 2.5 μg/mL, the cells were collected for real-time polymerase chain reaction (PCR) to assess gene expression associated with muscle differentiation. The cells were collected and lysed using TRIzol reagent, and the total RNA was isolated according to the manufacturer's protocol. The RNA concentration was measured using a NanoDrop One spectrophotometer (NanoDrop Technologies, United States). Complementary DNA (cDNA) was synthesized from 1 μg of RNA using a reverse transcription kit (Vazyme, China) according to the manufacturer's instructions. Real-time PCR was subsequently performed using specific primers for the muscle differentiation markers MyoD (Sangon Biotech, China) and NFATc1 (Sangon Biotech), along with a SYBR Green or TaqMan PCR master mix. The PCR reactions were run on a real-time PCR machine under appropriate thermal cycling conditions. The relative gene expression levels were quantified using the $2^{-\Delta\Delta C_T}$method, with glyceraldehyde-3-phosphate dehydrogenase used as the internal control. Data were analyzed to compare the effects of different treatment conditions on the expression of muscle-specific genes.

2.7.2 Immunofluorescence assay

According to the PCR results, the C2C12 cells were differentiated and cultured for 5 days at a concentration of 2.5 μg/mL, and MyHC expression was analyzed using immunofluorescence. The experimental groups were as follows: GO (>500 nm, 2.5 μg/mL) with horse serum, GO (<500 nm, 2.5 μg/mL) with horse serum, GO (>500 nm) without horse serum, GO (<500 nm) without horse serum, and a control group without GO. The cells were then treated as described in Section 2.6 for 5 days to promote myotube formation. Following the differentiation period, the cells were fixed with 4% paraformaldehyde at 24°C for 15 min. The cells were permeated with 0.1% Triton X-100 (Bio Froxx, Germany) for 10 min. The cells were blocked with 3% BSA for 30 min to prevent nonspecific binding. The primary antibody against MyHC (1:200, ABclonal, China, myosin heavy chain, a marker of muscle development and differentiation) was incubated with the cells overnight at 4°C. Then, the cells were incubated with a fluorescently labeled secondary antibody (1:500, Jackson, United States) for 1 h at room temperature in the dark. Following additional washes, the nuclei were stained with DAPI for 5 min. Images were captured using a fluorescence microscope (LEICA DM2000LED, China) and analyzed with ImageJ.

2.8 MC3T3-E1 cell treatment

The C2C12 cells were cultured in six-well plates in DMEM supplemented with 2% horse serum to induce differentiation. This setup served as the control group. For the experimental group, the cells were cultured under identical conditions but with the addition of GO (diameter >500 nm, 2.5 μg/mL) to assess its impact on exosome production. After 5 days of treatment, the culture media from both the control and experimental groups were collected separately, and the exosomes were isolated using ultracentrifugation. The media were centrifuged at 300 × g for 10 min to remove cell debris, followed by centrifugation at 10,000 × g for 30 min to pellet the exosomes. MC3T3-E1 cells (CL-0710, Pricella) were cultured in the MC3T3-E1 cell culture medium (CM-0710, Pricella) until they reached 70%–80% confluence.

The exosomes derived from the C2C12 cells, which were cultured with or without GO, were added to the MC3T3-E1 cells at a concentration of 50 μg/mL and incubated for 48 h. In the experimental group, the MC3T3-E1 cells were treated with the exosomes derived from the C2C12 cells exposed to GO and 2% horse serum, whereas the control group received exosomes from the C2C12 cells cultured with 2% horse serum alone.

2.9 RNA sequencing analysis

Based on the finding that GO at a concentration of 2.5 μg/mL and particle sizes of >500 nm can promote the proliferation and myogenic differentiation of C2C12 cells, this GO size and concentration were used for RNA sequencing (RNA-seq). The C2C12 cells were differentiated under three conditions: (A) 2% horse serum, (B) a combination of 2% horse serum and GO (diameter >500 nm, 2.5 μg/mL), and (C) GO

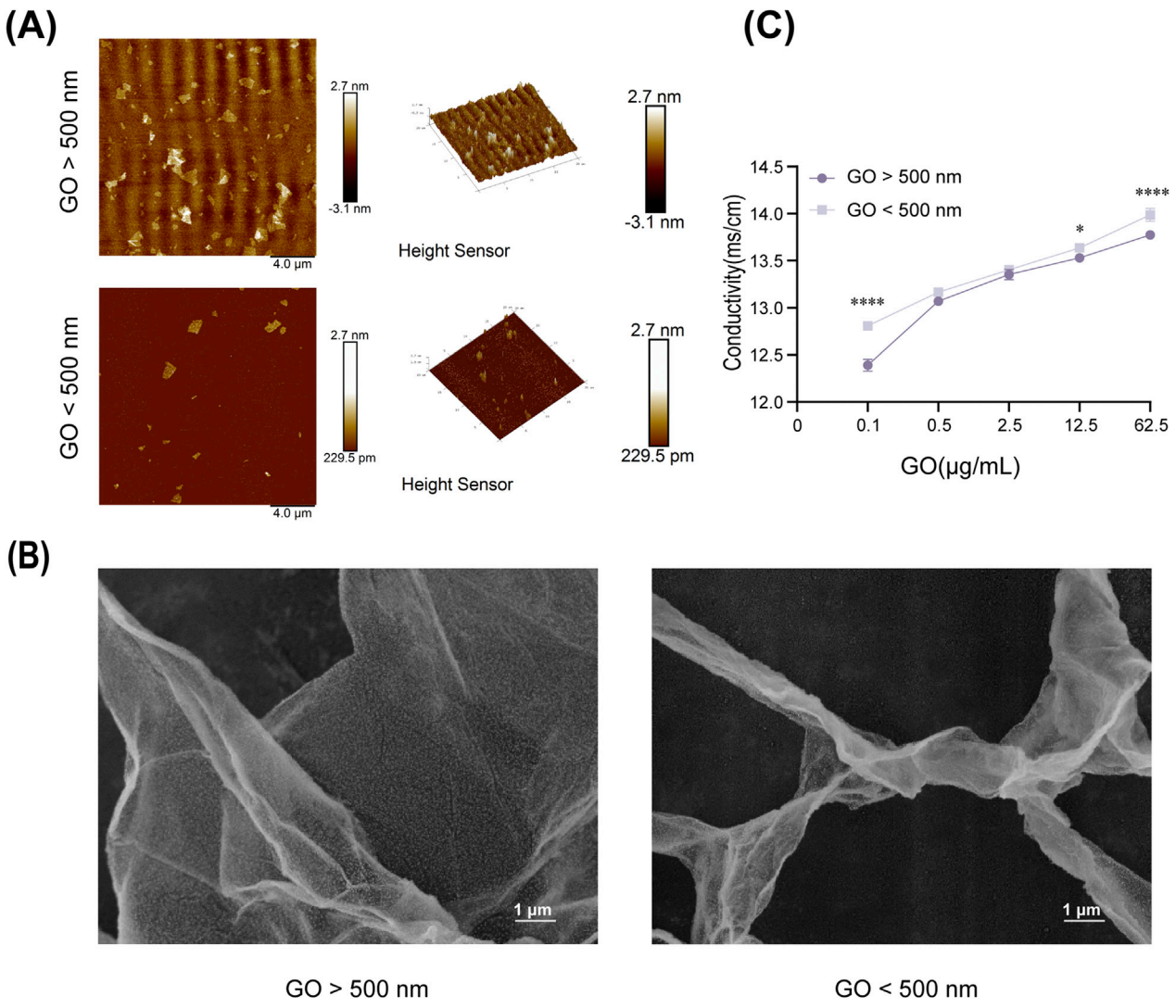

FIGURE 1
Physical and chemical properties of graphene oxide (GO). **(A)** Atomic force microscopy images of GO (diameter >500 nm) and GO (diameter <500 nm). Scale bars = 4 µm. **(B)** Scanning electron microscopy images of GO at ×10,000 magnification. **(C)** Conductivity of GO at different concentrations (0.1–62.5 µg/mL) and diameters (*$P < 0.05$, ****$P < 0.0001$).

(diameter >500 nm, 2.5 µg/mL). After a 5-day differentiation period, the cells from each condition were collected for RNA-seq analysis.

In a parallel experiment, the MC3T3-E1 cells were exposed to the exosomes derived from the C2C12 cells cultured under the aforementioned conditions. Following 48 h of exosome treatment, the MC3T3-E1 cells were harvested, and the total RNA was extracted using a commercial RNA extraction kit according to the manufacturer's instructions. RNA quality and quantity were assessed using a NanoDrop spectrophotometer and an Agilent Bioanalyzer. The RNA samples were subsequently prepared for sequencing by generating libraries and performing RNA-seq using Illumina. The resulting raw sequencing data were analyzed to determine gene expression levels.

2.10 Statistical analysis

All data are expressed as means ± standard deviations. The statistically significant differences between groups were analyzed using one-way or two-way analysis of variance in GraphPad Prism 9.5. Differences with p-values of <0.05 were considered statistically significant.

3 Results

3.1 Characterization of different sheet sizes of GO

The AFM and SEM results revealed clear differences in the surface morphology and structure of GO sheets of various sizes. The larger GO sheets exhibited a more uniform surface topology, whereas the smaller GO sheets displayed more irregular structures (Figures 1A,B).

In terms of conductivity, measurements indicated that the electrical conductivity of GO significantly improved with increasing concentration, regardless of the sheet size (Figure 1C). At the same concentration, smaller GO sheets exhibited slightly

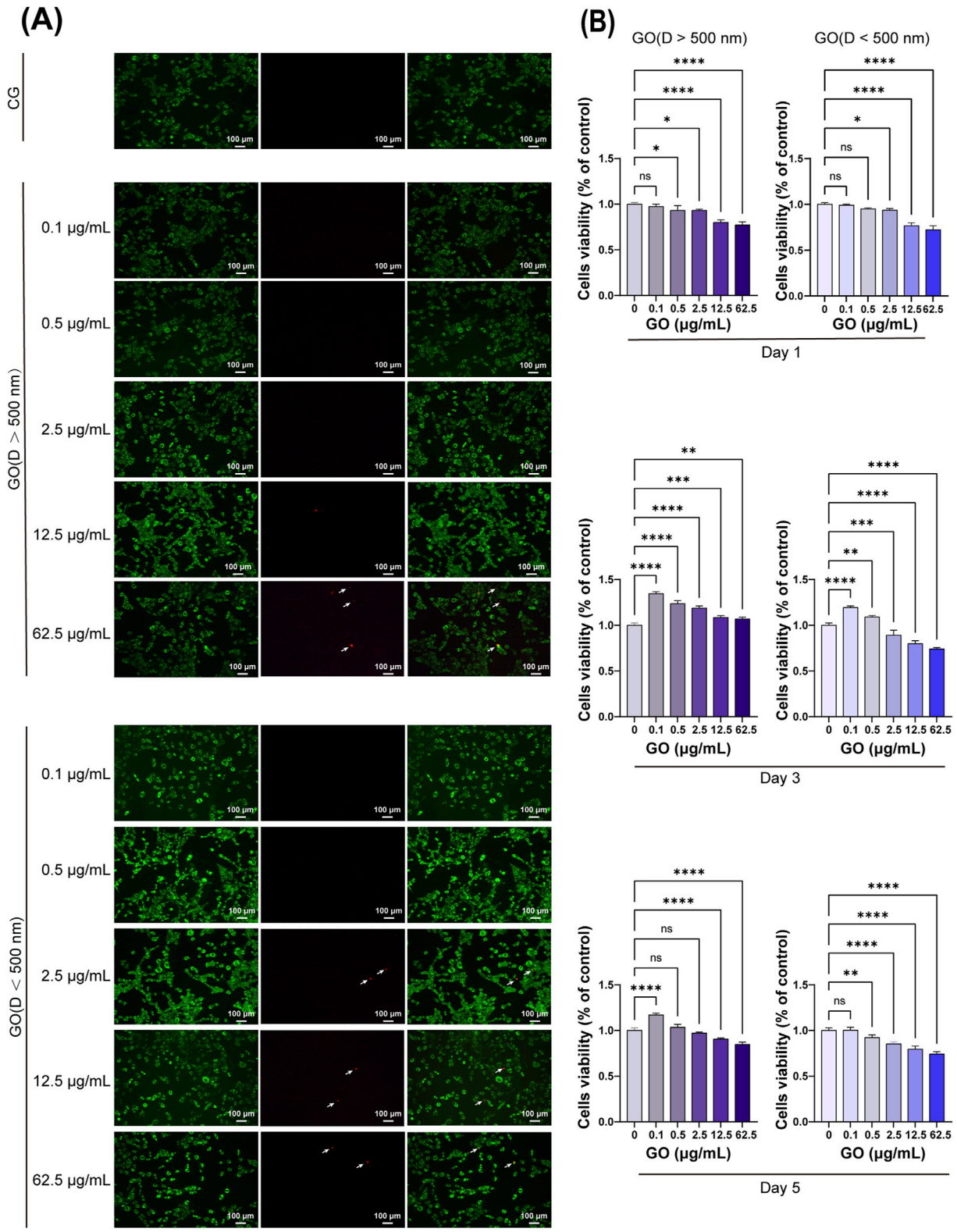

FIGURE 2
Cytotoxicity of graphene oxide (GO) with different concentrations and diameters. **(A)** Fluorescence images show the results of the live/dead staining with viable cells appearing green and dead cells (white arrow) appearing red. Scale bars = 100 μm. CG represents the conventional culture medium control group without GO. **(B)** CCK-8 assay results on days 1, 3, and 5 (n = 4, *p < 0.05, **p < 0.01, ***p < 0.001, ****p < 0.0001).

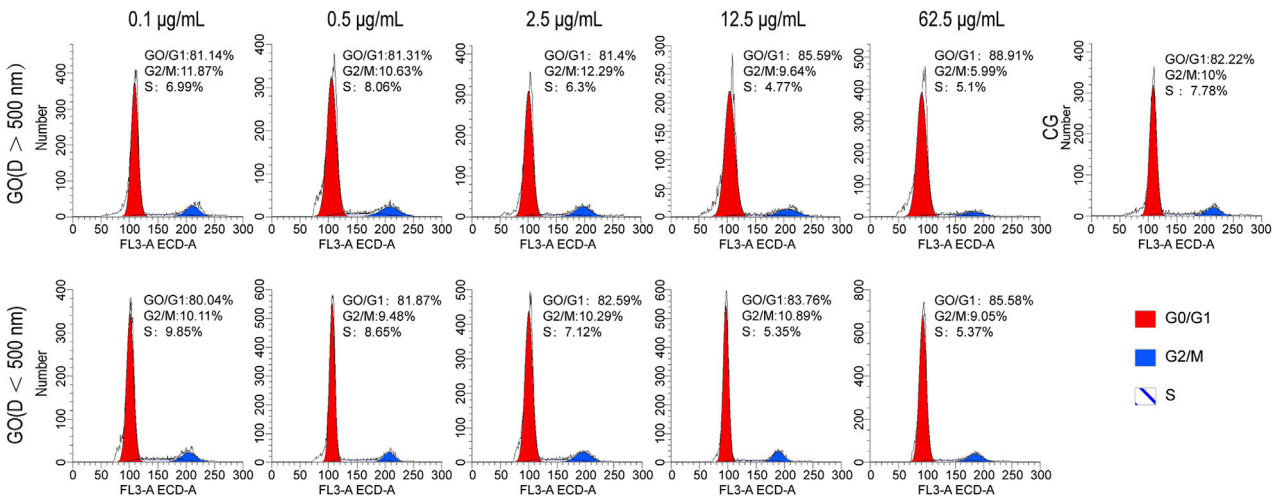

FIGURE 3
Cell cycle analysis of C2C12 cells treated with graphene oxide (GO); CG represents conventional culture medium control group without GO.

higher electrical conductivity than larger GO sheets, possibly because of their increased surface area and better charge mobility (Kim et al., 2017).

3.2 Effects of GO on C2C12 cell viability

In the CCK-8 assay evaluating the effects of GO on C2C12 cells, on the third day of culture, low concentrations of GO with sheet diameters of >500 nm were found to promote C2C12 cell proliferation (Figure 2B). By the fifth day, GO at concentrations of ≤2.5 μg/mL did not exert cytotoxic effects, indicating good biocompatibility at lower doses. However, at concentrations of ≥12.5 μg/mL, GO induced significant cytotoxicity, reducing cell viability. Moreover, smaller GO sheets (<500 nm) were found to be more cytotoxic than larger sheets, likely because of their higher surface area and increased interaction with cellular membranes. These results highlight the importance of the size and concentration of GO in determining its biocompatibility with C2C12 cells. Low concentrations of larger GO sheets appeared to support cell growth, whereas higher concentrations and smaller sheets exerted cytotoxic effects.

Live and dead staining experiments were conducted on myoblasts cultured for 1 day with various concentrations and sizes of GO. The results demonstrated that GO concentrations from 0.1 μg/mL to 12.5 μg/mL with particle sizes of >500 nm did not cause cell death, similar to that observed in the control group (Figure 2A). However, at a concentration of 62.5 μg/mL, few dead cells were detected. For GO with particles sizes of <500 nm, concentrations ranging from 0.1 μg/mL to 2.5 μg/mL did not induce cell death; however, at concentrations of >12.5 μg/mL, costaining with both calcein-AM and PI was observed. This costaining indicates that some cells exhibited compromised membrane integrity while still being capable of metabolizing calcein-AM, suggesting that these cells are in a state of stress or early apoptosis.

The flow cytometry analysis of C2C12 myoblasts cultured with varying concentrations and diameters of GO for 1 day revealed that when the concentration of GO was <12.5 μg/mL, its impact on cell cycle progression was relatively mild compared with that in higher concentrations. At 2.5 μg/mL, the distribution of cells in the G0/G1, G2/M, and S phases closely mirrored that of the control group, indicating minimal interference with the cell cycle (Figure 3). However, at a higher concentration of 62.5 μg/mL, a notable increase in the number of cells in the G0/G1 phase and a corresponding decrease in the number of cells in the G2/M and S phases were observed, suggesting that elevated concentrations of GO induce cell cycle arrest at the G0/G1 phase, potentially limiting cell division.

3.3 Effects of GO on C2C12 cell migration

According to the CCK8 results, the control group without GO was compared with the groups treated with GO at 0.5 and 2.5 μg/mL (<500 nm and >500 nm). The cell migration analysis revealed that treatment with GO enhanced the migration rate of myoblasts compared with that in the control group without GO. Alternatively, treatment with 2.5 μg/mL GO with particle sizes of >500 nm resulted in a more pronounced increase in myoblast migration, significantly enhancing cellular motility compared with the that in control group and the 0.5 μg/mL condition (Figures 4A,B). These results suggest that GO influences myoblast migration in a concentration-dependent manner, with higher concentrations of larger GO sheets (diameter >500 nm, 2.5 μg/mL) exerting a more substantial effect on promoting cell mobility.

3.4 Effects of GO on the cytoskeleton of C2C12 cells

Cytoskeletal experiments revealed that GO influenced the cytoskeletal organization and morphology of C2C12 cells in a concentration-dependent manner. In the control group without GO, the actin filaments were well-organized, supporting the

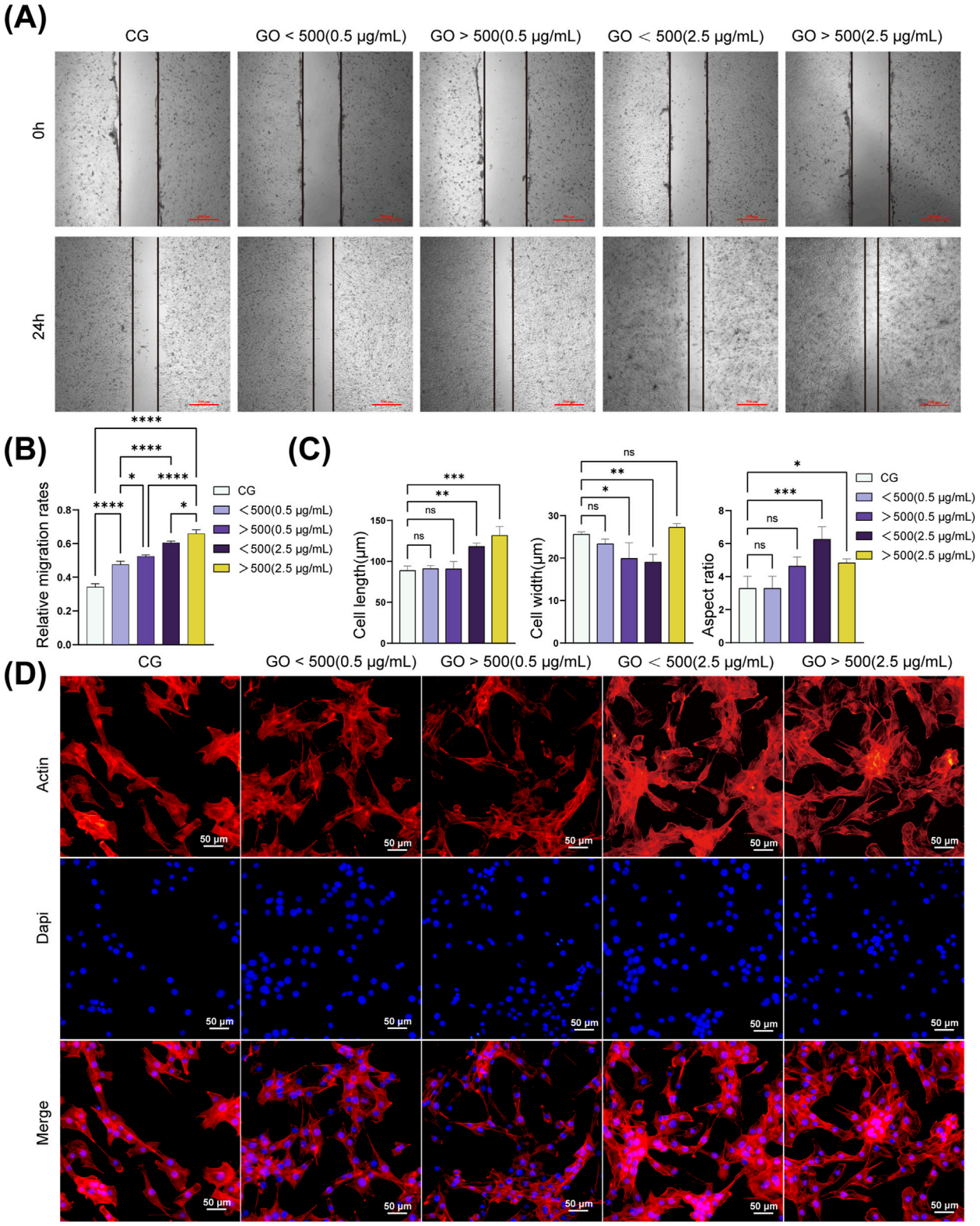

FIGURE 4
Migration and cytoskeleton of C2C12 cells treated with graphene oxide (GO). **(A,B)** Representative images and quantitative analysis of the scratch assay in C2C12 cells. (**$p < 0.01$, ***$p < 0.001$, ****$p < 0.0001$). **(C)** Morphology analysis of C2C12 cells. (*$p < 0.05$, **$p < 0.01$, ***$p < 0.001$; n = 50 cells per condition). **(D)** Cytoskeleton of C2C12 cells treated with GO. Red: F-actin (phalloidin), blue: nuclei (DAPI). CG represents conventional culture medium control group without GO. Scale bars = 4 μm.

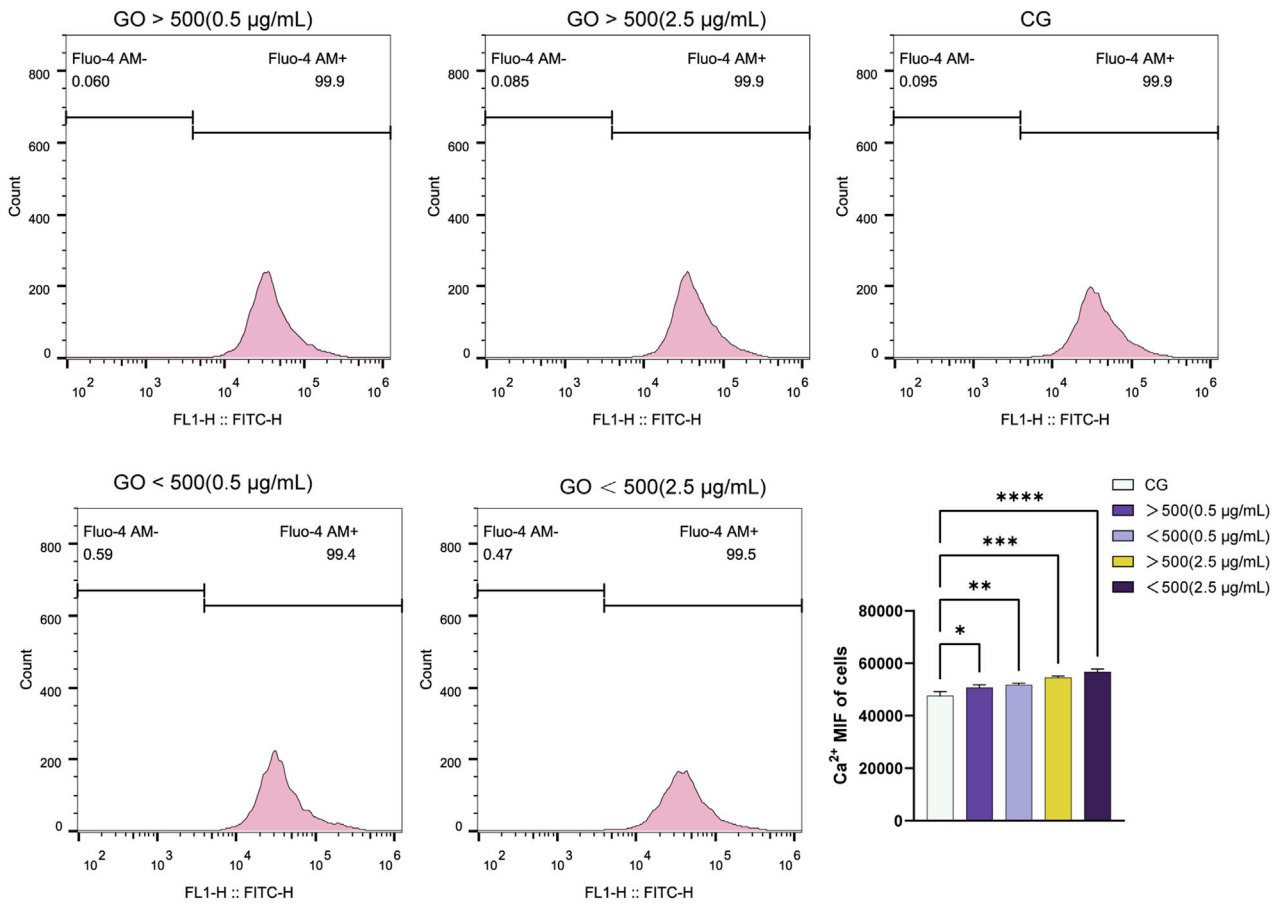

FIGURE 5
Fluorescence curve and quantitative analysis of calcium ion flux in C2C12 myoblasts treated with graphene oxide (GO) (*$p < 0.05$, **$p < 0.01$, ***$p < 0.001$, ****$p < 0.0001$).

typical spindle-shaped morphology of myoblasts with moderate migration. At a concentration of 0.5 μg/mL, both smaller GO sheets (diameter <500 nm) and larger GO sheets (diameter >500 nm) slightly enhanced cytoskeletal integrity and motility, with well-maintained actin filaments and improved cell spreading (Figure 4D). At 2.5 μg/mL, the GO sheets, particularly those with diameters of >500 nm, promoted cytoskeletal reorganization, resulting in pronounced stress fiber formation, enhanced cell adhesion, and a substantial improvement in cell migration. Quantitative analysis of the cytoskeleton revealed that treatment with 0.5 μg/mL GO exerted minimal effects on both cell length and width. At a concentration of 2.5 μg/mL, an increase in the cell length and aspect ratio was observed. Notably, GO with diameters of >500 nm increased the cell width, whereas GO with diameters of <500 nm decreased the cell width, accompanied by an increase in the aspect ratio (Figure 4C).

3.5 Effects of GO on calcium ion flow in C2C12

Flow cytometry analysis of calcium ion flux revealed that higher concentrations of GO, particularly at 2.5 μg/mL, induced greater fluorescence intensity of calcium ions than at concentration of 0.5 μg/mL. Moreover, the particle size of GO influenced the fluorescence intensity, with GO with diameters of <500 nm exhibiting slightly higher calcium ion flux than GO with diameters of >500 nm at the same concentration (Figure 5). Cells treated with 2.5 μg/mL GO—particularly the smaller-sized GO sheets (<500 nm)—showed more pronounced calcium signaling responses. This finding suggests that increased conductivity associated with increased GO concentration and surface area (for smaller particles) enhanced calcium ion influx. The enhanced electrical conductivity of GO appears to facilitate the entry of calcium ions through the cell membrane, likely by modulating ion channel activity, which in turn activates intracellular signaling pathways.

3.6 Effects of GO on C2C12 cell differentiation

PCR was performed to assess the expression of the *NFATc1* and *MyoD* genes. The results demonstrate a synergistic effect between GO and horse serum, leading to a significant upregulation of *MyoD* expression. At concentrations below 2.5 μg/mL, the expression levels

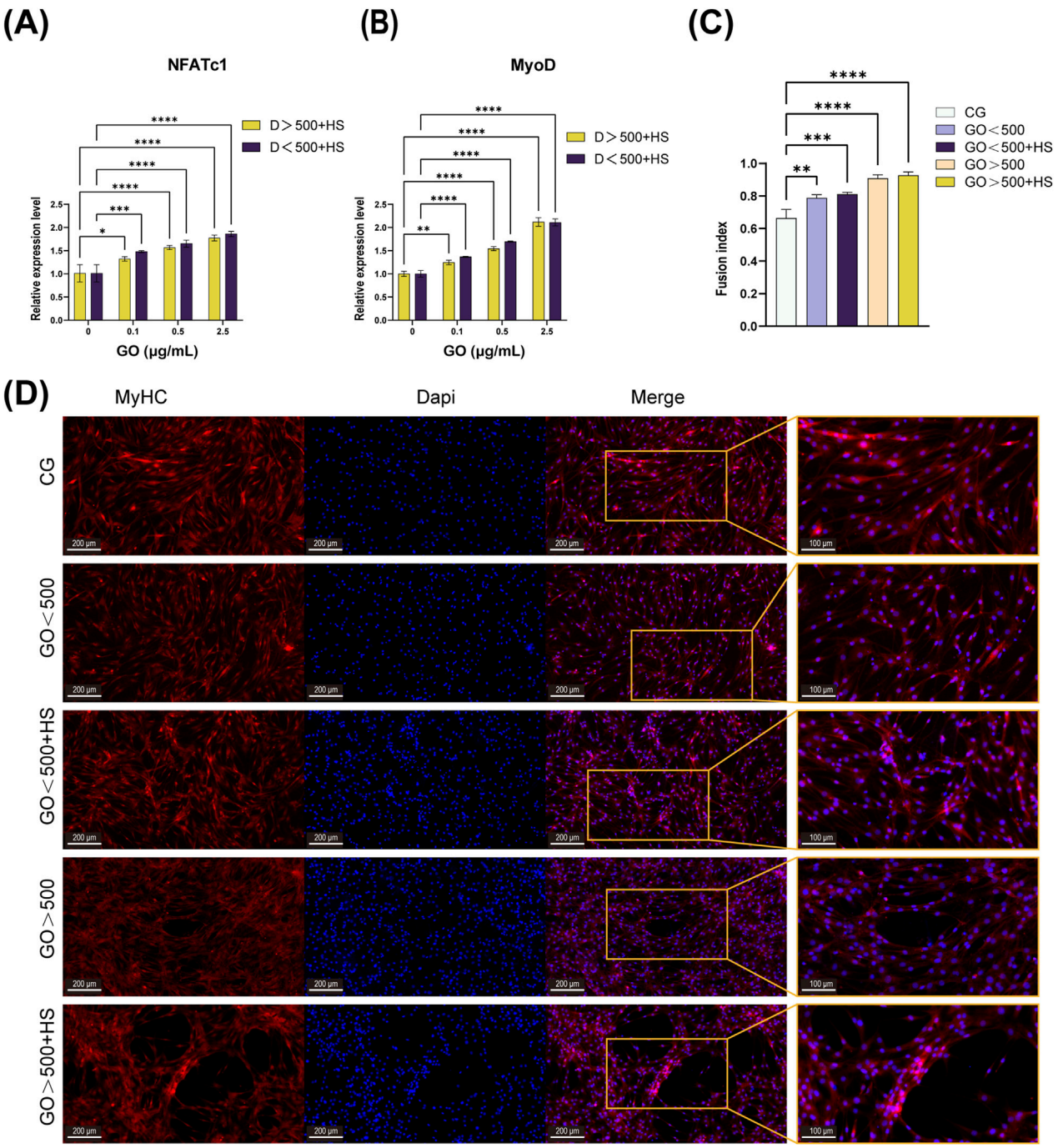

FIGURE 6
Effects of graphene oxide (GO) on C2C12 cell differentiation. **(A,B)** Polymerase chain reaction (PCR) results of *NFATc1* and *MyoD* after 5 days of differentiation in cultures with only horse serum and GO combined with horse serum ($n = 3$, $*p < 0.05$, $**p < 0.01$, $****p < 0.0001$). **(C,D)** Immunofluorescence image and fusion index analysis of MyHC after 5 days of differentiation with or without GO ($**p < 0.01$, $***p < 0.001$, $****p < 0.0001$). CG means a control group containing only 2% horse serum without GO.

of *NFATc1* and *MyoD* increased in correlation with the electrical conductivity of GO. However, at a concentration of 2.5 μg/mL, GO with a larger size induced higher *MyoD* expression compared to its smaller counterpart (Figures 6A,B).

Immunofluorescence analysis revealed that GO combined with 2% horse serum enhanced the formation of multinucleated myotubes and promoted myoblast fusion, regardless of the GO diameter (Figure 6C). Meanwhile, GO with diameters of >500 nm combined with 2% horse serum not only synergistically promoted the formation of multinucleated myotubes but also increased the length and diameter of the myotubes (Figure 6D). These results suggest that GO size, along with the differentiation medium, influences both the fusion process and the elongation of myotubes, with larger GO having a more pronounced effect.

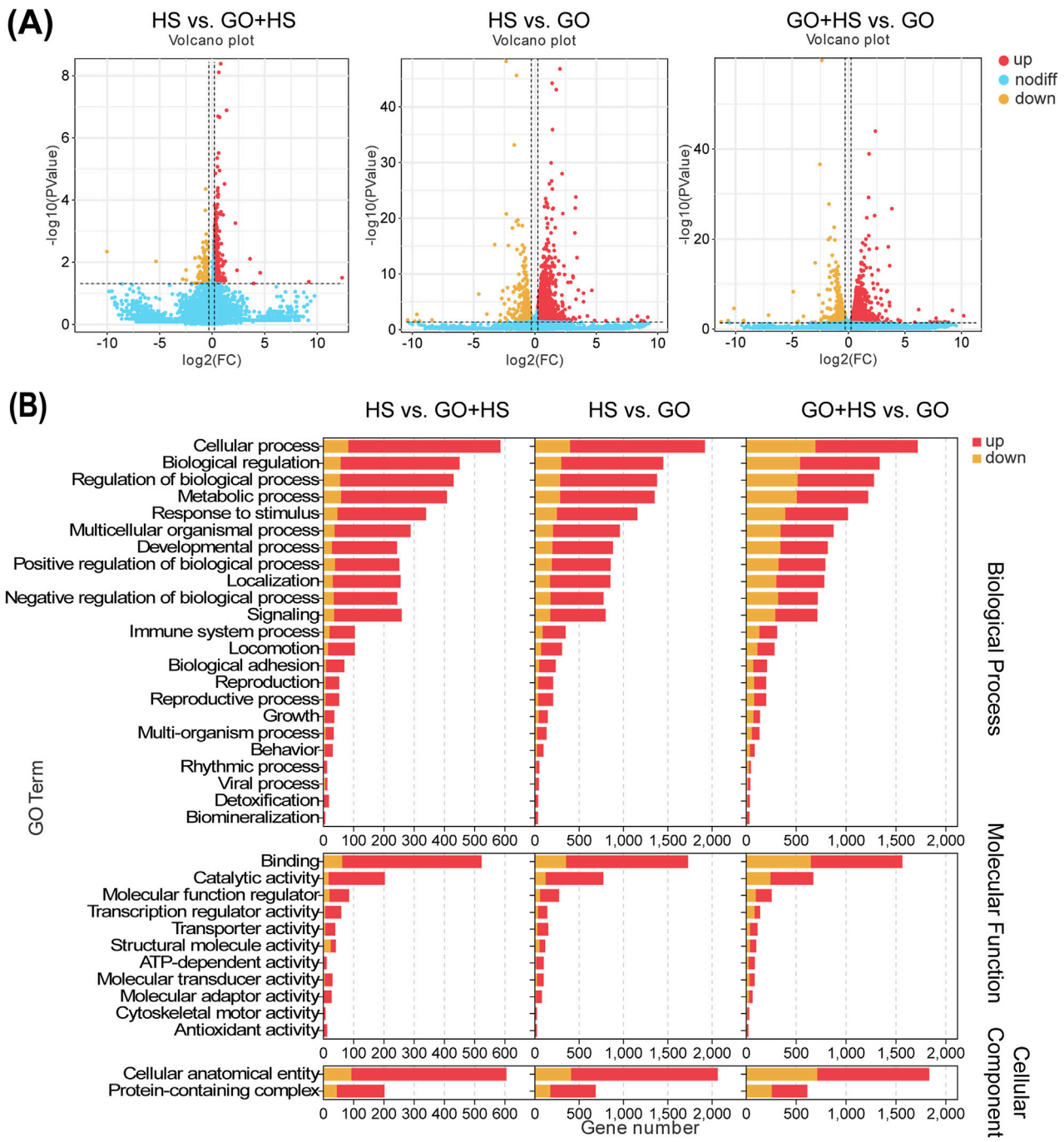

FIGURE 7
Summary of differentially expressed genes (DEGs) of C2C12 cells after 5 days of differentiation in cultures with horse serum, graphene oxide (GO), and GO combined with horse serum. **(A)** Volcano plot displaying an overview of the DEGs. HS represents the control group with 2% horse serum and no GO; GO + HS indicates the experimental group with GO and 2% horse serum. GO refers to the experimental group with GO but without horse serum. **(B)** GO channel enrichment statistical histogram.

The C2C12 cells were differentiated under three conditions: GO, horse serum, and GO combined with horse serum. RNA-Seq analysis revealed distinct gene expression changes in all the groups compared with those in the control group (containing 2% horse serum). In the GO plus horse serum group, 563 genes were upregulated and 93 were downregulated, whereas, in the GO-only group, 1,758 genes were upregulated and 425 were downregulated (Figure 7A).

GO treatment upregulated binding and catalytic activities, suggesting enhanced protein interactions and enzymatic activity. In cellular components, increase in the amount of cellular anatomical entities and protein-containing complexes indicates cytoskeletal remodeling. Biological processes remained dominated by cellular processes, biological regulation, and metabolism, implying enhanced differentiation and metabolic activity,

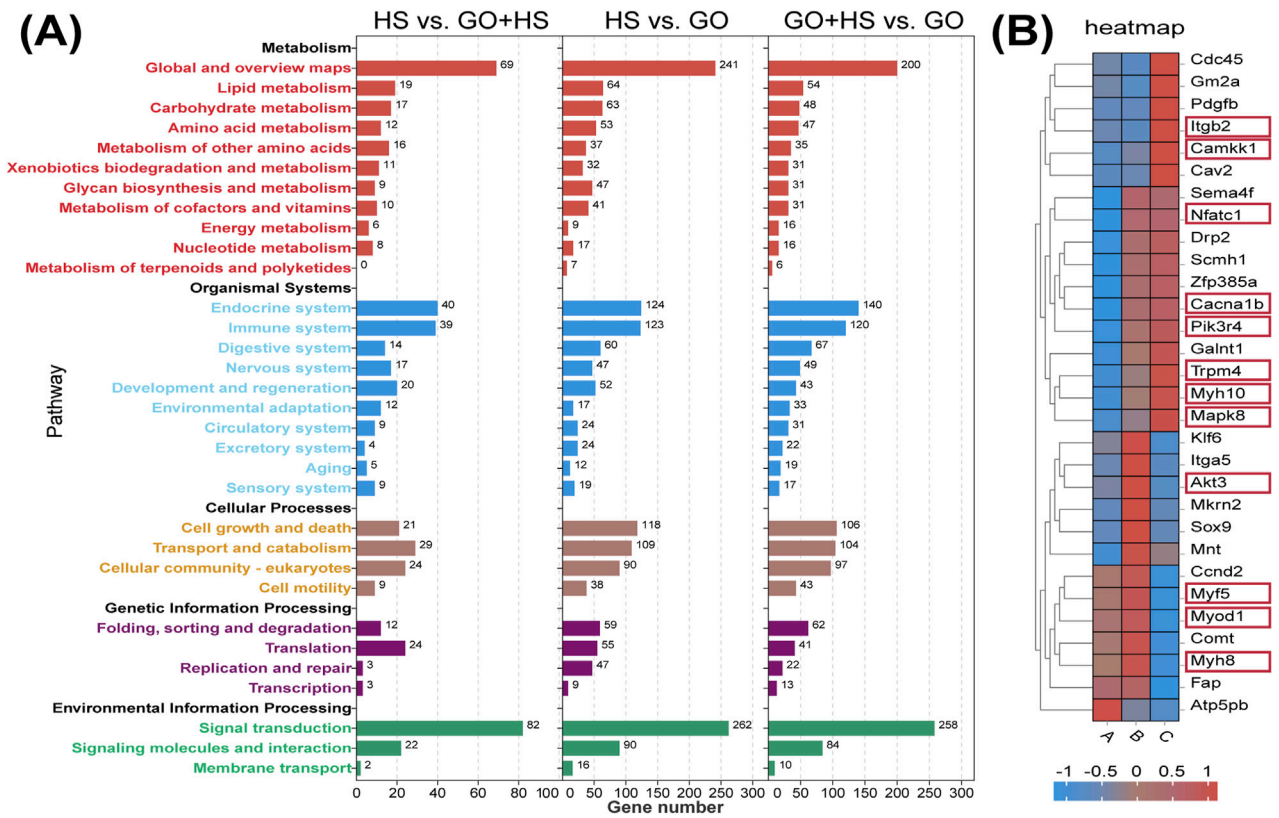

FIGURE 8
KEGG analysis results and differential gene expression analysis. **(A)** KEGG pathway enrichment histogram. **(B)** RNA-seq gene expression heat maps. **(A)** Control group with 2% horse serum and no graphene oxide (GO). **(B)** Experimental group with GO and 2% horse serum. **(C)** Experimental group with GO without horse serum.

especially in the GO plus horse serum group (Figure 7B). KEGG analysis revealed strong enrichment in metabolic and regulatory pathways, with horse serum partially mitigating GO-induced changes. GO significantly influenced signal transduction, with minor differences between the GO and GO plus horse serum groups, suggesting that horse serum modulates but does not override the effects of GO (Figure 8A).

In the GO plus horse serum group, the genes associated with muscle differentiation, including *MyoD1*, *Myf5*, and *MyH8*, were significantly upregulated, indicating enhanced myogenesis. Furthermore, the genes associated with the PI3K-Akt signaling pathway, such as *Pik3r4*, were upregulated in the GO plus horse serum and GO-only groups. *Akt3* was significantly upregulated, specifically in the GO plus horse serum group. The *Myo9b* gene, which is associated with cell adhesion, also exhibited elevated expression in both the treatment groups compared with that in the control group. The upregulation of *NFATc1* suggested that GO activated the NFAT signaling pathway, which has been implicated in the regulation of muscle growth and regeneration (Meissner et al., 2007). This activation is potentially linked to the enhanced electrical conductivity of GO, which can modulate intracellular signaling cascades. These findings collectively highlight the positive effects of GO and horse serum on myogenic differentiation and related signaling pathways (Figure 8B).

3.7 Effect of exosomes on MC3T3-E1 cells after C2C12 cell differentiation with or without GO

RNA-Seq analysis of MC3T3-E1 cells treated with the exosomes derived from C2C12 cells cultured with GO revealed the upregulation of 26 genes and the downregulation of 18 genes compared to that in the control group (Figure 9A).

The GO-treated exosomes exhibited changes in cellular processes, biological regulation, biological process regulation, and metabolic processes. This finding suggests that the exosomes derived from GO-cultured C2C12 cells affects the metabolic activities and growth of MC3T3-E1 cells. Additionally, changes in functions such as catalytic activity and other functional aspects were observed (Figure 9B). In the experimental group, significant upregulation was observed for genes such as *Tbx2* (involved in cell differentiation and development), *PDGFRB* (a receptor critical for cell proliferation), and *COL12A1* (a collagen essential for the ECM structure) (Chen et al., 2001; Bretaud et al., 2019; Khayal et al., 2018). Furthermore, *TRIB3* (involved in stress response and metabolic regulation), *SLC22A15* (a transporter), and *CORO6* (important for cell migration) were upregulated (Bai et al., 2021). Alternatively, genes such as *CXCL5* and *CXCL3* (encoding chemokines related to immune cell recruitment), *C3*

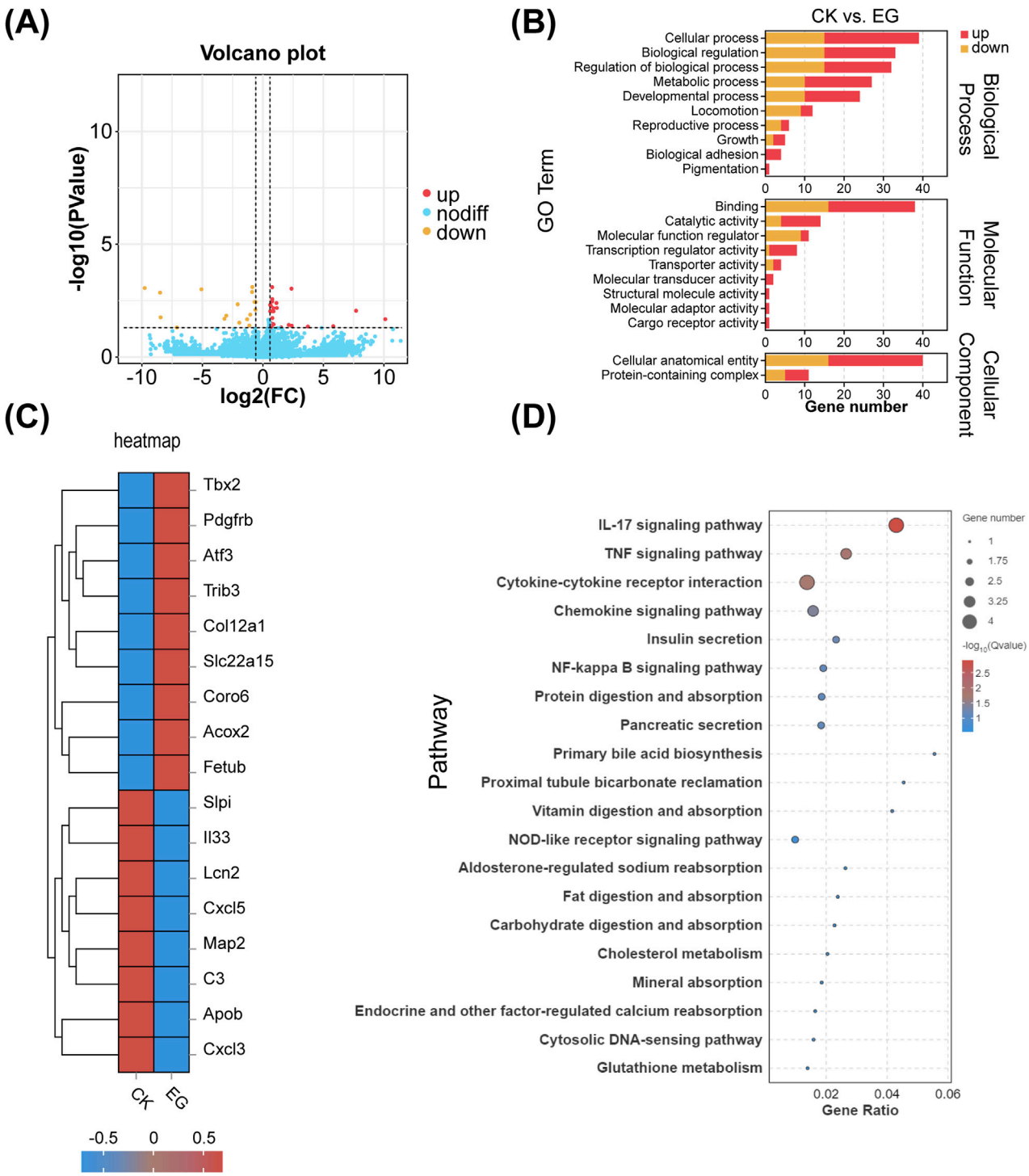

FIGURE 9
Effects of exosomes on MC3T3 cells after C2C12 cell differentiation with or without graphene oxide (GO). **(A)** Volcano plots. **(B)** Comparison of GO enrichment. **(C)** RNA-seq gene expression heat maps. **(D)** KEGG pathway concentration statistical bubble chart (CK represents the control group of MC3T3-E1 cells treated with normal medium, whereas, EG represents the experimental group of MC3T3-E1 cells treated with exosomes derived from C2C12 cells cultured with GO).

(encoding a complement system component), and *ApoB* (encoding a lipoprotein negatively correlated with bone mineral density) were downregulated (Figure 9C) (Zhu et al., 2022). The differential genes are primarily enriched in the IL-17 and TNF signaling pathways (Figure 9D).

4 Discussion

Herein, GO promoted C2C12 myoblast proliferation at diameters of >500 nm and concentrations of 2.5 μg/mL. CCK-8 assay and flow cytometry analysis revealed that the cytotoxicity of

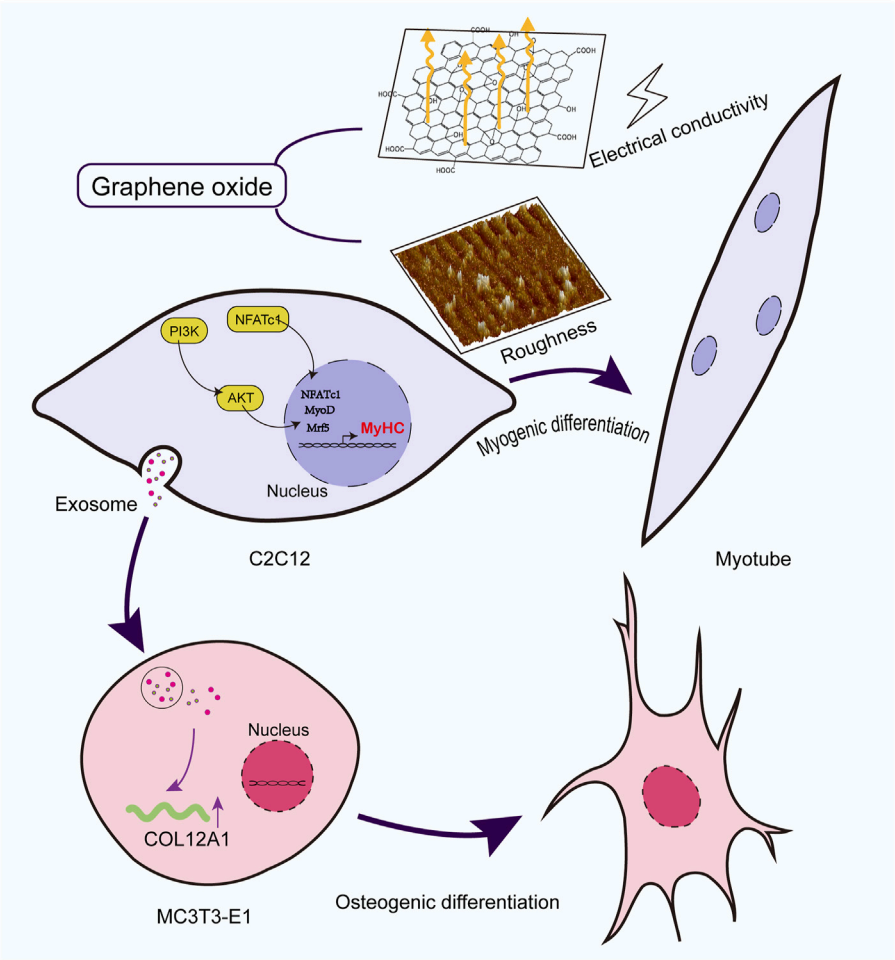

FIGURE 10
Mechanism diagram of GO promoting skeletal muscle complex regeneration.

GO is dose-dependent, with low concentrations exhibiting high biocompatibility (Mittal et al., 2016).

At the same concentration, GO with a larger diameter exhibited lower electrical conductivity (Figure 1C), which corresponded with the observed calcium ion influx across various concentration gradients (Figure 5). Notably, our evaluation of myogenic differentiation via PCR revealed that the expression of myogenic differentiation markers generally increased with increasing conductivity (across different sizes and concentrations of GO; Figures 6A,B). However, at a concentration of 2.5 μg/mL, the larger-sized GO (>500 nm) significantly enhanced myogenic gene expression than the smaller-sized GO. We speculate that this difference can be attributed to the superior biocompatibility of the larger GO sheets. GO exhibits excellent myogenic differentiation ability, mainly because of its electrical conductivity and surface morphology. Calcium ions (Ca^{2+}) can activate *NFATc1* (Kar et al., 2011). Increased GO conductivity plays a significant role in supporting the expression of *MyoD* and enhancing myogenic differentiation, with effects likely mediated through the regulation of Ca^{2+} channels and the subsequent activation of intracellular signaling cascades. The conductivity of GO appears to influence membrane electrical activity, facilitating the activation of voltage-gated calcium channels on the surface of C2C12 cells. This process enables the influx of Ca^{2+} ions into cells, which is essential for the various signaling pathways involved in muscle differentiation. An increase in intracellular calcium concentration can stimulate the calcineurin/NFATc1 pathway. Calcineurin, a calcium/calmodulin-dependent phosphatase, is activated by an increase in Ca^{2+} ions. Upon activation, calcineurin dephosphorylates NFATc1, causing it to translocate into the nucleus where it acts as a transcription factor to regulate genes involved in muscle differentiation and growth. The upregulation of NFATc1 in response to GO treatment indicates that GO's conductivity helps trigger this pathway, which is essential for the regulation of genes such as *MyoD*—an early marker and driver of myogenic differentiation (Zammit, 2017). Moreover, the conductive properties of GO enhance cellular membrane activity, likely promoting the sustained activation of PI3K-Akt (Xu et al., 2024). This pathway plays a pivotal role in regulating growth and differentiation by phosphorylating and activating various downstream targets, including myogenic regulatory factors, such as MyoD (Xu and Wu, 2000). These

observations are consistent with those reported in previous studies highlighting the effects of conductive materials on skeletal muscle cell differentiation, wherein conductivity has been shown to improve gene expression and cell arrangement required for effective differentiation (Dong et al., 2020; Wang et al., 2021; Dong et al., 2017).

GO promoted the upregulation of adhesion-related genes, such as *ITGB2* and *GM2A*, in C2C12 cells. Cytoskeletal immunofluorescence results further confirmed that GO enhanced cell adhesion, likely due to the increased surface roughness of GO, which improves cell adhesion by providing more contact points and increasing the surface area for cell–material interactions (Taylor et al., 2017). This promotes stronger attachment, further promoting the diffusion of cells and the stability of the differentiation process.

Furthermore, previous studies have reported that GO-based materials promote osteogenic differentiation and antimicrobial activity in MC3T3-E1 osteoblasts (Daulbayev et al., 2022; Park et al., 2016; Chen et al., 2016). Despite these insights, limited research has been conducted on the effects of GO in the broader musculoskeletal system. Herein, MC3T3-E1 cells were cultured with the exosomes derived from C2C12 myoblasts differentiated in the presence of GO; these exosomes upregulated genes such as *PDGFRB*, *COL12A1*, and *TBX2*, while downregulating inflammation-related genes such as *C3* (Liu et al., 2022). This indicates that GO can help create a favorable microenvironment for bone formation and repair. The dual effects of GO on muscle and bone cells highlight its potential as a therapeutic strategy for addressing musculoskeletal complex injuries, degenerative diseases, and age-related declines in musculoskeletal integrity (Figure 10).

Future studies on GO applications should investigate its systemic effects on different cell types within the musculoskeletal system and potential immune responses to GO. Furthermore, exploring potential synergies between GO and other regenerative approaches, such as stem cell therapies and growth factor delivery, could further enhance muscle and bone tissue engineering outcomes. Another key area for further investigation is the role of the exosomes derived from C2C12 myoblasts in mediating GO's beneficial effects on MC3T3-E1 cells. Analyzing the exosome cargo—including specific proteins, microRNAs, and metabolites—may reveal new signaling pathways and mechanisms that drive osteogenic differentiation and ECM formation. Identification of the factors associated with the exosomes responsible for these effects could lead to new therapeutic possibilities. Finally, previous studies have highlighted the significant potential of GO-based scaffolds for *in vivo* applications, particularly in the fields of tissue engineering and regenerative medicine (Jo et al., 2020; Gwon et al., 2024; Valencia et al., 2018). Based on these insights and our current findings, we believe that the GO formulation presented herein—with a diameter of >500 nm and a concentration of 2.5 μg/mL, which demonstrated the highest bioactivity *in vitro*—can be combined with other materials to construct composite scaffolds for the *in vivo* repair of skeletal muscle defects. However, the practical feasibility and therapeutic efficacy of this approach remain to be further validated through comprehensive animal studies.

5 Conclusion

GO with diameters of >500 nm and at concentrations of 2.5 μg/mL promotes balanced enhancement of C2C12 cell proliferation and myogenic differentiation. The increased electrical conductivity of GO stimulates calcium ion flow across the cell membrane and the upregulation of *NFATc1* and *MyoD* genes, thereby promoting the myoblast differentiation of C2C12 cells. GO enhances cell adhesion and promotes the upregulation of adhesion-related genes. Furthermore, the exosomes derived from GO-treated myoblasts upregulate genes such as *PDGFRB*, *COL12A1*, and *TBX2* while downregulating inflammation-related genes such as *C3*. These findings provide valuable insights into optimizing GO size, concentration, electrical conductivity, and surface roughness for improved biocompatibility and differentiation of both myoblasts and osteoblasts. This study highlights the potential of GO as a therapeutic material for simultaneous muscle and bone regeneration, facilitating the repair of the musculoskeletal complex.

Data availability statement

The original contributions presented in the study are included in the article/Supplementary Material, further inquiries can be directed to the corresponding authors.

Author contributions

YC: Formal Analysis, Investigation, Methodology, Visualization, Writing – original draft, Writing – review and editing. ZZ: Formal Analysis, Investigation, Methodology, Writing – review and editing. YS: Investigation, Methodology, Writing – review and editing. XL: Investigation, Methodology, Writing – review and editing. YH: Investigation, Methodology, Writing – review and editing. CL: Conceptualization, Formal Analysis, Investigation, Writing – review and editing. JL: Funding acquisition, Project administration, Supervision, Writing – review and editing.

Funding

The author(s) declare that financial support was received for the research and/or publication of this article. The authors gratefully acknowledge the financial support of the National Natural Science Foundation of China (82071160, 82370933, 82470946, and 82271027).

Conflict of interest

The reviewer YO declared a shared affiliation with the author(s) to the handling editor at the time of review.

The authors declare that the research was conducted in the absence of any commercial or financial relationships that could be construed as a potential conflict of interest.

Generative AI statement

The author(s) declare that no Generative AI was used in the creation of this manuscript.

Publisher's note

All claims expressed in this article are solely those of the authors and do not necessarily represent those of their affiliated organizations, or those of the publisher, the editors and the reviewers. Any product that may be evaluated in this article, or claim that may be made by its manufacturer, is not guaranteed or endorsed by the publisher.

Supplementary material

The Supplementary Material for this article can be found online at: https://www.frontiersin.org/articles/10.3389/fbioe.2025.1574145/full#supplementary-material

References

Bacakova, L., Filova, E., Parizek, M., Ruml, T., and Svorcik, V. (2011). Modulation of cell adhesion, proliferation and differentiation on materials designed for body implants. *Biotechnol. Adv.* 29 (6), 739–767. doi:10.1016/j.biotechadv.2011.06.004

Bahrami, S., Baheiraei, N., and Shahrezaee, M. (2021). Biomimetic reduced graphene oxide coated collagen scaffold for *in situ* bone regeneration. *Sci. Rep.* 11 (1), 16783. doi:10.1038/s41598-021-96271-1

Bai, X. S., Zhang, P., Liu, Y. S., Hao, L., Lv, L. W., and Zhou, Y. S. (2021). TRIB3 promotes osteogenic differentiation of human adipose-derived mesenchymal stem cells levelled by posttranscriptional regulation of mir-24-3p. *Chin. J. Dent. Res.* 24 (4), 235–249. doi:10.3290/j.cjdr.b2440815

Berrio, M. E., Oñate, A., Salas, A., Fernández, K., and Meléndrez, M. F. (2021). Synthesis and applications of graphene oxide aerogels in bone tissue regeneration: a review. *Mater. Today Chem.* 20, 100422. doi:10.1016/j.mtchem.2021.100422

Bretaud, S., Nauroy, P., Malbouyres, M., and Ruggiero, F. (2019). Fishing for collagen function: about development, regeneration and disease. *Seminars Cell Dev. Biol.* 89, 100–108. doi:10.1016/j.semcdb.2018.10.002

Catalano, A., Vita, G. L., Bellone, F., Sframeli, M., Distefano, M. G., La Rosa, M., et al. (2022). Bone Health in duchenne muscular dystrophy: clinical and biochemical correlates. *J. Endocrinol. Investigation* 45, 517–525. doi:10.1007/s40618-021-01676-4

Chagarlamudi, H., Corbett, A., Stoll, M., Bibat, G., Grosmann, C., Matichak Stock, C., et al. (2017). Bone health in facioscapulohumeral muscular dystrophy: a cross-sectional study. *Muscle Nerve* 56 (6), 1108–1113. doi:10.1002/mus.25619

Chen, J., Zhang, X., Cai, H., Chen, Z., Wang, T., Jia, L., et al. (2016). Osteogenic activity and antibacterial effect of zinc oxide/carboxylated graphene oxide nanocomposites: preparation and *in vitro* evaluation. *Colloids Surfaces B Biointerfaces* 147, 397–407. doi:10.1016/j.colsurfb.2016.08.023

Chen, J.-R., Zhong, Q., Wang, J., Cameron, R. S., Borke, J. L., Isales, C. M., et al. (2001). Microarray analysis of Tbx2-directed gene expression: a possible role in osteogenesis. *Mol. Cell. Endocrinol.* 177 (1-2), 43–54. doi:10.1016/s0303-7207(01)00456-7

Chen, M.-C., Sun, Y.-C., and Chen, Y.-H. (2013). Electrically conductive nanofibers with highly oriented structures and their potential application in skeletal muscle tissue engineering. *Acta Biomater.* 9 (3), 5562–5572. doi:10.1016/j.actbio.2012.10.024

Corona, B. T., Rivera, J. C., Owens, J. G., Wenke, J. C., and Rathbone, C. R. (2015). Volumetric muscle loss leads to permanent disability following extremity trauma. *J. Rehabilitation Res. Dev.* 52 (7), 785–792. doi:10.1682/jrrd.2014.07.0165

Daulbayev, C., Sultanov, F., Korobeinyk, A. V., Yeleuov, M., Taurbekov, A., Bakbolat, B., et al. (2022). Effect of graphene oxide/hydroxyapatite nanocomposite on osteogenic differentiation and antimicrobial activity. *Surfaces Interfaces* 28, 101683. doi:10.1016/j.surfin.2021.101683

Dong, R., Ma, P. X., and Guo, B. (2020). Conductive biomaterials for muscle tissue engineering. *Biomaterials* 229, 119584. doi:10.1016/j.biomaterials.2019.119584

Dong, R., Zhao, X., Guo, B., and Ma, P. X. (2017). Biocompatible elastic conductive films significantly enhanced myogenic differentiation of myoblast for skeletal muscle regeneration. *Biomacromolecules* 18 (9), 2808–2819. doi:10.1021/acs.biomac.7b00749

Duan, D., Goemans, N., Takeda, S., Mercuri, E., and Aartsma-Rus, A. (2021). Duchenne muscular dystrophy. *Nat. Rev. Dis. Prim.* 7 (1), 13. doi:10.1038/s41572-021-00248-3

Dumont, N. A., Bentzinger, C. F., Sincennes, M., and Rudnicki, M. A. (2015). Satellite cells and skeletal muscle regeneration. *Compr. Physiol.* 5 (3), 1027–1059. doi:10.1002/cphy.c140068

Fukuda, T., Takeda, S., Xu, R., Ochi, H., Sunamura, S., Sato, T., et al. (2013). Sema3a regulates bone-mass accrual through sensory innervations. *Nature* 497 (7450), 490–493. doi:10.1038/nature12115

Gielen, E., Dupont, J., Dejaeger, M., and Laurent, M. R. (2023). Sarcopenia, osteoporosis and frailty. *Metabolism* 145, 155638. doi:10.1016/j.metabol.2023.155638

Global, R. (2019). Global, regional, and national burden of 12 mental disorders in 204 countries and territories, 1990-2019: a systematic analysis for the Global Burden of Disease Study 2019. *Lancet Healthy Longev.* 9 (2), 137–150. doi:10.1016/s2215-0366(21)00395-3

Gwon, Y., Park, S., Kim, W., Park, S., Sharma, H., Jeong, H. E., et al. (2024). Graphene hybrid tough hydrogels with nanostructures for tissue regeneration. *Nano Lett.* 24 (7), 2188–2195. doi:10.1021/acs.nanolett.3c04188

Han, I. K., Song, K., Jung, S., Jo, Y., Kwon, J., Chung, T., et al. (2023). Electroconductive, adhesive, non-swelling, and viscoelastic hydrogels for bioelectronics. *Adv. Mater.* 35 (4), 2203431. doi:10.1002/adma.202203431

He, C., He, W., Hou, J., Chen, K., Huang, M., Yang, M., et al. (2020). Bone and muscle crosstalk in aging. *Front. Cell Dev. Biol.* 8, 585644. doi:10.3389/fcell.2020.585644

Herrmann, M., Engelke, K., Ebert, R., Müller-Deubert, S., Rudert, M., Ziouti, F., et al. (2020). Interactions between muscle and bone—where physics meets biology. *Biomolecules* 10 (3), 432. doi:10.3390/biom10030432

Izumiya, M., Haniu, M., Ueda, K., Ishida, H., Ma, C., Ideta, H., et al. (2021). Evaluation of MC3T3-E1 cell osteogenesis in different cell culture media. *Int. J. Mol. Sci.* 22 (14), 7752. doi:10.3390/ijms22147752

Jo, S. B., Erdenebileg, U., Dashnyam, K., Jin, G.-Z., Cha, J.-R., El-Fiqi, A., et al. (2020). Nano-graphene oxide/polyurethane nanofibers: mechanically flexible and myogenic stimulating matrix for skeletal tissue engineering. *J. Tissue Eng.* 11, 2041731419900424. doi:10.1177/2041731419900424

Jung, I., Dikin, D. A., Piner, R. D., and Ruoff, R. S. (2008). Tunable electrical conductivity of individual graphene oxide sheets reduced at "low" temperatures. *Nano Lett.* 8 (12), 4283–4287. doi:10.1021/nl8019938

Kar, P., Nelson, C., and Parekh, A. B. (2011). Selective activation of the transcription factor NFAT1 by calcium microdomains near Ca2+ release-activated Ca2+ (CRAC) channels. *J. Biol. Chem.* 286 (17), 14795–14803. doi:10.1074/jbc.m111.220582

Kenry, Lee, W. C., Loh, K. P., and Lim, C. T. (2018). When stem cells meet graphene: opportunities and challenges in regenerative medicine. *Biomaterials* 155, 236–250. doi:10.1016/j.biomaterials.2017.10.004

Khayal, L. A., Grünhagen, J., Provazník, I., Mundlos, S., Kornak, U., Robinson, P. N., et al. (2018). Transcriptional profiling of murine osteoblast differentiation based on RNA-seq expression analyses. *Bone* 113, 29–40. doi:10.1016/j.bone.2018.04.006

Kim, S. G., Wang, S. H., Ok, C. M., Jeong, S. Y., and Lee, H. S. (2017). Lateral diffusion of graphene oxides in water and the size effect on the orientation of dispersions and electrical conductivity. *Carbon N. Y.* 125, 280–288. doi:10.1016/j.carbon.2017.09.054

Laumonier, T., and Menetrey, J. (2016). Muscle injuries and strategies for improving their repair. *J. Exp. Orthop.* 3 (1), 15. doi:10.1186/s40634-016-0051-7

Lee, C., Wei, X., Kysar, J. W., and Hone, J. (2008). Measurement of the elastic properties and intrinsic strength of monolayer graphene. *Science* 321 (5887), 385–388. doi:10.1126/science.1157996

Liu, J., Saul, D., Böker, K. O., Ernst, J., Lehman, W., and Schilling, A. F. (2018). Current methods for skeletal muscle tissue repair and regeneration. *Biomed. Res. Int.* 2018, 1984879–11. doi:10.1155/2018/1984879

Liu, K., Yu, Y., Tong, M., Tang, B., and Shi, X. (2022). Increased level of complement C3 in patients with osteoporosis and enhanced osteogenic ability in osteoblasts with complement component 3 knockdown. doi:10.21203/rs.3.rs-1444255/v2

Lu, W., Chao, T., Ruiqi, C., Juan, S., and Zhihong, L. (2018). Patient-derived xenograft models in musculoskeletal malignancies. *J. Transl. Med.* 16 (1), 107–116. doi:10.1186/s12967-018-1487-6

Luong-Van, E. K., Madanagopal, T. T., and Rosa, V. (2020). Mechanisms of graphene influence on cell differentiation. *Mater. Today Chem.* 16, 100250. doi:10.1016/j.mtchem.2020.100250

Meissner, J. D., Umeda, P. K., Chang, K., Gros, G., and Scheibe, R. J. (2007). Activation of the β myosin heavy chain promoter by MEF-2D, MyoD, p300, and the calcineurin/NFATc1 pathway. *J. Cell. Physiology* 211 (1), 138–148. doi:10.1002/jcp.20916

Mittal, S., Kumar, V., Dhiman, N., Chauhan, L. K. S., Pasricha, R., and Pandey, A. K. (2016). Physico-chemical properties based differential toxicity of graphene oxide/reduced graphene oxide in human lung cells mediated through oxidative stress. *Sci. Rep.* 6 (1), 39548. doi:10.1038/srep39548

Moiseeva, V., Cisneros, A., Sica, V., Deryagin, O., Lai, Y., Jung, S., et al. (2023). Senescence atlas reveals an aged-like inflamed niche that blunts muscle regeneration. *Nature* 613 (7942), 169–178. doi:10.1038/s41586-022-05535-x

Nuge, T., Liu, Z., Liu, X., Ang, B. C., Andriyana, A., Metselaar, H. S. C., et al. (2021). Recent advances in scaffolding from natural-based polymers for volumetric muscle injury. *Molecules* 26 (3), 699. doi:10.3390/molecules26030699

Papaefthymiou, P., Kekou, K., and Ozdemir, F. (2022). Orofacial manifestations associated with muscular dystrophies: a review. *Turkish J. Orthod.* 35 (1), 67–73. doi:10.5152/turkjorthod.2021.21021

Park, K. O., Lee, J. H., Park, J. H., Shin, Y. C., Huh, J. B., Bae, J.-H., et al. (2016). Graphene oxide-coated guided bone regeneration membranes with enhanced osteogenesis: spectroscopic analysis and animal study. *Appl. Spectrosc. Rev.* 51 (7-9), 540–551. doi:10.1080/05704928.2016.1165687

Safari, B., Davaran, S., and Aghanejad, A. (2021). Osteogenic potential of the growth factors and bioactive molecules in bone regeneration. *Int. J. Biol. Macromol.* 175, 544–557. doi:10.1016/j.ijbiomac.2021.02.052

Safiri, S., Kolahi, A., Cross, M., Hill, C., Smith, E., Carson-Chahhoud, K., et al. (2021). Prevalence, deaths, and disability-adjusted life years due to musculoskeletal disorders for 195 countries and territories 1990–2017. *Arthritis and Rheumatology* 73 (4), 702–714. doi:10.1002/art.41571

Şelaru, A., Herman, H., Vlăsceanu, G. M., Dinescu, S., Gharbia, S., Baltă, C., et al. (2022). Graphene–oxide porous biopolymer hybrids enhance *in vitro* osteogenic differentiation and promote ectopic osteogenesis *in vivo*. *Int. J. Mol. Sci.* 23 (1), 491. doi:10.3390/ijms23010491

Seo, H.-J., Cho, Y.-E., Kim, T., Shin, H.-I., and Kwun, I.-S. (2010). Zinc may increase bone formation through stimulating cell proliferation, alkaline phosphatase activity and collagen synthesis in osteoblastic MC3T3-E1 cells. *Nutr. Res. Pract.* 4 (5), 356. doi:10.4162/nrp.2010.4.5.356

Sousa-Victor, P., García-Prat, L., and Muñoz-Cánoves, P. (2022). Control of satellite cell function in muscle regeneration and its disruption in ageing. *Nat. Rev. Mol. Cell Biol.* 23 (3), 204–226. doi:10.1038/s41580-021-00421-2

Stamnitz, S., and Klimczak, A. (2021). Mesenchymal stem cells, bioactive factors, and scaffolds in bone repair: from research perspectives to clinical practice. *Cells* 10 (8), 1925. doi:10.3390/cells10081925

Taylor, A. C., González, C. H., Miller, B. S., Edgington, R. J., Ferretti, P., and Jackman, R. B. (2017). Surface functionalisation of nanodiamonds for human neural stem cell adhesion and proliferation. *Sci. Rep.* 7 (1), 7307. doi:10.1038/s41598-017-07361-y

Valencia, C., Valencia, C. H., Zuluaga, F., Valencia, M. E., Mina, J. H., and Grande-Tovar, C. D. (2018). Synthesis and application of scaffolds of chitosan-graphene oxide by the freeze-drying method for tissue regeneration. *Molecules* 23 (10), 2651. doi:10.3390/molecules23102651

Wang, Y., Wang, Q., Luo, S., Chen, Z., Zheng, X., Kankala, R. K., et al. (2021). 3D bioprinting of conductive hydrogel for enhanced myogenic differentiation. *Regen. Biomater.* 8 (5), rbab035. doi:10.1093/rb/rbab035

Wong, S. H. M., Lim, S. S., Tiong, T. J., Show, P. L., Zaid, H. F. M., and Loh, H.-S. (2020). Preliminary *in vitro* evaluation of chitosan–graphene oxide scaffolds on osteoblastic adhesion, proliferation, and early differentiation. *Int. J. Mol. Sci.* 21 (15), 5202. doi:10.3390/ijms21155202

Xu, Q., Dai, W., Li, P., Li, Q., Gao, Z., Wu, X., et al. (2024). Piezoelectric film promotes skin wound healing with enhanced collagen deposition and vessels regeneration via upregulation of PI3K/AKT. *Nano Res.* 17 (8), 7461–7478. doi:10.1007/s12274-024-6717-z

Xu, Q., and Wu, Z. (2000). The insulin-like growth factor-phosphatidylinositol 3-kinase-Akt signaling pathway regulates myogenin expression in normal myogenic cells but not in rhabdomyosarcoma-derived RD cells. *J. Biol. Chem.* 275 (47), 36750–36757. doi:10.1074/jbc.m005030200

Zammit, P. S. (2017). Function of the myogenic regulatory factors Myf5, MyoD, Myogenin and MRF4 in skeletal muscle, satellite cells and regenerative myogenesis. *Seminars Cell and Dev. Biol.* 72, 19–32. doi:10.1016/j.semcdb.2017.11.011

Zhang, R.-N., Bao, X., Liu, Y., Wang, Y., Li, X.-Y., Tan, G., et al. (2023). The spatiotemporal matching pattern of ezrin/periaxin involved in myoblast differentiation and fusion and Charcot-Marie-tooth disease-associated muscle atrophy. *J. Transl. Med.* 21 (1), 173. doi:10.1186/s12967-023-04016-7

Zhu, R., Xu, Y., Wang, Z., Li, H., Song, M., Wan, H., et al. (2022). Higher serum apolipoprotein B level will reduce the bone mineral density and increase the risk of osteopenia or osteoporosis in adults. *Front. Cell Dev. Biol.* 10, 1054365. doi:10.3389/fcell.2022.1054365

frontiers | Frontiers in Immunology

TYPE Original Research
PUBLISHED 01 September 2025
DOI 10.3389/fimmu.2025.1626337

Check for updates

OPEN ACCESS

EDITED BY
Elizabeth Vinod,
Christian Medical College and Hospital, India

REVIEWED BY
Palash Mandal,
Charotar University of Science and Technology, India
Qiang Ding,
Zhejiang Chinese Medical University, China

*CORRESPONDENCE
Huan Xiao
402276678@qq.com
Qiushi Wei
weiqshi@126.com

†These authors have contributed equally to this work and share first authorship

RECEIVED 12 May 2025
ACCEPTED 04 August 2025
PUBLISHED 01 September 2025

CITATION
Peng P, Tian J, Lin K, Fang W, Yao F, Yang X, Hou W, Xiao F, Lu S, He W, He M, Xiao H and Wei Q (2025) Single-cell RNA-seq reveals a repair pattern in cystic lesions in steroid induced osteonecrosis of the femoral head. *Front. Immunol.* 16:1626337.
doi: 10.3389/fimmu.2025.1626337

COPYRIGHT
© 2025 Peng, Tian, Lin, Fang, Yao, Yang, Hou, Xiao, Lu, He, He, Xiao and Wei. This is an open-access article distributed under the terms of the Creative Commons Attribution License (CC BY). The use, distribution or reproduction in other forums is permitted, provided the original author(s) and the copyright owner(s) are credited and that the original publication in this journal is cited, in accordance with accepted academic practice. No use, distribution or reproduction is permitted which does not comply with these terms.

Single-cell RNA-seq reveals a repair pattern in cystic lesions in steroid induced osteonecrosis of the femoral head

Peng Peng[1,2†], Jiaqing Tian[3†], Kun Lin[4†], Weihua Fang[4], Fangming Yao[4], Xiaoqiang Yang[4], Wenyuan Hou[4], Fangjun Xiao[4], Shun Lu[4], Wei He[2,5,6], Mincong He[5,6], Huan Xiao[7]* and Qiushi Wei[2,5,6]*

[1]Guangdong Provincial Second Hospital of Traditional Chinese Medicine, Guangzhou, China, [2]National Key Laboratory of Traditional Chinese Medicine Syndrome, Guangzhou, China, [3]The Fifth Clinical College of Guangzhou University of Chinese Medicine, Guangzhou, China, [4]Guangzhou University of Chinese Medicine, Guangzhou, China, [5]Guangdong Research Institute for Orthopedics and Traumatology of Chinese Medicine, Guangzhou, China, [6]Department of Orthopaedics, The Third Affiliated Hospital, Guangzhou University of Chinese Medicine, Guangzhou, China, [7]Department of Orthopedics, Bijie Traditional Chinese Medicine Hospital, Bijie, China

Background: Studies have indicated that cystic lesions play a crucial role in the repair processes of steroid-induced osteonecrosis of the femoral head and its subsequent collapse. Here, we employed single-cell RNA sequencing (scRNA-seq) technology to investigate the transcriptomic landscape and repair mechanisms of cystic lesions in SIONFH.
Methods: We applied scRNA-seq combined with computational approaches to characterize distinct cell subsets and their molecular signatures within cystic lesions from three SIONFH patients. Additionally, histological assays were conducted to observe pathological manifestations of these lesions.
Results: Eight cell types were identified in cystic lesions of SIONFH. Among them, chondrocytes were divided into five subgroups. Among them, chondrocytes were divided into five subgroups: homeostatic chondrocytes (HomC), fibrocartilage chondrocytes (FC), prehypertrophic chondrocytes (preHTC), inflammatory chondrocytes (InflamC), and hypertrophic chondrocytes (HTC). Additionally, histological assays showed the presence of chondrocytes and a transition zone from chondrocytes to bone tissue within the cystic lesions. Notably, we report that one of the HTC clusters with CLIC3+ expression exhibited a strong involved in bone mineralization, osteoblast differentiation, and cell differentiation.
Conclusion: We have delineated the cellular heterogeneity and molecular signatures of cystic lesions in SIONFH. The results reveal a distinct repair program within these lesions, which might be driven by chondrocyte hypertrophy and might culminate in osteogenic differentiation.

KEYWORDS

steroid-induced osteonecrosis of the femoral head, single-cell RNA sequencing, chondrocyte, cystic lesions, osteogenic differentiation

1 Introduction

Steroid-induced osteonecrosis of the femoral head (SIONFH) represents a predominant subtype of non-traumatic ONFH, constituting nearly 40% of clinical cases (1, 2). This debilitating orthopedic condition arises primarily from prolonged high-dose glucocorticoid exposure - an unavoidable therapeutic necessity for managing various systemic diseases despite its iatrogenic consequences. The multifactorial pathogenesis involves complex interplay among genetic susceptibility, vascular compromise, metabolic disturbances (particularly lipid dysregulation), and elevated intraosseous pressure, collectively culminating in ischemic bone marrow necrosis and subsequent femoral head collapse (3). Characteristic radiographic progression manifests through three hallmark features: initial crescent sign formation, development of cystic lesions, and ultimately articular surface collapse - the latter serving as the definitive radiological threshold for advanced disease staging (4). This terminal collapse event precipitates rapid joint degeneration, leading to refractory hip pain, progressive mobility impairment, and in most cases, inevitable requirement for total hip arthroplasty.

Emerging evidence indicates that cystic lesions potentiate femoral head collapse risk, accelerate SIONFH progression, and adversely impact long-term prognostic outcomes (5). According to the Association Research Circulation Osseous (ARCO) staging system, cystic lesions represent a pathognomonic feature of Stage II osteonecrosis of the femoral head, radiographically characterized by subchondral radiolucent foci (6). Pathologically, these lesions predominantly consist of fibrous granulation tissue (7). The pathogenesis of cystic lesions formation remains elusive. Current models postulate that aberrant mechanical loading on sclerotic rims induces osteoclastic resorption, initiating a cystogenic cascade (8). It has been established that cystic lesions are associated with the collapse of the femoral head and disease prognosis in SIONFH (5). However, the reparative potential of cystic lesions in SIONFH remains largely unexplored. Lakhotia et al. observed varying degrees of new bone ingrowth in the cystic areas after femoral varus derotation osteotomy of ONFH patients using computed tomography (9). He et al. also found that spontaneous reparative transformation in subsets of cystic lesions during disease progression (10). These findings demonstrate that cystic lesions possess bone repair potential. Nevertheless, the underlying biological mechanisms remain to be elucidated.

Single-cell RNA sequencing (scRNA-seq) is a high-throughput sequencing technique that enables sequencing at the individual cell level (11). By sequencing the transcriptome of individual cells, scRNA-seq provides spatiotemporal dynamics of cellular processes, gene expression patterns, and cell heterogeneity. This technology possesses the capability to discern distinct cell types and acquire knowledge regarding physiological and pathological processes of certain disease. ScRNA-seq holds considerable clinical significance in domains such as oncology, immunology, and embryonic development (12–14). Presently, the majority of investigations on cystic lesions based on imaging and histological methods. Nevertheless, the utilization of scRNA-seq technology in studying cystic lesions remains unexplored.

Therefore, this study aims to systematically investigate the transcriptomic heterogeneity and aberrant repair mechanisms within cystic lesions of SIONFH using scRNA-seq technology. Our analysis delineates the cellular atlas of cystic lesions and identifies a pathological repair cascade characterized by chondrocyte hypertrophy with subsequent osteogenic differentiation, which might to be a hallmark of this unique microenvironment.

2 Materials and methods

2.1 Clinical specimen collection

All cystic lesions specimens were obtained from SIONFH patients undergoing total hip arthroplasty at the Third Affiliated Hospital of Guangzhou University of Chinese Medicine. Research protocols involving human subjects were approved by the Ethics Committee of the Third Affiliated Hospital of Guangzhou University of Chinese Medicine (approval number: GYH202101-04). All participants in this study were asked for Informed consent. The clinical and demographic characteristics of the patients were collected from medical records (Supplementary Table 1). The representative imaging data information are shown in Supplementary Figure 1.

2.2 Single-cell suspension preparation

After acquirement, fresh samples were washed with phosphate-buffered saline (PBS), then minced into approximately 1-millimeter pieces on ice. Tissue fragments were digested with 0.2% collagenase II (#2195526, Gibco, USA) in DMEM solution at 37°C for 2 h. The digested suspension was filtered through a 70-μm cell strainer. After centrifugation at 500 x g for 8 minutes, erythrocytes were lysed using erythrocyte lysis buffer.

2.3 Single-cell RNA-seq using 10x genomics chromium

According to the manufacturer's instructions, the Chromium Single Cell 3e V2/V3 Kit was used to construct the scRNA-seq library. Briefly, cells were loaded into Chromium microfluidic chips with 3' chemistry and barcoded using 10x Chromium Controller. Then, RNA from the barcoded cells underwent reverse transcription, followed by cDNA amplification and library construction. Sequencing was performed on an Illumina NovaSeq 6000 system.

2.4 Cell clustering and annotating

Gene expression levels were processed using the LogNormalize method of the"Normalization"function in the Seurat package. Dimensional reduction was conducted via principal components

analysis (PCA). Batch effects were removed using Harmony (v0.1.0). The top 20 principal components were selected for clustering analysis in our default workflow. Identified clusters were visualized with the t-distributed stochastic neighbor embedding (t-SNE). Cell types were annotated by combining cellular biomarkers from previous articles and Gene Ontology (GO) analysis.

2.5 Gene enrichment analysis

Enrichment analysis included GO enrichment analysis and Kyoto Encyclopedia of Genes and Genomes (KEGG) enrichment analysis. Enrichment analysis were performed using the enrichGO and enrichKEGG functions of the clusterProfiler (V 3.18.0) R package.

2.6 Cell–cell communication analysis

To identify potential intercellular interactions, we performed cell–cell communication analysis using the CellPhoneDB Python package (version 2.1.7) (15). CellPhoneDB primarily utilizes the profiles information of receptors in one cell type and ligands in another cell type to infer interactions between different cell types. We identified the most relevant cell type-specific interactions between ligands and receptors and visualized the inferred intercellular communication networks for each ligand-receptor pair and each signaling pathway by circle plots.

2.7 Pseudotime analysis

Pseudotime analysis was performed using Monocle2 (version 2.14.0) to characterize chondrocyte differentiation (16). Per standard protocol, integrated gene expression data were imported into Monocle2, Cells were ordered based on differentially expressed genes (DEGs) between chondrocytes subclusters. Employing the DDRTree method for dimensionality reduction and using default parameters in Monocle2 for cell ordering, we inferred the differentiation trajectories of chondrocytes.

2.8 Histological analysis

Stereotactic whole section sampling of the femoral head was used. Each specimen were sectioned at 5-mm intervals, and the portion of each section containing cystic lesions was sampled. Specimens were fixed in 4% paraformaldehyde (PFA) solution (G1101–500 ML Servicebio, Wuhan, China) for 2 days at room temperature. After decalcified by 10% EDTA solution, samples were embedded in paraffin and serially cut into 5 μm-thick sections. Following a previously reported procedure, every fifth section of two sections were selected and stained with Safranin-O/fast green (#G1371, Solarbio, Beijing, China), hematoxylin and eosin (H&E) (#C0105, Beyotime), and Alisin blue (#C0155M, Beyotime) to evaluate histological characteristic (17). After that, the sections were observed under a digital section scanner (3DHISTEC, Pannoramic MIDI).

2.9 Immunofluorescence and immunohistochemical staining

The dewaxing and rehydration process was performed on paraffin-embedded sections.

To perform immunofluorescent staining, sections were blocked with endogenous catalase blocker for 15 min and 3% BSA (MP Biomedicals, Cat.# 0218054990) for 40 min. Then, sections were incubated overnight at 4°C with primary antibodies as follows: MMP13 (rabbit, 1:1000, 66034-1-IG, 2C8F3, PROTEINTECH GROUP, USA), COL10A1 (1:100; Proteintech Group, Inc), SPP1 (1:100; Proteintech Group, Inc) and RUNX2 (1:100; Proteintech Group, Inc). After that, sections were stained with secondary antibody for immunohistochemical staining (IHC) (horseradish peroxidase-conjugated anti-mouse&rabbit: absin, Cat.# 996, [1:200]) or immunofluorescence staining (IF) (Goat pABs to Rb IgG (Alexa Fluor® 488): Abcam, Cat.# ab150081; Goat pABs to Ms IgG (Alexa Fluor® 555): Abcam, Cat.# ab150118, [1:200]) for 2 h at room temperature. Sections were washed with PBST three times and stained with hematoxylin for IHC or DAPI (Invitrogen, Cat.# D1306) for IF. Sections were visualized with the confocal fluorescence microscope (LSM800, Carl Zeiss, Germany) or digital section scanner (3DHISTEC, Pannoramic MIDI).

2.10 Western blot

Femoral head bone samples from three femoral neck fracture (FNF) and three SIONFH patients were obtained after total hip arthroplasty. Cystic lesions and bone sample were collected and immediately frozen in liquid nitrogen. Tissue lysates were prepared using RIPA buffer (Beyotime, P0013B) with protease inhibitors (Beyotime, P0013B). Protein concentrations were determined by BCA assay (Beyotime, P0009). Samples (30 μg/lane) were resolved on 10% SDS-PAGE gels and transferred to PVDF membranes (Beyotime, FFP20). After blocking with 5% non-fat milk (Beyotime, P0216) in TBST (1 h, RT), membranes were incubated overnight at 4°C with primary antibodies: anti-SPP1 (1:1000; Abcam, ab58632), anti-RUNX2 (1:800; CST, #94808), anti-ColoA1 (1:800; CST, #94808), anti-MMP3(1:800; CST, #94808), anti-CLIC3 (1:800; CST, #94808), anti-GAPDH (1:5000; Proteintech, 60004-1-Ig). Following TBST washes (3 × 10 min), HRP-conjugated secondary antibodies (1:5000; Affinity, S0001) were applied (1 h, RT). Signals were detected with ECL substrate (Beyotime, P0018S) using a ChemiDoc MP System (Bio-Rad).

2.11 RT-qPCR

Total RNA isolation was conducted using TRIzol reagent (Invitrogen, Carlsbad, CA, USA) per manufacturer guidelines.

Complementary DNA (cDNA) was synthesized employing a reverse transcription kit (Takara, Tokyo, Japan) according to established protocols. The polymerase chain reaction amplification profile comprised: initial denaturation (95°C, 1 min), followed by 40 cycles of denaturation (95°C, 20 s), primer annealing (55°C, 20 s), and extension (72°C, 30 s). GAPDH served as the endogenous control. All reactions were performed in triplicate, with relative quantification determined via the 2-ΔΔCq method. Primer sequences are documented in Supplementary Table 2.

2.12 Statistical analysis

SPSS software (version 23.0) was used to perform statistical analysis. Data were presented as mean values ± SD. Shapiro-Wilk test and Levene method were used for the estimation of the data normal distributions and homogeneity of variance, respectively. For the comparation of mean values between two groups, paired or unpaired two-tailed Student's t test was used. One-way or two-way analysis of variance (ANOVA) followed by Tukey's *post-hoc* tests were used to assess the statistical significance of the mean values of more than two groups. Differences with $p < 0.05$ indicates statistical significance.

3 Result

3.1 Cell clusters in cystic lesions

To determine cellular subtypes and their genetic characteristics, we obtained three cystic lesion specimens from the hip joints of three SIONFH patients and performed scRNA-seq analysis (Figure 1A). In total, 30,224 individual cells were obtained for subsequent analysis after strict quality filtration (Supplementary Figure 2). Based on t-SNE analysis, 16 distinct cluster cells were identified based on unbiased cell type recognition (Supplementary Table 3). Among them, eight major cell types were defined by specific marker genes, including endothelial cells (ECs) (expressing PECAM1, PLVAP, and FLT1), fibroblasts cells (FBs) (expressing THY1, PDGFRB, COL1A1, and COL1A2), chondrocytes (expressing ACAN, SOX9, and COL2A1), monocytes cells (expressing PLAC8), macrophages (expressing CD163, CD68, and MRC1), T cells (expressing CD3D, CD3E, and CD8A), mast cells (expressing TPSAB1, TPSB2, and KIT), and osteoclasts (expressing ACP5, CTSK, and MMP9) (Figures 1B–D). To gain a deeper understanding of the function on different cell types, GO enrichment analysis was conducted. Each cell type-specific gene displayed high enrichment in the GO terms expected (Supplementary Figure 3, Supplementary Table 4). For example, genes that are specifically expressed in ECs cluster are significantly enriched in angiogenesis and vasculature development; specific genes of chondrocyte cluster are significantly enriched in cartilage condensation and chondrocyte differentiation; specific genes of osteoclast cluster are significantly enriched in osteoclast differentiation. These analyses strongly support the accuracy of our cell-type assignments.

3.2 Identification of FBs and ECs

Through cluster analysis of the FBs, five subclusters (Supplementary Figure 4A) were identified. Among them, three major cell types were defined by specific marker genes. Myofibroblast cells (Myo_FBs) cluster was enriched in genes controlling the angiogenesis, muscle contraction, smooth muscle contraction, and muscle organ development, with high expression levels of ACTA2 and TAGLN (Figures 2A, C, Supplementary Figures 4B, E). Osteogenic fibroblast cells (Osteogenic_FBs) cluster was high in genes associated with collagen fibril organization, osteoblast differentiation, and skeletal system development, showing an upregulation of GJA1, MMP2, and COL1A1 (Figures 2A, C, Supplementary Figures 4B, E). Additionally, cells in the inflammatory fibroblast cells (Inflammatory_FBs) cluster were significantly enrich in immune response, cell surface receptor signaling pathway, and inflammatory response, with high expression levels of CXCR4, IL32, and PTPRC (Figures 2A, C, Supplementary Figures 4B, E).

To investigate ECs heterogeneity in cystic lesions, four subclusters (Supplementary Figure 4C) were identified. We identified four empirically defined populations: vein endothelial cells (Vein_ECs), artery endothelial cells (Artery_ECs), endothelial mesenchymal transition endothelial cells (EndMT_ECs), and lymphatic endothelial cells (Lymphatic_ECs) (Figure 2B). Vein_ECs was identified as cluster with high expression of genes related to blood coagulation and angiogenesis, including ACKR1 and VWF (Figure 2D, Supplementary Figures 4D, F). Artery_ECs were highly enriched in angiogenesis, aortic valve morphogenesis, and response to mechanical stimulus, with high expression with HEY1, IGFBP3, and EFNB2 (Figure 2D, Supplementary Figures 4D, F). EndMT_ECs cluster was enriched in genes associated with collagen fibril organization, extracellular matrix organization, and ossification, including COL1A1, COL1A2 and THY1 (Figure 2D, Supplementary Figures 4D, F). Additionally, cells in the Lymphatic_ECs cluster were mainly enriched in immune response, defense response to virus, and inflammatory response, with upregulated expression of CD69 and CXCR4 (Figure 2D, Supplementary Figures 4D, F). Immunofluorescence analysis confirmed the expression of these FB and EC markers in cystic lesions (Figure 2E).

3.3 Identification of macrophage cells

Through cluster analysis of macrophages, 12 subclusters (Supplementary Figure 5A) were identified. Among them, three major cell types were defined by specific marker genes (Figure 3A), including M1 macrophages (expressing IL1B and CD80), M2 macrophages (expressing MRC1 and CD163), and M2/M1 macrophages (expressing IL1B, CD80, MRC1 and CD163) (Figure 3B, Supplementary Figure 5B) (18, 19). Trajectory analysis revealed that M2/M1 macrophages and M2 macrophages can transform into M1 macrophages over time (Figure 3C). A dynamic pattern of gene expression changes along the entire lineage differentiation trajectory is displayed in Figure 3D. The marker genes of M2/M1 macrophages and M2 macrophages such as MRC1

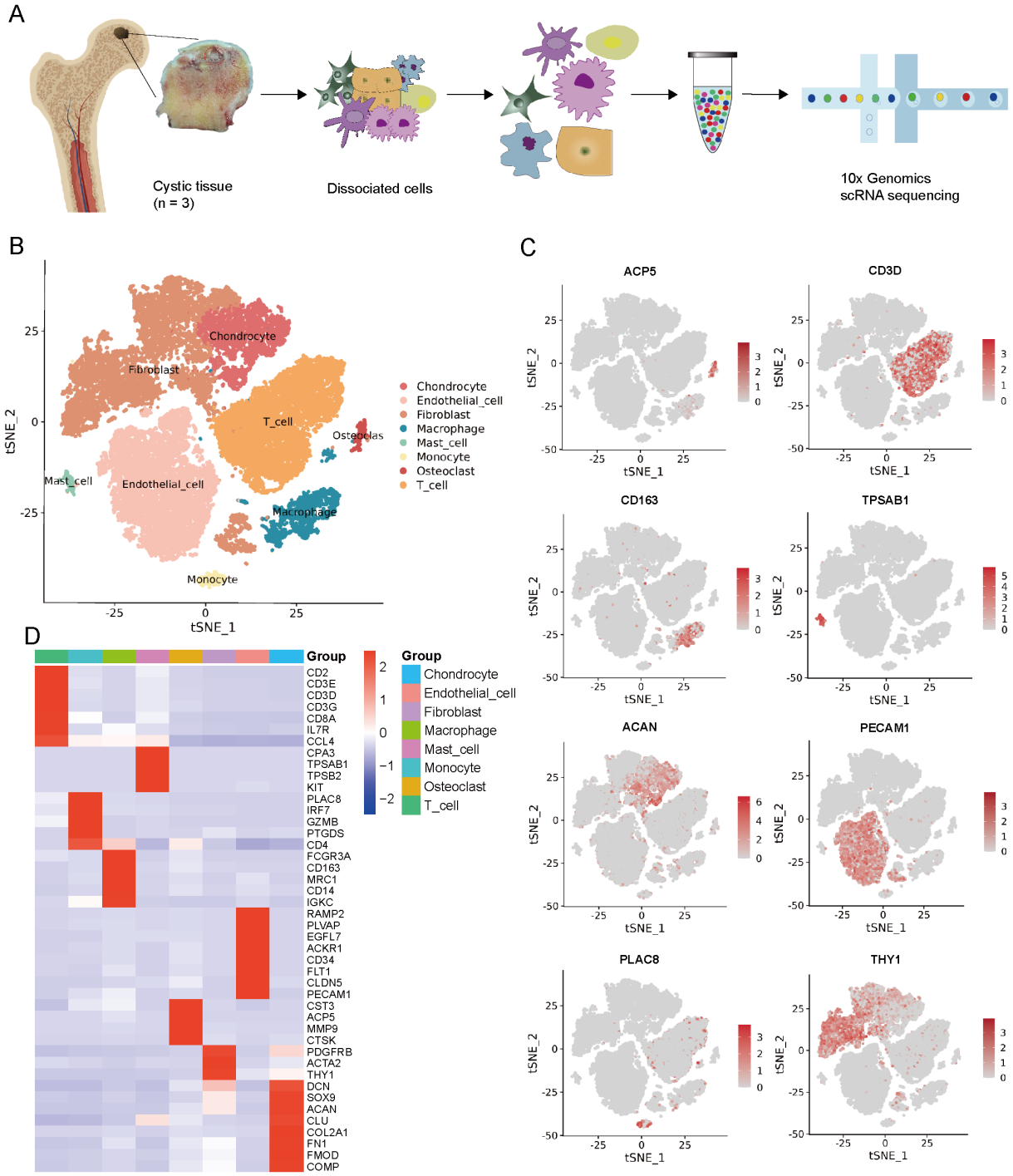

FIGURE 1
Single-cell RNA-seq of cystic lesions in SIONFH. **(A)** Schematic workflow of the experimental strategy. **(B)** t-SNE plot showing eight cell clusters in cystic lesions. **(C)** t-SNE plots showing eight cell type identified by marker gene expression (ACP5: osteoclasts; CD3D: T cells; CD163: macrophages; TPSAB1: mast cells; ACAN: chondrocytes; PECAM1: endothelial cells; PLAC8: monocytes cells; THY1: fibroblasts cells). **(D)** Heatmap plot showing scaled expression of canonical cell type-associated genes for clusters. SIONFH, steroid-induced osteonecrosis of the femoral head; scRNA-seq, Single-cell RNA sequencing; t-SNE, t-distributed stochastic neighbor embedding.

and CD163 decreased along pseudotime progression; while the marker genes of M1 macrophages such as CD80 and IL1B gradually increased along pseudotime progression (Figure 3E). Immunofluorescence analysis confirmed high CD163 expression in cystic lesions (Supplementary Figure 5C).

3.4 Identification of chondrocyte cells

To determine the identify of chondrocytes clusters, we identified five putative subclusters based on several transcriptomic studies of human chondrocytes, including: homeostatic

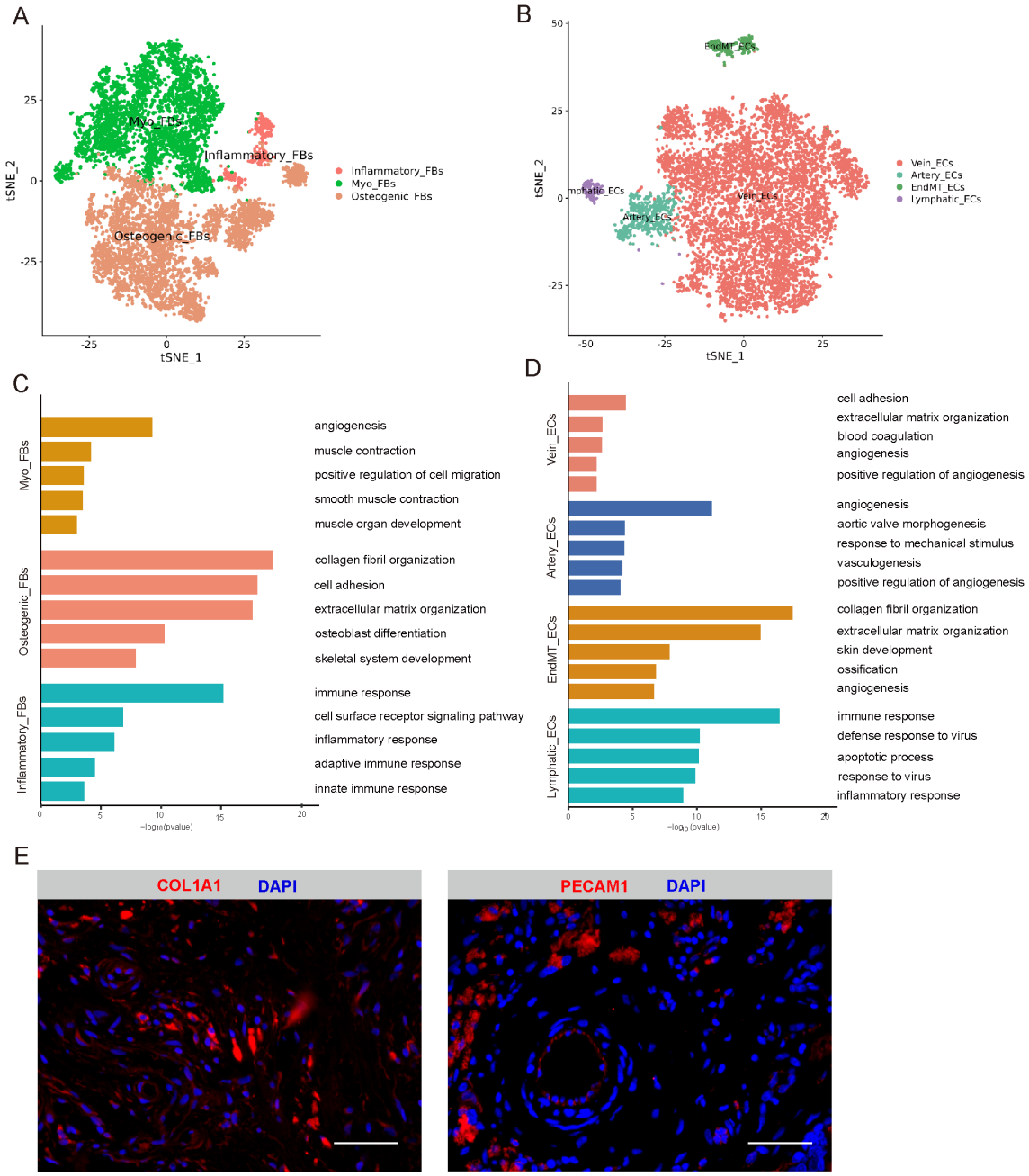

FIGURE 2
Identification of FBs and ECs. **(A)** t-SNE plot showing three subclusters of FBs. **(B)** t-SNE plot showing four subclusters of ECs. **(C)** The enriched GO terms results of marker genes of three cell subcluster of FBS. **(D)** The enriched GO terms results of marker genes of four cell subcluster of ECs. **(E)** Immunofluorescence expression of marker genes of FBs and ECs, respectively. Scale bar, 50 μm. t-SNE, t-distributed stochastic neighbor embedding; FBs, fibroblasts cells; ECs, endothelial cells; GO, gene ontology.

chondrocytes (HomC), fibrocartilage chondrocytes (FC), prehypertrophic chondrocytes (preHTC), inflammatory chondrocytes (InflamC), and hypertrophic chondrocytes (HTC) (Figure 4A) (20, 21). Representative markers for HomC, FC, preHTC, InflamC, and HTC were revealed (Figures 4B, C), representing new combinations of genes to distinguish chondrocyte populations. In addition, the GEO term revealed that HomC cluster was mainly enriched in negative regulation of growth and cellular zinc ion homeostasis; FC cluster was enriched in collagen fibril organization and actin filament organization; preHTC cluster was highly enriched in cartilage condensation and chondrocyte differentiation; InflamC cluster with high expression of genes related to immune response and inflammatory response; HTC cluster was significantly enriched in ossification, collagen catabolic process, osteoblast differentiation, and cell differentiation (Figure 4D). To further validate the

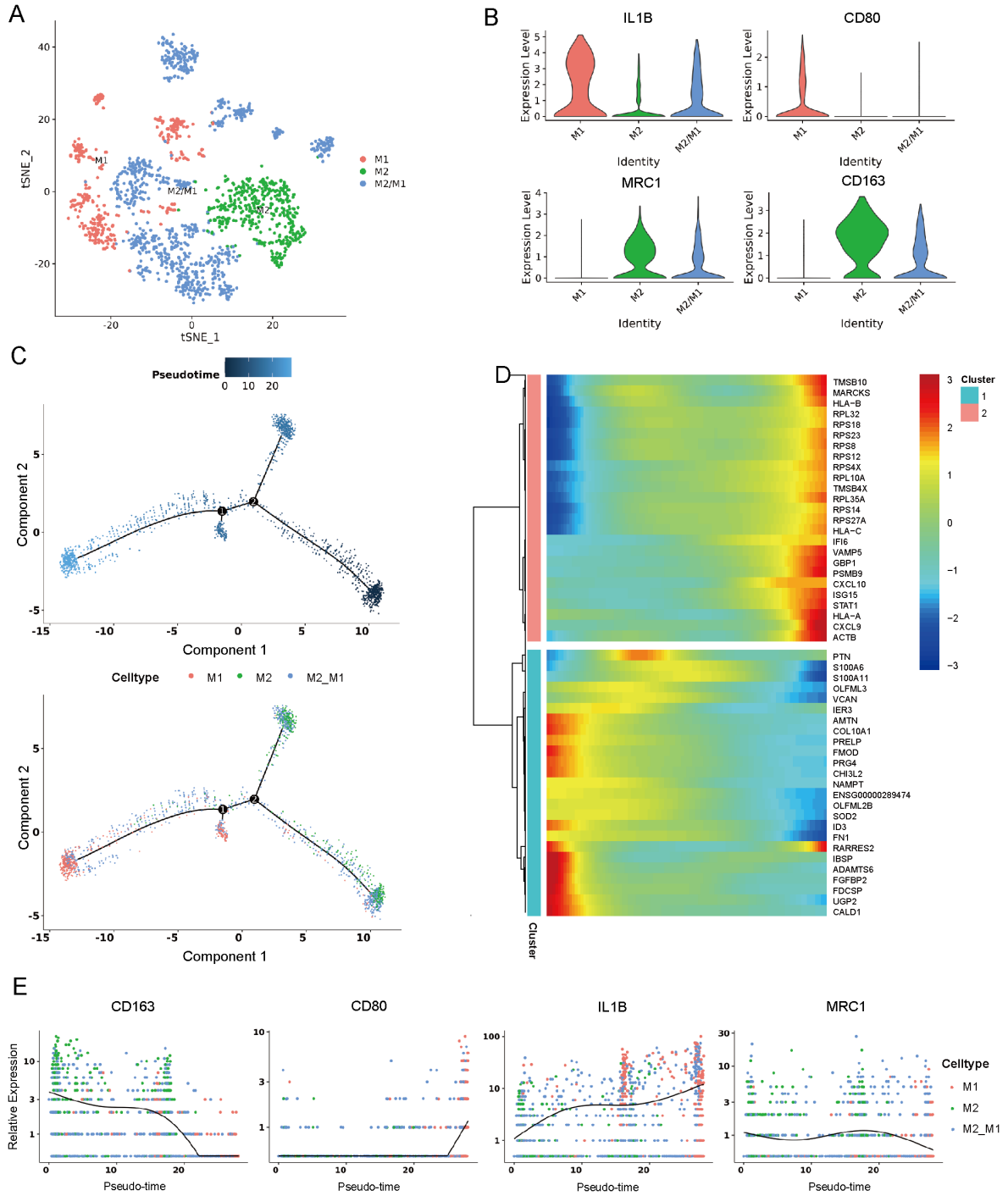

FIGURE 3
Identification of macrophage cells. **(A)** t-SNE plot showing three subclusters of macrophage cells. **(B)** Violin plots showing three cell type identified by marker gene expression (IL1B and CD80: M1 macrophages; MRC1 and CD163: M2 macrophages; IL1B, CD80, MRC1 and CD163: M2/M1). **(C)** Trajectory analysis of three subclusters of macrophage cells. **(D)** Dynamic pattern of gene expression changes along the entire lineage differentiation trajectory. **(E)** Expression of macrophage markers on a pseudo-time scale. t-SNE, t-distributed stochastic neighbor embedding.

differentiation process of chondrocytes, pseudotime analysis was conducted. The pseudotime trajectory axis derived from Monocle indicated that preHTC were existed in the start of the trajectory and the front of HTC, InflamC and HomCs distributed along trajectory, HTC and FC were mainly existed in the end, suggesting that the pseudotime trajectory conforms to the regular pattern of chondrocytes differentiation (Figure 4E). Additionally, we performed H&E staining, Alcian blue staining, and Safranin O-fast green staining to evaluate histological characteristic of the cystic lesions (Figure 5). Figure 5A showed the cystic lesions obtained from necrosis femoral head. H&E staining showed the presence of a certain number of chondrocytes and HTC at the edge of the cystic

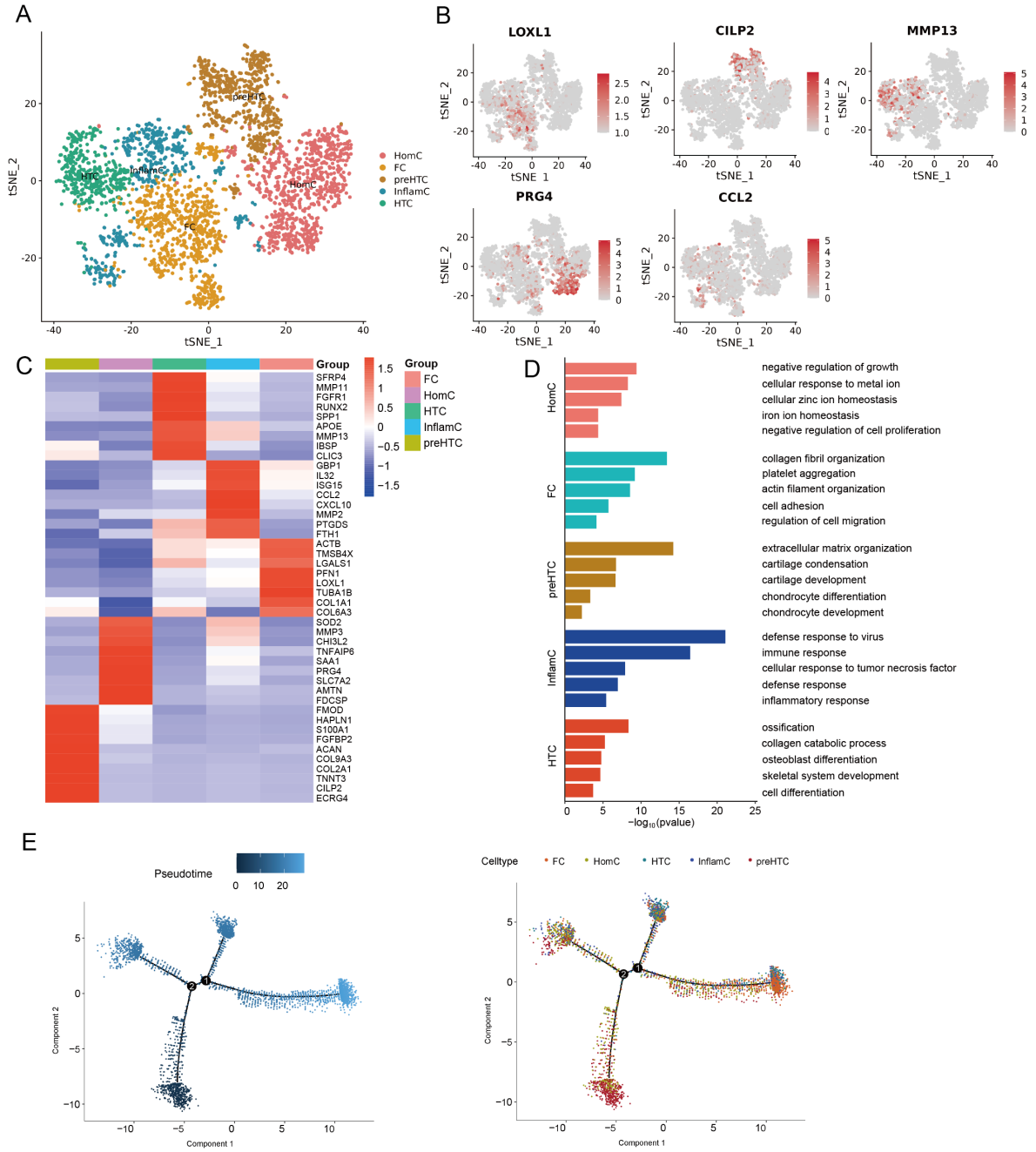

FIGURE 4
Identification of chonrocytes cells. **(A)** t-SNE plot showing five subclusters of chonrocytes cells. **(B)** t-SNE plots showing five cell type identified by marker gene expression (LOXL1: FC; CILP2: preHTC; MMP13: HTC; PRG4: HomC; CCL2: InflamC). **(C)** Heatmap plot showing scaled expression of canonical cell type-associated genes for five subclusters of chonrocytes cells. **(D)** The enriched GO terms results of marker genes of five subcluster of chonrocytes cells. **(E)** Trajectory analysis of five subcluster of chonrocytes cells. t-SNE, t-distributed stochastic neighbor embedding; FC, fibrocartilage chondrocytes; preHTC, prehypertrophic chondrocytes; HTC, hypertrophic chondrocytes; HomC, homeostatic chondrocytes; InflamC, inflammatory chondrocytes; GO, gene ontology.

lesions (Figure 5B). Alcian blue and Safranin O-fast green staining indicated that these cells were surrounded by a certain amount of cartilage matrix (Figure 5B). Meanwhile, we found a transition from cartilage tissue to bone matrix, suggesting the presence of a transitional zone from cartilage to bone tissue within the cystic lesions (Figure 5B).

3.5 Identification of HTC

To characterize the features of the HTC cluster, we divided the HTC cluster into three subclusters (Figure 6A). Among them, HTC.1 was identified as osteogenics-related cluster with high expression of genes enriched in ossification, bone mineralization,

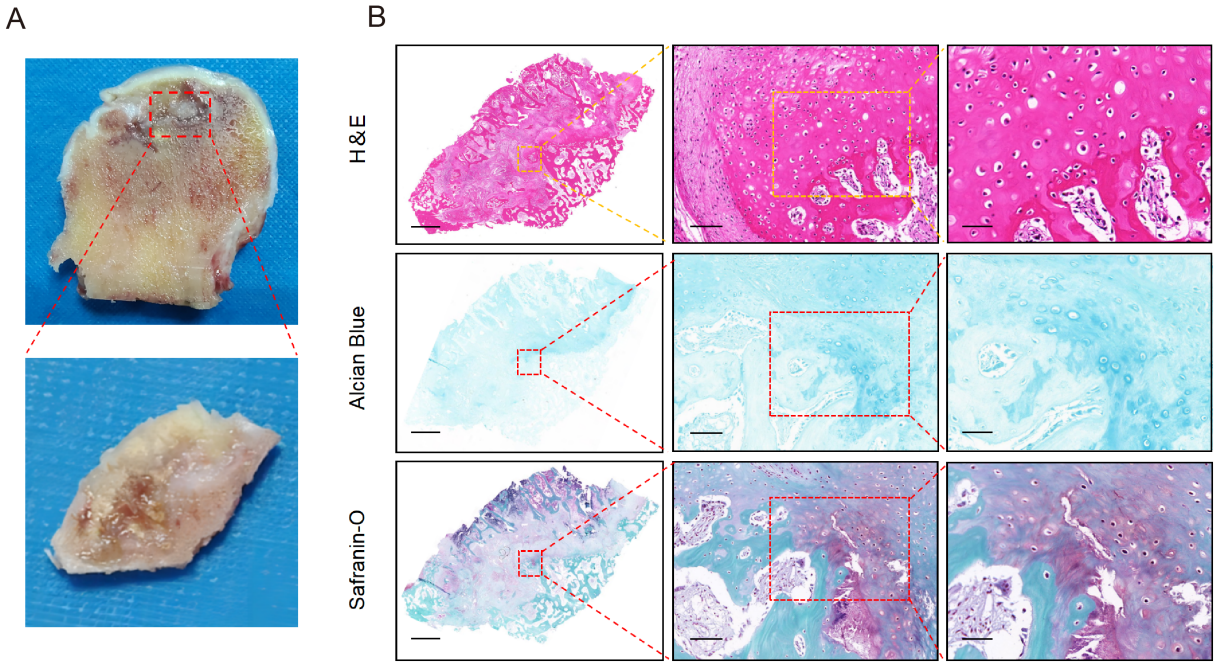

FIGURE 5
The pathological manifestations of cystic lesions. **(A)** The macroscopic appearance of cystic lesions in femoral head from SIONFH patients. **(B)** The results of H&E staining, Alcian blue staining, and Safranin O-Fast Green staining. Scale bar: left, 2.5 mm; middle, 100 μm; right, 50 μm. SIONFH, steroid-induced osteonecrosis of the femoral head.

and osteoblast differentiation, MAPK and PI3K-Akt signaling pathway, with high expression levels of SPP1, RUNX2, and MMP13 (Figures 6B, C). HTC.2 cluster expressed unique markers that enriched in extracellular matrix organization and protein digestion and absorption, including ASPN and NDUFA4L2 (Figures 6B, C). HTC.3 cluster expressed high levels of SFRP4 and MMP11, with functional enrichment in immune response, iron ion homeostasis, and negative regulation of cell differentiation, along with KEGG pathway enrichment in ferroptosis signaling (Figures 6B, C). In order to explore the possible mechanisms of endochondral ossification for HTC, we further detected the significant key genes involved in this process. CLIC3, a marker gene associated with chloride ion channel, was calculated via DEGs by comparing HTC.1 to HTC.2 and HTC.3 (Figure 6D). There is a great difference in the expression multiples between three clusters of HTC, indicating that CLIC3 is a specific gene for regulating the differentiation of HTC into osteoblasts. Western blot and RT-qPCR analyses revealed that both protein and gene expression levels of osteogenic markers (SPP1 and RUNX2), hypertrophic chondrocyte (HTC) markers (COL10A1 and MMP13), and CLIC3 were markedly elevated in cystic lesions compared to those in bone samples from FNF patients (Figures 6E, F). Immunohistochemical analysis revealed a high expression of osteogenic markers (SPP1 and RUNX2), HTC markers (COL10A1 and MMP13), and CLIC3 at the edge of the cystic lesions (Figure 6G). The results of immunofluorescence analysis were consistent with that of immunohistochemical analysis (Supplementary Figure 6).

3.6 Cellular interaction in cystic lesions

We identified eight types of cells, including four types of immune cells, repair-related cells like fibroblasts and endothelial cells and other cells like chondrocyte and osteoclast. Through CellChat analysis, we obtained a network map of interactions between cells (Figure 7A), and detected 75 significant ligand-receptor pairs among these 8 cell types, further categorizing them into 31 signaling pathways, including SPP1, MIF, VISFATIN, VEGF, CXCL, CCL, and MIF pathways (Figure 7B). The output of this analysis is a set of communication patterns linking cell populations with signaling pathways, whether in the context of output signals (treating cells as senders) or input signals (treating cells as receivers). The application of this analysis revealed three outgoing signaling patterns and four incoming signaling patterns (Figure 7C). For instance, the output indicated that all immune cells and osteoclasts exhibit outgoing signals characterized by pattern 1, representing multiple pathways including but not limited to SPP1, GALECTIN, CXCL, VEGF, and CCL. Fibroblasts and endothelial cells exhibit outgoing signals characterized by pattern 2, representing MK, PERIOSTIN, PTN, ANGPT, FGF among others. Chondrocytes exhibit outgoing signals characterized by pattern 3, representing ANGPTL, SEMA3, ncWNT among others. On the other hand, the communication signal patterns of target cells show that incoming signals from all immune cells are characterized by pattern 3, representing MIF, GALECTIN, CXCL, ANNEXIN, TNF, IL16 among others. Incoming signals from chondrocytes and fibroblasts are characterized by pattern 1, including TGFβ, GAS, PDGF, FGF

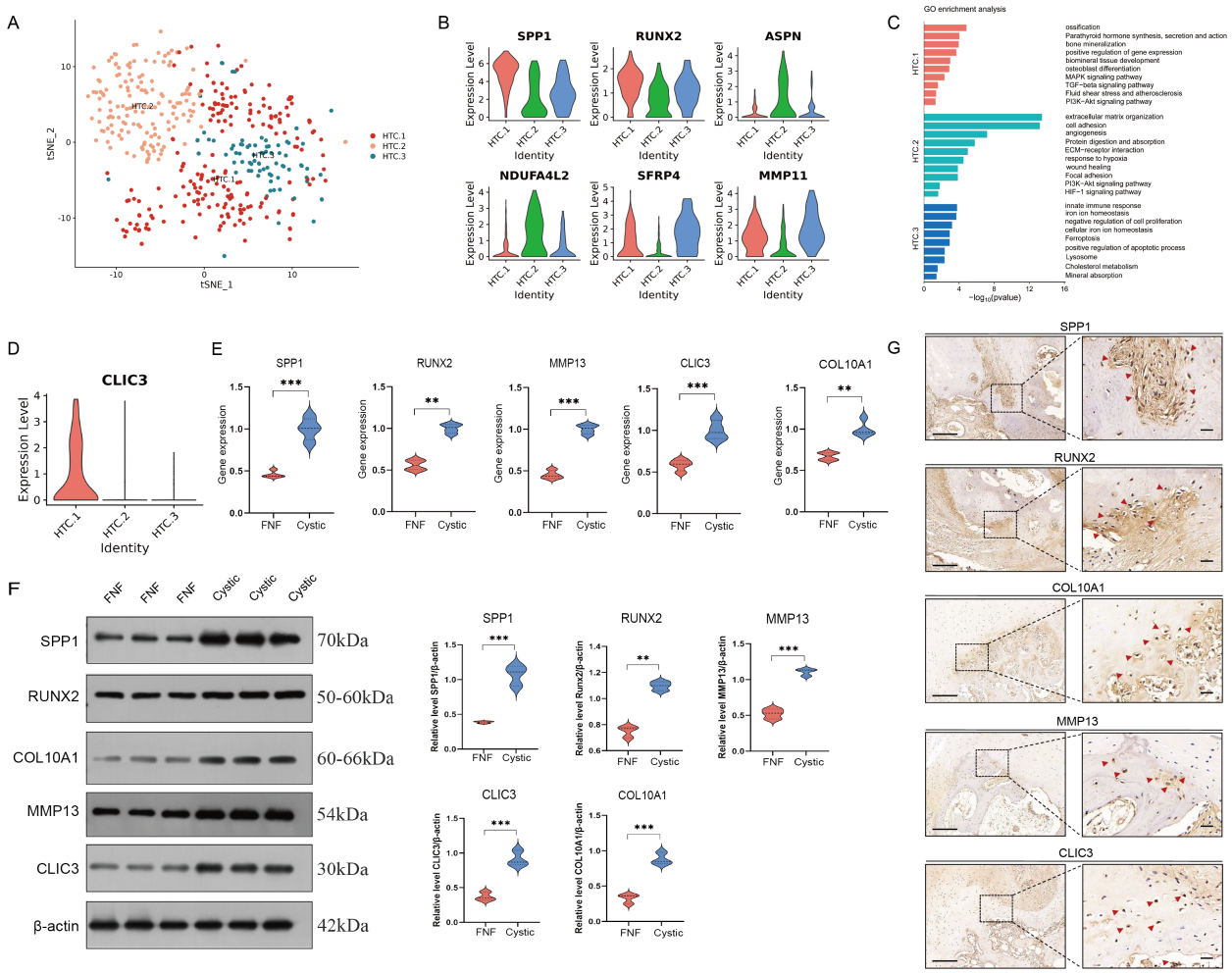

FIGURE 6
Identification of HTC cells. **(A)** t-SNE plot showing three subclusters of HTC. **(B)** Violin plots showing three cell type identified by marker gene expression (SPP1 and RUNX2: HTC.1; ASPN and NDUFA4L2: HTC.2; SFRP4 and MMP11: HTC.3). **(C)** The enriched GO terms results of marker genes of three subcluster of HTC. **(D)** The expression level of CLIC3 was significantly increased in HTC.1 cluster. **(E)** RT-qPCR analyses revealed that the gene expression levels of SPP1, RUNX2, COL10A1, MMP13, and CLIC3 were elevated in cystic lesions compared to those in FNF bone samples. **(F)** Western blot analyses revealed that the gene protein expression levels of SPP1, RUNX2, COL10A1, MMP13, and CLIC3 were elevated in cystic lesions compared to those in FNF bone samples. **(G)** Immunohistochemical expression of SPP1, RUNX2, COL10A1, MMP13, and CLIC3 in cystic lesions. Scale bar: left, 250 μm; right, 50 μm. HTC, hypertrophic chondrocytes; GO, gene ontology. **p < 0.01; ***p < 0.001.

among others. Incoming signals from endothelial cells are characterized by pattern 2. Incoming signals from osteoclasts are characterized by pattern 4, representing CSF, RANKL among others. We also found the FGF signaling network inferred by CellChat indicates that chondrocytes are the main source of receptors (Figure 7D). It exhibits weak autocrine activity in chondrocytes, primarily achieved through the ligand-receptor pair FGF1/FGFR1, but mainly secreted by fibroblasts, primarily through the ligand-receptor pair FGF7/FGFR1 (Figure 7E).

4 Discussion

SIONFH is an intractable orthopedic condition with disability risk (22, 23). Current conventional approaches focusing on imaging feature identification and clinical symptom management in hip preservation therapy have demonstrated limited efficacy. Emerging evidence suggests that targeting necrotic femoral head repair mechanisms may represent a promising therapeutic strategy. Previous studies have demonstrated the regenerative capacity of cystic lesions, yet their underlying pathophysiology and repair mechanisms remain unknown (9, 10). In this study, we employed scRNA-seq technology to characterize the transcriptome profile of cystic lesions for the first time. Significantly, we identified a novel osteogenic differentiation repair pattern mediated by hypertrophic chondrocytes, providing mechanistic insights into femoral head regeneration (Figure 8).

Eight cell populations were identified in cystic lesions, including endothelial cells, fibroblasts, chondrocytes, tissue stem cells, macrophages, T cells, osteoclasts, and monocytes. Previous studies have indicated that the pathological characteristics of cystic lesions include fibrous granulation tissue (7). Consistent with this, gross

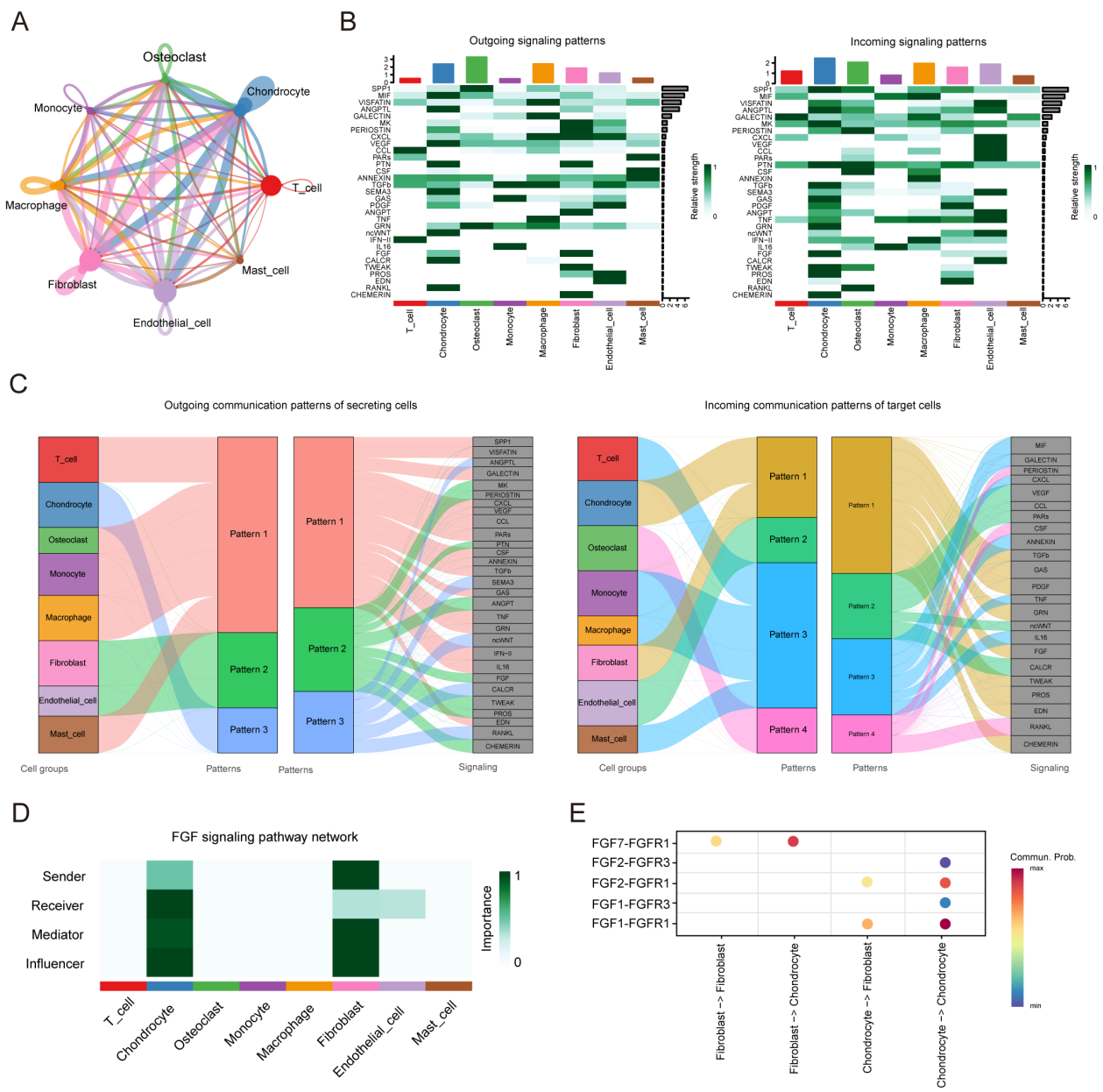

FIGURE 7
CellChat analysis of the communications between eight cell types in cystic lesions. **(A)** Analysis of the number of interactions among different cell types. **(B)** Overview of the outgoing signaling and incoming signaling of eight cell types. **(C)** Overview of the outgoing communication patterns of secreting cells and incoming communication patterns of target cells. **(D)** Communication roles played by eight cell types in FGF signaling pathway. **(E)** Bubble plot showing the ligand-receptor between fibroblasts and chondrocytes.

examination of numerous necrotic femoral head specimens revealed substantial red or grayish-white tissue within the cystic lesion areas, exhibiting histological characteristics consistent with granulation or fibrotic tissue. Quantitative analysis confirmed fibroblasts as the predominant cellular component, validating the scRNA-Seq methodology employed in this study. Subgroup analysis of fibroblasts identified three distinct subtypes: Myo_FBs, Osteogenic_FBs, and Inflammatory_FBs. Several reports suggested that fibroblasts possess intrinsic osteogenic differentiation capacity independent of pluripotent stem cell transition (24, 25). Our scRNA-Seq data suggest active fibroblast participation in osseous repair processes within cystic lesions, though the exact molecular mechanisms require further elucidation. The results also revealed a significant proportion of endothelial cells. Studies have shown a close relationship between angiogenesis and bone formation, where H-type blood vessels have shown potential to induce bone formation, concurrent with higher expression levels of EMCN and PECAM-1 within these vessels (26). Therefore, promoting neovascularization represents a promising therapeutic strategy to prevent femoral head collapse in SIONFH. We found that both Vein_ECs and Artery_ECs are highly enriched in angiogenesis biological processes within the endothelial cell

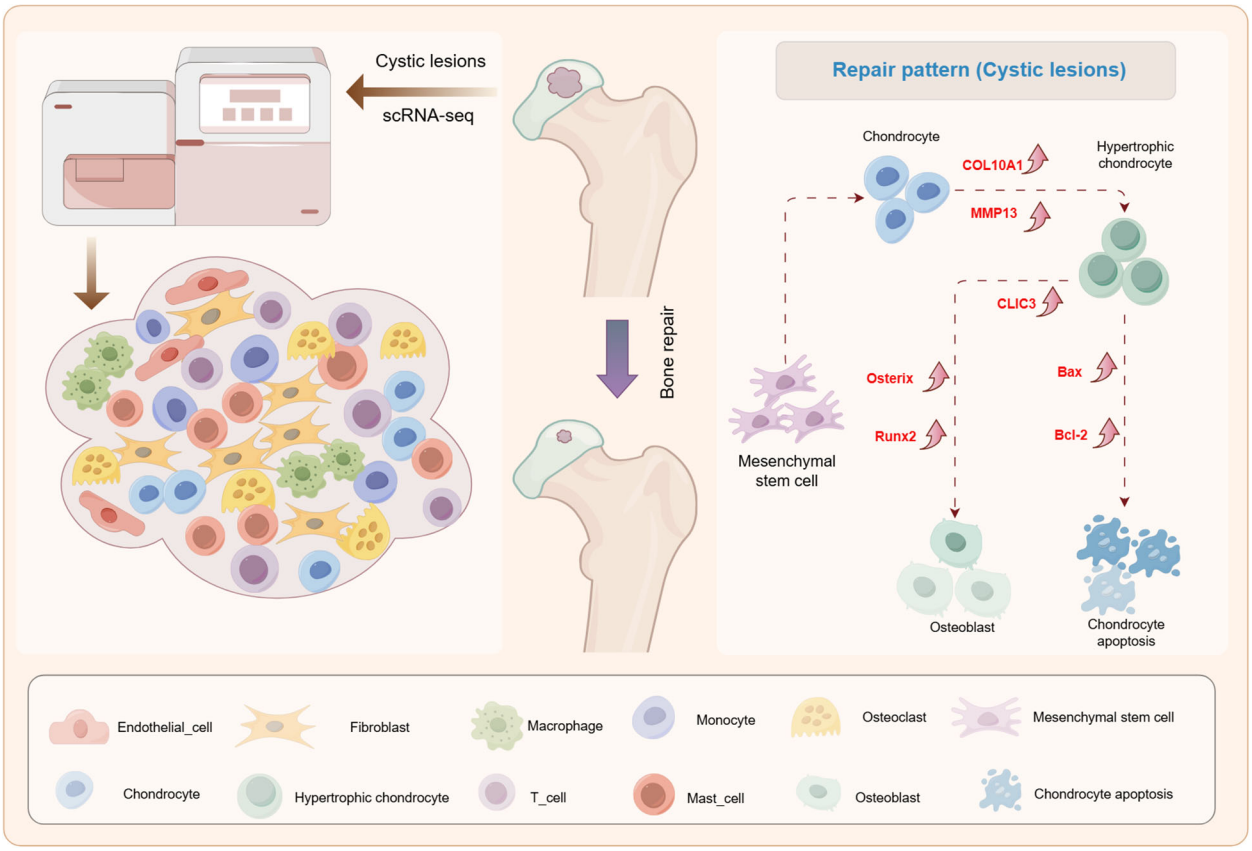

FIGURE 8
A graphical scheme of revealing the single-cell transcriptomic landscape of cystic lesions and the existence of a repair pattern involving chondrocyte hypertrophy and subsequent osteogenic differentiation in cystic lesions in SIONFH.

subgroups, which may contribute to the repair of cystic change in SIONFH.

Accumulating evidence in recent years highlights the indispensable role of bone immunology in the pathogenesis of SIONFH (27, 28). Immune cells can regulate the activation and function of various bone cells (osteoblasts, osteoclasts, mesenchymal stem cells, etc.), thereby regulating the processes of bone formation and repair (29). In this study, we observed significant immune cell infiltration in cystic lesions, including T cells, macrophages, monocytes, and mast cells. Consistent with previous studies, histological and bioinformatics analyses of ONFH revealed that the necrotic tissue contains a large number of immune cell infiltrations, such as macrophages, T lymphocytes, and B lymphocytes, implicating immune cells in ONFH onset and progression (30–32). The stimulation and inhibition of osteoblasts and osteoclasts by T cells are closely related to T cell subpopulations and cytokines, mainly achieved through the RANKL/RANK/OPG system (27). Macrophages, a type of "proliferative" immune cell, play a key role in the innate immune response. Macrophages can be "polarized" into different phenotypes based on their microenvironment, that is, "classically activated" M1 macrophages have pro-inflammatory effects, while "selectively activated" M2 macrophages have anti-inflammatory effects (33). Building on this, we identified three macrophage subtypes within the lesions. Pseudotemporal analysis found that M2/M1 macrophages and M2 macrophages can be transformed into M1 macrophages over time, indicating that in the local immune microenvironment of SIONFH cystic lesions, macrophages continuously polarize towards M1, leading to an increase in the M1/M2 ratio and causing imbalance of bone immunity, which may be one of the pathogenic mechanisms of SIONFH. Curcumin can prevent inflammation-mediated osteocyte apoptosis in a mouse model of glucocorticoid-related femoral head necrosis by inhibiting the polarization of M1 macrophages (34). Mongolicin can regulate inflammation and promote bone formation by inhibiting the TLR4/NF-κB pathway and M1 macrophage polarization, reducing the incidence of femoral head osteonecrosis and alleviating pathological manifestations within the femoral head (35). Therefore, inhibiting M1 macrophage polarization represents a promising therapeutic strategy for SIONFH.

Interestingly, we identified chondrocytes within the cystic lesions. Our analysis distinguished five chondrocyte subtypes based on established markers from prior articular cartilage scRNA-seq studies (20, 21). The pseudotime trajectory axis derived from Monocle matched well with cell types and the cell arrangement in the pseudospace trajectory corresponded to spatial relationships of the cells. Bone formation occurs via intramembranous ossification or endochondral

ossification (36). In endochondral ossification, there are three major models of transdifferentiation of chondrocytes to osteoblasts. Recently, growing evidences revealed that chondrocytes will mature and hypertrophy, and that they do not apoptose, but instead differentiate directly into osteoblasts and subsequently into osteocytes (37, 38). Consistent with this, we found that HTC were enriched in ossification, collagen catabolic process, and osteoblast differentiation. Cluster analysis revealed a distinct HTC.1 subpopulation with significant involvement in ossification and bone mineralization. We further conducted pathological observations on the cystic lesions. Through H&E, Alcian blue, and Safranin O-fast green staining, we observed the presence of chondrocytes and HTC and a transition zone from chondrocytes to bone tissue within the cystic lesions. The results of immunohistochemistry and immunofluorescence also indicated high expression of HTC markers and osteogenesis-related gene at the edge of the cystic lesions. Numerous studies have revealed that a multitude of signaling and transcription factors are critical for endochondral bone formation, including BMP (Bone Morphogenetic Proteins) signaling, Wnt/β-catenin signaling, Indian hedgehog (Ihh) pathway, and FGF signaling (39–41). Lyu et al. demonstrated that intraperitoneal injection of the BMP signaling inhibitor LDN193189HOU in mice rescues osteogenic activation in chondrocytes (42). Runx2, a core regulatory gene of osteogenic differentiation, exhibits dual functionality during chondrocyte-to-osteoblast transition: promoting chondrocyte hypertrophy while simultaneously activating osteoblast differentiation programs. Previous studies confirm that excessive activation of Runx2 accelerates chondrocyte catabolism (43). Consistent with this, our findings via Western blot, RT-qPCR, and immunohistochemistry analyses showed significantly elevated Runx2 expression levels within cystic lesions regions. Meanwhile, expression of the hypertrophic marker COL10A1 and catabolic enzyme MMP13 was markedly increased, providing direct evidence for chondrocyte hypertrophy and osteogenic transdifferentiation within cystic lesions. Notably, we found that a type of CLIC3^{+}HTC might be associated with ossification, indicating that these cells are potentially involved in osteogenic process in cystic lesions. CLIC3 is a soluble protein that regulates chloride conductance and cell growth. Previous study reported that CLIC3 is a key gene modulating osteoblast differentiation and enhancing bone formation (44). It may regulate osteoblast differentiation via cytoskeleton-associated signaling processes. In addition, the KEGG analysis showed that HTC.1 were enriched in MAPK signaling pathway, indicating that CLIC3 may regulate osteoblast differentiation through MAPK signaling pathway, but this requires further investigation.

The strength of this study is that we provide the first single-cell transcriptomic landscape of cystic lesions in SIONFH. In addition, the results of scRNA-seq analysis revealed a repair pattern of HTC differentiating into osteoblast in cystic lesions. In terms of limitations, first, the sample size is relatively small, and subsequent scRNA-seq studies will require more samples. Second limitation is the lack of an animal model for cystic changes, which prevents us from validating our findings *in vivo*. Third, although our findings delineate a repair pattern in SIONFH cystic lesions, the current cohort was confined to Chinese patients; future multi-ethnic studies are required to verify this pattern's universality.

5 Conclusion

In summary, we have delineated the cellular heterogeneity and molecular signatures of cystic lesions in SIONFH. Our research reveal a distinct repair program within these lesions, which might be driven by chondrocyte hypertrophy and might culminate in osteogenic differentiation. These findings will provide novel therapeutic targets for the repair of necrotic bone in SIONFH.

Data availability statement

The data presented in this study have been deposited in the Gene Expression Omnibus (GEO) repository under accession number GSE290411. These data are publicly available.

Ethics statement

The studies involving humans were approved by The Ethics Committee of the Third Affiliated Hospital of Guangzhou University of Chinese Medicine. The studies were conducted in accordance with the local legislation and institutional requirements. The participants provided their written informed consent to participate in this study.

Author contributions

PP: Data curation, Writing – original draft, Writing – review & editing. J-qT: Data curation, Writing – original draft. KL: Methodology, Project administration, Writing – original draft. WF: Methodology, Project administration, Writing – original draft. FY: Methodology, Supervision, Writing – review & editing. XY: Data curation, Formal analysis, Writing – original draft. WYH: Supervision, Validation, Writing – original draft. FX: Conceptualization, Data curation, Writing – review & editing. SL: Writing – review & editing. WH: Conceptualization, Writing – review & editing. MH: Conceptualization, Data curation, Writing – review & editing. HX: Writing – review & editing. QW: Conceptualization, Writing – original draft, Writing – review & editing.

Funding

The author(s) declare financial support was received for the research and/or publication of this article. This study was supported by the National Natural Science Foundation of China (grant number 82004392 and 82274544), the major project of "double first-class" and high-level university disciplines collaborative innovation team of Guangzhou University of Traditional Chinese Medicine (grant number 2021XK05); the Foundation of Guangdong Research Institute for Orthopedics and Traumatology of Chinese Medicine for Youth Scientists (grant number GYH202201-01); the key project of Guangdong Institute of Orthopedics and Traumatology of Chinese

Medicine (GYH202101-04), National Key Laboratory of Traditional Chinese Medicine Syndrome Open Fund Project (SKLKY2024B0019); the China postdoctoral Science Foundation (2024M750819); Guangdong Provincial Medical Research Fund Project(A2025133) and Bijie Science and Technology Bureau 'the open competition project' (no. BST Major Project No.1,2022).

Conflict of interest

The authors declare that the research was conducted in the absence of any commercial or financial relationships that could be construed as a potential conflict of interest.

Generative AI statement

The author(s) declare that no Generative AI was used in the creation of this manuscript.

Any alternative text (alt text) provided alongside figures in this article has been generated by Frontiers with the support of artificial intelligence and reasonable efforts have been made to ensure accuracy, including review by the authors wherever possible. If you identify any issues, please contact us.

Publisher's note

All claims expressed in this article are solely those of the authors and do not necessarily represent those of their affiliated organizations, or those of the publisher, the editors and the reviewers. Any product that may be evaluated in this article, or claim that may be made by its manufacturer, is not guaranteed or endorsed by the publisher.

Supplementary material

The Supplementary Material for this article can be found online at: https://www.frontiersin.org/articles/10.3389/fimmu.2025.1626337/full#supplementary-material

References

1. Birla V, Vaish A, Vaishya R. Risk factors and pathogenesis of steroid-induced osteonecrosis of femoral head - A scoping review. *J Clin Orthop Trauma*. (2021) 23:101643. doi: 10.1016/j.jcot.2021.101643

2. Zhang J, Cao J, Liu Y, Zhao L. Advances in the pathogenesis of steroid-associated osteonecrosis of the femoral head. *Biomolecules*. (2024) 14:667. doi: 10.3390/biom14060667

3. Motta F, Timilsina S, Gershwin ME, Carlo S. Steroid-induced osteonecrosis. *J Transl Autoimmun*. (2022) 5:100168. doi: 10.1016/j.jtauto.2022.100168

4. Shi S, Luo P, Sun L, Xie L, Yu T, Wang ZC, et al. Prediction of the progression of femoral head collapse in ARCO stage 2-3A osteonecrosis based on the initial bone resorption lesion. *Br J Radiol*. (2021) 94:20200981. doi: 10.1259/bjr.20200981

5. Zhang Z, Lin T, Zhong Y, Song W, Yang P, Wang D, et al. Effect of femoral head necrosis cystic area on femoral head collapse and stress distribution in femoral head: A clinical and finite element study [published correction appears in Open Med (Wars). *Open Med (Wars)*. (2022) 17:1282–91. doi: 10.1515/med-2022-0506

6. Sugano N, Atsumi T, Ohzono K, Kubo T, Hotokebuchi T, Takaoka K. The 2001 revised criteria for diagnosis, classification, and staging of idiopathic osteonecrosis of the femoral head. *J Orthop Sci*. (2002) 7:601–5. doi: 10.1007/s007760200108

7. Resnick D, Niwayama G, Coutts RD. Subchondral cysts (geodes) in arthritic disorders: pathologic and radiographic appearance of the hip joint. *AJR Am J Roentgenol*. (1977) 128:799–806. doi: 10.2214/ajr.128.5.799

8. Gao F, Han J, He Z, Li Z. Radiological analysis of cystic lesion in osteonecrosis of the femoral head. *Int Orthop*. (2018) 42:1615–21. doi: 10.1007/s00264-018-3958-z

9. Lakhotia D, Swaminathan S, Shon WY, Moon JG, Dwivedi C, Hong SJ. Healing process of osteonecrotic lesions of the femoral head following transtrochanteric rotational osteotomy: A computed tomography-based study. *Clin Orthop Surg*. (2017) 9:29–36. doi: 10.4055/cios.2017.9.1.29

10. He XM, He MC, Yang P, Zhang QW, Chen ZQ, He W, et al. The therapeutic effect of huo xue tong luo capsules in association research circulation osseous (ARCO) stage II osteonecrosis of the femoral head: A clinical study with an average follow-up period of 7.95 years. *Front Pharmacol*. (2021) 12:773758. doi: 10.3389/fphar.2021.773758

11. Slovin S, Carissimo A, Panariello F, Grimaldi A, Bouche V, Gambardella G, et al. Single-cell RNA sequencing analysis: A step-by-step overview. *Methods Mol Biol*. (2021) 2284:343–65. doi: 10.1007/978-1-0716-1307-8_19

12. Tao Y, Ma Y, Gu L, Zhang Y, Zhang Q, Zhou L, et al. Single-cell RNA sequencing reveals Shen-Bai-Jie-Du decoction retards colorectal tumorigenesis by regulating the TMEM131-TNF signaling pathway-mediated differentiation of immunosuppressive dendritic cells. *Acta Pharm Sin B*. (2025) 15:3545–60. doi: 10.1016/j.apsb.2025.05.013

13. Lin J, Huang L, Li W, Xiao H, Pan M. Unraveling the oxidative stress landscape in diabetic foot ulcers: insights from bulk RNA and single-cell RNA sequencing data. *Biol Direct*. (2025) 20:79. doi: 10.1186/s13062-025-00672-5

14. Riegel D, Romero-Fernández E, Simon M, Adenugba A, Singer K, Mayr R, et al. Integrated single-cell profiling dissects cell-state-specific enhancer landscapes of human tumor-infiltrating CD8+ T cells. *Mol Cell*. (2023) 83:622–636.e10. doi: 10.1016/j.molcel.2022.12.029

15. Lv Z, Han J, Li J, Guo H, Fei Y, Sun Z, et al. Single cell RNA-seq analysis identifies ferroptotic chondrocyte cluster and reveals TRPV1 as an anti-ferroptotic target in osteoarthritis. *EBioMedicine*. (2022) 84:104258. doi: 10.1016/j.ebiom.2022.104258

16. Qiu X, Hill A, Packer J, Lin D, Ma Y, Trapnell C. Single-cell mRNA quantification and differential analysis with Census. *Nat Methods*. (2017) 14:309–15. doi: 10.1038/nmeth.4150

17. Lihua C, Zhiyin T. Microplastics aggravates rheumatoid arthritis by affecting the proliferation/migration/inflammation of fibroblast-like synovial cells by regulating mitochondrial homeostasis. *Int Immunopharmacol*. (2023) 120:110268. doi: 10.1016/j.intimp.2023.110268

18. Murray PJ. Macrophage polarization. *Annu Rev Physiol*. (2017) 79:541–66. doi: 10.1146/annurev-physiol-022516-034339

19. Tian Z, Yang S. Integrating the characteristic genes of macrophage pseudotime analysis in single-cell RNA-seq to construct a prediction model of atherosclerosis. *Aging (Albany NY)*. (2023) 15:6361–79. doi: 10.18632/aging.204856

20. Ji Q, Zheng Y, Zhang G, Hu Y, Fan X, Hou Y, et al. Single-cell RNA-seq analysis reveals the progression of human osteoarthritis. *Ann Rheum Dis*. (2019) 78:100–10. doi: 10.1136/annrheumdis-2017-212863

21. Li H, Jiang X, Xiao Y, Zhang Y, Zhang W, Doherty M, et al. Combining single-cell RNA sequencing and population-based studies reveals hand osteoarthritis-associated chondrocyte subpopulations and pathways. *Bone Res*. (2023) 11:58. doi: 10.1038/s41413-023-00292-7

22. Wu CT, Kuo FC, Yen SH, Lin PC, Wang JW, Lee M, et al. Impaction bone grafting augmented with a wire coil by the lightbulb technique for osteonecrosis of the femoral head. *J Arthroplasty*. (2022) 37:2063–70. doi: 10.1016/j.arth.2022.04.034

23. Wei QS, Hong GJ, Yuan YJ, Chen ZQ, Zhang QW, He W. Huo Xue Tong Luo capsule, a vasoactive herbal formula prevents progression of asymptomatic osteonecrosis of femoral head: A prospective study. *J Orthop Translat*. (2018) 18:65–73. doi: 10.1016/j.jot.2018.11.002

24. Knaup I, Symmank J, Bastian A, Neuss S, Pufe T, Jacobs C, et al. Impact of FGF1 on human periodontal ligament fibroblast growth, osteogenic differentiation and inflammatory reaction *in vitro*. Einfluss von FGF1 auf Wachstum, osteogene Differenzierung und inflammatorische Stressreaktion humaner Parodontalligamentfibroblasten in *vitro*. *J Orofac Orthop*. (2022) 83:42–55. doi: 10.1007/s00056-021-00363-6

25. Ceylan M, Schoenmaker T, Hogervorst JMA, Jansen IDC, Schimmel IM, Prins CM, et al. Osteogenic differentiation of human gingival fibroblasts inhibits osteoclast formation. *Cells*. (2024) 13:1090. doi: 10.3390/cells13131090

26. Kusumbe AP, Ramasamy SK, Adams RH. Coupling of angiogenesis and osteogenesis by a specific vessel subtype in bone. *Nature*. (2014) 507:323–8. doi: 10.1038/nature13145

27. Ma J, Ge J, Gao F, Wang B, Yue D, Sun W, et al. The role of immune regulatory cells in nontraumatic osteonecrosis of the femoral head: A retrospective clinical study. *BioMed Res Int*. (2019) 2019:1302015. doi: 10.1155/2019/1302015

28. Zhang Q, Sun W, Li T, Liu F. Polarization behavior of bone macrophage as well as associated osteoimmunity in glucocorticoid-induced osteonecrosis of the femoral head. *J Inflammation Res*. (2023) 16:879–94. doi: 10.2147/JIR.S401968

29. Saxena Y, Routh S, Mukhopadhaya A. Immunoporosis: role of innate immune cells in osteoporosis. *Front Immunol*. (2021) 12:687037. doi: 10.3389/fimmu.2021.687037

30. Vicaş RM, Bodog FD, Fugaru FO, Grosu F, Badea O, Lazar L, et al. Histopathological and immunohistochemical aspects of bone tissue in aseptic necrosis of the femoral head. *Rom J Morphol Embryol*. (2020) 61:1249–58.

31. Zhao J, Zhang X, Guan J, Su Y, Jiang J. Identification of key biomarkers in steroid-induced osteonecrosis of the femoral head and their correlation with immune infiltration by bioinformatics analysis. *BMC Musculoskelet Disord*. (2022) 23:67. doi: 10.1186/s12891-022-04994-7

32. Wang B, Gong S, Shao W, Han L, Li Z, Zhang Z, et al. Comprehensive analysis of pivotal biomarkers, immune cell infiltration and therapeutic drugs for steroid-induced osteonecrosis of the femoral head. *Bioengineered*. (2021) 12:5971–84. doi: 10.1080/21655979.2021.1972081

33. Viola A, Munari F, Sánchez-Rodríguez R, Scolaro T, Castegna A. The metabolic signature of macrophage responses. *Front Immunol*. (2019) 10:1462. doi: 10.3389/fimmu.2019.01462

34. Jin S, Meng C, He Y, Wang X, Zhang Q, Wang Z, et al. Curcumin prevents osteocyte apoptosis by inhibiting M1-type macrophage polarization in mice model of glucocorticoid-associated osteonecrosis of the femoral head. *J Orthop Res*. (2020) 38:2020–30. doi: 10.1002/jor.24619

35. Zhu D, Yu H, Liu P, Yang Q, Chen Y, Luo P, et al. Calycosin modulates inflammation via suppressing TLR4/NF-κB pathway and promotes bone formation to ameliorate glucocorticoid-induced osteonecrosis of the femoral head in rat. *Phytother Res*. (2021) 35:2824–35. doi: 10.1002/ptr.v35.5

36. Aghajanian P, Mohan S. The art of building bone: emerging role of chondrocyte-to-osteoblast transdifferentiation in endochondral ossification. *Bone Res*. (2018) 6:19. doi: 10.1038/s41413-018-0021-z

37. Xiong J, Ma R, Xie K, Shan C, Chen H, Wang Y, et al. Recapitulation of endochondral ossification by hPSC-derived SOX9+ sclerotomal progenitors. *Nat Commun*. (2025) 16:2781. doi: 10.1038/s41467-025-58122-9

38. Shu HS, Liu YL, Tang XT, Zhang XS, Zhou B, Zou W, et al. Tracing the skeletal progenitor transition during postnatal bone formation. *Cell Stem Cell*. (2021) 28:2122–2136.e3. doi: 10.1016/j.stem.2021.08.010

39. Wang K, Ma C, Feng JQ, Jing Y. The emerging role of cell transdifferentiation in skeletal development and diseases. *Int J Mol Sci*. (2022) 23:5974. doi: 10.3390/ijms23115974

40. Houben A, Kostanova-Poliakova D, Weissenböck M, Graf J, Teufel S, Mark K, et al. β-catenin activity in late hypertrophic chondrocytes locally orchestrates osteoblastogenesis and osteoclastogenesis. *Development*. (2016) 143:3826–38. doi: 10.1242/dev.137489

41. Salazar VS, Gamer LW, Rosen V. BMP signalling in skeletal development, disease and repair. *Nat Rev Endocrinol*. (2016) 12:203–21. doi: 10.1038/nrendo.2016.12

42. Lyu Z, Da Y, Liu H, Wang Z, Zhu Y, Tian J. Chsy1 deficiency reduces extracellular matrix productions and aggravates cartilage injury in osteoarthritis. *Gene*. (2022) 827:146466. doi: 10.1016/j.gene.2022.146466

43. Wu X, Lai Y, Chen S, Zhou C, Tao C, Fu X, et al. Kindlin-2 preserves integrity of the articular cartilage to protect against osteoarthritis. *Nat Aging*. (2022) 2:332–47. doi: 10.1038/s43587-021-00165-w

44. Brum AM, van der Leije CS, Schreuders-Koedam M, Verhoeven J, Janssen M, Dekkers DH, et al. Identification of chloride intracellular channel protein 3 as a novel gene affecting human bone formation. *JBMR Plus*. (2017) 1:16–26. doi: 10.1002/jbm4.10003

Frontiers in
Cell and Developmental Biology

Explores the fundamental biological processes of life, covering intracellular and extracellular dynamics.

The world's most cited developmental biology journal, advancing our understanding of the fundamental processes of life. It explores a wide spectrum of cell and developmental biology, covering intracellular and extracellular dynamics.

Discover the latest Research Topics

See more →

Frontiers

Avenue du Tribunal-Fédéral 34
1005 Lausanne, Switzerland
frontiersin.org

Contact us

+41 (0)21 510 17 00
frontiersin.org/about/contact